Titre: Title:	Analysis of the Geomechanical Behavior of Two Adjacent Backfilled Stopes Based on Two and Three Dimensional Numerical Simulations
Auteur: Author:	Nooshin Falaknaz
Date:	2014
Type:	Mémoire ou thèse / Dissertation or Thesis
Référence: Citation:	Falaknaz, N. (2014). Analysis of the Geomechanical Behavior of Two Adjacent Backfilled Stopes Based on Two and Three Dimensional Numerical Simulations [Thèse de doctorat, École Polytechnique de Montréal]. PolyPublie. https://publications.polymtl.ca/1610/

URL de PolyPublie: PolyPublie URL:	https://publications.polymtl.ca/1610/
Directeurs de recherche: Advisors:	Michel Aubertin, & Li Li
Programme: Program:	Génie minéral

UNIVERSITÉ DE MONTRÉAL

ANALYSIS OF THE GEOMECHANICAL BEHAVIOR OF TWO ADJACENT BACKFILLED STOPES BASED ON TWO AND THREE DIMENSIONAL NUMERICAL SIMULATIONS

NOOSHIN FALAKNAZ

DÉPARTEMENT DES GÉNIES CIVIL, GÉOLOGIQUE ET DES MINES
ÉCOLE POLYTECHNIQUE DE MONTRÉAL

THÈSE PRÉSENTÉE EN VUE DE L'OBTENTION

DU DIPLÔME DE PHILOSOPHIAE DOCTOR

(GÉNIE MINÉRAL)

DÉCEMBRE 2014

UNIVERSITÉ DE MONTRÉAL

ÉCOLE POLYTECHNIQUE DE MONTRÉAL

Cette thèse intitulée :

ANALYSIS OF THE GEOMECHANICAL BEHAVIOR OF TWO ADJACENT BACKFILLED STOPES BASED ON TWO AND THREE DIMENSIONAL NUMERICAL SIMULATIONS

presentée par : FALAKNAZ Nooshin

en vue de l'obtention du diplôme de : Philosophiae Doctor

a été dûment acceptée par le jury d'examen constitué de :

M. SIMON Richard, Ph. D., président

M. AUBERTIN Michel, Ph. D., membre et directeur de recherche

M. LI Li, Doctorat., membre et codirecteur de recherche

M. MBONIMPA Mamert, Ph. D., membre

M. GRABINSKY Murray, Ph. D., membre externe

DEDICATION

I dedicate this work to

my husband ARASH and my son ARYA

my precious and beloved parents

&

my beloved country IRAN and my people.

ACKNOWLEDGEMENTS

I would like to express my deepest gratitude to my research supervisor Prof. ***Michel Aubertin*** for his open-ended support, guidance and extremely valuable advices in this project. This thesis have happened because of he inspired me through his devotion to academia. In addition to his help in writing the articles, and my dissertation, he has always given very generously his time to discuss various aspects of this project. Special thanks to my co-director Prof. *Li Li* who has given very precious advices during this project.

I would like to thank the industrial NSERC polytechnique-UQAT chair on Environment and Mine Wastes Management and from the Research Institute on Mines and the Environment (RIME UQAT-Polytechnique; RIME-IRME.ca) for financial support of this project.

I would also like to thank my friends, my colleagues and other members of RIME-IRME research group who helped me during this study.

I would like to conclude this section by thanking my husband *Arash*, my son *Arya* and my parents in *Iran* for their love, support and inspiration. My husband, ***Arash Khosravi***, has always supported me to start my Ph.D and helped me unconditionally during these years. I owe him a special gratitude.

RÉSUMÉ

L'industrie minière génère de grandes quantités de rejets qui peuvent être utilisés dans des chantiers souterrains pour contrôler les mouvements du massif rocheux et fournir un lieu de travail plus sûr pour les mineurs et les équipements. La compréhension du comportement mécanique de ces matériaux est une question cruciale pour prévenir les instabilités et réduire les risques. Il est important d'évaluer l'état des contraintes dans ces chantiers pour assurer une application sécuritaire du remblai. Au cours des dernières années, beaucoup de travail a été réalisé afin d'évaluer les contraintes dans les chantiers remblayés uniques (isolés). La distribution des contraintes dans les chantiers uniques a notamment été analysée en fonction des paramètres de résistance au cisaillement du remblai, de la géométrie du chantier, des pressions interstitielle de l'eau et des conditions de remplissage. A ce jour, l'analyse du comportement du remblai n'a pas pris en compte l'effet de l'excavation d'ouvertures multiples, qui peuvent influencer l'ampleur et la distribution des contraintes, des déformations et des déplacements de la paroi. La plupart des études ont également considéré la masse rocheuse comme un matériau élastique, ce qui ne reflète pas bien sa réponse réelle.

L'objectif principal de ce projet de doctorat était d'analyser le comportement de deux chantiers remblayés adjacents créés en séquence, en utilisant des simulations numériques. Les simulations ont tenu compte de l'effet des différents paramètres tels que les propriétés du remblai, la géométrie des chantiers, la largeur du pilier, la profondeur des ouvertures, la résistance du massif rocheux, l'état des contraintes naturelles, et le séquence d'excavation et de remplissage. Ces simulations ont montré que la contrainte de cisaillement qui se développe près du massif produit effet d'arche dans les deux chantiers. Ces effet est plus prononcé dans les chantiers remblayés étroits. Les résultats montrent aussi que la répartition finale des contraintes dans la première ouverture remblayée, après la création du chantier voisin, dépend largement des propriétés du remblai. Ces résultats montrent comment divers facteurs peuvent influer sur l'amplitude et la distribution des contraintes dans le premier chantier remblayé, suite à la création d'une seconde ouverture. Les résultats des simulations sont aussi comparés avec des solutions analytiques existantes.

Lorsque le massif rocheux est considéré comme ayant un comportement élasto-plastique, l'ampleur des contraintes, les déplacements des parois et les déformations du remblai sont

différentes des valeurs obtenues pour un comportement élastique. Les résultats révèlent aussi des effets combinés de la réponse du massif et d'autres caractéristiques, y compris la géométrie des chantiers (taille et espacement), leur profondeur, l'état des contraintes naturelles, ainsi que les propriétés du remblai.

La résistance minimale du remblai nécessaire pour maintenir la stabilité d'une face exposée lors du retrait d'un mur de support a également été étudiée en utilisant des solutions analytiques et numériques. Les résultats montrent que certaines ces solutions analytiques t ne semblent pas bien refléter le comportement réel du remblai et les mécanismes menant à la rupture. Les résultats de simulations en 3D indiquent également que la géométrie du chantier peut grandement affecter la résistance requise pour le remblai exposé.

Il est également montré que le comportement mécanique des chantiers remblayés dépend de leur longueur (i.e. troisième dimension), en plus des autres facteurs déjà identifiés. L'ampleur des contraintes et leur distribution, les déplacements des rocheuses, et les déformations sont également affectés par cette troisième dimension. Ces résultats montrent également que la réponse de deux chantiers adjacents de longueur finis est différente de celle des chantiers de longueurs infinis (i.e. analysés en 2D).

ABSTRACT

The mining industry generates large amount of waste materials which can be used in underground stopes to control ground movement and provide a safer work place for workers and equipments. Understanding of the mechanical behavior of these materials is a critical issue to prevent problem risks. It is important to assess the stress state in these stopes to ensure safe application of the backfill. In recent years, much work has been conducted to evaluate the stresses in single backfilled stopes. To date most research has focused on analyzing the behavior of backfill in isolated stopes without taking into account the effect of the excavation of two adjacent openings. However, reaction of neighboring stope, can influence the magnitude and distribution pattern of stresses, wall displacements and strain within an existing backfilled stope.

The main objective of this project was to analyze the behavior of two adjacent backfilled stopes created in sequence using numerical simulations (FLAC and FLAC^{3D}), taking into consideration the effect of different parameters such as backfill properties, stope geometry, pillar width, stope depth, rock mass strength parameters, and excavation and filling sequence. These simulations show that shear stresses develop near the rock mass wall and produce an arching effect in both stopes. Such arching effect is more pronounced in narrow backfilled stopes. The simulation results further indicate that the stress distribution in the first backfilled opening, following the creation of a second one, largely depends on the fill properties and other relevant parameters. These results show how these factors may affect the stress magnitude and distribution during and after the creation of a second opening. The simulations results are also compared with existing analytical solutions developed for isolated stopes.

When the rock mass behaves according to a elasto-plastic, the stress magnitude and pattern, wall displacements and backfill strains are significantly different from those obtained for an elastic rock mass behavior. The results shown here reveal the combined effects of the non-linear rock mass response and other characteristics including stopes geometry (size and spacing) and depth, natural stress state, and backfill properties. It is shown that the yielding of the backfill is affected by the rock mass behavior, and by other parameters such as backfill properties and stope geometry.

The minimum strength of the backfill required to maintain stability of an exposed face during removal of the support wall is also investigated using numerical simulations conducted

with FLAC^{3D}. The results show that existing analytical solutions may not reflect the actual behavior of the backfill and related failure mechanism. The results also show how the stope geometry and backfill properties affect the required strength for the exposed backfill.

Additional simulations conducted with FLAC^{3D} also show that the mechanical behavior of the backfilled stope depends on the stope length (third dimension). The stress magnitude and distribution, rock wall displacements and backfill strain are also affected by the stope third dimension.

TABLE OF CONTENTS

LIST OF TABLES

LIST OF FIGURES

LIST OF SYMBOLS AND ABBREVIATIONS

AWR	after front wall removal
B:	stope width (m)
BWR	before front wall removal
c′:	backfill cohesion (kPa)
c_{rm}:	cohesion of rock (kPa)
C_u:	coefficient of uniformity
D:	distance between stopes (pillar width) (m)
D_{60},D_{30}, D_{10}:	particle diameter at which 60%, 30% and 10% pass the mesh size (mm)
E:	backfill modulus
E_r:	rock mass elastic modulus
E_{rm}:	rock mass deformation modulus
e :	void ratio
e_{max} :	void ratio of backfill in loosest state
e_{min} :	void ratio of backfill in densest state
$G_{:}$	shear modulus
h:	depth (m) in the backfill
H:	stope height (m)
H_b :	total height of backfill in the stope (m)

I_d : density index

K: earth pressure coefficient for the backfill

K_a: active earth pressure coefficient

K_o: earth pressure coefficient at rest

K_r: earth pressure coefficient in the rock mass

k : hydraulic conductivity

L: stope length (m)

L_d: drift length (m)

n: porosity (%)

RMR : rock mass rating

s: deviatoric stress, radius of the Mohr-circle of stress (kPa).

t: mean stress, center of the Mohr-circle of stress (kPa)

UCS: uniaxial compressive strength (MPa)

z: stope depth (m)

α: sliding plane angle (°)

β: stope inclination (°)

γ: unit weight of backfill (kN/m^3)

γ_r: unit weight of rock (kN/m^3)

γ_{sat}: unit weight of saturated backfill (kN/m^3)

γ_{sub}: unit weight of submerged backfill (kN/m^3)

δ_h: horizontal displacement of rock walls (m)

δ_m: friction angle of fill/wall interface for wet backfill (°)

δ_{max}: maximum total displacement of open face (m)

δ_{sat}: friction angle of fill/wall interface for saturated backfill (°)

ε_h : horizontal strain of backfill

v: backfill Poisson's ratio

v_r: rock mass Poisson's ratio

σ_1: major principal stress (kPa)

σ_3: minor principal stress (kPa)

σ_h: horizontal stress (kPa)

σ_v: vertical stress (kPa)

ψ' : backfill dilatancy angle (°)

ϕ': internal friction angle of backfill (°)

ϕ_r: internal friction angle of rock (°)

ϕ_{rm}: internal friction angle of rock mass (°)

$\Delta\delta_h$: maximum difference between the horizontal displacements

$\Delta\sigma_h$: maximum difference between the horizontal stresses

$\Delta\sigma_v$: maximum difference between the vertical stresses

LIST OF APPENDICES

INTRODUCTION

Backfill can play an important role in underground mining operations by improving the wall stability around stopes and by reducing ore waste. The environmental and economic benefits of returning part of the tailings or waste rock underground are also part of the rationale behind backfilling (Hassani and Archibald, 1998).

A good understanding of the complex behavior of backfill and its interaction with the surrounding rock mass is a key step in assessing ground stability issues. Many researchers (e.g. Thomas, 1969; Ouellet et al. 1998b; Belem et al. 2000; Benzaazoua et al. 2004; Potvin et al. 2005; Helinski *et al.* 2007; Pirapakaran, 2008) carried out comprehensive studies to investigate the effect of various parameters on the mechanical behavior of backfills. There is generally a good agreement on how the binder content and curing time can influence the properties of the backfill materials. The majority of results show that the compressive strength and cohesion of the backfill increase as the curing time progresses and the binder proportion increases. Also, the compressive strength and elastic modulus of backfill tend to increase with the decreasing void ratio (same as other geotechnical materials).

These investigations also confirm that even the strongest backfills are soft (deformable) in comparison with the surrounding rock mass. This difference in stiffness and strength between these two materials generates a load transfer along the interfaces, which may create a significant arching effects in relatively narrow openings (e.g. Li et al. 2003). This phenomenon is well known in geotechnique (Handy and Spangler, 2007). Arching takes place in different types of materials such as soil, backfill and powder. It has also been analyzed for various situations such as the stress distribution around underground excavations (Terzaghi, 1943; Ladanyi and Hoyaux, 1969; Iglesia et al. 1999), earth pressure on retaining walls (Spangler and Handy, 1984; Take and Valsangkar, 2001), and underground conduits in ditches (Marston, 1930; McCarthy, 1988; Spangler, 1962). In mine stopes, the backfill is less rigid than the surrounding rocks, and tends to settle under its own weight after placement. Therefore, a portion of the overburden's weight is transferred to the rigid abutments due to frictional interaction between the fill and the surrounding walls, following the movement of backfill materials between the unyielding walls. The shear resistance along the interfaces prevents this downward movement and thus, reduces the

stress magnitude imposed within this yielding material at depth. Therefore, the stresses on the surrounding rigid rock mass increase.

Two and three-dimensional analytical solutions, often based on the Marston (1930) approach proposed for backfilled trenches, have been developed for evaluating the stress distribution in vertical single (isolated) backfilled stopes (e.g. Aubertin et al. 2003; Li et al. 2005; Pirapakaran and Sivakugan 2007; Li and Aubertin, 2008) and in inclined backfilled openings (e.g. Winch, 1999; Caceres, 2005; Sing et al. 2011; Ting et al. 2011, 2014; Li et al. 2013). Some of these solutions have been further developed to take into account the effect of pore water pressures PWP (Li and Aubertin 2009b, 2009c; Fahey et al. 2009). Mitchell et al. (1982) have proposed a solution that is commonly used to estimate the required strength of cemented backfill placed in stopes with an open face. This solution was later modified by Zou and Nadarajah (2006), Dirige et al. (2009), and Li and Aubertin (2012, 2014) to consider additional factors.

Physical-experimental models and in-situ measurements have been carried out to investigate the behavior of an isolated backfilled stope. Physical models tested by Mitchel et al. (1982) also showed the influence of arching on stress state within the stope with exposed faces. The measurements carried out by Take and Valsangkar (2001) and Pirapakaran (2008) have shown that the stress transfer in narrow backfilled openings and the effect of different parameters. Knutsson (1981) and Belem et al. (2004) reported in-situ measurements in stopes and on barricades. Thompson et al. (2011, 2012) also carried out in-situ measurements in stopes and on barricades. Furthermore, they investigated the effect of binder content, filling rate, geochemistry of ore body and pore water pressure on the stress state within these stopes.

Numerical modeling is another commonly used approach to analyze the behavior of backfilled stopes and barricades. Many different software codes, such as FLAC and FLAC^{3D}, PHASES2, PLAXIS and SIGMA/W, have been used to evaluate the stress state of the stopes and verify the results of analytical solutions in these structures. For instance, Li et al. (2003, 2005, 2007), Li and Aubertin (2009a, 2009b, 2009c, 2009d, 2009e, 2009f), and Pirapakaran (2008) have carried out a series of numerical simulations using FLAC to assess the stresses distribution in single stopes. The influence of different parameters was investigated, including backfill properties, stope geometry and pore water pressure. They often obtained a good agreement between the numerical and analytical solutions for the stress state in isolated backfilled stopes.

Other numerical analyses have been conducted by Helinski et al. (2007, 2010, 2011), Pirapakaran and Sivakugan (2007), Fahey et al. (2009), and El Mkadmi et al. (2011, 2014) to evaluate the influence of backfill properties, fill-wall interface characteristics, filling rate and pore water pressure. Numerical simulations have also been performed to assess the required strength of cemented paste backfill with an exposed face (Dirige et al. 2009; Karima et al. 2013; Emad and Mitri, 2013, Emad et al. 2014; Li and Aubertin, 2014).

In practice, underground mines generally include several stopes to recover the ore. To date however, little work has been done on the response of multiple stopes excavated in sequence. The influence of creating and filling neighboring stopes on the backfill response has not yet investigated. This is nonetheless an important issue, as the stress state in and around multiple openings may vary with the excavations geometry, position and creation sequence, as will be shown in this thesis.

The main purpose of this thesis is to develop a modeling approach, which would help mining operations predict the stresses, displacements and strain due to the creation of a second opening near an existing backfilled stope. The secondary motivation for this thesis is to investigate the influence of fill properties, stope geometry and rock mass parameters on the stress distribution, displacements and strains within the first backfilled stope when the rock mass behaves as elastic or elasto-plastic materials. Mining engineers can then use these results for selecting the size and location of the two adjacent stopes and to determine if the required backfill properties, considering also the rock mass characteristics. In addition, this approach gives a better evaluation of the minimum required strength of exposed cemented backfill, as a function of stope geometry and excavation sequence.

For this purpose, a comprehensive numerical study was conducted using more than 300 simulations. The backfill was incorporated into the FLAC model components. The first stope was excavated in one step (layer) and filled with four layers (steps). Then, the second stope was excavated in four steps (layers) from bottom to top and filled with four layers (steps). This project also involved numerical simulations under 2D (plane strain) and 3D conditions. The stress distribution within the first and second backfilled stopes was studied and compared with that of a single stope. The rock walls displacements and backfill strain in the first backfilled stope were also obtained. The simulation results specifically show how the excavation and backfilling of the

second stope affects the response of the first backfilled opening. The results are presented in terms of stresses, displacements and strains. The results illustrate how key parameters influence both the stress magnitude and distribution pattern, which can become much more complex in the case of two neighboring stopes. The influence of stope geometry and backfill strength parameters on the behavior and stability of exposed cemented backfill was also simulated. In all these cases, the numerical results were also compared with existing analytical solutions.

This thesis is structured as follows: Chapter 1 reviews the literature related to mine backfilling. Chapter 2 presents the research objectives, hypothesis and the methodology. Chapter 3 and 4 present the main results obtained using numerical simulations conducted with FLAC to determine the stress distribution and wall displacements in adjacent backfilled stopes when the simulating rock mass is elastic; these chapters also address the influence of different parameters on the stresses and displacements, including backfill and rock mass properties and stope geometry. Chapter 5 presents the simulation results for two adjacent backfilled stopes in an elasto-plastic rock mass; the influence of different parameters is also evaluated. Chapter 6 provides the results in terms of the stress state and displacements of the backfill in the primary stope (using FLAC^{3D}) when the secondary stope is mined out. Chapters 3 to 6 are presented in the form of manuscripts that have been submitted to peer-reviewed journals. Chapters 3 to 6 are the accepted or submitted papers; because of this paper format, there will be overlaps and repetitions between the chapters. Chapter 7 also addresses the effect of the third dimension on the stress distribution of two adjacent backfilled stopes using FLAC^{3D}, considering different backfill properties and stope geometry. Stresses are generally shown in kPa, while displacements and strains are shown in cm and %, respectively. The interpretation of the results shown in these chapters are context dependent and, in some cases, may involve engineering judgment from the author. When describing and comparing the results, differences are generally considered "significant" only when they could influence the engineering decision making process. Chapter 8 discusses these findings. The last Chapter includes a conclusion and recommendations for future work.

CHAPTER 1 LITERATURE REVIEW

Mining is a major industry in Canada. Many mines are based on underground operations, which are using mining methods that can be divided into three categories: naturally supported, supported and caving (unsupported) methods (Hartman et al. 1992; Brady and Brown, 1993). Mine backfill provides global support for rock walls and surrounding ground, often using waste rock or tailings (with or without cement).

Even the strongest backfill is soft in comparison with the adjacent rock mass (e.g. Appendix G for typical properties). When the backfill is placed in the stope, the difference between the mechanical properties of these two materials induces stress redistribution in the backfill and adjacent rock. The backfill deformation under its own weight produces a load transfer along the interfaces with the rock, due to the movement of the backfill material along unyielding walls. The shear resistance along the interfaces partly prevents this movement and reduces the stress magnitude within the yielding materials at depth; this phenomenon is known as an arching effect. Accurate evaluation of the stress distribution in rock mass and backfill materials is an essential issue for the design of backfilled stopes and barricades (e.g. Hassani and Archibald 1998; Aubertin et al. 2003; Pirapakaran, 2008).

This chapter presents a summary of some mining methods, backfill properties, as well as a review of arching effects within mining openings (using analytical solutions and numerical models), and a few results from in-situ measurements.

1.1 Mining Methods

Depending on the ore location, mining methods can be divided into two major types: surface mining and underground mining.

Surface Mining

This method is used when the ore deposits are located close to the surface. There are several surface mining methods such as strip mining, open pit mining, placer mining, hydraulic mining and dredging. Among them, open pit and strip mining are most often used (Hartman et al. 1992; Darling, 2011). Open pit mining involves digging a large hole in the ground using four basic operations including drilling, blasting, loading and hauling. Strip mining is used when a

seam of ore is located very close to the surface and covered by thin layers of soil or rock overburden (e.g.Pirapakaran, 2008).

Underground Mining

Underground mining methods are used to extract the minerals from the earth at depth and to reduce the amount of waste materials. It requires equipments and people to work underground. Providing a safe working place is one of the most important issues in underground mining. According to Brady and Brown (1993), underground mining methods can be divided into three major categories: self-supported, supported and caving (unsupported). This classification is based on the type of ground support. In caving methods, the ground is allowed to collapse under its own weight, sometimes up to the ground surface. Room and pillar mining, shrinkage stoping, sublevel stoping, and VCR (vertical crater retreat) are examples of self-supported mining methods, whereas (artificially) supported mining methods usually mean cut-and-fill mining methods. Stope backfilling is the most common methods to provide global ground support in underground mines. This method involves filling the underground stopes and support the excavated spaces using the supporting properties of backfill materials. As the backfill is usually relatively weak, it is often strengthen by adding a binder such as Portland cement. Typical properties of backfills are given in Appendix G.

1.2 Backfill classification

Backfill is often made of waste materials released from ore extraction and processing operation. There are different types of backfill such as hydraulic fill, paste fill and rock fill (Hassani and Archibald, 1998). Some of the major factors influencing the selection of backfill type are the physical and the mechanical properties of the ore and rock mass, fill strength requirements and mining methods. Mine backfills can be cemented or un-cemented.

Hydraulic fill (or slurry fill) includes mill tailings, sand or waste rock materials, water. It can also be made with or without binder. The pulp density of hydraulic fill is between 65-75% by weight. This type of fill must be transported in pipelines at higher velocities than the critical settling velocity to prevent deposition of solids. The hydraulic conductivity of slurry fills varies between 10^{-5} to 10^{-6} m/s (Grice, 2001). According to Potvin et al. (2005), the maximum amount

of particles finer than 10 μm should be limited to 10% to reach the adequate hydraulic conductivity.

Paste backfill was introduced by Robinsky (1975) as a non-segregating slurry known as thickened tailings. As a backfill, it includes the full mill tailings, a binder and water. Paste backfill has high solid content in the range of 75% to 85% by weight, depending on the particle size distribution and solid relative density. It often contains at least 15% of particles smaller than 20 μm, required to achieve reliable paste flow and act as a lubricant for the flow in the pipelines (Potvin et al. 2005). Sufficient water is added to reach the required paste consistency, i.e. about 200 mm of slumps (by the standard slump test). Cement is added (around 3%-7% by weight) to the mixture at the surface or prior to the fill placement in the stope (Belem et al., 2000).

Waste rock produced from underground or surface mining can be used in stopes with or without cement as rock fill. The cement can be added before the placement of rock fill in the stope or after placement. Consolidated rock fill (CRF) consists of relatively fine waste rock aggregates mixed with a slurry (at 5% to 6% cement content) to produce a 50% to 60% pulp density (Hassani and Archibald, 1998).

1.3 Backfill properties

The backfill properties should be selected to provide the optimum extraction of minerals based on the support requirements. In order to design a backfill material, it is necessary to study its physical and mechanical characteristics. A good understanding of these characteristics enables modification of the backfill material, quality control as well as design evaluation and final optimization according to the target properties. The final cost can then be assessed.

1.3.1 Physical properties

A backfill material consists of three different phases. The physical properties of this multi-phase material depend on the physical properties of each of these phases. The water content w is a basic characteristic, which influences the unit weight and mechanical properties of the backfill (Hassani and Archibald, 1998). Therefore, it is necessary to determine the water content in the backfill to reach the desirable backfill mechanical properties. Depending on the initial water content and hydraulic conductivity of the backfill as well as underground conditions, the

in-situ water content usually varies between 15 to 22% for a hydraulic fill. The material strength, stiffness and the hydraulic conductivity are affected by the void ratio as well. A typical void ratio *e* is 0.25 to 0.75 for a slurry fill and 0.5 to 0.85 for rock fill (Scoble and Piciacchia, 1987; Hassani and Archibald, 1998). Porosity, n ($= \frac{e}{1+e} \times 100\%$), typically varies from 20% to 48% for hydraulic fill and 35% to 42% for high-density slurry fill (Mitchell et al. 1975).

The strength and stiffness are also affected by the density index, I_D ($= \frac{(e_{max}-e)}{(e_{max}-e_{min})} \times 100\%$); where e_{max}, e_{min} are the void ratio in the loosest and densest states, respectively. The density index of hydraulic fill after placement in a stope is typically between 50-60% (Scoble and Piciacchia, 1988). Potvin et al. (2005) classified backfill based on the density index as loose, medium or dense (see Table 1.1).

Table 1.1: Density index for hydraulic fills (after Potvin et al. 2005)

Density index, I_D (%)	**State**
0-15	Very loose packing
15-30	Loose packing
30-60	Medium dense packing
60-85	Dense packing
85-100	Very dense packing

It is also useful to classify backfills according to their particle size distribution and density. Typically, paste backfill contains a widely graded size distribution with at least 15% of grains finer than 20 μm. The coefficient of uniformity, C_u ($= \frac{D_{60}}{D_{10}}$), is another factor that affects the backfill behavior. Particles of different sizes can influence porosity, permeability, strength and the percolation rate of the backfill. A well graded fill has a lower void ratio and smaller saturated hydraulic conductivity (*k*) in comparison with a uniform graded fill (Hassani and Archibald, 1998).

1.3.2 Mechanical properties

Backfill structure must be stable during and after placement. It must also be able to remain stable during the extraction of adjacent stopes and sustain the increased loading. The mechanical properties of backfill change over time and can be investigated by different

laboratory tests such as uniaxial compression tests, triaxial compression tests and direct shear tests. The unconfined compression test is commonly used to obtain the uniaxial compressive strength (UCS) of cemented fill. Belem et al. (2000) investigated the mechanical behavior of cemented paste backfill made with mine tailings, which was mixed with three different types of binder: ordinary Portland cement (PC), fly-ash based binder (FP) and slag based binder (SP). Three different proportions of binders (3 wt%, 4.5wt% and 6 wt %) were used. The short (28 days), mid (91 days) and long term (112 days) mechanical behavior of paste backfill were measured using a series of uniaxial compression tests. The results showed that for a given type of binder (Figure 1-1a), the compressive strength and Young's modulus are proportional to the amount of binder; a higher binder content gives a higher compressive strength and higher elastic modulus. Also, for a given amount of binder (fixed percentage), the compressive strength of cemented paste backfill can vary with the type of binder (Figure 1-1b), while the elastic modulus is almost unchanged for these binders (Belem et al. 2000).

(a)

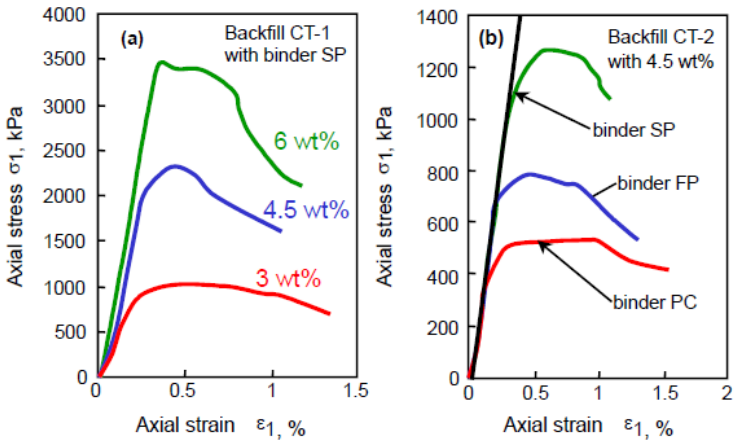

(b)

Figure 1-1: Uniaxial compressive strength of paste fill after 112 days of curing; results for: a) different proportion of binder; b) different type of binder (after Belem et al. 2000)

The compressive strength of paste backfill is time-dependent. Benzaazoua et al. (2004) investigated the effect of curing time on the strength properties of six paste backfills from different Canadian hard rock mines. They also studied the effect of the chemical composition of mine tailings and mixing water, binder types and binder proportions. Their results showed that for a given type of binder, the compressive strength of the paste backfill usually increases with the curing time and the binder proportion (Figure 1-2). They reported that different strength can be obtained from different binder types for a given tailing. In addition, Young's modulus

increases with increasing binder content for all types of mixtures. These results are in good agreement with those obtained by Belem et al. (2000). A similar investigation was conducted by Pirapakaran (2008). The results showed that the unconfined compressive strength of paste backfill increases with the binder content.

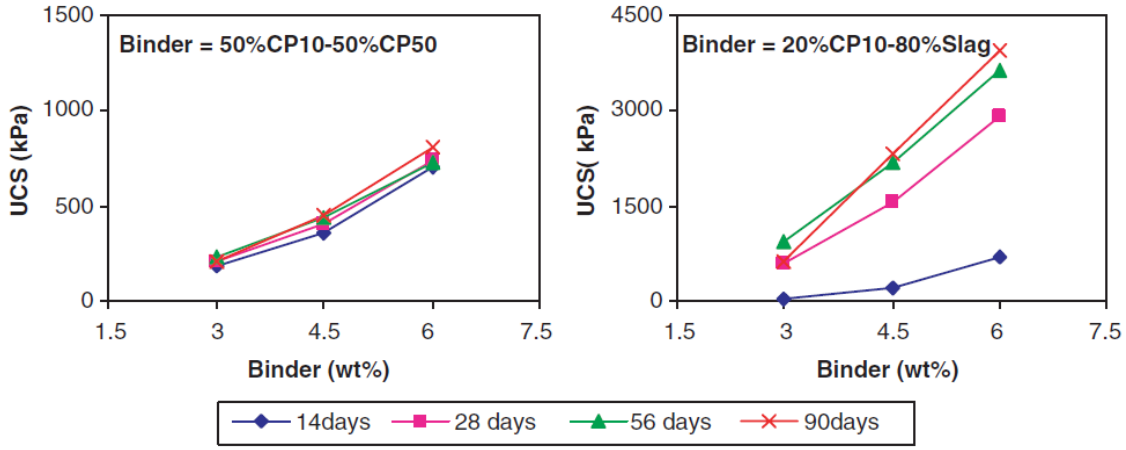

Figure 1-2: Effect of binder proportion on the mechanical strength of paste backfill as a function of curing time (after Benzaazoua et al. 2004)

Benzaazoua et al. (2004) also carried out a study on the effect of tailing's chemistry. They showed that tailings with higher sulphide content may have higher strength. Their results also showed that an increase in the water content of the mixture resulted in lower compressive strength.

The effect of particle size distribution on the hydration process of the binders and the compressive strength development of backfill was also investigated by various authors. The majority of these studies (Thomas, 1969; Ouellet et al. 1998a; Benzaazoua et al. 2004; Helinski et al. 2007; Pirapakaran, 2008) have shown that a backfill with coarser particles showed a higher compressive strength than a backfill with finer particles. Similar investigations were also conducted on the mechanical properties of hydraulic fills by Thomas (1969) and Helinski et al. (2007). They reported that the compressive strength increased as the cement content and curing time increased.

The shear strength parameters of backfill, including internal friction angle (ϕ), cohesion (c) and the friction angle (δ) along the interface of rock and back fill, are important characteristics, which can be used in stability analysis. Belem et al. (2000) investigations also

showed that for a given type of binder, the highest cohesion was obtained with the higher binder content (Figures 1-3). Barrett (1973) carried out triaxial compression laboratory tests on cemented hydraulic fills; the results indicated that cohesion increased with curing time.

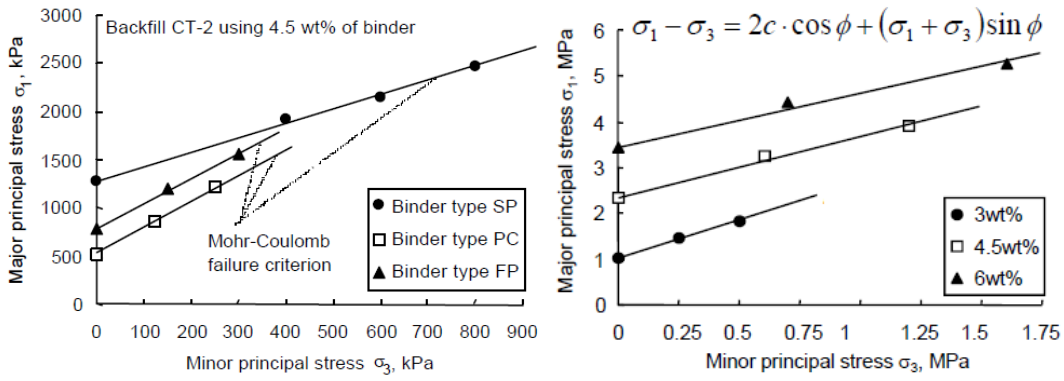

(a) (b)

Figure 1-3: Variation of shear strength of paste backfill due to: a) binder type; b) binder proportion (after Belem et al. 2000)

Veenstra (2013) carried out laboratory tests to investigate the strength and consolidation properties of seven different paste fills from three different mines. The results of these tests were used as input parameters for numerical models. He reported that the friction angles for most of the paste backfills varied between 34° to 40°. The results also showed that backfill cohesion was increased with time for low binder content. For high binder content, it increased and then decreased with the curing time. The maximum cohesion for low (2% to 4.5%) binder content paste fill was about 300 kPa, while it reached 600 kPa for a high (6.5% to 8.5%) binder content.

1.3.3 Hydro-mechanical properties

The hydraulic properties of backfill depend on water content and void ratio. These parameters influence the densification and drainage of the backfill and also its stress-strain response. The hydraulic conductivity is affected by the binder content; higher binder content typically results in a lower hydraulic conductivity. Also, the hydraulic conductivity tends to decrease as the applied stress increases (Pierce et al. 1997). Helinski et al. (2007) showed that a decrease in void ratio reduced the hydraulic conductivity of cemented fills.

Moreover, Helinski et al. (2011) carried out triaxial compression tests on cemented paste backfill for investigating the effect of curing time. The results revealed that the hydraulic conductivity decreased during the hydration process of cement.

Godbout et al. (2007) investigated the effect of binder on the saturated hydraulic conductivity of paste backfill. They reported that hydraulic conductivity decreased with an increase in the binder content. The type of binder content may also influence the hydraulic conductivity and its evolution.

In mining backfills, the self-weight consolidation occurs naturally due to gravity. Excess pore water pressure is then dissipated over time. Hydraulic fills are consolidated rapidly due to a relatively large hydraulic conductivity. In paste backfill, the hydraulic conductivity is low and consolidation occurs more slowly. In addition, cementation bonds may prevent consolidation (Potvin et al. 2005).

Belem et al. (2002) studied the effect of load application and consolidation on the mechanical strength of paste backfill under drained (and undrained) conditions. The tailings from a hard rock mine were mixed with 5 wt% of Portland cement (types I and V). The results of this study showed that the loading of drained backfill leads to rapid drainage, which favors the formation of hydrates and increases the UCS of drained samples (Figure 1-4). For undrained paste backfill samples, the load application increased the pore pressure, which leads the breakage of cement bonds and a reduction of the UCS.

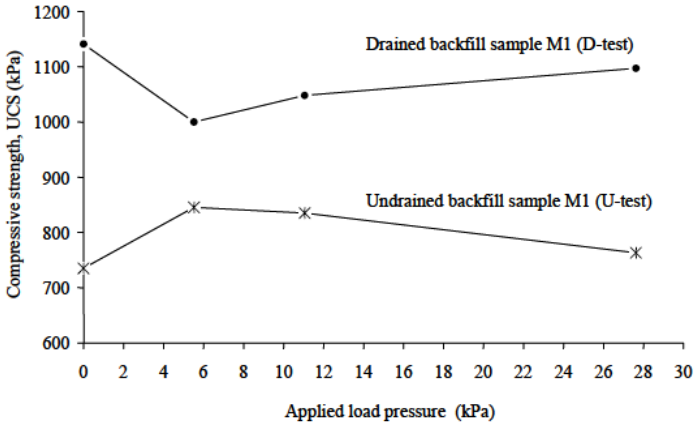

Figure 1-4: Influence of applied load on the UCS of paste backfill (after Belem et al. 2002)

The results of this study also showed that the UCS of the drained samples was higher than those obtained from undrained samples. In addition, the UCS of drained paste fill usually tends to increase with an increase in the applied load, while the UCS of undrained samples is typically reduced with increasing load.

Fahey et al. (2009) investigated the consolidation behavior of backfill in a stope during curing. They reported that the increased compressive strength obtained for specimens cured under stress is due to the increase in density achieved by compressing the specimens.

1.4 Stress distribution and arching effects

Arching can develop under various conditions in and around underground excavations (Terzaghi, 1943; Ladanyi and Hoyaux, 1969; Iglesia et al. 1999), along retaining walls (Spangler and Handy, 1985; Take and Valsangkar, 2001), and above underground conduits in ditches (Marston, 1930; Spangler, 1962; McCarthy, 1988). It can also happen in mining stopes where the backfill, which is less rigid than the surrounding rock, settles under its own weight after placement. A portion of the overburden weight is then transferred to the rigid abutments due to frictional interaction between the fill and the surrounding walls, following the movement of backfill. The shear resistance along the interfaces partly prevents this downward movement and thus, reduces the stress magnitude in the yielding material at depth. Therefore, the stresses in this surrounding rigid rock mass increase while, the vertical stress in the lower part of the opening under the main arch is reduced in comparison with the overburden stress (e.g. Aubertin et al. 2003; Li et al. 2003; Falaknaz et al. 2013). A typical arching phenomenon is illustrated in Figure 1-5. This figure shows that the stresses are typically lower along the walls than at the vertical central line (VCL); also, both the vertical and horizontal stresses are smaller than the overburden pressures, especially at depth (as will be shown below).

There are different ways to evaluate arching including analytical equations, physical models, in-situ measurements and numerical models. These will be described in the following.

1.4.1 Analytical solutions

Analytical solutions are usually simple and easy to use, compared with numerical simulations. They are relatively popular tools for evaluating the stress magnitude within stopes.

In the following, two and three-dimensional analytical solutions for vertical and inclined stopes are presented.

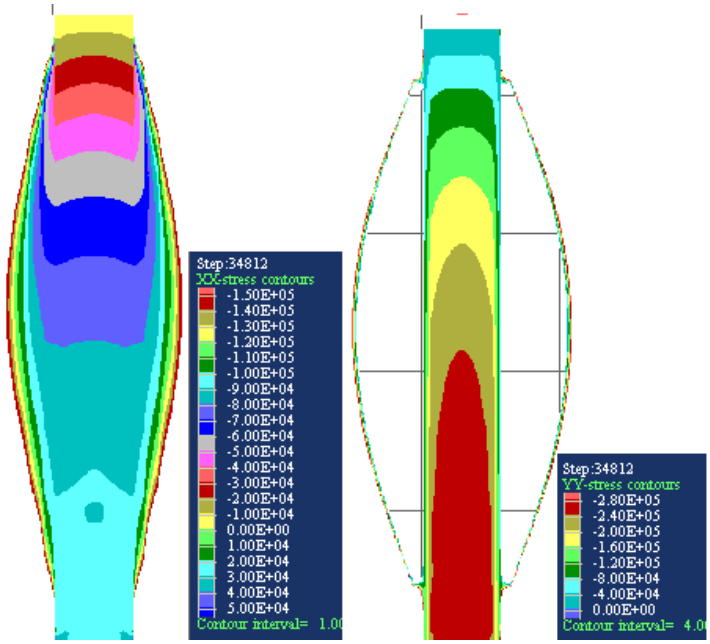

Figure 1-5: A typical arching phenomenon in a backfilled stope: a) vertical stress; b) horizontal stress (Falaknaz et al. 2013, see also Chapter 3)

1.4.1.1 2D analytical solutions

Marston's solution

Marston (1930, see also in McCarthy, 1988) provided a solution based on limit equilibrium, under plane strain to assess the arching phenomenon in vertical openings for cohesionless fill material. This solution was proposed for conduits in ditches, but it can be adapted to evaluate the stresses (in kPa) within narrow backfill stopes (Aubertin et al. 2003). This solution can be written as follows:

$$\sigma_v = \frac{\gamma B}{2\mu K}\left[1 - exp\left(-\frac{2\mu K H}{B}\right)\right] \quad (1\text{-}1)$$

$$\sigma_h = \sigma_v K \quad (1\text{-}2)$$

where μ (= tan δ) is the friction coefficient along the walls (δ is the friction angle (°) along these walls); B is the stope width (m); γ is the backfill unit weight (kN/m^3); H is the stope height (m) and K is the earth pressure coefficient.

Terzaghi's solution

Terzaghi's solution (1943) was developed based on that of Marston, by adding the effect of cohesion, *c*. It can be written as follows:

$$\sigma_v = \frac{\gamma B - 2c}{2K tan\emptyset}\left[1 - exp\left(-\frac{2KHtan\emptyset}{B}\right)\right] \quad (1\text{-}3)$$

where ϕ is the internal friction angle (°) of the backfill material.

Modified Marston's solution

The modified Marston's solution was proposed by Aubertin et al. (2003) for two-dimensional vertical stopes with a cohesionless backfill. Figure 1-6 shows a vertical stope and the acting forces.

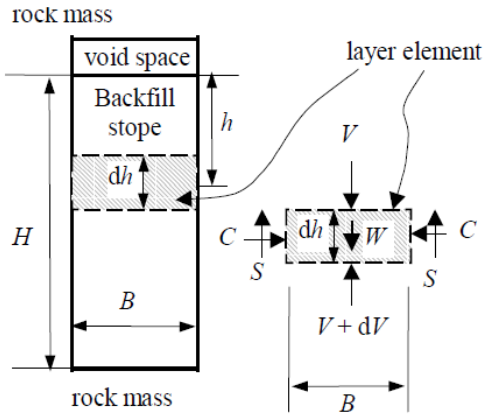

Figure 1-6: A vertical backfill stope and acting forces on the layer element (after Aubertin et al. 2003)

These resulting stresses can be written as:

$$\sigma_v = \gamma B\left[\frac{1-\exp\left(-\frac{2KHtan\phi'}{B}\right)}{2Ktan\phi'}\right] \quad (1\text{-}4)$$

$$\sigma_h = \gamma B\left[\frac{1-\exp\left(-\frac{2KHtan\phi'}{B}\right)}{2tan\phi'}\right] = K\sigma_v \quad (1\text{-}5)$$

Again, ϕ' is the internal friction of the fill material (°); γ is the unit weight of the backfill (kN/m^3) and *K* is the earth reaction coefficient. Based on the wall movements and the material characteristics, the value of *K* can be expressed as: (McCarthy, 1988):

$K = K_o = 1\text{-}\sin\phi'$ At rest condition (1-6)

$K = K_a = tan^2(45 - \frac{\phi'}{2})$ Active condition (Rankine solution) (1-7)

$K = K_P = tan^2(45 + \frac{\phi'}{2})$ Passive condition (Rankine solution) (1-8)

Equations 1-4 and 1-5 were proposed for narrow backfilled stopes under fully drained condition (with $u = 0$). In most cases, the earth reaction coefficient in active condition ($K = K_a$) is considered for analytical calculations (Li et al. 2003, Sobhi et al. 2014).

The horizontal and vertical stresses obtained by this solution are less than the overburden stress (γz) due to arching effects (see results in section 1.3.3.1). A series of numerical calculations were conducted by Li et al. (2003, 2007) and Li and Aubertin (2009a) for vertical stopes using FLAC (a numerical code based on the finite difference method, from Itasca, 2002) to verify the analytical solution results. The results of their investigations will be presented in section 1.4.3.1.

Li et al. (2005) extended these equations for cohesive materials, the corresponding formulations can be written as follows (in 2D):

$$\sigma_v = \frac{\gamma B - 2c(1+\tan\alpha\tan\phi)}{2K tan\phi'}\left[1 - \exp\left(-\frac{2KHtan\phi'}{B}\right)\right] \quad (1\text{-}9)$$

$$\sigma_h = K\sigma_v \quad (1\text{-}10)$$

where c is the fill cohesion (kPa); α is an angle based on fill condition and K is the earth pressure coefficient based on the wall movements and the material characteristics.

These solutions (Aubertin, et al. 2003; Li et al. 2005) assume uniformly distributed stress across the width of the stope. Li and Aubertin (2008) proposed the following alternative solution with a stress distribution factor (DF) related to an arch geometry:

$$\sigma_{vx} = \gamma B\left(\frac{1-\exp\left(-\frac{2K\,h\,tan\delta}{B(1-DF)}\right)}{2K\,tan\delta}\right).\left[1 - a\left(\frac{x}{B}\right)^b\right] \quad (1\text{-}11)$$

$$\sigma_h = \gamma B\left[\frac{1-\exp\left(-\frac{2K\,h\,tan\delta}{B(1-DF)}\right)}{2tan\delta}\right] \quad (1\text{-}12)$$

where x is the distance from the center line of the stope ($x \leq \frac{B}{2}$) having a width B; a and b are parameters that control the curvature of the stress distribution and DF is the distribution factor defined as follows:

$$DF = \frac{a}{2^b(b+1)} = \frac{2^{\left(1-\lambda_1\frac{H}{B}\right)}tan^{-\lambda_2}(\phi_0+\phi\prime)}{2^b(b+1)} \quad (1\text{-}13)$$

In these equations, the reference friction angle ϕ_0 =50°, while the distribution parameters λ_1 = 0.02, λ_2 = 0.1, and b = 3. Li and Aubertin (2008) compared numerical calculations with the results obtained by the modified solution to verify the effect of the distribution factor. Some results of this study will be showed in section 1.4.3.1.

Effect of pore water pressure

Li and Aubertin (2009c) proposed an analytical solution to evaluate the stress distribution in submerged vertical backfilled stope under plane strain (2D) equilibrium conditions, as shown in Figure 1-7. The effective vertical and horizontal stresses for partially submerged conditions can then be defined as:

$$\sigma_v' = \frac{B\,\gamma_{sub}}{2K_s\,tan\phi'}\left[1-\exp\left(-\frac{2K_s\,(h-H_m)}{B}tan\phi'\right)\right]+\frac{B\,\gamma_m}{2K\,tan\phi}\left[1-\exp\left(-\frac{2K\,H_m}{B}tan\phi\right)\right]\times$$

$$\exp\left(-\frac{2K_S(h-H_m)}{B}\right)tan\phi' \quad (1\text{-}14)$$

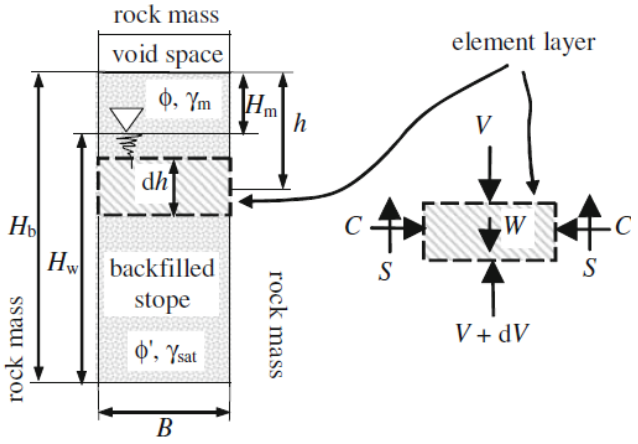

Figure 1-7: A vertical backfill stope under partially submerged condition in 2D (after Li and Aubertin, 2009c)

where H_m (m) is the height of wet backfill above the phreatic surface; H_w (m) is the height of the water in the stope; H_b (m) is the total height of the backfill in the stope; B is the stope width (m); γ_m and γ_{sat} (kN/m^3) are the unit weight of the fill above and below the phreatic surface, respectively; γ_{sub} (= $\gamma_{sat} - \gamma_w$) is the submerged unit weight of the backfill (kN/m^3); γ_w is the unit weight of water (kN/m^3), K_s is the effective reaction coefficient for the saturated backfill (based on K_a for an active condition). The wet backfill has the friction angle ϕ (°) while the saturated backfill has the effective friction angle ϕ'(°). This solution shows that an increase in the fill friction angle reduces the effective stresses in the backfill. An increase of the stope width causes an increase in the effective stresses of backfill. A comparison between the effective stress distribution obtained using numerical simulations and those obtained using Eq. 1-14 will be presented in section 1.4.3.1.

Li and Aubertin (2010a) extended this solution to include the effect of positive pore water pressure in vertical backfilled stopes considering a non-uniform vertical stress along the stope width. When the backfill is completely submerged ($h > H_m$), the effective non-linear vertical stress can be expressed as follows:

$$\sigma_{vx}' = \sigma_{vo}' \left\{ 1 - \mathrm{DF_{sat}} \left(\frac{|x|}{B} \right)^3 \right\} \tag{1-15}$$

with :

$$\sigma_{vo}' = \frac{B.\gamma_{sub}}{K_{sat} tan\delta_{sat}} \left\{ 1 - \exp\left[\frac{(\langle H_m \rangle - h).K_{sat}}{B(1-DF_{sat}/4)} \tan\delta_{sat} \right] \right\} + \frac{B.\gamma_m}{K_m tan\delta_m} \left\{ 1 - \exp\left[\frac{\langle H_m \rangle . K_m}{B(1-DF_m/4)} \tan\delta_m \right] \right\} \times$$

$$\exp\left[\frac{(\langle H_m \rangle - h).K_{sat}}{B(1-DF_{sat}/4)} \tan\delta_{sat} \right] \tag{1-16}$$

where x is the distance from the vertical center line ($-B/2 \le x \le B/2$); σ'_{vx} is the non-uniform vertical stress across the width of the stope (kPa); σ'_{vo} is the vertical stress along the center line of the stope (x=0); δ_m is the interface friction angle (°) ($\delta_m \le \phi_m$) and K_m is the active reaction coefficient$\left(= \frac{1-sin\phi_m}{1+sin\phi_m}\right)$. The MacCauley brakets are defined as $\langle H_m \rangle = \left(\frac{H_m + |H_m|}{2}\right)$. The distribution factor in the saturated backfill is:

$$DF_{sat} = \frac{2^{-(2+\frac{H_b}{100B})}}{tan^{0.1}(50^\circ + \emptyset_{sat})} \tag{1-17}$$

This solution indicates that both effective vertical and horizontal stresses decrease below the water table due to pore water pressure, while the total vertical and horizontal stresses tend to increase by the water pressure.

Inclined stopes

The solutions presented above have been proposed for stopes with vertical walls. Other methods have been developed for inclined walls. For instance, Caceres (2005) developed an analytical solution based on Marston's theory and the results obtained from numerical calculations for an inclined stope filled by rock fill. This solution can be written as follows for the vertical stress along the central line:

$$\sigma_v = \left[\frac{\gamma.L}{2K\ tan\emptyset}\right].sin^2\beta\left[1-\exp\left(\frac{2.z\ .K\ tan\emptyset}{L\ sin^2\beta}\right)\right] \quad (1\text{-}18)$$

$$K = 1.4sin^2\emptyset - 2\sin\emptyset + 1 \qquad 0 < \emptyset \leq 40 \quad (1\text{-}19)$$

Where L is the stope span (m); z is the height of the fill (m); K is the coefficient of lateral earth pressure obtained from numerical simulations (FLAC); γ is the unit weight of the fill (kN/m^3); and β is the stope wall angle (°). The effect of cohesion is neglected here.

Ting et al. (2011) proposed another analytical solution for backfilled stopes bounded by two parallel inclined walls, as shown in Figure 1-8. It was assumed that the adhesion between the rock face and the backfill is equal to the cohesion of the backfill. The shear stress along the interface of the backfill to hanging wall and footwall is considered same as for Caceres (2005).

The stresses are expressed as follows:

$$\sigma_v = \frac{\gamma.B-2(c(1+sin2\beta tan\delta))}{2K'\ tan\delta}\left(1-e^{-2K'\left(\frac{z}{B}\right)tan\delta}\right)+qe^{-2K'\left(\frac{z}{B}\right)tan\delta} \quad (1\text{-}20)$$

With:

$$K' = \frac{1+k}{2}+\frac{1-K}{2}cos2\beta + Ktan\delta sin2\beta \quad (1\text{-}21)$$

Where H is the height of stope (m); B is width of the stope (m); β is stope wall angle to the horizontal line (°); δ is the interface friction angle ($\delta = \frac{2}{3}\phi$); c is the cohesion of the backfill (kPa); γ is the fill unit weight (kN/m^3); q is the surcharge (kPa) and K is the earth pressure coefficient. Ting et al. (2011) compared the results obtained using the proposed expression with

other analytical solutions as well as with some numerical results for several special cases. Their results indicated that the combination of the arching effect and stope inclination can cause 65-70% reduction of the vertical stress at depth.

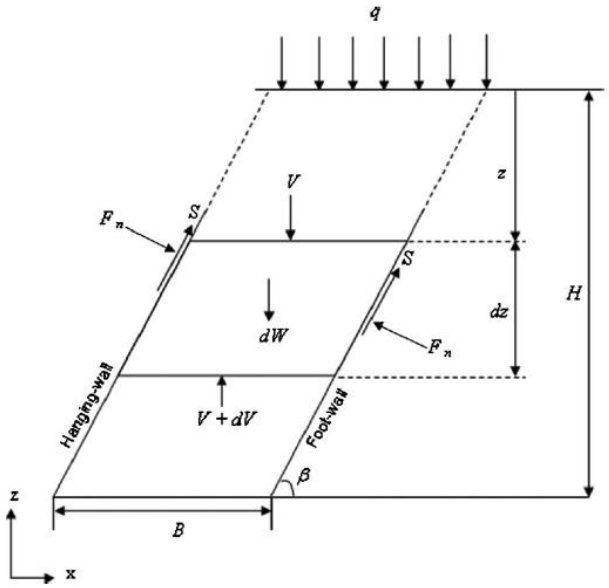

Figure 1-8: Characteristics of an inclined backfilled stope (after Ting et al. 2011)

Ting et al. (2014) recently proposed another analytical solution for backfilled stope with two non-parallel inclined walls with both walls are leanings to the same side at different angles, α and β to the horizontal (Figure 1-9).

The expression for the vertical stress at depth z is:

$$\sigma_v = -\frac{(R-Sz)}{T} + \frac{S(P-Qz)}{T(T+Q)} + \left(q + \frac{R}{T} - \frac{SP}{T(T+Q)}\right)\left[\left(1 - \frac{Qz}{P}\right)^{\frac{1}{a}}\right]^{-T} \quad (1\text{-}22)$$

$$P = B + \frac{H(tan\alpha - tan\beta)}{tan\beta\, tan\alpha}, \qquad Q = \frac{tan\alpha - tan\beta}{tan\beta\, tan\alpha}, \qquad S = \frac{\gamma(tan\alpha - tan\beta)}{tan\beta\, tan\alpha} \quad (1\text{-}23)$$

$$T = \frac{(tan\alpha - tan\beta)}{tan\beta\, tan\alpha} - K_1 tan\phi - K_2 tan\phi - K_2 cot\beta + K_1 cot\alpha \quad (1\text{-}24)$$

$$R = \gamma B - c(1 + sin2\alpha tan\phi) - c(1 + sin2\beta tan\phi) - csin2\beta cot\beta + csin2\alpha cot\alpha + \frac{\gamma H(tan\alpha - tan\beta)}{tan\beta\, tan\alpha} \quad (1\text{-}25)$$

$$K_1 = \frac{1+k}{2} + \frac{1-K}{2} cos2\alpha + Ktan\phi sin2\alpha \quad K_2 = \frac{1+k}{2} + \frac{1-K}{2} cos2\beta + Ktan\phi sin2\beta \quad (1\text{-}26)$$

Where B = stope width at the base (m), B_T = stope width at top (m), H = height of the stope (m), α = wall inclination at hanging wall (°), β = wall inclination at footwall; γ, c = unit weight and cohesion of the fill, respectively; K = lateral earth pressure; z is fill depth measured from top of the backfill. In this solution, the rock-wall interface is considered very rough so that the interface friction angle δ is taken as the friction angle of the backfill, ϕ. They showed that the results obtained using this analytical solution are in good agreement with those obtained from numerical simulations using FLAC when $\alpha \leq \beta$.

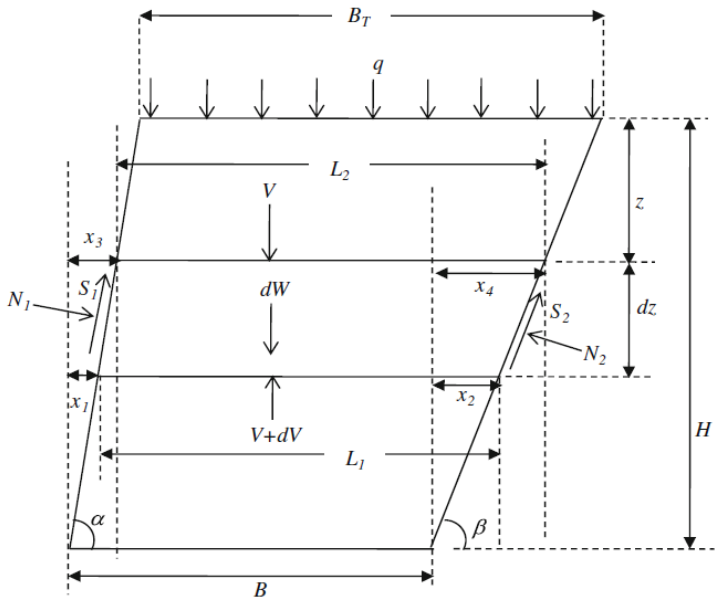

Figure 1-9: An inclined backfill stope with non-parallel walls (after Ting et al. 2014)

Singh et al. (2011) also developed an analytical solution for inclined backfilled stopes with two parallel walls, as shown in Figure 1-10. The expression for the vertical stress can be written as follows:

$$\sigma_v = \frac{(\gamma\delta B sin^2\alpha cosec\delta - 2c)}{2(sin^2\delta + Kcos^2\delta)tan\delta}\left\{1 - exp\left(\frac{8(sin^2\delta + Kcos^2\delta)tan\delta sin\delta}{B[2(1+K)\delta - (1-K)sin2\delta cos2\alpha]sin^3\alpha}z\right)\right\}$$

$$+\sigma_o exp\left(-\frac{8\left(sin^2\delta + Kcos^2\delta\right)tan\delta\, sin\delta}{B[2(1+K)\delta - (1-K)sin2\delta\, cos2\delta]sin^3\alpha}z\right) \qquad (1\text{-}27)$$

where B = stope width at the base (m), H = height of the stope (m), α = wall inclination (°); γ, c = are the unit weight and cohesion of the fill, respectively; K = lateral earth pressure; z is stope depth from top surface. In this solution, the fill-wall friction angle δ is taken as the friction angle of backfill, ϕ. The vertical stress obtained using this solution for the vertical stope is higher than

those stresses reported by Aubertin et al, (2003), Caceres (2005), Pirapakaran and Sivakugan (2007) and lower than those shown by Marston (1930).

Li et al. (2013) developed an analytical solution for the stresses in backfilled symmetrical openings (trenches) with non-parallel inclined walls, based on Marston solution. Figure 1-11 shows the model used to develop this solution.

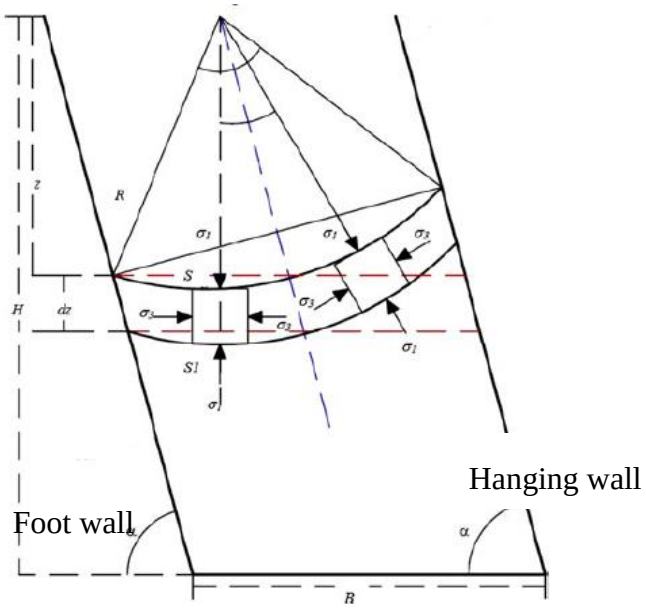

Figure 1-10: An inclined backfill stope with parallel walls (after Singh et al. 2011)

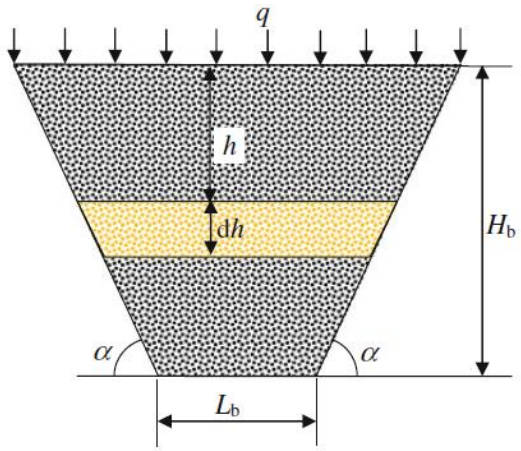

Figure 1-11: A trench with inclined walls (after Li et al. 2013)

The equation for the vertical stress can be written as:

$$\sigma_v = \frac{\gamma.D}{2(\lambda-1)}.(1-\frac{2.h}{D})\left\{1-\left(1-\frac{2h}{D}\right)^{\lambda-1}\right\}+q\left(1-\frac{2h}{D}\right)^{\lambda} \quad (1\text{-}28)$$

where:

$$D = L_b tan\alpha + 2H_b; \quad \lambda = K_a(tan\alpha . tan\delta + 1) - 1 \tag{1-29}$$

where α is the angle of the walls (°), δ is the friction angle of interface between the backfill and the wall (°), H_b is the thickness of the backfill (m), L_b is the width of the ditch at its base (m), γ is the unit weight of the backfill (kN/m^3), h is the depth of layer element (m). A good agreement was obtained between the vertical stress calculated by these solutions and numerical results obtained with FLAC.

1.4.1.2 Analytical solutions in 3D

In many geotechnical structures, one size is much larger than the others. These problems can be solved using plane strain (2D) condition (Hustrulid et al, 1989; Iglesia, et al, 1999; Aubertin, et al, 2003). However, when the stope length is small, three-dimensional solutions should be used to obtain a more realistic estimation of the stress distribution. Some of those 3D solutions are presented below.

Van Horn (1964) proposed the following three-dimensional solution for vertical stopes.

$$\sigma_v = \frac{\gamma\left(\frac{B\,L}{L+B}\right)-2c}{2K_r\,tan\delta}\left(1 - exp\left(\frac{-4\,K_r\,H\,tan\delta\,(L+B)}{LB}\right)\right) \tag{1-30}$$

$$\sigma_h = \frac{\sigma_h}{\sigma_v}\sigma_v \tag{1-31}$$

This solution is based on Marston's theory and inherits its restrictions. For instance, this theory uses Coulomb criterion along the rock and fill interface, which is not always appropriate when dealing with porous media. In addition, in this theory vertical stress is uniformly distributed across the stope width.

Winch (1999) introduced a 3D analytical solution for vertical stopes based on Terzaghi (1943) limit equilibrium solution. The vertical normal stress of fill (kPa) is:

$$\sigma_{vT} = \sigma_{vO} + \frac{\frac{w.l.\gamma}{2R\,(w+l)} - (c + K.\sigma_{vo}\,tan\phi)}{Ktan\phi}\left[1 - e^{\frac{-2R\,(l+w)}{l.w}K.tan\phi(z-z_o)}\right] \tag{1-32}$$

where w is the wall width (m); l is the wall length (m); z_o is the height of the fill at which the arching starts (m); z is the stope height; σ_{vo} is the vertical normal stress (kPa) at $z = z_o$; R is the

ratio of active length to total length of the stope; and *K* is the earth pressure coefficient which can take two values, i.e. K_o= *1- sinϕ* or $K_a = tan^2(45 - \frac{\phi}{2})$.

Li et al. (2005) proposed a 3D analytical solution for vertical backfilled stopes based on the Marston's solution for cohesive (cemented) backfill. Figure 1-12 shows a three-dimensional vertical narrow backfilled stope and all of the forces acting on a layer element. The four walls can have different properties. In this figure, *H* is the stope height (m); *B* is the stope width (m) and *L* is the stope length (m).

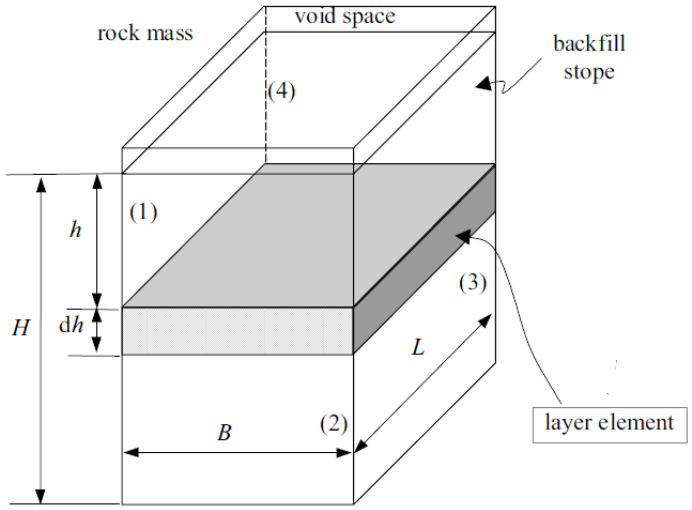

Figure 1-12: A 3D vertical backfill stope with the acting forces on the layer element (after Li et al. 2005)

The vertical and horizontal stresses across the horizontal plane at position *h* can be expressed as follows:

$$\sigma_{vh} = \frac{\gamma - (\kappa_{13}B^{-1} + \kappa_{24}L^{-1})}{(\lambda_{13}B^{-1} + \lambda_{24}L^{-1})}(1 - exp[-h((\lambda_{13}B^{-1} + \lambda_{24}L^{-1})]) \quad (1\text{-}33)$$

$$\sigma_{hhi} = K_i\,\sigma_{vh} + 2c\tan\alpha_i \quad (1\text{-}34)$$

$$\lambda_{13} = K_1\,tan\delta_1 + K_3\,tan\delta_3 \quad (1\text{-}35)$$

$$\lambda_{24} = K_2\,tan\delta_2 + K_4 tan\delta_4 \quad (1\text{-}36)$$

$$\kappa_{13} = c_1 + c_3 + 2c(tan\,\alpha_1\tan\delta_1 + tan\,\alpha_3\tan\delta_3) \quad (1\text{-}37)$$

$$\kappa_{24} = c_2 + c_4 + 2c(tan\,\alpha_2\tan\delta_2 + tan\,\alpha_4\tan\delta_4) \quad (1\text{-}38)$$

where δ_i and c_i (i = 1-4) are the friction angle (°) and the cohesion (kPa) of the i^{th} fill-wall interface (i = 1-4). The value of K_i (i = 1-4) is based on Rankine' active case. α_i (i = 1 - 4) is the angle of the failure plane from the horizontal (at-rest α_i = 0, active $\alpha_i = (\frac{\phi}{2} - 45°)$. When the friction angle of the fill material ϕ'_b is larger than the friction angle of the interface ($\phi'_b \geq \delta_i$), then the yielding takes place along the fill-wall interface. In the opposite case ($\phi'_b \leq \delta_i$), failure occurs in the fill material. The friction angle of the wall-fill interface δ is typically taken as the fill friction angle ϕ.

Comparisons between the vertical and horizontal stresses calculated using the 3D solution with the results obtained with the 2D solution showed that both stresses are usually smaller with the 3D solution, as illustrated in Figure 1-13. This difference is due to the larger shear stress mobilized along the third dimension on the fill-wall interface (which is neglected in the 2D solution). A higher fill-wall friction angle results larger arching effects and less stresses at depth in the backfill. An increase in the cohesion of the fill material also decreases the stresses within the stope. This solution does not consider the effects of the distribution factor (DF) on the vertical stresses in the backfill. A non-linear stress distribution across the width was introduced by Li and Aubertin (2010a).

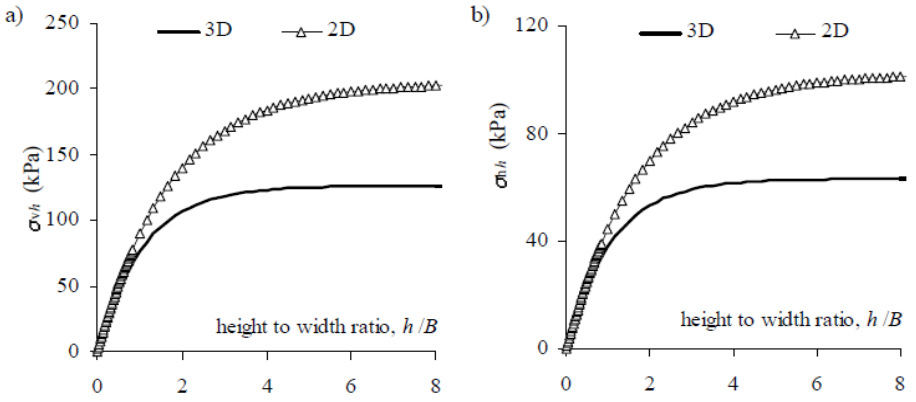

(a) (b)

Figure 1-13: Calculated values of the: a) vertical stress; b) horizontal stress (versus ratio *h/B*). In these cases B = 6 m, L=10 m (in 3D), c =1 kPa, $\delta = \phi$ = 30°, γ =20 kN/m^3, K=K_o= 0.5, (after Li et al. 2005)

Pirapakaran and Sivakugan (2007) also proposed a 3D solution for vertical stopes with different shapes (rectangular, circular and square). The vertical and horizontal stresses distributed within the stope can be expressed as:

$$\sigma_v = \frac{\gamma w}{2Ktan\delta}\left(\frac{l}{l+w}\right)\left[1 - exp\left\{-2\left(\frac{l+w}{lw}\right)Khtan\delta\right\}\right] \quad (1\text{-}39)$$

$$\sigma_v = \frac{\gamma w}{2tan\delta}\left(\frac{l}{l+w}\right)\left[1 - exp\left\{-2\left(\frac{l+w}{lw}\right)Khtan\delta\right\}\right] \quad (1\text{-}40)$$

where w is the stope width (m); h is the stope depth (m); l is the stope length (m); K is the coefficient of earth pressure ($K = K_o$) and δ is the friction angle of the fill/wall interface which is assumed to be 0.67ϕ. All walls have the same properties. Seven aspect ratios l/w (stope length/stope width) from 1 to 7 were considered to calculate the vertical stress within the stope. It was observed that for all aspect ratio, the vertical normal stresses were considerably less than the overburden pressure. In addition, the lowest vertical normal stress was reported for square and circular stopes in which the aspect ratio is equal to 1 (Figure 1-14). This solution is a specific case of the Extended-3D Marston's theory (Li et al, 2005) for various cross sections in which the cohesion is zero.

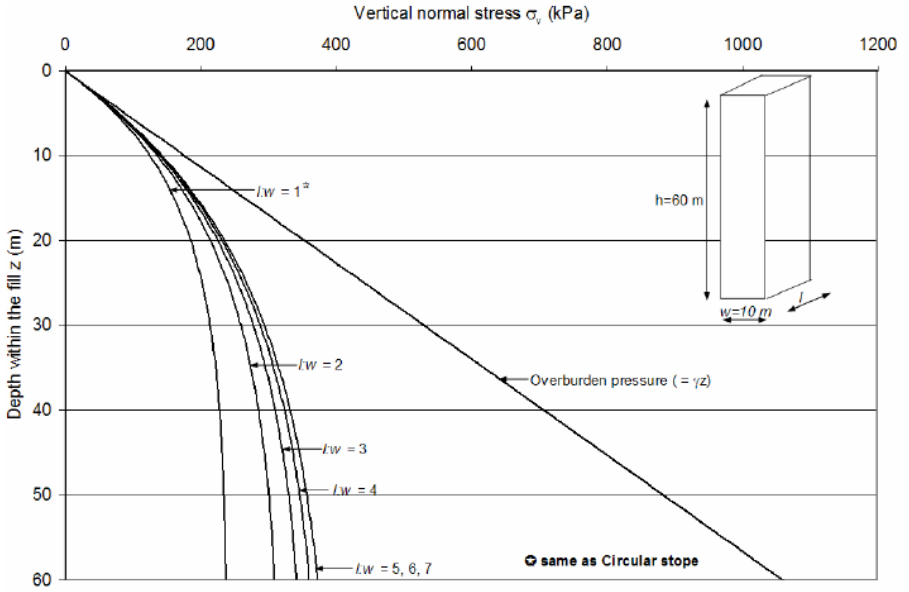

Figure 1-14: Vertical normal stress within the stope for different stope aspect ratios (l/w) using 3D solution (after Pirapakaran, 2008)

Submerged 3D stopes

Li and Aubertin (2009b) extended their 3D analytical solution for the case of submerged vertical backfilled stopes subjected to surface load, p_o (kPa). Figure 1-15 shows a schematic diagram of a vertical backfilled stope and a layer element. The opposite walls are considered to have the same properties. The layer element is located below the water table ($h \geq H_m, u_w = \gamma_w H_b$), which is under static equilibrium in the vertical direction. The effective vertical and horizontal stresses across the horizontal plane at position *h* can be obtained from the following equations:

$$\sigma'_{vh} = \frac{\gamma_m - 2c_m(\lambda_{1m}B^{-1}+\lambda_{2m}L^{-1})}{M_m}(1-\exp(-H_m M_m))\exp\big((H_m-h)M_{sat}\big) + \frac{\gamma_{sub} - 2c_{sat}(\lambda_{1sat}B^{-1}+\lambda_{2sat}L^{-1})}{M_{sat}}(1-\exp\big((H_m-h)M_{sat}\big) + P_o exp[(H_m-h)M_{sat} - H_m M_m] \quad (1\text{-}41)$$

$$\sigma'_{hhi} = K_{isat}\sigma'_{vh} + 2c_{sat}tana_{isat} \quad (1\text{-}42)$$

$$M_{sat} = 2(K_{1sat}B^{-1} + K_{2sat}L^{-1})tan\delta_{sat} \quad (1\text{-}43)$$

$$M_m = 2(K_{1m}B^{-1} + K_{2m}L^{-1})tan\delta_m \quad (1\text{-}44)$$

$$\lambda_{1sat} = 1 + 2tana_{1sat}tan\delta_{sat} \quad (1\text{-}45)$$

$$\lambda_{2sat} = 1 + 2tana_{2sat}tan\delta_{sat} \quad (1\text{-}46)$$

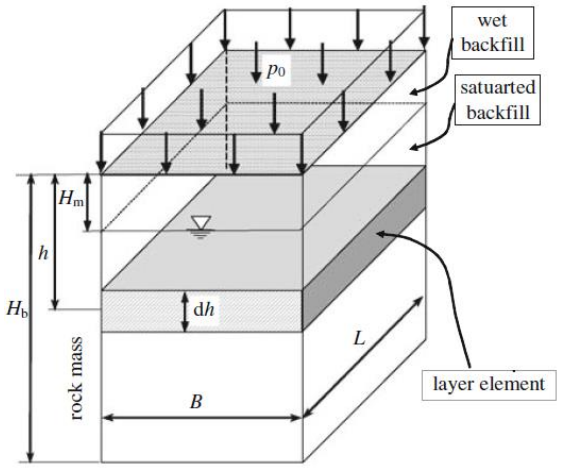

Figure 1-15: A 3D vertical backfilled stope in the presence of water (after Li and Aubertin, 2009b)

In this figure, ϕ_m (°) and c_m (Pa) are the internal friction angle and cohesion of the wet (moist) backfill; ϕ_{sat} (°) and c_{sat} (Pa) are the internal friction angle and cohesion of the saturated backfill; δ_m and δ_{sat} (°) are the friction angles of the fill/wall interface for the wet and saturated backfill, respectively; γ_{sub} (= $\gamma_{sat} - \gamma_w$) is the submerged unit weight of the backfill (kN/m^3). The opposing walls have the same properties.

The results from this solution show that the effective stresses are lower than the overburden pressure due to arching effects. Also, the slope of the vertical and horizontal stresses distribution is changing at the phreatic surface level (Figure 1-16). Furthermore, both effective vertical and horizontal stresses are reduced below the water table due to pore water pressure. The results also showed that an increase of the stope width produced an increase in both vertical and horizontal effective stresses.

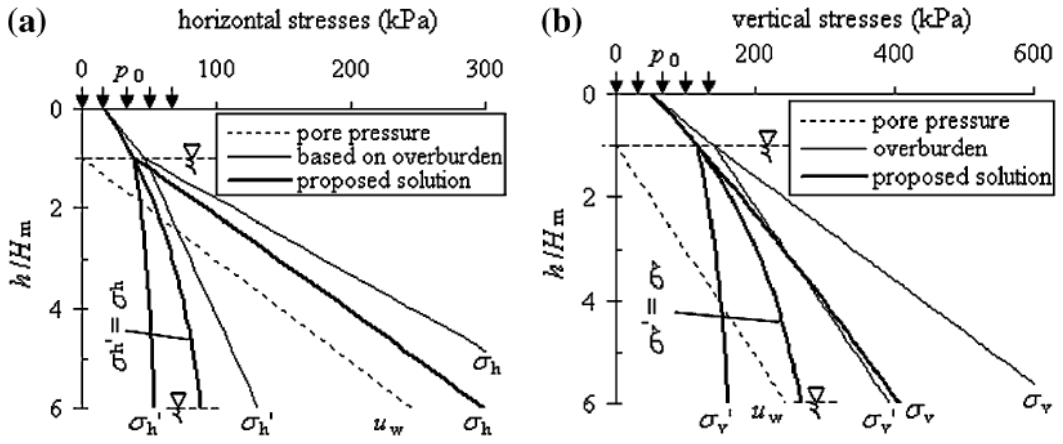

Figure 1-16: (a) Vertical; (b) horizontal stresses (total and effective) versus elevation h; $K=K_a$, phreatic surface is at H_m = 5m, B =10 m, L = 20m, ϕ = 30°, γ = 18 kN/m^3, saturated fill is $\phi_m = \phi_{sat} = \delta_m = \delta_{sat}$ = 30, γ_{sat} = 20 kN/m^3, p_o = 50 kPa (after Li and Aubertin, 2009c)

1.4.1.3 Backfilled stopes with an open face

Mitchell et al. (1982) developed a 3D analytical solution based on the limit equilibrium method for an exposed fill mass, as shown in Figure 1-17. It is considered that failure occurs within a block through a sliding plane forming a wedge. The shear resistance between the fill and the stope walls is due to fill cohesion only, which prevents sliding of the block. The cohesion required to maintain the stability of the block can be expressed as:

$$FS = \frac{\tan \emptyset}{\tan \alpha} + \frac{2cL}{(H - \frac{B \times \tan \alpha}{2})(\gamma L - 2c_b) \sin 2\alpha} \quad (1\text{-}47)$$

$$c = \frac{\gamma H}{2\,(\frac{H}{L} + tan\alpha)} \quad (1\text{-}48)$$

where α is the angle of the failure plane to horizontal ($45° + \frac{\emptyset}{2}$); ϕ is the internal friction angle (°) of the backfill material (often assumed $\phi = 0$); c_b is the bond cohesion along the sidewalls and the backfill interface (kPa); γ is the fill unit weight (kN/m^3); L is block's length (m); w is block's width (m); H is the height of the block (m); and FS is the factor of safety. This solution will be reviewed in Chapter 6.

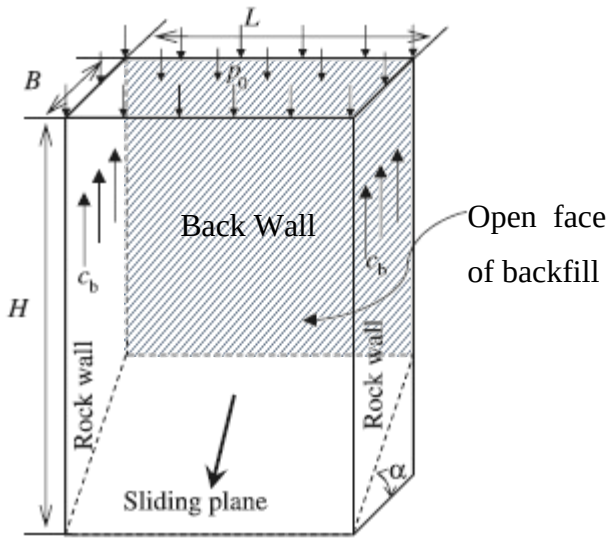

Figure 1-17: A confined block with an open face (after Mitchell et al. 1982)

Dirige et al. (2009) also proposed an analytical solution based on Mitchel's solution, but with different assumptions to estimate the required strength and factor of safety of the backfill in an inclined stope as shown in Figure 1-18. For this solution, the hanging wall is considered as a free surface without shear resistance, while the footwall resistance is assumed constant and equal to the fill cement bond shear strength. For an ore body inclined less than 90° with relatively smooth walls, the safety factor is:

$$FS = \frac{tan\phi}{tan\alpha} + \frac{\frac{cLW}{\cos \alpha}}{F_v sin\alpha} + \frac{cos\beta tan\phi}{sin\alpha} \quad (1\text{-}49)$$

where α (= 45°+ ϕ/2) is the angle of the failure plane within the fill (°); ϕ is the friction angle (°); β is the hanging wall/footwall dip (°); c is the fill cohesion (kN/m^2); L and W are the stope/backfill length and width (m) respectively.

The vertical force applied by the weight of the potential sliding block (kN) is given by:

$$F_v = (\gamma WLH^*) - ((\gamma WLH^*)cos\beta\ tan\phi) \quad (1\text{-}50)$$

where γ is the fill unit weight (kN/m^3); H^* = H- (L. $tan\alpha$)/2 (m); H is the fill height (m). For rough rock wall surfaces, the safety factor is written as:

$$FS = \frac{tan\phi}{tan\alpha} + \frac{\frac{cLW}{\cos\alpha}}{F_v sin\alpha} + \frac{cos\beta tan\phi}{sin\alpha} + \frac{\frac{cLH^*}{sin\beta}}{F_v\ sin\alpha} \quad (1\text{-}51)$$

with:

$$F_v = (\gamma WLH^*) - \left\{\left(\frac{cLH^*}{\sin\beta}\right) + ((\gamma WLH^*)cos\beta\ tan\phi)\right\} \quad (1\text{-}52)$$

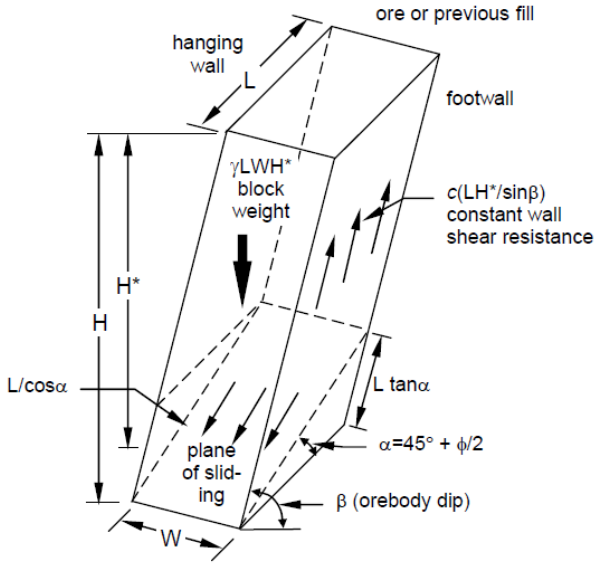

Figure 1-18: A confined inclined block with an open face (after Dirige et al. 2009)

Their calculations showed that the fill stability increases with decreasing stope width and height, orebody inclination, increasing binder content and wall roughness. This limit equilibrium solution relies on a number of assumptions that may not all be realistic, such as postulating that the cohesion along the sidewalls is equal to the backfill cohesion, the frictional strength along these sidewalls is nil, and the mobilized strength along the back wall of the stope is negligible (e.g. Li and Aubertin, 2012, 2014).

Li and Aubertin (2012) proposed a modified solution for an exposed backfill based on the Mitchel et al. (1982) solution, considering the effect of the friction angle along the fill-wall interfaces and the cohesion along the back wall. This solution is valid for backfilled stopes with a high ($H/B \geq \tan\alpha$) and ($H/B < \tan\alpha$) low aspect ratio (stope height/stope width). The following is obtained from the Modified Mitchel (MM) solution for stopes with a high aspect ratio (HAR):

$$FS = \frac{\tan \emptyset}{\tan \alpha} + \frac{2c}{[p_o + (H - \frac{B \times \tan \alpha}{2})(\gamma L - 2c_b)] \sin 2\alpha} \quad (1\text{-}53)$$

$$c = \frac{(p_o + \gamma(H - (B \times tan\, \alpha)/2)}{\left[\left(FS - \frac{\tan \emptyset}{\tan \alpha}\right) \sin 2\alpha\right]^{-1} + r_b\,(H - \frac{B \times \tan \alpha}{2})/L} \quad (1\text{-}54)$$

where r_b (= c_b/c; from 0 to 1) is the adherence ratio of the fill-rock interface, p_o is the surcharge due to different of sources. For backfilled stopes with a low aspect ratio (LAR), the factor of safety and required cohesion can be expressed by:

$$FS = \frac{\tan \emptyset}{\tan \alpha} + \frac{2c}{[p_o + H(\frac{\gamma}{2} - \frac{c.r_b}{L})] \sin 2\alpha} \quad (1\text{-}55)$$

$$c = \frac{p_o + \gamma(H/2)}{2\left[\left(FS - \frac{\tan \emptyset}{\tan \alpha}\right) \sin 2\alpha\right]^{-1} + r_b H/L} \quad (1\text{-}56)$$

The modified Mitchell (MM) solution better correlates with Mitchell et al. (1982) experimental results. The MM solution used the same basic assumptions adopted by Mitchell et al. (1982), but there is little practical data or simulation results to justify these assumptions. The only source available for verification of the results comes from some shear box and unconfined compression test results. Addressing some of these questionable assumptions lead to the development of a new analytical solution by Li and Aubertin (2014) to define the exposed backfill strength based on the displacements and apparent failure mechanism. The wedge model is then divided into an upper rectangular block and a lower triangular wedge. The upper part is assumed to move along the vertical direction while the lower part moves in a direction parallel to the sliding plane. The *FS* and the value *c* are expressed as:

$$FS = \frac{\tan \emptyset}{\tan \alpha} + \frac{c\left(\frac{1}{\cos \alpha} + r_{bs}\frac{H'}{L}\right) + \frac{\left(\frac{\gamma}{M} - p_1\right)\left[\frac{1 - \exp(-MH')}{MH'} - 1\right] + \gamma H'/2}{1 + L/B}}{\left(p_1 + \frac{\gamma H'}{2}\right) \sin \alpha} \quad (1\text{-}57)$$

$$c = \frac{D'(p_o + \gamma(H-H') - G') + A'\gamma H'[1-L/B]\sin\alpha - \gamma\left(\frac{C'}{M} + \frac{H'}{2}\right)}{\left(l + \frac{L}{B}\right)B' + D'(H-H')\left(\frac{2r_{bs}}{L} + \frac{r_{rb}}{B}\right)} \quad (1\text{-}58)$$

$$p_1 = p_o - G' + (H-H')\left\{\gamma - c\left(\frac{2r_{bs}}{L} + \frac{r_{bb}}{B}\right)\right\} \quad (1\text{-}59)$$

$$G' = \frac{1}{1+\frac{L}{B}}\left\{\gamma(H-H') + (P_O - \frac{\gamma}{M})[1 - \exp(-(H-H')M]\right\} \quad (1\text{-}60)$$

$$A' = FS - \frac{\tan\emptyset}{\tan\alpha} \qquad B' = \frac{1}{cos\alpha} + r_{bs}\frac{H'}{L} \qquad C' = \frac{1-\exp(-MH')}{MH'} - 1$$

$$D' = A'\left(1 + \frac{L}{B}\right)sin\alpha + C' \qquad H' = B\,tan\alpha \quad (1\text{-}61)$$

where r_b (considered identical for the side walls and back wall, i.e., $r_b = r_{bb} = r_{bs}$) varies from 0 to 1 for frictionless walls ($\delta = 0$) and for fully frictional interfaces along the side walls ($\phi = \delta$). The factor of safety given here tends to increase slightly and linearly with the backfill cohesion when $r_b = 0$. When the interface cohesion is similar to the backfill cohesion ($r_b = 1$), the factor of safety increases, more markedly with the latter. The backfill stability is also improved when mobilized friction is considered along the interfaces (rough wall), compared with frictionless interfaces. These solutions will be reviewed with more details in Chapter 6.

1.4.1.4 Horizontal pressure on barricades

A barricade is a brick, concrete or lattice structure constructed to retain the backfill material within the stope. A saturated backfill is susceptible to generate mudflow of fine-grained material. Therefore, a well-design barricade is required. In the following, a few analytical methods proposed for the design of barricades are summarized.

Mitchell et al. (1975) first proposed the following solution to estimate the load applied by the backfill on barricades:

$$F_h = \tfrac{1}{2}\gamma H^2 W_d K_o \quad (1\text{-}62)$$

where F_h is the total horizontal barricade load (kN), W_d is the drift width (m); H_d is the drift height (m); K_o is the at-rest earth pressure coefficient and H is the total height of the fill in the stope (m). This solution neglects the frictional stress redistribution along the walls. Modified equations proposed by Mitchell (1992) can be written as:

$F_h = \frac{1}{2}\gamma H^2 W_d K$ for $H < H_d$ (1-63)

$F_h = \frac{1}{2}\gamma H_d (H - \frac{H_d}{2}) W_d K$ for $H \geq H_d$ (1-64)

Smith and Mitchell (1982) and Mitchell and Roettger (1984) proposed another solution to address the frictional stress transfer to the abutments. In this solution, the horizontal normal stress σ_h and the load P on the barricade are expressed as follows:

$\sigma_h = 0.4\gamma H(1 - 0.6\frac{l}{W_d})]$ (1-65)

$P = 0.2\gamma H^2 (w_d - 0.6l)$ for $H \leq H_d$ (1-66)

$P = 0.2\gamma H_d (2H - H_d)(w_d - 0.6l)$ for $H > H_d$ (1-67)

where l is the set-back distance between the bulkhead and the stope wall brow (m). The horizontal stress is linearly increased with the backfill height, while the influence of barricade height on the horizontal stress is neglected. Furthermore, where the drift width w_d is very large, no stress is transferred along the drift. The influence of the barricade height on the horizontal stress is neglected in this solution.

Li and Aubertin (2009d) have proposed a 3D analytical solution to evaluate the stresses on barricades for fully drained backfills ($u = 0$), based on Figure 1-19.

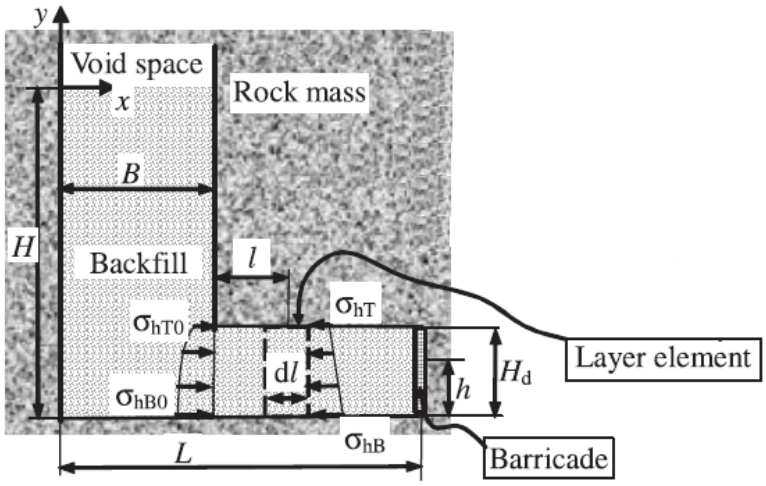

Figure 1-19: A vertical backfill stope with an access drift under fully drained (u = 0) condition (after Li and Aubertin, 2009d)

For a cohesionless backfill, the horizontal stress σ_h in the drift and the load P on the barricade are:

$$\sigma_h = [\frac{h}{H_d}\sigma_{hTO} + (1-\frac{h}{H_d})\sigma_{hBO}]exp[-l\frac{2tan\delta}{K_{dl}}(\frac{1}{H_d}+\frac{K_{dt}}{W_d})] \quad \text{for} \quad H \geq H_d \qquad (1\text{-}68)$$

$$\sigma_h = \sigma_{hBO}(1-\frac{h}{H})exp[-l\frac{2tan\delta}{K_{dl}}(\frac{1}{H}+\frac{K_{dt}}{W_d})] \quad \text{for} \quad H < H_d \qquad (1\text{-}69)$$

$$P = \frac{H_d W_d}{2}(\sigma_{hBO}+\sigma_{hTO})exp[\frac{-2tan\delta}{K_{dl}}(\frac{1}{H_d}+\frac{K_{dt}}{W_d})(L-B)] \quad \text{for} \quad H \geq H_d \qquad (1\text{-}70)$$

$$P = \frac{HW_d}{2}\sigma_{hBO}exp[\frac{-2tan\delta}{K_{dl}}(\frac{1}{H_d}+\frac{K_{dt}}{W_d})(L-B)] \quad \text{for} \quad H < H_d \qquad (1\text{-}71)$$

$$\sigma_{hTO} = \frac{\gamma}{M}\{1-exp[-K_s M(H-H_d)]\} \qquad \sigma_{hBO} = \frac{\gamma}{M}\{1-exp[-K_s MH]\} \qquad (1\text{-}72)$$

$$M = 2\,(B^{-1}+W_s^{-1})tan\delta \qquad (1\text{-}73)$$

In these equations, L is the distance between the stope wall and the barricade (m); l is the horizontal distance between the vertical element and the stope entrance (m); h is the element height (m); w_s is the stope length (m); H is the backfill height (m); H_d and W_d are the height and the width of the access drift (m); W_s is the stope length (m); δ is the friction angle of the wall-fill interface (°); ϕ is the fill friction angle (°) and K_{dl} and K_{dt} are the earth pressure coefficient in the longitudinal and transverse direction of drift, respectively (based on Rankine's theory); σ_{hTO} and σ_{hBO} are the horizontal normal stresses at the top and base level of the drift.

The influence of backfill properties and drift geometry on the stress distribution in the drift is shown in Figure 1-20. It is seen that an increase in the fill friction angle decreases the stress magnitude in the drift. It is also observed that when the width or the height of the drift increases, the stress transfer to the walls is reduced and the pressure on the barricade increases.

Li and Aubertin (2009e) developed a complementary analytical solution to evaluate the effective and total stresses on barricades under partially or fully submerged conditions. Figure 1-21 shows a schematic diagram of a vertical backfilled stope with the access drift. For a cohesionless backfill, the effective horizontal stress σ'_h in the drift at elevation h is expressed as:

$$\sigma'_h = [\frac{h}{H_d}\sigma'_{hTO} + (1-\frac{h}{H_d})\sigma'_{hBO}]exp[-l\frac{2tan\delta_{sat}}{K'_{dl}}(\frac{1}{H_d}+\frac{K'_{dt}}{W_d})] \qquad H_b \geq H_d \qquad (1\text{-}74)$$

$$\sigma'_h = (1-\frac{h}{H_d})\sigma'_{hBO}exp[-l\frac{2tan\delta_{sat}}{K'_{dl}}(\frac{1}{H_d}+\frac{K'_{dt}}{W_d})] \qquad H_b < H_d \qquad (1\text{-}75)$$

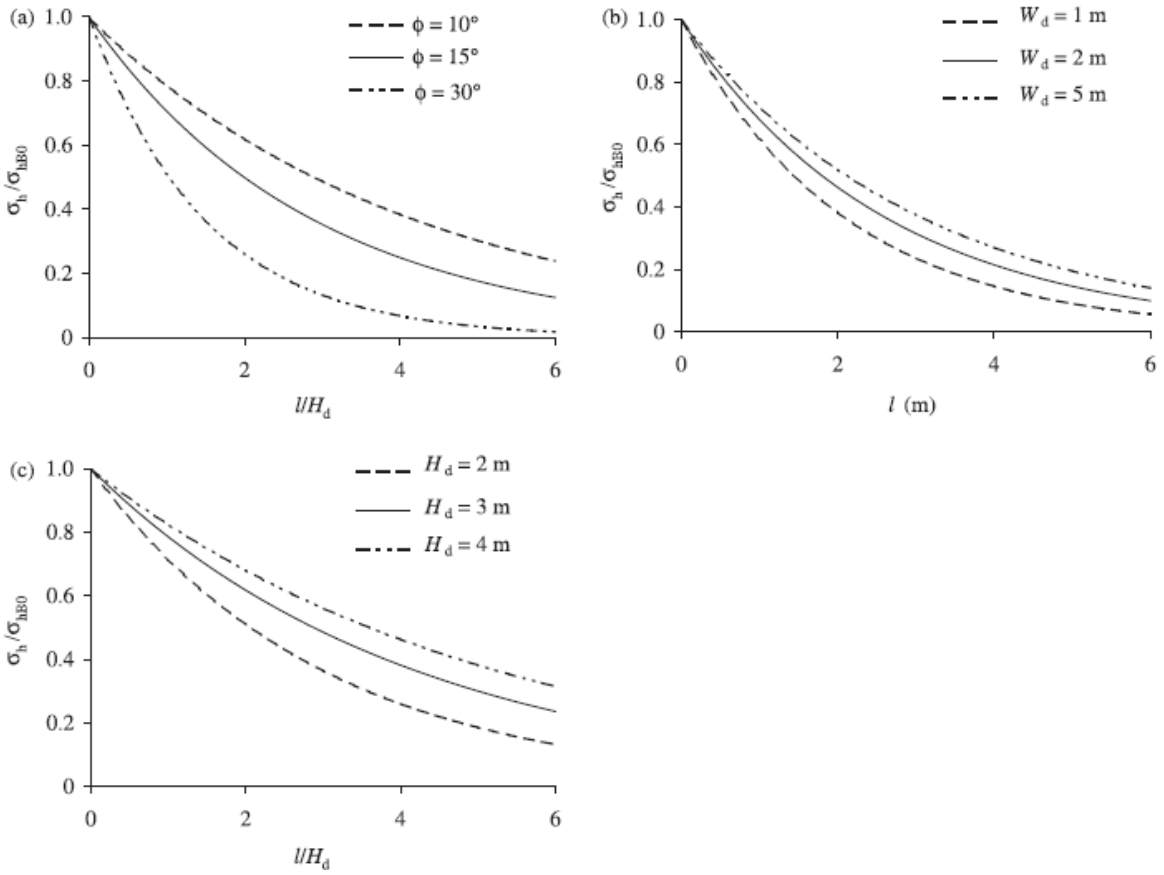

Figure 1-20: Horizontal stress distribution with different: a) backfill friction angle; b) drift width; c) drift height, along the drift, at *h* =1m (after Li and Aubertin, 2009d)

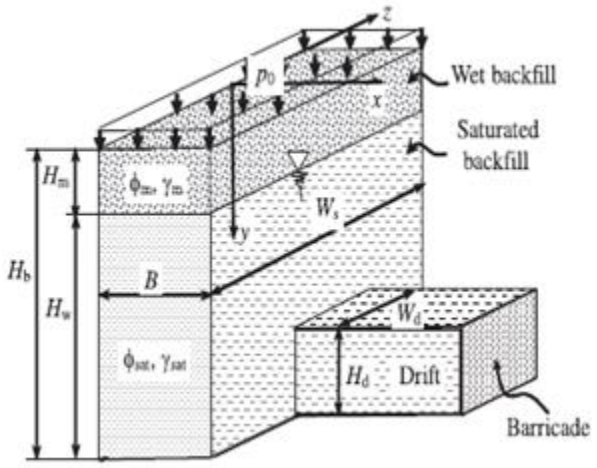

Figure 1-21: A 3D view of vertical backfilled stope and access drift with barricade (after Li and Aubertin, 2009e)

The total pressure (kN/m^2) applied on the barricade in submerged condition becomes:

$$P = \frac{w_d H_d}{2}\left\{(\sigma'_{hBO} + \sigma'_{hTO})exp\left[-\frac{2tan\delta_{sat}}{K'_{dl}}\left(\frac{1}{H_d}+\frac{K'_{dt}}{w_d}\right)l\right] + \gamma_w(2H_w - H_d)\right\} \quad (1\text{-}76)$$

where σ'_{hBO} and σ'_{hTO} are the effective horizontal stresses at the top and base of the drift in the stope entrance (kPa); K'_{dt} (=K'_a) and K'_{dl} (=K'_p) are the reaction coefficients of the saturated backfill in the transversal and longitudinal directions of drift axis by substituting ϕ_{sat}' (effective friction angle of saturated backfill); H_b is the backfill height (m); H_d is the height of access drift; H_w is the height of saturated backfill in the stope; w_d is the drift width (m); γ_w is the unit weight of water (kN/m^3); and δ_{sat} is the friction angle along the interface of saturated fill and the rock walls (°).

These solutions indicate that in all cases (when $u > 0$), the total normal stresses are larger than the effective stresses along the drift. An increase of fill friction angle decreases both the total and effective stresses in the drift. It was also shown that both the total and effective stresses increase as the width or the height of the drift increases. The same tendencies were also observed for a drift under drained condition.

1.4.2 Physical models and in-situ measurements

Physical models and experimental measurements in the field can be used to investigate the behavior of backfilled stopes. Analytical solutions and numerical models can also be verified using such measurements. In the following, some of the physical models and in-situ measurements performed for backfilled stopes are described.

1.4.2.1 Physical models and related testing results

Mitchell et al. (1982) carried out 26 intermediate scale tests (2 m in height) on a physical model (made with wood) to investigate the stability of exposed cemented backfill, as shown in Figure 1-22. They reported that when the walls are closer together, the required cement strength could be decreased. Their investigations also showed that arching could have a significant influence on the stress transfer within the stope and its stability. In addition, they conducted several direct shear tests and unconfined compressive tests to determine the materials properties. The results of this study were used to develop and verify this 3D analytical solution (presented in section 1.4.1.3).

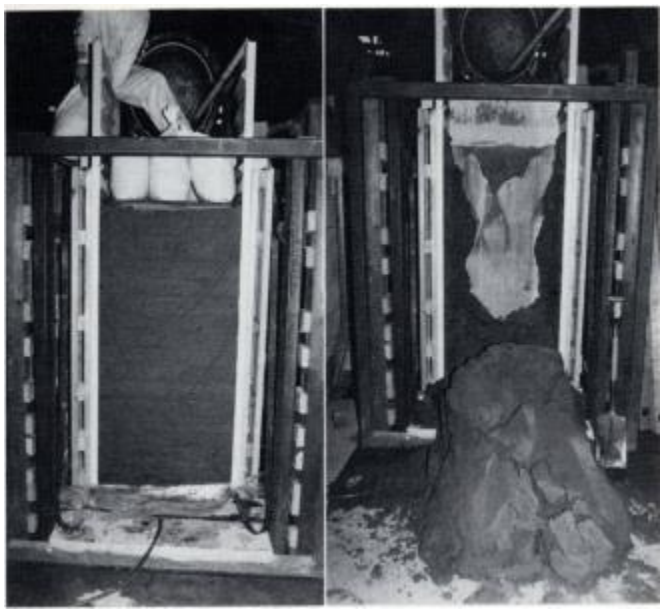

Figure 1-22: General views of: a) the model frame, b) failure test with a surcharge (Mitchell et al. 1982)

Take and Valsangkar (2001) conducted a series of centrifuge tests to evaluate the use of flexible earth pressure cells to measure lateral earth pressure in backfill behind retaining walls. The results of this study showed that the lateral earth pressures measured with calibrated cells were less than the overburden stresses. It was also observed that rougher walls significantly reduced the lateral earth pressures. They concluded that the average interface friction angle of the backfill could be used to estimate the earth pressure distribution based on the arching theory.

Euler and Aldrich (2002) carried out centrifuge tests on model of paste filled stopes, to quantify the effects of arching on the behaviour of sill mat during undercut mining. The sill mat was made with paste fill and mixed with higher cement content; it was placed at the bottom of the stope to a thickness of at least the width of the stope. The model tests indicated that arching developed as a function of frictional effects and cohesion between the fill and rock. The sill mat was stable in all cases. It was also observed that the frictional effects, and thus degree of arching, increased with an increase in wall roughness.

Pirapakaran (2008) developed a laboratory model to measure the average vertical stress at the bottom of a stope, considering different parameters. Two circular and two square model stopes (100 mm and 150 mm width or diameter and 600 mm and 900 mm height) were constructed to investigate the effect of stope geometry on the stress distribution within a

hydraulic fill. Arching developed within the circular and square stopes, and it increased with an increase in surface roughness. The vertical normal stresses in the circular stopes (for both sizes, 100×600 mm and 100×900 mm) were about 85% of the stresses measured in square stopes during and after filling (Figure 1-23). Pirapakaran (2008) has also performed direct shear tests on 12 different hydraulic fill samples to evaluate the internal friction angle (ϕ) and the interfacial angle (δ) of hydraulic fills. He reported that the friction angle and interfacial friction angle increased with the density index I_D. Moreover, the results showed that the internal friction angle ϕ is typically larger than the interfacial friction angle δ at any relative density and surface roughness. This difference increases as the density index increases from very loose to dense.

Fall and Nasir (2010) have studied cemented paste backfill (CPB) - wall interface strength parameters using laboratory direct shear tests. Two types of wall materials were used, i.e., concrete and brick. Figure 1-24a shows the impact of curing time on the friction angle along the CPB-concrete and CPB-brick interfaces and on the internal friction angle (ϕ) of CPB. The results showed that the interface friction angle (δ) is not affected by the wall materials in this case.

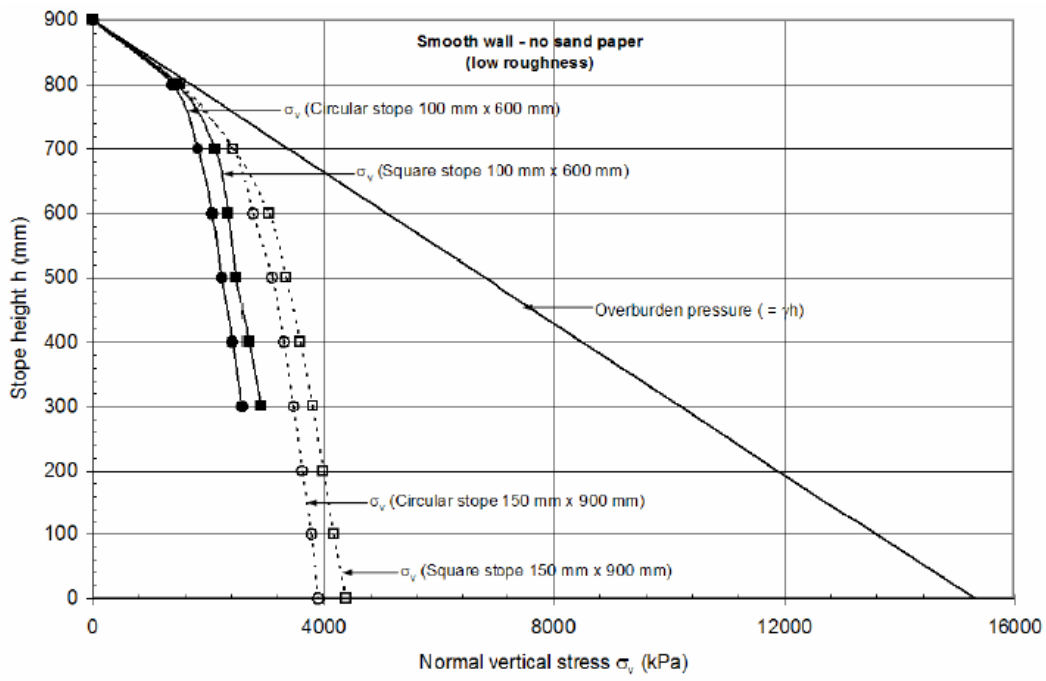

Figure 1-23: Vertical stress measured along square and circular stopes during experimental tests on physical models (after Pirapakaran, 2008)

This angle tended to increase when the curing time progressed. Their results also showed that shear strength parameters (c and ϕ) of CPB-concrete and CPB-brick are very similar. The normalized friction angle of the interface (δ /ϕ) was higher than 0.6 regardless of the curing time (Figure 1-24b). They reported that the interface friction angle $\delta > \frac{2}{3}\phi$ when the curing time progresses. They also observed that the cohesion along the interfaces was typically much smaller than the backfill cohesion.

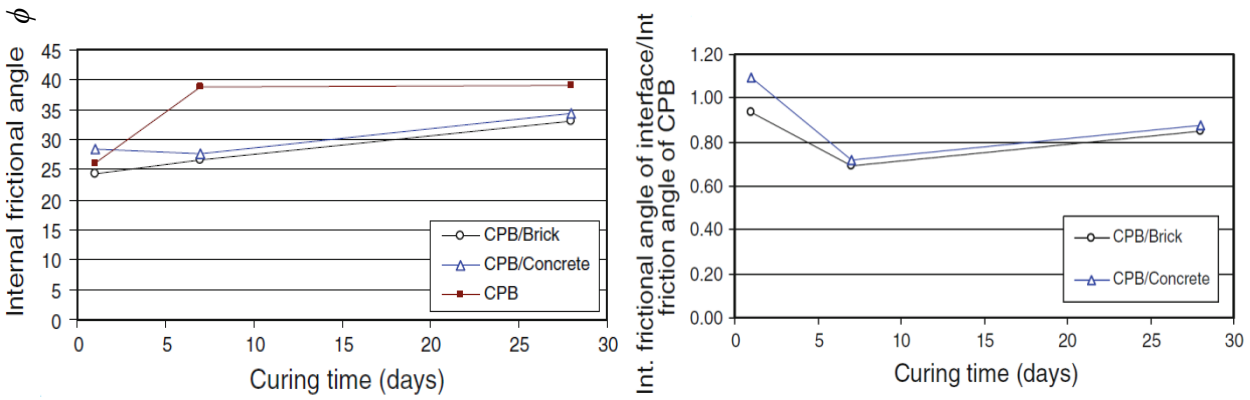

(a) (b)

Figure 1-24: Time dependent behaviour: a) evaluation of the internal friction angle (ϕ) of the backfill CPB and at the interfaces CPB-brick and CPB-concrete; b) evaluation of the ratio of interface friction angle (δ) at the interfaces CPB-brick and CPB-concrete to internal friction angle (ϕ) of the CPB (after Fall and Nasir, 2010)

1.4.2.2 In-situ measurements

Knutsson (1981) carried out in-situ stress and convergence measurements perpendicular to the hanging wall within three inclined stopes. The length to width ratio of the stopes was almost 10 (or higher). The vertical and horizontal stresses were measured perpendicular to the hanging wall. The stresses were also calculated based on an analytical solution considering the inclination of the orebody. They reported that the measured stresses were reduced significantly due to arching effects.

Ouellet and Servant (1998b) have measured pressures in a stope filled by cemented hydraulic backfill (initial solid density of 50 to 65%, mixed with 6.5% cement by weight) and on a barricade. They used total pressure cells and piezometers installed at the stope floor and on the barricade. The stope height and width were 45 m and 15 m, respectively; the hanging wall and

footwall were at 70° to the horizontal. The measured results showed that the total pressure exerted on the barricade increased during the first days of filling and then decreased as the pore water pressures dissipated. The total and effective stresses at mid-height of the stope also increased during filling (Figure 1-25). They concluded that the hydraulic conductivity of the backfill was affected by the presence of layers of coarser materials. The numerical results obtained using SEEP/W suggested that the hydraulic conductivity of the backfill was anisotropic when the sequence of backfilling extended over many days.

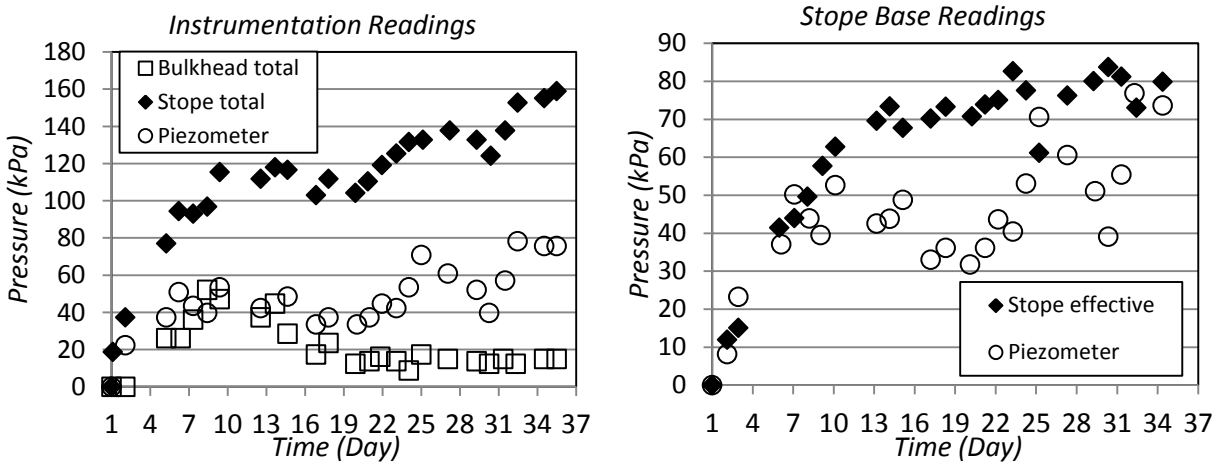

(a) (b)

Figure 1-25: Pressure readings vs time for pressure cells and piezometers: a) total stress; b) effective vertical stress in the stope and on the barricade (after Ouellet and Servant, 1998b)

Belem et al. (2004) measured the stresses within paste backfilled stopes and on barricades during and after filling at the Doyon gold mine. The two stopes dimensions were 3 m × 23 m and 22 m high, and 12 m × 21 m and 30 m high as shown in Figure 1-26a. Eight earth pressure cells (TPC) were installed at various points, including the stope floor, the plug/residual fill interface, the lower wall and the barricade. The paste fill was composed of gold mine tailings mixed with 3% (wt) of Portland cement and slag. The pressure values measured during and after filling showed that the pressures gradually increased during backfilling and decreased after 10 days. They reported that the internal longitudinal pressure (σ_x) in the pastefill was higher than the transversal (σ_y) and vertical pressures (σ_z), presumably due to arching effects. The lateral pressure measured on the barricade indicated that the pressure increased and reached its

maximum when the fill height was about 22 m. It remained unchanged with the placement of additional paste fill as shown in Figure 1-26b.

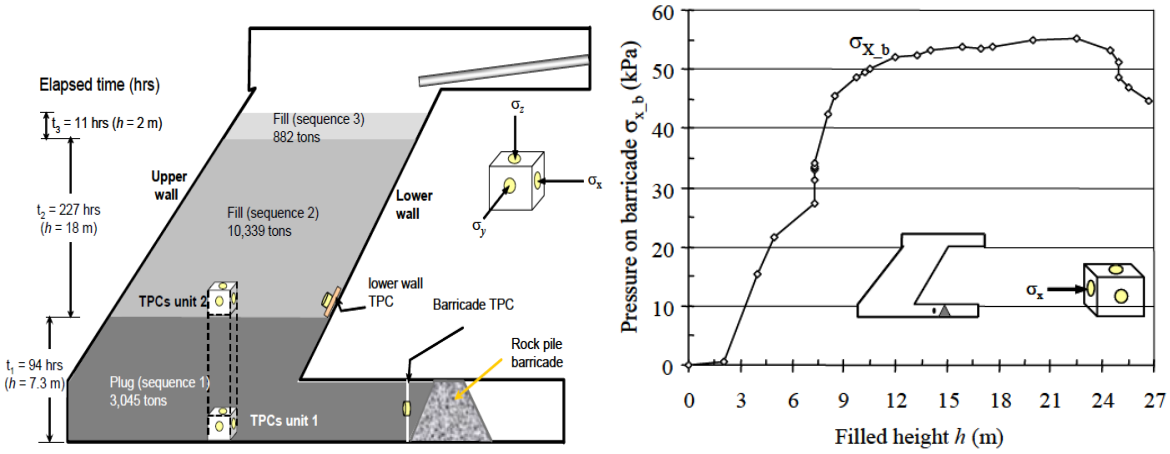

(a) (b)

Figure 1-26: General views of : a) the filling of the stope with cement paste in three sequences, b) variation of the lateral pressure $\sigma_{x\text{-}b}$ on the barricade as a function of the filling height (after Belem et al. 2004)

Le Roux et al. (2005) carried out a field investigation on the Golden Giant mine's paste fill to assess the in-situ properties and to provide data required for mix design optimization. The paste fill was composed of tailings mixed with Portland cement and fly-ash at a binder content of 1 to 6%. A self-boring pressure meter (SBP) was used to measure the field strength of the paste fill. They also conducted laboratory tests on similar laboratory prepared paste fill specimens to compare the results with in-situ data. The results showed that the undrained shear strength and shear modulus of the field materials measured by the SBP were respectively between 50% to 80% and 100% to 150% higher than those obtained from laboratory prepared CPB samples. In addition, the laboratory tests on undisturbed samples of CPB obtained at the mine using drilling techniques indicated that the undisturbed block samples had a higher void ratio and lower cohesion than the laboratory prepared CPB samples. However, the friction angles were almost the same for the unsaturated block samples and the laboratory prepared CPB samples as addressed in Table 1.2.

Table 1.2: The strength properties of the field CPB and laboratory prepared CPB (after Le Roux et al. 2005)

Strength property	Undisturbed block sample		Laboratory prepared CPB (3% binder at 56 days)
	Saturated	Unsaturated	
Void ratio	1.2	1.2	1
Degree of saturation	99%	92%	99%
ϕ'	19-27	32-37	35
c' (kPa)	55-98	47-60	101
E (MPa)	25-47	12-17	35.9
UCS (kPa)	175-240	110-130	384

Helinski et al. (2007) investigated the evolution of the vertical total stress (σ_v) and pore water pressure (u) during filling of two mine stopes at the KB gold mine and the SNM (Sally Malay mine) located in Western Australia. At the KB mine, the stope height is 40 m with a plan dimension of 15×18 m, and a single 6 m wide× 6 m tall drawpoint at the center of one of the long sides. The stope was filled with paste fill. Pore water pressures and total vertical stresses were monitored at the center of the stope floor using piezometers and total pressure cells. The results showed that the measured value of σ_v was less than the total overburden pressure (Figure 1-27a).

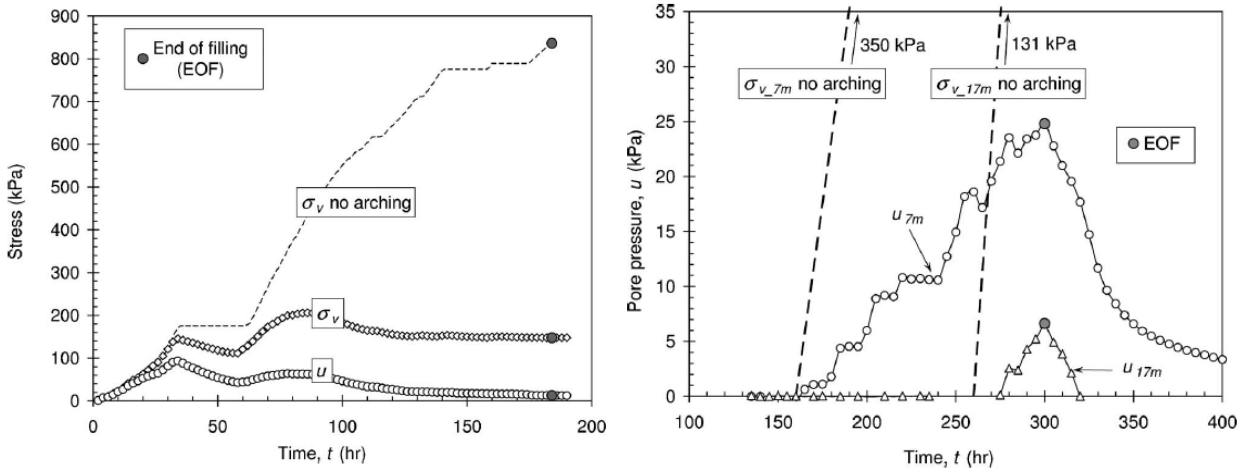

(a) (b)

Figure 1-27: In situ measurement of pore water pressure (u) and total vertical stress (σ_v) at the base of the stope at: a) the KB Mine, b) the SNM Mine

The results also indicated that σ_v and u initially increased at the same rate as the overburden pressure. After 20 hours, effective stresses started to develop. When filling is suspended (from 34 to 58 h) σ_v and u were reduced and the effective stress increased due to

further consolidation. The results obtained at theSNM , in a stope 23 m in height and a plan dimension of 10 m ×12 m, and two 6 m wide × 6 m tall drawpoint, showed that the rate of increase in pore water pressure was significantly less than the rate of total stress increase due to the consolidation taking place during placement (Figure 1-27b). The results also indicated that the pore water pressure increased during filling and was reduced when the filling was terminated (at 300 *h*).

Thompson et al. (2009, 2011, 2012) and Grabinsky (2010) have studied the evolution of total earth pressures and pore water pressures using a series of instrumented points installed within backfill stopes and close to fill fences. The total earth pressure cells (TEPCs) and piezometers measured the total stresses, pore water pressures and temperature changes during hydration of paste fill in two stopes at the Inmet's Cayeli mine in Turkey, two stopes at Kidd mine and one stope at Williams mine in Canada. These stopes have different geometries and were filled at different rates. The stope height and width varied between 15 to 53 m and 8 to 30 m, respectively. The barricades height and width were between 5 to 6 m and 5 to 10 m, respectively. All measuring devices were installed in a cage connected to the data acquisition system. The results for the Cayeli mines (Figure 1-28a to 1-28c) and the Kidd mine (Figure 1-28d) are presented here. Three instrument cages including TEPC and piezometer were vertically installed at the center of stopes at the Cayeli mines. Also, three total pressure cells and piezometers were attached directly to the fill barricades (Figure 1-28a). Figure 1-28b shows the total earth pressure, pore-water pressure and temperature measured for the 685 stope (Cage 3). It can be seen that the pressure increased gradually during the first filling and then the total pressures were equal to the pore water pressure. Also, the vertical stress was equal to the horizontal stress. During the 2.85 day pour, the horizontal pressures initially decreased and the pore water pressure was reduced at a faster rate than the total earth pressures. However, the total vertical stress increased faster than the horizontal stress during this period. The temperature in the backfill also increased due to cement hydration. Figure 1-28c also shows the effect of the filling rate of CPB on the pressure in a stope. It can be seen that the pressure increased as a function of the filling rate.

The results from the Kidd mine (Figure 1-28d) also showed that the highest total earth pressures were measured in the bottom third of the stope, in vertical direction. The lower rise rate and relatively higher binder content lead to lower barricade pressures. They reported that a higher binder content can increase the pressure between 12 and 18 hours. The results also revealed that

the pressure decreases with the distance into the drift. Their investigations also showed that the differences in geochemistry of orebody influence the hydration rate and barricade's pressure.

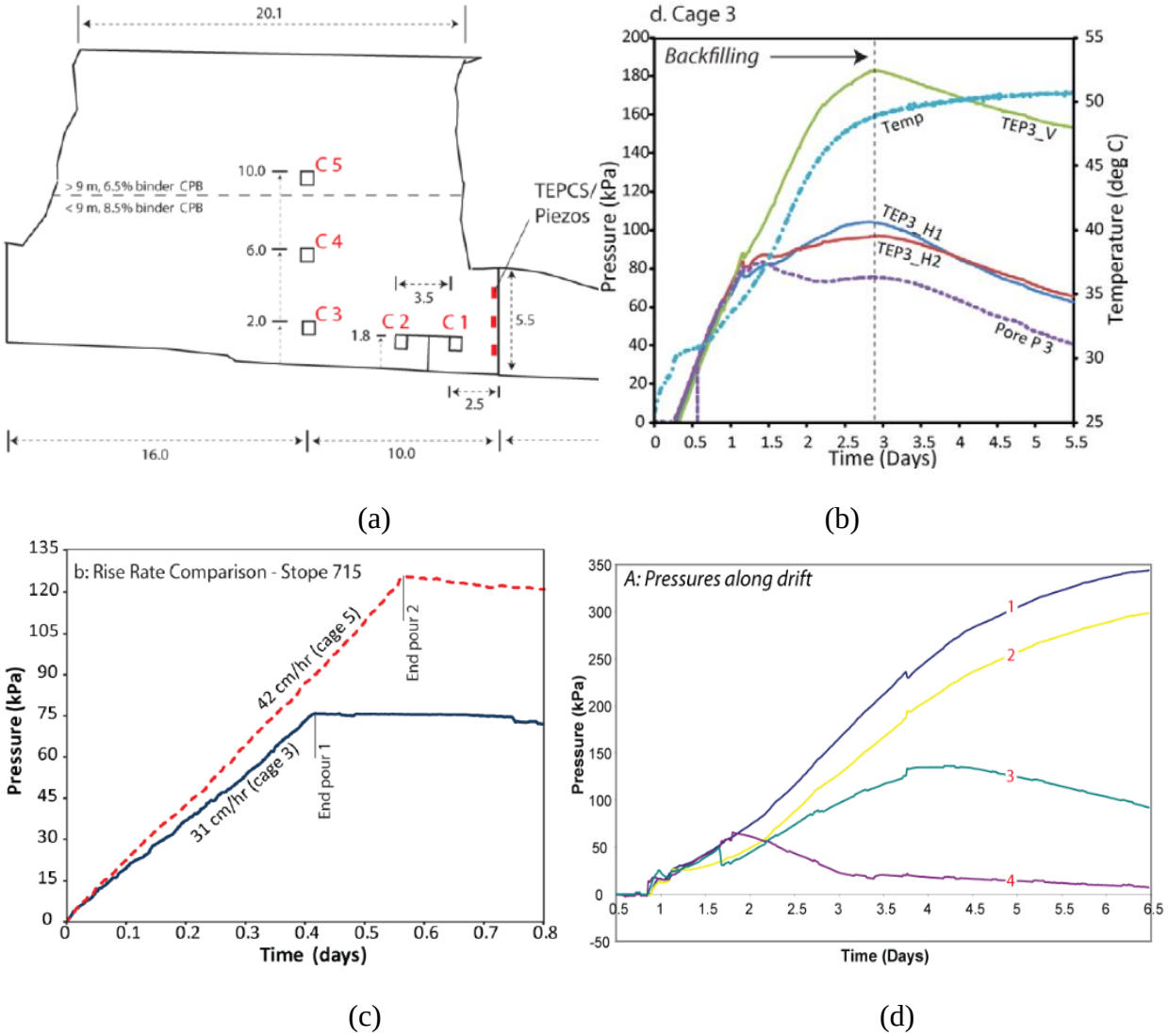

Figure 1-28: In situ measurement in the Cayeli mine (a to c) and the Kidd mine (d): a) cross section of the instruments, b) an example of total earth pressure (TEP), pore water pressure (Pore P) and temperature measured at C_3, c) pressures measured for two CPB filling rates in the 715 stope at C_3 and C_5, d) total earth pressure along the long axis of the stope for $C_{1\text{-}4}$ and fill barricade (after Thompson et al. 2009, 2011, 2012)

1.4.3 Numerical modeling

Numerical models are commonly used to evaluate and validate analytical solutions and to solve complicated problems that cannot be solved using such analytical solutions. Numerical

simulations can use different constitutive models, input parameters and boundary conditions to study the mechanical behavior and deformation of the models. Numerical investigations have been carried out using different software to study the stress distribution in vertical and inclined backfill stopes (e.g. Hustrulid et al., 1989; Bloss, 1992; Coulthard, 1999; Pierce, 2001; Aubertin et al., 2003; Rankine, 2004; Li et al., 2003, 2007; Li and Aubertin 2009a, 2010a; Helinski et al., 2007, 2010, 2011; Pirapakaran, 2008; Veenstra, 2013; El Mkadmi et al., 2014). In the following section, some of the numerical simulations for backfilled stope and barricades will be presented and discussed.

1.4.3.1 Simulations with FLAC

Li et al. (2003) have used FLAC (in 2D) to study the arching effect within a narrow backfilled stope and to compare the results with the analytical solution of Aubertin et al. (2003). They considered the rock mass as homogenous, isotropic and linear elastic, while the back fill behavior is elasto-plastic according to Mohr-Coulomb criterion. The geometry and the material properties used for these simulations are shown in Figure 1-29. It was considered that the whole stope was excavated and filled instantly. The wall convergence was zero. The results showed that the stresses are less than the overburden pressures due to arching effects (Figure 1-30). The results also indicated that the stresses are non-uniformly distributed within the stope. This result is not in accordance with most analytical solutions, which assume that both stresses are uniformly distributed across the width.

Li and Aubertin (2008) introduced a distribution factor (DF) in the Modified Marston solution (Aubertin et al. 2003) to account for the non-uniform distribution of the vertical stress along the stope width (as mentioned, in section 1.4.1.1). To verify this modified solution, additional numerical calculations have been performed using FLAC. The results showed that the modified solution represents the vertical stress well along the centre line and also the horizontal stress in the entire stope, as illustrated in Figure 1-31. These results indicate that the modified solution Li and Aubertin (2008) gives better results in comparison with the Modified Marston solution of Aubertin et al. (2003).

Li et al. (2007) and Li and Aubertin (2009a) conducted a series of numerical modeling using multistep filling (in layers) to investigate the stress distribution within vertical and inclined stopes. Figure 1-32a shows the inclined stope used for the numerical calculations. The results

revealed that the stress magnitude increases nonlinearly with depth *h*. In the lower part of the stope, the vertical stress along the footwall is larger than along the hanging wall as seen in Figure 1-32c. However, the horizontal stress close to the base of the stope is higher along the hanging wall than along the footwall due to stress transfer (Figure 1-32b).

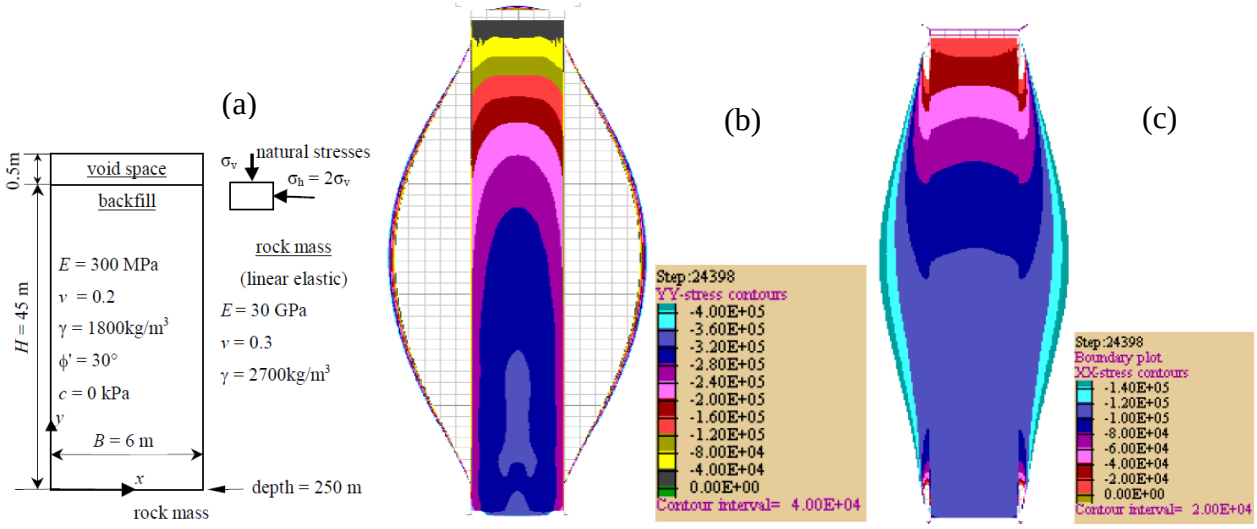

Figure 1-29: (a) A vertical backfilled stope with the main properties of rock mass and backfill; Stress distribution in the backfill stope calculated with FLAC ; b) vertical stress; c) horizontal stress (after Li et al. 2003)

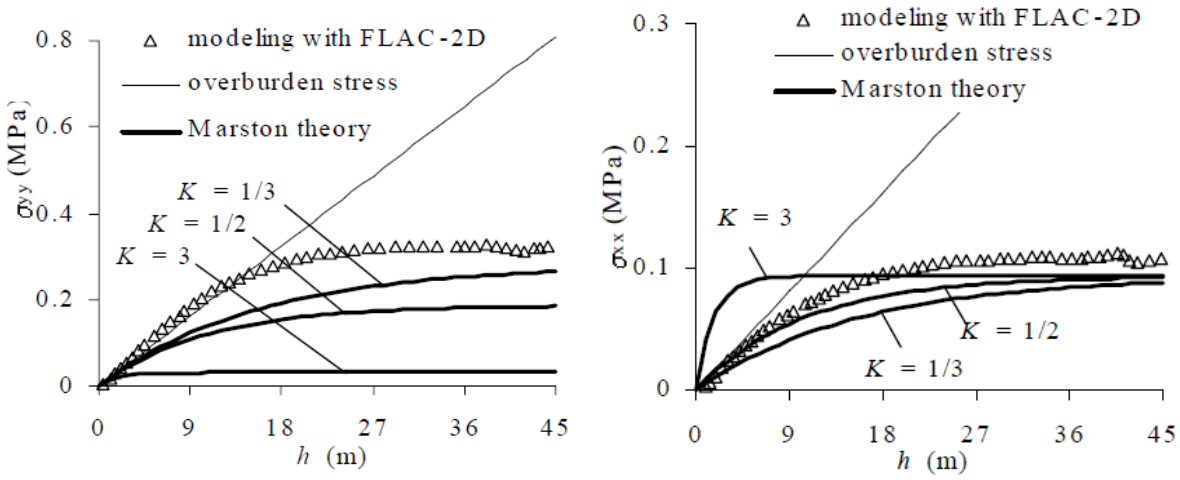

Figure 1-30: The stress distribution along the vertical central line obtained by the numerical and analytical solutions; a) vertical stresses, b) horizontal stresses (after Li et al. 2003)

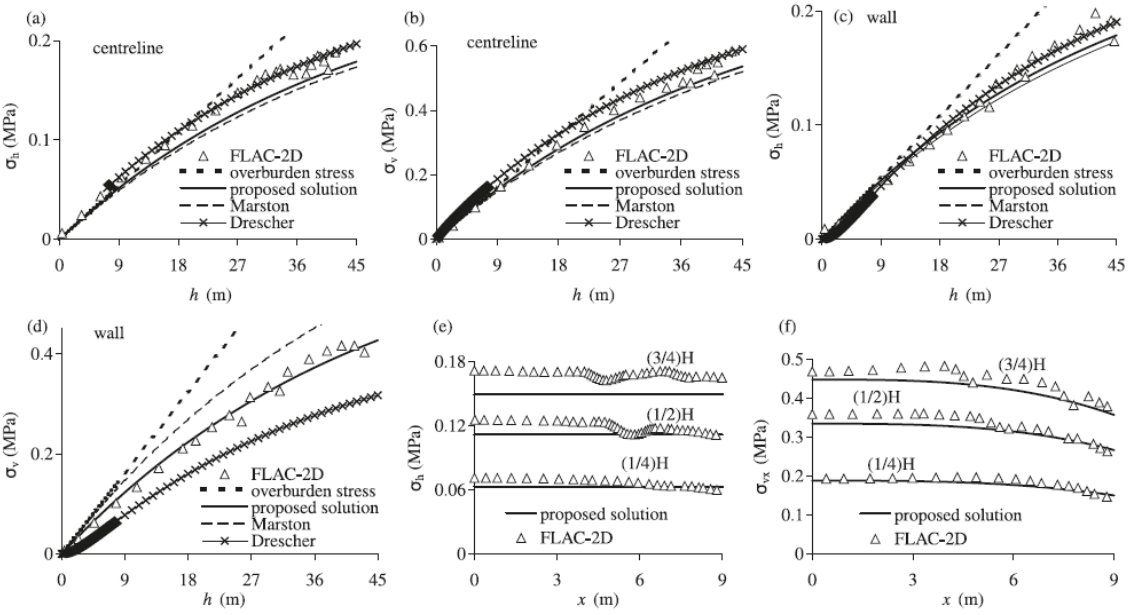

Figure 1-31: Vertical σ_v and horizontal σ_h stresses for H = 45m, B = 18m, ϕ =30°; a) σ_h along the central line; b) σ_v along the central line; c) σ_h along the wall; d) σ_v along the wall; e) σ_h at different depth across the width; f) σ_{vx} at different depth across the width (after Li and Aubertin, 2008)

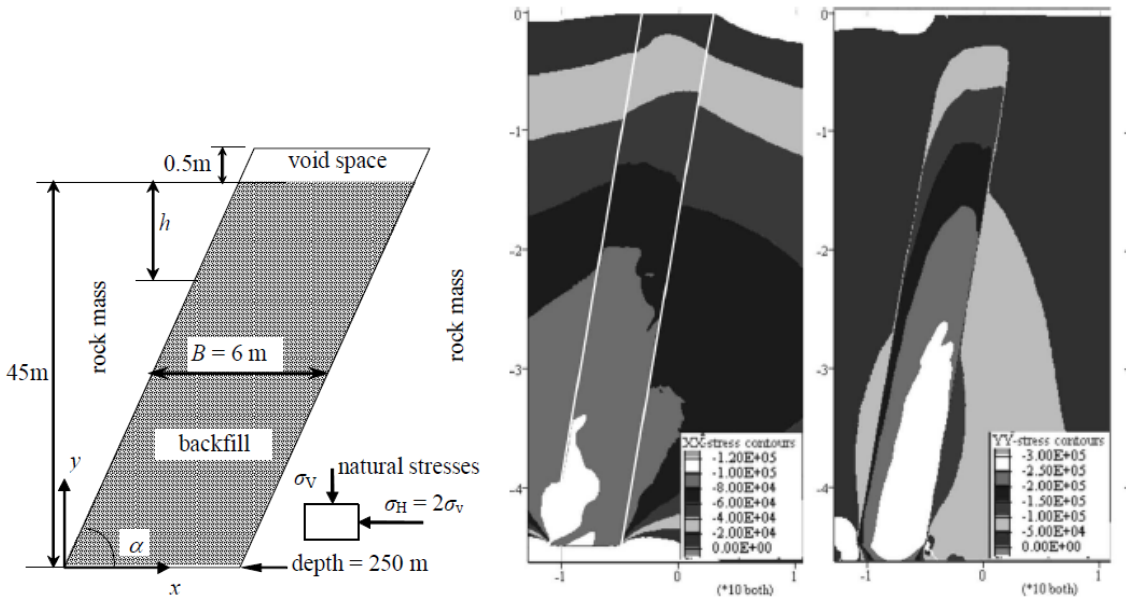

(a) (b) (c)

Figure 1-32: (a) An inclined backfilled stope simulated with FLAC; stress distribution obtained using FLAC: a) horizontal stress; b) vertical stress, simulations for stope inclination α = 80°, γ =18 kN/m^3, ν = 0.2, ϕ'=30°, ψ' = 0° (after Li and Aubertin, 2009a)

Li and Aubertin (2007, 2009a) also investigated the influence of different parameters including stope inclination and stope width, backfill modulus and Poisson's ratio, internal friction angle, cohesion and dilatancy angle of the backfill. They showed that the horizontal stresses are not affected by the stope inclination α along the central line and hanging wall as shown in Figure 1-33.

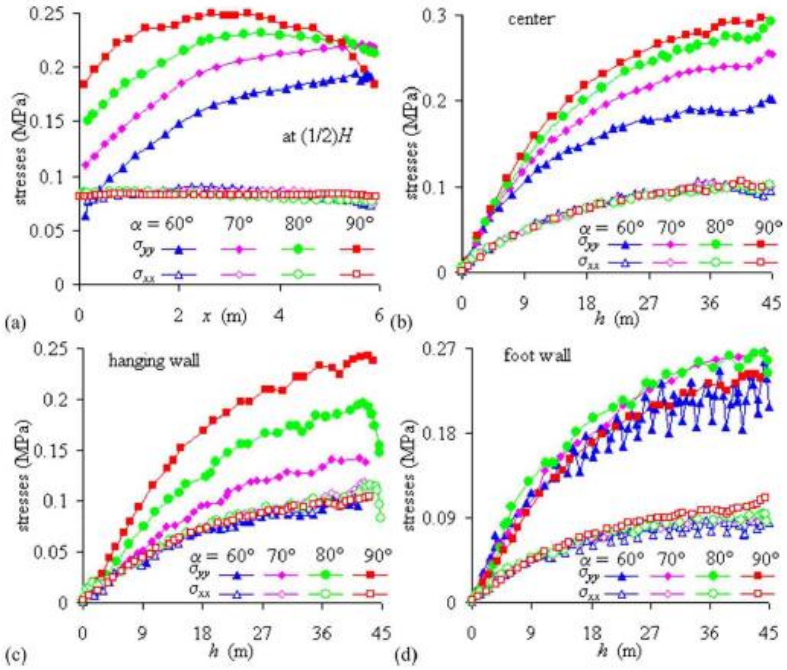

Figure 1-33: Stress variation for different stope inclination α: a) at mid height of the stope; b) along central line; c) along hanging wall; d) along the foot wall (after Li et al. 2009a)

A decrease in the stope inclination (with respect to the horizontal) decreases the vertical stress within the backfill close to the hanging wall. Near the footwall, the vertical stress tends to increase as the inclination angle decreases from 90° to 70° and then decreases for more a inclined stope (60°). It was also observed that a decrease in the stope width tends to increase the arching effect and reduce the magnitude of the horizontal and vertical stresses within the stope (Figure 1-34). They reported that the backfill modulus E has little influence on the stress distribution in the stope.

Also, when Poisson's ratio is increased, the vertical stress tends to decrease, but the horizontal stress is almost insensitive to variation of Poisson's ratio. It was also shown that both the horizontal and vertical stresses tend to decrease with an increase in the friction angle ϕ' and

backfill cohesion c' as seen in Figures 1-35 and 1-36. The simulation results showed that the vertical stress is reduced when the dilatancy angle increases (Figure 1-37).

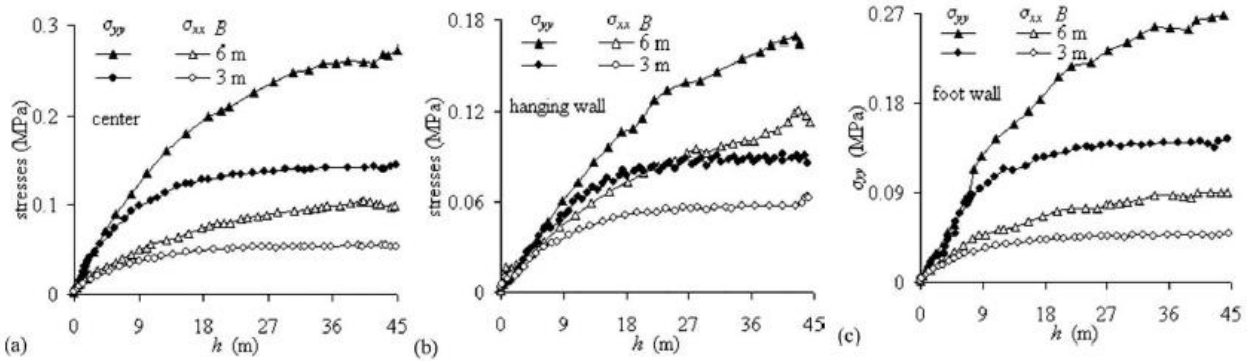

Figure 1-34: Stress variation for two stope widths: a) along the central line; b) along the hanging wall; c) along the foot wall (α = 75°) (after Li and Aubertin, 2009a)

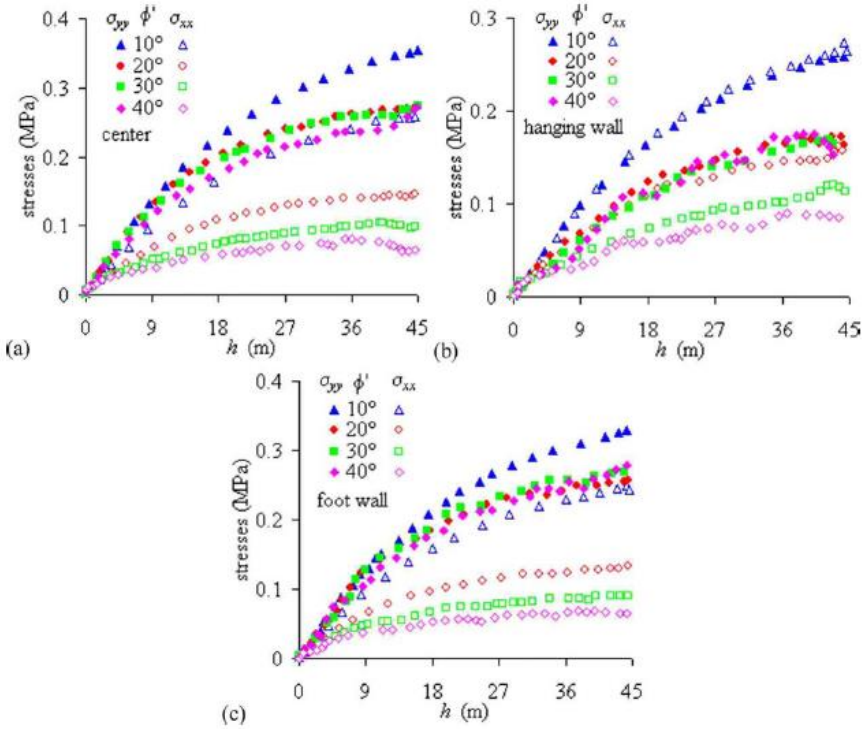

Figure 1-35: Stress variation for different backfill friction angle ϕ': a) along the central line; b) along the hanging wall; c) along the foot wall (α = 75°) (after Li and Aubertin, 2009a)

The influence of the layering sequence on the results provided by numerical simulations was also investigated by Li and Aubertin (2009a). Figure 1-38 shows the results obtained with one step using the pseudodynamic and pseudostatic methods and also for a multilayer filling

simulation (for cohesionless backfill). It can be seen that pseudodynamic and pseudostatic simulations with one filling step tend to overestimate the stress state in comparison to a multilayer sequence. The results showed that the stress distribution for the stope filled with four layers can be considered as representative of the static solution; adding more layers does not have a significant influence on the results. Similar results were obtained by Pirapakaran and Sivakugan (2007) for multistep filling simulations under a static loading.

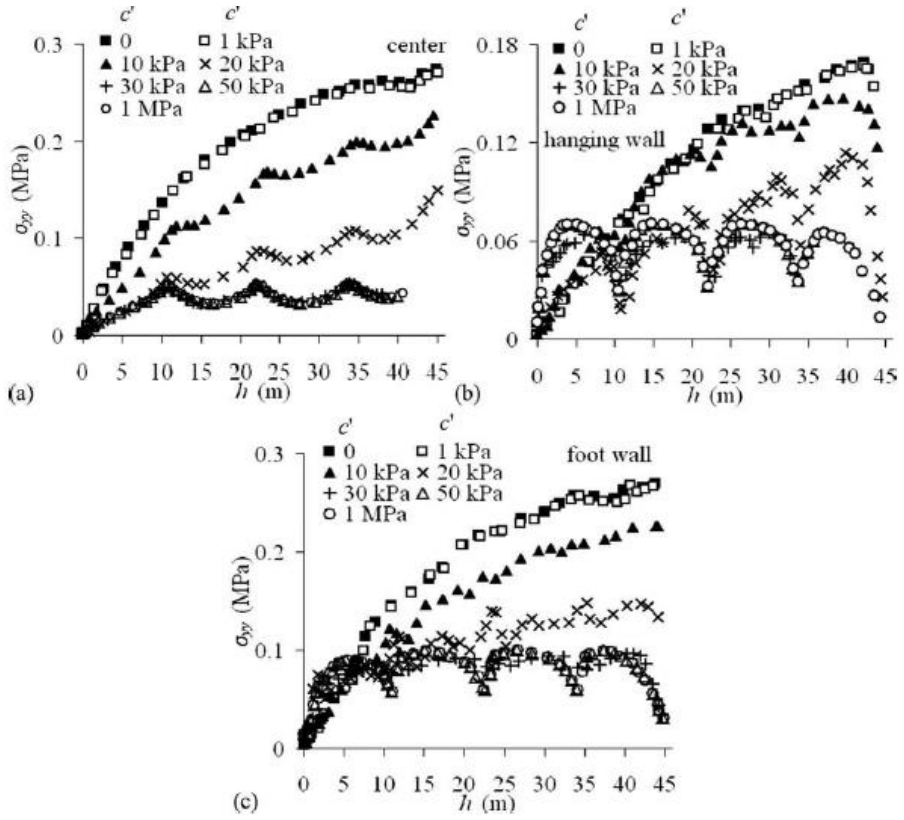

Figure 1-36: Stress variation for different backfill cohesion c' (multi-step filling): a) along the central line; b) along the hanging wall; c) along the foot wall (α = 75°) (after Li and Aubertin, 2009a)

Li and Aubertin (2009c) have carried out additional simulations to verify the analytical solutions developed for submerged backfill (see section 1.4.1.1). Three different conditions were simulated, including a submerged backfill with a water table at the backfill surface, a backfill under water and a partially submerged backfill. A good agreement was observed between the numerical simulation results and those obtained from the analytical solutions for submerged conditions as shown in Figure 1-39 (presented in section 1.4.1.1).

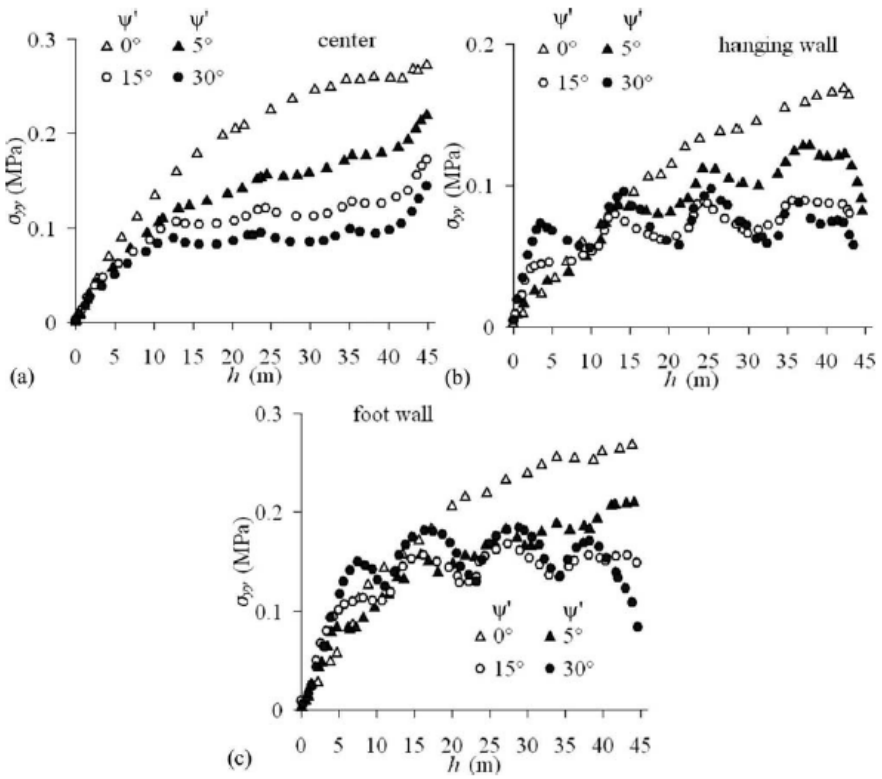

Figure 1-37: Stress variation for different backfill dilatancy angle ψ' (multi-step filling): a) along the central line; b) along the hanging wall; c) along the foot wall (α = 75°) (after Li and Aubertin, 2009a)

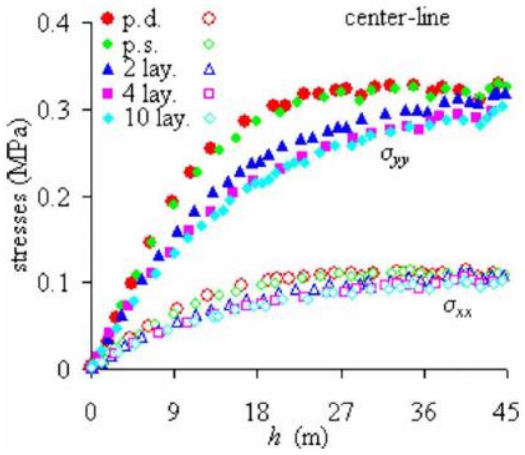

Figure 1-38: Stress distribution obtained with multistep simulation along the central line (after Li and Aubertin, 2009a)

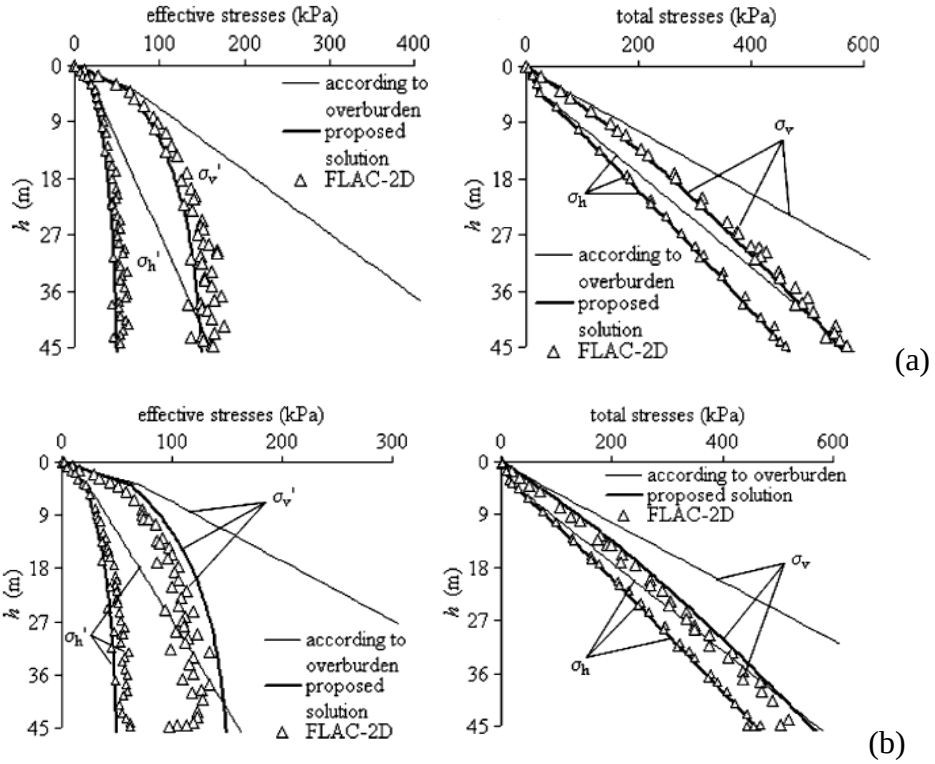

Figure 1-39: Vertical and horizontal effective and total stresses: a) along the VCL; b) near the wall calculated by proposed analytical and numerical solution; partially submerged condition (after Li and Aubertin, 2009c)

These results also indicated that the effective stresses obtained by the numerical and analytical calculations are smaller than the overburden pressure, especially at larger depth, due to arching effects. Under partially submerged conditions, the slope of effective stress curves changes at the phreatic surface and then tends to be almost independent of stope depth for the conditions analyzed here (Figure 1-39). The results also showed that the effective stresses are affected by the fill properties and the stope geometry; for instance, the effective stresses along the vertical central line tends to decrease as the friction angle increases from 20° to 40°.

Pirapakaran (2008) studied the stress distribution within a two dimensional narrow stope and three-dimensional circular and square backfilled stopes. He included interface elements between the rock and backfill in his modeling using FLAC. The input parameters such as rock mass and fill properties are the same as Li et al. (2003), except for the internal friction angle (ϕ = 35°), dilatancy angle (ψ = 5°) and ratio between the interfacial friction angle (δ) and the internal friction angle (ϕ) which are 0.75 to 0.92, respectively.

Two circular stopes and two square stopes with 100 mm width (or diameter) and 600 mm and 900 mm height, were simulated. They reported that for the same stope width or diameter, the vertical stresses obtained for circular stopes were lower than those obtained for the square stopes. The results also showed that the trends followed by the vertical normal stresses were similar for both circular and square sections when the surface roughness was low, medium and high. These normal stresses usually decreased with an increase in the surface roughness at the stope depth. The results obtained using FLAC for circular and FLAC^{3D} for square stopes showed a good agreement with the experimental results. The effect of different parameters on the stress distribution within square and circular stopes was also studied by Pirapakaran (2008). He reported that an increase in the fill friction angle and cohesion increases the arching effect and reduces the vertical normal stress in circular, square and narrow (2D) backfilled stopes. The same results were obtained by Li et al (2003, 2007, 2009a) for vertical and inclined narrow backfilled stopes.

Veenstra (2013) used FLAC and FLAC^{3D} to investigate the stresses of early age cemented paste backfill in a single stope. The influence of different parameters, including stope geometry, filling rate, backfill properties (friction angle, cohesion, Poisson's ratio and hydraulic conductivity) has also been studied. He showed that an increase in the backfill friction angle and cohesion leads to a decrease in the stresses within the stope. The results indicated that Poisson's ratio had little impact on stresses. The simulations also indicated that the stresses increased with an increase of the stope width, while inclining a stope decreased the stresses and changed the stress pattern in the stope. These results are in accordance with those obtained by others, including Li et al. (2007, 2009a), for vertical and inclined narrow backfilled stopes. The investigation of the filling rate revealed that longer pour time decreased the stresses in the stope due to increased drainage and hydration time, while a short pour time lead to increased stresses. Similar observations have been reported by El Mkadmi et al. (2011, 2014), as described in the following sub-sections.

Veenstra (2013) also used the results of in-situ measurements to verify the numerical results. For this purpose, six instrumented stopes were monitored, i.e. four stopes from the Çayeli Bakir Mine, a stope from Williams Mine and a stope from Kidd Mine. Each stope has different stope geometry (and filling rate, see section 1.4.2.2). Both 2D and 3D models were used; the model geometry was taken from cavity monitoring surveys generated by the mines. The results of

these models were compared to the in-situ measurements. The results were obtained along three directions, including *z*-direction in dark blue, *y*-direction in red and *x*-direction in green. The simulation results of the cages closer to the stope center had the best agreement with the instrumentation results (Figure 1-40a), while the drift simulation results did not show such good agreement with the measurements (Figure 1-40b). All simulation results showed the same tendencies as the instrumentation results, i.e. the stresses increased, decreased, and increased again with the changing filling-rate. He concluded that the simulations were replicating the in-situ observations. It was also observed that a faster rise rate generated higher stresses due to limited time for drainage. The results revealed that the simulation results changed by moving the measurement location.

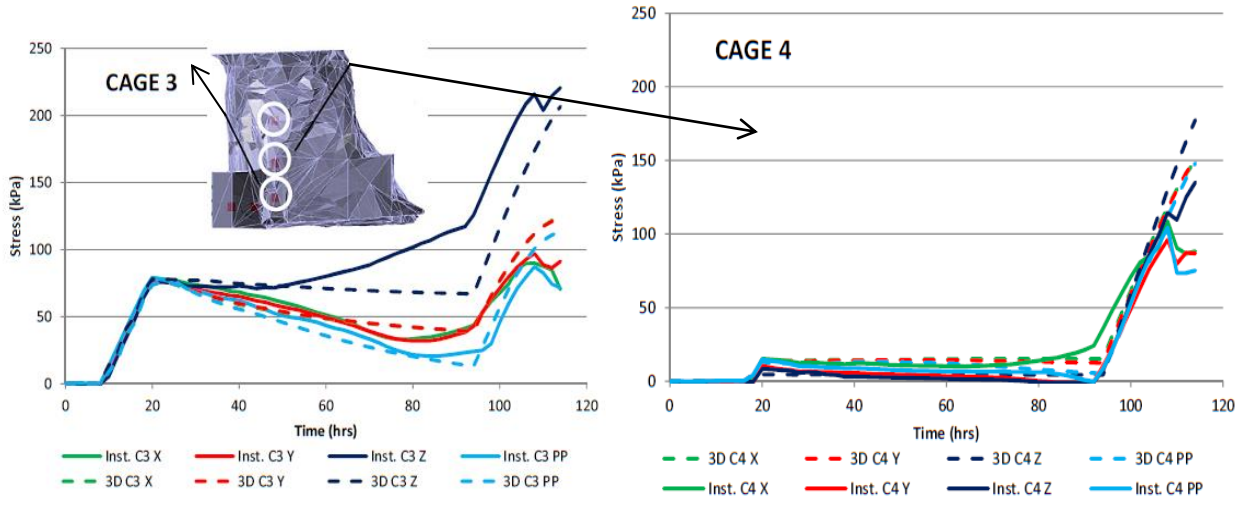

(a) (b)

Figure 1-40: Simulations results and in-situ measurements data for stope 715-N22 at Çayeli Bakir Mine: a) near the drift, b) near the stope center (after Veenstra, 2013)

Dirige et al. (2009) studied backfill behavior during adjacent pillar mining using FLAC ^{3D}. Stopes with different sizes (3 m wide, 15 m long and 30 m high; 7.5 m wide, 15 m long and 40 m high) and rock wall conditions (including smooth and rough) were simulated. They also investigated the effect of stope width, height, inclination, and wall roughness on the stability of cemented backfill during adjacent pillar mining. The results showed that for inclined stopes with smooth rock walls, the backfill failure was driven by the fill self-weight. The resisting forces developed on the footwall-fill contact and fill failure plane tended to prevent this failure. For inclined stopes with rough rock walls, this roughness contributed to the stability of the backfill

during removal of adjacent stope. In this case, the resisting forces developed on the fill failure plane tended to prevent the failure of paste fill. The results also showed that stopes with rough walls were considerably stable, while the stopes with smooth rock walls could become stable by increasing the binder content.

Li and Aubertin (2014) recently investigated the required strength of backfill in a stope using FLAC^{3D} when an adjacent stope was mined out. Two adjacent stopes, each having H = 40 m, L = 8 m and B = 10 m, were considered. The first stope was created and the fill was placed in the stope in 8 layers (after convergence of the elastic rock mass). The behavior of the exposed backfill was investigated after the secondary stope was mined out. The results showed how the stability of the exposed backfill varied with the backfill strength.

1.4.3.2 Simulations with SIGMA/W

El Mkadmi et al. (2011, 2014) carried out numerical simulations with the finite element code SIGMA/W (GEOSLOPE, 2008) to investigate the influence of drainage, consolidation and filling rate on the total and effective stress distribution within the stopes and on barricades. Figure 1-41 shows the geometry and the boundary conditions used for an instantaneously and a sequentially filled stope. Three conditions were simulated, including: dry backfill, a rapidly filled stope with progressive drainage, and a sequentially filled stope with drainage. The results obtained for the dry condition indicated that the vertical and horizontal stresses along the center line of the stope were less than the overburden pressure due to arching effects. For the initially saturated backfill with progressive drainage, the total vertical stress was observed to be equal to the overburden pressure just after the stope was instantaneously filled.

They reported that the initial vertical stress increased linearly with depth. The pore water pressure developed in the backfill was then equal to the total vertical stress, as seen in Figure 1-42. As time progressed, the pore water pressure and the total vertical stress decreased. At the early time of backfilling, the effective vertical stress was nil. The effective vertical stress increased and arching effects were progressively developed within the backfilled stope when drainage progressed. The results also indicated that when the pore water pressure is fully dissipated, the total vertical stress was very similar to the one in a dry backfill. This investigation also showed that very high total stresses were generated by rapid filling (5m/5hours) in comparison with intermediate and slow filling rates. Under the quick filling conditions, there was

little arching and the short term effective stress was almost nil. Drainage could lead to pore water pressure dissipation if there is enough time before adding new layers. The load on the barricade is also reduced with drainage and negative pore water pressure (suction) can develop during and after filling.

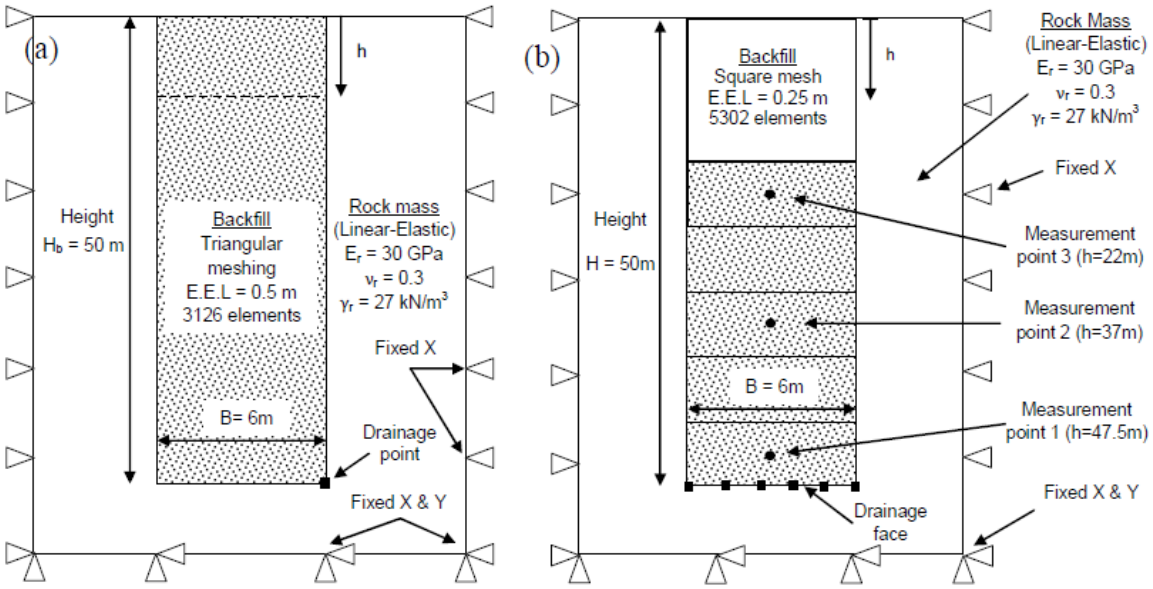

Figure 1-41: Barricade and stope geometry: a) instantaneously filled stope; b) a stope with vertical drainage and sequential filling (after El Mkadmi et al. 2011)

1.4.3.3 Simulations with other software

The stress distribution within backfilled stope was studied using other softwares and the effect of different parameters on stress state was also studied. In the following, some of these studies are briefly presented.

Simulations with PLAXIS

Fahey et al. (2009) used Plaxis to simulate the stress state in a saturated backfilled stope. Two types of backfill were considered for this investigation, i.e. a dry cohesionless backfill and a fully saturated backfill. They investigated the influence of different parameters on stress distribution within the filled stope with dry cohesionless fill materials. In addition, the behavior of a fully saturated backfill was simulated to study the vertical stress at the base of stopes at the

end of an undrained filling, at the end of consolidation of the fill, and at the end of drawdown of the water table.

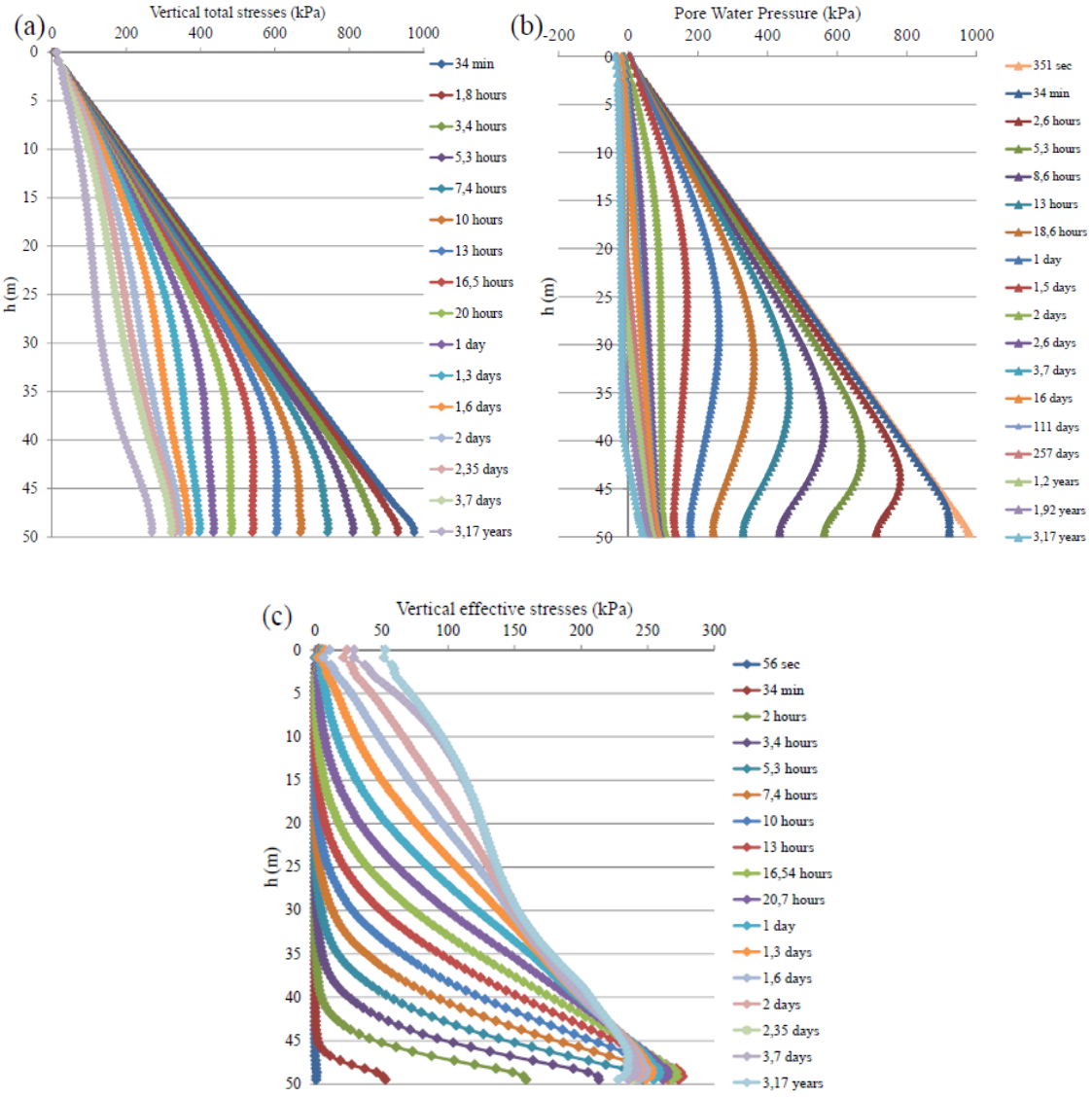

Figure 1-42: Investigation of the: a) total vertical stress and; b) PWP; c) effective vertical stresses of saturated backfilled stope along the VCL for an instantaneously filled stope (after El Mkadmi et al. 2011, 2014)

The results indicated that both stresses were reduced when the stope width decreased due to more stresses being transferred to the walls; similar results were obtained by Li et al. (2003, 2007), Pirapakaran (2008), and Li and Aubertin (2009a). The results also showed that an increase in the dilatancy angle tended to decrease both the horizontal and vertical stresses, as also

observed by Li et al. (2007, 2009a). They also reported that the increase of Young's modulus had no effect on the stress distribution within the stope, while an increase in Poisson's ratio up to v = 0.4 tended to decrease the stresses in the stope. These results are in good agreement with other simulation results, such as those obtained by Li et al. (2007, 2009a) with FLAC.

For initially saturated conditions, the behavior of the backfill depends on the hydraulic conductivity of the materials and rate of filling. Two cases were considered by Fahey et al. (2009), i.e. undrained and drained conditions. They reported that arching effects could not develop with completely undrained filling, which occured if the permeability of the backfill was low relative to the filling rate. The total vertical and horizontal stresses were equal to each other and also equal to the overburden pressure. In this situation, the barricade should be designed using the full overburden weight. They also showed that the pore water pressure and total vertical stresses tended to decrease with consolidation, while the effective stresses increased. When the water table is at the base of the stope and enough time is allocated for full consolidation, the total stresses were reduced and the effective stresses were increased. The pore water pressures were assumed to be hydrostatic and nil above the water table.

Simulations with Minefill 2D

Helinski et al. (2007) developed a two-dimensional finite element model named Minefill 2D to simulate the filling process and the loads imposed on a barricade. This software can be used for both hydraulic and paste fills. The influence of material properties and filling sequences on the loads can be also investigated. This model is fully coupled to simulate consolidation and considers stiffness, strength, hydraulic conductivity and self-desiccation. In this investigation, the water table is allowed to rise and fall according to volumetric strains and flows through the upper material layer; a fully saturated condition is assumed throughout the filling process. Three types of backfills were considered, i.e., two paste fills (A, B) and one hydraulic fill (C). They concluded that hydraulic conductivity and chemical reactions may have had a considerable influence on the stress state.

The results of this study also indicated that a decrease of binder content could increase the pore water pressure and the loads imposed on the barricade (as reported by Belem et al. 2004). They reported that the self-desiccation (i.e. net water volume change as a result of chemical

reactions during the hydration process) could reduce the pore water pressure on the barricade and increase the consolidation by up to 75%; few others have reported similar results.

PHASES2

Aubertin et al. (2003) conducted numerical simulations using the finite element code PHASES 2 (RocScience, 2002) to study the response of vertical and inclined backfilled stopes. The results showed that a proportion of the stresses in the stopes were transferred to the rock walls. The results revealed that the analytical solution might overestimate the load transferred to the walls. The numerical results also showed that the vertical and horizontal stresses were larger than those due to the overburden pressure; this response was caused by the inward convergence of the walls that squeezed the fill and increased the internal pressure in the stope.

1.5 Summary and conclusion

Arching is an important phenomenon in mine backfilled stopes. It needs to be evaluated in a realistic manner. In this chapter, typical physical and mechanical properties of backfill have been presented to properly understand the backfill behavior. Different methods have been introduced to estimate the stress state in mine stopes, including analytical solutions, physical models, in-situ measurements and numerical modeling. The solutions presented in this chapter often neglect several factors. For instance, the 2D analytical solutions are based on simplified assumptions and are only applicable for relatively simple conditions such as plane strain. When the length of the backfilled stope is small, these solutions become inappropriate. Moreover, these solutions do not account for more complex stope geometries. All of these solutions are derived from Marston's solution which uses Coulomb criterion in the backfill and along the rock and fill interface. The use of this criterion is not always appropriate when dealing with porous media. In addition, Marston's solution assumes that the earth reaction coefficient K depends on the fill properties but not on the position in the stope. Another limitation relates to the use of the limit equilibrium method which assumes that the shear strength is fully mobilized along the entire fill-wall interface. Furthermore, the wall properties are usually assumed similar.

Although three-dimensional analytical solutions have been developed to overcome some of the existing limitations in 2D analytical approaches, these solutions are only applicable for specific cases and also have several restrictions. For instance, such solutions apply to regular

geometric shapes such as square, rectangular and circular stopes and cannot be used for more complex stope geometries. The stope inclination is an important factor that is neglected in the 3D analytical solutions. The effect of consolidation, drainage, water flow, strength gain with curing time, rate of filling and progressive placement, negative pore water pressure (or suction) and excavation sequence are equally neglected in 2D and 3D analytical solutions. In some cases, parameters in (semi) analytical solutions were obtained from an optimization technique using a series of numerical simulations or experimental data. Validation of the numerical models with these semi-analytical solutions can be less reliable.

Laboratory tests and in-situ measurements have been carried out by various researchers to evaluate the influence of different parameters on backfill behavior. The laboratory test and in-situ measurements can also be used to validate numerical and analytical results for a single stope. However, there are a very limited number of physical models and in-situ measurements on arching effects. In addition, these measurements are more expensive and time-consuming than analytical and numerical solutions.

Comprehensive laboratory studies were carried out to evaluate the backfill properties, including stiffness and strength, which play a significant role in the safety and economy of mining operations (Appendix G). Comparisons have shown that the strength and stiffness obtained from in situ paste fill are typically higher than those obtained using samples prepared in the laboratory.

Numerical simulations are commonly used to assess a wide variety of conditions, including simplified to complex stope geometry, different input parameters and the complex layout of the stopes and barricades. Many different software, such as FLAC, PHASES2, FLAC^{3D}, PLAXIS and SIGMA/W, have been used to evaluate the stress state and verify the results of analytical solutions.

In most of the above-mentioned studies, two-dimensional programs were used. The influence of consolidation and hydration processes have also been neglected in most of the simulations. The rock mass behavior is considered elastic, which may not be in accordance with in-situ cases. Moreover, all the above-mentioned simulations were carried out for a single stope, and did not take into account the influence of the multiple excavations on the response of

backfilled stopes. The stability analysis of exposed backfilled stopes was also limited to a few simulated cases..

In practice, underground mines generally include several stopes to recover the ore. The influence of excavating adjacent openings on the backfill response has not yet been investigated in detail, and there are few solutions available for their analysis and design. This is nonetheless an important issue, as the stress state in and around multiple openings is known to depend on the excavations geometry, position and creation sequence (e.g. Brady and Brown 1993; Villaescusa 2003; Hoek 2007). To date, however, very little work has been done on the response of multiple stopes excavated in sequence in terms of displacement of the rock walls, local strain, and stress distribution in the backfill. Also, in some cases, the response of the rock mass is better represented by an elasto-plastic model (Brady and Brown 2004; Hoek, 2007). This in turn may influence the interaction between the rock mass and backfill.

This dissertation presents new modeling results obtained with FLAC and FLAC^{3D} for the case of two neighboring stopes, created one after another, considering different backfill and rock mass properties, stope geometry and rock mass behavior. The results of this study illustrate how these key factors influence both the magnitude and distribution pattern of the stresses, which can become much more complex in the case of two neighboring stopes. Also, a comprehensive investigation of exposed backfill in stopes due to mining out the adjacent stope is carried out to assess the stress state and the required strength of backfill.

CHAPTER 2 RESEARCH OBJECTIVE

Mining includes the exploration, extraction, and processing of minerals located below the earth's surface. Mining is necessary for mankind to access minerals, materials and energy. Despite many economic benefits from mining operations, this industry may include negative impacts on the environment during and after mining operations. The most important issues include the general and local stability of the excavated mine, selected structures, and production of waste materials during excavation. Careful considerations should be adopted to minimize the negative effects of mining operation and to provide a safe work place (Hoek and Brown, 1980).

In a mining operation, a large amount of waste materials is released from the extract and ore processing. Waste management and disposal are among the most important challenges in the mining industry (Aubertin et al. 2002). Nowadays, backfilling is one of the best ways to use these by-products. Backfill materials are placed into excavated stopes to provide a safer working place and to support the ground. This may allow the extraction of adjacent walls, while reducing the environmental impacts due to the waste materials. Ground control being the main goal of backfilling, it is necessary to have a good understanding of the backfill mechanical behavior in the stopes and its interaction with the surrounding rock mass.

As the vast majority of mine backfills are softer (more deformable) than the adjacent rock mass, the difference in stiffness between these two materials often generates stress redistribution from the backfill to the adjacent walls. In recent years, much work has been done to develop analytical solutions for evaluating the stress distribution in single backfilled stopes with two and three-dimensional equations. Numerical simulations have also been carried out to evaluate the stress state in single backfilled stopes. The influence of different parameters including stope geometry, backfill properties, filling rate and water pressure on the stress distribution within located stopes has also been assessed. However, there are still many other factors that should be considered to obtain representative solutions. One of these is the influence of the sequence of excavation on response of multiple backfilled stopes. The stress state within stopes excavated in an elasto-plastic rock mass is another aspect which has been neglected in most previous investigations. The stability of exposed backfill in stopes also needs to be studied further.

2.1 Problem statement

In practice, underground mines generally include several stopes to recover the ore, but the influence of excavating adjacent openings on the backfill response has not yet been investigated in details, and there are few solutions available for their analysis and design. This is nonetheless an important issue, as the stress state in and around multiple openings is known to depend on the excavations geometry, position and creation sequence. There is a limited knowledge about how a backfilled stope behaves during excavation and filling of an adjacent one.

This dissertation deals with the assessment of fill response, in terms of arching effects and stress developments within two adjacent stopes created in sequence. The goal of this thesis is to develop a numerical modeling approach to investigate the stress and strain distributions in multiple stopes in which the influence of different parameters, such as fill properties, stope geometry, pillar width, natural stress state and properties of rock mass, and excavation sequence, will be considered. In addition, the effect of rock wall removal on the stress distribution within a backfilled stope is assessed for different geometries and backfill strength. This project essentially involved conducting simulations of two adjacent stopes using 2D and 3D numerical models. The results of these simulations will be compared with those obtained from analytical solutions. The influence of many factors is analysed here, but the effect of pore water pressures is not taken into account in this study.

2.2 Thesis objectives

The overall objective of this thesis was to determine the stress distribution within two adjacent backfilled stopes and the related backfill behavior. These can be divided into sub-objectives:

1- Conduct a review of the past and current methods for modeling single backfilled stopes
2- Develop 2D and 3D numerical models of two adjacent stopes (based on those applied to single backfilled stopes), incorporating the effect of excavation and filling of the second stope with the following capabilities:
    - account for the stress-strain behavior and displacements in the two adjacent stopes

- replicate different backfill and rock mass properties and stopes location (depth and distance)
- use complex 2D and 3D stope geometries
- use different constitutive models for the rock mass and backfill
- model different excavation and filling sequences

3- Investigate the required strength of exposed backfill with particular reference to stope geometry and excavation sequence
4- Validate the numerical models using analytical solutions to demonstrate the model capacity.

2.3 Relevance of the thesis

The stability of the underground mining spaces is one the most important issues worldwide. In mining, the risk of stope and barricade failure demands a high level of safety in mine design. A good understanding of the backfilled stope behavior and stability is required to maximize safety and minimize costs. Numerical methods have often been applied for backfilled stopes, but few studies have been carried out to evaluate the geomechanical behavior of backfill materials in more than one excavation, considering different parameters, including backfill properties, stope geometry and excavation sequence.

Development of numerical models for two excavations created one after the other will improve the design of multiple stopes. It may also be possible to modify analytical solutions based on the numerical simulations results obtained for two stopes.

This thesis provides a basic approach for the optimum design of multiple backfilled stopes, considering the influence of various factors. Also, the backfill properties and stope geometry needed for the stability of exposed backfill during mining of a secondary stope can be evaluated. The results of this investigation also give the stress magnitudes based on the distance and geometry of two stopes in 3D.

2.4 Contributions

This research will contribute to the analysis and design of backfilled stopes and help better address geo-mechanical challenges in underground mining. This research may lead to following benefits for the mining industry:

- Significant cost saving by an improved assessment of the required backfill strength
- Significant reduction of the risks due to failures and increased productivity following improved predictions of the stresses, wall displacements and strains within two adjacent backfilled stopes
- Optimization of backfill properties and size and location of adjacent stopes

The scientific contribution of this project is a thesis that includes the following four manuscripts submitted to peer reviewed journals:

1- Falaknaz, N., Aubertin, M., Li. L. Numerical Analyses of the Stress State in Two Neighboring Stopes Excavated and Backfilled in Sequence, *International journal of Geomechanics, ASCE,* Submitted in Feb 2013; accepted Nov 2014.

2- Falaknaz, N., Aubertin, M., Li. L. A numerical investigation of the geomechanical response of adjacent backfilled stopes, *Canadian geotechnical journal,* Submitted in Feb 2014; under revision following comments from reviewers.

3- Falaknaz, N., Aubertin, M., Li. L. Evaluation of the stress state in two adjacent backfilled stopes within an elasto-plastic rock mass, *Geotechnical and geological Engineering journal,* Submitted in Jul 2014.

4- Falaknaz, N., Aubertin, M., Li. L. Stability analyses of backfill in mine stopes with an open face, *Canadian geotechnical journal,* Submitted in Oct 2014.

Two other conference papers (Falaknaz et al. 2013, 2014) were also published in the course of this doctoral work.

It should be noted that the four manuscripts included in this Thesis (Chapters 3 to 6) are based on those initially submitted to journals (with some minor corrections, usually requested by

the evaluation committee). Corrections made later (as requested by the Reviewers and Editors, and others), before publication in journals, are not included here. The final published papers may thus differ from the versions appearing in the Thesis.

2.5 Outline of the thesis

Chapter 1 provides an overview of the backfill types, arching effects, previous analytical and numerical solutions, physical models and in-situ measurements within underground mines. Chapter 2 introduces the problem statement, objectives and the relevance of the thesis.

Chapter 3 gives the main results obtained using both analytical and numerical solutions to determine the stress distribution and wall displacements in two adjacent stopes considering different parameters, including backfill friction angle, dilatancy angle and cohesion, stope width and stope depth. In this chapter, it was assumed that the Poisson's ratio v and internal friction angle ϕ of the backfill are independent parameters, as was usually the case in previous numerical investigations. The conceptual models for the numerical simulations, with modification of the existing models for vertical stopes using FLAC will be presented in this chapter.

Chapter 4 presents the main results obtained for similar backfilled stopes, but with dependent values for the Poisson's ratio and the internal friction angle of the backfill. Also, the influence of pillar width for both cohesionless and cohesive backfill, natural stresses in the rock mass and its elastic modulus, are evaluated. The results are presented in terms of stresses, wall displacements and backfill strains. In this chapter, the response of backfill will also be assessed in terms of the stress path induced by the excavation and filling process.

Chapter 5 contains the main results obtained for two adjacent backfilled stopes with an elasto-plastic rock mass behavior. The results obtained using both elastic and elasto-plastic behaviors were compared. The influence of different parameters, including stope width, pillar width, stope depth, natural stresses in the rock mass, modulus and shear strength parameters of the rock mass is also addressed in this chapter. The rock wall displacements and backfill strains were monitored during excavation and filling sequences and will be presented in this chapter. The stress path in the backfill is also provided when rock mass is considered as an elasto-plastic material.

Chapter 6 investigates the stress state and displacements in a primary stope using FLAC^{3D} when a secondary stope is mined out. The required backfill strength and the factor of safety for different stope geometry were also evaluated. The sliding plane angle is also calculated for different stope geometry. The results are compared with the existing analytical solutions. Because of their self-contained format (as journal manuscripts), Chapters 3 to 6 contain overlaps and repetitions. Chapter 7 includes the effect of the third dimension on the stress distribution in two adjacent backfilled stopes, using FLAC^{3D}. The influence of different parameters, including stope width and depth, backfill friction angle and cohesion is also investigated in this chapter.

Some of the simulations results are presented in the form of isocontours, as FLAC output, with the commonly used sign convention i.e. compression stresses are negative and tensiles stresses are positive; however, other graphs (prepared with excel) are based on the usual rock mechanics sign convention, i.e. compression stresses (and strains) are positive and the tensiles stresses (and strains) are negative.

Chapter 8 contains a summary and general discussion on the results obtained in this investigation.

The last chapter includes a conclusion and recommendations for future studies. Some additional results are presented in the Appendices.

CHAPTER 3 ARTICLE 1: NUMERICAL ANALYSES OF THE STRESS STATE IN TWO NEIGHBORING STOPES EXCAVATED AND BACKFILLED IN SEQUENCE

Nooshin Falaknaz, Michel Aubertin, and Li Li

This article was accepted to International journal of Geomechanics, ASCE, Submitted in Feb 2013, Accepted in Nov 2014.

Abstract: Backfilling of underground stopes is commonly used in the mining industry. The stress state in these stopes has to be evaluated to ensure safe application of the backfill. In recent years, much work has been conducted to assess the stresses in single backfilled stopes. The stress distribution in stopes may also be affected by the excavation of multiple openings. This paper presents key results obtained from numerical simulations of two adjacent vertical stopes created in sequence. The results illustrate the influence of stope geometry (size and spacing), natural stress state, backfill properties, and excavation (and filling) sequence on the stress distribution in both stopes. The simulations indicate that the stress distribution in the first backfilled opening, following the creation of the second one, largely depends on the fill properties. These results also show how these factors may affect the stress magnitude and distribution pattern in the case of two adjacent stopes, when the creation of a second opening influences the response of the first one. It is also demonstrated that the second backfilled stope tends to behave in a manner similar to that of a single (isolated) stope, where a classical arching effect often dominates the stress distribution.

Keywords: Multiple stopes; Mine backfill; Excavation sequence; Stresses; Numerical modeling.

3.1 Introduction

Backfills are placed in underground openings to improve ground control conditions around mine stopes and prevent excessive deformation of the surrounding rock mass. In addition, backfills can increase the stiffness and strength of rock mass by raising the local confining pressure. Environmental and economic considerations are also part of the rationale behind stope backfilling, which can furthermore contribute to a reduction of the amount of wastes disposed on the surface, hence limiting their impact and the related costs (Hassani and Archibald 1998; Benzaazoua et al. 2008).

Ground control being the main goal of backfilling, it is necessary to have a good understanding of the backfill mechanical behaviour in stopes and its interaction with the surrounding rock mass. The intrinsic response of backfill can vary widely depending on its constituents. In this regard, various studies have shown that the behavior of backfills is affected by the grain size distribution of the solid phase, amount and type of binder, and characteristics of the water (e.g. Hassani and Archibald, 1998; Belem et al. 2000; Benzaazoua et al. 2004; Potvin et al. 2005; Rankine and Sivakugan, 2007). These investigations have also demonstrated that the vast majority of mine backfills are softer (more deformable) than the adjacent rock mass (at least in the case of hard rock mines). The difference in stiffness between these two materials can generate stress redistribution from the backfill to the adjacent walls. This stress transfer, confirmed by in-situ stress measurements (e.g. Knutsson 1981; Hustrulid et al. 1989; Belem et al. 2004; Thompson et al. 2011, 2012), is associated with an arching effect, which is a well-known phenomenon in soil mechanics (Handy and Spangler, 2007) and for other problems involving particulate materials (e.g. Cowin, 1977; Blight 1986).

In recent years, much work has been done to develop analytical solutions, based on the Marston (1930) backfilled trench approach, for evaluating the stress distribution in single backfilled stopes with two and three dimensional equations (Aubertin et al. 2003; Li et al. 2005; Li and Aubertin, 2008). These solutions have further been modified to take into account the effect of pore water pressures PWP (Li and Aubertin 2009b, c), while others have introduced changes for stopes with inclined walls (e.g. Ting et al. 2011).

Another approach commonly used to investigate this stress state relies on numerical modeling. The influence of different factors, including backfill properties (Li et al. 2003;

Pirapakaran and Sivakugan, 2007; Fahey et al. 2009; Li and Aubertin, 2009a), geometry of the opening (Li et al. 2007; Li and Aubertin, 2009a), filling rate, consolidation and evolving fill characteristics (El Mkadmi et al. 2011a, b, 2014), has been investigated through simulations to assess their effect on the stresses developing within single stopes and on barricades. In practice, underground mines generally include several stopes to recover the ore, but the influence of excavating adjacent openings on the backfill response has not yet been investigated in details, and there are few solutions available for their analysis and design. This is nonetheless an important issue, as the stress state in and around multiple openings is known to depend on excavations geometry, position and creation sequence (e.g. Brady and Brown, 1993; Villaescusa, 2003; Hoek, 2007). The importance of this aspect for the design of backfilled stopes is specifically demonstrated with the results presented here.

In this paper, new modeling results obtained with FLAC are presented for the case of two neighboring stopes created one after the other. The results show the influence of various factors, including stope geometry, natural stresses in the rock mass, backfill properties, and excavation (and filling) sequence, on the stress state in both backfilled stopes. The paper illustrates how these key factors influence both the magnitude and distribution pattern of stresses, which can become much more complex in the case of two neighboring stopes. The simulation results more specifically show how the excavation and backfilling of the second stope affect the response of the first backfilled opening, in terms of displacement of the walls, local strain, and stress distribution in the stope.

3.2 Simulation with FLAC

While analytical solutions are very useful, their application is usually limited to simple cases with regular geometry and idealized material properties. Numerical models are more flexible and versatile tools in comparison with analytical solutions. These can be used to solve complex problems using different constitutive models, input parameters and boundary conditions. Previous works conducted by the authors and by other groups has shown that the commercial code FLAC (Itasca, 2002) is a useful tool to investigate the response of backfill in stopes. This is a two-dimensional finite difference program that uses an explicit Lagrangian calculation scheme and a mixed-discretization zoning technique. The discretization must be optimized to define a mesh that gives stable and precise results, for realistic computation time. In this investigation, the

models were built after testing various mesh sizes to determine a valid solution. Quadrilateral elements are used in the models, with a coarser mesh for the elastic rock region and a finer mesh inside and near the backfilled stope. The number of elements for a single stope or two adjacent stopes depends on the stope geometry and model size. The total size of the model is another key aspect, as the location of the external boundaries must not influence the results, while maintaining the model domain to a realistic size. This optimum model size may vary when the stopes geometry changes. This assessment was performed early in this investigation, and the location of the boundaries has been adjusted for each case (more information is included in Falaknaz, 2014; Appendix A).

3.2.1 Single stope

Figure 3-1(a) shows a model used to analyse the response of a typical vertical backfilled stope (Case 0 in Table 3.1). The rock mass and backfill properties are given in Table 3.1, with the stope geometry. These characteristics, which are loosely based on typical hard rock mining operations located in Abitibi (Quebec, Canada), are also used for other cases listed in Table 3.1.

In these calculations, the rock mass is considered homogeneous, isotropic and linearly elastic; the following parameters have been used: E_r = 30 GPa (Young's modulus), υ_r = 0.33 (Poisson's ratio), γ_r = 27 kN/m^3 (unit weight). The properties of the backfill (with and without cement) used in the numerical analyses have been adapted from laboratory testing results (taken from: Belem et al. 2000; Pirapirakan, 2008; Veenstra, 2013). The fill behaviour follows an elasto-plastic law with the Mohr-Coulomb criterion. Its mechanical properties are described by E, υ, γ, with the effective internal friction angle ϕ', cohesion c', and dilatancy angle ψ' (with $\phi' \neq \psi'$ for a non-associated flow rule).

The reference stope width is 6 m, and it is filled to a height of 45 m, with 0.5 m of void space left at the top. The natural in-situ vertical stress σ_v in the rock mass is obtained by considering the overburden weight, for a depth z (at the base of the opening) of 300 m (Case 0). The natural horizontal stress in the rock mass σ_h is taken as twice the vertical stress σ_v (i.e. $\sigma_h = K_r \sigma_v = 2 \gamma_r z$) based on a typical situation encountered in the Canadian Shield (Herget 1988; Arjang 1996, 2004); additional values of the natural earth pressure coefficient (or stress ratio) K_r in the rock mass have also been investigated by Falaknaz (2014, Chapter 4), but these results are not presented here.

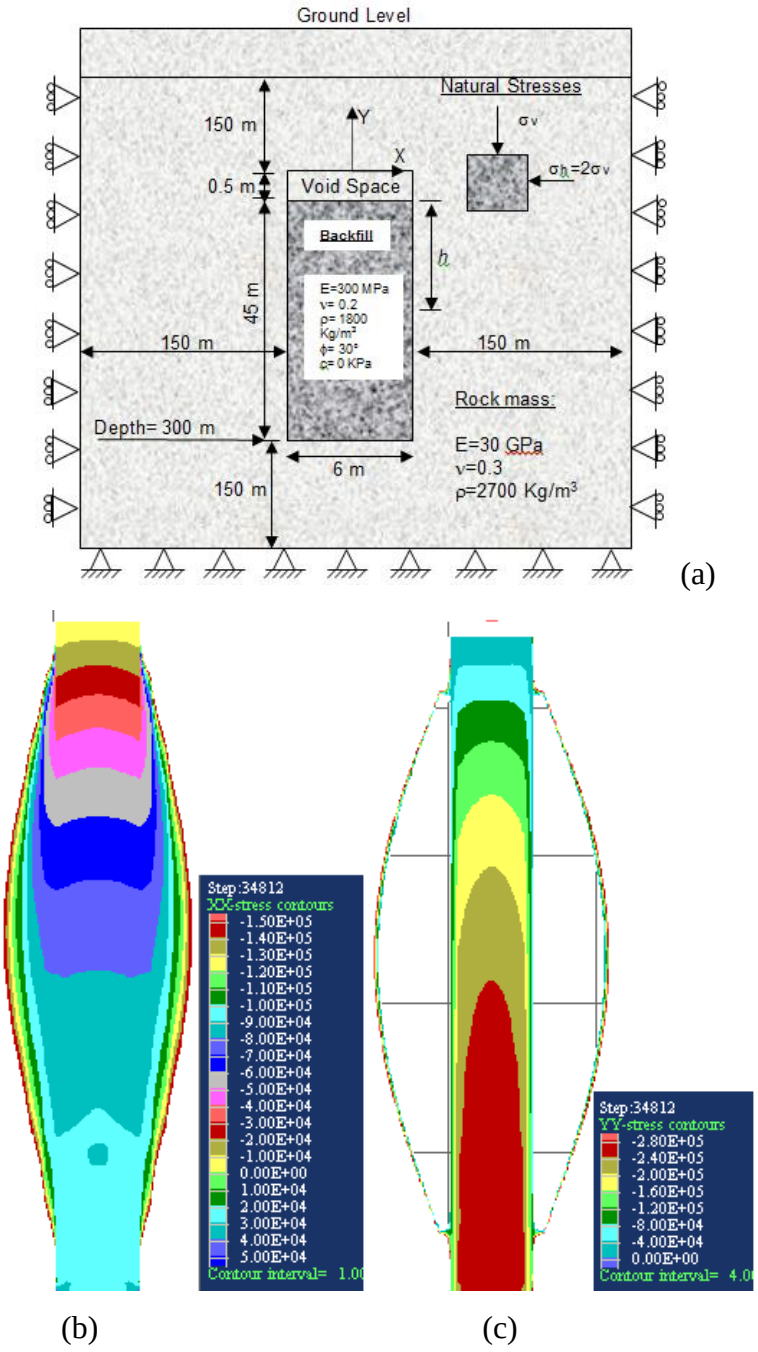

Figure 3-1: Backfilled stope model for the base case (Case 0): (a) schematic view (not to scale), with properties and boundary conditions used for the simulations with FLAC; numerical simulation results with isocontours of (b) horizontal stresses and (c) vertical stresses distributions at the end of filling (see Table 3.1 for details)

Table 3.1: Parameters used in the numerical simulations, including stope size, backfill properties, and number of elements in the mesh (with height h = 45 m, pillar width D = 8 m, and backfill modulus E = 300 MPa)

Cases	*Width B* (m)	*v*	ϕ' (º)	ψ' (º)	*c'* (kPa)	*Depth of stope base z* (m)	Number of elements
0 (Base)	6	0.2	30	0	0	300	104×262
1a,b,c	6	0.2	25, 30, 35	0	0	300	124×262
2a,b	6, 18	0.3	35	0	0	300	var
3a to e	6	0.3	35	0	1, 20, 50, 100, 300	300	124×262
4a,b	6	0.3	35	17.5, 35	1, 20	300	124×262
5a,b	6	0.3	35	0	0	400,2000	160×352

The conditions imposed around the outer perimeter of the model prevent horizontal displacement on both sides, while vertical displacements are allowed. Displacements at the bottom of the model are prevented along both axes. A relatively coarse mesh (from 5 m near the model boundaries to 1 m near stope walls) is used for the elastic rock region while a finer mesh is used for the backfill (i.e. 0.5 m grid size). The number of elements is 104×262 for the single stope. Gravity is the initial condition applied to the model.

The sidewalls of a stope created by blasting are typically very rough and irregular, so shearing tends to occur in the backfill itself. Therefore, there is no (planar) interface element between the backfill and rock mass in the numerical models (see Li et al. 2003 and Li and Aubertin, 2009a for a discussion on this issue).

The stope is excavated instantly and the rock region is allowed to reach stress-strain equilibrium. The backfill is then placed in four layers; a larger number of layers would not influence significantly the stress state under these conditions (Li and Aubertin 2009a). The simulated stress distribution and wall convergence are monitored during the excavation and filling of the stope.

Figures 3-1(b) and 3-1(c) show the distribution of the vertical and horizontal stresses in the backfilled stope at the end of filling for a backfill internal friction angle ϕ' = 30º (other material parameters are given in the caption and in Table 3.1). These results show that both the horizontal and vertical stresses tend to be smaller along the walls than in the central part of the stope at a given elevation. This is typical of stopes where a strong arching effect develops (e.g. Li et al. 2003, 2005). Figure 3-2 shows the stress distribution along the vertical center line (VCL) and along the walls, obtained from FLAC for the (base) Case 0.

The figure also shows the stresses obtained from the analytical solution proposed by Li and Aubertin (2008), which is a modified version of Marston's (1930) solution initially developed for trenches and later adapted for backfilled stopes (Aubertin et al. 2003; Li et al. 2003). This solution can be expressed as follows for the vertical and horizontal stresses at depth *h* (Li and Aubertin, 2008):

$$\sigma_{vx} = \gamma B \left(\frac{1-\exp\left(-\frac{2K\,h\,tan\phi'}{B(1-DF)}\right)}{2K\,tan\phi'} \right).\left[1 - a\left(\frac{x}{B}\right)^{b}\right] \qquad (3\text{-}1)$$

$$\sigma_h = \gamma B \left(\frac{1-\exp\left(-\frac{2K\,h\,tan\phi'}{B(1-DF)}\right)}{2tan\phi'} \right) \quad (3\text{-}2)$$

In these equations, B is the stope width (m); K is the earth pressure coefficient in the backfill, which is taken as the Rankine active coefficient [$K = K_a = \tan^2(45° - \phi'/2)$]; x is the distance from the center line of the stope ($x \leq \frac{B}{2}$); a and b are parameters that control the vertical stress distribution along the width; DF is the distribution factor defined as follows:

$$DF = \frac{a}{2^b(b+1)} \quad (3\text{-}3)$$

$$\text{with } a = 2^{\left(1-\lambda_1\frac{H}{B}\right)} tan^{-\lambda_2}(\phi_0 + \phi') \text{ and } \quad b = 3 \quad (3\text{-}4)$$

In these equations, the values of ϕ_0 =50°, λ_1 = 0.02 and λ_2 = 0.1 have been obtained from an optimisation technique applied to a series of numerical simulations (Li and Aubertin, 2008).

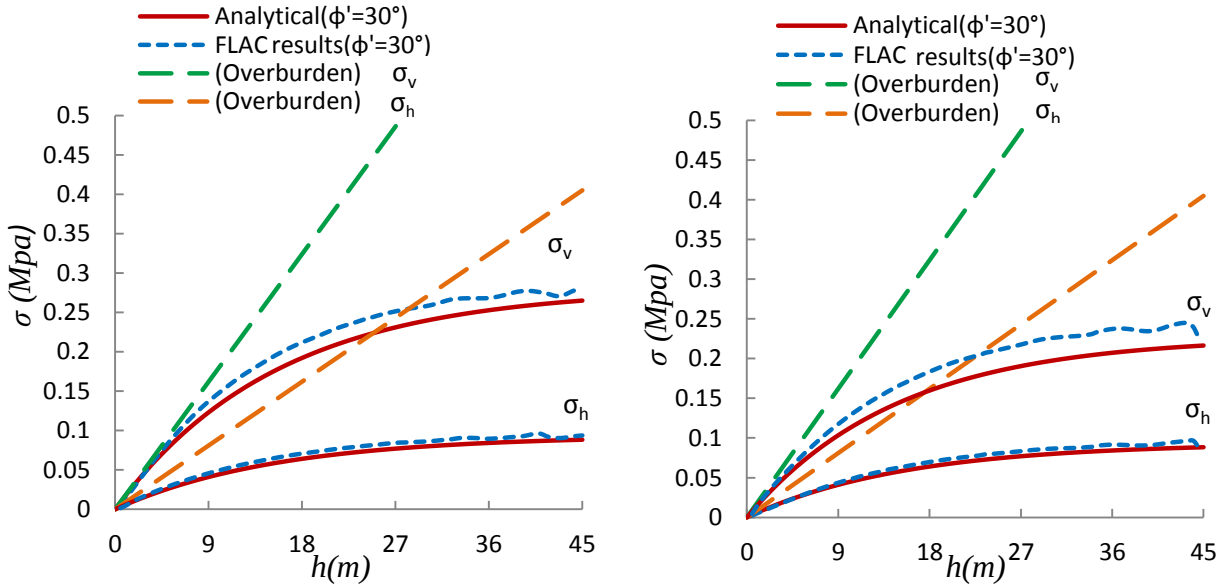

(a) (b)

Figure 3-2: Horizontal and vertical stresses along (a) the VCL and (b) walls of a single stope (base Case 0) obtained using the analytical (Eqs. 3-1 to 3-2) and numerical (using FLAC) solutions; the overburden pressures (with $\sigma_v = \gamma h$ and $\sigma_h = K_o\ \sigma_v$; $K_o = 1\text{-}sin\phi'$) at different elevations h are also shown

This type of solution (with an arching effect) has been successfully compared with experimental results taken from the literature (Li et al. 2005; Li and Aubertin 2009a). The results shown in Figure 3-2 will serve as a basis (Case 0) for the analyses presented in the following.

3.2.2 Two adjacent stopes

Figure 3-3 shows the model with two backfilled stopes located near each other (Case 1, Table 3.1). The model size is adjusted for all cases, so that the external boundaries are far enough from the openings not to affect the calculations. For instance, for two adjacent stopes with B = 6 m or 18 m, the boundaries are located 150 m from the stope walls in both directions. The distance between the two stopes is 8 m for Case 1 (and others cases identified in Table 3.1). The rock mass and backfill properties are the same as in the base Case 0 (Figure 3-1 and Table 3.1). As in all the cases simulated here, the natural in-situ horizontal stress σ_h is twice the vertical stress σ_v in the rock mass. The boundary conditions applied to the rock region are presented in Figure 3-3.

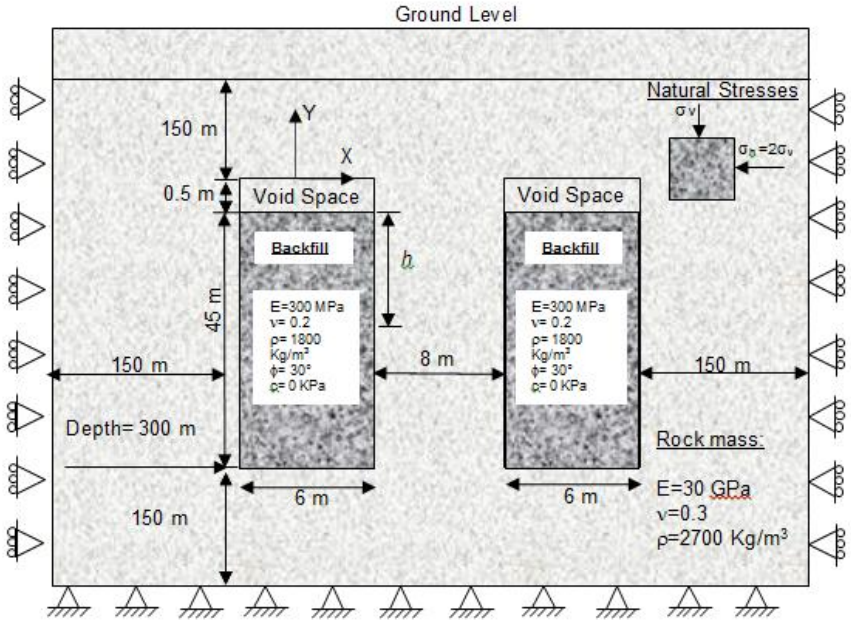

Figure 3-3: Schematic view of the boundary conditions, size and properties applied for simulating the response of two vertical backfilled stopes (not to scale) in plane strain (with an earth pressure coefficient K_r = 2 in the rock mass)

The first stope is excavated instantly and the rock mass is allowed to reach equilibrium under the imposed stresses (including rock weight). The backfill in this first stope is placed in four layers, leading to a stress distribution similar to that shown in Figure 3-2 before the second opening is created. Then, the second stope is excavated in four layers (or steps) from the bottom to the top and then filled in four layers.

The stress distribution and wall convergence of the first stope is monitored during the excavation and filling of the second stope. Again, a relatively coarse mesh (element size of 5 m close to the model boundaries, down to 1 m close at the stope walls) is used for the elastic rock region while a finer mesh is used for the backfill (element size of 0.5 m x 0.5 m). Table 1 gives the details of the simulations performed. It is seen in this table that the number of elements for the two stopes simulations varies according to the stope size and distance between them. For instance, the number of elements is 124×262 for stopes with B = 6 m and 172×262 for stopes with B = 18 m.

The distribution of vertical and horizontal stresses in the backfilled stopes obtained using FLAC at the end of filling of the second stope is shown in Figure 3-4 (Case 1, for 2 stopes having the same size as in Case 0). The results show that both the horizontal and vertical stresses tend to be smaller along the walls than in the central part of the stopes at a given elevation. There is thus an arching effect developing in both stopes, but the stress distributions are somewhat different in the two openings. These distributions are nonetheless fairly similar to those obtained for a single stope (Case 0, Figures 3-1 and 3-2).

Figure 3-5 shows the stress distribution in the first stope along the vertical central line (VCL) during excavation (Fig. 3-5a) and filling (Fig. 3-5b) of the second stope. As can be seen, there is an important transfer of the backfill load to the walls, associated with the arching effect seen in Figure 3-4. It is also observed that during excavation of the second stope, the vertical and horizontal stresses change in the first stope (Fig. 3-5a). For the first two excavation steps of the second stope, the horizontal stresses tend to decrease in the first stope (from a maximum of about 170 kPa to 50 kPa at h = 26 m) due to displacement of right wall. These stresses then increase at depth (up to 81 kPa), but decrease in the upper part after the third step; the horizontal stresses remain almost constant for the third and fourth steps of excavation.

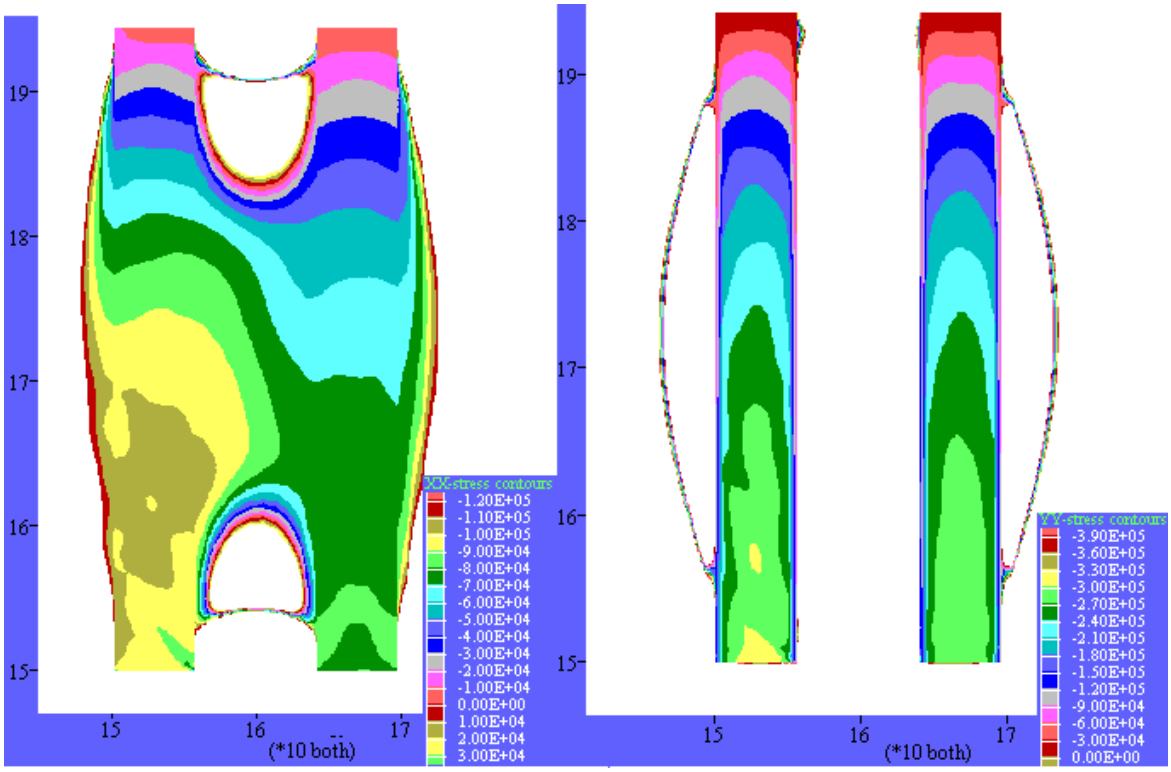

(a) (b)

Figure 3-4: Numerical simulation results showing the non-symmetric stress state in the two adjacent backfilled stopes at the end of filling of the second stope (Case 1b): (a) horizontal stresses σ_h; (b) vertical stresses σ_v. These stresses can be compared with those obtained for a single stope (Case 0, Figure 3-1)

During the extraction of first two rock layers of the second stope, the vertical stresses in the first (backfilled) stope tend to decrease (by up to 60%), especially near mid-height. The horizontal displacement of the right wall (illustrated in Fig. 3-7b, presented below) leads to this stress decrease in the first stope. These stresses increase upon the third excavation step and then tend to return to the earlier magnitude for the last two stages.

During backfilling of the second stope, the horizontal stresses along the VCL of the first stope tend to increase with the filling steps (Fig. 3-5b, left), but the changes are much less than during the excavation steps. The vertical stresses in the first stope are not sensitive to the filling steps taking place in the second stope (Fig. 3-5b, right).

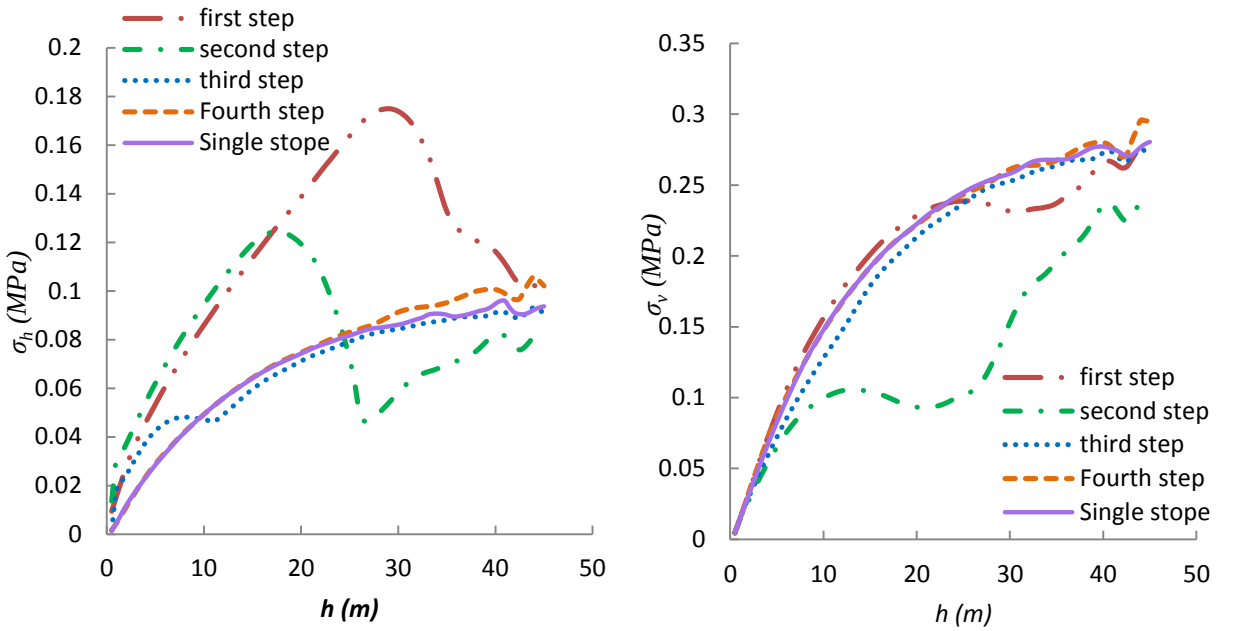

(a)

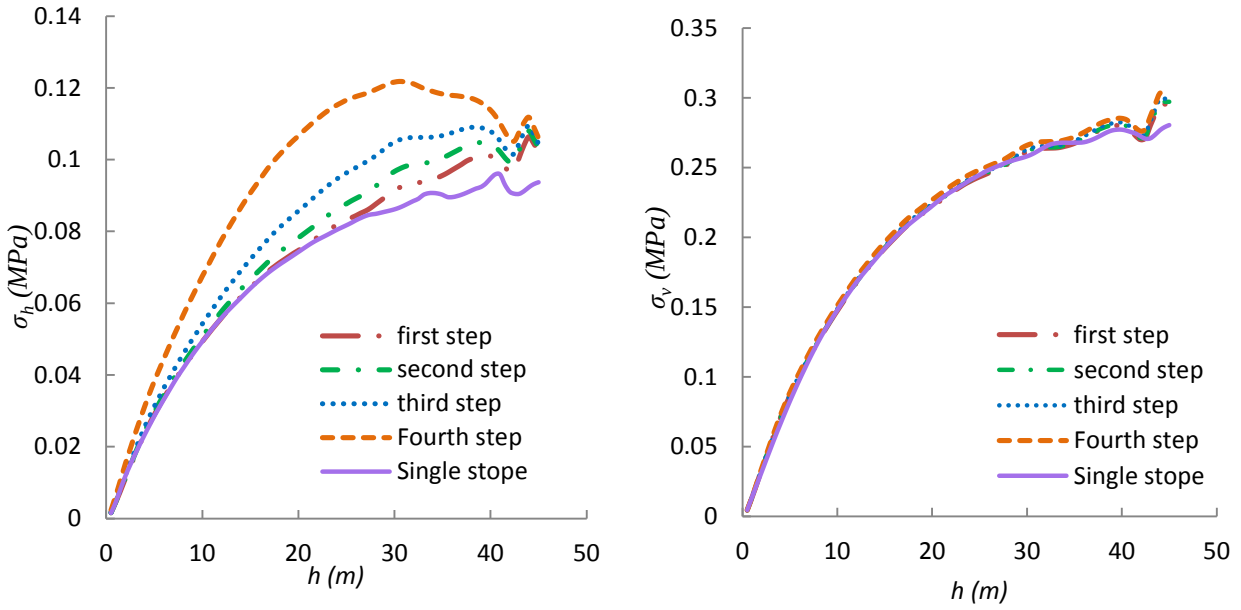

(b)

Figure 3-5: Horizontal (left) and vertical (right) stresses along VCL of the first backfilled stope (Case 1b), (a) during the 4 steps for excavating the second stope; (b) during the 4 steps for filling the second stope; the results for the single stope (Case 0) are also shown

Figure 3-5 shows the stress distributions within a single stope and within the two adjacent stopes after excavation and filling. As can be seen on the left hand side of this figure, the

horizontal stresses along the vertical central line of the first stope after excavation of the second one is almost identical to that obtained for a single backfilled stope (and for the second stope after backfilling). However, the horizontal stresses increase (by up to 40% near mid-height) after filling of the second stope. Hence, these results (Fig.3-5b, left hand side) indicate that the horizontal stresses in the first stope are significantly influenced by filling of the second stope in Case 1. It is also seen in Figure 3-5 (right hand side) that the excavation and filling bear little effect on the vertical stresses along the VCL of the first stope, where the magnitude is the same as for a single stope.

The results also show that the horizontal and vertical stresses along the vertical central line (VCL) of the second stope are quite similar to those obtained along the VCL of a single backfilled stope after filling. Thus, it may be considered that the backfill response along the VCL of the second opening is practically the same as that obtained for a single vertical stope, for which the stresses can be estimated using the analytical solution given above (Eqs. 3-1 and 3-2).

Figure 3-6 shows the horizontal and vertical stresses along the left and right walls of both stopes after excavation and filling of the second stope (Case 1). It can be seen that the horizontal stresses in the backfill along the left and right walls of the first stope are almost similar to the horizontal stresses along the walls of a single vertical stope.

The horizontal stresses along the walls tend to increase in the first stope (especially near mid-height) with filling of the second stope. The vertical stresses along the walls of the first stope, after excavation and filling of the second opening, are close to those obtained for a single backfilled stope (see also Figure 3-5). Again, the final horizontal and vertical stresses obtained in the backfill along the walls of the second stope (after the whole process of excavation and filling) are almost identical to those obtained for a single stope.

The variation of the stress state in the first backfilled stope during the creation and subsequent filling of the second opening can be related to movements of the rock walls. The horizontal displacements δ_h of the right and left (rock) walls of the first stope during the excavation and filling of second stope are shown in Figures 3-7 and 3-8. The vertical displacements have also been computed; the simulated results (not presented here; see Appendix B in Falaknaz, 2014, for details) indicate that these vertical displacements are much smaller (by

about an order of magnitude) than the horizontal ones, and that their effect on the stress state in the backfill is much less significant.

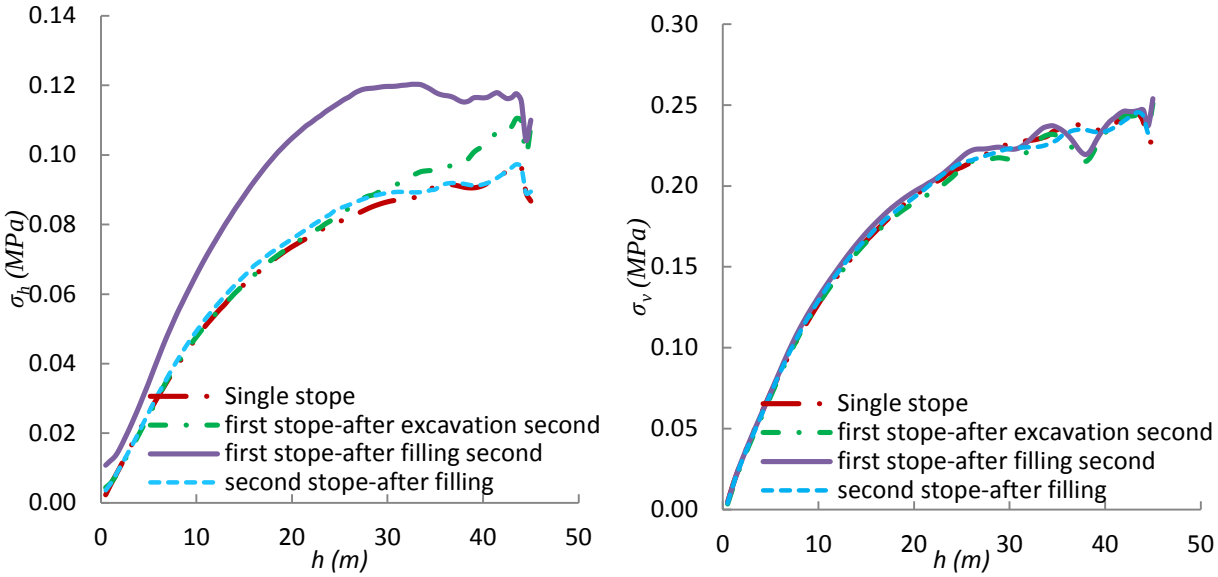

(a)

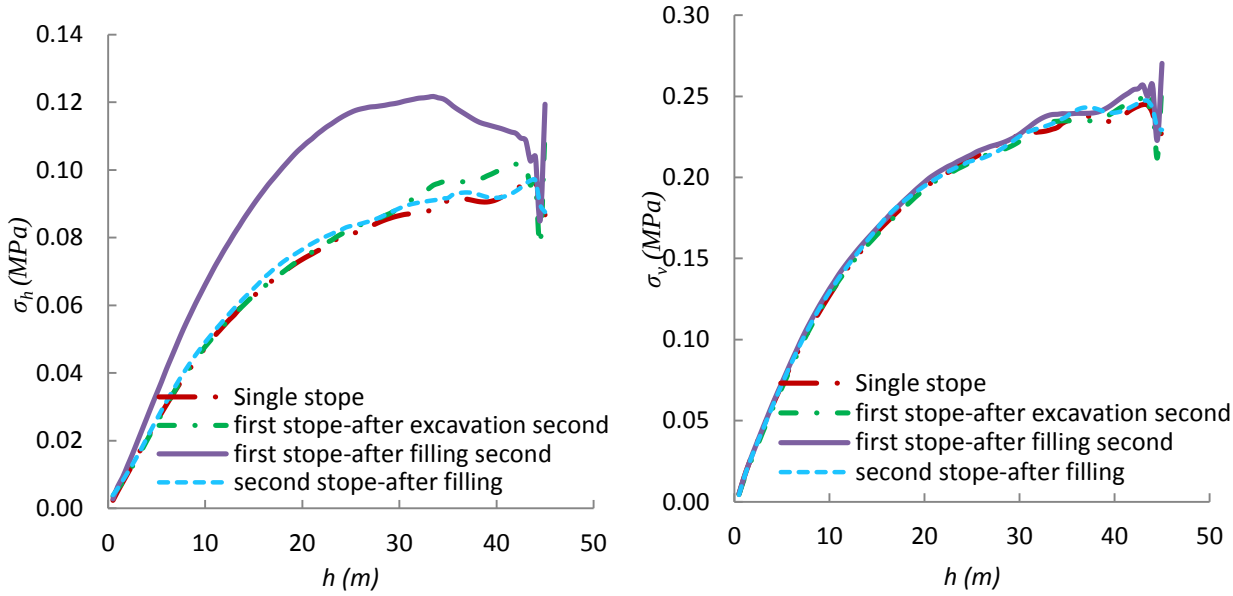

(b)

Figure 3-6: Horizontal (left) and vertical (right) stresses along the (a) left wall and (b) right wall of the first and second stopes, after excavation and filling of the latter (Case 1b); the results for the single stope (Case 0) are also shown

The horizontal displacements δ_h along the left wall (taken at 0.5 m from the rock wall), shown in Figure 3-7(a), goes from about 2 cm (first step, single backfilled stope) to 2.16 cm toward the right during the four excavation steps of the second stope. This indicates that the horizontal displacement of the left wall is not significantly affected by the excavation of the adjacent stope. The horizontal displacement δ_h along the right wall of the first stope (Fig. 3-7b) evolves with the excavation steps, going left and then right (from a maximum of about -2.2 cm - leftward - upon the first step to -0.07 cm upon the fourth excavation step at mid-height).

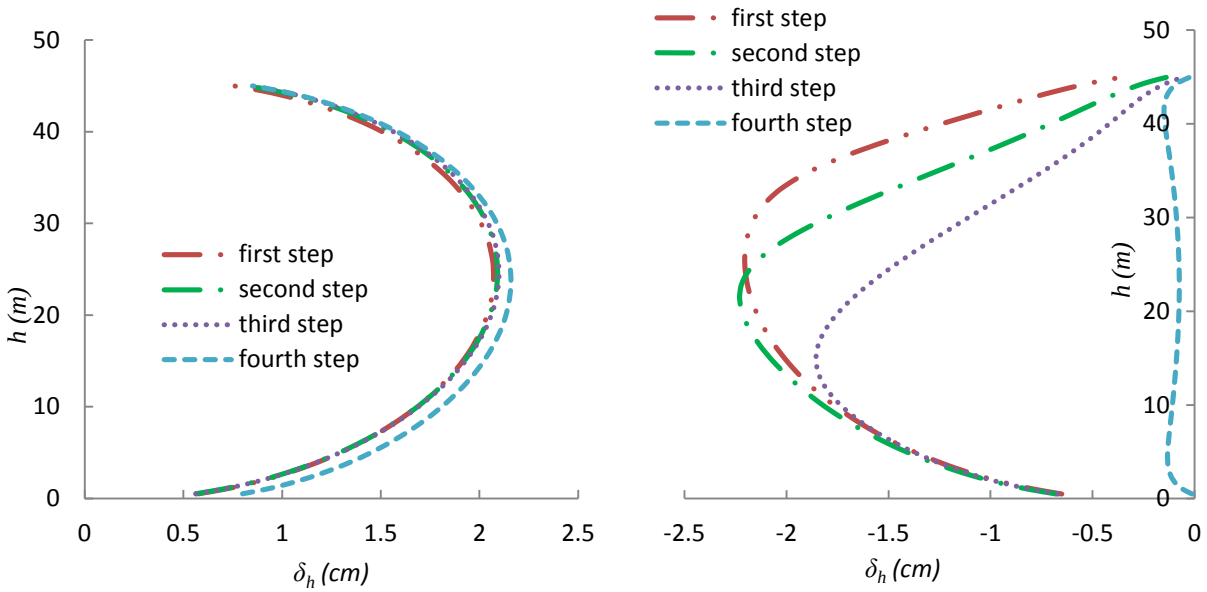

Figure 3-7: Horizontal displacements δ_h along the (a) left wall and (b) right wall of the first stope during the excavation (4 steps) of the second stope (Case 1b)

The δ_h along the left wall of the first backfilled opening are not affected by the filling process (Fig. 3-8a). However, the horizontal displacements at mid-height of the right wall increase with the filling steps from -0.07 cm upon the first step of filling to -0.12 cm at the end of filling of the second stope (Fig. 3-8b). These results show that the right wall moves inward (i.e. within the first stope) during the 4 steps of filling of the second stope. The maximum horizontal displacement during the excavation of the second stope is about 2 cm, while it is about 0.12 cm during filling. These displacements help understand the changes in the horizontal stresses observed in the first stope during excavation and filling of the second stope (Figures 3-5 and 3-6). The vertical displacements (not shown here, Appendix B in Falaknaz, 2014) are much smaller

(about 0.1 to 0.2 cm) than δ_h during the excavation steps and these remain unchanged during filling of the second stope.

The δ_h along the left wall of the first backfilled opening are not affected by the filling process (Fig. 3-8a). However, the horizontal displacements at mid-height of the right wall increase with the filling steps from -0.07 cm upon the first step of filling to -0.12 cm at the end of filling of the second stope (Fig. 3-8b). These results show that the right wall moves inward (i.e. within the first stope) during the 4 steps of filling of the second stope. The maximum horizontal displacement during the excavation of the second stope is about 2 cm, while it is about 0.12 cm during filling. These displacements help understand the changes in the horizontal stresses observed in the first stope during excavation and filling of the second stope (Figures 3-5 and 3-6). The vertical displacements (not shown here, Appendix B in Falaknaz, 2014) are much smaller (about 0.1 to 0.2 cm) than δ_h during the excavation steps and these remain unchanged during filling of the second stope.

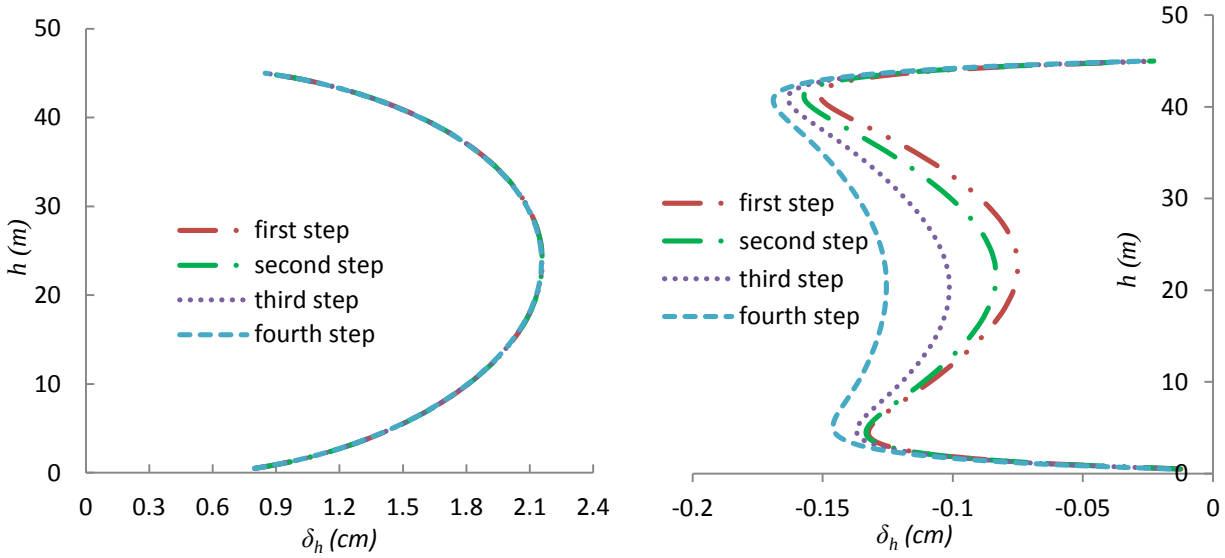

(a) (b)

Figure 3-8: Horizontal displacements δ_h along the (a) left wall and (b) right wall of the first stope during filling (4 steps) of the second stope (Case 1b)

The horizontal strain ε_h in the backfill along the VCL of the first stope during excavation and filling of the second stope is presented in Figure 3-9. As this strain is not given directly by FLAC, it has been calculated with a user-defined (FISH) function based on the horizontal

displacements along two vertical axes. The figure indicates that the horizontal strain ε_h increases to about -0.35 % at mid-height of the first stope during the excavation of the second stope, and then becomes constant during filling.

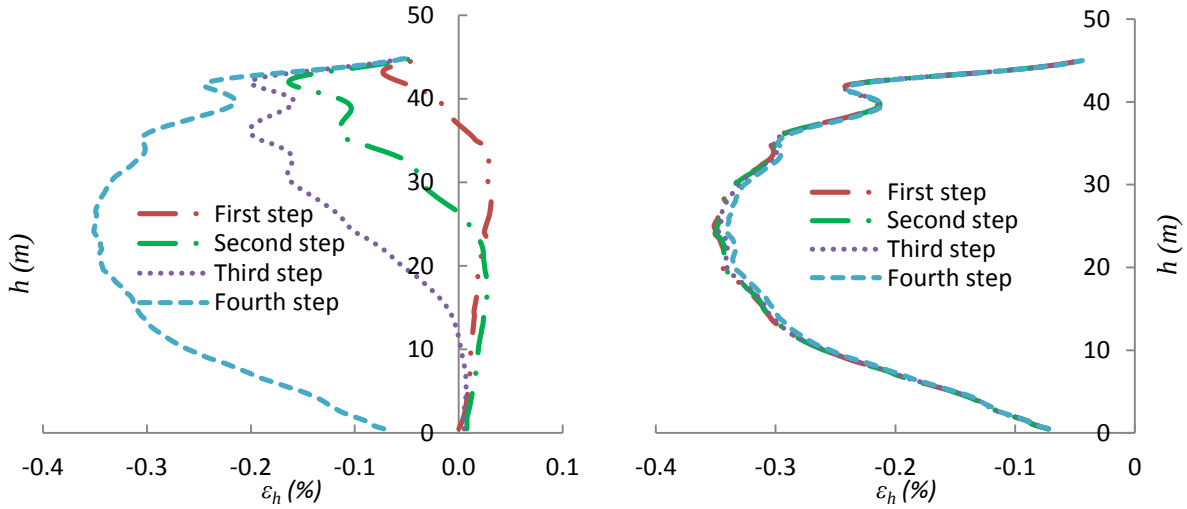

Figure 3-9: Horizontal strain ε_h along the VCL of the first backfilled stope during (a) excavation (4 steps) and (b) filling (4 steps) of the second stope (Case 1b)

3.3 Influence of different parameters

Additional numerical simulations have been conducted to investigate the influence of various parameters on the stress distribution within the two neighboring stopes. Results from a series of calculations are presented in the following to assess the effect of varying the stope size (width B), openings depth (or natural stress state), and the backfill internal friction angle (ϕ'), cohesion (c'), dilation angle (ψ'). The results are presented in terms of the stresses along the VCL and walls of the first stope. As the final stresses obtained for the second backfilled stope are again very close to those of the isolated stope, these are not shown here (Appendix B in Falaknaz, 2014).

3.3.1 Stope Width *B*

The influence of the width on the stress distribution within a single backfilled stope has been investigated by Li and coworkers (Li et al. 2005, 2007; Li and Aubertin, 2008, 2009a), but this aspect has not yet been assessed for two adjacent stopes (to the authors knowledge). In the

next simulation (Case 2), both stopes have a width B = 18 m and space of 8 m. The boundaries are again located 150 m from the stopes walls. There are 172×262 elements in the mesh, with a size that varies with the distance from the walls. The boundary conditions and rock and backfill properties are presented in Table 3-1. Figure 3-10 shows the isocontours of the stresses within the two stopes. It is seen that the stresses distributions are more irregular within the first stope, in comparison to Case 1 with B = 6 m (see Figure 3-4). In addition, there is less arching in both stopes when the width increases (as expected). Displacements are also more pronounced in Case 2.

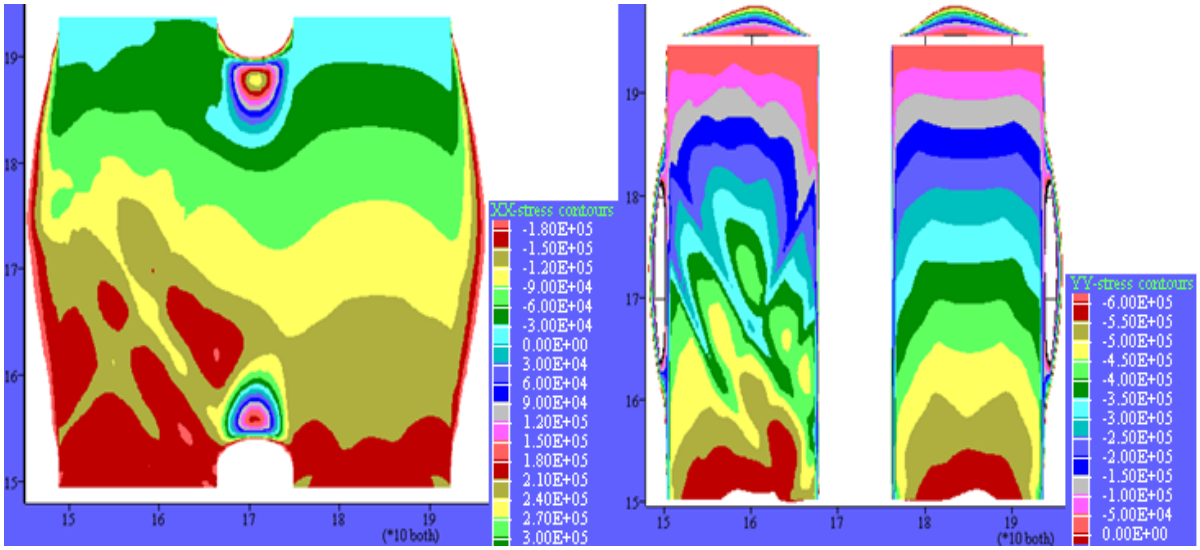

(a) (b)

Figure 3-10: Distribution of the (a) horizontal stresses σ_h and (b) the vertical stresses σ_v in the two adjacent backfilled stopes at the end of filling of the second stope, for stopes having a width B = 18 m (Case 2)

The stresses along the vertical central line and walls of the first stope after excavation of the second one are shown in Figure 3-11 (for both stopes). These results show that both the horizontal and vertical stresses tend to be smaller along the walls than in the central part of the first stope at a given elevation (after excavating and filling of the second stope). It is also observed that an increase of the stope width (from 6 m for Case 1 to 18 m for Case 2) leads to larger horizontal and vertical stresses. The stress increase in the first stope can reach up to 50% at depth along the VCL (σ_v = 580 kPa, σ_h = 200 kPa for stope width of 18 m, and σ_v = 290 kPa, σ_h =

100 kPa for stope width of 6 m) and near the walls (σ_v = 480 kPa, σ_h = 210 kPa for width of 18 m, and σ_v = 258 kPa, σ_h = 110 kPa for width of 6 m), after excavation and filling of the second stope.

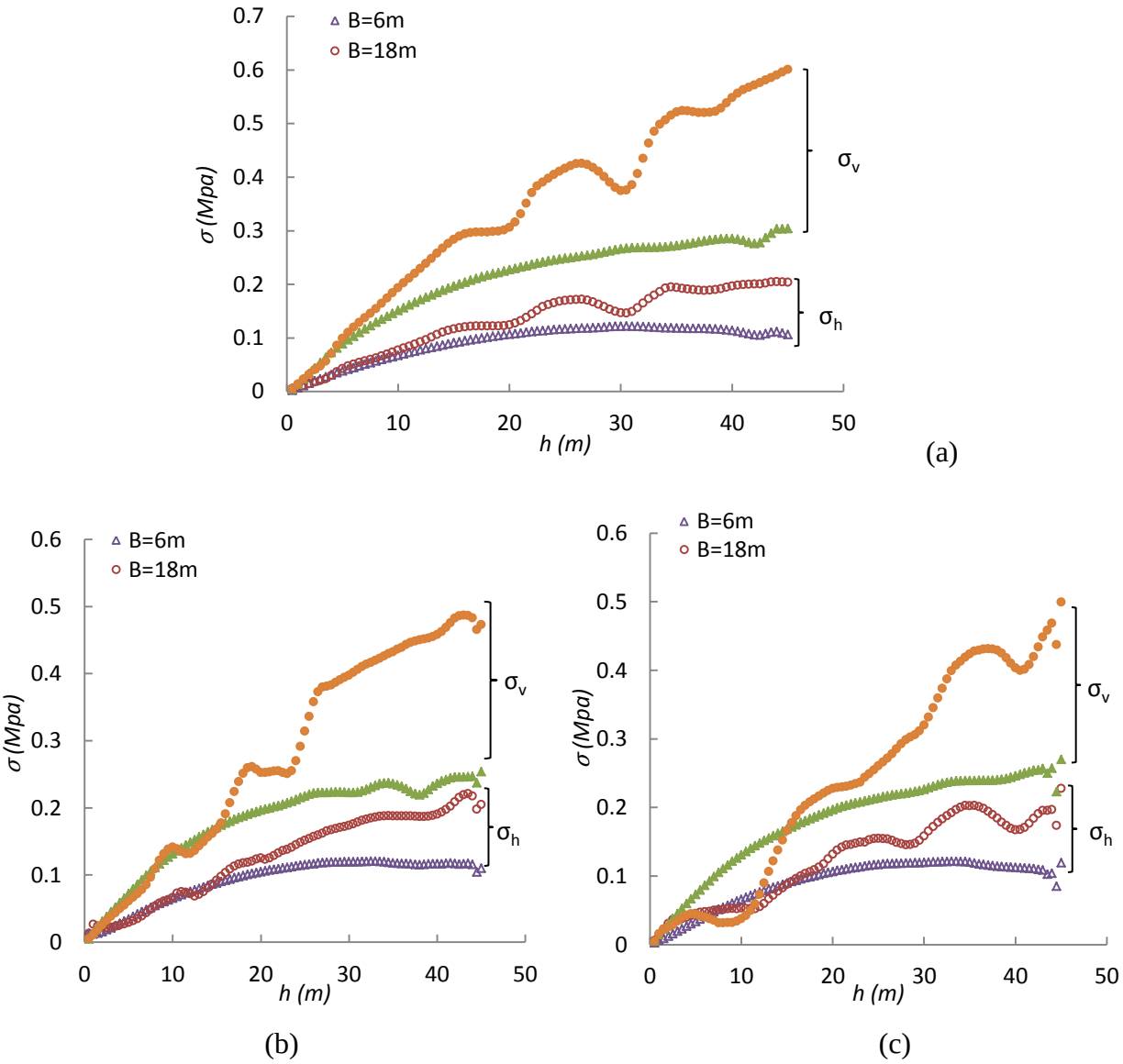

Figure 3-11: Effect of stope width *B* on the vertical and horizontal stresses in the first backfilled stope along the (a) VCL; (b) left wall; (c) right wall after excavation and filling of the second stope (Case 2)

In this Case 2, the vertical stresses in the first stope remain almost unchanged during filling of the second opening; this is due to the larger stresses in the pillar, which are then less sensitive to the additional pressures due to filling of the second stope. These results indicate how the size of the openings influences the way the stress state evolves in the first stope during the

excavation and filling of the second stope. The influence of stope size can also be seen through the horizontal displacements δ_h along the walls of first stope (after excavation and filling of the second stope), which are shown in Figure 3-12.

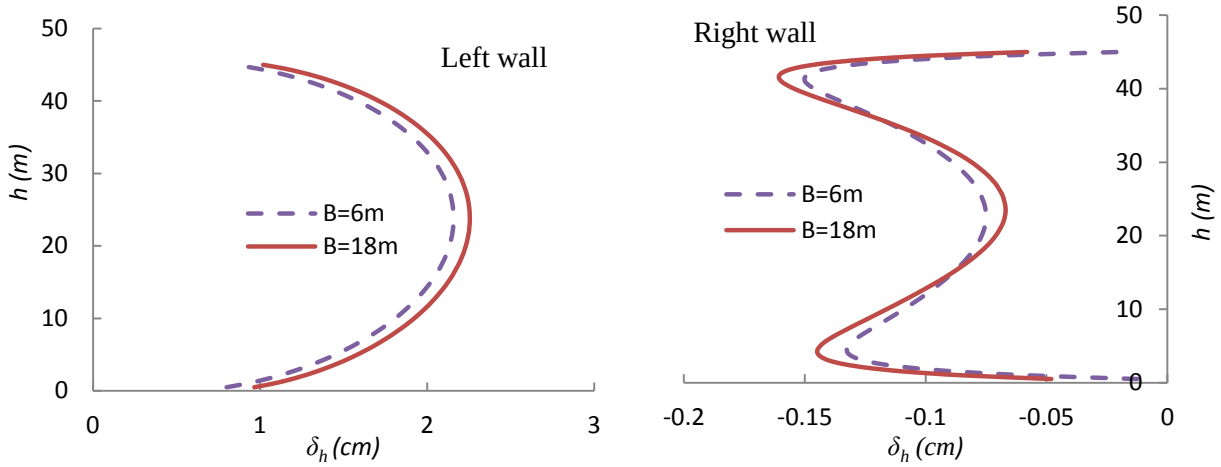

(a)

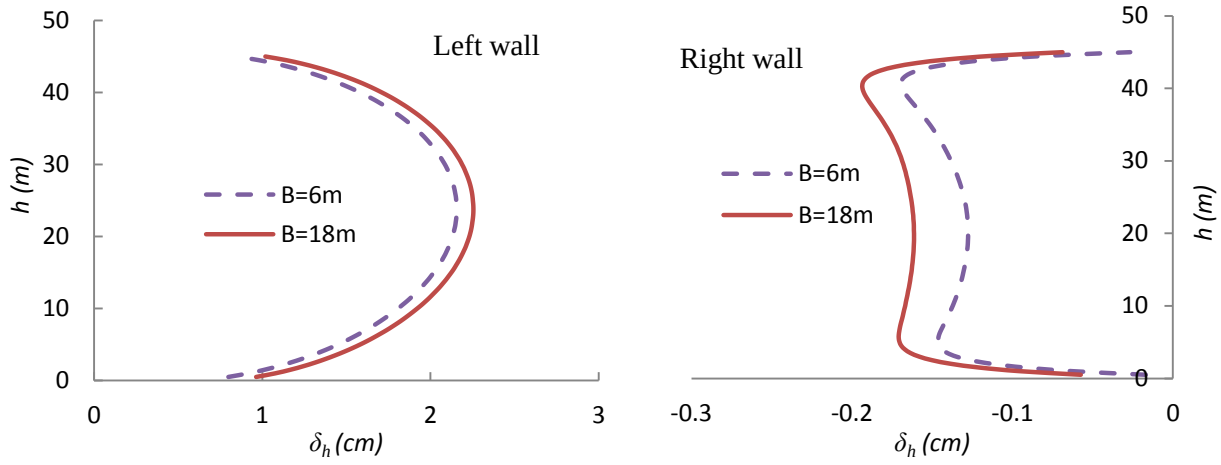

(b)

Figure 3-12: Horizontal displacements δ_h in the first stope along the left wall and right wall after (a) excavation and (b) filling of the second stope (Case 2)

It is seen that the horizontal displacements of the left wall increase with stope width, by up to 0.226 cm at mid-height (i.e. compare Fig. 3-12a with Fig. 3-7a). The δ_h of the right wall also tends to increase with B in the upper and lower parts of the stope, but it decreases somewhat near mid height after excavation of the second stope. The horizontal displacement of the right wall increases with B by up to 0.16 cm near mid-height and by about 0.19 cm at depth of the first stope after filling of the second stope, as seen in Figure 3-12b. The vertical displacements (not

shown here, Appendix B, in Falaknaz, 2014), which remain much smaller than the horizontal ones (except for the top wall), are also sensitive to the stope width, but this does not seem to influence much the stresses in the backfill. As with the stresses (Fig. 3-10), the horizontal strains in the backfill become more irregular in the larger stope (see Appendix B, in Falaknaz, 2014, for more details).

3.3.2 Depth of the openings

Many underground mines are operating at great depth; such is the case for instance with Agnico-Eagle's LaRonde mine, in Abitibi, which has a maximum depth exceeding 2000 m. As this can be a key factor, simulations were also conducted to investigate the influence of the depth of the openings, considering the base of the two stopes located at 400 m and 2000 m below the ground surface (Case 5, Table 3.1); this increases the natural stresses proportionally. Both stopes have a width B= 6 m and the distance between the two stopes D = 8 m. The boundaries are located 240 m from the stope walls. There are 161×353 elements in the mesh, with sizes that vary according to the distance from the walls. The boundary conditions and rock and backfill properties are same as Case 1 (with ϕ' = 35º). Figure 3-13 shows the stresses along the VCL and walls of the first stope located at both depths (2000 m and 400 m) after excavation and filling of the second stope.

It is seen that the horizontal stresses in the first stope are affected by the stope depth, particularly below mid-height where these increase significantly by a factor of up to 2 along the VCL and by up to a factor of 1.6 along the walls of the first stope (Figure 3-13). The vertical stresses also increase with the stopes depth in the lower part of the first backfilled stope. However, in this case, the vertical stresses magnitudes are not sensitive to filling of the second stope (as this added fill pressure is too small to significantly affect the displacements in the pillar and the stress state in the first stope).

The horizontal displacements δ_h along the walls of first stope (after excavation and filling of the second stope) are shown in Figure 3-14. It can be seen that the displacement of the left wall increases with depth by up to 5 times, from 3 cm (depth of 400 m) to 15.8 cm (depth of 2000 m) near mid-height, while the horizontal displacement of the right wall is increased by a factor of up to 10, from 0.13 cm (depth of 400 m) to 1.076 cm (depth of 2000 m) near mid-height of the first

stope. The maximum horizontal strains ε_h (Fig. 3-14c) in the backfill also increase (from -0.5% to about -2.5%) with the stopes depth.

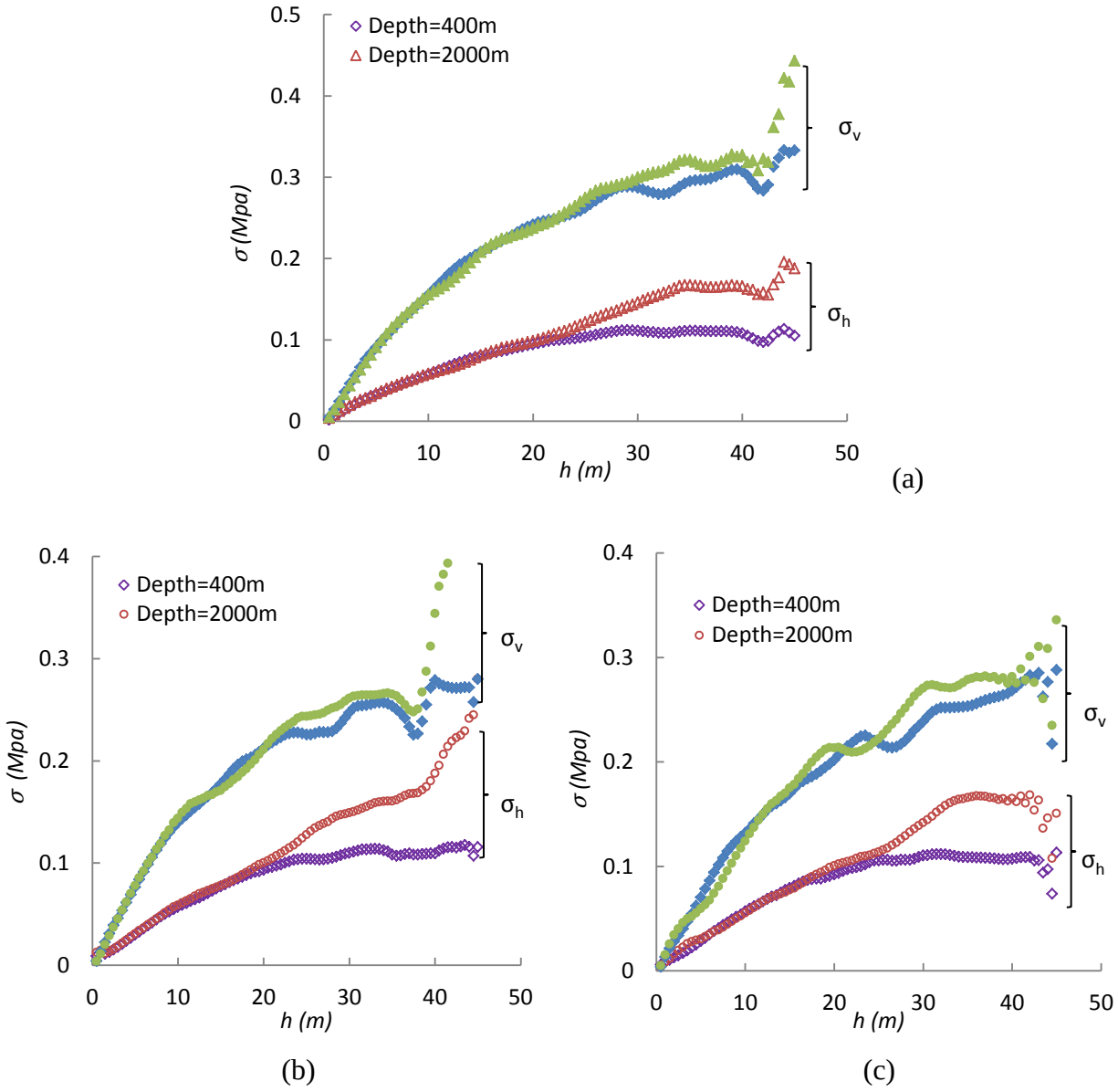

Figure 3-13: Effect of stope depth *z* (base of the opening, distance from the surface) on the vertical and horizontal stresses in the first backfilled stope along the (a) VCL, (b) left wall, and (c) right wall, after excavation and filling of the second stope (Case 5)

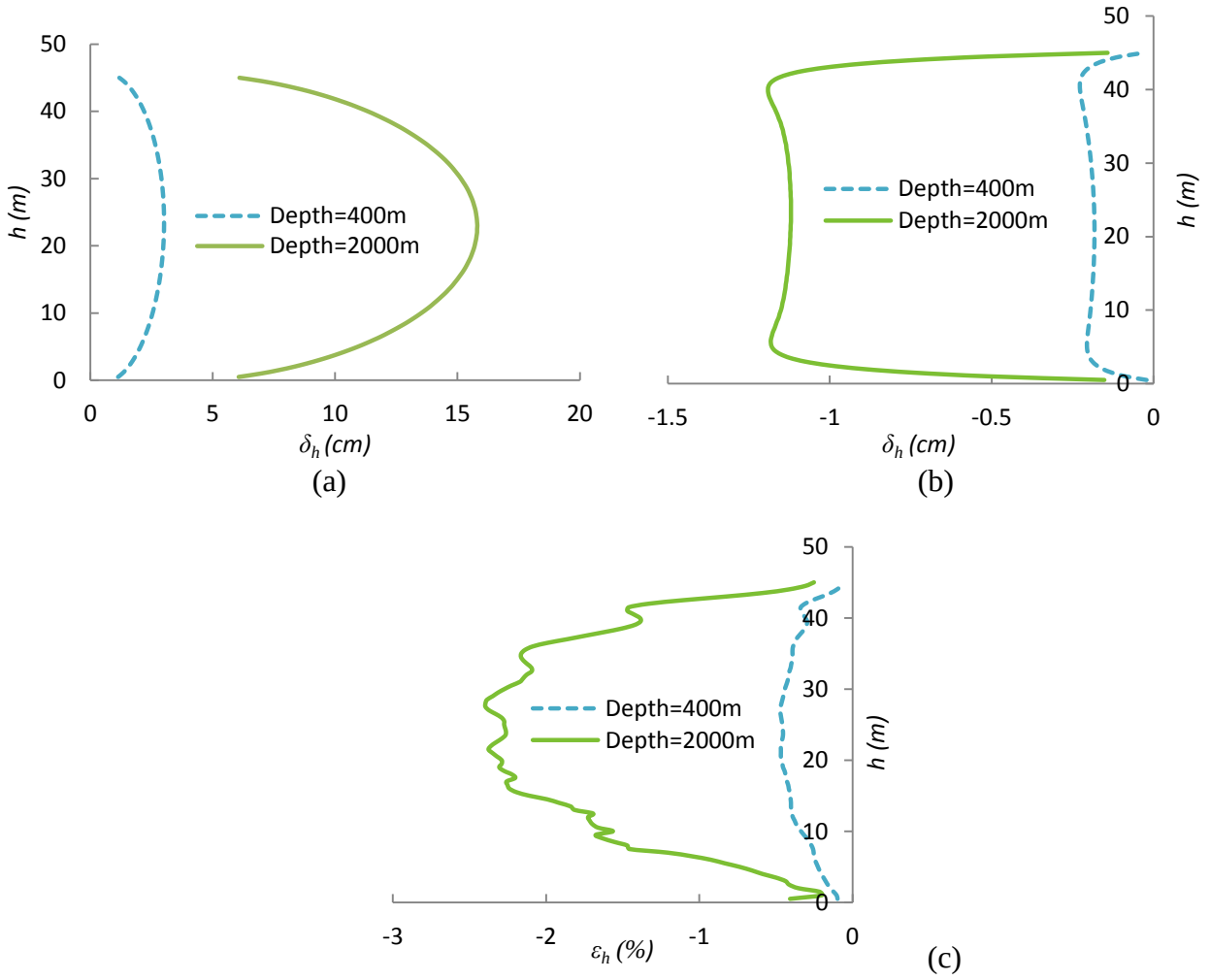

Figure 3-14: Horizontal displacements δ_h in the first backfill stope along the (a) left wall and (b) right wall; (c) horizontal strain ε_h along the VCL; the results are shown after excavation and filling of the second stope (Case 5)

3.3.3 Internal friction angle ϕ'

It is well known that the fill properties can have a major influence on the stress state in a single backfilled stope (Li et al. 2003; Li and Aubertin, 2008, 2009a), so it can be expected that these will also affect the response in the case of two neighboring stopes. This aspect is investigated here through Cases 1a,b, c. (for $\phi' = 25^o$, 30^o, 35^o, respectively; n.b. a value $\phi' = 35°$ is considered realistic for backfill made with tailings from hard rock mines).

Figure 3-15 presents the stresses along the VCL, left, and right wall of the first stope as a function of angle ϕ' (after excavation and filling of the second stope) after excavation (a) and

filling (b) of the seconde stope. It is seen that an increase in the friction angle from 25° to 35º (and of the corresponding Poisson ratio υ, based on Jaky's (1948) relationship tends to decrease the horizontal stresses by up to 30% (i.e. by 0.0853 MPa) in the backfill near the base of the stope (Fig. 3-15a); the vertical stresses appear much less sensitive to this increase (Figure 3-15b).

It can be seen that as the friction angle increases, the horizontal stresses decrease significantly (by up to 30% at the mid-height), while the vertical stresses increase marginally. These observations correspond well to results obtained by the authors (Li et al. 2007, Li and Aubertin, 2009a) for a single backfilled stope. Figure 3-16 shows the horizontal and vertical stresses obtained from the numerical simulations and from the analytical solution (based on Eqs. 3-1 and 3-2, with $K = K_a$) considering different friction angles.

The results indicate that the horizontal and vertical stresses along the vertical central line (Fig. 3-16a) and walls (Fig. 3-16b) of the second stope (after filling) are similar to those obtained for a single stope (Case 0); these stresses are slightly higher than those given by the analytical solution. The horizontal stresses in the first stope after filling of the second opening are larger than in the latter along the VCL and walls (compare with Fig. 3-6a, 3-6b left and Fig. 3-5b left). The vertical stresses along the VCL and walls of the first stope are fairly similar to those obtained using the numerical and analytical solutions for a single stope and for the second stope as presented in Figures 3-6a, 3-6b (right) and Figure 3-5b (left).

3.3.4 Cohesion c' and Dilation Angle ψ'

The cohesion c' of cemented backfill is also expected to influence the stress distribution (Li et al. 2005, Li and Aubertin, 2009a). Simulations results (Case 3) shown in Figure 3-17 indicate that an increase in cohesion c' (from 1 to 300 kPa) tends to reduce the horizontal stresses in the first backfilled stope (by up to 80% at mid-height of the stope). However, this effect is limited to relatively small values of c', as the stresses become almost insensitive to a variation of the backfill cohesion for $c' \geq 100$ kPa (in this case). The stresses obtained for a backfill cohesion $c' = 0$ and 1 kPa are practically the same, showing a typical arching effect (the latter can thus be considered as quasi-cohesionless). In addition, it is seen that both stresses distributions are irregular along the VCL, with a trend that becomes wavy, particularly for the horizontal stresses.

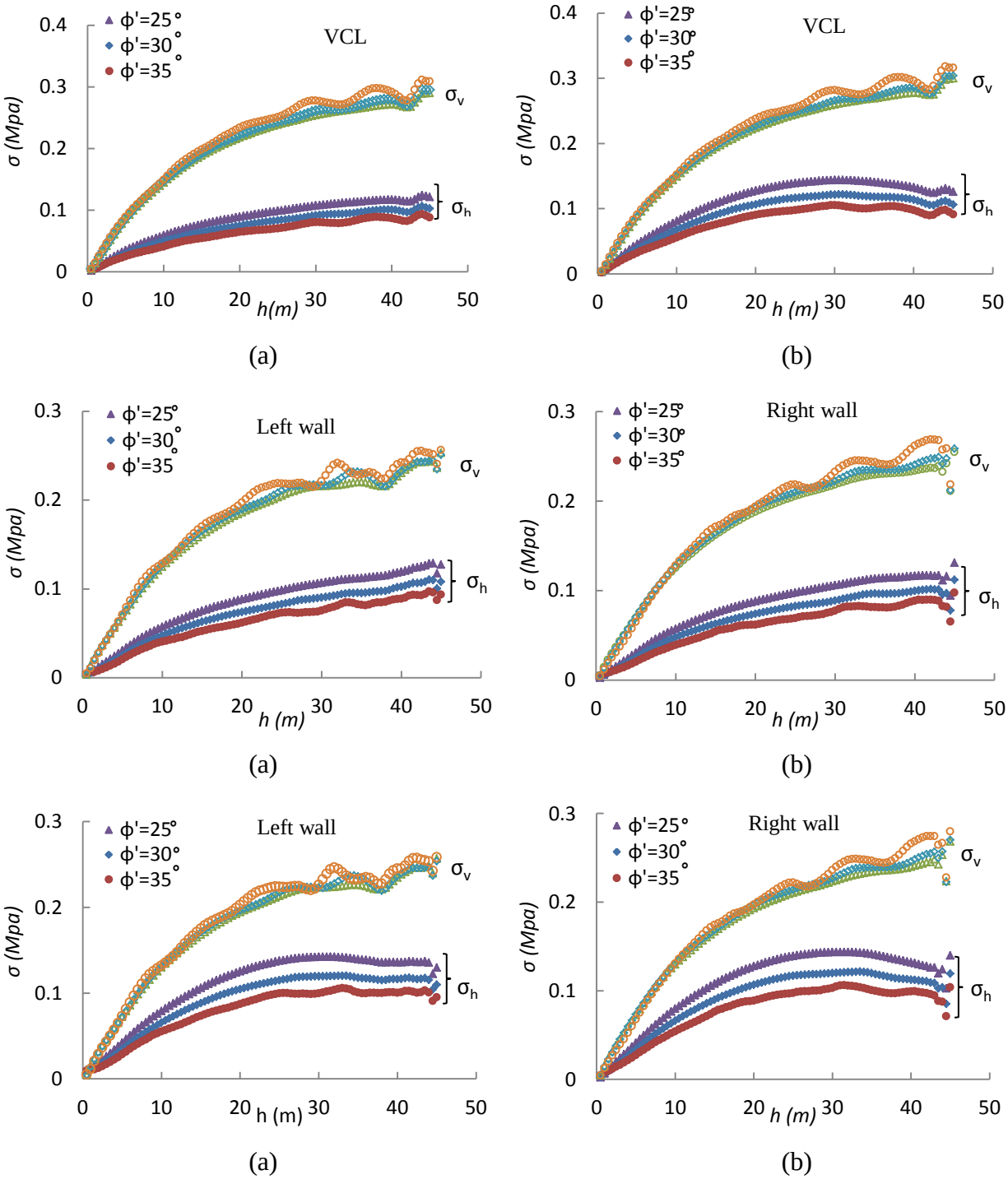

Figure 3-15: Effect of backfill internal friction angle ϕ' on the stress distribution along the VCL and the left and right walls in the first backfilled stope, after (a) excavation and (b) filling of the second stope (Cases 1a,b,c)

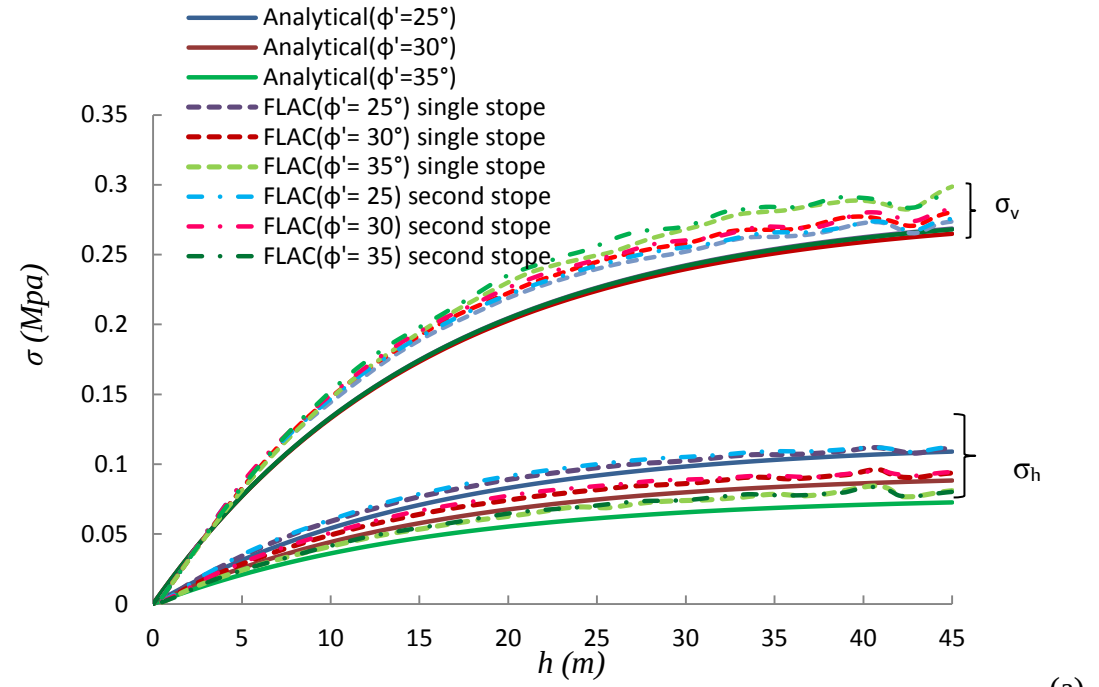

Figure 3-16: Vertical σ_v and horizontal stresses σ_h along the (a) VCL and (b) walls of the second backfilled stope (Case 1a,b,c) and a single backfilled stope (Case 0) obtained using the analytical (Eqs. 3-1 to 3-2) and numerical (using FLAC) solutions for different internal friction angles

The position of the peaks is related to the sequence of excavation (4 steps) and filling (4 steps). Cohesion of the backfill leads to a beam-like behavior for each layer with $c' \geq 20$ kPa (as discussed by Li and Aubertin, 2009a). The stresses along the VCL of the first stope show a local

maximum near the top of each layer and a local minimum at their base when the cohesion $c' > 1$ kPa; this type of behavior is not seen for cohesionless backfill (Figure 3-17).

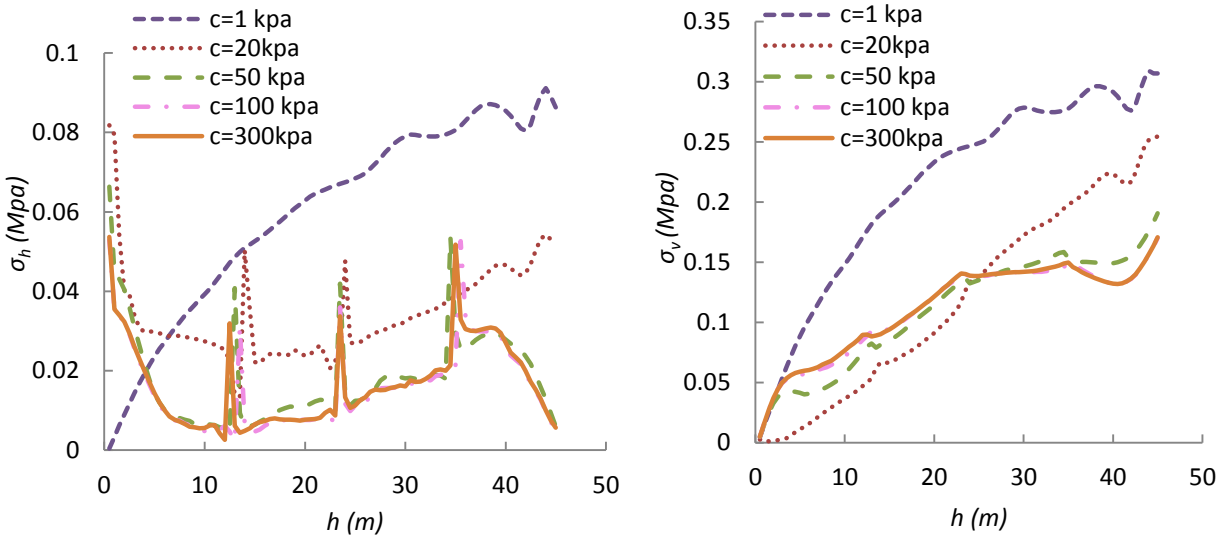

(a)

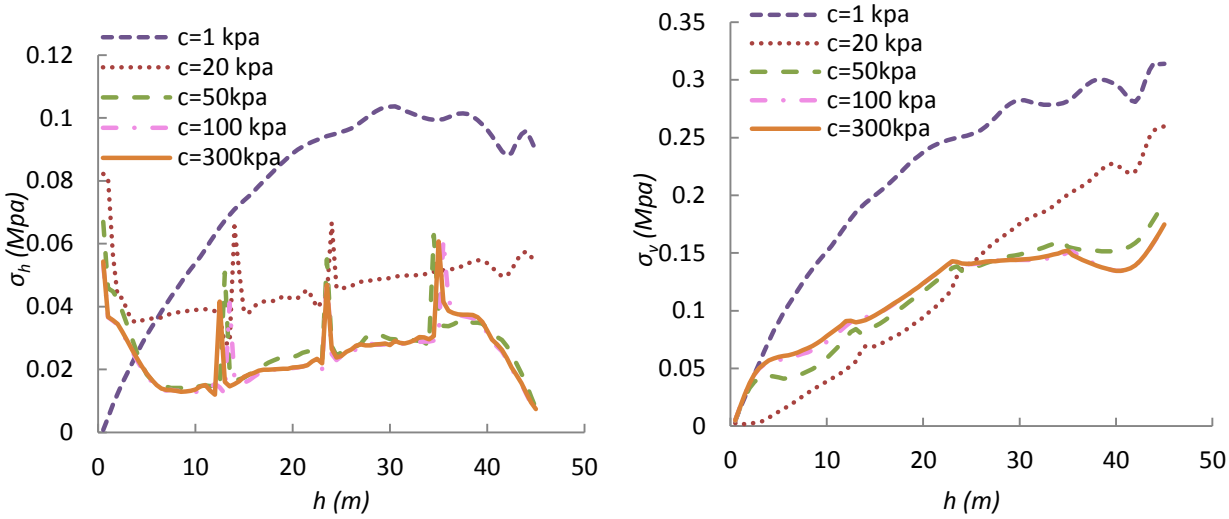

(b)

Figure 3-17: Effect of backfill cohesion c' on the stress distribution along the VCL of the first stope after (a) excavation and (b) filling of the second stope (Case 3)

Figure 3-18 shows the stress state along the walls of the first stope as a function of backfill cohesion. An increase of c' from 1 kPa to 50 kPa decreases the horizontal stresses by about 80% (i.e. down to 15.3 kPa along the left wall and 11.8 kPa along the right wall) at mid-height near the walls. The vertical stresses along the walls also decrease when cohesion increases

to about 20 kPa (by up to 45 % at mid-height); the vertical stresses along the walls become almost insensitive to any further increase of cohesion for $c' \geq 100$ kPa. During filling of the second stope, both stresses along the walls of the first stope remain unchanged.

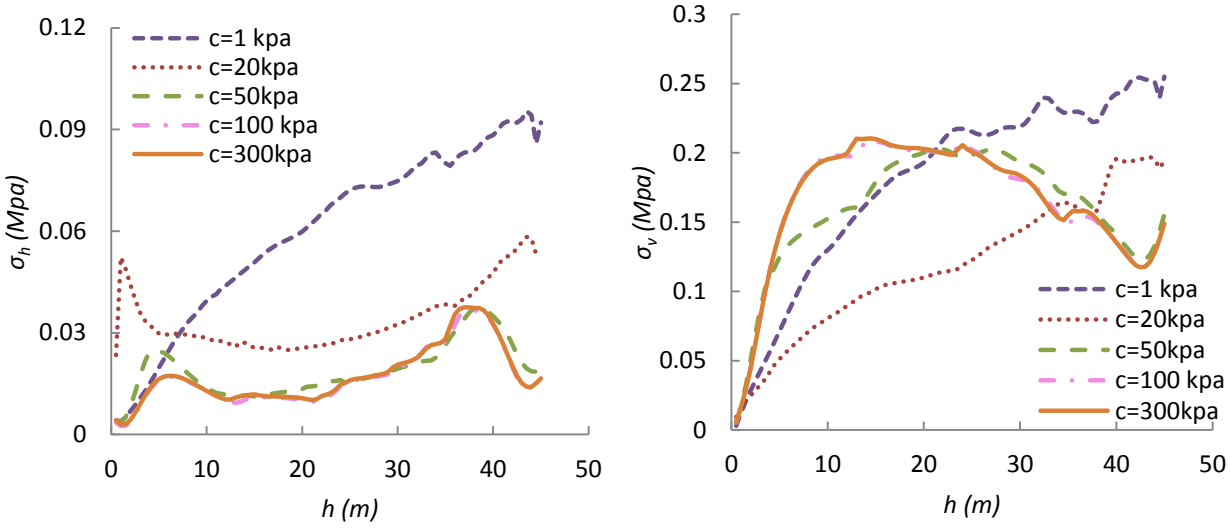

(a)

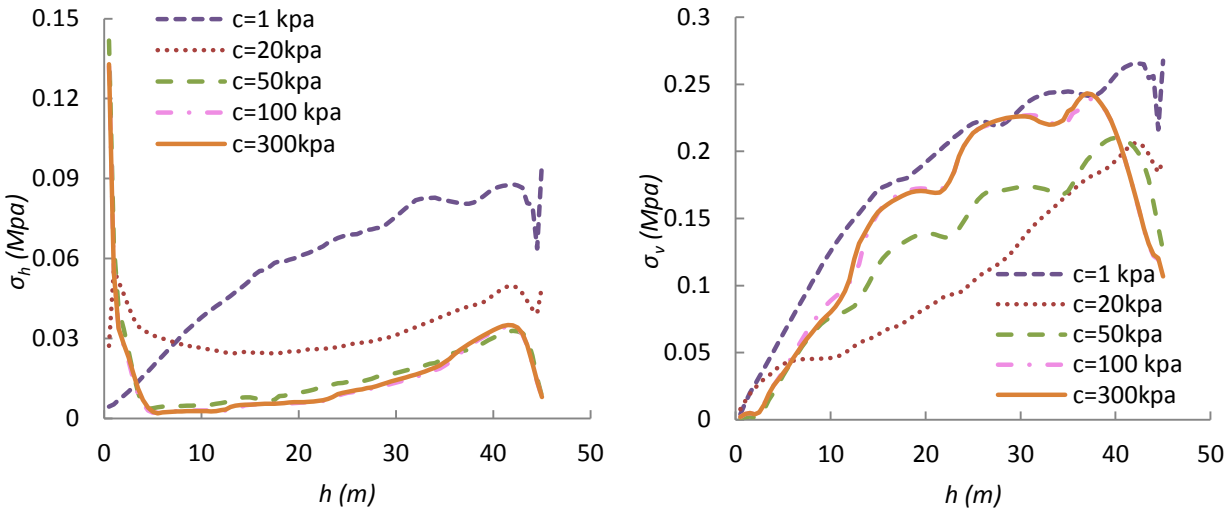

(b)

Figure 3-18: Effect of backfill cohesion c' on the stress distribution along the (a) left wall and (b) right wall of the first stope, after excavation of the second stope (Case 3)

Simulations results shown in Figures 3-17, 3-19 and 3-20 also indicate that for a given value of the backfill cohesion and internal friction angle, an increase of the dilation angle ψ' (from 0° in Case 3, Fig. 3-17b, to 17.5° and 35° in Case 4, Fig. 3-19 and 3-20) tends to reduce (by

up to about 15%), the stresses along the VCL and walls in the first backfilled stope (after excavation and filling of the second stope).

These results also indicate that the backfill cohesion has a more pronounced effect on the horizontal stresses than the dilation angle. Li et al. (2007) and Li and Aubertin (2009a) have obtained similar trends for isolated backfilled stopes with vertical and inclined walls.

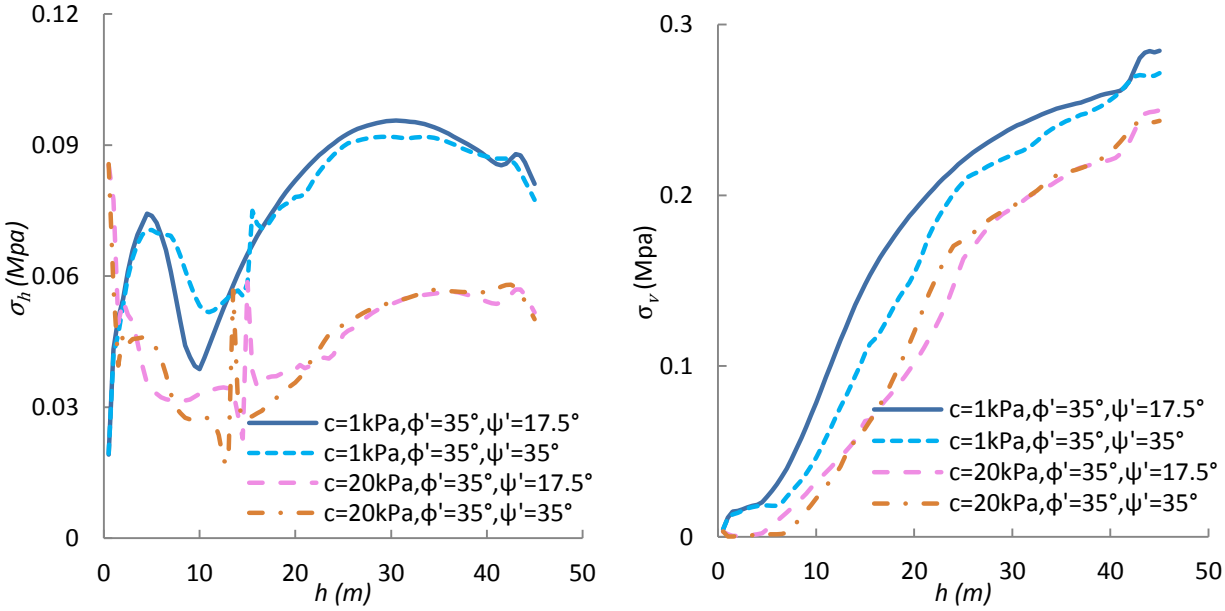

Figure 3-19: Effect of backfill cohesion c', internal friction angle ϕ' and dilation angle ψ' on the stress distribution along the VCL of the first stope after excavation and filling of the second stope (Case 4)

3.4 Discussion

3.4.1 Stress distribution in isolated and adjacent stopes

In this paper, simulations results obtained with FLAC, in 2D, are used to assess the effect of creating a second opening on the stress state in an existing backfilled stope. An important outcome of these calculations is that the stress distribution in the first backfilled stope can be more complex, and much less uniform, than the one in a single stope (e.g. Figures 3-1, 3-4 and 3-10), due to a more elaborate loading path associated with the excavation and filling of the second stope (Chapter 4, in Falaknaz, 2014).

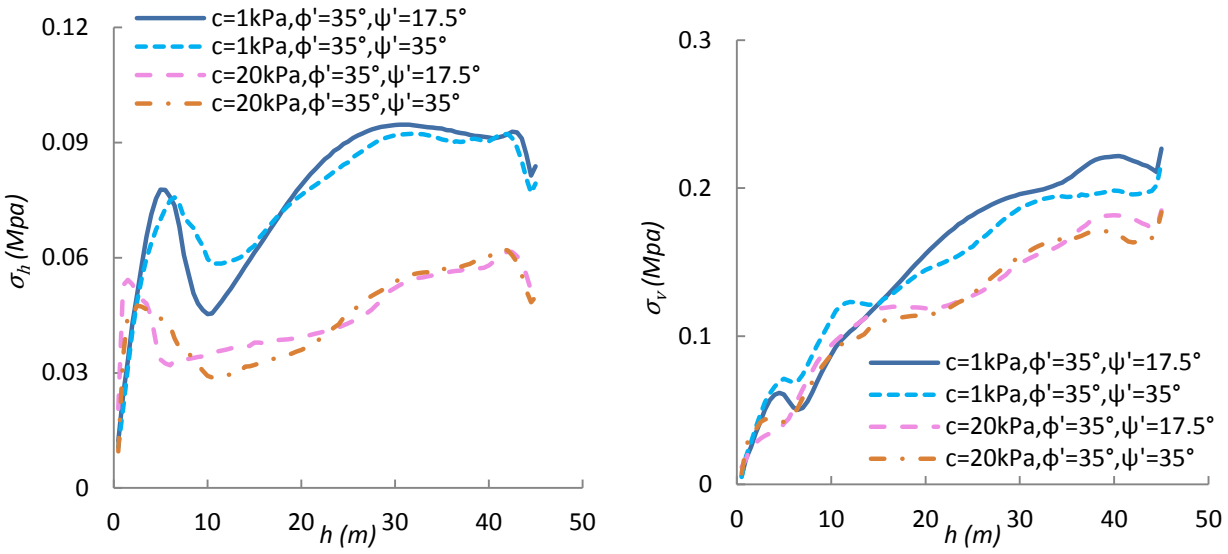

(a)

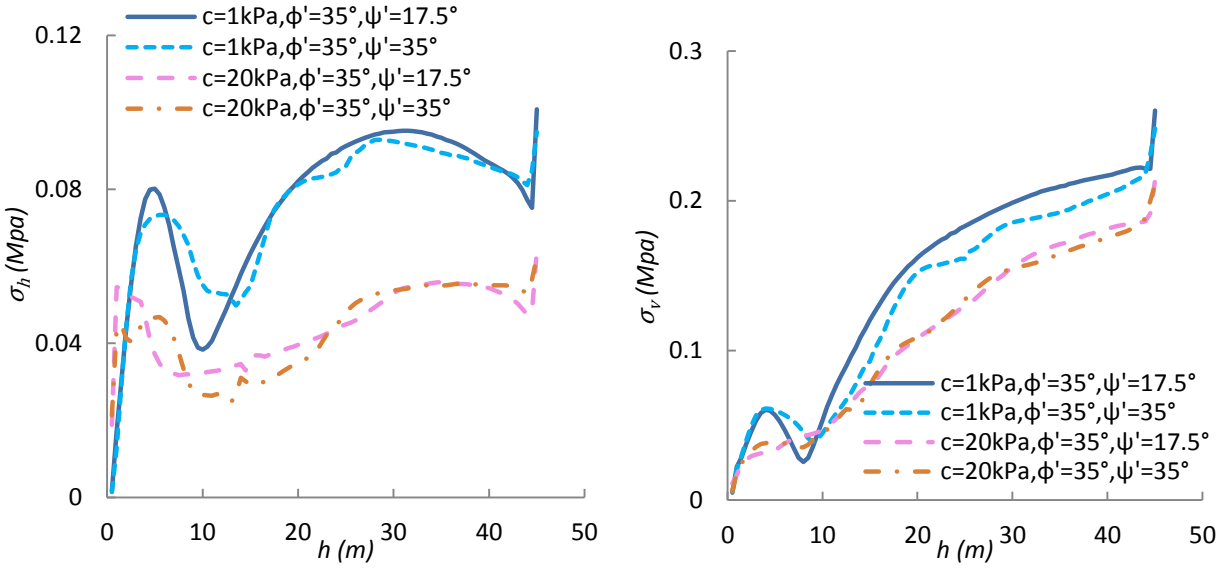

(b)

Figure 3-20: Effect of backfill cohesion c', internal friction angle ϕ' and dilation angle ψ' on the stress distribution along the (a) left wall and (b) right wall of the first stope after excavation and filling of the second stope (Case 4)

It is also observed that the horizontal stresses in the backfill along the VCL and walls of the first stope tend to increase (by up to 40% near mid-height) during filling of the second stope. Their magnitude then becomes significantly higher than those obtained for a single stope (Figures 3-5 and 3-6, left hand side). However, the vertical stresses along the VCL and walls of the first stope are fairly similar to those obtained for a single stope (Figures 3-5 and 3-6, right hand side).

The results also indicate that the final stress distributions in the second stope is fairly similar to the one obtained for an isolated stope (Figures 3-4 and 3-6). Moreover, these results suggest that the analytical solution proposed Li and Aubertin (2008) for a single stope can be used to estimate the stresses along the walls and the VCL of the second backfilled stope after filling the latter, as shown in Figure 3-16. But this solution may not be appropriate to evaluate the horizontal stresses in a backfilled stope when a new opening is created nearby.

3.4.2 Limitations and ongoing work

The results shown here apply to plane strain conditions when the effect of the third dimension can be neglected, as is commonly the case for many mine sites (and for a majority of published investigations). As this situation may not be representative of some in-situ backfilled stopes, additional work is underway to simulate the response of two stopes in 3D, considering the same influence factors investigated here in 2D (Chapter 7 in Falaknaz, 2014); these results will be included in upcoming publications.

Also, the behavior of the rock mass was considered to be linear-elastic, but this may not reflect its actual response (especially under large natural stresses or for weaker rock masses). Therefore, additional simulations are being conducted to assess the influence of a non-linear behaviour of the rock mass on the stress distribution of neighboring backfilled stopes.

Work is also underway to assess the effect of a backfill exposure that can take place after removing one of the stope walls (i.e. when a neighboring stope is created immediately next to the first one); this aspect of the investigation specifically focusses on the stability of the backfill open face (Li and Aubertin 2012, 2014; Chapter 6 in Falaknaz, 2014).

The ongoing numerical investigation further includes other factors such as the backfill stiffness, stope height, size of the pillar between the two openings, earth pressure coefficient K_r ($= \sigma_h / \sigma_v$) in the rock mass, and number of layers used to excavate and fill the two stopes; the corresponding results are included in Falaknaz (2014, Chapter 4).

3.5 Conclusion

This paper presents the main results of a numerical investigation conducted with FLAC on the behavior of two neighboring backfilled stopes to evaluate the effect of backfill properties,

stope geometry, and excavation and filling sequence on stress distribution within the backfill. The results presented here indicate that the second backfilled stope tends to behave in a manner similar to a single stope, where arching effects often dominate the stress distribution. The simulated horizontal and vertical stresses distributions in the second stope are in a good agreement with those calculated with an analytical solution previously developed by Li and Aubertin (2008) for a single stope. However, the stress distributions can be quite different in the two stopes, because those in the first backfilled opening may be significantly influenced by the excavation and filling of the neighboring stope.

The results specifically show how the stress distribution in the first backfilled opening varies during the creation of the second one and how it is influenced by the fill material properties. For instance, the simulations indicate that an increase of the fill internal friction angle ϕ' (from 25º to 35º) leads to a decrease of the horizontal stresses (by up to 30% near the stope base in this case). The stresses also diminish with an increase of the backfill cohesion, particularly in the range 1 kPa < c' < 100 kPa; within this range, the horizontal stress in the first backfilled stope can be reduced by up to 80%, while the vertical stress decreases by up to 60% (for the conditions considered here). There is also an effect of the backfill dilation angle ψ', but it is much less significant.

The simulations also illustrate how the stress state in the first backfilled stope may change as a function of the width and depth of the openings. The results demonstrate that an increase of the width (from 6 m to 18 m) tends to decrease arching effect and to increase the stress magnitude in the stopes (by up to 50% at base of the first stope). A larger depth increases the stresses in the pillar, the displacements of the walls, and the corresponding stresses within the first backfilled stope, which can be raised by factor of up to 2 along the VCL for a depth that goes from 400 m to 2000 m. The results shown here help our understanding of how the creation of a neighboring stope can affect the stress state in an existing backfilled opening.

Acknowledgements

The authors acknowledge the financial support from NSERC and from the partners of the Industrial NSERC Polytechnique-UQAT Chair on Environment and Mine Wastes Management

(2006-2012) and of the Research Institute on Mines and the Environment (RIME UQAT-Polytechnique; www.irme.ca).

References

Arjang, B. (2004). Database on Canadian in situ ground stresses. CANMET Division Report MMSL, 01-029 (TR).

Arjang, B. (1996). In situ ground stresses in the Abitibi Mining District. CIM Bulletin, **89**(996): 65-71.

Aubertin, M., Li, L., Arnold, S., Belem, T., Bussiere, B., Benzaazoua, M., and Simon, R. (2003). Interaction between backfill and rock mass in narrow Stopes. Proc., Soil and Rock America 2003, P.J. Culligan, H. H. Einstein, and A. J. Whittle, eds., Verlag Glückauf Essen VGE, Essen, Germany, 1, 1157–1164.

Belem, T., Benzaazoua, M., and Bussière, B. (2000). Mechanical behaviour of cemented paste backfill. Proc., 53th Can. Geotech. Conf., CGS, Montreal, 1, 373-380.

Belem, T., Harvey, A., Simon, R., and Aubertin, M. (2004). Measurement and prediction of internal stresses in an underground opening during its filling with cemented fill. Proc., of the 5th Int. Symp. on Ground Support, Australia Center for Geomechanics, Perth, Australia, 619–630.

Benzaazoua, M., Fall, M., and Belem, T. (2004). A contribution to understanding the hardening process of cemented pastefill. Miner. Eng., **17(**2): 141-152.

Benzaazoua, M., Bussiere, B., Dermers, I., Aubertin, M., Fried, E., and Blier, A., (2008). Integrated mine tailings management by combining environmental desulphurization and cemented paste backfill: Application to mine Doyon. Miner. Eng., **21**(4): 330-340.

Blight, G.E. (1986). Pressure exerted by materials stored in silos. Part I: Coarse materials. Géotechnique, **36**(1): 33-46.

Brady, B.H.G., and Brown, E.T. (1993). Rock Mechanics for Underground Mining. (2nd edn). Chapman & Hall, London, U.K.

Cowin, S.C. (1977). The theory of static loads in bins. J. Applied Mech., **44**(3): 409-412.

El Mkadmi, N., E. M., Aubertin, M., and Li, L. (2011a). The effect of transient drainage on the tress state in backfilled mine stopes. Proc., 2011 Pan-Am CGS Geotech. Conf., University of Toronto, #1139, 7p.

EL Mkadmi, N., Aubertin, M., and Li, L. (2011b). Numerical analysis of the early response of paste backfill in a vertical stope. Mines without Borders. CIM, Montreal, 68-78.

El Mkadmi, N., Aubertin, M., and Li, L. (2014). Effect of drainage and sequential filling on the behavior of backfill in mine stopes. Can. Geotech. J., **51**(1): 1-15.

Fahey, M., Helinski, M., and Fourie, A. (2009). Some aspects of the mechanics of arching in backfilled stopes. Can. Geotech. J., **46**(11): 1322-1336.

Handy, R., and Spangler, M. (2007). Geotechnical engineering: Soil and Foundation principles and practice, 5th Ed. McGraw Hill, New York.

Hassani, F., and Archibald, J. (1998). Mine backfill. Canadian Institute of Mine, Metallurgy and Petroleum, Montreal, Canada.

Herget, G. (1988). Stresses in rock. A.A.Balkema, Rotterdam, The Netherland.

Hoek, E. (2007). Practical rock engineering. Hoek's Corner (Rock Science). <https://www.rocscience.com/education/hoeks_corner> (Mar. 15, 2014).

Hustrulid, W., Qianyuan, Y., and Krauland, N. (1989). Modeling of cut and- fill mining systems, Näsliden revisited. Innovation in mining backfill technology, F. P. Hassani, M. J. Scoble, and T. R. Yu, eds, A.A.Balkema, Rotterdam, The Netherlands, 147–164.

Itasca. (2002). FLAC version 5.0. Users Manuals. ITASCA Consulting Group, Minneapolis, Minnesota, USA.

Jaky, J. (1948). Pressure in silos. Proceedings of the 2nd International Conference on Soil Mechanics and Foundation Engineering, A.A.Balkema, Rotterdam, The Netherland, 1, 103-107.

Knutsson, S., (1981). Stresses in the hydraulic backfill from analytical calculations and in-situ measurements. Proc., Conf. on Application of Rock Mech. to Cut and Fill Mining., Institution of Mining and Metallurgy, London, 261–268.

Li, L., Aubertin, M., Simon, R., Bussiere, B., and Belem, T. (2003). Modeling arching effects in narrow backfilled stopes with FLAC. Proc., the 3th Int. FLAC symp., R. Brummer, P. Andrieux, C. Detournay, and R. Hart, eds, A.A.Balkema, Rotterdam, Netherlands, 211-219.

Li, L., Aubertin, M., and Belem, T. (2005). Formulation of a Three Dimensional Analytical Solution to Evaluate Stress in Backfilled Vertical Narrow Openings. Can. Geotech. J., **42**(6): 1705-1717.

Li, L., Aubertin, M., Shirazi, A., Belem, T., and Simon, R. (2007). Stress distribution in inclined backfilled stopes. MINEFILL 2007, Canadian Institute of Mining, Metallurgy and Petroleum, Montreal, Canada.

Li, L., and Aubertin, M. (2008). An improved analytical solution to estimate the stress state in subvertical backfilled Stopes. Can. Geotech. J., **45**(10): 1487-1496.

Li, L., and Aubertin, M. (2009a). Numerical investigation of the stress state in inclined backfilled stopes. Int. J. Geomech., **9**(2): 52-62.

Li, L., and Aubertin, M. (2009b). A three-dimensional analysis of the total and effective stresses in submerged backfilled Stopes. Geotech. Geol. Eng., **27**(4): 559-569.

Li, L., and Aubertin, M. (2009c). Influence of water pressure on the stress state in stopes with cohesionless backfill. Geotech. Geol. Eng., **27**(1): 1-11.

Li, L., and Aubertin, M. (2012). A modified solution to assess the required strength of backfill in mine stopes. Can. Geotech. J., **49**(8): 994-1002.

Li, L., and Aubertin, M. (2014). An improved method to assess the required strength of cemented backfill in underground stopes with an open face. Int. J. of Mining Science and Technology, 4, in press.

Marston, A. (1930). The theory of external loads on closed conduits in the light of latest experiments. Bulletin 96, Iowa Engineering Experiment Station, Ames, Iowa.

Pirapakaran, K., and Sivakugan, N. (2007). Arching within hydraulic fill stopes. Geotech. Geol. Eng., **25**(1): 25-35.

Pirapakaran, K. (2008). Load-deformation characteristics of minefills with particular reference to arching and stress developments. PhD Thesis, James Cook University, Australia.

Potvin Y, Thomas E, and Fourie A. (2005). Handbook on mine fill. Australian Centre for Geomechanics, The University of Western Australia, Nedlands, Australia.

Rankine, R.M., and Sivakugan, N., 2007. Geotechnical properties of cemented paste backfill from Cannington Mine, Australia. Geotech. Geol. Eng., **25**(4): 383-393.

Ting, C.H., S.K. Shukla, and N. Sivakugan. (2011). Arching in soils applied to inclined mine stopes. Int. J. Geomech., **11**(1): 29-35.

Thompson, B.D., Bawden, W.F., and Grabinsky, M.W. (2011). In Situ monitoring of cemented paste backfill pressure to increase backfilling efficiency. CIM J., **2**(4): 1-10.

Thompson, B., Bawden, W., and Grabinsky, M. (2012). In situ measurements of cemented paste backfill at the Cayeli Mine. Can. Geotech. J., **49**(7): 755–772.

Veenstra, R. (2013). A design procedure for determining the in situ stresses of early age cemented paste backfill. PhD Thesis, University of Toronto, Canada.

Villaescusa, E. (2003). Global extraction sequence in sublevel stoping. Twelfth Int. Symp. on Mine Planning and Equipment Selection, Western Australian School of Mines, WA, Australia, (1): 9-17.

CHAPTER 4 ARTICLE 2: A NUMERCIAL INVESTIGATION OF THE GEOMECHANICAL RESPONSE OF ADJACENT BACKFILLED STOPES

Nooshin Falaknaz, Michel Aubertin, and Li Li

This article was submitted to Canadian geotechnical journal, Submitted in Feb 2014, under revision following comments from reviewers.

Abstract: Backfilling of mine stopes helps provide a safe work place underground. The interaction between the backfill and surrounding rock mass has to be evaluated to ensure the secure application of backfill. This critical issue has led to much work on the stress state in single (isolated) backfilled stopes. However, the stress distribution in multiple openings that interact with each other has not yet been investigated as thoroughly. In this paper, the authors are using numerical simulations to evaluate the response of two adjacent backfilled stopes created in sequence. The simulations results, presented in terms of stresses, displacements and strains, illustrate the influence of different parameters including backfill strength, pillar width, stope depth, rock mass stiffness, natural stress state, and excavation and filling sequence. Complementary aspects are also considered. A discussion follows on some of the characteristics and limitations of this investigation.

Keywords: Underground openings; Mine backfill; Two adjacent stopes; Stress analyses; displacements; Numerical modeling.

Résumé: Le remblayage des chantiers miniers aide à fournir un lieu de travail souterrain sécuritaire. L'interaction entre le remblai et le massif rocheux doit être évaluée pour assurer l'application sécuritaire du remblai. Cette question cruciale a conduit à de nombreux travaux sur l'état des contraintes dans les chantiers remblayés uniques isolés. Toutefois, la distribution des contraintes dans des ouvertures multiples qui interagissent les unes avec les autres n'a pas encore été étudiée de façon spécifique. Dans cet article, les auteurs utilisent des simulations numériques afin d'évaluer la réponse des deux chantiers remblayés adjacents créés en séquence. Les résultats des simulations, présentés en termes de contraintes, de déplacements et de déformations, montrent l'influence des différents paramètres, incluant la résistance de remblai, la largeur du pilier, la profondeur du chantier, la rigidité du massif rocheux, l'état des contraintes naturelles et la séquence d'excavation et de remplissage. Des aspects complémentaires sont aussi abordés. La discussion porte sur quelques-unes des caractéristiques et des limitations de cette investigation.

Mots clés: Excavations souterraines; Remblais miniers; Excavations multiples; Analyse des contraintes; Déplacements; Modélisation numérique.

4.1 Introduction

Backfill can play an important role for the success of underground mining operations by improving the wall stability around stopes and by reducing ore dilution. The environmental and economic benefits of returning part of the tailings or waste rock underground are also part of the rationale behind backfilling (Hassani and Archibald, 1998; Benzaazoua et al. 2008).

A good understanding of the mechanical behavior of the backfill and its interaction with the surrounding rock mass is a key step to assess the geomechanical response of backfilled stopes and related ground stability issues. Different types of backfill may have quite different properties, depending on their constituents, including the grain size of the solids and the type and proportion of binder (e.g., Belem et al. 2000; Benzaazoua et al. 2004; Potvin et al. 2005). Nonetheless, even the strongest backfills are soft (deformable) in comparison with the surrounding rock mass. This difference in stiffness and strength between these two materials tends to produce a load transfer along the interfaces due to the downward settlement of the backfill, which may create a significant arching effect in relatively narrow openings (e.g. Li et al. 2003). This phenomenon, well known in geotechnique (Handy and Spangler, 2007) has been confirmed by various measurements in the laboratory (e.g. Li et al. 2005; Pirapirakan, 2008) and in underground backfilled stopes (Knutsson, 1981; Hustrulid et al. 1989; Belem et al. 2004; Thompson et al. 2011, 2012).

Analytical solutions, often based on the Marston (1930) approach proposed for backfilled trenches, have been developed for evaluating the stress distribution in single (isolated) backfilled stopes (e.g. Aubertin et al. 2003; Li et al. 2005; Caceres, 2005; Pirapakaran and Sivakugan, 2007; Li and Aubertin, 2008; Sing et al. 2011; Ting et al. 2011, 2014). Numerical modelling is another commonly used approach to evaluate the stress state in isolated backfilled stopes, and to investigate the influence of different parameters such as backfill properties, fill-wall interface characteristics, filling rate and pore water pressures (e.g. Li et al. 2003, 2007, 2010a; Hassani et al. 2008; Li and Aubertin, 2008, 2009a, 2009b; Helinski et al. 2007, 2010; Pirapakaran and Sivakugan 2007; Fahey et al. 2009, El Mkadmi et al. 2011a, 2011b, 2014; Sivakugan et al. 2013;Veenstra 2013; Veenstra et al. 2013; Emad et al. 2014).

To date however, little work has been done on the response of multiple stopes excavated in sequence. The influence of creating and filling neighboring stopes on the backfill response is

investigated in this paper using the code FLAC (Itasca, 2002). In the following, new simulations results are presented for the case of two adjacent stopes considering different backfill and rock mass properties, pillar width, depth and natural stress state, and excavation and filling sequence. The results illustrate how these parameters can influence the stress distribution, wall displacements, and strain in backfilled openings. These show that there can be significant differences between the response of single (isolated) and neighboring stopes.

4.2 Modeling approach and simulated cases

Previous works conducted by the authors and various other groups have shown that the code FLAC (Itasca, 2002) is a convenient tool to analyze the stress state in backfilled stopes. This two-dimensional finite difference program uses an explicit Lagrangian calculation scheme and a mixed-discretization zoning technique to solve numerically the equations defining the stresses and displacements in and around the underground openings.

The mesh size and boundary locations of each model constructed with FLAC here have been adapted to obtain representative results. For this purpose, the models were built after testing various mesh sizes to determine a stable numerical solution. Optimization has led to the use of a coarser mesh for the elastic rock region and a finer mesh inside the backfilled stopes. The number of elements depends on the geometry and model size. Also, the external boundaries have been placed far enough to avoid any influence on the results obtained inside and near the stopes. This assessment was performed for each simulation, considering stope distance and depth, rock mass properties and other factors summarized in Table 4-1; typical model characteristics are given below (with more details provided in Appendix A in Falaknaz, 2014). The cases identified in Table 4-1 include the Reference case for a single opening, and 8 cases (0 to 7) for models with two stopes, with one or two parameters varied in the different simulations.

4.3 Assumption for the backfill properties

The degree of arching in a backfilled stope has been shown to be influenced by the backfill properties, including its internal friction angle of the backfill, ϕ' and Poisson's ration ν (e.g. Li et al. 2003, 2007; Li and Aubertin, 2009a). The value of these parameters is also known

to influence the ratio between the horizontal σ'_h and vertical σ'_v stresses, given by the earth reaction coefficient, K:

$$K = \frac{\sigma'_h}{\sigma'_v} \quad (4\text{-}1)$$

At rest, when there is no horizontal strain, the value of K is related to the Poisson's ratio, ν, according to (Aysen, 2002; Blight, 1986):

$$K_o = \frac{\nu}{1-\nu} \quad (4\text{-}2)$$

The earth reaction coefficient at rest can also be estimated from the relationship proposed by Jaky (1948) for normally consolidated granular soils:

$$K_o = 1 - \sin \emptyset' \quad (4\text{-}3)$$

Equations (4.2) and (4.3) are sometimes considered equivalent (e.g. McCarthy, 2007). These lead to a relationship between ν and ϕ', which can be expressed as follows:

$$\nu = \frac{1-sin\phi'}{2-sin\phi'} \quad (4\text{-}4)$$

The values of the shear modulus G (= $\frac{E}{2(1+\nu)}$) and bulk modulus K_b (= $\frac{E}{3(1-2\nu)}$) of the material then also depend on the value of ϕ'. In most investigations on the response of backfills in underground openings, the values of ϕ' and ν have been treated as independent variables. In the simulations conducted here, these values are related to each other through Equation 4. This aspect is addressed again near the end of the paper.

4.4 Analyses of the stress state in a single stope

Figure 4-1 shows the characteristics of the Reference case model (Table 4.1) used to simulate the response of a single stope, with the imposed boundary conditions, geometry, and material properties; simulations results are also shown in this figure. The rock mass is considered homogeneous, isotropic and linearly elastic, with the following parameters: E_r = 30 GPa (Young's modulus), ν_r = 0.3 (Poisson's ratio), γ_r = 27 kN/m^3 (unit weight). The fill behaves as an elasto-plastic material, with the Mohr-Coulomb criterion. Its mechanical properties are defined

by E_b, ν_b, γ_b, ϕ', and by its cohesion c' and dilatancy angle ψ' (with $\psi' < \phi'$ for the non-associated flow rule adopted here). The reference stope width is 6 m, and it is filled to a height of 45 m, with 0.5 m of void space left at the top. The natural in-situ vertical stress σ_v in the rock mass is obtained by considering the overburden weight for a depth z of 300 m. The natural in-situ horizontal stress σ_h in the rock mass is twice the vertical stress σ_v, based on a fairly typical situation encountered in the Canadian Shield (i.e. $K_r = \sigma_h / \sigma_v = 2$). Vertical displacements are allowed in the model while the horizontal displacement is prevented on both sides by using fixed condition (Fig.4-1a).

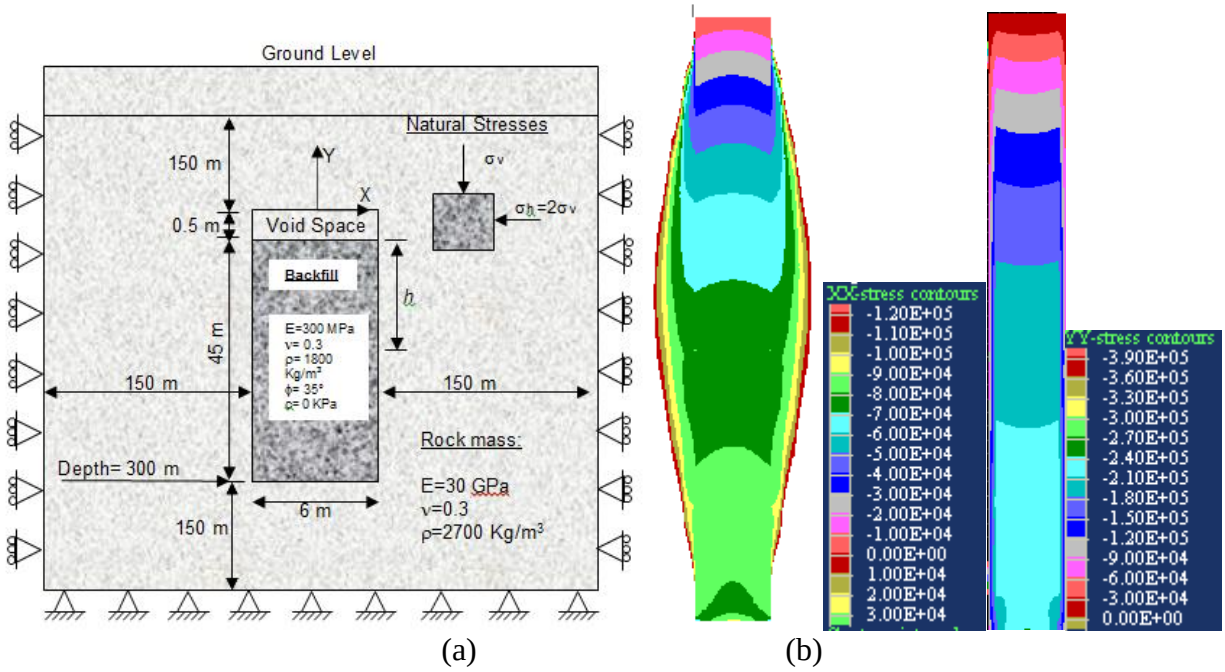

(a) (b)

Figure 4-1: Single backfilled stope (Reference case): (a) a schematic view of the boundary conditions, size and properties applied for a single stope (not to scale), in plane strain, (b) numerical modeling results showing the horizontal (left) and vertical (right) stress distributions at the end of filling of the second stope (see Table 4.1 for details)

All displacements are prevented at the bottom of the model. A relatively coarse mesh (from 5 m near the model boundaries to 1 m near stope walls) is used for the elastic rock region, while a finer mesh is used for the backfill (i.e. 0.5 m grid size). The number of elements is 104×262 (H × V) for the single stope (Reference case). Gravity is applied as the initial condition.

Table 4.1: Parameters used in the numerical simulations, including stope size and material properties (with H = 45 m and E_b = 300 MPa)

Cases	B (m)	ν_b	ϕ' (º)	c' (kPa)	E_r *(GPa)*	*Pillar width* D(m)	*Depth of stope z base* (m)	K_r (σ_h/σ_v)	*Number of Layers*
Reference	6	0.3	35	0	30	0	300	2	4
0a,b,c	6	0.36, 0.3, 0.26	25, 35, 40	0	30	8	300	2	4
1	18	0.36	25	0	30	8	300	2	4
2a,b,c	6	0.3	35	0	30	8,24,60	300	2	4
3a,b	6	0.3	35	20,50	30	8,24,60	300	2	4
4a,b,c	6	0.3	35	0	30	8	400	1,2,4	4
5a,b,c	6	0.3	35	0	2,10,30	8	300	2	4
6a,b,c	6	0.3	35	0	2.10.30	8	2000	2	4
7	6	0.36, 0.33, 0.3,0.2	25, 30, 35	0	30	8	300	2	4
8	6	0.3	35	0	30	8	300	2	4,7,10

The excavation of the whole stope is completed instantly and the convergence takes place before the backfill is placed in the stope in four layers (as suggested by Li and Aubertin, 2009a). The stress state and displacements can be monitored during the excavation and filling of the stope. Figure 4-1b shows the distribution of the vertical and horizontal stresses in the backfilled stope at the end of filling. These results, which are similar to those of Li and Aubertin (2009a), show that both stresses are smaller along the walls than in the central part of the stope at a given elevation; these stresses are lower than the overburden pressures due to arching.

4.5 Analyses of two adjacent stopes – Base Case

The base model and calculation results are presented for two adjacent stopes in Figure 4-2 (Case 0, Table 4.1). The rock mass and backfill properties are shown in Figure 4-2a (and Table 4.1). As mentioned above, the model size was adjusted so that the external boundaries are far enough from the openings to avoid any significant influence on the calculation results. For instance, for two adjacent stopes each having a width B = 6 m, a height H = 45 m, and separated by a distance D = 8 m (pillar width between the two stopes), the boundaries are located 150 m from the stope walls in both directions. The boundary conditions applied to the rock region are also shown in Figure 4-2a.

In these simulations, the left stope is excavated first (in one step) and the rock walls are allowed to move. The backfill is then placed in this first stope in four layers, leading to a stress distribution similar to that shown in Figure 4-1 (for a single stope, reference case). The second opening is then excavated in four steps (from the bottom, up) and filled in four layers. A relatively coarse mesh (element size of 5 m close to the model boundaries, down to 1 m close at the stope walls) is used for the elastic rock region, while a finer mesh is used for the elasto-plastic backfill (typical element size of 0.5 m x 0.5 m). Table 4.1 gives other details for Case 0 and for the other simulations (Cases 1 to 8).

4.5.1 Stress State

The stress distribution and wall convergence in the first stope are monitored during the excavation and filling of the second stope. The simulation results obtained at the end of the excavation and filling process, shown in Figure 4-2b, indicate that an arching effect is developing in both stopes, but with different stress states.

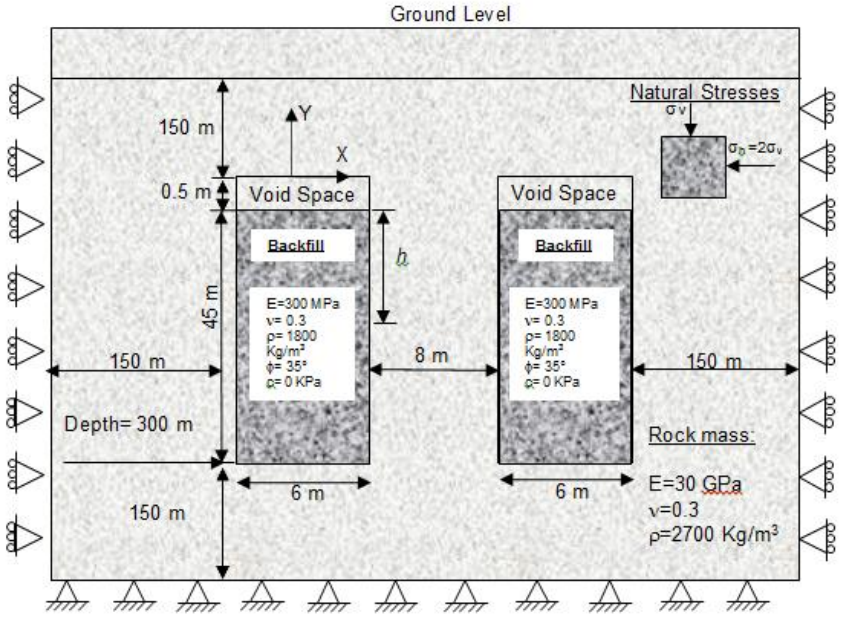

(a)

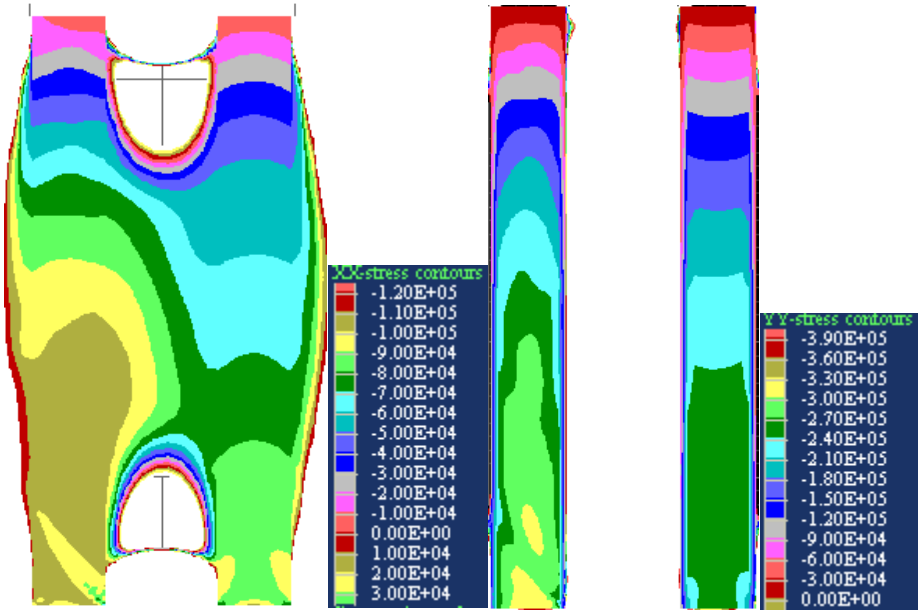

(b)

Figure 4-2: Case 0b: (a) schematic view of the boundary conditions, size and properties applied for the simulations of the two backfilled stopes (not to scale), (b) modeling results showing the horizontal (left) and vertical (right) stress distributions in the two adjacent backfilled stopes at the end of filling of the second stope

The distributions obtained for the second stope are seen to be fairly similar to those obtained for a single stope (Reference Case, Figure 4-1). However, the simulated stresses in the

first backfilled stope are quite different from those obtained for a single stope (or for the second stope). Figure 4-3 shows the stresses along the vertical central line (VCL) within a single stope (Reference Case) and in the two adjacent stopes (Case 0) after excavation and filling. The results in Figure 4-3a indicate that the horizontal stresses in the first stope after excavation of the second one and in the second stope after backfilling are close to those obtained for a single stope. It is also seen that the horizontal stresses increase, by up to 40% near mid-height, after complete filling of the second stope. Figure 4-3b shows that the final vertical stresses along the VCL of the second stope are somewhat higher than those obtained for a single stope; these are smaller than the stresses in the first stope after excavation and subsequent filling of the second stope.

These results indicate that the horizontal and vertical stresses differ for the two stopes, and that those stresses in the second stope can also differ from those obtained for a single backfilled stope. There is thus an effect of the neighboring openings on the stress state in already backfilled stopes.

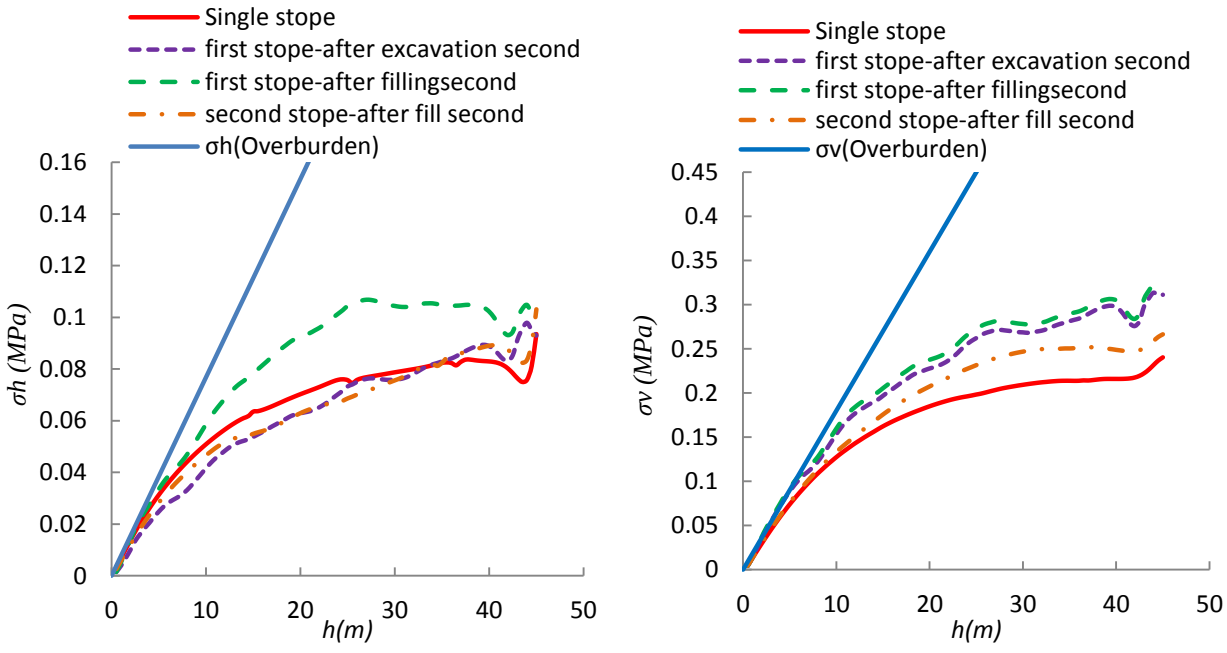

(a) (b)

Figure 4-3: Horizontal (a) and vertical (b) stresses along the VCL of the first backfilled stope; the resultants are shown for a single stope (reference case) and for the first and second stopes after excavation and filling of the latter (Case 0b)

4.5.2 Horizontal Displacements and Strains

The variation of the stresses in the two adjacent backfilled stopes can be related, at least in part, to movements of the rock walls during the excavation and filling sequence. Figure 4-4 shows the horizontal displacements of the left and right (rock) walls for an isolated stope (Reference Case) and of the first and second stopes during the excavation steps (stages) used to create the second opening in the model (Case 0). For the first stope, the final displacements obtained for the single (isolated) stope correspond to the first step that precedes the creation of the second stope; this is followed by four excavation stages to create the second stope (and by four filling stages for this second stope, as described below and in Figure 4-5). There are thus five steps (curves) for the first stope in Figure 4-4a, and four steps (curves) for the second stope being created in four excavated layers in Figure 4-4b.

It is seen that the horizontal displacements δ_h along the left wall of the first stope (left side of Figure 4-4a), at mid-height, goes from about 2 cm (first step, single stope) to 2.16 cm toward the right during the four excavation steps of the second stope. This indicates that the additional horizontal displacements of this left wall are relatively small during the excavation of the second stope. The horizontal displacements along the right wall of the first stope (Fig. 4-4a, right side), at mid-height, evolve quite differently with the excavation of the second stope, going left (increasing displacement) and then right (decreasing displacements), from about -2 cm in the first step (isolated stope) to only -0.075 cm for the last excavation step. At the end of the excavation steps, the horizontal displacements along the right wall of the first stope are smaller than those obtained for the left wall.

The horizontal displacements along the walls of the second stope are shown in Figure 4-4b. It is seen that the left wall of this stope is progressively moving right, toward the newly created opening (as expected). At mid-height, the displacement goes from about -2 cm to the left (after the first excavation step) to about 0.26 cm to the right after the complete excavation of the second stope. This progressive displacement toward the right is fairly similar to the one obtained for the right wall of the first stope (Fig. 4-4a) during the same stages.

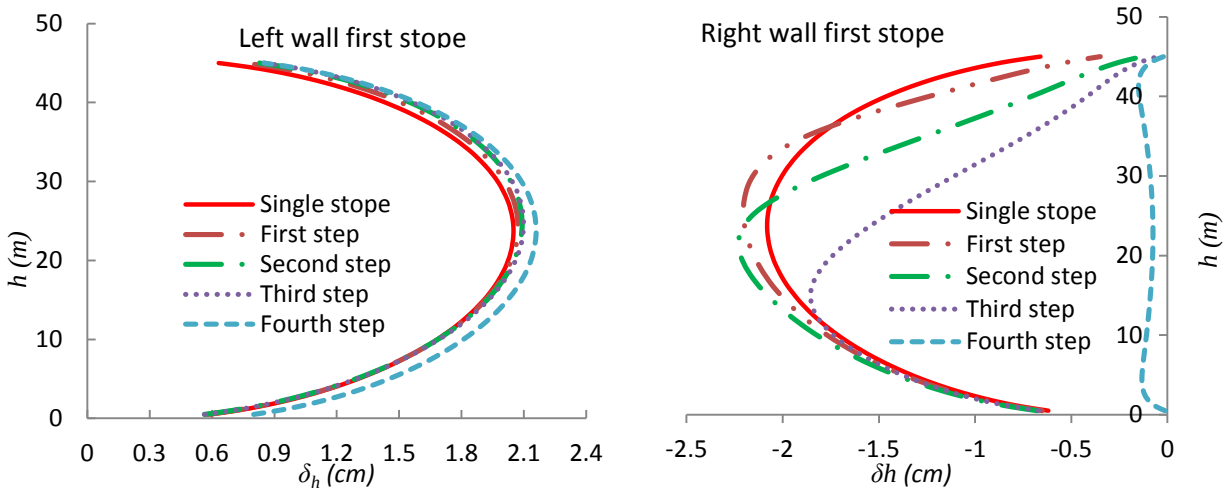

(a)

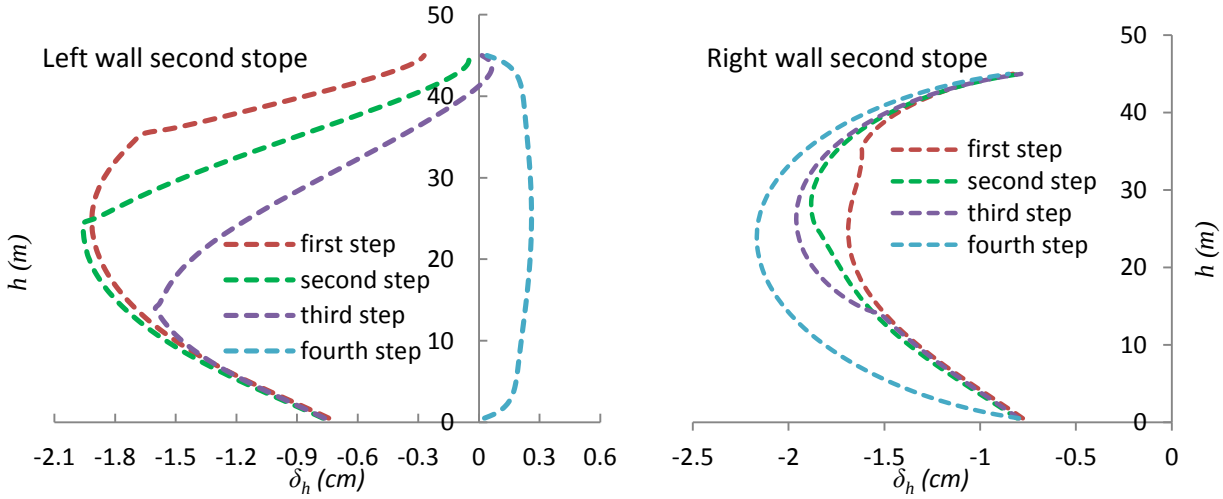

(b)

Figure 4-4: Horizontal displacements δ_h along the left wall (left side) and right wall (right side) of: (a) the first stope; (b) second stope, during excavation of the second stope (Case 0b)

The horizontal displacements along the right wall of the second stope (Figure 4-4b, right side) are going leftward, toward the newly created void space; at mid-height, the displacement goes from about -1.67 cm (first excavation step) to -2.16 cm (last step) to the left.

Figure 4-5 shows the horizontal displacements δ_h of the walls of both stopes during the four filling steps applied to the second stope. The δ_h along the left wall of the first backfilled stope is not affected by the filling process (Figure 4-5a, left side). Much more significant horizontal displacements, leftward, are obtained along the right wall of the first stope during the

filling steps of the second stope (Fig. 4-5a, right side); hence, adding the backfill in the second stope affects the displacement of this wall. A similar horizontal displacement, toward left, is also seen along the left wall of the second stope during the filling process (Figure 4-5b, left side). These two walls (on each side of the pillar) are moving leftward by about 0.05 cm during the four filling steps. The right wall of the second stope remains almost unmoved during filling of this stope (Figure 4-5b, right side).

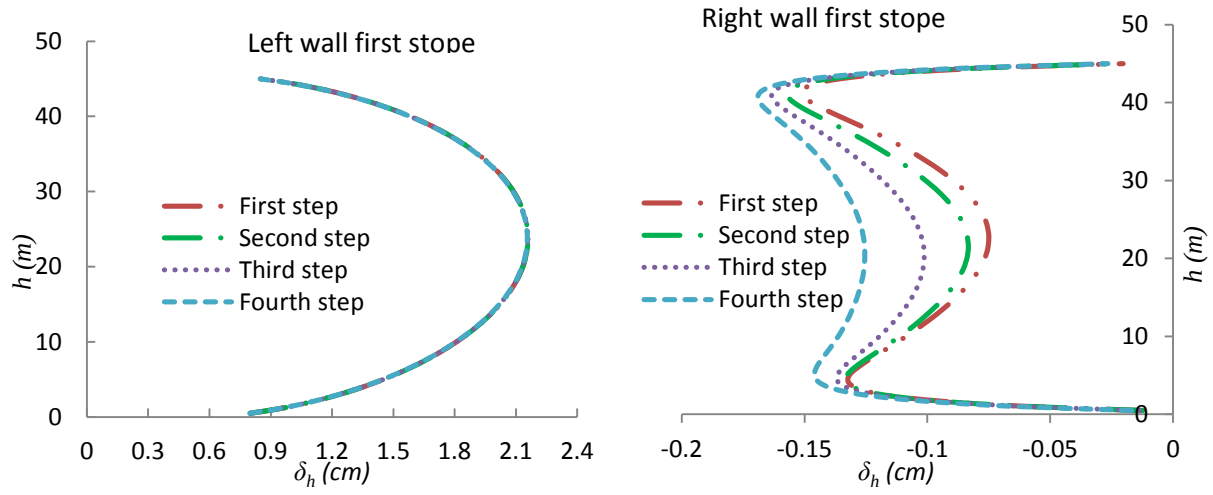

(a)

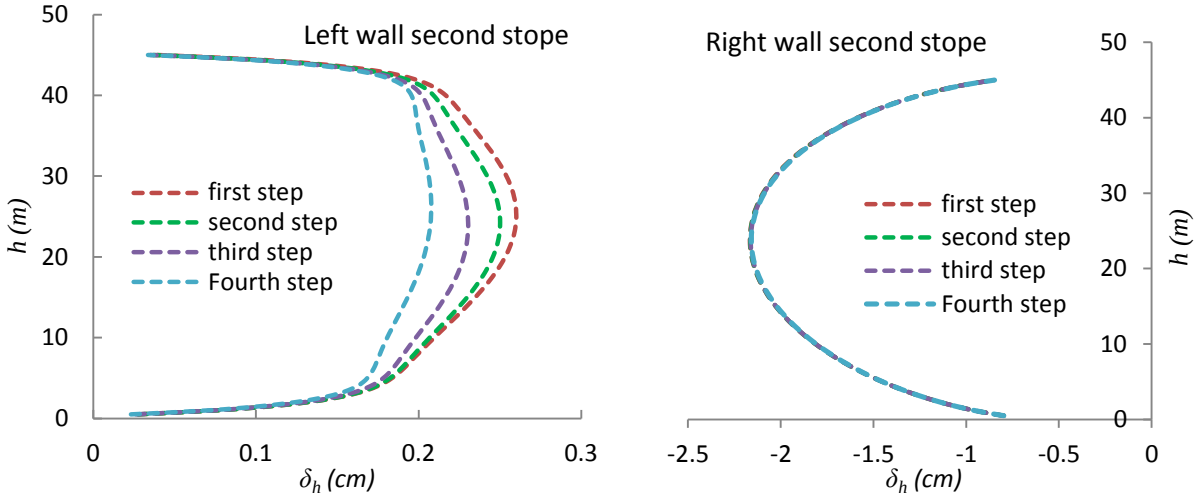

(b)

Figure 4-5: Horizontal displacements δ_h along the left wall (left side) and right wall (right side) of (a) the first stope; (b) second stope, during filling of the second stope (Case 0b)

These displacements shown in Figures 4-4 and 4-5 help understand the evolution of the stresses observed in the first and second backfilled stopes during the excavation and filling sequence (Figure 4-3). As can be seen, when the right wall of the first backfilled stope moves right toward the second stope during the excavation of the latter, the stresses along the VCL and walls of the first stope tend to decrease. During the filling of the second stope, the right wall of the first stope moves leftward, producing an increase of the stresses along the walls and VCL in this first stope. However, this increase produced by filling of the second stope is not as significant as the changes associated with the excavation process, due to the smaller displacements observed along the rock walls.

The vertical displacements along the walls have also been computed. These simulations results (not shown here) indicate that these vertical displacements are much smaller (by about an order of magnitude) than the horizontal ones, so that their effect on the stress state in the backfill is much less significant (see Appendix C for details in Falaknaz, 2014).

The horizontal strains ε_h in the backfill have been calculated in the central part of the openings (along the VCL) for the single stope (Reference Case) and for the two neighboring stopes (Case 0). As this strain is not given directly by FLAC, an average horizontal strain has been evaluated with a user-defined (FISH) function based on the horizontal displacements along two vertical axes located near each other, separated by an initial distance of 0.5 m.

Figure 4-6a shows that the horizontal strain ε_h in the first backfilled stope reaches about - 0.35% at mid-height during the excavation of the second stope; it remains almost constant during filling of the latter. Results shown in Figure 4-6b indicate that the horizontal strains, at mid-height, in the single stope (Reference Case) are smaller than those obtained in the second stope after backfilling. These strains are much smaller than those obtained in the first stope, when the adjacent stope is created. These average strains also lead to a better understanding of the responses observed during the simulations of the backfilled stopes.

4.6 Parametric analysis

The results presented above for the Reference and Base cases indicate that the stresses within a single stope and in two neighboring backfilled stopes can be quite different. In the following, it will be shown that the differences can vary with various parameters, including the

value of the backfill friction angle ϕ', stope width B, pillar width D, natural stress state in the rock mass (through coefficient K_r) and its Elastic modulus E_r.

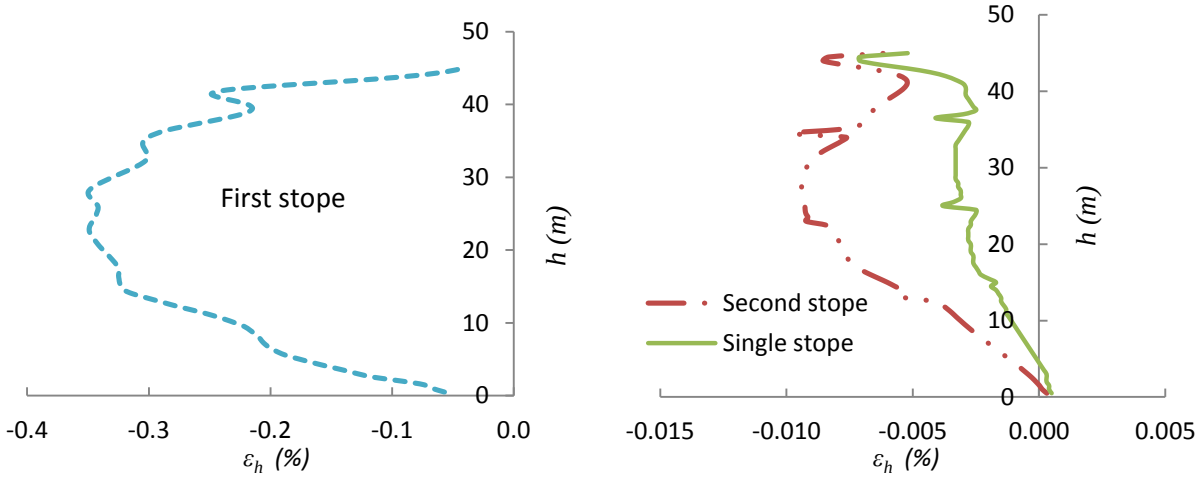

(a) (b)

Figure 4-6: Horizontal strain ε_h along the VCL of (a) the first and (b) single stope and second stope (in the backfill) after filling of the second stope obtained (Case 0b)

4.6.1 Internal friction angle ϕ' of the backfill

Figure 4-7 presents the results obtained for Case 0 (ϕ' = 25°, 30°, 35° and 40°) after excavation and filling of the second stope; the variation of the internal friction angle ϕ' of the backfill is accompanied by a change in the Poisson's ratio v (according to Eq. 4-4), as indicated in Table 4.1. One sees that when the backfill friction angle increases from 25° to 40°, the horizontal stresses along the VCL of the first stope decrease, while the vertical stresses remain almost unchanged (Falaknaz et al, 2013). These observations are somehow in good agreement with the results obtained by Li et al. (2007) and Li and Aubertin (2009a) for a single backfilled stope.

4.6.2 Stope width *B*

The effect of stope width B on the stress magnitude was also investigated. When the stope width is 18 m (Case 1), the final horizontal and vertical stresses along the VCL of first backfilled stope are larger than those obtained for stopes having a width of 6 m (Figure 4-8). This is due in part to the larger stresses in the pillar (which produce more displacements along the walls) and to a less pronounced arching effect when the stope width increases. The simulations results (not

shown here, Appendix C) also indicate that an increase of the stope width (from 6 to 18 m) reduces the differences between the vertical stresses (along the VCL) obtained for an isolated stope and for the second backfilled stope.

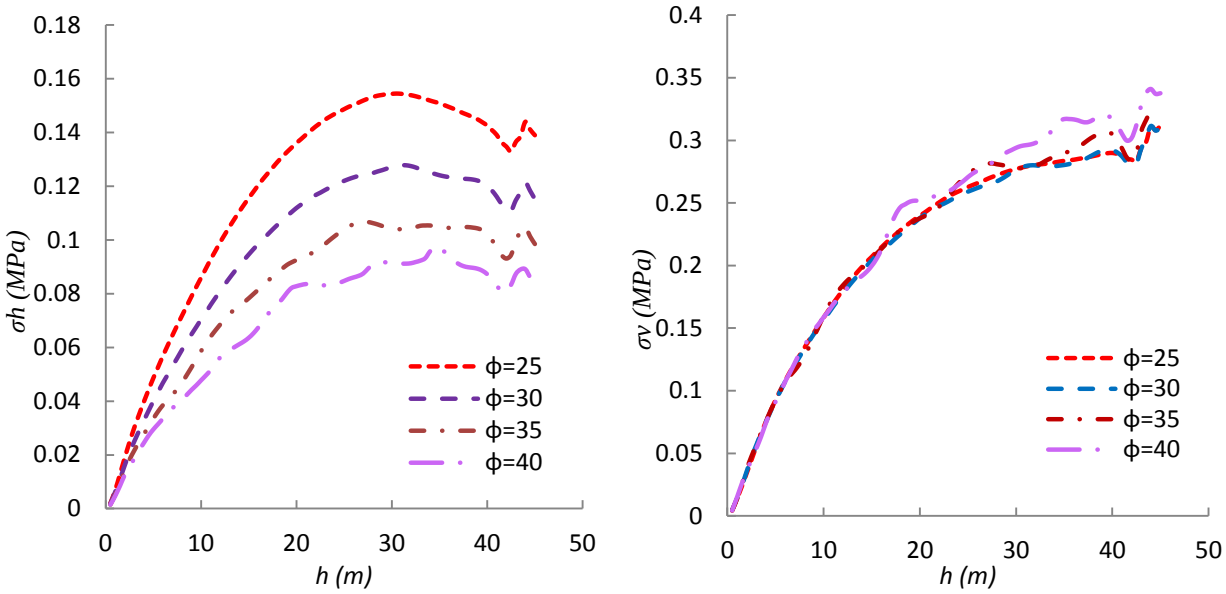

(a) (b)

Figure 4-7: Effect of the internal friction angles ϕ' of the backfill on the horizontal (a) and vertical (b) stresses along VCL of the first backfilled stope (Case 0)

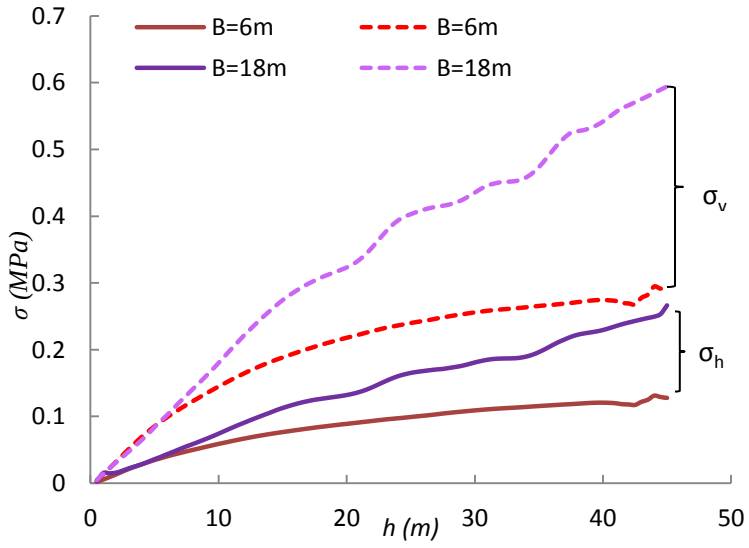

Figure 4-8: Effect of stope width B on the horizontal σ_h and vertical σ_v stresses along VCL of the first backfilled stope (Case 1)

4.6.3 Pillar width *D*

The influence of the distance between the two openings was assessed for stopes having a width B = 6 m, for a cohesionless backfill (Case 2) and for backfills with cohesion (Case 3). The distance between the stopes was varied between 8 m to 60 m. Again, the model boundaries are located far enough from the stope walls to avoid any significant influence on the results. The number of elements in these models was 124×262 (D = 8 m), 140×262 (D = 24 m) and 204×332 (D = 60 m), with a mesh size that varied with the distance from the stope walls. The boundary conditions and materials properties are the same as for Case 0.

4.6.3.1 Cohesionless backfill

Figure 4-9 shows the stresses along the VCL and along the walls of the first stope, after excavation of the second stope (for D = 8 m, 24 m and 60 m, Cases 2a,2b, Table 4.1). It is seen that the horizontal and vertical stresses along the VCL of the first backfilled stope are not affected by the pillar width D, when considering the excavation of the second stope (Figure 4-9a). However, the horizontal stresses in the first stope along the VCL after backfilling of the second stope tend do decrease somewhat when the pillar width D increases, while the vertical stresses remain almost unchanged (Figure 4-9b). More specifically, the horizontal stresses decrease when the D increases from 8 m to 24 m, and these remain essentially unchanged for D = 24 and 60 m.

The same observations can be observed along the walls of the first stope for the different values of D, after excavation (Figure 4-10a) and filling (Figure 4-10b) of the second stope. A thicker pillar is thus less affected by the filling of the second stope, which produces smaller displacements of its walls when D increases; the stresses in the first stope are also less influenced by the filling when the pillar is wider (as expected).

The horizontal displacements δ_h along the walls of the first stope, after the excavation of the second stope, are shown in Figure 4-11. It can be seen that the pillar width D does not affect much the rightward displacement of the left wall (Figure 4-11a). However, when the pillar width increases, the rightward movement of the right (pillar) wall increases by a factor of up to 16, from - 0.075 cm (D = 8 m) to -1.223 cm (D = 60 m) near mid-height (Figure 4-11b). The maximum horizontal strain ε_h along the VCL in the backfill also decreases (from - 0.35% to about - 0.12%) with an increase of the pillar width D (Figure 4-11c).

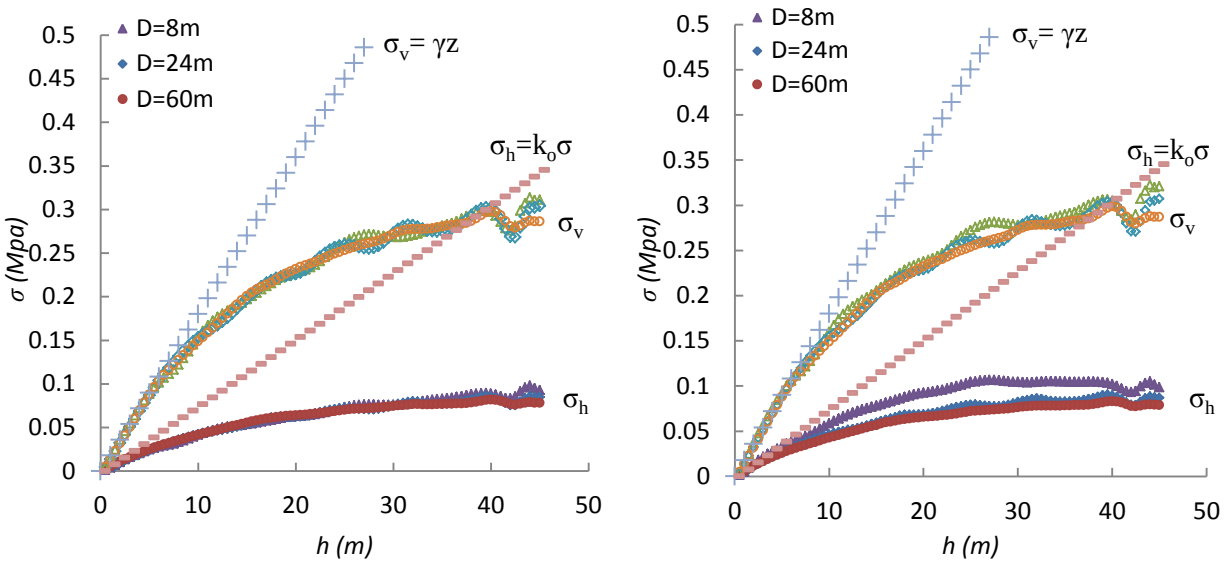

(a) (b)

Figure 4-9: Effect of pillar width *D* on the distribution of the vertical and horizontal stresses in the first stope along the VCL after: (a) excavation; (b) filling of the second stope (Case 2)

4.6.3.2 Cohesive backfill

Cohesion of the backfill due to addition of a binder may significantly affect the stress state in backfilled stopes (Li and Aubertin, 2009a; El Mkadmi et al. 2013). This effect is also clearly perceived from the simulation results shown in Figure 4-12 (when compared with other results shown above). This figure shows the stresses along the VCL of the first stope, for different pillar width *D* after excavation of the second stope for a cemented (cohesive) backfill (Cases 3a,3b, Table 4.1). Two cohesion values are considered here: c' = 20 kPa and 50 kPa (in addition to c' = 0 for Case 2).

For both values of the backfill cohesion, it is seen that the horizontal and (to a lesser extent) vertical stresses in the first stope become quite different than those obtained for the granular backfill (Figures 4-9 and 4-10); for instance, near the base of the stope with a 60 m wide pillar, σ_v = 280 kPa and σ_h = 76 kPa for c' = 0 kPa ; σ_v = 217 kPa and σ_h = 41 kPa for c' = 20kPa; σ_v = 114 kPa and σ_h = 3 kPa for c' = 50kPa. It is also observed that for c' = 20 kPa (Fig. 4-12a), the stresses along the VCL of the first stope (and also along the walls, not shown here,

Appendix C) are not affected significantly by the pillar width *D* after the excavation of the second stope.

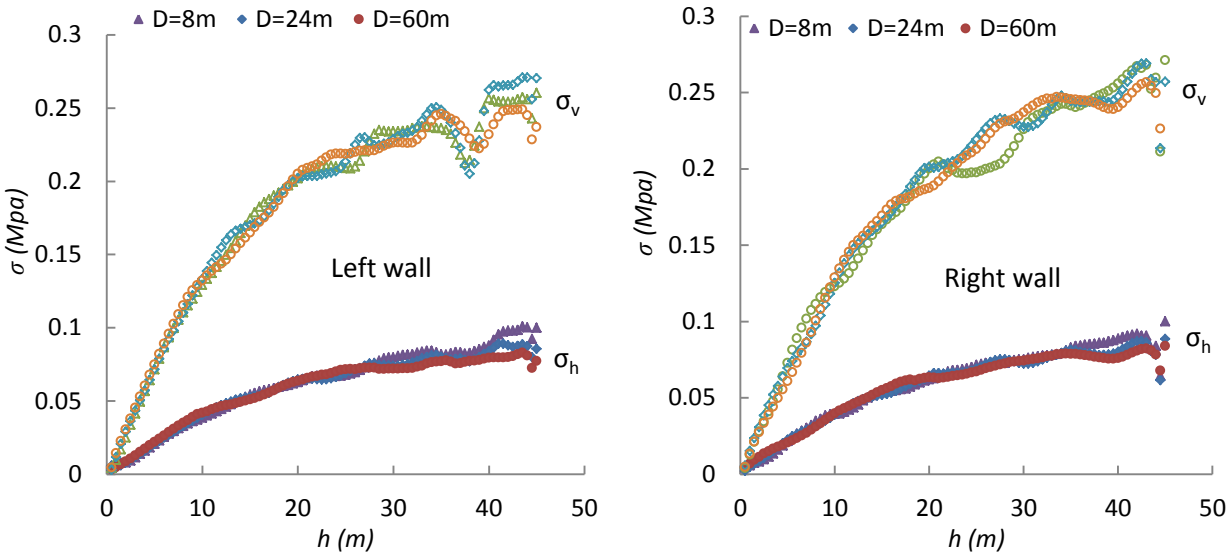

(a)

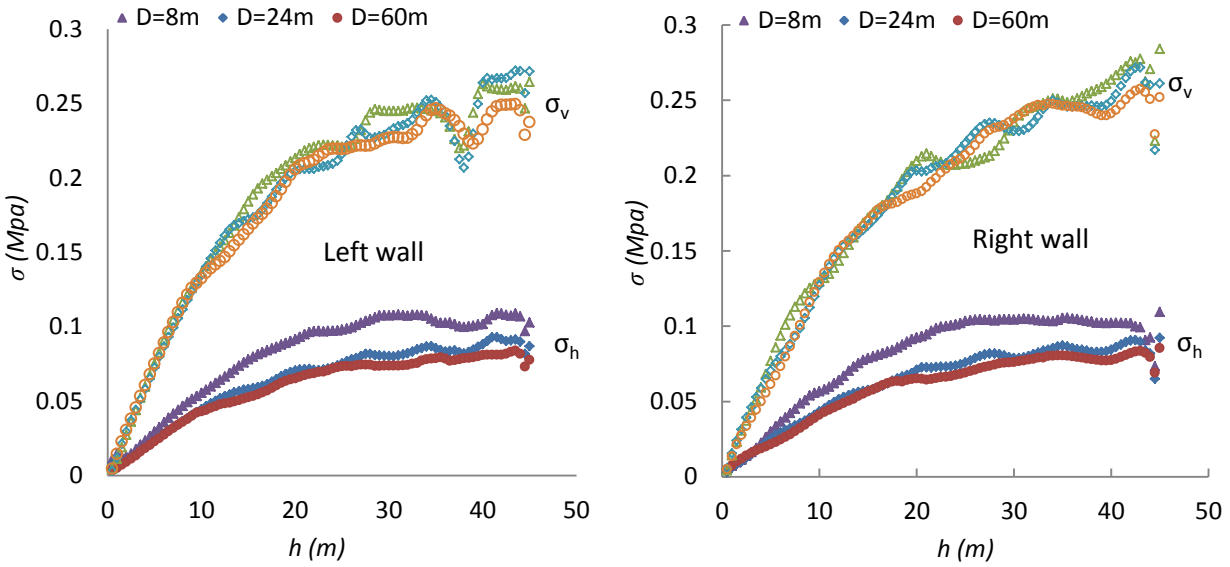

(b)

Figure 4-10: Effect of pillar width *D* on the distribution of the vertical and horizontal stresses in the first stope along the left wall (left side) and right wall (right side) in the backfill after: (a) excavation; (b) filling of the second stope (Case 2)

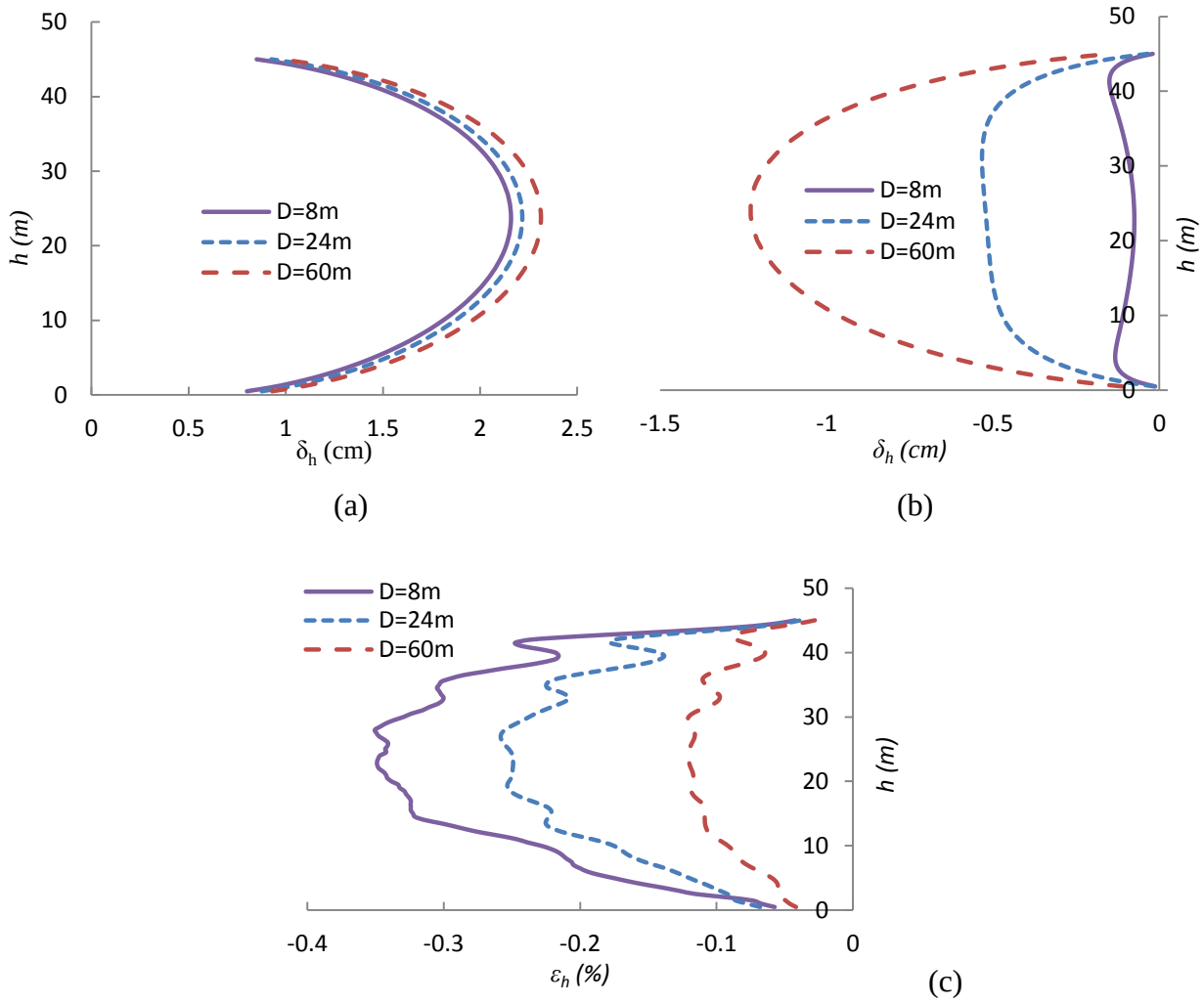

Figure 4-11: Effect of pillar width D on the horizontal displacements δ_h in the first stope along the: (a) left wall; (b) right wall; (c) horizontal strains ε_h in the backfill along the VCL after excavation of the second stope (Case 2)

After filling of the latter, the horizontal stresses tend to decrease somewhat when the pillar width D increase, while the vertical stresses remain almost unchanged (Figure 4-12a, right side). For c' = 50 kPa (Fig. 4-12b), the vertical stresses along the VCL of the first stope (and also along the walls, not shown here, Appendix C in Falaknaz, 2014) tend to decrease more significantly (compare to Fig. 4-12a) with an increase of the stope distance after the excavation and filling of the second stope.

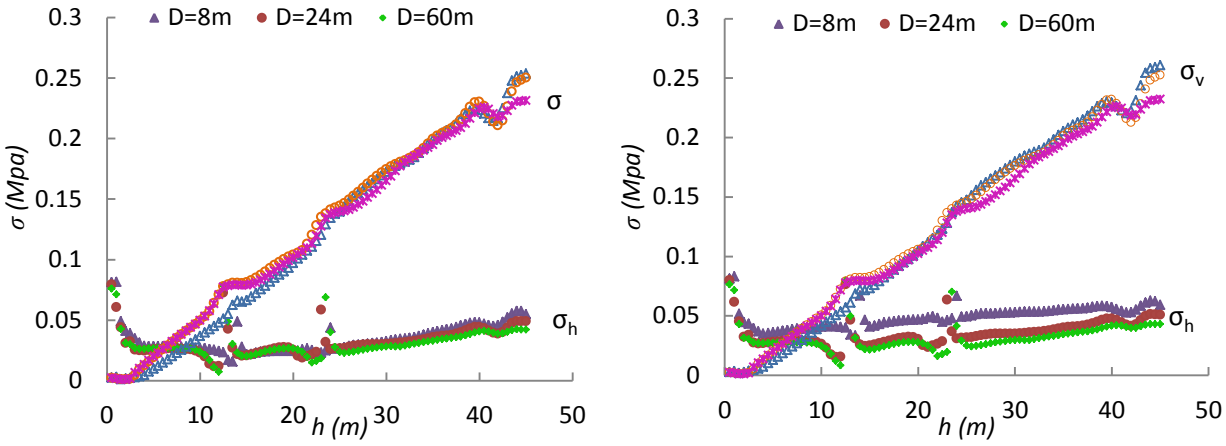

(a)

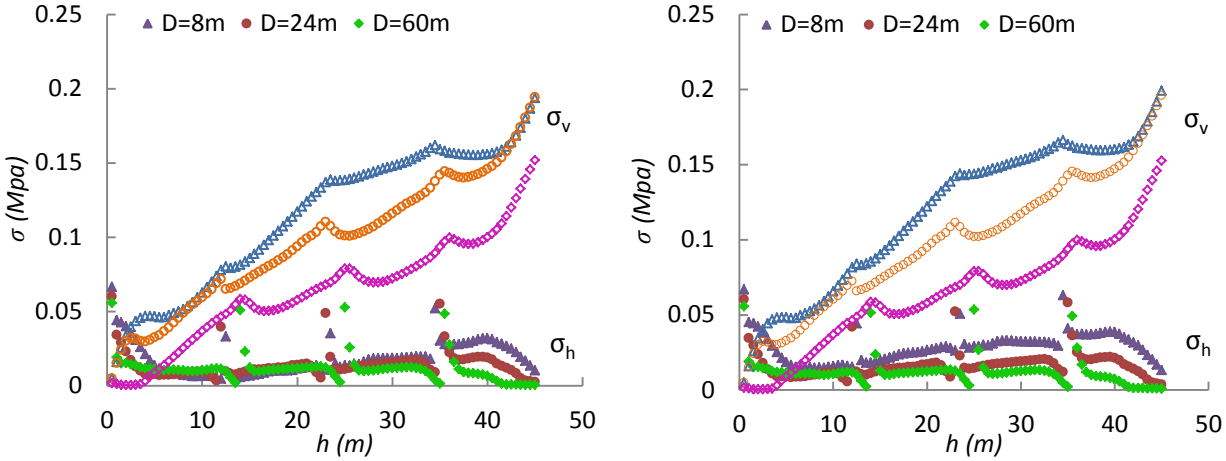

(b)

Figure 4-12: Effect of pillar width *D* on the distribution of the vertical and horizontal stresses along the VCL of first stope after excavation (left side) and filling (right side) of the filled stope for: (a) Case 3a with c' = 20 kPa; (b) Case 3b with c' = 50 kPa

In this case, an increase in the pillar width *D* leads to a decrease of the vertical stresses along the VCL by up to 50% near mid-height (σ_v = 133 kPa for *D* = 8 m, and σ_v = 67 kPa for *D* = 60 m), after excavation of the second stope. For Case 3b, the horizontal stresses, which are much smaller than the vertical stresses, are not affected as much as the latter by the stope distance (although there is a significant effect of *D* here also).

For cases with a cemented backfill (c' =20 kPa and 50 kPa), the horizontal displacements and along the VCL (and walls) of the first stope (not shown here, Appendix C in Falaknaz, 2014) are almost similar to those obtained for c' = 0 kPa (Figure 4-11). Hence, the shear strength of the

backfill does not have influence on the rock walls horizontal displacements (for the conditions considered here).

4.6.4 Natural stresses in the rock mass

The natural stress ratio $K_r = \sigma_h/\sigma_v$ (with $\sigma_v = \gamma z$, where z is depth and γ is the rock unit weight) in a rockmass can vary widely in the earth crust (e.g. Hoek et al, 2002). The effect of K_r on the reponse of backfilled stopes was assessed with additional simulations. In this Case 4, the stopes are located at a depth of 400 m below the ground surface; this depth was selected to avoid the boundary effect on the results (especially when the natural stresses are increased). The model boundaries are located 240 m from the stopes. Figure 4-13 presents the stresses along the VCL of the first stope, for different stress ratios K_r (= 1, 2, 4), after excavation of the second stope (Table 4.1). The results indicate that an increase in the value of K_r, from 1 to 4, tends to produce an increase in the horizontal stresses in the backfill, particularly below mid-height, by up to 25% ; similar increase were also obtained for the left and right walls (results not shown here, Appendix C in Falaknaz, 2014). The vertical stresses appear less sensitive to the values of K_r. Also, the simultations indicate that the stresses in the first stope tend to increase sligthly during filling of the second stope for all values of K_r (results not shown here, details given in Appendix C in Falaknaz, 2014).

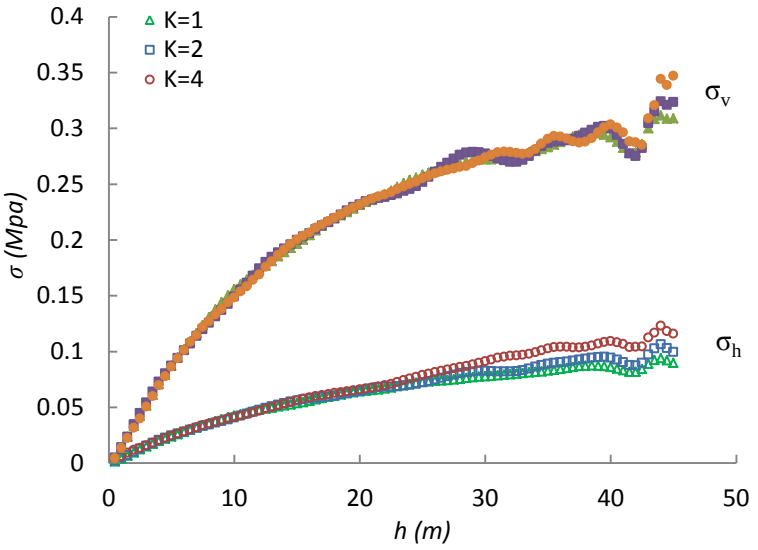

Figure 4-13: Effect of K_r value on the distribution of the vertical and horizontal stresses in the first stope along the VCL after excavation of the second stope (Case 4)

Figure 4-14 shows the influence of the value of K_r on the horizontal displacements along the walls of the first stope (after excavation of the second stope), and the horizontal strains in the backfill along the VCL.

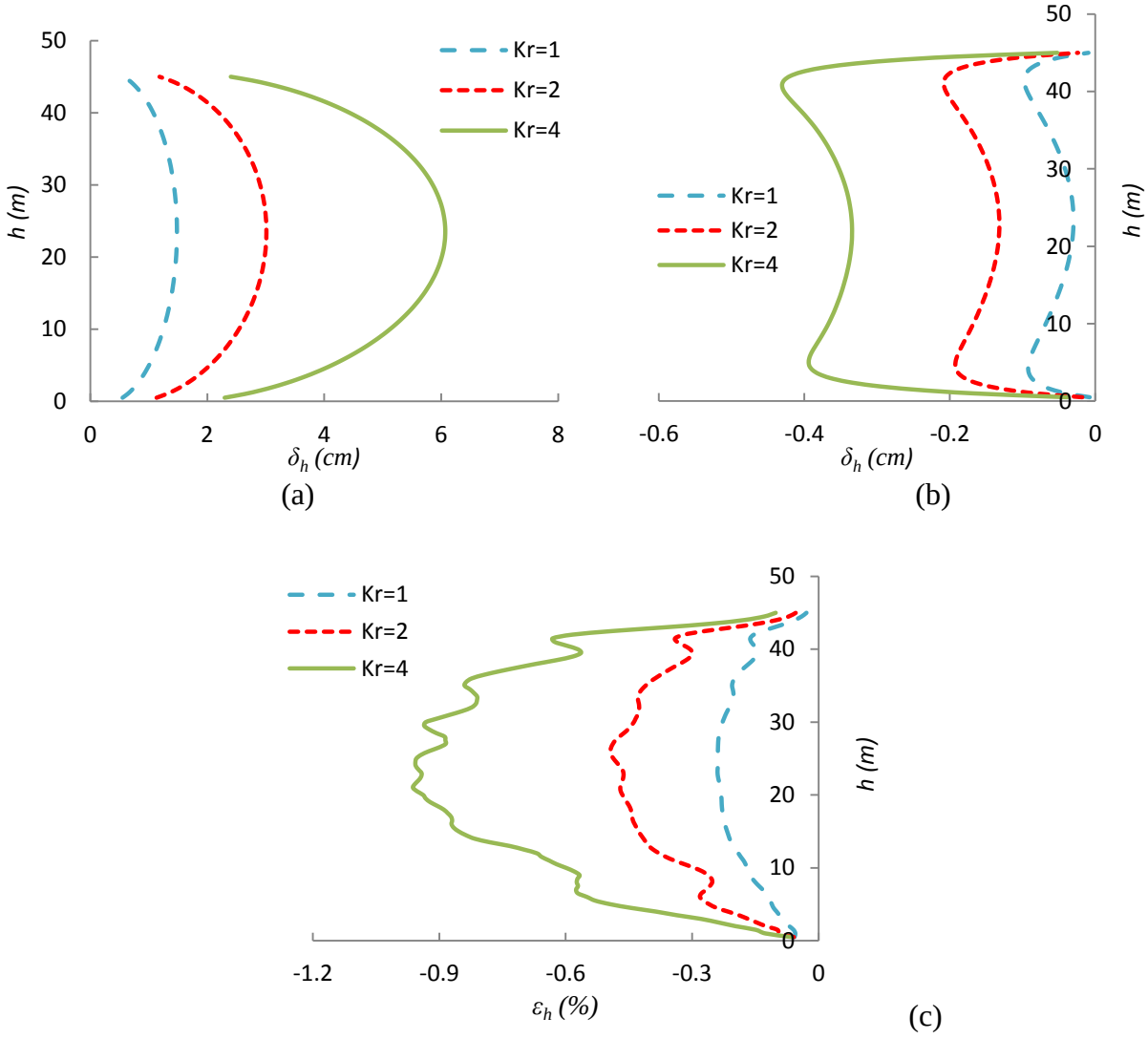

Figure 4-14: Effect of the K_r value on the horizontal displacements δ_h in the first stope along the (a) left wall and (b) right wall; (c) horizontal strains ε_h in the backfill after excavation of the second stope (Case 4)

It is seen that the horizontal displacements of the left wall (Fig. 4-14 a) tend to increase with the value of K_r, by up to 5 times at mid-height (where the maximum horizontal displacement δ_h is 1.48 cm for K_r = 1 and 6.06 cm for K_r = 4), and up to 10 times (δ_h = - 0.03 cm for K_r = 1 and

- 0.334 cm for K_r = 4) for the right wall (Fig. 4-14b). The maximum horizontal strains ε_h in the backfill increase by up to 4 times, from - 0.24% for K_r = 1 to - 0.94% for K_r = 4 (Fig. 4-14c).

4.6.5 Depth *z* and Elastic modulus E_r of the rock mass

The rock stiffness, represented here by its elastic modulus E_r, may also affect the stress distribution within the two adjacent stopes, as illustrated by the results of Case 5. The results shown in Figure 4-15 indicate that a decrease of the elastic modulus E_r, from 30 GPa to 2GPa, leads to higher horizontal and vertical stresses along the VCL of the first stope (and also along the walls – not shown here, Appendix C in Falaknaz, 2014), particularly in the deeper parts. The maximum horizontal stress at depth along the VCL in the first stope increases by factor of about 3 (i.e. σ_h = 92 kPa for E_r = 30 GPa, and σ_h = 242 kPa for E_r = 2 GPa) and the vertical stress increases by factor of about 2 (σ_v = 311 kPa for E_r = 30 GPa, and σ_v = 504 kPa for E_r = 2 GPa). These stresses do not change much during backfilling of the second stope.

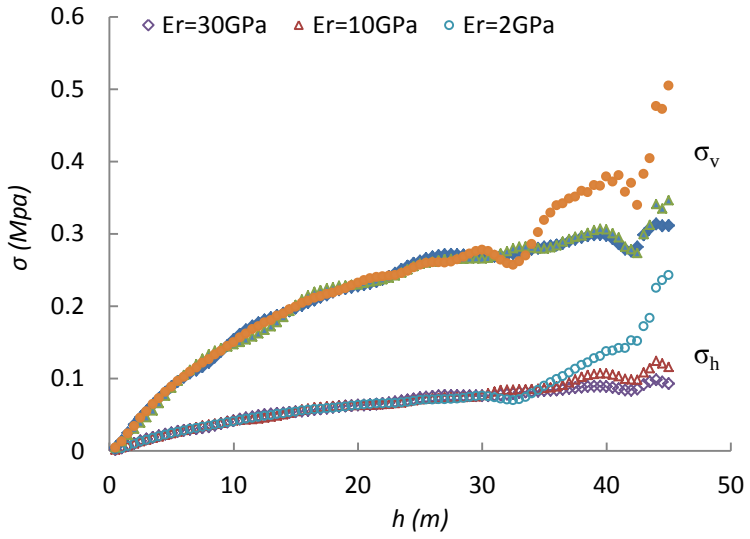

(a)

Figure 4-15: Effect of rock modulus E_r on the distribution of the vertical and horizontal stresses in the first stope along the VCL after excavation of the second stope (Case 5)

As expected, the horizontal displacements along the walls and the horizontal strains along the VCL tend to increase when the elastic modulus of rock mass decreases (Figure 4-16). The horizontal displacement δ_h (Fig. 4-16a) of the left wall is 2.15 cm for E_r = 30 GPa and 32 cm for E_r = 2 GPa at mid-height; also is δ_h = - 0.075 cm for E_r = 30 GPa and -1.12 cm for E_r = 2 GPa for the right wall. The average horizontal strain ε_h (Fig. 4-16c) also tends to increase when the elastic

modulus E_r decreases, from - 0.35% near mid-height for E_r = 30 GPa to about - 4.8% for E_r = 2 GPa.

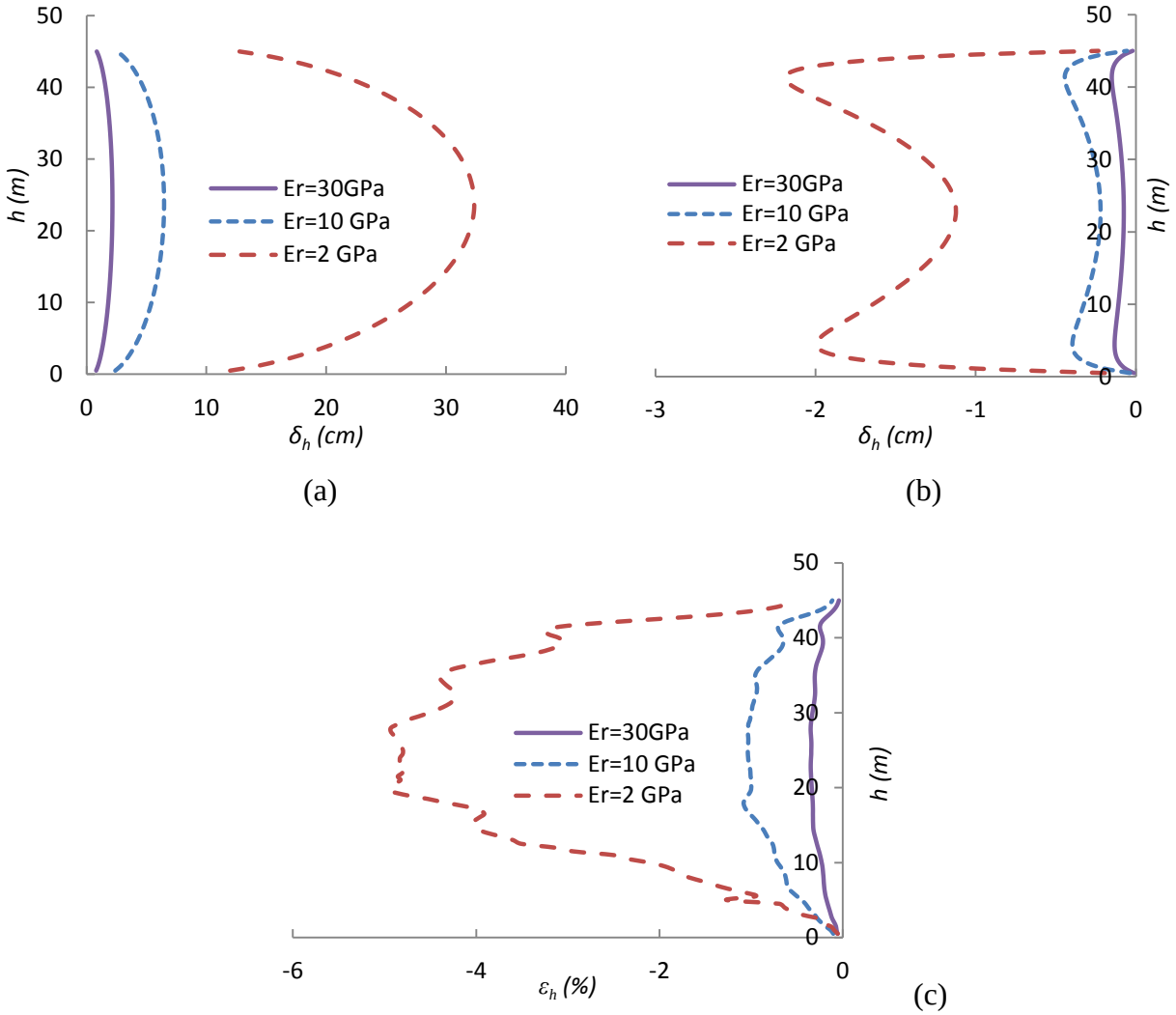

Figure 4-16: Effect of rock modulus E_r on the horizontal displacements δ_h in the first stope along the (a) left wall and (b) right wall; (c) horizontal strains ε_h in the backfill after excavation of the second stope (Case 5)

The stresses obtained at a larger depth of 2000 m are shown in Figure 4-17 (Case 6, Table 4.1). These results show that an increase of the stope depth, from 300 m to 2000 m, leads to larger horizontal and vertical stresses along the VCL. More specifically, the maximum horizontal stress along the VCL of the first stope increases by a factor of about 2, from σ_h = 93 kPa (depth of 300 m) to σ_h = 182 kPa (depth of 2000 m) for E_r = 30 GPa, and by a factor of about 3.5, from σ_h = 242 kPa (depth of 300 m) to σ_h = 840 kPa (depth of 2000 m) for E_r = 2 GPa (Figure 4-17a); the

latter value seems unrealistic, considering the excessive displacements that are obtained for this very low modulus (see below). The vertical stresses are also affected by an increase of the stope depth, but to a lesser extent, as shown in Figure 4-17b. The increase reaches a factor of about 1.4, from σ_v = 311 kPa (depth of 300 m) to σ_v = 433 kPa (depth of 2000 m) for E_r = 30 GPa, and a factor of about 1.7, from σ_v = 504 kPa (depth of 300 m) to σ_v = 877 kPa (depth of 2000 m) for E_r = 2GPa. Similar tendencies are also observed for the stresses along the walls of the first backfill stope (Appendix C in Falaknaz, 2014).

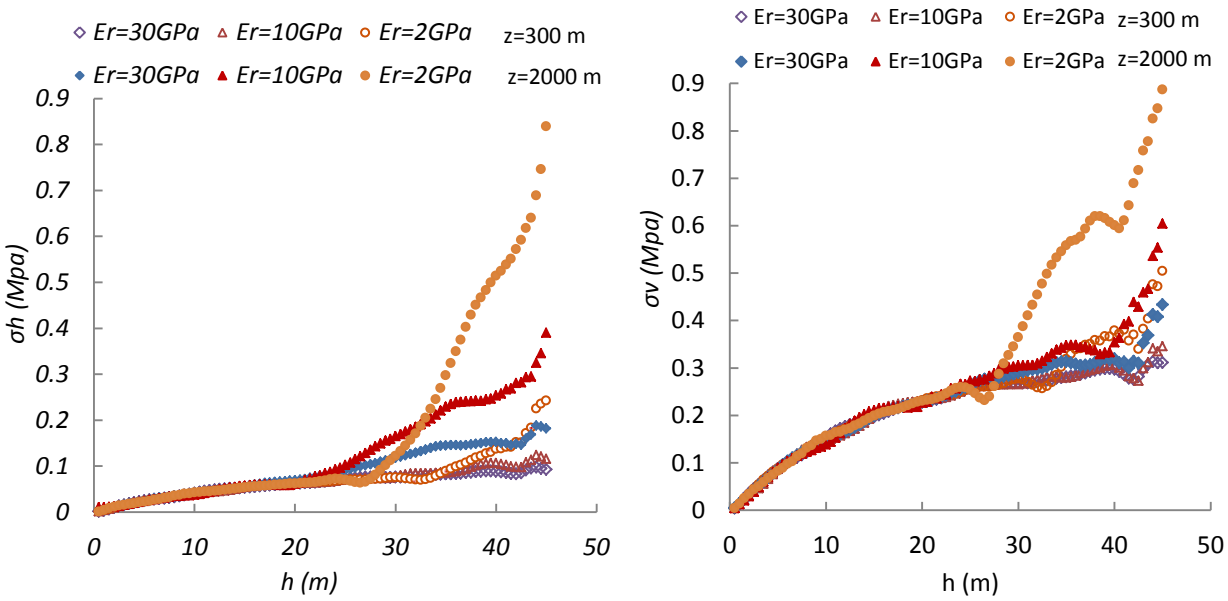

(a) (b)

Figure 4-17: Effect of rock modulus E_r and depth z on the distribution of the (a) horizontal and (b) vertical stresses in the first stope along the VCL in the backfill after excavation of the second stope (Case 6).

The horizontal displacements δ_h along the walls of the first stope (after the excavation of the second stope) are shown in Figure 4-18, for depth of 300 m and 2000 m, for different rock mass modulus. It can be seen that the maximum displacement δ_h of the left wall increases with depth, by up to 7 times, from 2.16 cm (depth of 300 m) to 15.8 cm (depth of 2000 m) for E_r = 30 GPa. For the very low modulus value E_r = 2 GPa, δ_h goes from 32 cm (depth of 300 m) up to 2.36 m (depth of 2000 m) near mid-height of the first stope; these values are unrealistically large, and are shown here for indicative purposes only, to illustrate the potential effect of a weak rock mass modulus.

The leftward horizontal displacement δ_h of the right wall near mid-height of the first stope is also largely increased, by a factor of up to 10, from -0.075 cm (depth of 300 m) to -1.076 cm (depth of 2000 m) for E_r = 30 GPa, and by a factor of up to 14, from -1.12 cm (depth of 300 m) to -16 cm (depth of 2000 m) for the small modulus E_r value of 2 GPa.

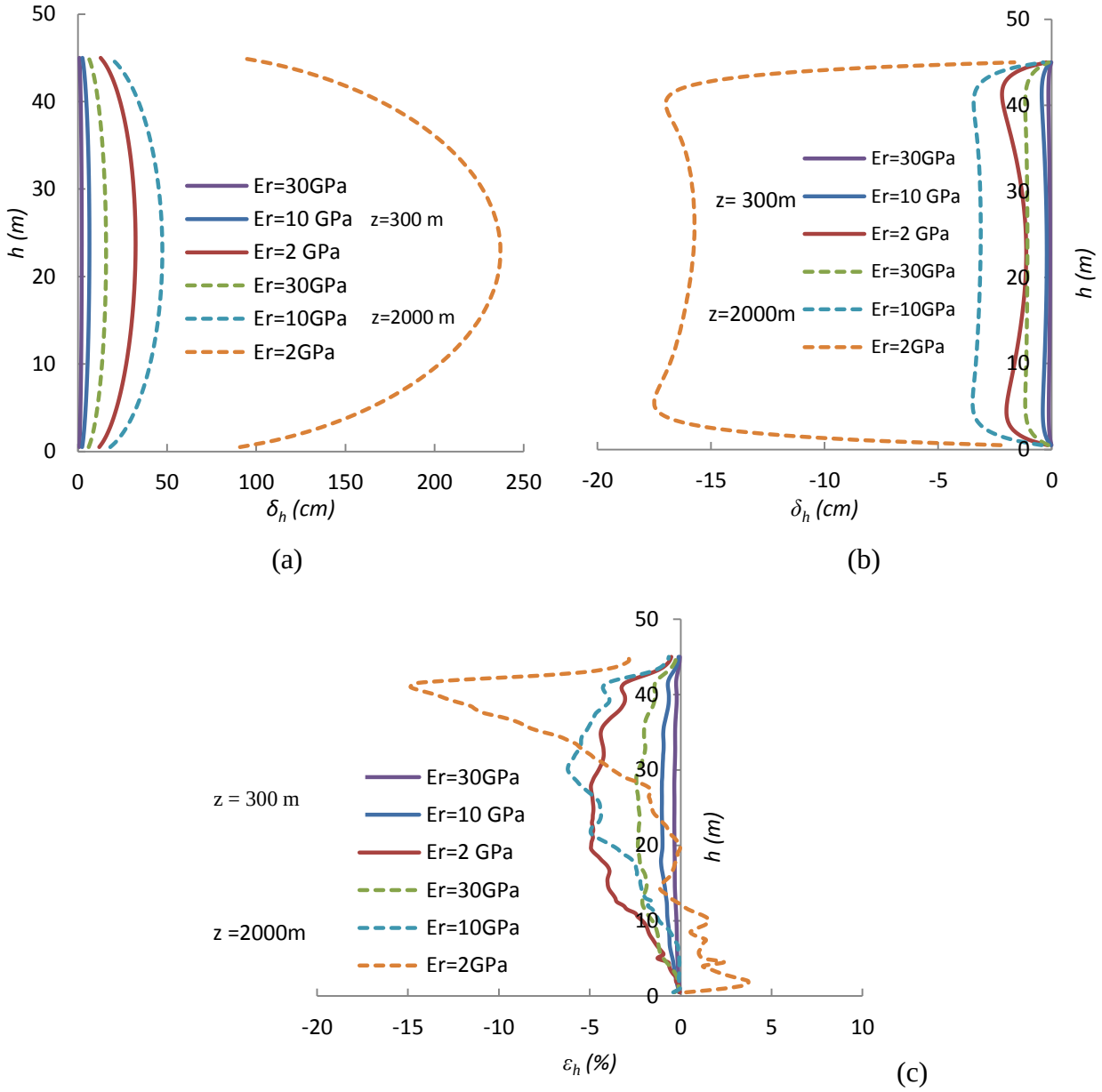

Figure 4-18: Effect of rock modulus E_r and depth z on the horizontal displacements δ_h in the first stope along the (a) left wall and (b) right wall; (c) horizontal strains ε_h along the VCL in the first backfilled stope after excavation of the second stope (Case 6)

The maximum average horizontal strains ε_h (Fig. 4-18c) in the backfill also increases significantly with the stope depth, from - 0.35% (depth of 300 m) to about - 2.5% (depth of 2000 m) for E_r =30 GPa, and from -5% (depth of 300 m) to about - 14.5% (depth of 2000 m) for E_r = 2 GPa (again, the latter value appears unrealistic, considering the large displacement involved).

The simulations also indicate that when the rock mass modulus decreases and the stope depth increases, the backfill near the top of the stope may tend to move upward, as it is pushed by the horizontal displacement of the walls (results not shown here, Appendix C in Falaknaz, 2014); this was also observed for a single stope with a relatively large convergence of the walls (Aubertin et al. 2003).

4.7 Discussion

4.7.1 Relationship between ϕ' and ν

In this paper, FLAC was used to assess the effect of creating two neighboring stopes created in sequence on the stress distribution in the backfill, for plane strain conditions. Various other aspects can have an effect on the stresses and displacements in the backfilled stopes. One of these is related to the assumptions used to define two of the key backfill properties. As stated above, the numerical analyses conducted here are based on the existence of an explicit relationship between the values of ϕ' and ν, as expressed by Equation 4-4. This assumption is different from the one commonly used in many previous analyses, where these two parameters were treated as being independent from each other (implicitly). The influence of this assumption on the results were compared with simulations that considered independent values for ϕ' and ν for two adjacent stopes (Case 7) as shown in Figure 4-19. As can be seen in this figure, there is a transfer of the backfill load to the each wall, associated with the arching effect, in all cases, with both assumptions.

The simulations indicate that for the first two excavation stages of the second stope, the horizontal stresses in the first stope obtained with Eq. 4-4 are somewhat higher than those obtained using independent values for ϕ' and ν, while the vertical stresses are smaller than those obtained based on the latter assumption (results not shown here; details given in Appendix C in Falaknaz, 2014). There is no significant difference between the results obtained after the last two stages of excavation for these two assumptions.

Figure 4-19 also shows that both horizontal and vertical stresses based on Eq.4-4 (dash lines) are higher than those obtained using the independent values for ϕ' and v (solid lines) after filling of the second stope. As the friction angle increases from 25º to 35º, this difference between the results obtained with both assumptions tends to decrease.

In general, the simulation results obtained here indicate that the stresses obtained using these two different assumptions (ϕ' and v related or independent) show similar trends and have the same magnitude along the VCL of the first stope at the end of excavation and filling of the second stope. The same tendencies can be observed for the stresses along the walls of first backfilled stope (results presented in Appendix C in Falaknaz, 2014). The observed effects of ϕ' and v are also in good agreement with the tendencies observed by Li et al. (2007) and Li and Aubertin (2009a) for a single backfilled stope.

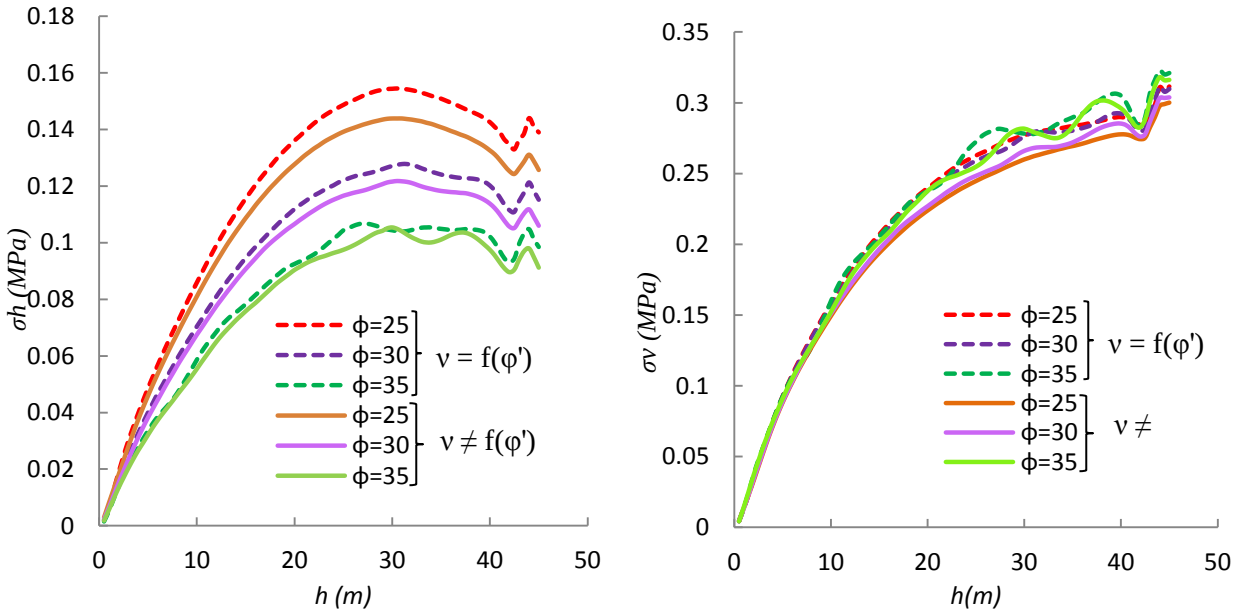

(a) (b)

Figure 4-19: Horizontal (a) and vertical (b) stresses along VCL in the first backfilled stope, using independent v and ϕ' values (Case 7, solid lines) and Eq.4-4 (Case 7, dash lines) after filling of the second stope

4.7.2 Simulation procedure

One of the other important factors that could also influence the simulated stresses, displacements, and strains in the backfilled stopes is the imposed excavation and filling sequence.

Case 8 considers this factor by simulating two stopes created and filled progressively (in up to 10 layers). In these simulations, the first stope is excavated in one step, and the elastic rock mass walls are allowed to converge in the opening. The backfill is then placed in the first stope in 4, 7 or 10 layers. This is followed by the excavation of the second stope in 4, 7 and 10 steps, and its filling in 4, 7 and 10 layers. Figure 4-20 shows the stress distributions in the first stope obtained for different numbers of steps (excavation and filling of the second stope) for a cohesionless backfill. The results indicate that the stresses obtained along the VCL of the first stope (and also along the walls, not shown here, Appendix C in Falaknaz, 2014) are almost the same for the different sequences. These results thus suggest that the simulations presented above (four steps for the excavation and filling of the second stope), do provide representative responses. These observations correspond well to the results obtained by Li and Aubertin (2009a) for a single stope.

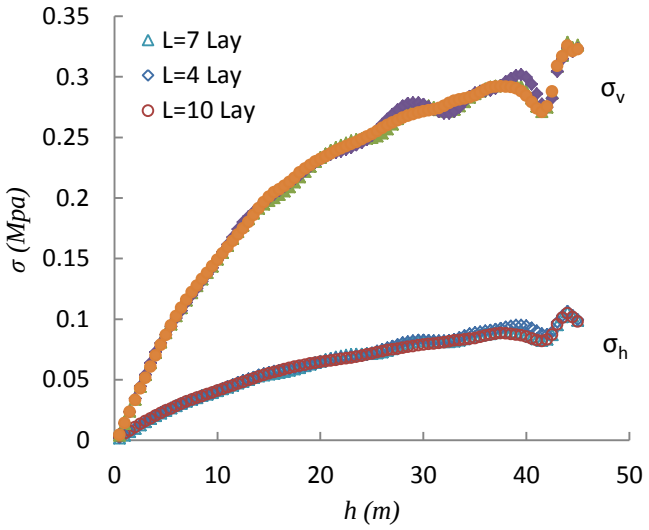

Figure 4-20: Effect of the filling sequence (4 to 10 layers) on the distribution of the vertical and horizontal stresses in the first backfilled stope along the VCL (Case 8)

4.7.3 Stress path

The stress distribution within backfilled stopes can also be assessed in terms of the stress path induced by the excavation and filling process. Examples of such stress path are illustrated here for points along the VCL of a single stope and of the first backfilled stope. The stress path

is presented in the *t*-*s* plane (Wood, 1990; also known as the q-p plane in 2D; e.g. Bowles, 1988; McCarthy, 2007) for 9 steps, starting with step 0 corresponding to the end of filling of the first stope (similar to a single stope) followed by 8 steps for the excavation and filling of the second stope. The two stress coordinates used to represent the stress path are defined as:

$$t = (\sigma_1 - \sigma_3)/2 \quad (4\text{-}5)$$

$$s = (\sigma_1 + \sigma_3)/2 \quad (4\text{-}6)$$

Where σ_1 and σ_3 are the major and minor principal stresses, respectively. The Coulomb criterion (in 2D) can then be expressed from these two stress variables as follow, for a cohesionless backfill (Wood, 1990):

$$t = s.sin\,\phi \quad (4\text{-}7)$$

This linear yield criterion is also shown with the results presented below. The stress paths obtained for three points located along the VCL of the first backfilled stope have been computed; these are point 1 (*h* = 9 m from the top of the backfill), point 2 (*h* = 18 m), and point 3 (*h* = 27 m). The stress path was monitored from step 0 that represent the condition at the end of filling of the first stope (similar to a single backfilled stope), followed by the excavation (4 steps) and filling (4 steps) of the second stope.

Figure 4-21 shows the stress path for the three points. Point 3 is used as an example to describe the process. At step 0, the stress state (*s* = 140 kPa, *t* = 63 kPa) is located below the yield criterion. With the first excavation step (of the second stope), there is a change in the stress state, with the mean stress increasing (*s* = 190 kPa) and the deviatoric stress decreasing (*t* = 17 kPa). For step 2, both the mean and deviatoric stresses are reduced (in comparison with steps 1 and 0). The stress state is then approaching the yield criterion. For the third and fourth steps (end of excavation) and fifth step (first step of filling), the backfill is loaded, both the mean and deviatoric stresses are increasing. During these steps, the stress path follows the linear yield criterion. During the last three filling steps (backfilling of the second stope), the deviatoric stress at point 3 (first stope) is reduced, while the mean stress *s* tends to increase, hence moving away from the yield criterion. This path is in general agreement with the evolution of the horizontal and vertical stresses along the VCL shown in Figure 4-3.

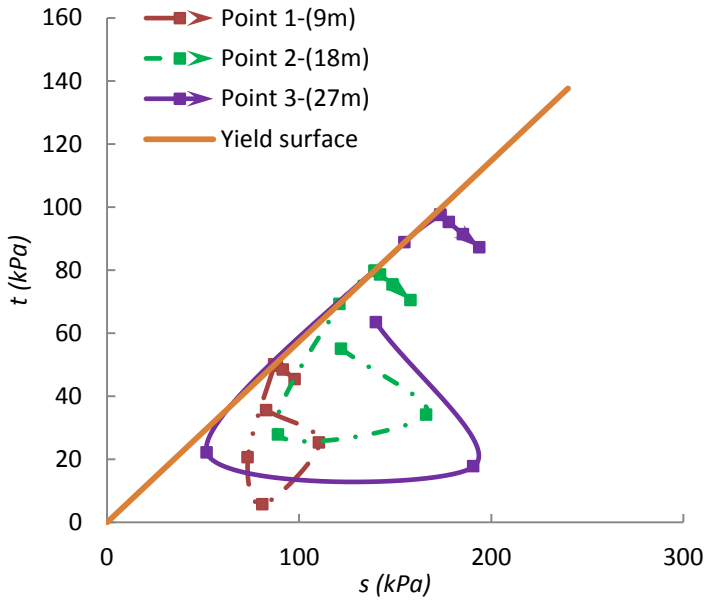

Figure 4-21: Stress path obtained in three different locations (z = 9 m, 18 m, 27 m from the top) along the VCL of the first backfilled stope during excavation and filling of the second stope

Figure 4-21 also shows the stress path at points 1 and 2. It is seen that although the stress magnitudes are different for the 3 points, the tendencies are the same for the paths. However, the intersection of the stress path with the yield surface does not always occur at the same time (step), indicating that different points along the VCL (and elsewhere) may respond somewhat differently during excavation and filling of the second stope.

Figure 4-22 shows relationships between the deviatoric stresses and the horizontal strains for the same three points in the first backfilled stope. The results indicate that the backfill in the stope is first unloaded (reduction of t), producing a positive (compression) strain, and then reloaded during the last excavation step and the four filling steps (for the second stope), producing an extension strain in the backfill.

It is also worth noting that such type of response, with yielding and unloading of the backfill in the first stope is different than the one observed for a single stope and for the second backfilled stope during the excavation and filling steps.

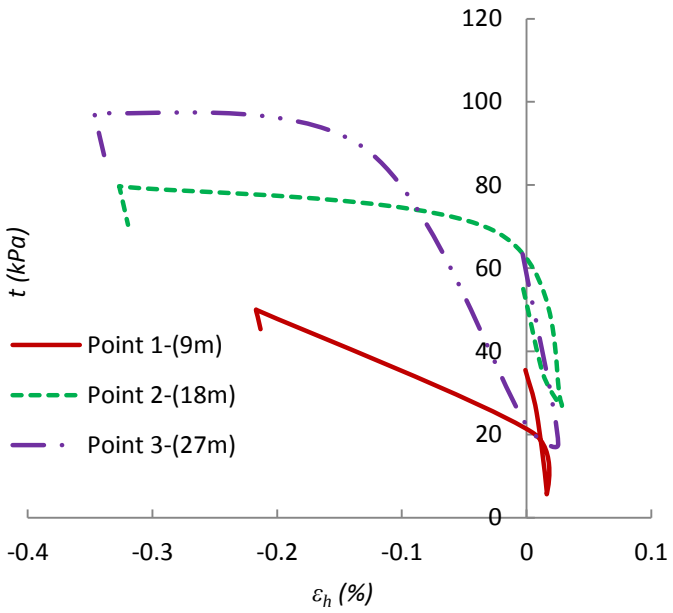

Figure 4-22: Deviatoric stresses and the horizontal strains ε_h obtained in three different locations along the VCL of the first backfilled stope during excavation and filling of the second stope

4.7.4 Final remarks

The simulations results presented here show that the response of backfill in neighboring (multiple) backfilled stopes can be different, and sometimes much more complex, than that obtained for isolated stopes.

Additional factors can also influence the stress state in stopes, such as the dilatancy angle ψ' and the generation and dissipation of pore water pressures in (initially) saturated backfills; these issues have been considered in other publications from the authors' group (El Mkadmi et al. 2011a, 2011b, 2014). The ongoing program also include simulations of adjacent stopes in 3D (instead of plane strain conditions) and the removal of one the walls of the stope containing a cemented backfill; these issues are addressed in Chapter 6 (Falaknaz, 2014).

The simulations conducted above have been based on the simplified assumption of an elastic behavior for the rock mass. This assumption may not be representative of actual behavior, particularly under large naturel (or induced) stresses or for relatively weak (or fractured) rock masses. In such cases, the response of the rock mass is better represented by an elasto-plastic model (Brady and Brown, 2004; Hoek, 2007). This in turn may influence the interaction between

the rock mass and backfill, as shown by complementary simulations that have recently been conducted. These calculations have shown that larger displacements can occur along the walls of stopes in such elasto-plastic media, which in turn affect the stresses in the backfill; more details on this aspect are provided in Chapter 5 (Falaknaz, 2014).

The numerical investigations results shown here indicate the creating a new stope near an existing backfilled opening may significantly influence the stress state in the latter. Unfortunately, there is no actual experimental data available (to the authors knowledge) to validate the simulations results. Therefore, additional work is needed to conduct measurements that could be used to calibrate and validate results from such numerical simulations; this is one of the main challenges ahead which will have to be addressed in future investigations.

4.8 Conclusion

This paper illustrates the main results of a numerical investigation on the behavior of two neighboring backfilled stopes aimed at evaluating the effect of various factors on the stresses and displacements in the opening; the main factors considered here include the rock mass properties, stopes geometry, depth and distance between the openings, and the excavation and filling sequence. The results indicate that the arching effect often dominates the stress distribution in the stopes. However, the stress distributions are different in the two stopes, and also distinct from those obtained for a single stope. The results presented here indicate that the second backfilled stope tends to behave in a manner similar to a single stope, where arching effects often dominate the stress distribution. The simulated horizontal and vertical stresses distributions in the second stope are in a good agreement with those calculated with the analytical solution developed by Li and Aubertin (2008) for a single stope. The stress distributions can however be quite different between the two stopes, as the stresses in the first backfilled opening may be significantly influenced by the excavation and filling of the neighboring stope. The results specifically show how the stress state in the first backfilled opening varies during creation of the second one, as a function of various factors, including, the rock mass modulus. A lower elastic modulus leads to larger stresses in the first backfilled stope due to larger horizontal displacements δ_h of the walls. The effect of a low rock mass stiffness can be amplified by greater depth and larger naturel stresses. The stresses in the first backfilled stope are not very sensitive to a variation of the earth reaction coefficient K_r in the rock or the rock mass modulus E_r, at least when the simulations are

conducted for an elastic rock mass. Results can however be quite different when the rock mass behaves in an elasto-plastic manner; in such cases, the stresses in the first backfilled stope may become much more sensitive to these parameters, as shown in the complementary calculations performed in Chapter 5 (Falaknaz, 2014).

The results also show that an increase in the pillar width D between the two stopes influence the stress state within the stopes, particularly when a cohesive backfill is used.

Another consideration addressed here is the effect of using a relationship between Poisson's ratio, v_b, and the internal friction angle, ϕ', to establish the backfill properties. According to Jaky's (1948) well known equation, these two parameters can be related through the earth reaction coefficient at rest, K_o. The use of this relationship between v_b and ϕ' may influence the stress distribution in the stopes, but this effect is generally small.

The stress distribution within backfilled stopes is also assessed in terms of the stress path induced by the excavation and filling process. It is shown that the stress paths obtained for different points along the VCL of the first backfilled stope can involve some loading and unloading (in terms of the mean and deviatoric stresses) and intersect the yield surface at various stages. Such unloading and reloading of the backfill affect its response, according to the induced stress state and yielding condition. This type of behavior is different from the one observed for a single stope and for the second backfilled stope during the excavation and filling steps.

Acknowledgements

The authors acknowledge the financial support from NSERC, from the partners of the Industrial NSERC Polytechnique-UQAT Chair on Environment and Mine Wastes Management and from the Research Institute on Mine and the Environment (RIME UQAT-Polytechnique).

References

Aubertin, M., Li, L., Arnold, S., Belem, T., Bussiere, B., Benzaazoua, M., and Simon, R. (2003). Interaction between backfill and rock mass in narrow stopes. *In* soil and rock America 2003, Vol. 1, pp. 1157–1164.

Aysen, A. (2002). Soil mechanics - Basic concepts and engineering applications. Lisse: Balkema.

Belem, T., Benzaazoua, M., and Bussière, B. (2000). Mechanical behavior of cemented paste backfill. *In* proceedings of 53th Canadian geotechnical conference, Montreal, Canada, Vol. 1, pp. 373-380.

Belem, T., Harvey, A., Simon, R., and Aubertin, M. (2004). Measurement and prediction of internal stresses in an underground opening during its filling with cemented fill. *In* Proceedings of the 5th international symposium on ground support in mining and underground construction, 28–30 September 2004, Perth, Western Australia. Edited by E. Villaescusa and Y. Potvin.Tayler and Francis Group, London, Australia. pp. 619–630

Benzaazoua, M., Fall, M., and Belem, T. (2004). A contribution to understanding the hardening process of cemented paste fill. Miner. Eng. **17**(2): 141-152.

Benzaazoua, M., Bussiere, B., Dermers, I., Aubertin, M., Fried, E., and Blier, A. (2008). Integrated mine tailings management by combining environmental desulphurization and cemented paste backfill: Application to mine Doyon, Quebec, Canada. Minerals Engineering. **21**(4): 330-340.

Blight, G.E. (1986). Pressure exerted by materials stored in silos. Part I: coarse materials. Géotechnique, **36**(1): 33-46.

Bowles, J.E. (1988). Foundation analysis and design. McGraw- Hill.

Caceres, C. (2005). Effect of backfill on longhole open stoping, MASc Thesis. Mining Engineering, University of British Columbia, 139 pp.

El Mkadmi, N., E. M., Aubertin, M., and Li, L. (2011a). The effect of transient drainage on the tress state in backfilled mine stopes. *In* proceeding 2011 Pan-Am CGS Geotechnical Conference, University of Toronto, #1139.

EL Mkadmi, N., Aubertin, M., and Li, L. (2011b). Numerical analysis of the early response of paste backfill in a vertical stope. Mines without borders, *In* proceedings of mines without Borders, CIM conference and exhibition, Montréal, 22–25 May 2011. Canadian institute of mining, metallurgy and petroleum (CIM), Montréal, Que. pp. 68–78.

EL Mkadmi, N., Aubertin, M., and Li, L. (2014). Effect of drainage and sequential filling on the behavior of backfill in mine stopes. Canadian Geotechnical Journal, **51**(1): 1-15.

Emad, M.Z., Mitri, H. and Kelly, C. (2014). Effect of blast-induced vibrations on fill failure in vertical block mining with delayed backfill. Canadian Geotechnical Journal, 2014, **51**(9): 975-983.

Fahey, M., Helinski, M., and Fourie, A. (2009). Some aspects of the mechanics of arching in backfilled stopes. Canadian Geotechnical Journal, **46**, pp. 1322-1336.

Falaknaz, N., Aubertin, M. and Li, L. (2013). Numerical investigation of the stress state in adjacent backfilled mine stopes. *In* proceedings of the Canadian geotechnical conference, GeoMontreal, Montreal, Canada.

Jaky, J. (1948). Pressure in silos. *In* proceedings of the 2nd International conference on soil mechanics and foundation engineering, Rotterdam: Balkema, Vol. 1, pp. 103-107.

Handy, R., and Spangler, M. (2007). Geotechnical engineering: Soil and Foundation principles and practice, 5th Ed. McGraw Hill., New York.

Hassani, F., and Archibald, J. (1998). Mine backfill. CD-Rom, Canadian institute of mine, metallurgy and petroleum. Montreal, CIM.

Hassani, F., Mortazavi, A., Shabani, M. (2008). An investigation of mechanisms involved in backfill-rock mass behaviour in narrow vein mining. The Journal of Southern African Institute of Mining and Metallurgy 108, 463-472.

Helinski, M., Fahey, M., and Fourie, A. (2007). Numerical modeling of cemented mine backfill deposition. Journal of Geotechnical and Geoenvironmental Engineering., **133**(10): 1308-1319.

Helinski, M., Fahey, M., and Fourie, A. (2010). Coupled two-dimensional finite element modeling of mine backfilling with cemented tailings. Canadian Geotechnical Journal, **47**(11): 1187-1200.

Hoek, E., Carranza-Torres, C.T., and Corkum, B. (2002). Hoek-Brown failure criterion 2002 edition. *In* proceeding of 5th North American rock mechanics symposium, Toronto. **1**: pp. 267-273.

Hustrulid, W., Qianyuan, Y., and Krauland, N. (1989). Modeling of cut and- fill mining systems, Näsliden revisited. Innovation in mining backfill technology, F. P. Hassani, M. J. Scoble, and T. R. Yu, eds., Balkema, Rotterdam, The Netherlands, pp. 147–164.

Itasca. (2000). FLAC version 5.0. Users manuals. ITASCA consulting group, Thresher square East, 708 South Third Street, Suite 310, Minneapolis, Minnesota, USA.

Knutsson, S. (1981). Stresses in the hydraulic backfill from analytical calculations and in-situ measurements. *In* proceedings of conference on application of rock mech. to cut and fill mining, institution of mining and metallurgy, London, pp. 261–268.

Li, L., and Aubertin, M. (2008). An improved analytical solution to estimate the stress state in subvertical backfilled stopes. Canadian Geotechnical Journal, **45**(10): 1487-1496.

Li, L., and Aubertin, M. (2009a). Numerical investigation of the stress state in inclined backfilled stopes. International Journal of Geomechanics, **9**(2): 52-62.

Li, L., and Aubertin, M. (2009b). A three-dimensional analysis of the total and effective stresses in submerged backfilled stopes. Geotechnical and Geological Engineering, **27**(4): 559-569.

Li, L., Aubertin, M., Simon, R., Bussiere, B., and Belem, T. (2003). Modelling arching effects in narrow backfilled stopes with FLAC. *In* proceedings of the 3th International FLAC symposium, 21-24 October 2003, Sudbury, Ontario, Canada, pp. 211-219.

Li, L., Aubertin, M., and Belem, T. (2005). Formulation of a three dimensional analytical solution to evaluate stress in backfilled vertical narrow openings. Canadian Geotechnical Journal, **42**(6): 1705-1717.

Li, L., Aubertin, M., Shirazi, A., Belem, T., and Simon, R. (2007). Stress distribution in inclined backfilled stopes. MINEFILL 2007, April 29- May 2, 2007, Montreal, Quebec, Canadian institute of mining, metallurgy and petroleum (CIM), #2510.

Li, L., Aubertin, M., and Shirazi, A. (2010). Implementation and application of a new elasto-plastic model based on a multiaxial criterion to assess the stress state near underground openings. ASCE International Journal of Geomechanics, **10**(1): 13-21.

Marston, A. (1930). The theory of external loads on closed conduits in the light of latest experiments. Bulletin 96, Iowa engineering experiment station, Ames, Iowa.

McCarthy, D.F. (1988). Essentials of soil mechanics and foundations: Basic geotechnics. 4th edition, Prentice Hall.

Pirapakaran, K. (2008). Load-deformation characteristics of minefills with particular reference to arching and stress developments. PhD Thesis. James Cook University, Australia.

Pirapakaran, K., and Sivakugan, N. (2007). Arching within hydraulic fill stopes. Geotechnique and Geological Engineering, **25**(1): 25-35.

Potvin Y, Thomas E, and Fourie A. (2005). Handbook on mine fill. Australian Centre for Geomechanics. ISBN 0-9756756-2-1.

Singh, S., Shukla, S. and Sivakugan., N. (2011). Arching in inclined and vertical mine stopes. Geotech. Geo. Eng. J. **29**(5): 685-693. doi:10.1007/s10706-011-9410-4.

Sivakugan, N., Widisinghe, S., and Wang, V. (2014). Vertical stress determination within backfilled mine stopes. International Journal of Geomechanics, **14**(5): 06014011.

Ting, C.H., S.K. Shukla, and N. Sivakugan. (2011). Arching in soils applied to inclined mine stopes. Int. J. Geomech. **11**(1): 29-35.

Ting, C.H., Sivakugan, N. Read, W., and Shukla, S.K. (2014). Analytical expression for vertical stress within an inclined mine stope with non-parallel walls. Geotech. Geol. Eng. **32**: 577-586.

Thompson, B.D., Bawden, W.F., and Grabinsky, M.W. (2011). In Situ monitoring of cemented paste backfill pressure to increase backfilling efficiency. CIM J. **2**(4):1-10.

Thompson, B., Bawden, W., and Grabinsky, M. (2012). In situ measurements of cemented paste backfill at the Cayeli Mine. Canadian Geotechnical Journal, **49**, pp. 755–772.

Wood, D. (1990). Soil behavior and critical state soil mechanics. Cambridge university press. ISBN 0-521-33782-8.

Veenstra, R. (2013). A design procedure for determining the in situ stresses of early age cemented paste backfill. PhD Thesis, University of Toronto, Canada.

Veenstra, R.L., Grabinsky, M.W., and Bawden, W.F. (2013). An Examination of the Failure Mechanisms in Modeled Cemented Paste Backfill, World Mining Congress, Montreal. 11-15 August 2013.

CHAPTER 5 ARTICLE 3: EVALUATION OF THE STRESS STATE IN TWO ADJACENT BACKFILLED STOPES WITHIN AN ELASTO-PLASTIC ROCK MASS

Nooshin Falaknaz, Michel Aubertin, and Li Li

This article was submitted to Geotechnical and geological Engineering journal, Submitted in Jul 2014, under revision following comments from reviewers.

Abstract: Backfill is used in the mining industry to improve the stability of underground openings and reduce the environmental impact due to the surface disposal of mine wastes. A critical issue for the design of backfilled stopes is the determination of the stress state in the backfill and surrounding rock mass. In recent years, much work has been conducted to assess the stresses in isolated backfilled stopes. Recent work performed by the authors indicates that the stress distribution in stopes may also be affected by the excavation of multiple openings. So far, simulations of adjacent stopes have been based on an elastic behavior for the rock mass, which may not reflect its actual response (especially under large stresses). This paper presents key results obtained from numerical simulations of two neighboring backfilled stopes excavated in sequence in an elasto-plastic rock mass. The simulations results illustrate the combined effects of the non-linear rock mass response and of other characteristics including stopes geometry (size and spacing) and depth, natural stress state, and backfill properties. These results indicate that, although arching effects tend to develop in all narrow stopes, the stress distribution in adjacent openings can be quite different for elastic or elasto-plastic rock mass behavior. The results presented here also illustrate the similarities and differences between the behavior of a single backfilled stope and of two adjacent stopes, depending on the rock mass properties and overall characteristics of the models.

Keywords: Two adjacent stopes; Mine backfill; Rock mass; Stresses; Strains; Wall displacements; Numerical modeling; Elastic; Elasto-plastic behavior.

5.1 Introduction

Backfills are commonly used in underground mine openings to improve ground stability and to reduce the amount of mining wastes disposed on the surface (e.g. Hassani and Archibald 1998; Benzaazoua et al. 2004). A critical issue for the design of backfilled stopes is a good understanding of the interaction that develops between the backfill and the surrounding rock mass (Aubertin et al. 2003; Li et al. 2003).

The response of a backfill can vary widely depending on its basic characteristics, including the solid grains properties, type and proportion of binder, and water quality. The complex behavior of mine backfill has been investigated through various laboratory and field studies (e.g. Boumiz et al. 1996; Ouellet et al. 1998; Belem et al. 2000; Potvin et al. 2005; Yilmaz et al. 2009; Thompson et al. 2012). These investigations have shown that, in most cases, there is a very large difference in stiffness between the backfill and surrounding rock mass (especially for base and precious metals mining). In turn, this may generate stress redistribution due to the interaction between the two media, which tends to reduce the pressures in narrow backfilled stopes. This phenomenon, often referred to as an arching effect (e.g. Knutsson, 1981; Mitchell et al. 1982; Pierce, 1997; Grice, 1998; Li et al. 2003), is well known in geotechnique (Handy, 1985; Harrop-Williams, 1989).

The stress distribution in stopes needs to be properly evaluated as it affects the backfilling operations and design of barricades constructed in drifts. In recent years, analytical solutions have been developed and applied to assess the stress state in single (isolated) backfilled stopes (Hustrulid et al. 1989; Aubertin et al. 2003; Li et al. 2003; Pirapakaran, 2008). Additional studies include specific developments to analyse particular conditions such as three-dimensional configurations (Li et al. 2005), varying stresses across the stope width (Li and Aubertin, 2008, 2010), and the effect of pore water pressures (Li and Aubertin 2009a, 2009b). These solutions have been validated, at least in part, using numerical modeling (Li et al. 2007; Pirapakaran and Sivakugan 2006; Sing et al. 2011; El Mkadmi et al. 2014) and experimental results (Li et al. 2005; Li and Aubertin, 2009a).

More recently, the stress state in adjacent backfilled stopes has also been investigated, considering the influence of different parameters such as fill properties, stope geometry and natural stress state in the rock mass (Falaknaz et al. 2013, 2014). These calculations have

essentially been based on the simplified assumption of a linear elastic behavior for the rock mass. This assumption may not be representative of the rock mass behavior, particularly under large naturel (or induced) stresses and for relatively weak (or fractured) rock. In such cases, the response of the rock mass is better represented by an elasto-plastic model (Brady and Brown, 2004; Hoek, 2007). This in turn may influence the interaction between the rock mass and backfill.

This paper presents key results from numerical simulations conducted with a non-linear model for the rock mass behavior. These calculations are aimed at analysing the response of two neighboring stopes created one after the other. The results include a comparison of the stresses, displacements and strains in the backfill for various conditions, taking into account various influence factors, including stopes geometry and distance, depth and natural stresses, backfill properties and excavation (and filling) sequence.

5.2 Conceptual models and rock mass behavior

The commercial code FLAC (Itasca, 2002) has commonly been used to assess the stresses in and around underground openings (Li et al. 2003, 2007; Pirapakaran and Sivakugan, 2006; Li and Aubertin, 2009a; Sivakugan et al. 2013; Veenstra, 2013). This is a two-dimensional (plane strain) finite difference program that uses an explicit Lagrangian calculation scheme and a mixed-discretization zoning technique. This code is well adapted to simulate the response of geo-engineering structures under stage construction.

Early in this investigation, simulations with different mesh sizes and boundary locations were conducted to identify valid models and stable results. Quadrilateral elements are used for the mesh, with coarser elements in the rock region far from the backfilled stopes and a finer mesh inside and near the stopes (including the plastic zone for the rock mass). The stopes geometry and overall model size are two key factors that affect the number of elements in the two stopes models. For each model, the location of the external boundaries was determined so that it would not influence the calculation results; the model size may thus vary with the stopes dimensions and properties of the rock mass (see details in Falaknaz, 2014; Appendix A).

The stress state in neighboring stopes is known to be related to the backfill and rock mass properties. In numerical simulations, the fill material is typically represented by an elasto-plastic

constitutive model such as the Mohr-Coulomb (Li et al. 2003; Li and Aubertin, 2009a), Modified Cam-Clay (El-Mkadmi et al. 2014) or other formulations (Li et al. 2010). As for the rock mass behavior, most simulations previously performed (by the authors and other groups) have considered it as linear elastic. However, such linear elastic response is not always appropriate when analyzing underground openings, particularly in the case of relatively fractured rock masses or for openings at large depth. In these cases, a nonlinear model is deemed preferable. In practice, an elasto-plastic formulation with the Mohr-Coulomb criterion is often considered for engineering applications (e.g. Brady and Brown, 2004; Hoek, 2007; Kaiser and Kim, 2008). This approach is adopted here to assess the response of backfilled stopes and of the surrounding rock mass, considering two conditions for the latter based on the rock mass rating (RMR) value (Bieniawski, 1989), i.e. good (RMR = 80) and fair (RMR = 60), as summarized in Table 5.1.

The properties of the filling material are provided below, with the other characteristics of the models used for simulating the response of the two backfilled stopes excavated and filled in sequence. The main results are also compared with those obtained for a single backfilled stope, which serves as a reference case.

5.3 Stress distribution in an isolated stope

Figure 5-1(a) shows a schematic view of the conceptual model that simulates a typical vertical backfilled stope (Case 0 in Table 5.2). The rock mass is considered homogeneous, isotropic and linearly elastic for Case 0a, with the following parameters: E_r = 30 GPa (Young's modulus), μ_r = 0.3 (Poisson's ratio), γ_r = 27 kN/m^3 (unit weight). For Case 0b, the rock mass follows an elasto-plastic behaviour, based on the Mohr-Coulomb yield condition; the following parameters have been used for the good quality rock mass: E_{rm} = 30 GPa (deformation modulus), μ_{rm} = 0.3, γ_{rm} = 27 kN/m^3, c_{rm} = 2 MPa (cohesion), ϕ_{rm} = 45° (friction angle) (based in part on values suggested by Hoek et al. 2002; Hoek 2007; see Table 5.1).

The properties of the backfill used in the numerical analyses have been adapted from laboratory tests results (mainly taken from Belem et al. 2000 and Veenstra 2013). As mentioned above, the simulated fill behaviour also follows an elasto-plastic constitutive law with the Mohr-Coulomb yield criterion. For Cases 0a and 0b, the backfill properties are controlled by the values of parameters E, μ, γ, ϕ, and c' given in Table 5.2 (and with a dilatancy angle $\psi' = 0$, i.e. a non-

associated flow rule). This reference vertical stope is 6 m wide and 45 m high, with 0.5 m of void space left at the top of the backfill.

The reference stope width *B* is 6 m, and it is filled to a height h of 45 m, with 0.5 m of void space left at the top (i.e. total height of the opening H = 45.5 m). The natural in-situ vertical stress σ_v in the rock mass is given by the overburden pressure for a depth *z* of 400 m (at the bottom of the stope), while the natural in-situ horizontal stress $\sigma_h = 2\ \sigma_v$ (based on a typical situation for the Canadian Shield; e.g. Arjang 2004). The conditions imposed around the outer perimeter of the model prevent horizontal displacements, but allow vertical displacements along the side boundaries; there are no vertical displacements at the bottom of the model. The number of elements is 104×262 for Cases 0a and 0b. As the sidewalls of stopes created by blasting are typically rough, shearing tends to occur in the backfill itself; therefore, the model does not contain (planar) interface elements between the backfill and rock mass.

The simulation initially involves applying gravity to the model. Following Li and Aubertin (2009a), the single stope is then excavated instantly and the backfill is placed in four layers after the rock region has reached stress-strain equilibrium. The stress distribution and wall convergence are monitored during the excavation and filling of the stope.

Figure 5-1(b) show the distribution of the stresses in the backfilled stope for Case 0a (EL model) and Case 0b (EP model) at the end of filling. These results show that the arching effect is well developed in both cases (as was expected from previous analytical and numerical results obtained by Li et al. 2003, 2005, for an elastic rock mass). The results shown here also indicate that the stresses are distributed in a similar manner for the elastic rock mass and the elasto-plastic rock mass (Fig. 5-1b), for the conditions simulated here.

Figure 5-2 shows the stress distributions along the vertical center line (VCL) and along the walls for Case 0a (elastic rock mass, EL) and Case 0b (elasto-plastic rock mass, EP). The figure also shows the overburden stresses in the backfilled stopes (with $\sigma_h = K_o\ \sigma_v$; with K_o= 1-sin ϕ') and the stresses obtained from the analytical solution proposed by Li and Aubertin (2008), which can be expressed as follows for the vertical and horizontal stresses.

$$\sigma_{vx} = \gamma B \left(\frac{1-\exp\left(-\frac{2K\,h\,tan\phi'}{B(1-DF)}\right)}{2K\,tan\phi'} \right).\left[1 - a\left(\frac{x}{B}\right)^b\right] \qquad (5\text{-}1)$$

$$\sigma_h = \gamma B \left(\frac{1-\exp\left(-\frac{2K\,h\,tan\phi\prime}{B(1-DF)}\right)}{2tan\phi\prime} \right) \quad (5\text{-}2)$$

In these equations, B is the stope width (m); K is the earth pressure coefficient in the backfill, which is taken as Rankine's active coefficient [$K = K_a = \tan^2(45° - \phi'/2)$]; h is the depth (m) in the backfill (h varies from 0 at the backfill surface to 45 m at the base of the stope); x is the distance (m) from the center line of the stope ($|x| \leq \frac{B}{2}$); a and b are parameters that control the vertical stress distribution along the width; DF is the distribution factor defined as follows:

$$DF = \frac{a}{2^b(b+1)} = \frac{2^{\left(1-\lambda_1\frac{H}{B}\right)}tan^{-\lambda_2}(\phi_0+\phi\prime)}{2^b(b+1)} \quad (5\text{-}3)$$

The reference friction angle ϕ_0 =50°, while the distribution parameters are given as follows: $\lambda_1 = 0.02$, $\lambda_2 = 0.1$, and b = 3 (for all calculations). Figure 5-2 indicates that the stresses obtained from the numerical simulation and analytical solution are close to each other. It can also be seen that the stresses along the VCL and walls of the single stope within an elastic (EL) rock mass are almost the same as those obtained for an elasto-plastic (EP) rock mass (Figure 5-2a, 5-2b).

This result was expected because the fill is added after the convergence of the wall (due to excavation) has taken place. Hence, the stresses in this isolated backfilled stope are not significantly affected by the rock mass constitutive behavior (for the conditions imposed here); as will be shown below, this is not necessarily the case for adjacent stopes created in sequence.

5.4 Stress distribution in two adjacent stopes

The following calculations have been conducted for an elastic (EL) and elasto-plastic (EP) rock mass that contains two adjacent stopes created one after the other. Figure 5-3 shows the conceptual model with the two backfilled stopes (Case 1, with characteristics given in Table 5.2). The model external boundaries are located far enough from the openings to avoid influencing the simulations results (as mentioned above; details shown in Appendix A in Falaknaz, 2014); for Case 1b for instance, the boundaries are located 350 m from the stope walls in all directions.

Table 5.1 : Rock mass parameters used in the numerical simulations with the elasto-plastic (EP) model (based on Bieniawski's 1989 RMR characterisation method and on values suggested by Hoek et al. 2002)

Rock type	*UCS_{intact} (uniaxial compressive strength) (MPa)*	*RMR (Rock mass rating)*	*c_{rm} (MPa)*	*ϕ_{rm}(°)*	*E_{rm} (GPa)*	*K_r (= σ_h/σ_v)*
Good	100	80	2	45	30	2
Fair	70-90	60	0.45	40	10	2

Table 5.2 : Backfill properties and stopes characteristics used in the numerical simulations (with H = 45. 5 m, with a void space of 0.5 m; h = 45 m; E = 300 MPa, μ = 0.3, c' = 0, ϕ' = 35°)

Cases	*B* (m)	*E_{rm} (GPa)*	*c_{rm}* (MPa)	*ϕ_{rm}* (°)	*Distance D* (m)	*Depth z* (m)	*K_r* (σ_h/σ_v)
0a, EL model; 0b, EP model (Base Case)	6	30	0, 2	0,45	8	400	2
1a,EL model ; 1b, EP model	6	30	0, 2	0,45	8	400	2
2 (EP model)	18	30	2	45	8	550	2
3 (EP model)	6	30	2	45	24,60	400	2
4 (EP model)	6	30	2	45	8	2000	2
5 (EP model)	6	30	2	45	8	400	1,4
6 (EP model)	6	10	0.45	40	8	400	2

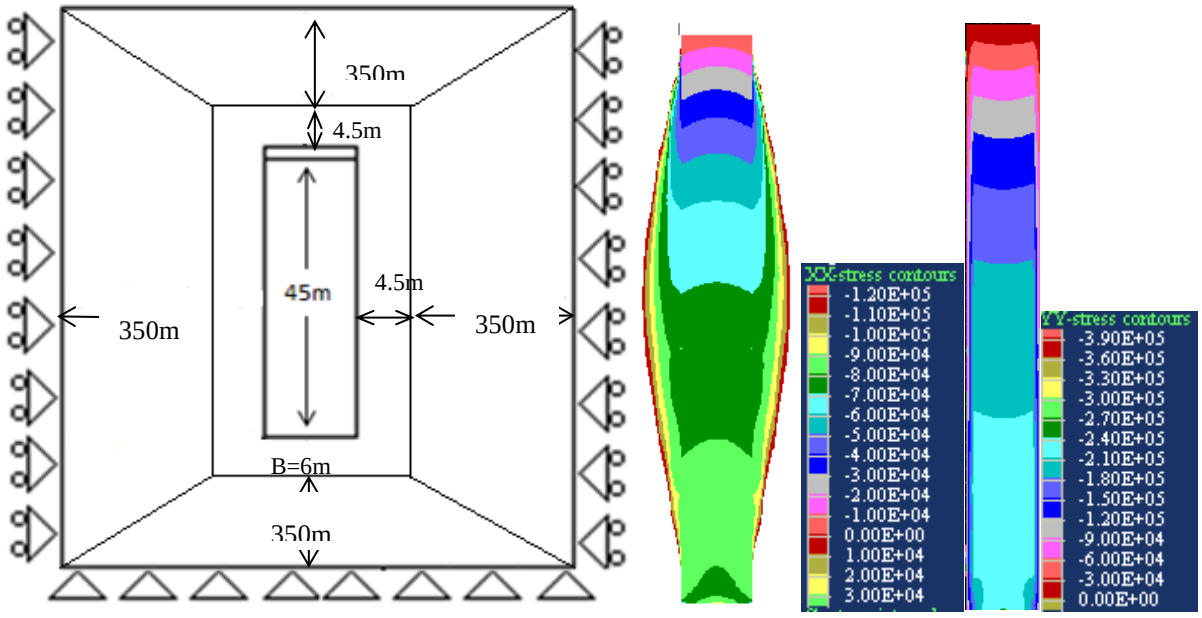

(a) (b

Figure 5-1 : Model of a single backfilled stope (h = 45m) which serves as the base (reference) case (Case 0); size (not to scale) and properties (a); simulated isocontours of horizontal (left) and vertical (right) stresses for (b) an elastic rock mass behavior (EL, Case 0a) and an elasto-plastic rock mass behavior (EP, Case 0b); similar stresses are obtained for the EP and EL models in this case

In the following simulations, the first stope is excavated in one step and the backfill is placed in four layers after the rock mass reaches an equilibrium under the imposed stresses (including rock weight). The second stope is then excavated in four equal steps and filled in four layers. In the case of two neighboring stopes, the stresses, displacements and strains evolve through 9 steps, starting with step 0 at the end of filling (similar to a single stope), followed by 8 steps for the excavation (4 steps) and filling (4 steps) of the second stope.

5.4.1 Stress state

After the first stope is created and filled, the stress distribution is similar to the one shown in Figure 5-1b (isolated stope). The stress distribution then changes with the walls displacement within the first stope when the second stope is excavated (in four steps) and filled (in four layers); these monitored features are presented for simulations conducted with EL and EP rock masses.

Figure 5-4 shows the stress distribution in the backfilled stopes obtained at the end of filling of the second stope (Case 1a, EL; and Case1b, EP).

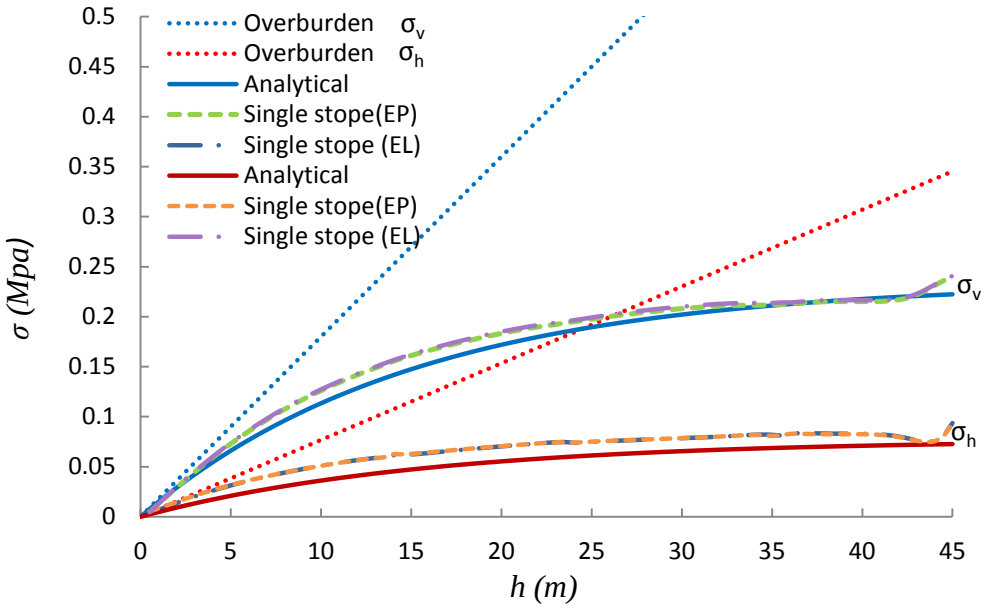

(a)

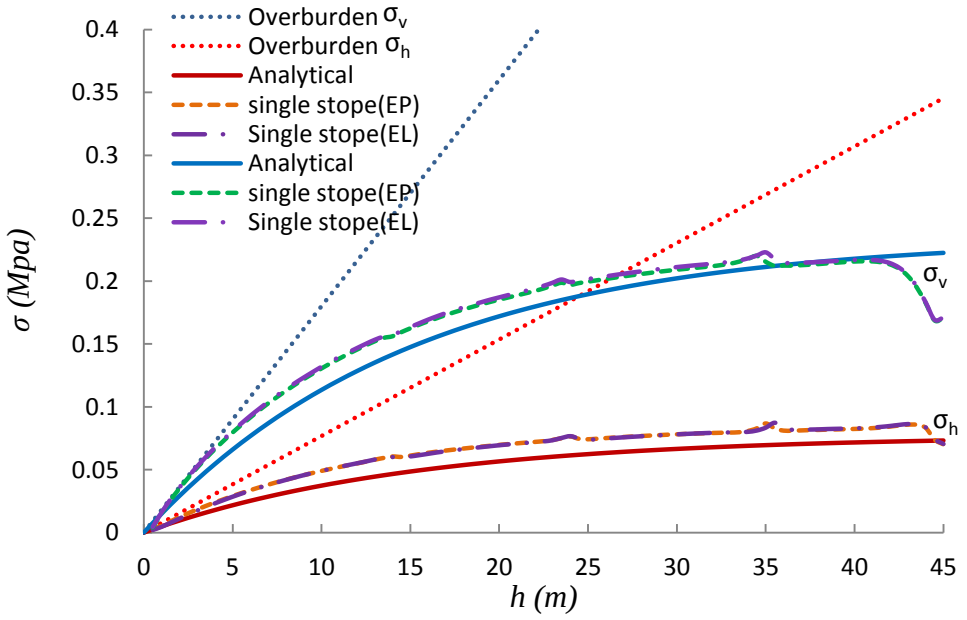

(b)

Figure 5-2: Horizontal and vertical stresses obtained along the (a) VCL and (b) walls of a single stope (Cases 0a, 0b) using the analytical (Eqs. 5-1 and 5-2) and numerical solutions; the overburden pressures (i.e. $\sigma_v = \gamma h$ and $\sigma_h = K_o\, \sigma_v$, with $K_o = 1\text{-}sin\phi'$) at different depth h are also shown

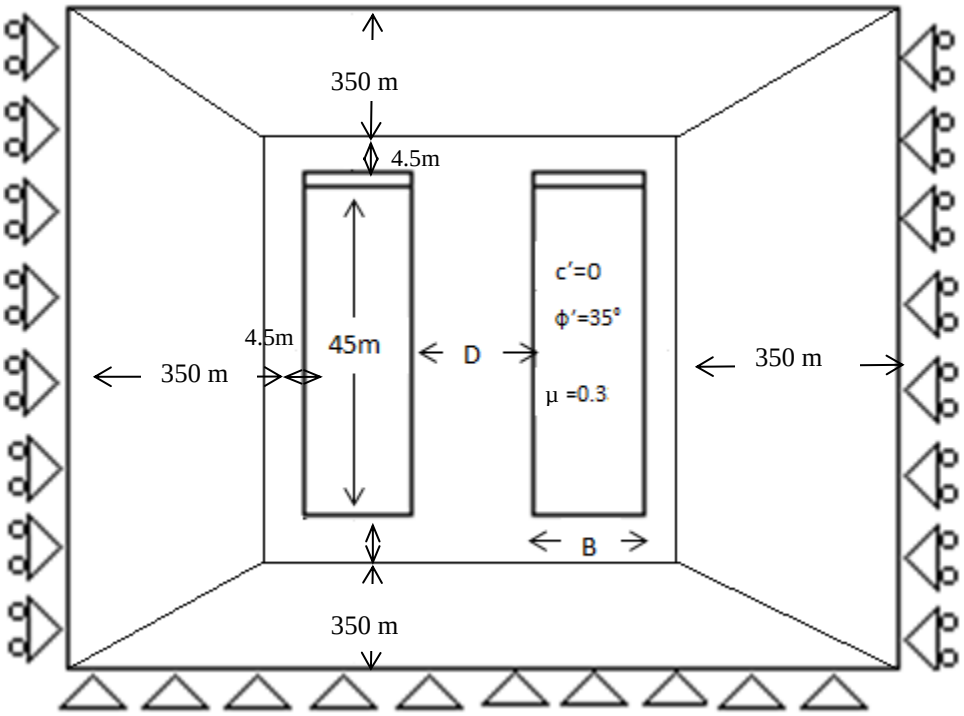

Figure 5-3: Conceptual model of two vertical backfilled stopes, with the boundary conditions, size and properties used for some of the simulations (not to scale)

The results indicate that arching is taking place in both stopes, due to the frictional shear stresses that limit the backfill downward movement. However, the stress distributions are different for the two stopes, and for the two types of rock mass behavior. It is observed that the stresses distributions are somewhat less uniform when the rock mass behaves according to the elasto-plastic model (Fig. 5-4b). Hence, the mechanical response of the rock mass (elastic or elasto-plastic) may influence the stresses in the backfilled stopes. This effect will be shown below to be related to differences in the displacements of the rock walls and strains in the backfill.

Figure 5-5 shows the stress distribution in the first stope along the vertical central line (VCL) for Cases 1a (EL) and 1b (EP) during excavation (Fig. 5-5a) and filling (Fig. 5-5b) of the second stope. The results indicate that there is a significant transfer of the backfill load to the walls, hence reducing the stresses at depth (compared to the overburden pressures shown in Figure 5-2). It is also seen that the horizontal and (to a somewhat lesser extent) vertical stresses obtained using the EP model for the rock mass can be much higher than those obtained using the EL model (especially during the first excavation steps – Fig. 5-5a).

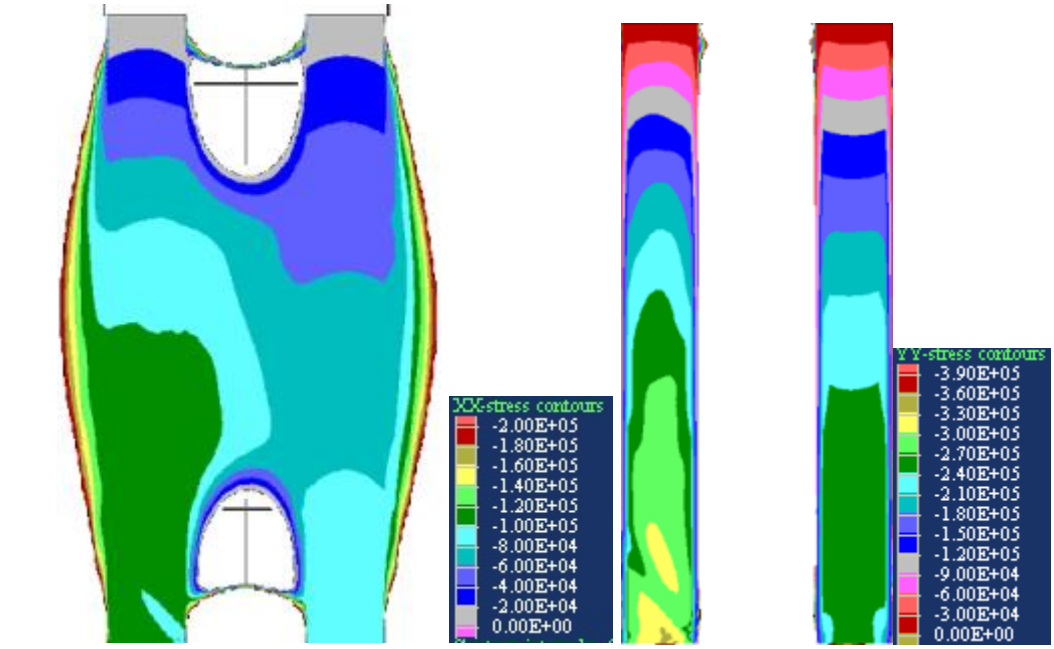

(a)

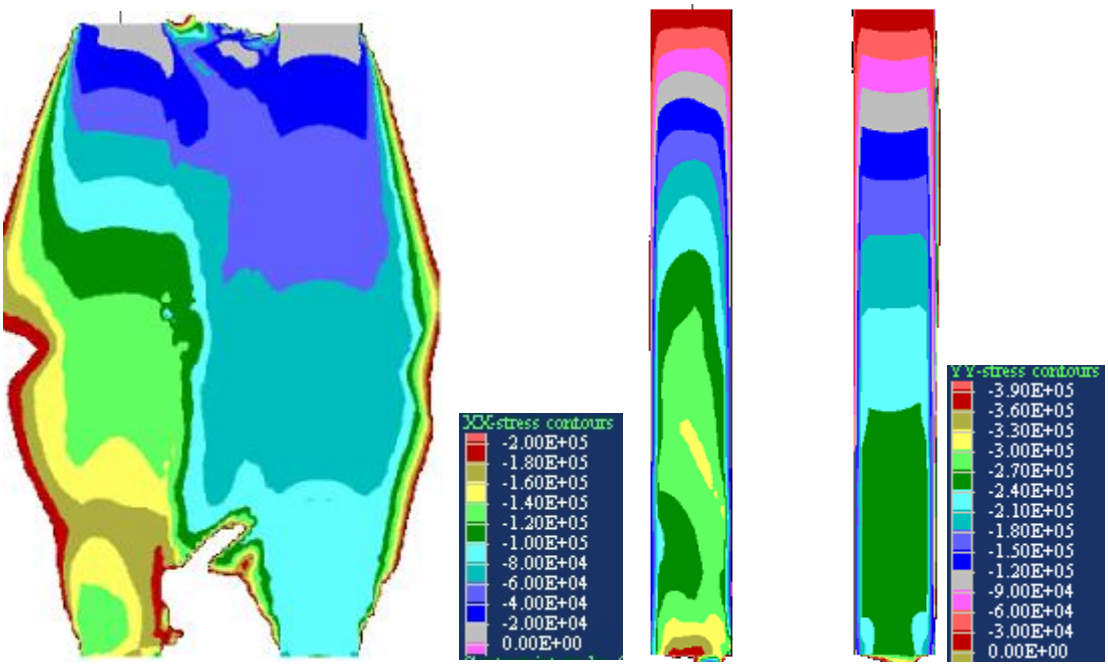

(b)

Figure 5-4: Numerical results showing isocontours of the horizontal (left side) and the vertical (right side) stresses for: (a) an elastic rock mass behavior (EL, Case 1a) and (b) an elasto-plastic rock mass behavior (EP, Case 1b)

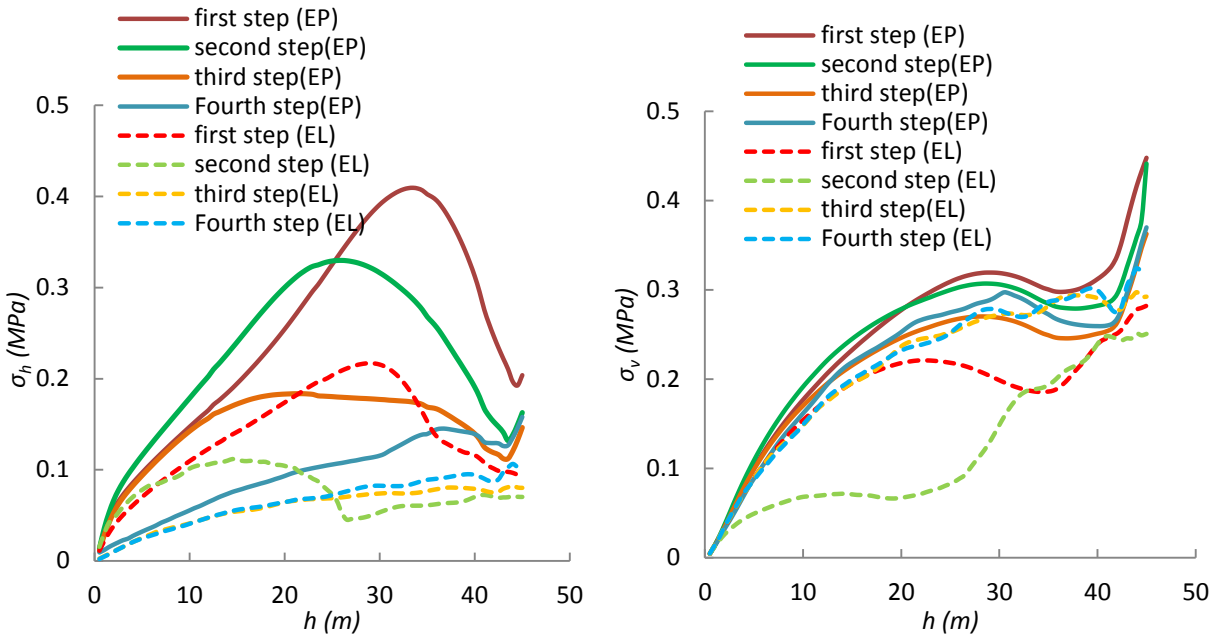

(a)

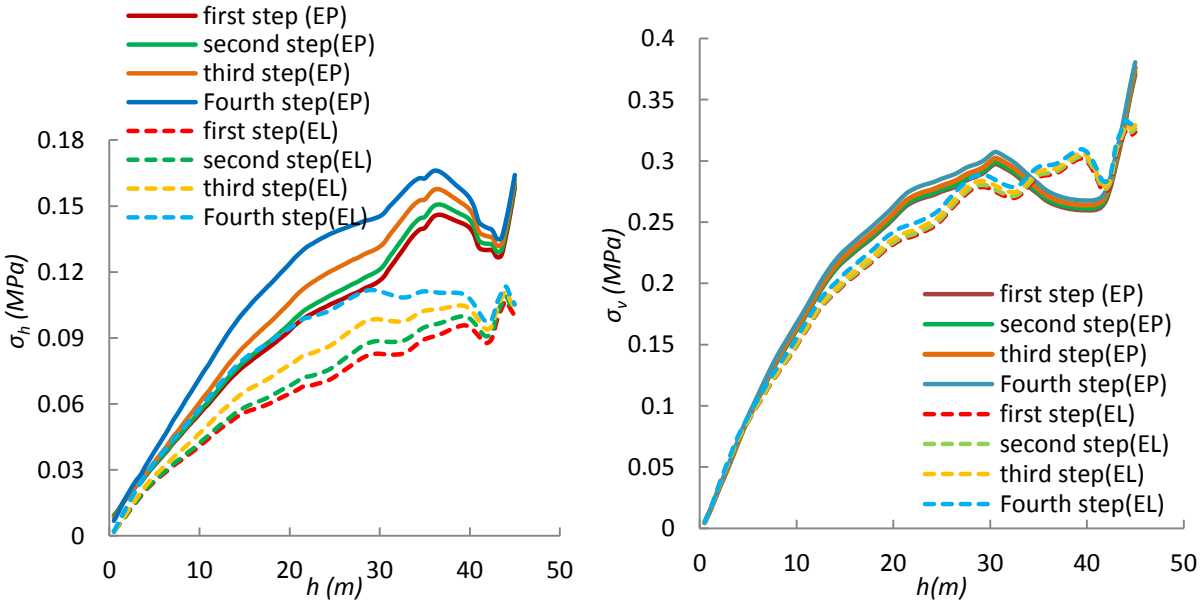

(b)

Figure 5-5 : Horizontal (left) and vertical (right) stress distributions along the VCL of the first backfilled stope for an elastic (EL, Case 1a) and elasto-plastic (EP, Case 1b) rock mass (a) during the 4 steps for excavating the second stope; (b) during the 4 steps for filling the second stope

More specifically, the simulations results indicate that the horizontal stresses σ_h along the VCL in Case 1b (EP model) tend to decrease progressively in the first stope, during the

excavation of the second stope (Figure 5-5a), from a maximum of about 409 kPa (after the first excavation step) to 132 kPa at h = 33 m (for the last step), i.e. a reduction of 68%. For Case 1a (EL model), the reduction of the maximum horizontal stress is about 62% (from 216 kPa for step 1 to 80 kPa for step 4).

The maximum vertical stresses σ_v along the VCL obtained with the EL model increases from 220 kPa (first excavation step) to 240 kPa (step 4), at the stope mid-height, while it decreases from 310 kPa (step 1) to 286 kPa (step 4) at h = 33 m for the EP model, during excavation of the second stope. Despite the divergences observed during the first excavation steps, the vertical stresses obtained for Cases 1a and 1b are quite similar after the fourth step of excavation of the second stope.

Figure 5-5b shows that during backfilling of the second stope, the horizontal stresses obtained with both rock mass models tend to increase, while the vertical stresses decrease. The horizontal stress along the VCL at mid-height increases by about 20%, (from 132 kPa to 158 kPa) for Case 1b (EP model), and it increases by about 30% (from 72 kPa to 103 kPa) for Case 1a (EL model). The vertical stresses along the VCL remain almost unchanged during filling of the second stope with both the EP and EL models.

These results thus indicate that the horizontal stresses in the first stope obtained with both models follow similar trends during excavation and filling of the second stope, although their magnitude is larger for the EP model at the end. The vertical stresses obtained using both EP and EL models are almost similar at the end of the filling steps. The same tendencies are also observed for the stresses along the walls of the first backfilled stope (not shown here; details in Appendix D in Falaknaz, 2014).

Figure 5-6(a) compares the stresses along the VCL in the two adjacent stopes (Case 1b) and the single stope (Case 0b) for an elasto-plastic (EP) rock mass, after excavation of the second stope and after its filling. It can be seen that the final horizontal and vertical stresses along the VCL of the first stope are larger than those obtained for a single stope and for the second backfilled stope. It is also seen that filling of the second stope increases the horizontal stresses by up to 20% near mid-height. This figure also shows that the horizontal stresses for a single stope and the second backfilled stope are almost identical at the end of the filling process for the EP model. The vertical stresses along the VCL of the second stope (Fig. 5-6a, Case 1b, left side) are

somewhat higher than those obtained for a single stope, but smaller than those obtained for the first stope (after complete excavation and filling of the second stope).

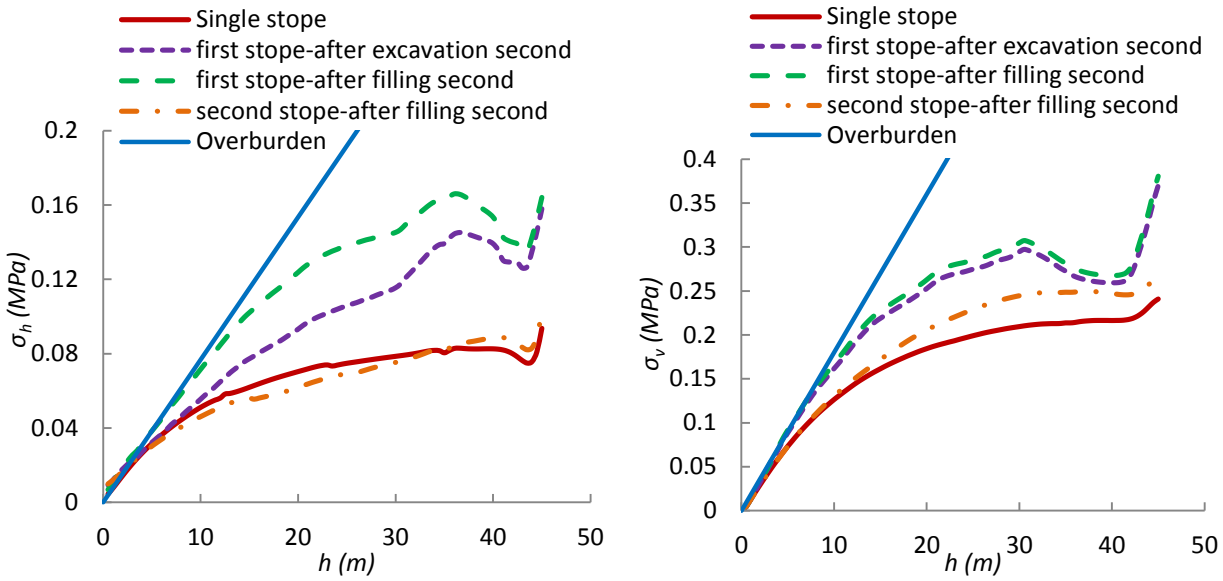

(a)

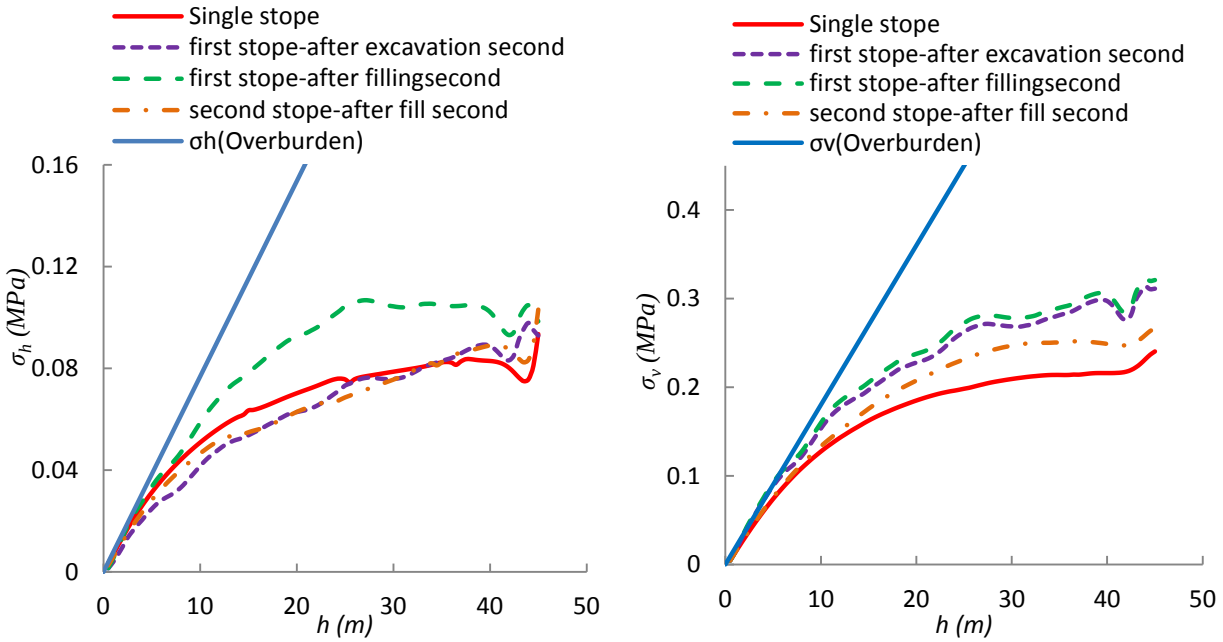

(b)

Figure 5-6: Horizontal (left) and vertical (right) stress distributions along VCL of the first backfilled stope, after excavation and filling of the second stope, for (a) an elasto-plastic rock mass behavior (EP, Case 1b) and (b) an elastic rock mass behavior (EL, Case 1a); the results along the VCL of the single and second stope are also shown

Figure 5-6(b) shows the results obtained with the elastic (EL) rock mass for the single stope (Case 0a) and the two adjacent stopes (Case 1a) after excavation and after filling of the second stope. Comparison with the results obtained with the EP rock mass (Fig. 5-6a) shows the differences between the two simulated cases.

It is seen that for the EL model, the horizontal stresses along the VCL (and walls, not shown here, Appendix D in Falaknaz, 2014) of the first stope remain almost unchanged after excavation of the second stope (Fig.5-6b, right side), while they tend to increase for the EP model (Fig.5-6a, right side).

However, the horizontal stresses for a single stope and for the second backfilled stope are almost identical at the end of the filling process for both EP and EL models. The vertical stresses show quite similar tendencies for the EP and EL models. The difference between the vertical stresses in the first stope (at the end of filling of the second stope) and in the second backfilled stope is more pronounced for the EP model than those for the EL model.

5.4.2 Displacements and strains

Figure 5-7 shows the simulated displacements of the walls of the first stope obtained with the EP and EL models, after excavation and filling of the second stope. It is seen that for the EP model (Case 1b), the horizontal displacements δ_h along the left wall of the first stope (Figure 5-7a), at mid-height, goes from about 17.31 cm (step 0; case similar to a single stope) to 17.51 cm (to the right) during the four excavation steps (of the second stope). Along the right wall of the first stope, the horizontal displacements (Fig. 5-7b) at mid-height evolves quite differently during excavation of the second stope, going left (increasing displacement) and then right (decreasing displacements), from about -17.2 cm for step 0 (isolated stope) to -17.45 cm for the first excavation step and then to -16.76 cm for the last excavation step. Hence, at the end of the excavation steps, the horizontal displacements along the right wall of the first stope are somewhat smaller than those obtained for the left wall. The results also indicate that, although the additional horizontal displacements δ_h of both walls are relatively small during the excavation of the second stope, they are in general agreement with the evolution of the stresses in the backfill.

The horizontal displacements δ_h of the walls of the first (and second) stopes are not affected noticeably by the filling process (not shown here, Appendix D in Falaknaz, 2014); this

explains why the stresses in the first backfilled stope are not changing much during filling of the second stope in these cases.

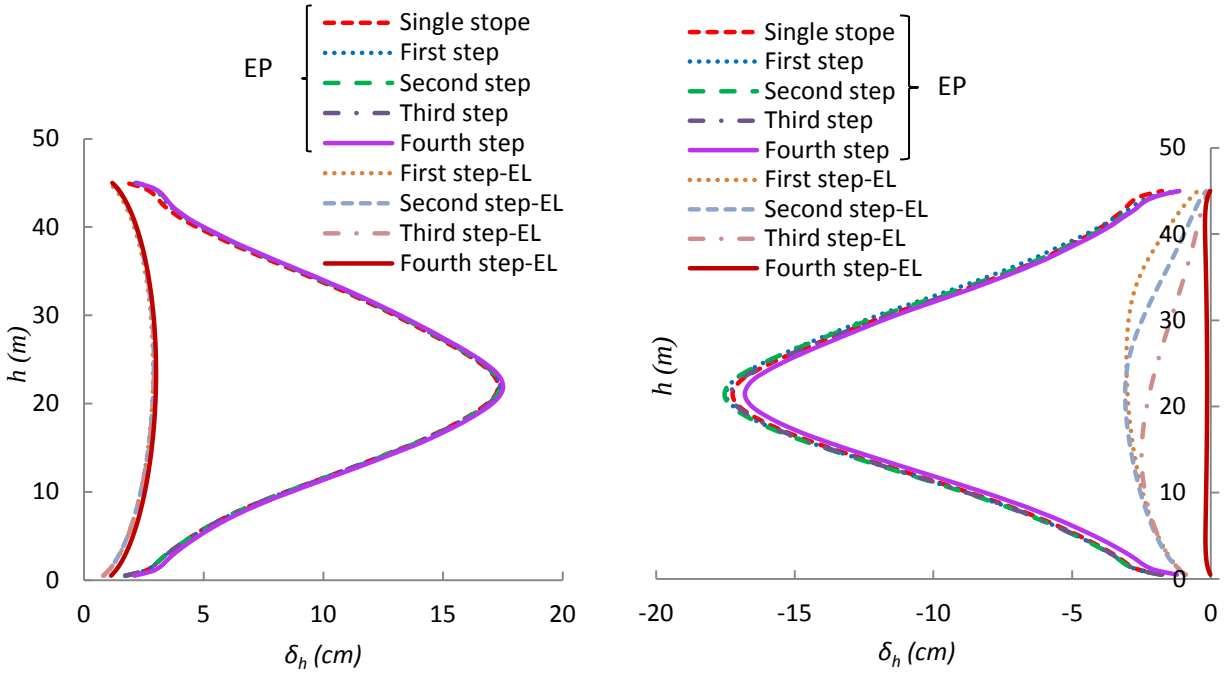

Figure 5-7 : Horizontal displacements δ_h along the: (a) left wall, (b) right wall of the first stope during excavation (4 steps) of the second stope for the EP model (Case 1b), and for the EL model (Case 1a); the horizontal displacements δ_h of the walls in a single stope with the EP model are also shown

The horizontal displacement δ_h at mid-height of the left wall (Fig. 5-7a) is increased from 2.9 cm (step 0) to 3.01 cm (after step 9) for the EL model and from 17.31 cm to 17.51 cm for the EP model, following excavation and filling of the second stope. For the same steps, δ_h at mid-height along the right wall is decreased from -3.02 cm (step 0) to - 0.131 cm (i.e. change of about 90 %) for the EL model and from -17.2 cm to -16.76 cm (about 4 %) for the EP model at the end of filling of the second stope (Fig.5-7b).

The horizontal strains ε_h in the backfill along the VCL of the first backfilled stope have also been calculated, using a FISH function introduced in FLAC (based on the horizontal displacements between two vertical axes located near each other). Figure 5-8 shows the evolution of the horizontal strains ε_h for the EL (Case la) and EP (Case 1b) models. In these figures, a positive strain is linked to compression, while a negative strain indicates extension. As seen in

Figure 5-8a for the EP model, the backfill in the first stope is initially subjected to positive (compressive) strains. Then, the horizontal strains decrease (becoming less positive) during the excavation steps. At the end of the excavation process, the maximum horizontal strain ε_h is negative (at -0.055%) for the EP model. The horizontal strains obtained with the EL model (Case 1a) is shown in Figure 5-8b.

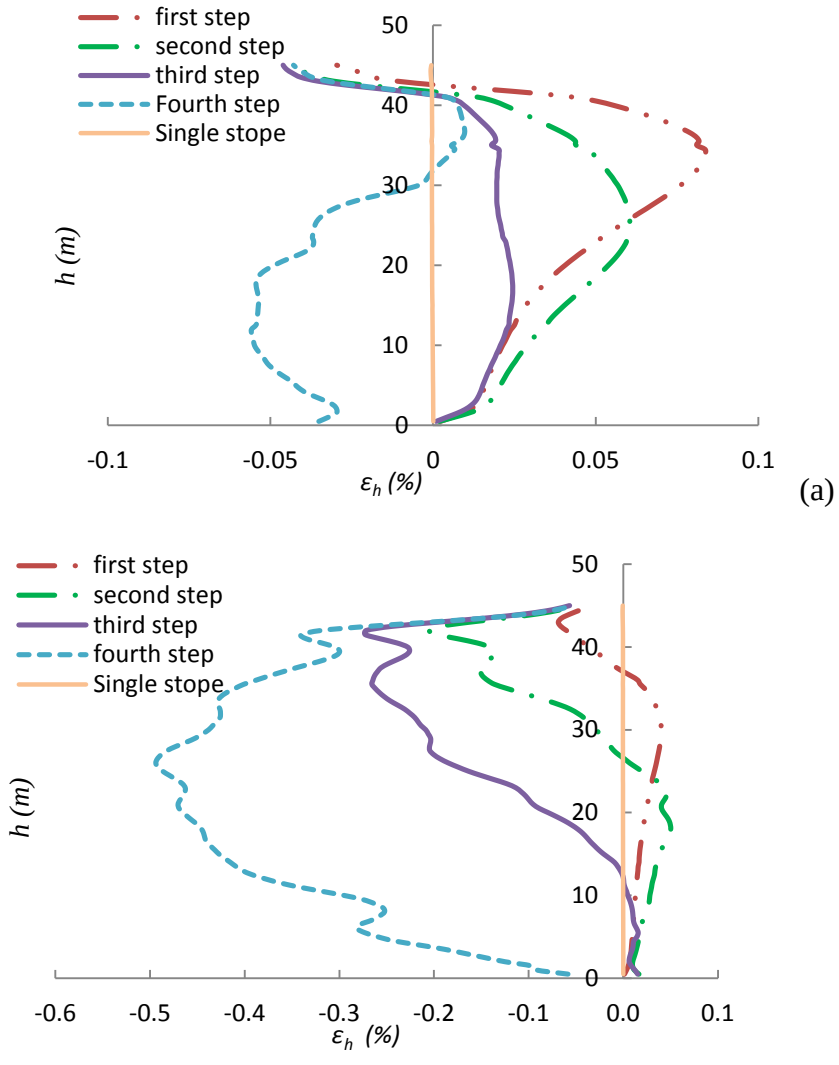

Figure 5-8 : Horizontal strain ε_h along the VCL of the first stope for: (a) an elasto-plastic rock mass behavior (EP, Case 1b) and (b) an elastic rock mass behavior (EL, Case 1a) after excavation of the second stope

The results indicate that the initially positive strains ε_h are less pronounced but nonetheless follow a similar tendency as for the EP model. The maximum horizontal strain ε_h at the end is much larger (at -0.49%) for the EL model.

5.4.3 Stress path

The response of the backfill in stopes can also be assessed in terms of the stress path induced by the excavation and filling process. Examples of such stress path are presented here for points located along the VCL of a single (isolated) stope and of the first (of two) backfilled stope (s) created in sequence. The stress path is presented in the t-s plane, which is also known as the q-p plane in 2D (e.g. Bowles, 1984; McCarthy, 2007). These two stress coordinates can be defined as (Wood, 1990):

$$t = (\sigma_1 - \sigma_3)/2 \quad (5\text{-}4)$$

$$s = (\sigma_1 + \sigma_3)/2 \quad (5\text{-}5)$$

Where σ_1 and σ_3 are the major and minor principal stresses (kPa), respectively. The Coulomb criterion (in 2D) is also shown graphically with the stress paths; it is expressed as follow (for a cohesionless backfill):

$$t = s.\sin\phi \quad (5\text{-}6)$$

In the case of the first of two neighboring stopes, the path follows the stresses through 9 steps, starting with step 0 at the end of filling (similar to a single stope), followed by 8 steps for the excavation (4 steps) and filling (4 steps) of the second stope. The stress paths through these 9 steps have been computed for three points located along the VCL: point 1 at h = 9 m (from the top of the backfill), point 2 at h = 18 m, and point 3 at h = 27 m.

Figure 5-9 shows the stress path for these three points for Case 1b (EP model) and Case 1a (EL model). Conditions at point 3 are used here to describe the path during the 9 steps. For the EP model (Figure 5-9a), the initial stress state (step 0), i.e. s = 140 kPa and t = 63 kPa, is located fairly close from the yield criterion. Upon the first excavation step (of the second stope), the mean stress s (= 335 kPa) increases while the deviatoric stress t (= 20 kPa) decreases; the path is thus moving away from the yield condition. For step 2, both stresses are decreasing to s = 317 kPa and t = 18 kPa. With the third and fourth steps (end of excavation) and fifth step (first step of

filling), the mean stress is progressively reduced while the deviatoric stresses is increasing (t = 88 kPa), hence getting closer to the yield surface. During the last three filling steps, the mean stress tends to increase (s =217 kPa) and the deviatoric stress decreases slightly (t = 77 kPa). The stresses at point 3 are thus approaching the yield criterion without reaching it during these 9 steps. The stress path thus follows a relatively complex trajectory, with the backfill in the first stope being initially loaded, then unloaded and reloaded during the excavation and filling steps (of the second stope). This path gives a different perspective for the evolution of the stresses along the VCL previously shown in Figure 5-6a.

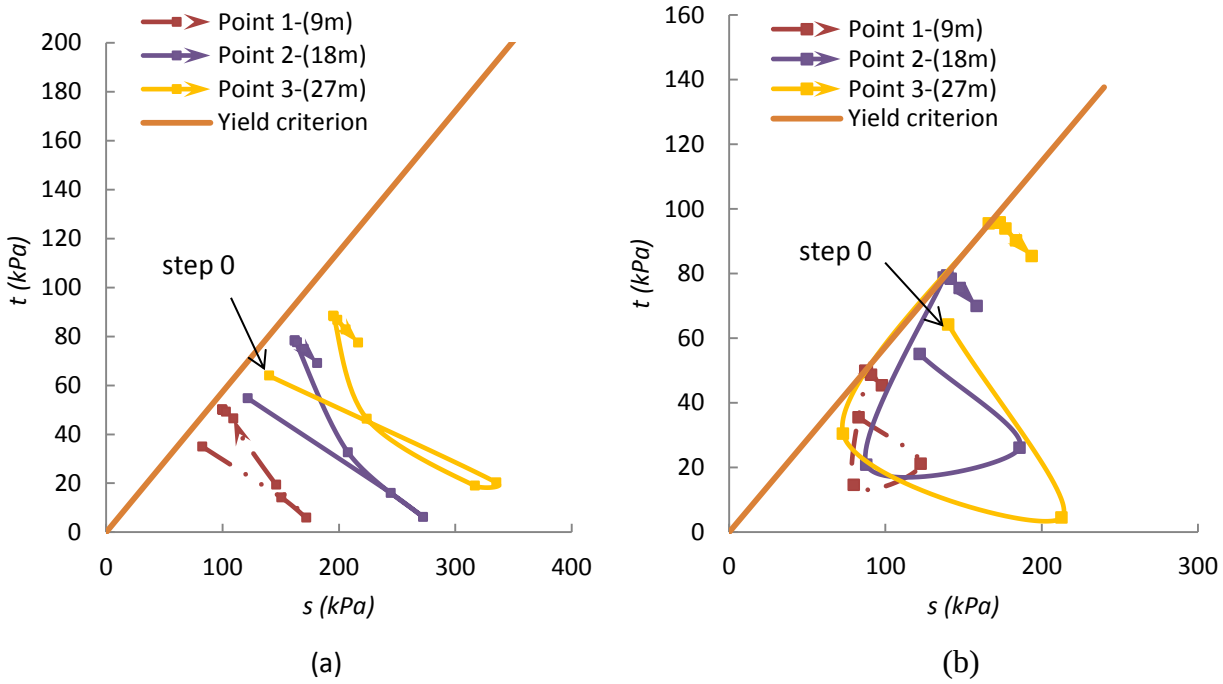

Figure 5-9 : Stress path at three different locations (h = 9 m, 18 m, 27 m from the top) along the VCL of the first stope for: (a) an elasto-plastic rock mass behavior (EP, Case 1b) and (b) an elastic rock mass behavior (EL, Case 1a) during the 9 steps (i.e. excavation and filling of the second stope)

Figure 5-9a also shows the stress path for points 1 and 2 located along the VCL of the first stope. Although, the stress tendencies are similar for the 3 points, the stresses t and s are somewhat smaller for points 1 and 2 (at shallower depths).

Figure 5-9b shows the stress path for Case 1a (EL model). It is seen that this stress path is different than the one observed for the EP model. These stress paths at all three points intersected

the yielding criterion at the end of the excavation steps and remain fairly close to it during filling (of the second stope).

Figure 5-10 shows the relationships between the mean stresses *s* and the horizontal strains ε_h for the same three points located in the first backfilled stope. These results indicate that the tendencies for the EP and EL models are also different. Figure 5-10a (EP model) shows that the backfill in the stope is first loaded (increase of *s*), producing positive strain (compression) and then unloaded during the next three steps of excavation producing a smaller strain in the last step (step 4), and then compressed during the four filling steps (for the second stope). In the EL model, the backfill is loaded (with an increase of the mean stress) and then unloaded by the second step of excavation and then reloaded during the rest of the excavation steps and the four filling steps. The results shown in Fig. 5-10 are in general agreement with the evolution of the stress paths shown in Fig. 5-9 and horizontal strains ε_h presented in Figure 5-8.

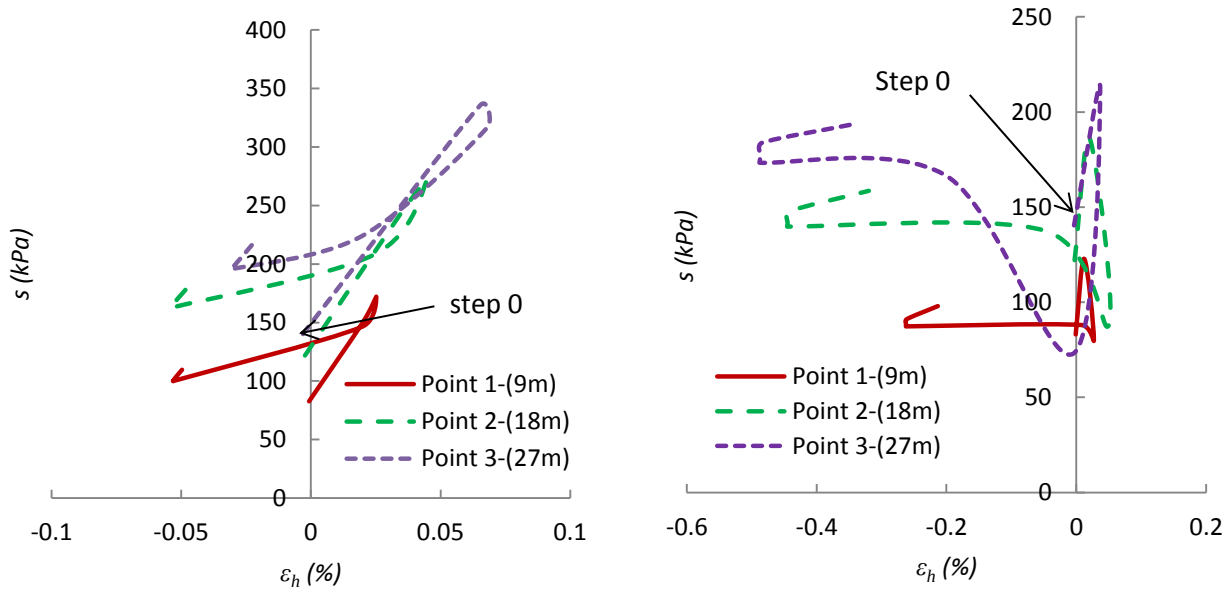

Figure 5-10 : Mean *s* stresses and horizontal strains ε_h at three different locations (h = 9 m, 18 m, 27 m from the top) along the VCL of the first backfilled stope for: (a) an elasto-plastic rock mass behavior (EP, Case 1b), (b) an elastic rock mass behavior (EL, Case 1a) during the 9 steps (i.e. excavation and filling of the second stope)

5.5 Effect of different parameters

A number of additional simulations have been conducted to assess the response of the two neighboring backfilled stopes located in an elasto-plastic (EP) rock mass, considering the influence of different model parameters including the stope width *B*, pillar size *D* (or horizontal distance between the two openings), depth and natural stress state, deformation modulus E_{rm} and strength parameters *c* and ϕ of the rock mass. The results are presented in the following in terms of the stresses, displacements and strains along the VCL and walls of the first stope.

5.5.1 Width *B*

The stresses along the VCL and walls obtained for different stope widths *B* (= 6 m and 18 m, Case 2 in Table 5.2), considering an elasto-plastic rock mass, are shown in Figure 5-11. In these simulations, the external boundaries of the model are located 500 m from the stope walls in all directions, with the base of both stopes located at a depth of 550 m.

Figure 5-11 indicates the stresses are larger (i.e. smaller arching effect) in the first stope (and also in the second stope, not shown here, Appendix D in Falaknaz, 2014) when the width increases from 6 m to 18 m. Near the base of the first stope, the results shown in Figure 5-11a give σ_v = 871 kPa and σ_h = 451 kPa for *B* = 18 m, while σ_v = 507 kPa and σ_h = 240 kPa for *B* = 6 m (after excavation and filling of the second stope). Similar trends are observed for the stresses along the stope walls (Fig. 5-11b, 5-11c). It can also be inferred from these results that a wider stope tends to produce more uniform stresses across its width.

The stope width *B* has a limited influence on the horizontal displacements δ_h along the walls of the first stope after the excavation and filling of the second stope. Additional results (not shown here) also indicate that the horizontal strains ε_h along the VCL of the first backfilled stope are smaller in the narrower stope after excavation and filling (step 9) of the second stope (Appendix D in Falaknaz, 2014).

Figure 5-12 shows the stress path for points 1 (*h* = 9 m form the top of the backfill), 2 (*h* = 18 m), and 3 (*h* = 27 m) in the first backfilled stopes considering *B* = 18m (Case 2, to be compared with Fig. 5-9a for *B* = 6m), during the excavation and filling of the second opening. Again, point 3 is used to describe the evolution of the stress path. Upon step 0 (isolated backfilled stope), the stress state is *s* = 259 kPa and *t* = 100 kPa, which is well below the yield criterion.

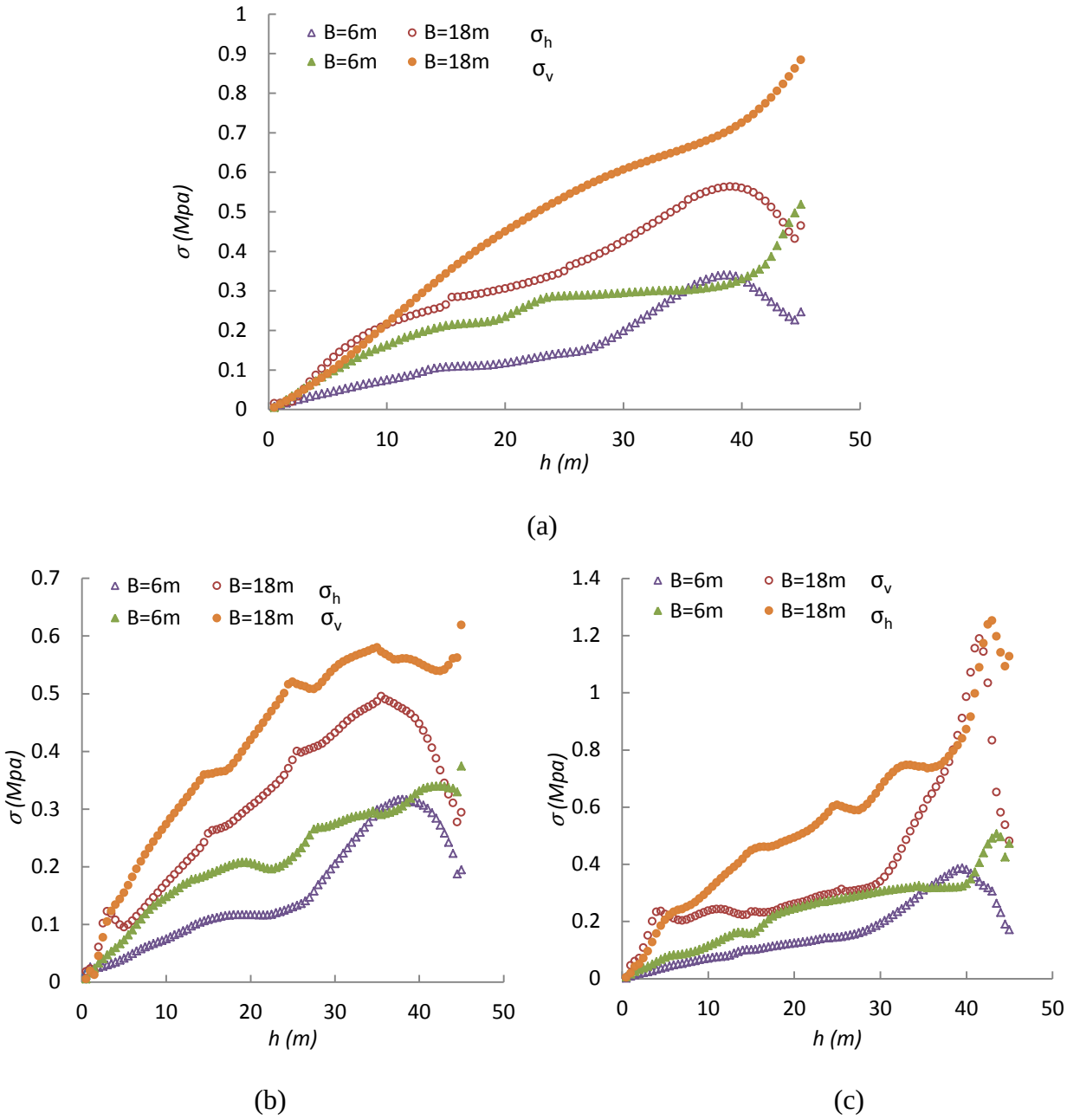

Figure 5-11: Effect of stope width *B* on the vertical and horizontal stresses in the first backfilled stope for an elasto-plastic rock mass behavior (EP) along the (a) VCL; (b) left wall; (c) right wall, after excavation and filling of the second stope (Case 2)

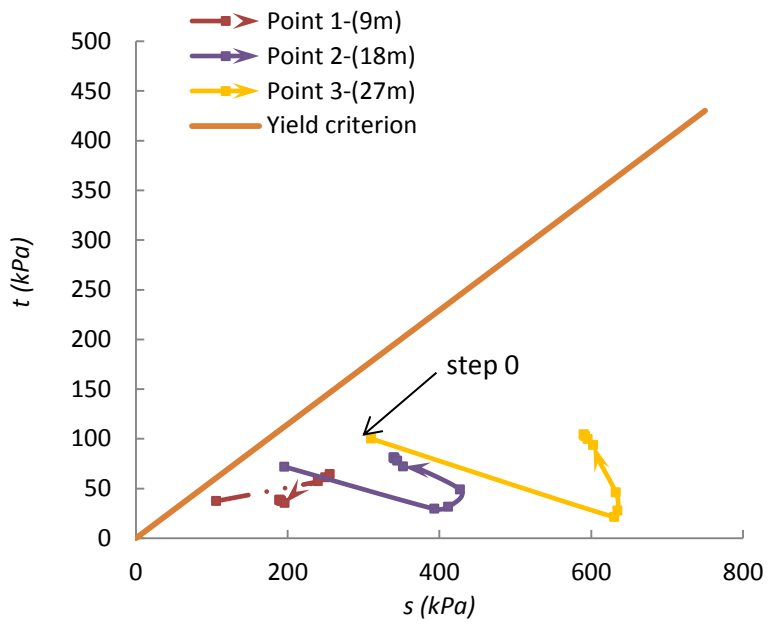

Figure 5-12: Effect of stope width *B* on the stress path at three different locations (*h* = 9 m, 18 m, 27 m from the top) along the VCL of the first backfilled stope during the 9 steps (i.e. excavation and filling of the second stope) (Case 2)

Following the first three steps of excavation (for the second stope), the mean stress increases (*s* = 538 kPa) and the deviatoric stress decreases (*t* = 46 kPa). Upon step 4, the mean stress decreases (*s* = 460 kPa), but the deviatoric stress is increased (*t* = 104). With the filling steps, the mean stress is slightly increased (*s* = 474 kPa) while the deviatoric stress slightly decreases (*t* = 94 kPa). As seen in Figure 5-12, this stress path does not intersect the linear yield criterion at point 3.

Figure 5-12 also shows the stress path for points 1 and 2 along the VCL of the first stope. It is seen that the stress magnitudes are different for these 2 points; the path is also somewhat distinct for point 1 located at a shallower depth.

5.5.2 Pillar width *D*

The influence of distance (or pillar width) *D* between two adjacent stopes has been evaluated with the elasto-plastic (EP) model to simulate the response of the rock mass (Case 3, Table 5.2). The distance between the two stopes varies from 8 m to 60 m. As with most simulations, calculations have been performed for openings having a width *B* = 6 m, at a depth z

= 400 m (for the base of the stopes). For these cases, the boundaries are typically located 360 m from the stope walls to avoid influencing the calculations results (in both directions and along both axes).

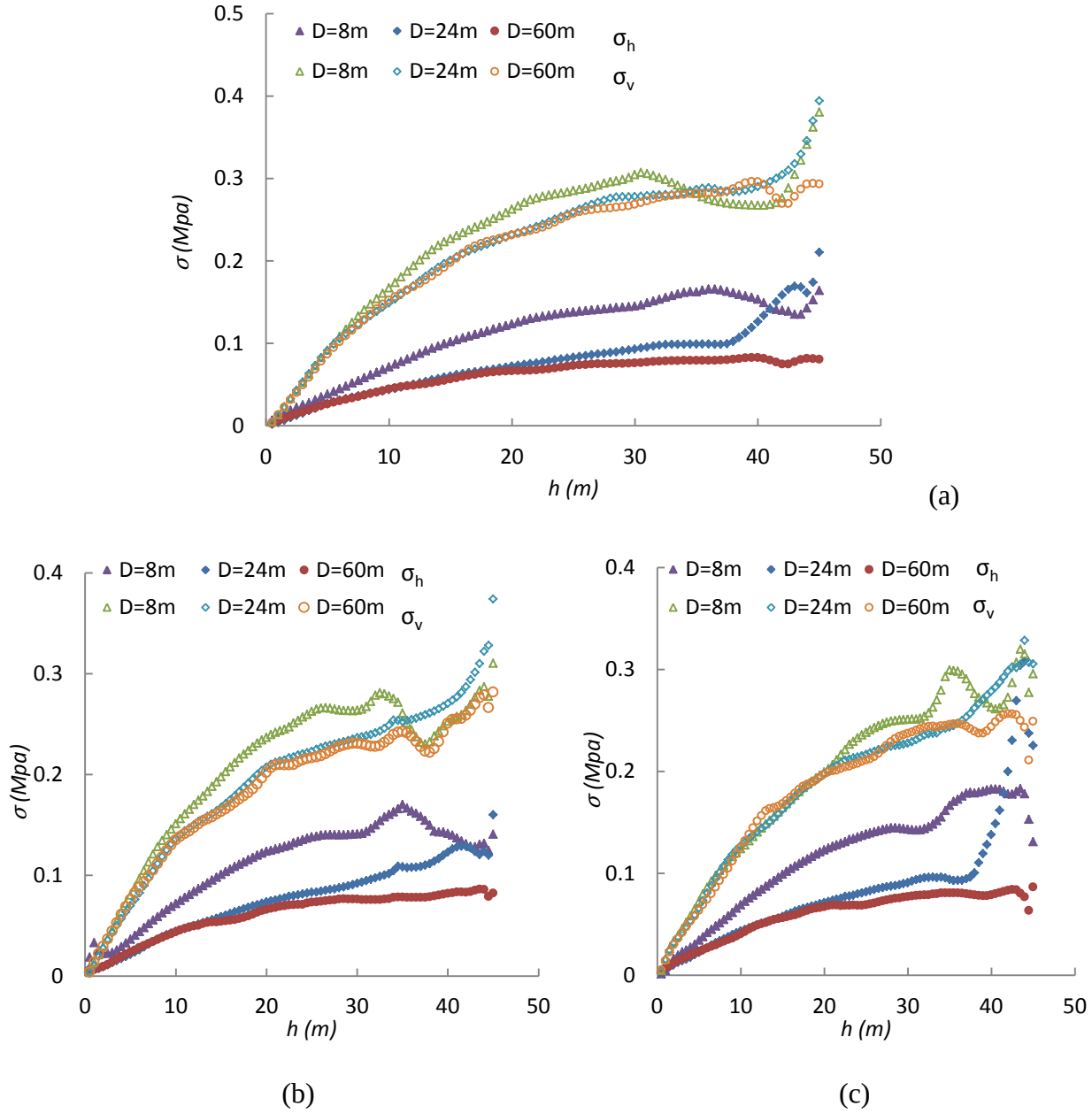

Figure 5-13 : Effect of pillar width *D* on the vertical and horizontal stresses in the first backfilled stope for an elasto-plastic rock mass behavior (EP) along the: (a) VCL; (b) left wall; (c) right wall, after excavation and filling of the second stope (Case 3)

The results shown in Figure 5-13 indicate that when the stope distance increases, the horizontal stresses in the first opening tend to decrease (by a factor of up to 2.5) along the VCL and walls (after excavation and filling of the second stope). For instance, near the base of the stope along the VCL, σ_h = 166 kPa for D = 8 m and σ_h = 79 kPa for D = 60 m; along the left wall, σ_h = 170 kPa for D = 8m and σ_h = 78 kPa for D = 60 m; along the right wall, σ_h = 166 kPa for D = 8 m and σ_h = 80 kPa for D = 60 m. The vertical stresses also tend to decrease, but to a lesser extent, when the distance between the stopes increases, especially when D goes from 8 m to 24 m; these stresses then remain almost unchanged for D increasing up to 60 m.

The horizontal displacements δ_h along the walls of the first stope are also affected by the distance between the openings (not shown here, Appendix D in Falaknaz, 2014). When the distance between the stopes decreases, the horizontal displacement of the right wall tends to increase at the end of filling of the second stope (step 9). The horizontal displacement of the left wall is not significantly affected by the pillar width.

The maximum horizontal strains ε_h (not shown here) are smaller in the first stope with narrower pillar (D = 8m and 24m) after filling of the second stope (step 9) due to an increase of the right wall displacement toward the left (Appendix D in Falaknaz, 2014).

Figure 5-14 shows the stress path for the same 3 points, considering different pillar widths (i.e. Case 3, with D = 24 and 60 m, to be compared with Fig. 5-9a for D = 8m). It is seen on Fig. 5-14a that for a pillar width of 24 m, the stress paths tendencies are similar to the ones obtained for D = 8m (Fig. 5-9a). In this case (D = 24 m), two of the stress paths (at points 1 and 2) intersect the yield surface upon the fourth step of excavation (of the second stope) while the other is very close.

When the pillar width is increased to 60 m, the stress paths are different from those obtained for D = 8 m and 24 m, as seen in Figure 5-14b. The stress state at point 3 upon step 0 is s = 140 kPa, t = 63 kPa (below the yield criterion).

Following the excavation and filling steps (for the second stope), the mean and deviatoric stresses increase (s = 169 kPa, t = 94 kPa), so the stress path intersects the linear yield criterion. The same tendencies can be seen for points 1 and 2 along the VCL of the first stope. It can be concluded that the stress path and its intersection with the yield surface are significantly affected by the pillar width.

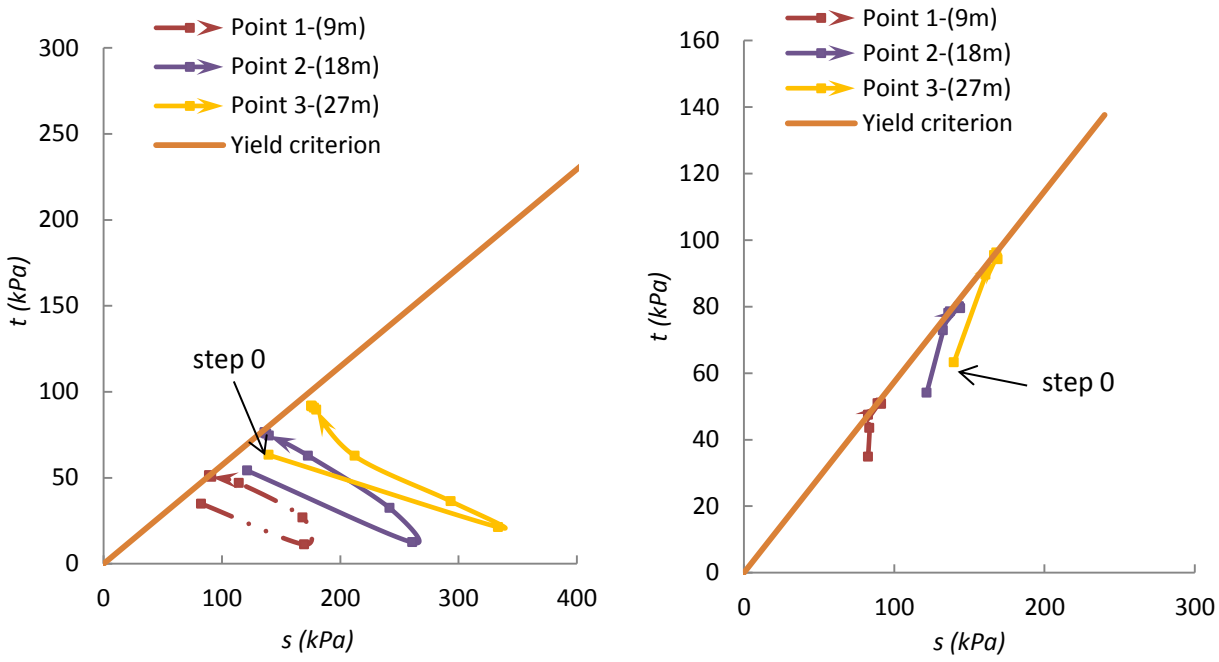

(a) (b)

Figure 5-14 : Effect of pillar width D on the stress path at three different locations (h = 9 m, 27 m, from the top) along the VCL of the first backfilled stope during the 9 steps (i.e. excavation and filling of the second stope) for: (a) D = 24m (Case 3); (b) D = 60m (Case 3)

5.5.3 Stope depth *z*

The effect of openings depth z on the stress state has also been investigated with the elasto-plastic (EP) model for the rock mass, considering the base of two stopes located at 400 m and 2000 m below the ground surface (Case 4, Table 5.2). The natural stresses are proportion to depth z. Both stopes have a width B= 6 m and the distance between the two stopes D = 8 m. The boundaries are located 360 m from the stope walls. Figure 5-15 shows the stresses along the VCL and walls of the first stope located at both depths after excavation and filling of the second stope. It is seen that the horizontal stresses in the first stope are significantly affected by the stope depth, particularly below mid-height where these increase significantly with z, by a factor of up to 25 along the VCL and walls. An abrupt change can be observed for a depth of 2000 m; the stresses in this first stope show a marked increase below mid-height. For instance, near the base of the first stope σ_h = 140 kPa for z = 400 m and σ_h = 3791 kPa for z = 2000 m, along the VCL; along the left wall, σ_h = 133 kPa for z = 400 m and σ_h = 3609 kPa for z = 2000 m; along the right wall,

σ_h = 180 kPa for z = 400 m and σ_h = 4209 kPa for z = 2000 m. The vertical stresses also increase with depth, by a factor of about 7 along the VCL and walls. For instance, along the VCL σ_v = 276 kPa for z = 400 m and σ_v = 2485 kPa for z = 2000 m. These large differences are related to the different trends in the stresses distributions for stopes at depth z of 400 m and 2000 m.

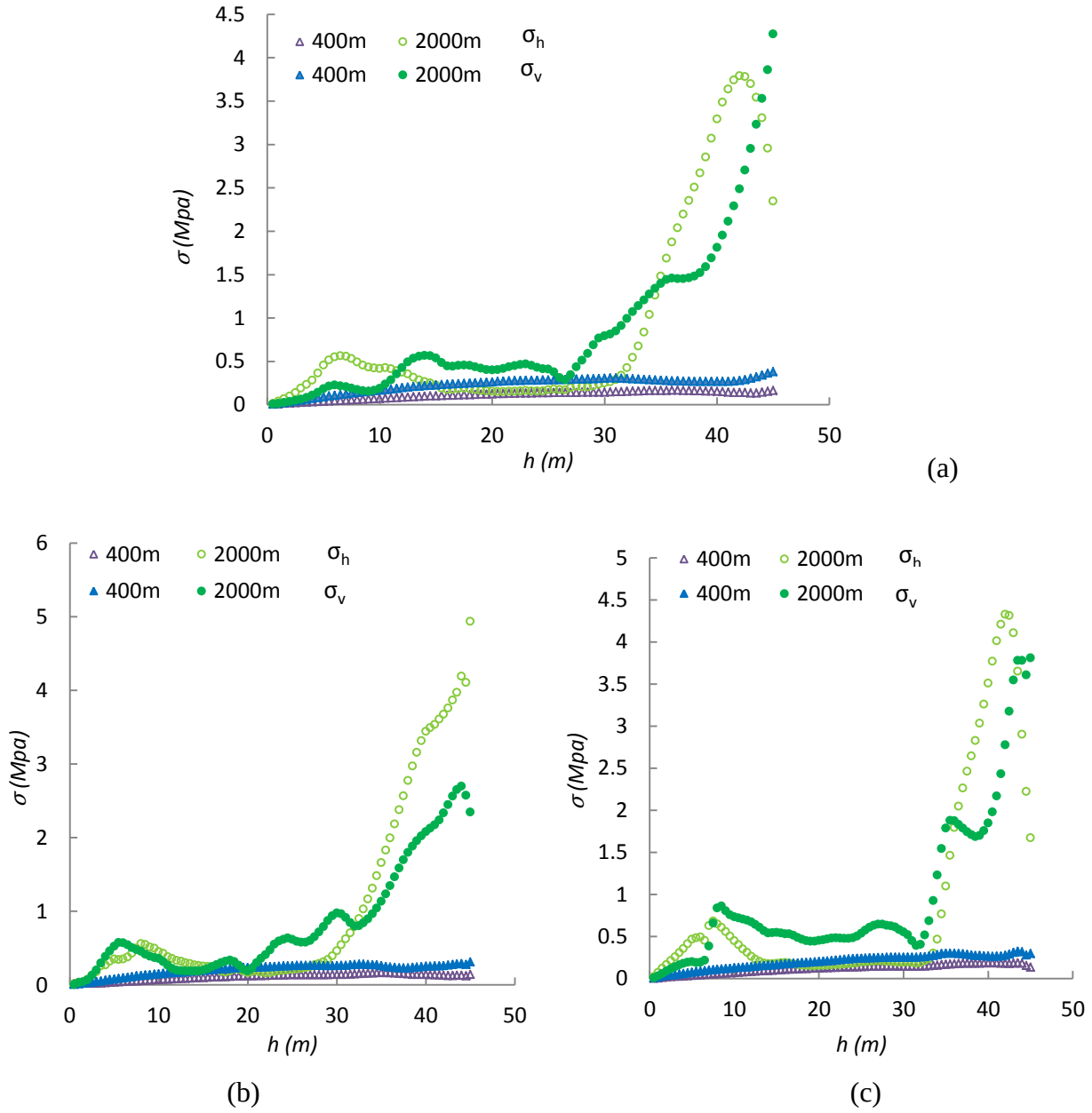

Figure 5-15 : Effect of stope depth z on the vertical and horizontal stresses in the first backfilled stope for an elasto-plastic rock mass behavior (EP) along the: (a) VCL; (b) left wall; (c) right wall, after excavation and filling of the second stope (Case 4)

As can be expected, the horizontal displacements δ_h along the walls of the first stope are also influence markedly by the stopes depth; When the stopes depth increases, the horizontal displacements of the walls (not shown here, Appendix D in Falaknaz, 2014) tends to increase (by a factor of up to 7) at the end of filling of the second stope (step 9). The maximum horizontal strains ε_h in the backfill also increase when the stope depth increases (about 5 times) from 400 m to 2000 m (more details are presented in Appendix D in Falaknaz, 2014).

Figure 5-16 shows the stress path for the three same points in stope 1, considering depth of z = 2000 m (i.e. Case 4, to be compared with Fig. 5-9a for z = 400 m). At point 3, the initial stress state upon step 0 (s = 139 kPa, t = 63 kPa) is located below the yield criterion. Following the first and second excavation steps (for the second stope), both mean and deviatoric stresses increase (s = 2042 kPa, t = 694 kPa). During the last two excavation steps and the first filling step, the mean (s = 249 kPa) and deviatoric stresses (t = 142 kPa) decrease. The stresses at point 3 are reaching the yield criterion at step 3, and remain along this line for the following steps. With the third and fourth filling steps, the mean stress increases (s = 270), while the deviatoric stresses decrease (t = 138 kPa). Fairly similar stress path tendencies are observed for points 1 and 2, with different stress magnitudes. The results indicate that the intersection of the stress path with the yield surface is affected by the stope depth.

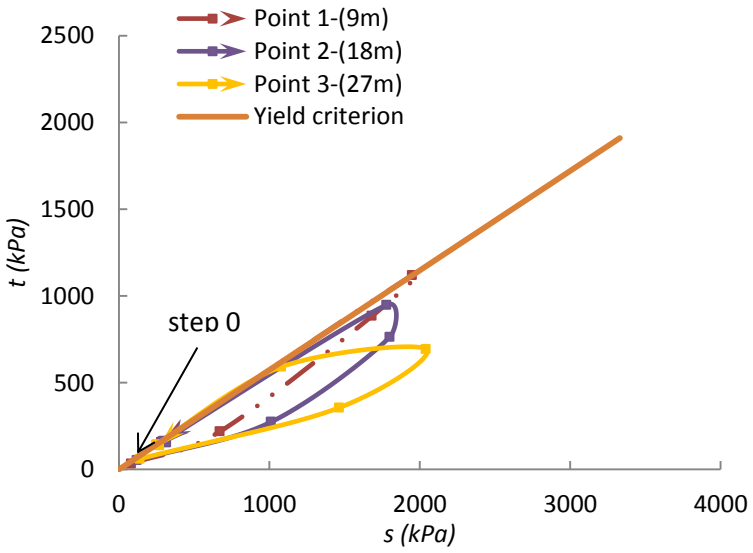

Figure 5-16: Effect of stope depth z on the stress path at three different locations (h = 9 m, 27 m, 45 m from the top) along the VCL of the first backfilled stope during the 9 steps (i.e. excavation and filling of the second stope) (Case 4)

5.5.4 Natural stress ratio in the rock mass, K_r

The natural stress ratio $K_r = \sigma_h/\sigma_v$ (with $\sigma_v = \gamma z$, where z is depth and γ is the rock unit weight) in a rockmass can vary widely with depth, orientation and location in the earth crust (e.g. Zoback, 1992; Hoek et al. 2002). The effect of K_r on the reponse of backfilled stopes was assessed with additional simulations (Case 5, z = 400 m). Figure 5-17 shows the stresses along the VCL and walls of the first stope, for different stress ratios K_r (= 1, 2, 4), after excavation and filling of the second opening. The results indicate that an increase in the value of K_r, from 1 to 4, tends to produce an increase in the horizontal stresses in the backfill, particularly below mid-height; This figure shows that the horizontal stresses around the mid part of the backfill are not sensitive to the value of the natural stress ratio, while these show an abrupt increase in the lower and upper parts when $K_r = 4$; the increase can then reach a factor of up to 3 (σ_h = 165 kPa for K_r = 1 and σ_h = 370 kPa for K_r = 4) along the VCL.

Similar increases were also obtained for the left wall (σ_h = 155 kPa for K_r = 1 and σ_h = 350 kPa for K_r = 4) and right wall (σ_h = 190 kPa for K_r = 1 and σ_h = 395 kPa for K_r = 4). The vertical stresses appear less sensitive to the values of K_r. The final vertical stresses along the VCL of the first tope remain almost unchanged when the K_r value goes from 1 to 2, and increase by a factor of up to 1.5 for K_r = 4. (i.e. σ_v = 267 kPa for K_r = 1 and σ_h = 369 kPa for K_r = 4). Similar results can be observed along the stope walls.

The horizontal displacements δ_h along the walls and the horizontal strain of backfill ε_h of the first stope are also affected by the value of K_r (see detailed results in Appendix D in Falaknaz, 2014).The horizontal displacements of the walls tend to increase with the value of K_r (by up to 25 times for the left wall and by y up to 30 times for the right wall), at the end of filling of the second stope (step 9). The maximum horizontal strain ε_h in backfill changes from -0.084% for K_r = 1 to 0.065% for K_r = 4 (upon step 9).

Figure 5-18 shows the stress path for the same three points, for different natural stress ratio (Case 5, with K_r = 1, 4, to be compared with Fig. 5-9a for K_r = 2). The stress path tendencies are fairly similar for the three values of K_r. More specifically, it can be seen in Fig. 5-18 that for K_r = 1, 4, the stress paths do not approach the yield criterion during the excavation and filling of the second stope, except for point 1 (Fig. 5-18a) that reaches the yield surface upon step 4 when

K_r = 1. The results indicate that the stress state and stress path can be significantly affected by the natural stress ratio in the rock mass.

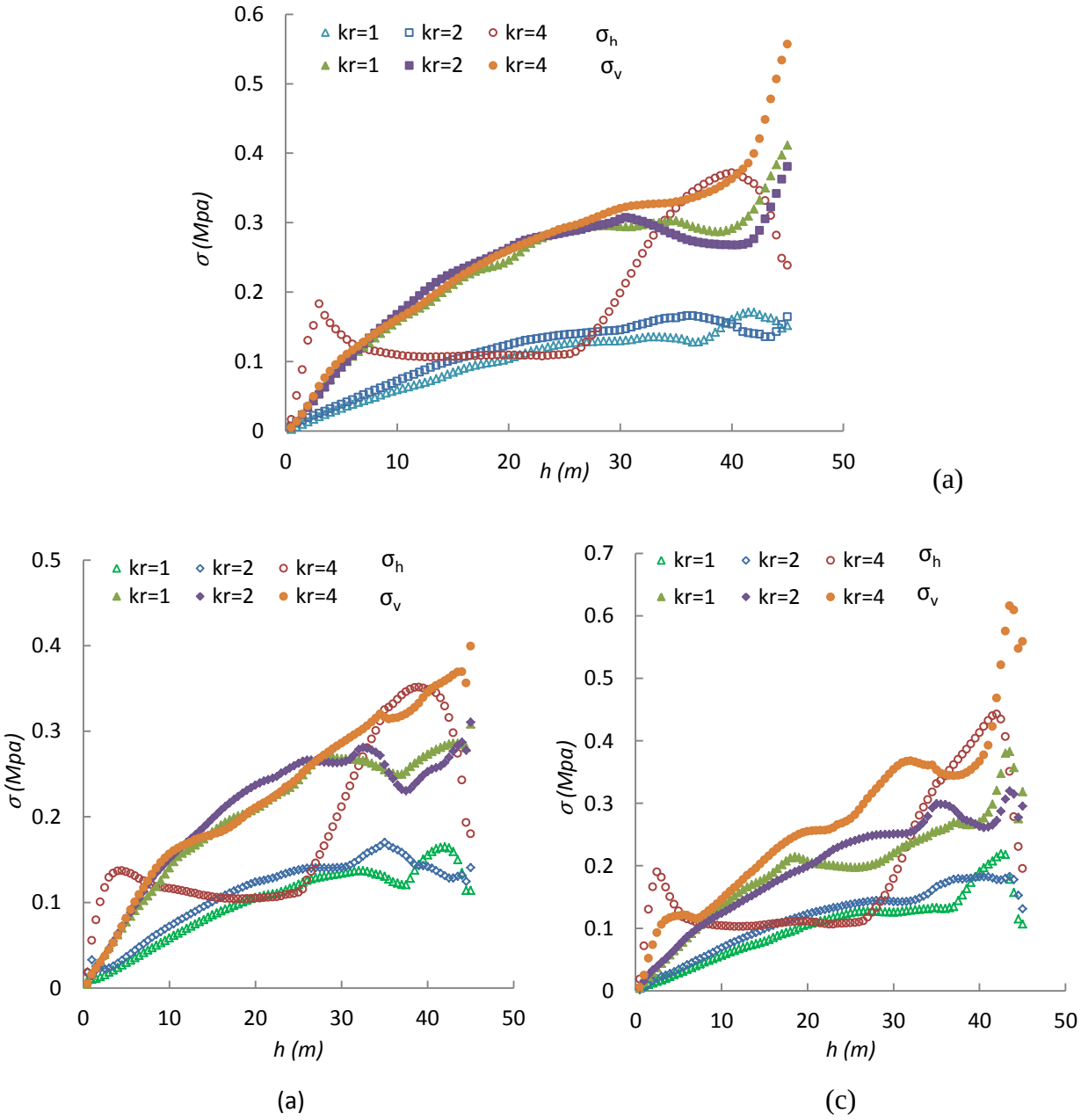

Figure 5-17: Effect of K_r on the vertical and horizontal stresses in the first backfilled stope for an elasto-plastic rock mass behavior (EP) along the: (a) VCL; (b) left wall; (c) right wall, after excavation and filling of the second stope (Case 5)

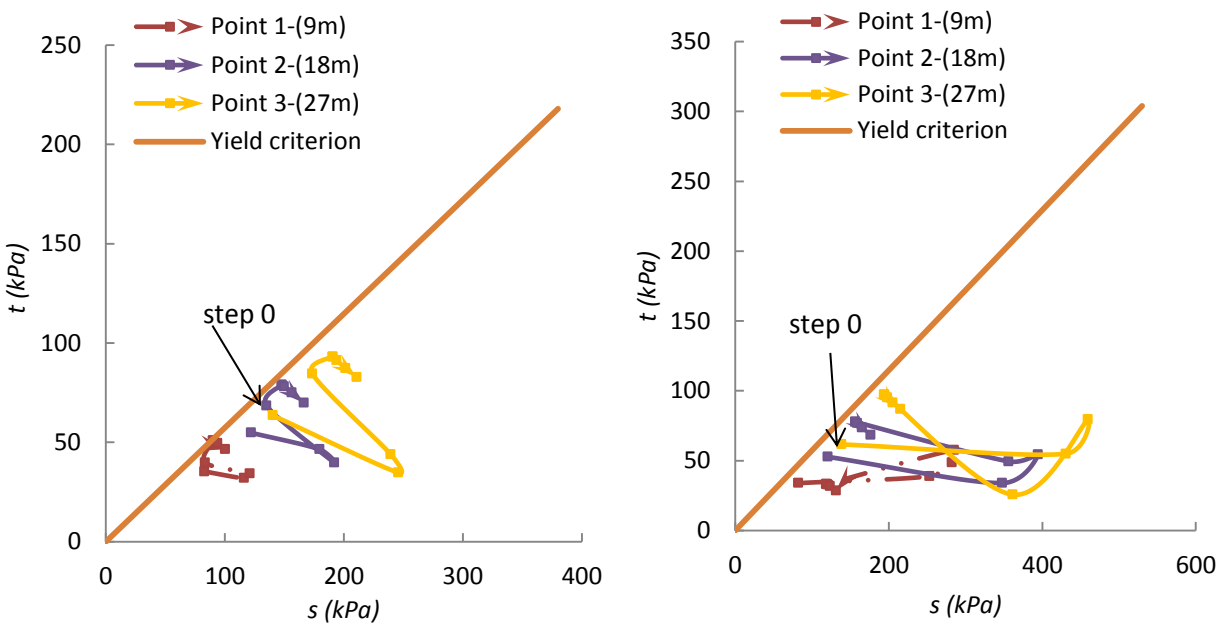

(a) (b)

Figure 5-18 : Effect of K_r on the stress path at three different locations (h = 9 m, 27 m, 45 m from the top) along the VCL of the first backfilled stope during the 9 steps (i.e. excavation and filling of the second stope) for: (a) K_r = 1 (Case 5); (b) K_r = 4 (Case 5)

5.5.5 Modulus E_{rm} and strength parameters c_{rm} and ϕ_{rm} of the rock mass

The stresses along the VCL and walls obtained for different deformation modulus E_{rm} (= 10 GPa and 30 GPa, Case 6 in Table 5.2) and yield strength parameters c_{rm} (= 0.45 MPa, 2 MPa) and ϕ_{rm} (= 40°, 45°) for the elasto-plastic rock mass (see Table 5.1) are shown in Figure 5-19. The results reveal that both stresses along the VCL and walls of the first stope tend to increase, particularly below mid-height, when the modulus of rock decreases to 10 GPa. This figure shows that the stresses in the top part of the backfill is not sensitive to the value of the modulus, while these increase fairly abruptly in the lower part when the modulus decrease. The horizontal stresses increase by a factor of about 6 near the base of the stope along the VCL (σ_h = 149 kPa for E_{rm} = 30 GPa, σ_h = 947 kPa for E_{rm} = 10 GPa), while the vertical stress increases by factor of about 3 (σ_v = 267 kPa for E_{rm} = 30 GPa and σ_v = 723 kPa for E_{rm} = 10 GPa), after excavation and filling of the second stope. The same trends are observed for the stresses along the stope walls (Fig. 5-19b, 5-19c).

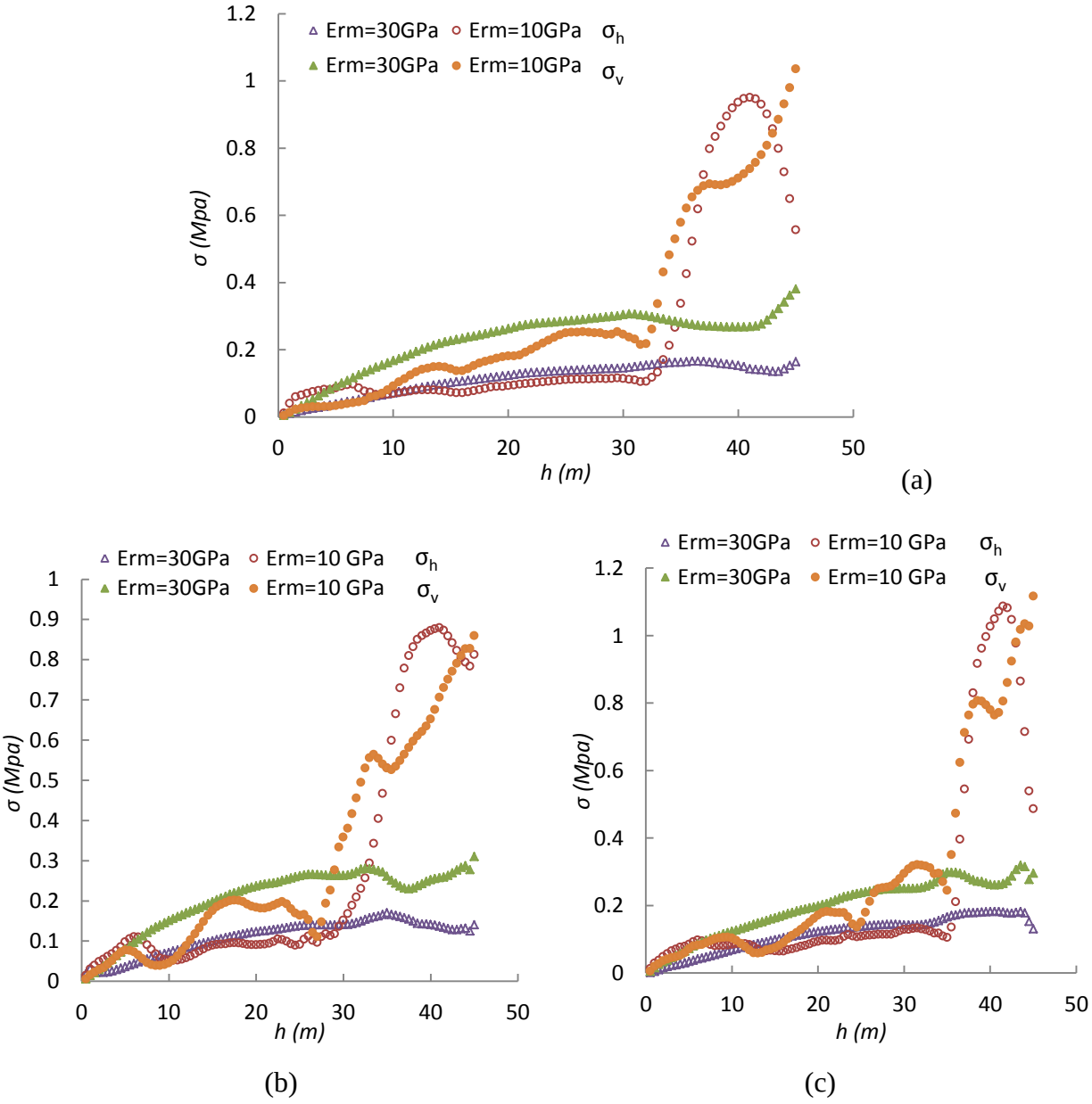

Figure 5-19 : Effect of rock modulus E_{rm} (and strength parameters, c_r, ϕ_r) on the vertical and horizontal stresses in the backfill of first stope for an elasto-plastic rock mass behavior (EP) along the: (a) VCL; (b) left wall; (c) right wall, after excavation and filling of the second stope (Case 6)

Again, the stresses in the backfill follow the displacements δ_h along the walls, which increase significantly (by up to 4 times at mid-height) when the rock mass modulus is decreased (upon step 9). The maximum horizontal strains ε_h in the backfill also increase, by up to 40 times,

when the deformation modulus decreases from 30 to 10 GPa (results not shown here; see Appendix D in Falaknaz, 2014).

Figure 5-20 shows the stress path for the three same points during the excavation and filling of the second opening, for the reduced rock mass modulus (Case 6, with E_{rm} = 10 GPa, to be compared with Fig. 5-9a with E_{rm} = 30 GPa). Point 3 is used again to describe this path. Upon step 0, the initial stress state (s = 145 kPa, t = 72 kPa) is located just below the yield criterion. The mean and deviatoric stresses increase (s = 653 kPa, t = 216 kPa) with the first and second excavation steps (for the second stope). During the last two excavation steps, both the mean and deviatoric stresses decrease (s = 150 kPa, t = 85 kPa) as the stress path reaches the yield criterion. During the filling steps, the mean stress is increasing (s = 182 kPa) while the deviatoric stress is reduced (t = 69 kPa), along the yield locus. The stress paths for points 1 and 2 follow fairly similar trend, intersecting the linear yield criterion.

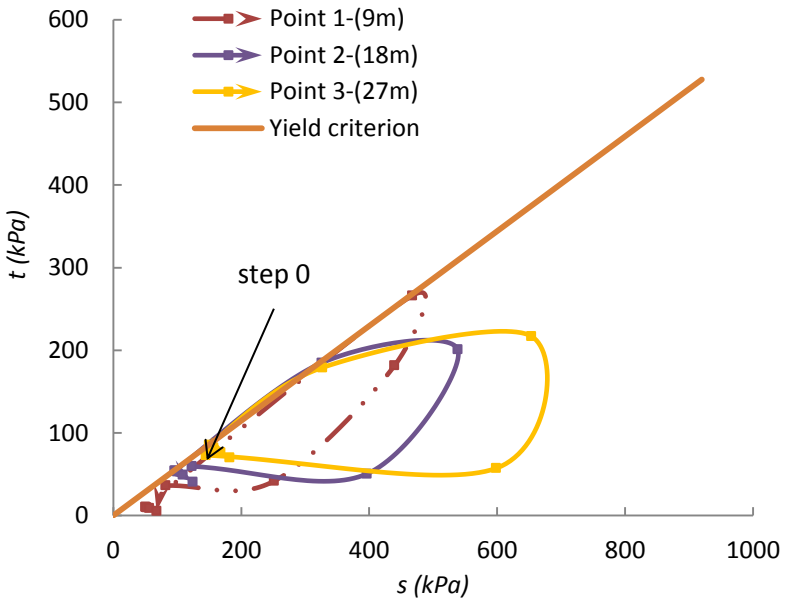

Figure 5-20 : Effect of rock modulus E_{rm} (and strength parameters, c_r, ϕ_r) on the stress path at three different locations (h = 9 m, 27 m, 45 m from the top) along the VCL of the first backfilled stope during the 9 steps (i.e. excavation and filling of the second stope) (Case 6)

5.6 Discussion

The results presented above illustrate how a backfilled stope behavior can be affected by the creation of a nearby opening during its excavation and filling, for a rock mass that obeys a

non-linear constitutive equation. Similar calculations have also been performed for two stopes in a linear elastic rock mass (Falaknaz et al. 2013; Falaknaz et al. 2014); it is thus worth commenting on the simulations results obtained with both types of model for the rock mass. Other aspects that may influence simulations results are also discussed briefly in this section.

5.6.1 EP vs EL model

The simulations with FLAC have been used here to assess the response of two backfilled stopes excavated and filled in sequence in a rock mass that obeys the classical elasto-plastic (EP) model. An important outcome of these calculations is that the stress distribution in the first stope can be less uniform (particularly below the mid-height) than the one obtained with the elastic (EL) model (e.g. Figures 5-13, 5-15, 5-17 showing an abrupt increase below mid-height). This difference is due, at least in part, to the more pronounced displacements of the walls when the rock mass is more deformable (i.e. with the EP model). The results also reveal that the stress distributions in a single backfilled stope and in the second of two stopes, are fairly similar for the EP and EL models, while higher stresses can be observed in the first backfilled stope with the EP model (Figures 5-4b, Figure 5-5 left side).

These results suggest that the analytical solution proposed Li and Aubertin (2008) for a single stope with the EL model can be used to estimate the stresses in a single and in the second stope, for both elastic and elasto-plastic rock masses.

The stress path along the VCL of the first stope shows the effect of the excavation and filling of the second stope. The mean and shear stresses do not evolve in a monotonous way, but follow a path that can get closer or farther from the yielding surface, in a manner that is different for both models. The results also indicate that the stress path can be significantly affected by various influence factors, such as stope depth, natural stress ratio and deformation modulus (strength parameters) of rock mass.

Key outcomes for the analysis of such factors can be summarized as follows:

- There is less arching when the width B of the openings increases with both EP and EL models. When the EP model is used, changing the width can lead to larger differences between the horizontal stresses and the vertical stresses after excavation and filling of the second stope. For instance, the maximum difference between the horizontal, $\Delta\sigma_h$, and

vertical stresses, $\Delta\sigma_v$, near the base of the first stope and along the VCL are $\Delta\sigma_h$ = 211 kPa and $\Delta\sigma_v$ = 364 kPa with the EP model when B goes from 6 m to 18 m, while $\Delta\sigma_h$ = 100 kPa and, $\Delta\sigma_v$ = 290 kPa with EL model. These stresses evolve along the same trend as the wall displacements with both EP and EL models.

- The EP model for the rock mass also produces larger differences for the horizontal and vertical stresses when the pillar width D is changed. For instance, the maximum difference between the horizontal stresses, near the base of the first stope along the VCL $\Delta\sigma_h$ = 87 kPa when D goes from 8 m to 60 m with the EP model, while $\Delta\sigma_h$ = 18 kPa with the EL model (after excavation and filling of the second stope). This is consistent with the movement of the walls and with the horizontal strain ε_h in the backfill, which is increased by a factor of about 2 with the EP model when D goes from 8 m to 60 m, while ε_h is decreased by about 65 % with the EL model. This behavior is due to the elastic response of the rock mass that produces reversible displacements upon unloading.
- The stresses in the first backfilled stope are less sensitive to an increase in the value of K_r with the EL model than with the EP model. This indicates that a change in mechanical behavior of elastic rock mass doesnot have influence on the backfill response. The results also indicate that a decrease of the rock mass modulus leads to more pronounced increase of the stresses when the EP model is used (compared with the EL model).

5.6.2 Simulation procedure

One of the other important factors that may also influence the results of the simulations, in terms of the calculated stresses, displacements, and strains, is the imposed excavation and filling sequence. In this study, the response of the two stopes is simulated by considering four excavated layers and four filling layers having equal height.

Additional calculations have been made considering layers with different thicknesses. The results of the simulations (not shown here; see Appendix D for details in Falaknaz, 2014) indicate that the horizontal stresses can be sensitive to the excavation steps used to create the second stope. However, the vertical stresses are almost insensitive to the excavation sequence for the second stope.

5.7 Conclusion

The main results of numerical simulations conducted to assess the behavior of two neighboring backfilled stopes in an elasto-plastic rock mass (EP model) have been presented. The influence of different parameters have also been taken into account including backfill properties, stope geometry, natural stress ratio in the rock mass, distance between the openings (pillar width) and rock mass modulus (shear strength of rock mass). These calculations results indicate that arching effects develop in all narrow stopes. Comparisons with simulations conducted with an elastic rock mass (EL model) shows that the stress distribution in adjacent openings can be quite different when considering an elasto-plastic rock mass behavior. The results also illustrate similarities and differences between the behavior of a single backfilled stope and of two adjacent stopes.

More specifically, the simulations indicate that an increase of the stope width B leads to an increase of the horizontal and vertical stresses, particularly near the stope base. The stresses tend to diminish with an increase of the pillar width, particularly in the lower part of the stope. An increase of the stope depth tends to increase the stress magnitude below the mid-height of the first stope. A larger natural stress ratio K_r increases the stresses in the pillar, displacements of the walls, and the corresponding stresses within the first backfilled stope. A smaller rock mass modulus (with smaller shear strength parameters) tends to increase the stresses in the backfill and the horizontal displacements δ_h of the rock walls.

The stresses distributions within the backfilled stopes have also been assessed in terms of the stress path induced by the excavation and filling process. The stress path along the VCL of the first stope indicates that the process can involve some loading and unloading (in terms of the mean and deviatoric stresses) during the various stages.

Acknowledgements

The authors acknowledge the financial support from NSERC and from the partners of the Industrial NSERC Polytechnique-UQAT Chair on Environment and Mine Wastes Management (2006-2012) and of the Research Institute on Mines and the Environment (RIME UQAT-Polytechnique; http://rime-irme.ca/).

References

Arjang, B. (1996). In situ ground stresses in the Abitibi Mining District. CIM Bulletin, **89**(996), 65-71.

Aubertin, M., Li, L., Arnold, S., Belem, T., Bussiere, B., Benzaazoua, M., and Simon, R. (2003). Interaction between backfill and rock mass in narrow Stopes. In: Proceedings of soil and rock America 2003, P.J. Culligan, H. H. Einstein, and A. J. Whittle, eds, Verlag Glückauf Essen VGE, Essen, Germany, 1, 1157–1164.

Bieniawski, ZT. (1989). Engineering rock mass classifications. Wiley, New York, 215 pp.

Belem, T., Benzaazoua, M., and Bussière, B. (2000). Mechanical behaviour of cemented paste backfill. In: Proceedings of 53th Canadian geotechnical. Conference, CGS, Richmond, 1, 373-380.

Benzaazoua, M., Fall, M., and Belem, T. (2004). A contribution to understanding the hardening process of cemented pastefill. Miner. Eng. **17**(2): 141-152.

Bowles, JE. (1988). Foundation analysis and design. McGraw- Hill.

Boumiz, A., Vernet, C., and Tenoudjit, FC. (1996). Mechanical properties of cement pastes and mortars at early ages – evolution with time and degree of hydration. Advn. Cem. Bas. Mat. 3: 94-106.

Brady, BHG., and Brown, ET. (2004). Rock mechanics for underground mining, 3rd edition. Kluwer, Dordrecht, 628 p.

El Mkadmi, N., Aubertin, M., and Li, L. (2014). Effect of drainage and sequential filling on the behavior of backfill in mine stopes, Can. Geotech. J. **51**(1): 1-15.

Falaknaz, N., Aubertin, M., and Li, L. (2014). A numerical modeling study to assess the stress distribution in two nearby backfilled openings created in sequence. In: Proceedings of the Canadian geotechnical conference, GeoRegina, Regina, Canada.

Falaknaz, N., Aubertin, M., and Li, L. (2013). Numerical investigation of the stress state in adjacent backfilled mine stopes. In: Proceedings of the Canadian geotechnical conference, GeoMontreal, Montreal, Canada.

Grice, T. (1998). Underground mining with backfill. Mine tailings disposal-2nd Annual Summit. Brisbane. Australia.

Handy, RL. (1985). The arch in soil arching. J Geotech Eng ASCE, **111**(3): 302–318.

Harrop-Williams, K. (1989). Arch in soil arching. J Geotech Eng. **115**(3):415–419.

Hassani, F., and Archibald, J. (1998). Mine backfill. Canadian institute of mine, metallurgy and petroleum, Montreal, Canada.

Hoek, E. (2007). Practical rock engineering. Hoek's Corner (Rock Science). <https://www.rocscience.com/education/hoeks_corner> (Apr. 15, 2014).

Hoek, E., Carranza-Torres, CT., and Corkum, B. (2002). Hoek-Brown failure criterion 2002 edition. In: Proceedings of 5th North american rock mechanics symposium, Toronto. 1: pp. 267-273.

Hustrulid, W., Qianyuan, Y., Krauland, N. (1989). Modeling of cut and- fill mining systems—Näsliden revisited. In: Hassani FP, Scoble MJ, Yu TR (eds) Innovation in mining backfill technology. Balkema, Rotterdam, pp 147–164.

Itasca, (2002). FLAC version 5.0. Users Manuals. ITASCA consulting group, Minneapolis, Minnesota, USA.

Kaiser, PK., Kim, BH. (2008). Rock mechanics advances of underground construction and mining. Keynote lecture, Korea rock mechanics symposium, South Korea, pp 1-16.

Knutsson, S. (1981). Stresses in the hydraulic backfill from analytical calculations and in-situ measurements. In: Proceedings of conference on application of rock mech. to cut and fill mining, Institution of mining and metallurgy, London, 261–268.

Li, L., Aubertin, M., Simon, R., Bussiere, B., and Belem, T. (2003). Modelling arching effects in narrow backfilled stopes with FLAC. In: Proceedings of the 3th Int. FLAC Symp, R. Brummer, P. Andrieux, C. Detournay, and R. Hart, eds, A.A.Balkema, Rotterdam, Netherlands, 211-219.

Li, L., Aubertin, M., and Belem, T. (2005). Formulation of a three dimensional analytical solution to evaluate stress in backfilled vertical narrow openings. Can. Geotech. J. **42**(6): 1705-1717.

Li, L., Aubertin, M., Shirazi, A., Belem, T., and Simon, R. (2007). Stress distribution in inclined backfilled stopes. MINEFILL 2007, Canadian Institute of Mining, Metallurgy and Petroleum, Montreal, Canada.

Li, L., and Aubertin, M. (2008). An improved analytical solution to estimate the stress state in subvertical backfilled Stopes. Can. Geotech. J. **45**(10): 1487-1496.

Li, L., and Aubertin, M. (2009a). Numerical investigation of the stress state in inclined backfilled stopes. Int. J. Geomech **9**(2): 52-62.

Li, L., and Aubertin, M. (2009b). Influence of water pressure on the stress state in stopes with cohesionless backfill. Geotech Geol Eng **27**(1): 1-11.

Li, L., Aubertin, M., and Shirazi, A. (2010). Implementation and application of a new elasto-plastic model based on a multiaxial criterion to assess the stress state near underground openings. ASCE Int. J. Geomech, **10**(1): 13-21.

McCarthy, DF., (1988). Essentials of soil mechanics and foundations: Basic geotechnics. 4th edition, Prentice Hall.

Mitchell, RJ. (1992). Centrifuge model studies of fill pressures on temporary bulkheads. CIM Bull, **85**(960): 48–54.

Ouellet, J., Bidwell, TJ., and Servant, S. (1998). Physical and mechanical characterisation of paste backfill by laboratory and in-situ testing. In: Proceedings of minefill'98, Brisbane, April 1998, pp. 249–254.

Pierce, ME. (1997). Laboratory and numerical analysis of the strength and deformation behaviour of paste backfill. Master's Thesis, Department of mining engineering, Queen's University, Kingston, Ontario, Canada.

Pirapakaran, K. (2008). Load-deformation characteristics of mine fills with particular reference to arching and stress developments. PhD Thesis, James Cook University, Australia.

Pirapakaran, K., and Sivakugan, N. (2006). Numerical and experimental studies of arching effects within mine fill stopes. In: Proceedings of the 6th International Conference on physical modelling in geotechnics, C. W. W. Ng, L. M. Zhang and Y. H. Wang, Eds., Taylor & Francis, Hong Kong, Vol. 2, 1519–1525.

Potvin, Y., Thomas, E., and Fourie, A. (2005). Handbook on mine fill. Australian centre for geomechanics, the University of Western Australia, Nedlands, Australia.

Sivakugan, N., Widisinghe, S., Wang, V. (2013). A note on vertical stress determination within the backfilled mine stopes. Int. J. Geomech, doi:10.1061/(ASCE)GM.1943-5622.0000367.

Singh, S., Shukla, S. and Sivakugan, N. (2011). Arching in inclined and vertical mine stopes. Geotech. Geo. Eng. J, **29**(5), 685-693. doi:10.1007/s10706-011-9410-4.

Thompson, B., Bawden, W., and Grabinsky, M. (2012). In situ measurements of cemented paste backfill at the Cayeli Mine. Can. Geotech. J, **49**(7): 755–772.

Veenstra, R. (2013). A design procedure for determining the in situ stresses of early age cemented paste backfill. PhD Thesis, University of Toronto, Canada.

Wood, D. (1990). Soil behavior and critical state soil mechanics. Cambridge university press. ISBN 0-521-33782-8.

Yilmaz, E., Benzaazoua, M., Belem, T., and Bussiere, B. (2009). Effect of curing pressure on compressive strength development of cemented paste backfill. Minerals Eng. 22:772-785.

Zoback, ML. (1992). First and second order patterns of tectonic stress: The world stress map project: J. of Geophysical Research, 97, p. 11,703–11,728.

CHAPTER 6 ARTICLE 4: STABILITY ANALYSES OF BACKFILL IN MINE STOPES WITH AN OPEN FACE

Nooshin Falaknaz, Michel Aubertin, and Li Li

This article was submitted to Canadian geotechnical journal, Submitted in Oct 2014.

Abstract: Backfilling of mine stopes contributes to ground control around large openings. Mining methods involving the use of cemented backfill pillars require the exposed face remains stable during removal of one of the support walls to create the adjacent stope. Determining the minimum strength of the backfill is thus a critical issue to avoid production and safety problems. Accordingly, a few studies have been conducted to assess the required strength of backfill in stopes with an open face. This paper presents 3D simulations results that investigate the response of exposed backfill during sequential excavation, considering the effect of stope geometry and material strength. Numerical modeling results are then compared with analytical solutions developed to obtain the required backfill strength. The simulations indicate that such analytical solutions are based on assumptions that do not reflect well the actual behavior of the backfill and the related failure mechanism. The analyses also show that the required strength obtained from the different solutions often does not correlate well with each other. Some of the characteristics, implications and limitations of this investigation are also discussed.

Keywords: Underground openings; cemented mine backfill; open face; required strength; numerical modeling, analytical solutions

Résumé : Le remblayage des chantiers miniers contribue au contrôle du terrain autour des grandes ouvertures. Les méthodes de minage qui impliquent l'usage de piliers de remblai cimenté reposent sur la stabilité de la face exposée durant l'enlèvement du mur de support pour créer le chantier voisin. Déterminer la résistance minimale du remblai est un élément critique pour éviter les problèmes de production et les risques pour la sécurité. En conséquence, quelques études ont été menées afin de déterminer la résistance requise du remblai dans les chantiers avec une face exposée. Cet article présente les résultats de simulations 3D visant à évaluer la réponse du remblai exposé durant l'excavation séquentielle, en considérant les effets de la géométrie du chantier et de la résistance du matériau. Les résultats des modélisations numériques sont comparés avec ceux issus des solutions analytiques développées pour obtenir la résistance minimale du remblai. Les simulations indiquent que ces solutions analytiques sont basées sur des hypothèses qui ne reflètent pas bien la réponse du remblai et le mécanisme de rupture. Les analyses montrent aussi que la résistance obtenue des diverses solutions ne sont pas corrélées entre elles. Certaines caractéristiques, implications et limitations liées à cette investigation sont également discutées.

Mots clés: Ouverture souterraine, remblai minier cimenté, face ouverte, résistance requise, modélisation numérique, solution analytique.

6.1 Introduction

Backfilling is used to improve the stability of the rock mass around underground mine stopes and to reduce ore dilution. The environmental and economic benefits of returning part of the tailings or waste rock underground are also part of the rationale behind the use of backfill (Hassani and Archibald, 1998; Benzaazoua et al. 2010).

Some mining operations apply extraction methods that involve primary and secondary stopes (such as the shrinkage stoping). The primary stopes are excavated and then filled with a cemented backfill. During excavation of the nearby secondary stope, one of the walls can be removed. In this case, the backfill forming a "pillar" in the primary stope must be able to stand on its own, without the support of this wall. The stability of the exposed backfill face during adjacent mining is thus a critical issue to control the risk for workers and equipment and the associated costs for the mining operation.

Mitchell et al. (1982) have proposed a solution that is commonly used to estimate the required strength of cemented backfill placed in primary stopes with an open face. This limit equilibrium solution is based on the sliding of the wedge toward the exposed face of a vertical opening. It relies on a number of assumptions that may not all be realistic, such as postulating that the cohesion along the sidewalls is equal to the backfill cohesion, the frictional strength along these sidewalls is nil, and the mobilized strength along the back wall of the stope is negligible (e.g. Li and Aubertin, 2012, 2014).

The solution proposed by Mitchell et al. (1982) was later modified by Zou and Nadarajah (2006) to include the effect of a surcharge load. Dirige et al. (2009) also proposed an analytical solution to estimate the required strength of exposed backfill in an inclined stope, based on the same type of assumptions.

Li and Aubertin (2012) reviewed these solutions and developed modified formulations, based on the Mitchell et al. (1982) model, considering backfilled stopes with a high aspect ratio (i.e. height H >> width B, as in the original solution) and a low aspect ratio, incorporating a surcharge on the top of backfill. This MM (Modified Mitchell) solution is recalled below (Section 6.4), together with the original solution.

Karima et al. (2013) recently conducted numerical simulations using the code 3DEC (Itasca) to assess the required strength of cemented paste fill with an exposed face. Their results suggest using a curing time of 14 days for a stable backfill when the adjacent stope is excavated. This investigation shows the effect of the mining cycle and percentage of cement on backfill stability.

Emad and Mitri (2013) and Emad et al. (2014) have studied the effect of static and dynamic loadings on the stability of the exposed backfill using FLAC^{3D} (Itasca, 2009). Their results indicate that, for the specific cases considered, static loading did not produce failure when the secondary stope was extracted. The dynamic analyses have shown that the extent of damage produced by blast vibrations may affect the response of exposed backfill. Li and Aubertin (2014) also showed results from recent numerical simulations conducted with FLAC^{3D} (Itasca, 2006), aimed at evaluating the geomechanical response of cemented backfill upon exposure of a vertical face. They also developed an analytical solution (presented below) partly based on these simulation results.

Despite many interesting outcomes from these preliminary numerical investigations, these have not led to a systematic analysis of the 3D behavior of backfill in stopes with an exposed face, and which considers key influence factors such as backfill properties, stope geometry, and excavation sequence. Also, to the authors' knowledge, the required backfill strength given by the analytical solutions mentioned above have not yet been compared with results from such 3D simulations. In this paper, results from numerical calculations are presented to illustrate the effect of important factors, including stope width *B*, length *L* and height *H*, fill properties, and excavation sequence, on the behavior and stability of exposed cemented backfill during mining of a secondary stope. The required strength obtained from numerical results is also compared with values given by the Mitchell et al. (1982) solution and by two alternative solutions recently presented by Li and Aubertin (2012, 2014).

6.2 Numerical modeling with FLAC^{3D}

Previous work conducted by the authors and various other groups has shown that the finite difference code FLAC and FLAC^{3D} (Itasca, 2009, 2014) can be used to assess the response of backfill in mine stopes. The latter is used here to investigate the three-dimensional behavior of

backfilled stopes with an open face. The mesh size and boundary locations of each model constructed with FLAC^{3D} have been adapted to obtain representative results. Planar symmetry models were built after testing various meshes to obtain stable numerical solutions. Quadrilateral elements were used in the models, with a coarser mesh for the elastic rock region and a finer mesh inside the backfilled stope. The number of elements can vary with the geometry and size of the model. The external boundaries have been placed far enough to avoid influencing the results obtained inside and near the stopes (as described for 2D simulations by Falaknaz et al. 2013, 2014).

The sidewalls of stopes created by drilling and blasting are typically very rough and irregular, so shearing tends to occur in the backfill itself. Therefore, these models do not include (planar) interface element between the backfill and rock mass (Li et al. 2003; Li and Aubertin, 2009).A series of three-dimensional models (Table 6.1) were used to simulate the response of backfilled stope with an open face. The effect of different stope geometries (Cases 1, 2, and 3) and excavation sequence (Cases 4, 5, and 6) has been evaluated, considering different backfill strength. The simulations are repeated for each geometry, with a varying value of *c*, to determine the required cohesion to maintain (or not) a stable condition; the critical value is thus obtained by progressively reducing the cohesion*c*, from one simulation to the other, until failure appears.

Figure 6-1 shows the characteristics of the base model. The rock mass is considered homogeneous, isotropic and linearly elastic, with the following properties: E_r = 30 GPa (Young's modulus), ν_r = 0.3 (Poisson's ratio), γ_r = 27 kN/m^3 (unit weight). The range of backfill properties introduced in the numerical analyses has been based on laboratory tests results reported by Hassani and Archibald, Belem et al. (2000), Potvin et al. (2005), and Veenstra (2013). The cemented fill behaves as an elasto-plastic material, according to the Mohr-Coulomb yield criterion. Its mechanical properties are defined by E, ν, γ, and by the internal friction angle ϕ (which is related here to Poisson's ratio ν, for consistency of the at-rest earth pressure coefficient K_o; Falaknaz et al. 2014), cohesion c', and dilatancy angle ψ' (with $\psi' = 0 < \phi'$ for the non-associated flow rule adopted here). A zero tension cut-off (Coulomb criterion) was adopted for these simulations; this conservative assumption was deemed acceptable because of the paucity of reliable experimental data on the tensile strength of cemented backfill. The backfill properties and stope characteristics for each case are summarized in Table 6.1.

Table 6.1: Backfill properties and stope characteristics adopted for the numerical simulations (stope depth z = 300 m; E = 300 MPa, ν= 0.3 and related ϕ' = 35°, γ = 18 kN/m3)

Cases (with variants)	*B* (m) (width)	*L* (m) (length)	*H* (m) (height)	*c* (kPa) (backfill cohesion)	Number of steps for front wall removal
$1_{L,\,c}$: $1_{9,10}$, $1_{9,30}$, $1_{30,60}$, $1_{30,\,85}$	6	9, 30	45	10, 30, 60, 85	1
$2_{B,\,c}$: $2_{25,20}$, $2_{25,30}$	25	9	45	20, 30	1
$3_{H,\,c}$: $3_{25,20}$, $3_{25,24}$	6	9	25	20, 24	1
4_{steps}: 4_1, 4_4, 4_7	6	12	45	30	1, 4, 7
5_{steps}: 5_1, 5_4	20	9	45	20	1,4
6_{steps}: 6_1, 6_4	6	9	20	20	1,4

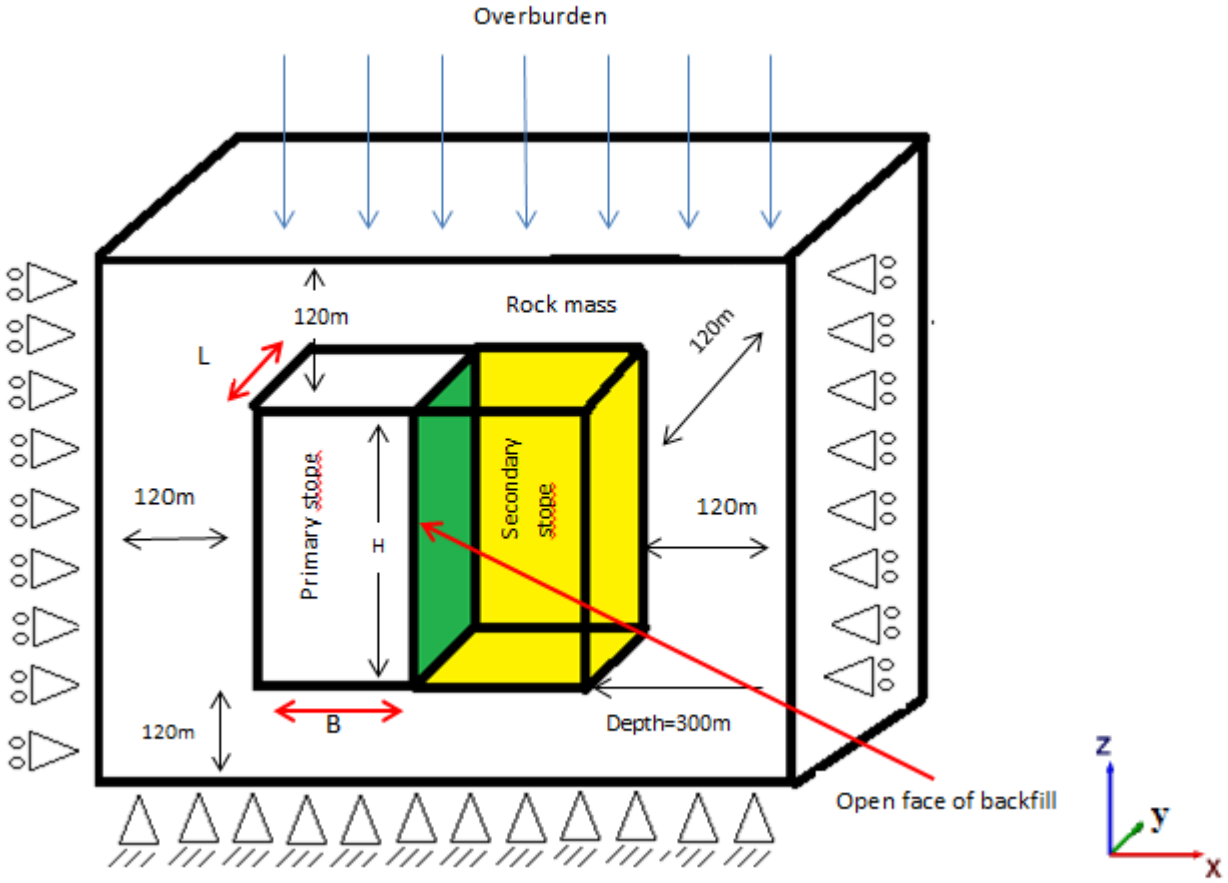

Figure 6-1: Model of two adjacent stopes with the size and boundary conditions (not to scale)

The natural in-situ vertical stress σ_v in the rock mass is obtained by considering the overburden weight for a depth z of 300 m (at the base of the stope). The natural in-situ horizontal stress σ_h in the rock mass is twice the vertical stress σ_v, based on a fairly typical situation encountered in the Canadian Shield (i.e. $K_r = \sigma_h / \sigma_v = 2$; e.g. Herget, 1988; Arjang, 2004).

Gravity is applied as the initial condition before the openings are created. Excavation of the primary stope is completed instantly (single step) and walls convergence takes place before the backfill is added in the stope in four layers (based on Li and Aubertin, 2009). The stress state and walls displacements are registered before excavation of the secondary stope. Then, one of the walls is removed to create the nearby stope in a single or multiple steps. The simulations are conducted using small-strain calculations to avoid interruption due to twisted elements; this is deemed reasonable as the focus lies here on the initiation of instability (rather than on extensive

yielding). The horizontal displacements of the four walls, i.e. front wall (open face), back wall and two side walls, are monitored during the calculations.

Calculation steps continue until the model reaches an equilibrium condition or an active collapse of the fill. The unbalanced forces are monitored to check equilibrium (or instability) at each stage. The stresses and displacements isocontours and magnitudes, the displacement vectors and strength/stress ratios are used to evaluated the response of the backfill and the main characteristics of the failure mechanism (when applicable). The stresses and displacements are determined along four vertical lines (Figure 6-2) in the primary backfilled stope, i.e. line AA′ (vertical central line, VCL), BB′ (side wall), CC′ (back wall) and DD′ (open face). The strength to stress ratio (equivalent to a factor of safety *FS*) is determined using the zone averaged effective shear stress and the yield strength given by the constitutive model (based on the Mohr-Coulomb criterion) as supplied by FLAC^{3D}.

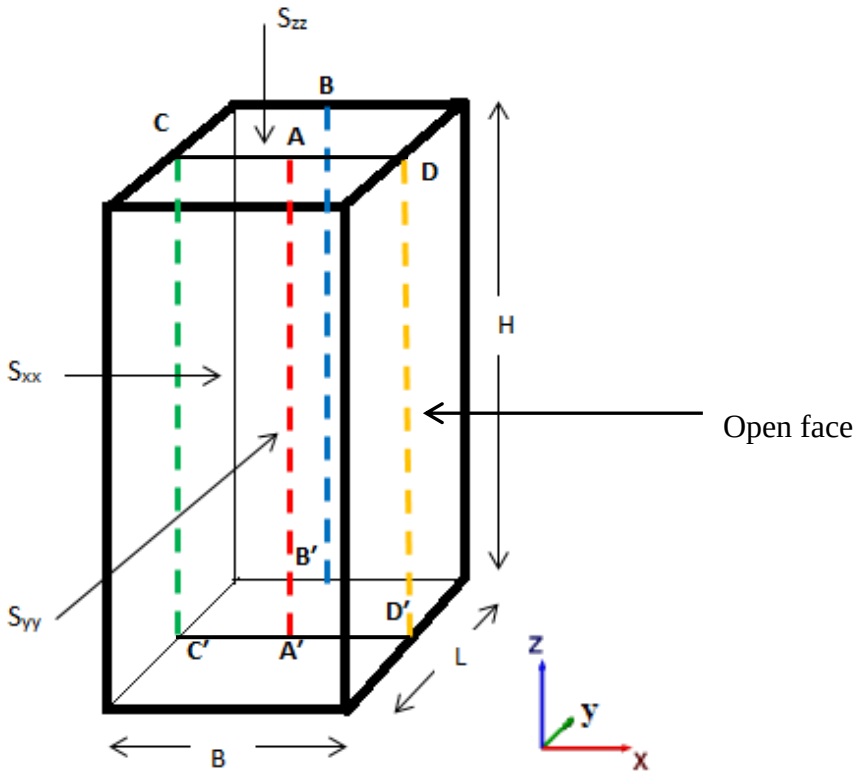

Figure 6-2: Model of a primary backfilled stope with the vertical lines used for presenting the results (not to scale)

6.3 Simulation results

A number of simulations have been conducted to assess the response of exposed backfill in primary stopes, considering the influence of different characteristics including the stope length *L*, width *B*, and height *H*, backfill strength, and excavation sequence (see Table 6.1). The simulations have been repeated with different cohesion values (which control backfill strength) to evaluate more specifically the stability of the backfill after removal of the front wall. The results are presented in terms of normal stresses, total displacements and factor of safety (strength/stress ratio) within the primary stope, considering removal of the support wall (secondary stope) in one (Cases 1-3) or more (Cases 4-6) steps.

6.3.1 Behavior of stopes with different lengths

Length L = 9 m

The influence of stope length *L* (m) on the response of an exposed backfill is evaluated for stopes having a width of *B* = 6 m (Case 1, Table 6.1). The simulations results obtained for stopes with a length *L* = 9 m and *c* = 10 kPa (Case $1_{9,10,}$ Table 6.1) or *c* = 30 kPa (Case $1_{9,30}$) and for *L*= 30 m and *c* = 60 kPa (Case $1_{30,60}$) or *c* = 85 kPa (Case $1_{30,85}$) are described in the following. Additional simulations results are introduced later when the failure condition (and required strength) is assessed.

The stresses distribution and walls displacements in the primary stope have been monitored during the removal of the front wall. Figure 6-3 shows the isocontours of the horizontal (S_{xx}) and vertical (S_{zz}) stresses (see orientations in Fig. 6-1) obtained along vertical plane C′A′D′-DAC (center of the stope, see Fig. 6-2) within the primary stope before (BWR, left side) and after (AWR, right side) front wall removal, for *c* = 10 kPa (Case $1_{9,10}$, Figure 6-3b) and *c* = 30 kPa (Case $1_{9,30}$, Figure 6-3a). As expected, the results shown in Fig. 6-3a (stable backfill) indicate that the vertical stress reduction due to arching, observed BWR when the 4 walls are in place (see also Li et al. 2005), is significantly reduced after removal of the front wall. The effect of the four layers used for filling the primary stope can also be seen in this figure. The situation illustrated in Fig. 6-3b, where the weaker backfill becomes unstable AWR (see also below) leads to significantly different results in this case.

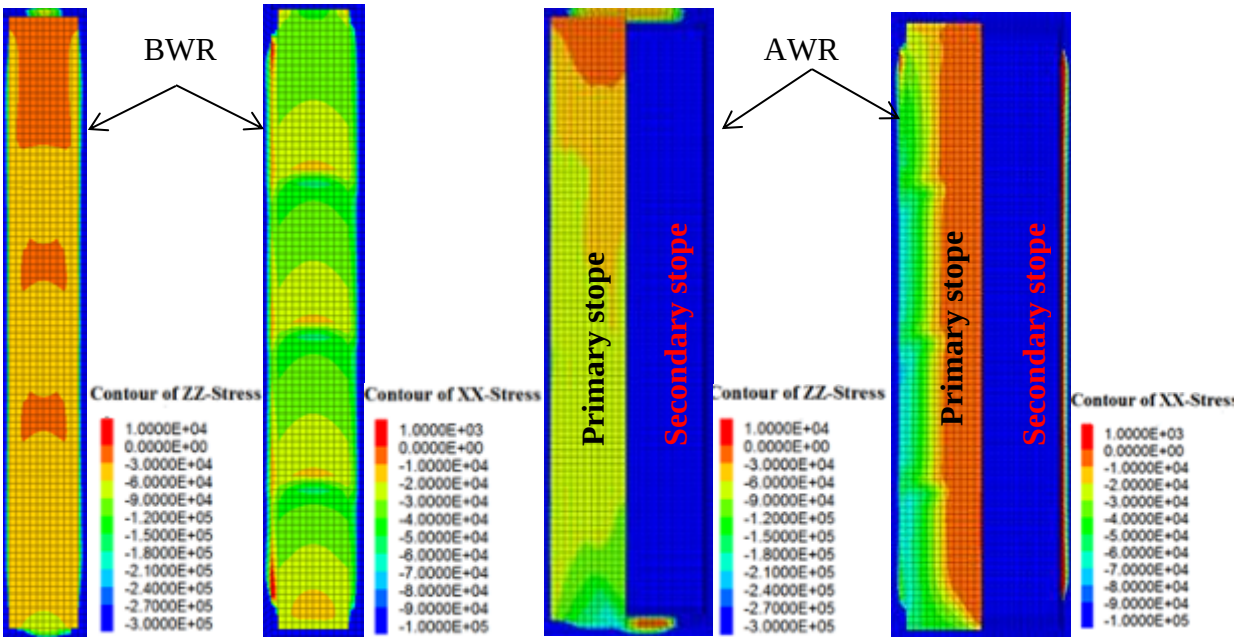

(a)

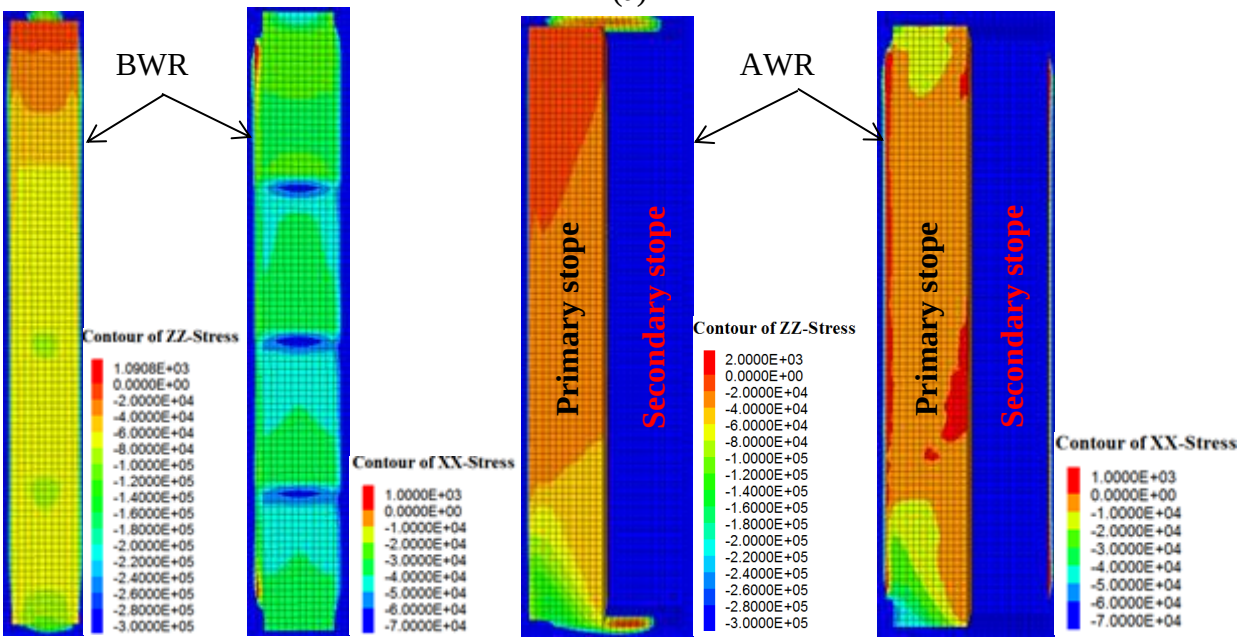

(b)

Figure 6-3: Vertical (s_{zz}) and horizontal (s_{xx}) stresses distributions obtained along the vertical plane C′A′D′-DAC (Fig. 6-2) in the primary backfilled stope before (BWR) and after (AWR) front wall removal: (a) with c = 30 kPa, (Case $1_{9,30,}$ stable backfill); (b) with c = 10 kPa (Case $1_{9,10,}$ unstable backfill)

It is seen here that the compressive horizontal stresses S_{xx} along the back wall and side walls BWR become tensile stresses AWR within the exposed backfill. A zone of instability developed from the top to mid-height of the exposed face, as shown below.

Figure 6-4 shows the horizontal stresses (S_{xx}, Fig. 6-4a; S_{yy}, Fig. 6-4b) along the VCL (line AA′ in Fig. 6-2) and the three walls (lines BB′, CC′, DD′) within the primary stope when c = 30 kPa (Case $1_{9,30}$) before (BWR) and after (AWR) removal of the front wall. In this case, the backfill remains stable upon removal of the front wall; stability is also confirmed when looking at the displacements and strength/stress ratio contours, as will be shown below (see Figures 6-6 and 6-7, presented in the following). It is seen that the horizontal stress S_{xx} (Fig. 6-4a), at mid-height, along the back wall (line CC′) increases by up to 2 times (i.e. from S_{xx} = 23 kPa BWR to S_{xx} = 54 kPa AWR); along the side walls (line BB′), it increases by up to 5 times (from S_{xx} = 15 kPa BWR to S_{xx} = 77 kPa AWR). However, this horizontal stress (at mid-height) tends to decrease along the stope VCL, by up to 45% (from S_{xx} = 18 kPa BWR to S_{xx} = 10 kPa AWR). The horizontal stresses S_{yy} (at mid-height) also increase along the back wall (line CC′) by up to 6 times (from S_{yy} = 17 kPa BWR to S_{yy} = 104 kPa AWR), along the side walls (line BB′) by up to 7 times (from S_{yy} = 21 kPa BWR to S_{yy} = 147 kPa AWR), and along the open face (i.e. along the axis perpendicular to the wall removed) by up to 3 times (from S_{yy} = 17 kPa BWR to S_{yy} = 49 kPa AWR), as seen in Figure 6-4b.

These results show that when the exposed backfilled face is stable, the horizontal stresses S_{xx} and S_{yy} along the walls BWR tend to increase as a result of removing of the front wall. Part of the stresses carried along the wall being removed is thus transferred to the remaining walls after creation of the adjacent stope.

The same observation applies to the vertical stresses S_{zz} (at mid-height) along the side walls and back wall (Fig.6-4c). For instance, along the back wall (line CC′), the stresses are increased by a factor of up to 2, from S_{zz} = 38 kPa (BWR) to 76 kPa (AWR); along the side walls (line BB′), the increase reaches about 2.5 times, from S_{zz} = 32 kPa (BWR) to 88 kPa (AWR). However, the vertical stresses tend to decrease along open face (line DD′) by up to 15%, from S_{zz} = 38 kPa (BWR) to 33 kPa (AWR).

These results also clearly show that non-negligible contact stresses exist along the fill-wall interfaces, on the three remaining walls after front wall removal. This important observation

is not in line with assumptions adopted by Mitchell et al. (1982) to develop his analytical solution (recalled below).

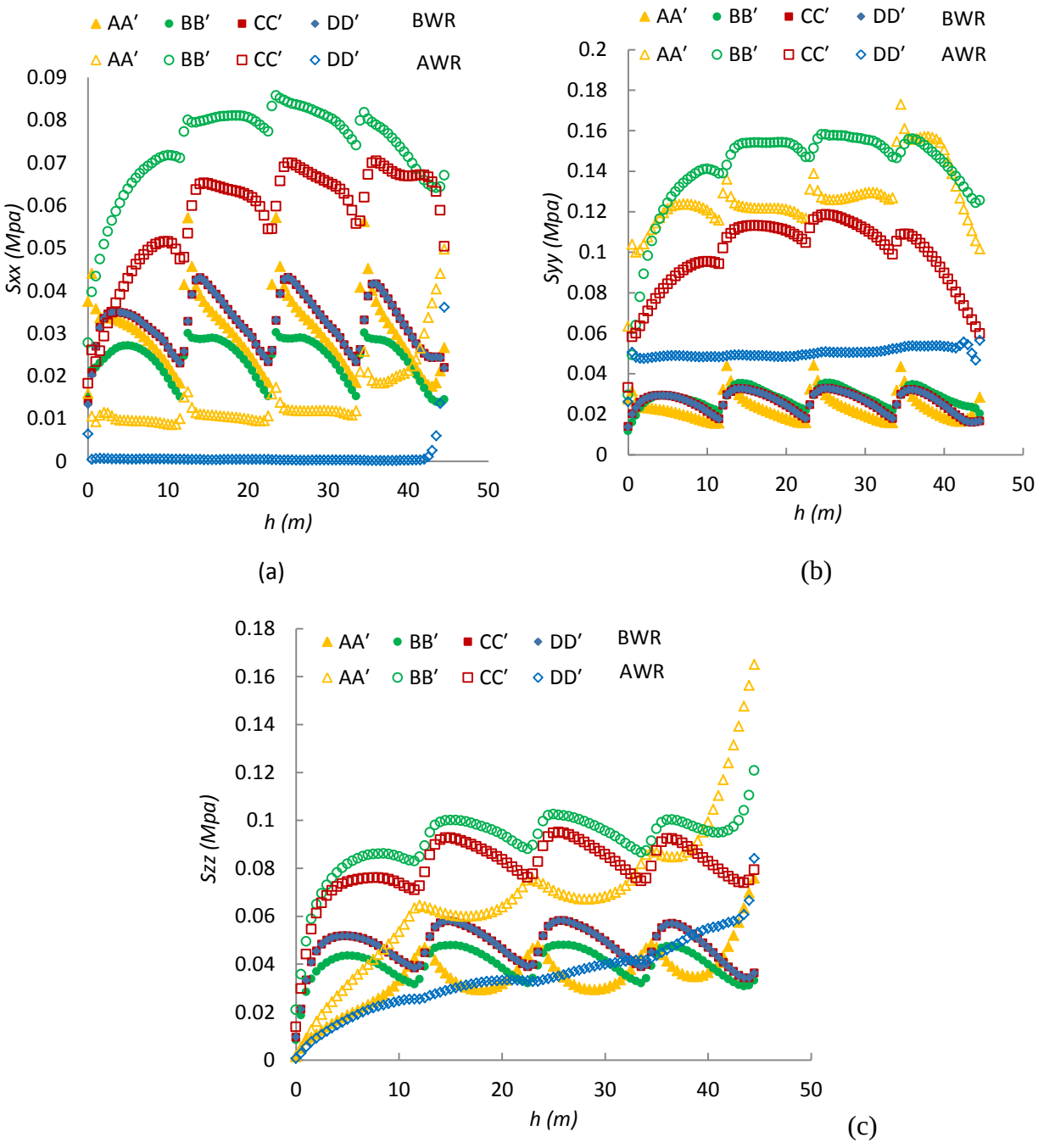

Figure 6-4: Horizontal stresses (a) S_{xx} and (b) S_{yy}, and (c) vertical S_{zz} stresses along the VCL (line AA′), back wall (line CC′), sidewalls (line BB′) and open face (line DD′) of the primary backfilled stope before (BWR) and after (AWR) front wall removal (Case $1_{9,30}$, stable backfill)

Figure 6-5 shows the stresses for the same stope, but with c = 10 kPa (Case $1_{9,10}$). In this case, the backfill becomes unstable upon removal of the front wall. It is seen that the horizontal S_{xx} (normal) stresses decrease significantly along the back wall (line CC′) at mid-height, from S_{xx} = 34 kPa BWR to S_{xx} = 0.9 kPa AWR, and along the side walls (line BB′), from S_{xx} = 25 kPa BWR to S_{xx} = -7 kPa AWR (Fig. 6-5a); tensile stresses thus appear within the cemented backfill AWR, particularly in the upper part of the stope (see Discussion below). The horizontal stresses S_{yy} also decrease along the back wall (line CC′) from S_{yy} = 25 kPa BWR to S_{yy} = 9 kPa AWR (at mid-height), along the side walls (line BB′) from S_{yy} = 34 kPa BWR to S_{yy} = 17 kPa AWR, and along the open face from S_{yy} = 25 kPa BWR to S_{yy} = 17 kPa AWR (Fig. 6-5b).

The vertical stresses S_{zz} (Fig. 6-5c) along the side walls and back wall also decrease when the front wall is removed for this case with an unstable backfill face. For instance, at mid-height along the back wall (line CC′), S_{zz} goes from about 54 kPa (BWR) to 18 kPa (AWR) near mid-height; along the side walls (line BB′), S_{zz} goes from 51 kPa (BWR) to 43 kPa (AWR); along open face (line DD′), S_{zz} is reduced from 54 kPa (BWR) to 37 kPa (AWR).

These results indicate that the vertical stress transfer to the rock walls, associated with arching, is significantly reduced after removal of the front wall. The behavior of the backfill in this case is thus quite different than the one observed for Case $1_{9,30}$; this is due to the instability induced by the removal of the front wall when the backfill cohesion is too low (i.e. c = 10 kPa).

Figure 6-6 shows the total displacements of the backfill and the movement orientation (arrows) after removal of the front wall (AWR) for L = 9 m, with c = 30 kPa (Fig. 6-6a) and c = 10 kPa (Fig. 6-6b). The effect of the four layers used for filling the primary stope can be also seen in the Fig. 6-6a (as was also the case for the stresses shown in Figure 6-3). These results confirm that the backfill becomes unstable AWR when the cohesion is 10 kPa (Case $1_{9,10}$), with the maximum (total) displacement of the open face δ_{max} reaching about 5 m (Fig. 6-6b). The backfill remains stable when the cohesion is 30 kPa (Case $1_{9,30}$) with δ_{max} = 3.5 mm (Fig. 6-6a). The angle of the sliding plane α at the base of the unstable backfilled stope, obtained from the simulation results, is about 56° (Fig. 6-6b).

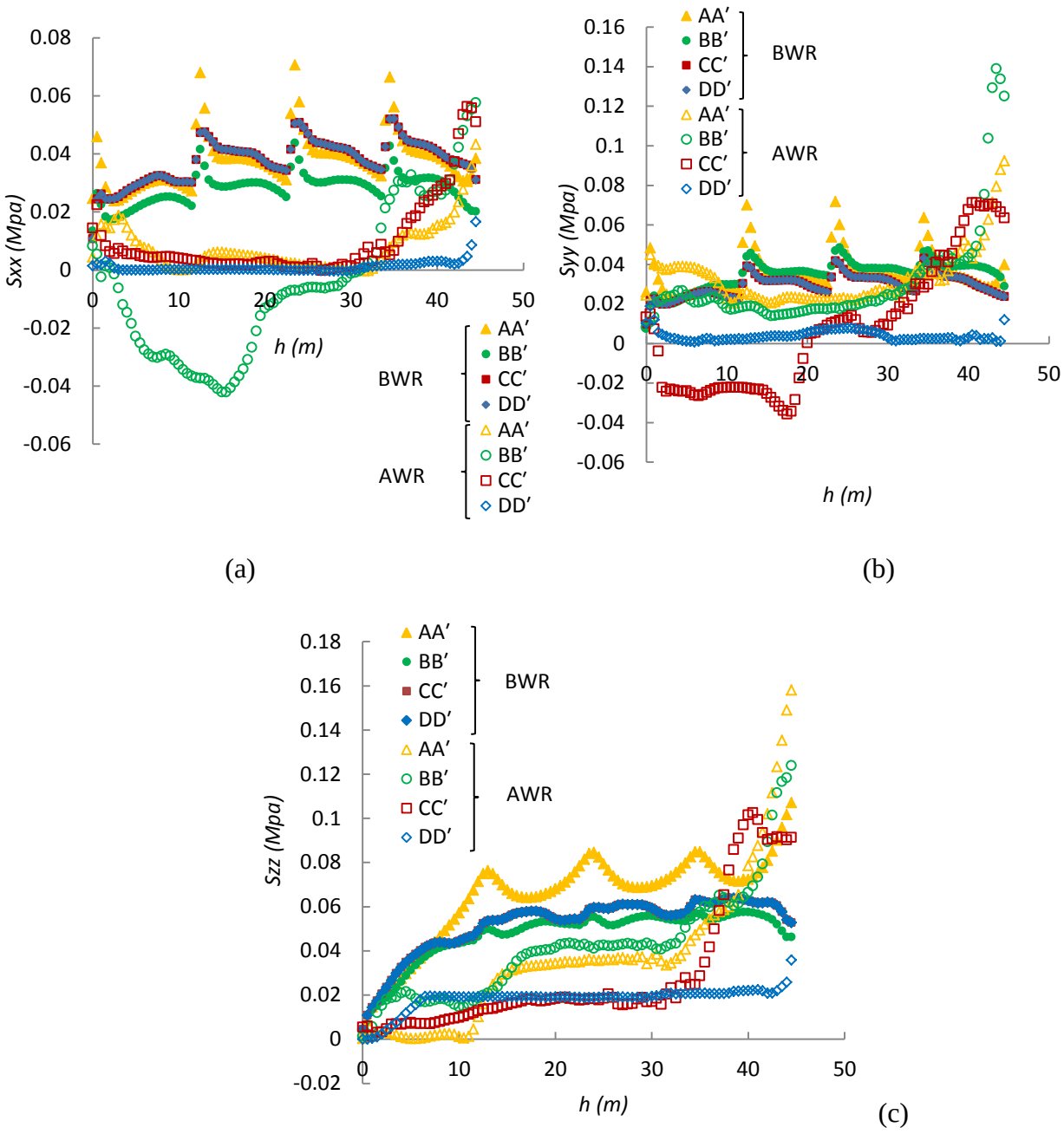

Figure 6-5: Horizontal stresses (a) S_{xx} and (b) S_{yy}, and (c) vertical S_{zz} stresses along the VCL (line AA′), back wall (lines CC′), sidewalls (line BB′) and open face (line DD′) of the primary backfilled stope before (BWR) and after (AWR) front wall removal; (Case $1_{9,10}$, unstable backfill)

Strength/stress ratio (or *FS*) contours are presented in Figure 6-7. A cohesion c = 30 kPa (Case $1_{9,30}$) leads to a strength/stress ratio ≥ 1 (Fig. 6-7a); the exposed backfill thus remains stable, confirming the small displacements shown in Figure 6-6a. For Case $1_{9,10}$ (Fig.6-7b), the

strength/stress ratio (*FS*) is less than unity, so a significant instability develops upon wall removal. A sliding plane is formed, creating a wedge that is fairly similar to the Mitchell et al. (1982) conceptual model (Figure 6-1), but with a slightly curved shape (observed also by Li and Aubertin 2014). Examination of the sliding plane in Figure 6-7b indicates that the sliding surface makes an angle $\alpha \approx 56°$ with the horizontal axis for Case $1_{9,10}$ (similarly to Fig. 6-6b). This angle is relatively close to the value postulated by Mitchell et al. (1982), i.e. $\alpha = 45° + \phi'/2 = 62.5°$ for $\phi' = 35°$ (see below).

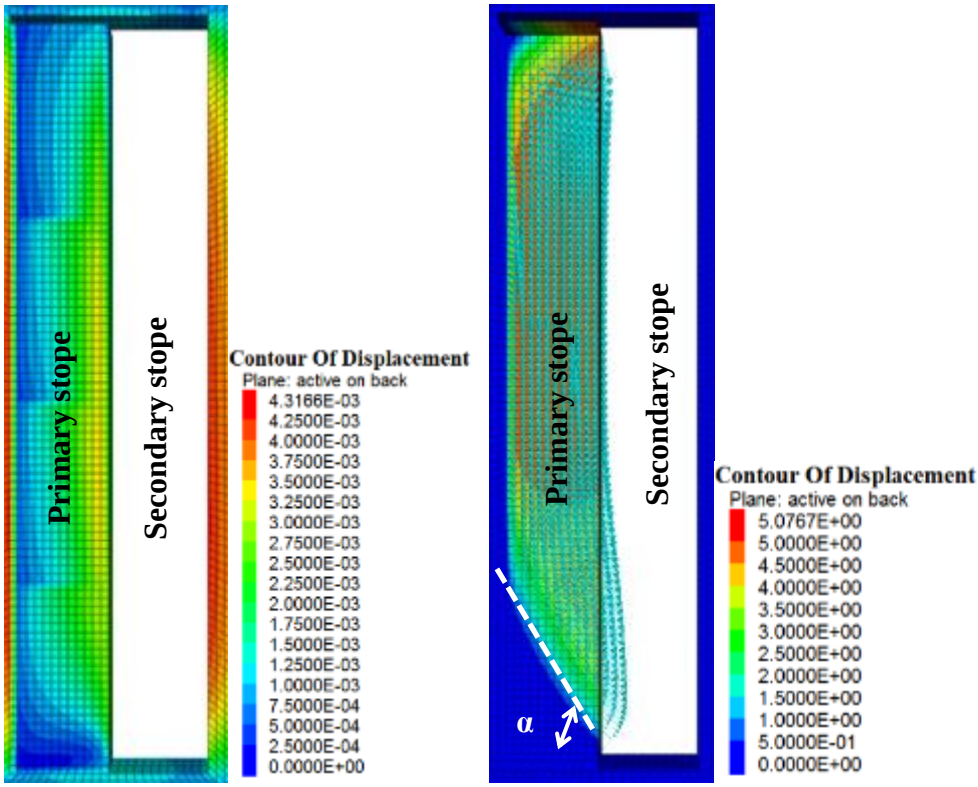

(a) (b)

Figure 6-6: Displacement isocontours on plane C′A′D′-DAC (Fig. 6-2) and displacement vectors toward the open face in the primary backfilled stope after (AWR) front wall removal (a) Case $1_{9,30}$, stable backfill (b) Case $1_{9,10}$ unstable case

Length L = 30 m

Figures 6-8 and 6-9 show the horizontal stresses S_{xx} along the VCL and the three walls within a primary stope having a larger length, L = 30 m, for two cohesion values, i.e. c = 85 kPa (Case $1_{30,85}$) and c = 60 kPa (Case $1_{30,60}$) before (BWR) and after (AWR) removal of the front wall. The latter case leads to an unstable backfill face (as indicated by the displacements and

strength/stress ratio shown later; see Figures 6-10 and 6-11 below), while the former is stable. It can be seen that the final horizontal (normal) stresses along the VCL and back wall (AWR) are smaller than those obtained before wall removal (BWR). For both Cases (Case $1_{30,85}$ and Case $1_{30,60}$), the horizontal stresses S_{xx} (normal) at mid-height decrease markedly along the back wall (line CC′), by up to 75% (from S_{xx} = 27 kPa BWR to S_{xx} = 7 kPa AWR, at mid-height), but these stresses remain positive, while S_{xx} increases along the side walls (line BB′), by up to 3 times (from S_{xx} = 15 kPa BWR to S_{xx} = 48 kPa AWR).

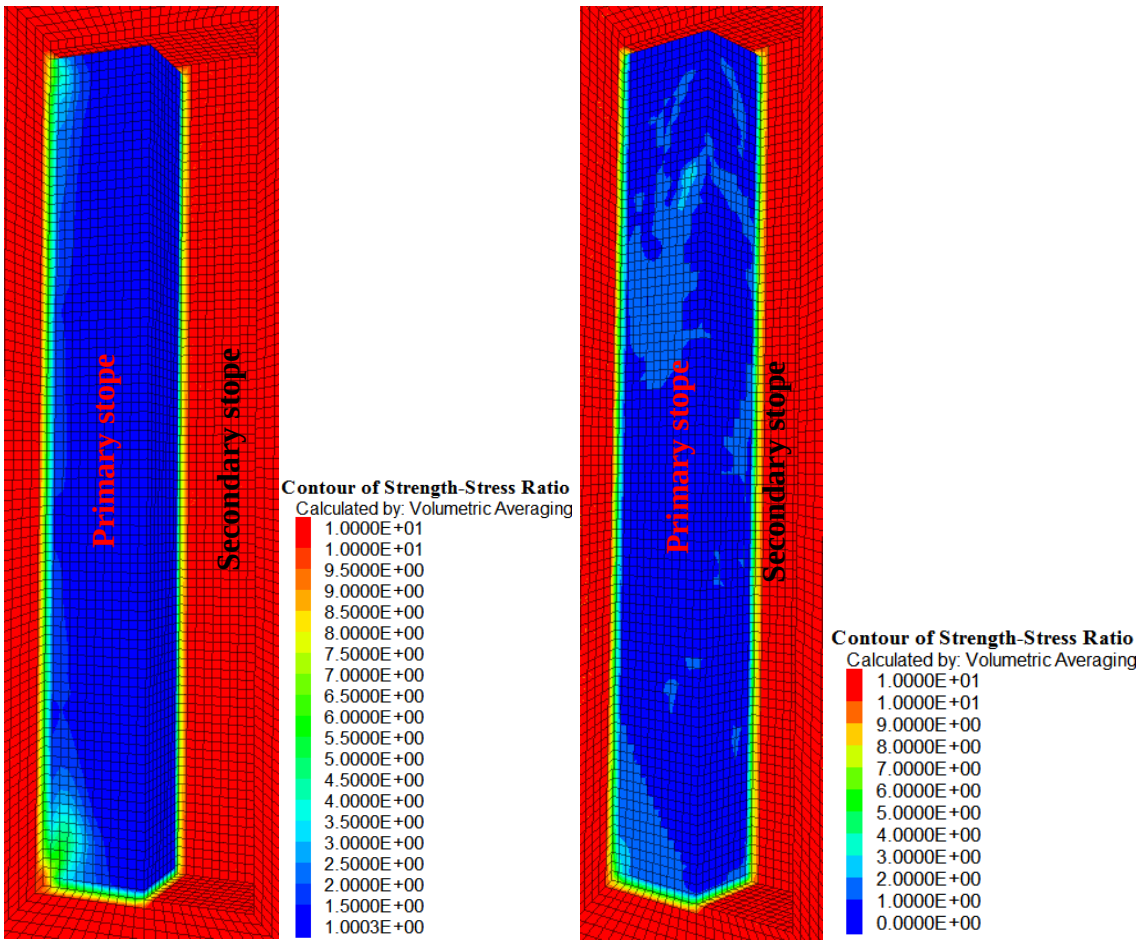

(a) (b)

Figure 6-7: Isocontours of strength/stress ratio (*FS*) in the primary backfilled stope after (AWR) front wall removal: (a) Case $1_{9,30}$, stable backfill (b) Case $1_{9,10}$, unstable backfill

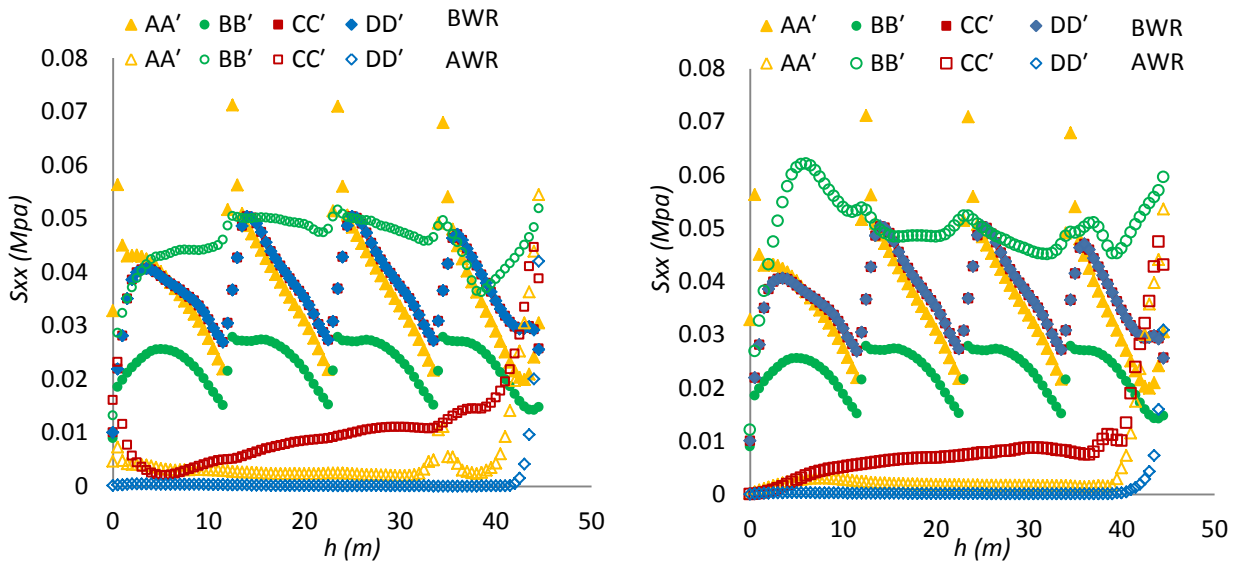

(a) (b)

Figure 6-8: Horizontal stresses S_{xx} in the primary backfilled stope along the VCL (line AA′), back wall (line CC′), sidewalls (line BB′) and open face (line DD′) before (BWR) and after (AWR) front wall removal: (a) Case $1_{30,85}$, stable backfill (b) Case $1_{30,60,}$ unstable backfill

Figure 6-9 shows the horizontal stresses S_{yy} along the VCL and three walls before (BWR) and after (AWR) removal of the front wall. For a stable backfill face (Case $1_{30,85}$), it is seen that the behavior of the backfill is quite different than the one observed for the unstable face (Case $1_{30,60}$). When the backfill is stable AWR, the final horizontal stresses S_{yy} along the VCL, back wall and sidewalls (AWR) are higher than those obtained before wall removal (BWR), as seen in Figure 6-9a. For instance, along the back wall (line CC′) S_{yy} goes from about 22 kPa (BWR) to 151 kPa (AWR) near mid-height; along the side walls (line BB′) S_{yy} goes from 23 kPa (BWR) to 154 kPa (AWR); along (and perpendicularly to) the open face (line DD′), S_{yy} is increased from 22 kPa (BWR) to 86 kPa (AWR). However, when the exposed backfilled face is unstable (Fig. 6-9b, Case $1_{30,60}$), the horizontal stress S_{yy} at mid-height decreases along the open face (i.e. along the axis perpendicular to the wall removed) by up to 50% (from S_{yy} = 22 kPa BWR to S_{yy} = 10 kPa AWR); the stresses S_{yy} tend to increase along the back wall (line CC′), by up to 10 times (from S_{yy} = 22 kPa BWR to S_{yy} = 227 kPa AWR at mid-height), and along the side walls (line BB′) by up to 7 times (from S_{yy} = 23 kPa BWR to S_{yy} = 168 kPa AWR). The vertical S_{zz} stresses in the stope generally tend to increase when the front wall is removed in both cases (not shown here, see details in Appendix E of Falaknaz, 2014).

Figure 6-10 presents the total displacements in the backfill for L = 30 m for two cohesion values, i.e. c = 85 kPa (Case $1_{30,85}$, Fig. 6-10a) and 60 kPa (Case $1_{30,60,}$ Fig. 6-10b). These results confirm that the backfill becomes unstable upon wall removal when the cohesion is 60 kPa; in this case, the maximum total displacement δ_{max} reaches 0.88m (Figure 6-10b) near the top of the stope; the angle of the sliding plane at the base is about 53°. The backfill remains stable when the cohesion is 85 kPa (Case $1_{30,85}$), with δ_{max} = 0.077m (Figure 6-10a). The displacements of the backfill along plane C′D′DC, particularly along the back wall, can help understand the stresses distributions shown for these and related cases.

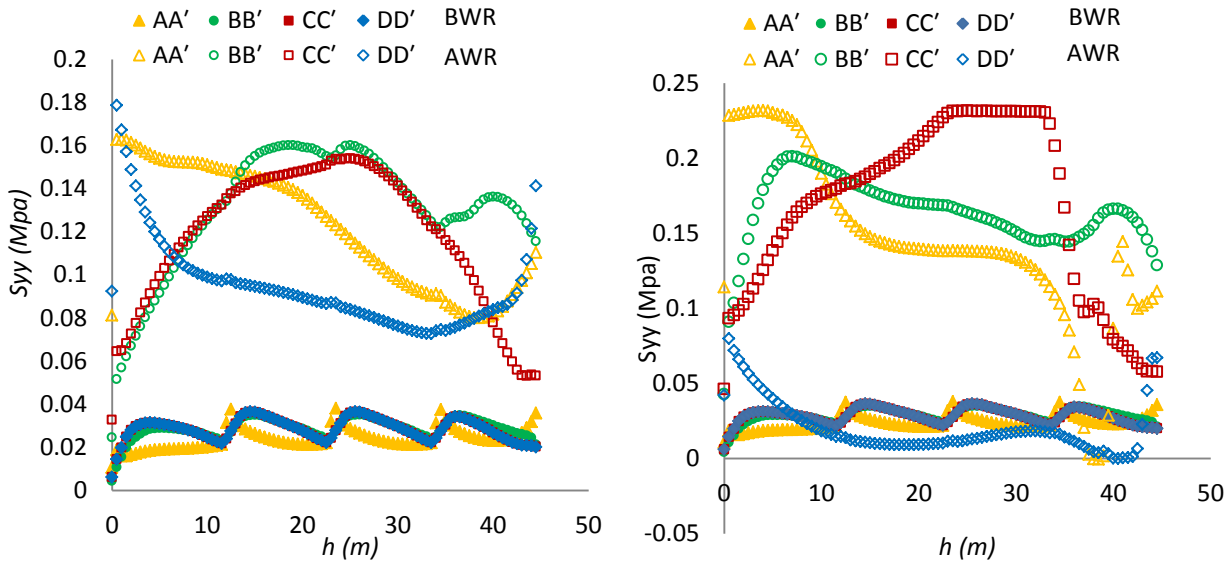

Figure 6-9: Horizontal stresses S_{yy} in the primary backfilled stope along the VCL (line AA′), back wall (lines CC′), sidewalls (line BB′) and open face (line DD′) before (BWR) and after (AWR) front wall removal: (a) Case $1_{30,85}$, stable backfill (b) Case $1_{30,60}$, unstable backfill

Figure 6-11 shows the effect of increasing the stope length to L = 30 m on strength/stress ratio (*FS)* contours; the results can be compared with those in Fig. 6-7 for L = 9 m. It is seen that a higher cohesion is required to maintain a stable face along the exposed backfill for the larger stope. The sliding plane corresponding to a strength/stress ratio < 1 makes an angle $\alpha \approx 53°$ (Fig. 6-11b) when c = 60 kPa (Case $1_{30,60}$, as in Fig. 6-10b). An increase of the cohesion to 85 kPa (Case $1_{30,85}$, Fig. 6-11a) increases the strength/stress ratio (*FS*) above unity, so the backfill face remains a stable.

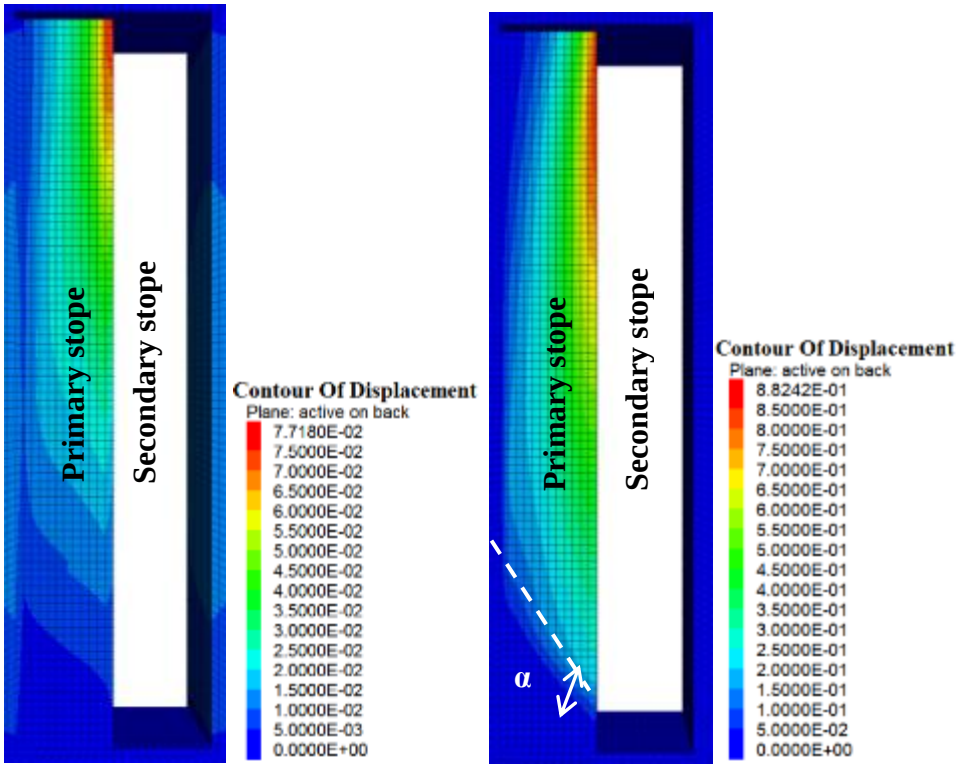

(a) (b)

Figure 6-10: Displacement isocontours along plane C′A′D′-DAC (Fig. 6-2) in the primary backfilled stope after (AWR) front wall removal with: (a) Case $1_{30,85}$, stable backfill (b) Case $1_{30,60,}$ unstable backfill; the sliding plane angle α can also be seen for Case $1_{30,60}$

These simulations results illustrate how the stability of the exposed face is influenced by the stope length and by the cohesion of the cemented backfill. These two factors may affect the response of the backfill in a very significant manner. A systematic comparison of the stability conditions obtained by numerical calculations and given by analytical solutions will be presented below.

6.3.2 Behavior of stopes with a larger width *B*

The calculations results presented above were obtained for B = 6 m (Case 1). The effect of stope width B (m) on the response of an exposed backfill is evaluated for stopes having a length L = 9 m and height H = 45 m (Case 2, Table 6.1), considering a stope width B = 25 m, for c = 30kPa (Case $2_{25,30}$, Table 6-1) or c = 20kPa (Case $2_{25,20}$, Table 6.1). Results from additional

simulations, with other values of *B*, are also presented below, when the failure conditions are assessed.

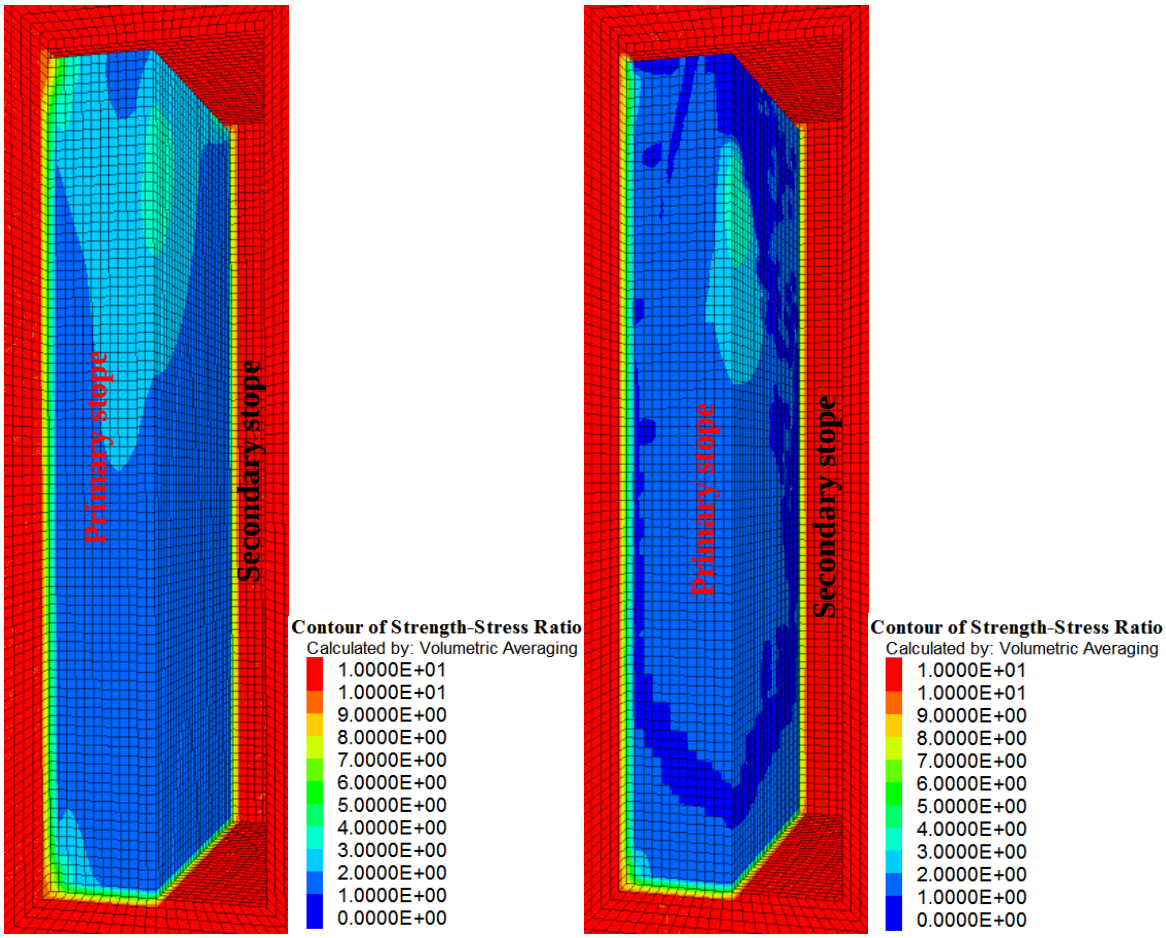

(a) (b)

Figure 6-11: Isocontours of strength/stress ratio (*FS*) in the primary backfilled stope after front wall removal with: a) Case $1_{30,85}$, stable backfill (b) Case $1_{30,60,}$ unstable backfill

Figure 6-12a shows the horizontal stress S_{xx} along the VCL (line AA′) and three walls (lines BB′, CC′, DD′) within the primary stope with B = 25, for c = 30 kPa (Case $2_{25,30}$), before (BWR) and after (AWR) removal of the front wall. In this case, the backfill remains stable AWR. It is seen that the horizontal stresses S_{xx} at mid-height increase considerably along the back wall (line CC′), by up to 3.5 times (from S_{xx} = 43 kPa BWR to S_{xx} = 150 kPa AWR) and by up to 2.5 times along the VCL and side walls (lines AA' and BB′; from S_{xx} = 35 kPa BWR to S_{xx} = 154 kPa AWR). The results for Case $2_{25,30}$ also reveal that the stresses, S_{yy} (not shown here, Appendix E in

Falaknaz, 2014) AWR exceed those BWR along the open face (i.e. along the axis perpendicular to the wall removed).

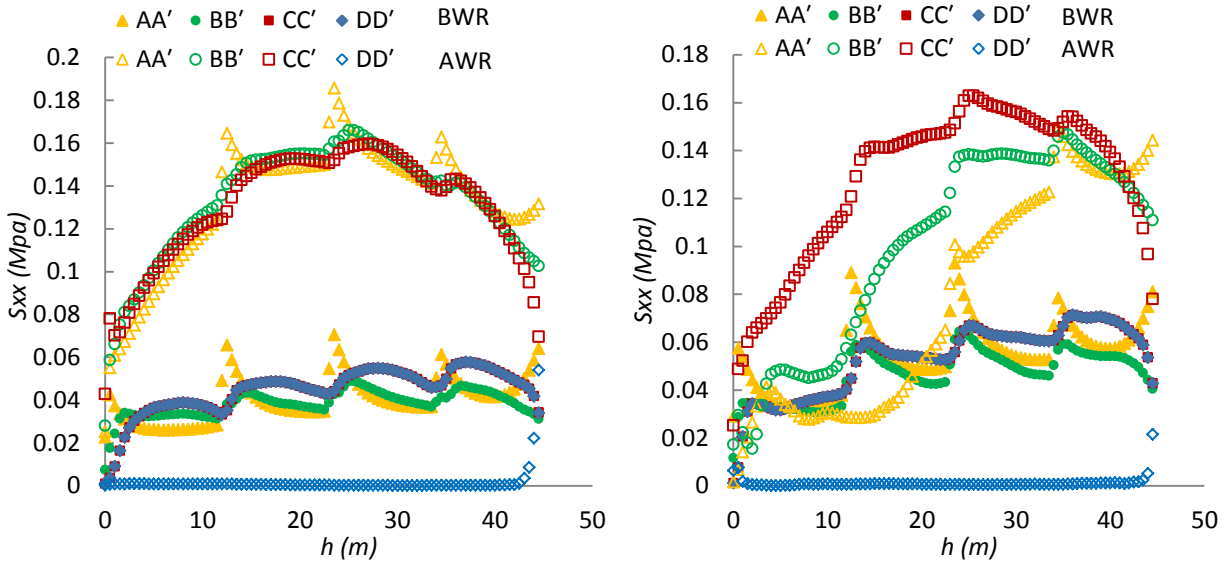

(a) (b)

Figure 6-12: Horizontal stresses S_{xx} in the primary backfilled stope for B = 25m along the VCL (line AA′), back wall (lines CC′), sidewalls (line BB′) and open face (line DD′) before (BWR) and after (AWR) front wall removal: (a) Case $2_{25,30}$, stable backfill (b) Case $2_{25,20,}$ unstable backfill

Figure 6-12b shows stresses for c = 20 kPa (Case $2_{25,20}$). In this case, the backfill becomes unstable upon removal of the front wall. It is seen that the horizontal stresses S_{xx} tend to increase along the back wall (line CC′), by up to 3 times (from S_{xx} = 52 kPa BWR to S_{xx} = 147 kPa AWR, near mid-height); these also increase along sidewalls (line BB′), by up to 2.5 times (from S_{xx} = 43 kPa BWR to S_{xx} = 114 kPa AWR), and along the VCL (line AA′), by up to 1.3 times (from S_{xx} = 49 kPa BWR to S_{xx} = 65 kPa AWR). Figure 6-12 shows that the behavior of the backfill is quite different for Case $2_{25,20}$, compared with the one observed for Case $2_{25,30}$, due to the instability induced by the removal of the front wall, when the backfill cohesion is too low.

Figure 6-13 shows the total displacements of the backfill after removal of the front wall (AWR) for B = 25m, with c = 30 kPa (Fig. 6-13a, Case $2_{25,30}$) and c = 20 kPa (Fig. 6-13b, Case $2_{25,20}$). These results confirm that the backfill is stable when the cohesion equals 30 kPa, with the maximum (total) displacement of the open face δ_{max} = 9 mm, while it is unstable when the

cohesion is 20 kPa with δ_{max} = 1.4 m (Fig. 6-13b). The angle of the sliding plane α at the base of the unstable backfill is about 64° (Fig. 6-13b), which is quite close to the value postulated by Mitchell et al. (1982) (i.e. $\alpha = 45° + \phi'/2 = 62.5°$ for $\phi' = 35°$).

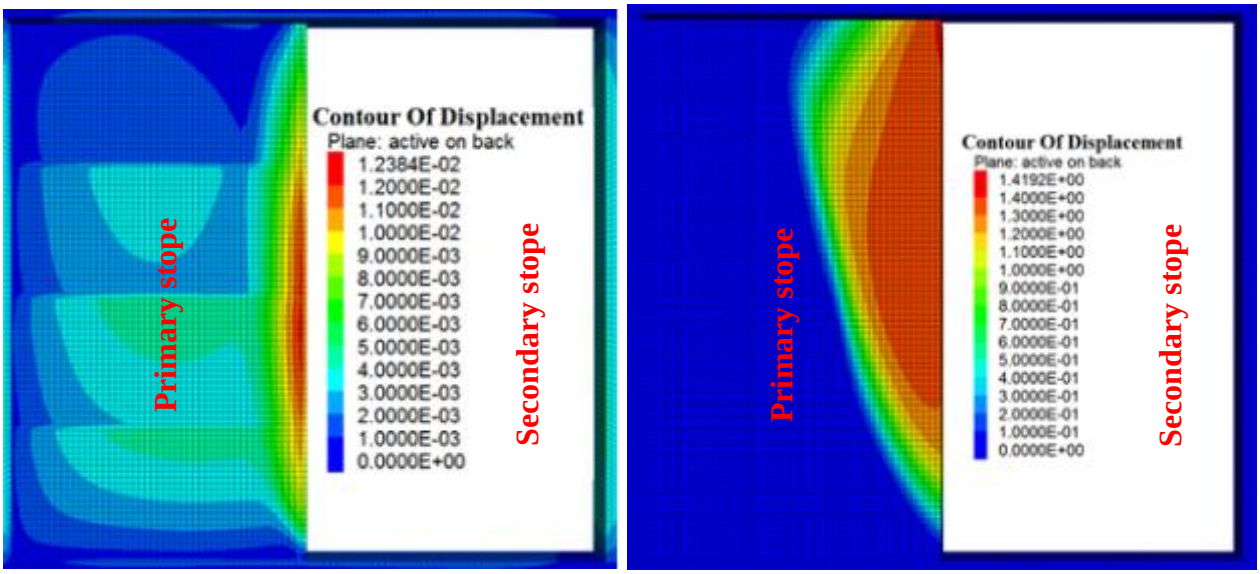

(a) (b)

Figure 6-13: Displacement contours of backfill along plane C′A′D′-DAC (Fig. 6-2) in the primary backfilled stope after (AWR) front wall removal: (a) Case $2_{25,30}$, stable backfill (b) Case $2_{25,20,}$ unstable backfill

Strength/stress ratio (*FS*) isocontours are presented in Figure 6-14. As can be seen, the backfill is unstable (*FS* < 1) for *c* = 20 kPa (Case $2_{25,20,}$ Figure 6-14b), in agreement with the large displacements shown in Figure 6-13b. An increase of the cohesion to 30 kPa (Case $2_{25,30}$, Figure 6-14a) leads to a strength/stress ratio above unity, so the backfill remains stable. These simulations confirm that the stability of an exposed backfill face can be sensitive to the stope width, when the cohesion is low.

6.3.3 Behavior of stopes with a smaller height *H*

The effect of stope height, *H*(m), on the response of exposed backfilled was also investigated, considering stopes having a length *L* = 9 m and a height *H* = 25 m (Case 3, Table 6.1). The simulations results shown here were obtained for *c* = 24 kPa (Case $3_{25,24}$) and *c* = 20 kPa (Case $3_{25,20}$); these are described in the following. Figure 6-15 shows the horizontal stresses

S_{xx} along the VCL (line AA′) and three walls (lines BB′, CC′, DD′) within the primary stope before (BWR) and after (AWR) front wall removal.

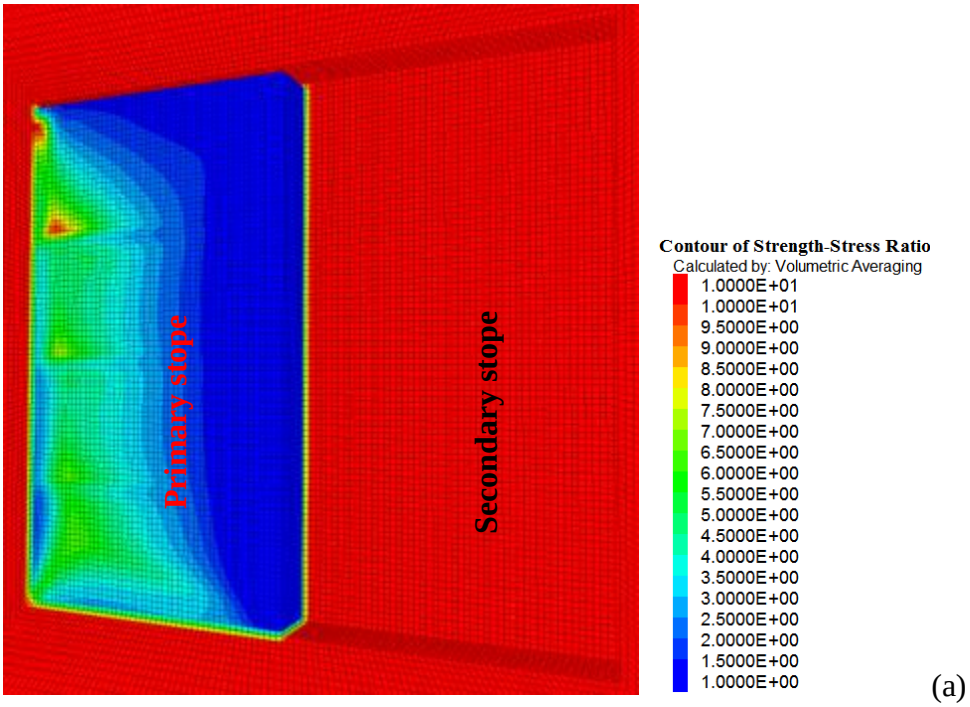

(a)

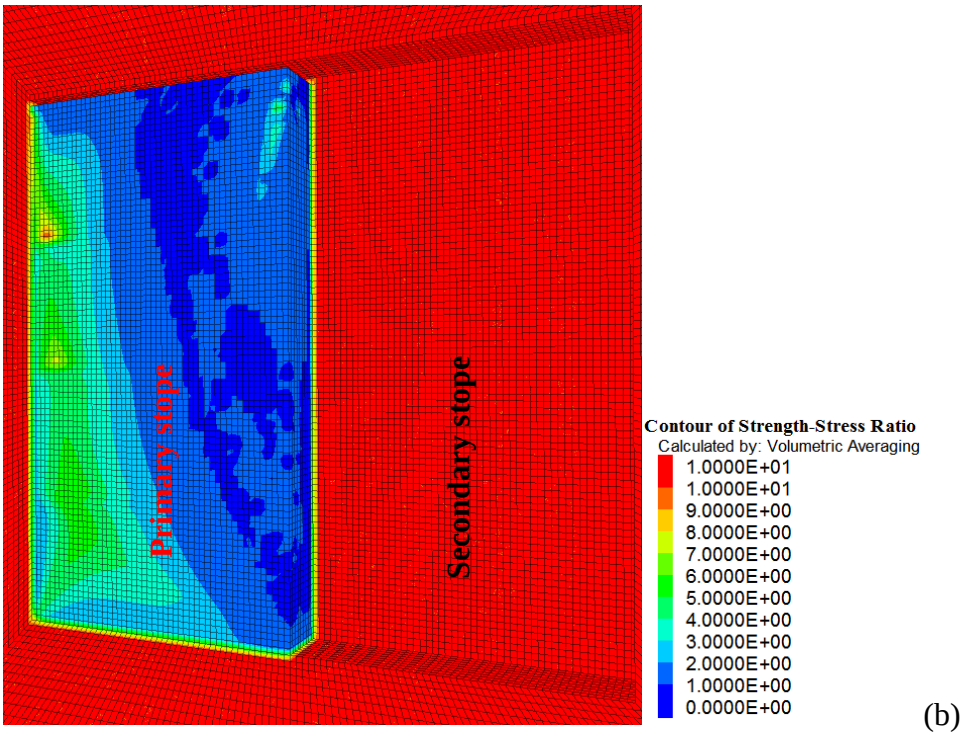

(b)

Figure 6-14: Isocontours of strength/stress ratio (*FS*) in the primary backfilled stope (B = 25 m) after front wall removal: (a) Case $2_{25,30}$, stable backfill (b) Case $2_{25,20,}$ unstable backfill

The simulation results indicate that backfill is stable AWR when c = 24 kPa. It is seen in Fig. 6-15a that in this case, the horizontal stress S_{xx} increases along the back wall (line CC′) by up to 2 times (from S_{xx} = 24 kPa BWR to S_{xx} = 44 kPa AWR), and also along the side walls (line BB′) by up to 3 times (from S_{xx} = 15 kPa BWR to S_{xx} = 44 kPa AWR). This horizontal stress tends to decrease along the VCL (line AA′), by up to 50% (from S_{xx} = 19 kPa BWR to S_{xx} = 8 kPa AWR).

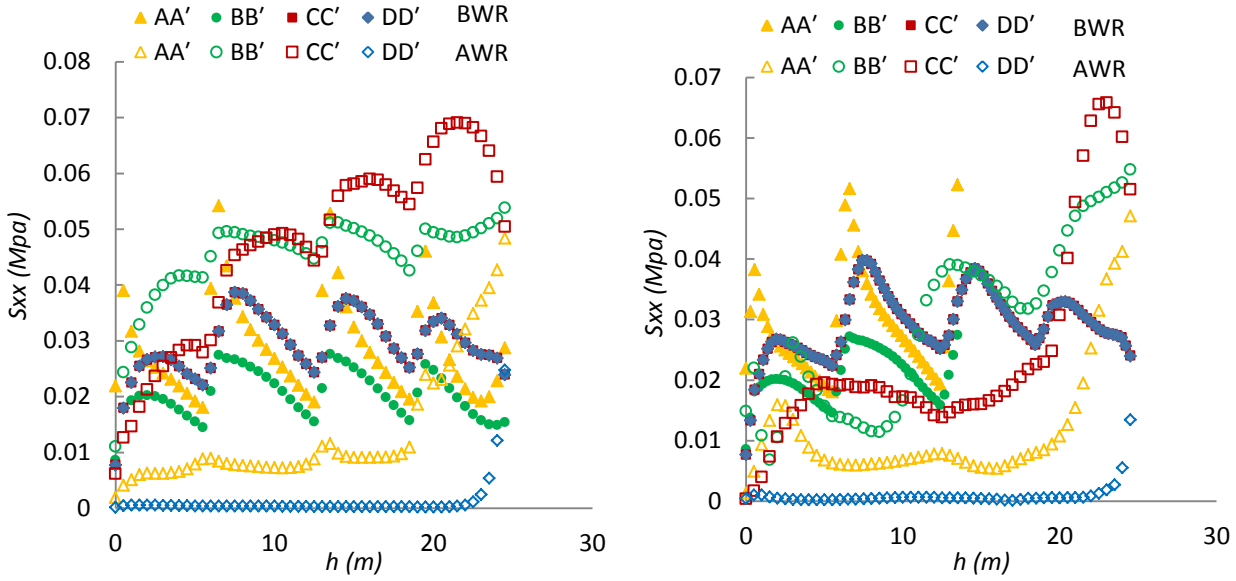

(a) (b)

Figure 6-15: Horizontal stresses S_{xx} in the primary backfilled stope (H = 25 m) along the VCL (line AA′), back wall (lines CC′), sidewalls (line BB′) and open face (line DD′) before (BWR) and after (AWR) front wall removal: (a) Case $3_{25,24}$, stable backfill (b) Case $3_{25,20,}$ unstable backfill

The results also indicate that the horizontal stresses S_{yy} (not shown here, see Appendix E in Falaknaz, 2014) along the three walls tend to increase as a result of removing of the front wall.

The horizontal stress S_{xx} for c = 20 kPa (Case $3_{25,20}$) are shown in Fig. 6-15b, for a backfill that becomes unstable AWR. It is seen that these horizontal stresses decrease considerably along the back wall (line CC′), from S_{xx} = 26 kPa BWR to S_{xx} = 14 kPa AWR near mid-height, and along the VCL (line AA′), from S_{xx} = 25 kPa BWR to S_{xx} = 7 kPa AWR. This horizontal stress tends to increase along the side walls (line BB′), from S_{xx} = 17 kPa to S_{xx} = 35 kPa near mid-height.

The horizontal S_{yy} and vertical S_{zz} stresses (not shown here) in the backfilled stope also tend to increase significantly when the front wall is removed (see details in Appendix E in Falaknaz, 2014).

Figure 6-16 shows the total displacements of the backfill AWR, for H = 25 m, with c = 24 kPa (Case $3_{25,24}$, Fig. 6-16a) and c = 20 kPa (Case $3_{25,20}$, Fig. 6-16b). These results indicate that the backfill remains stable when c = 24 kPa, with maximum (total) displacement of the open face δ_{max} = 4 mm, near the top, while it becomes unstable when cohesion c = 20 kPa, with δ_{max} = 0.44 m. The effect of the four layers used for filling the primary stope can also be seen in this figure. The slide plane angle α is about 64° at the base of unstable backfill, a value quite close to the theoretical angle of 62.5°. Strength/stress ratio (FS) contours presented in Figure 6-17 confirm that the backfill is unstable (strength/stress ratio < 1) for a cohesion of 20 kPa, while it remains stable (strength/stress ratio ≥ 1) for c = 24 kPa.

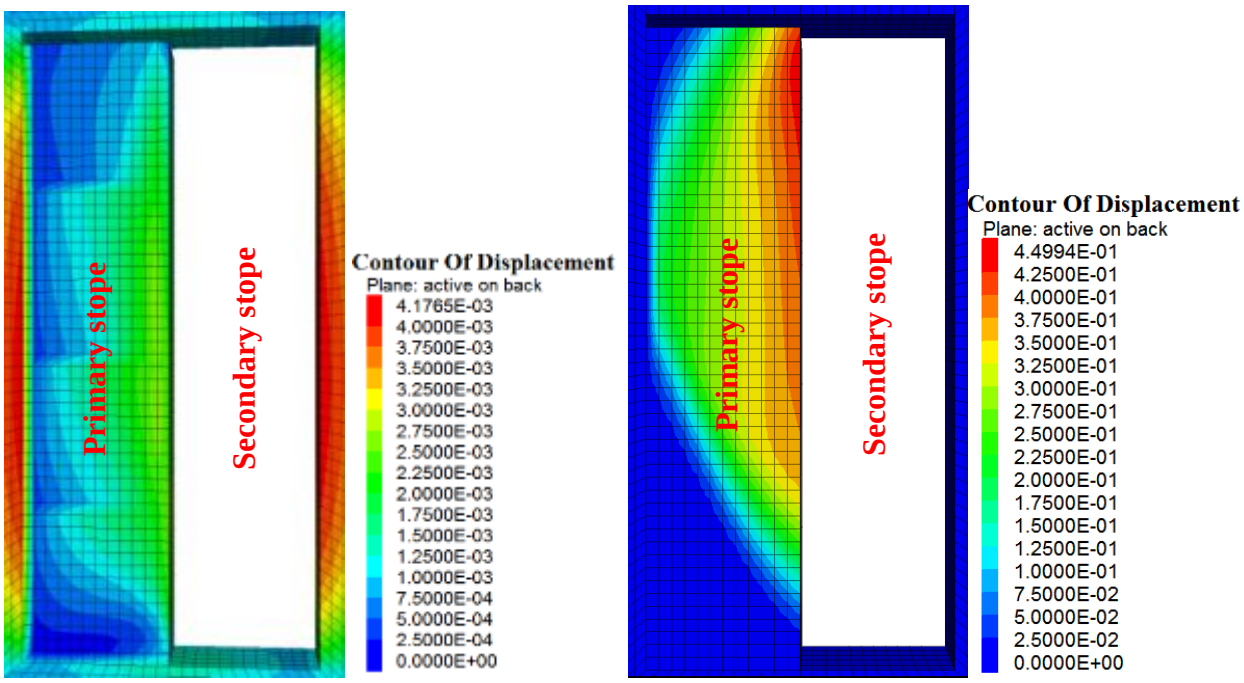

(a) (b)

Figure 6-16: Displacement isocontours in the primary backfilled stope (H = 25 m) after (AWR) front wall removal: (a) Case $3_{25,24}$, stable backfill (b) Case $3_{25,20,}$ unstable backfill

These simulations results confirm that the FS of the exposed backfill decreases with an increase of the stope height, for a given cohesion value. The stability can be improved by increasing the cohesion of the backfill.

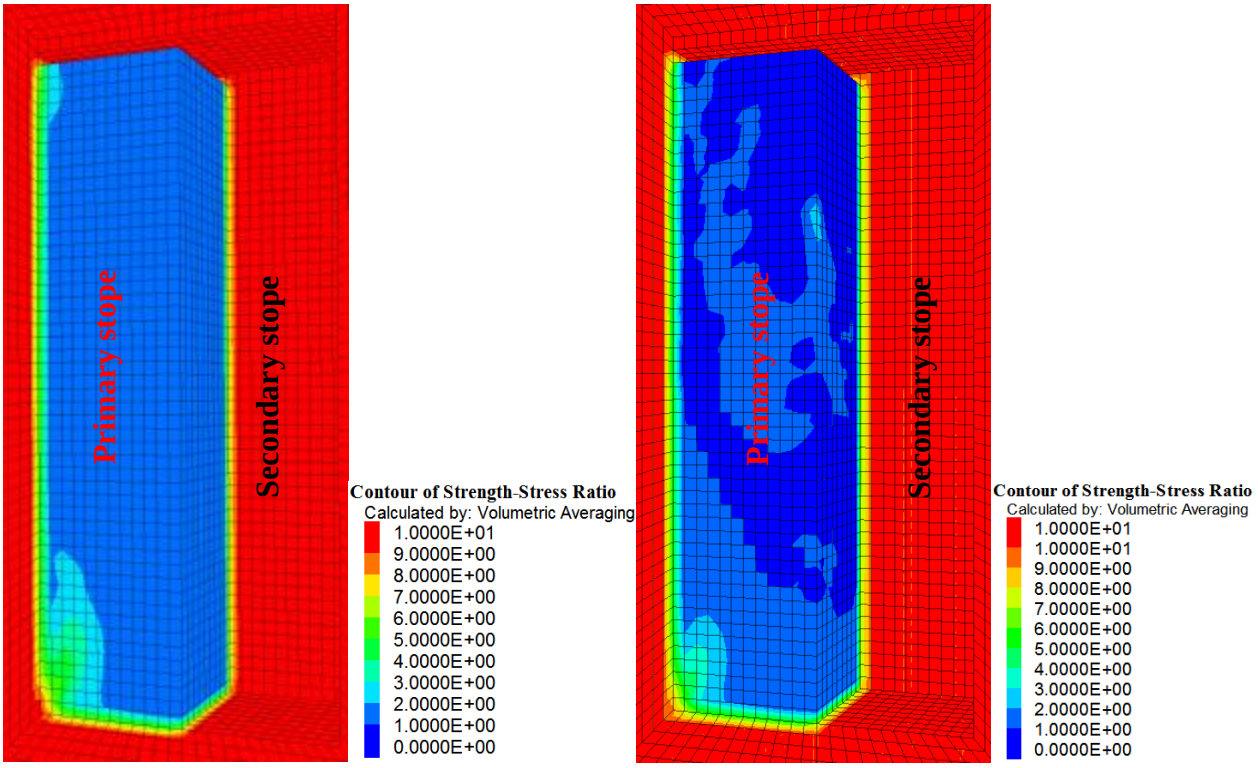

(a) (b)

Figure 6-17: Isocontours of strength/stress ratio (*FS*) in the primary backfilled stope (*H*= 25 m) after front wall removal: (a) Case $3_{25,24}$, stable backfill (b) Case $3_{25,20}$, unstable backfill

6.3.4 Effect of wall removal sequence

Numerical simulations results also revealed that the backfill response (in terms of stresses, displacements and stability) is affected by the front wall removal sequence. For instance, when the removal sequence goes from one step (excavation of the complete face) to four and seven steps (starting at the base of the stope; Cases 4_1, 4_4, 4_7), for a cohesion c = 30 kPa (and L = 12 m, B = 6 m, H = 45 m), the maximum displacement of the exposed face, δ_{max}, decreases from 0.15 m to 0.009 m (Figure 6-18), while the factor of safety *FS* (strength/stress ratio) increases from below unity for a single step (Case 4_1 , unstable case) to above one for 4 and 7 steps (Cases 4_4 and 4_7). The position at which the maximum displacement occurs also tends to change with the removal sequence, being close to top of the exposed backfill for Case 4_1, and near mid-height for Case 4_7. When the backfill cohesion c is relatively lower, at c = 20 kPa, (Cases 5_1 and 5_4), the value of *FS* (strength/stress ratio) becomes smaller than unity, leading to instability in all cases. Increasing the number of steps for the removal of the front wall then produces a reverse effect on

the displacements, as seen in Figure 6-19, with the displacements increasing from Case 5_1 to Case 5_4.

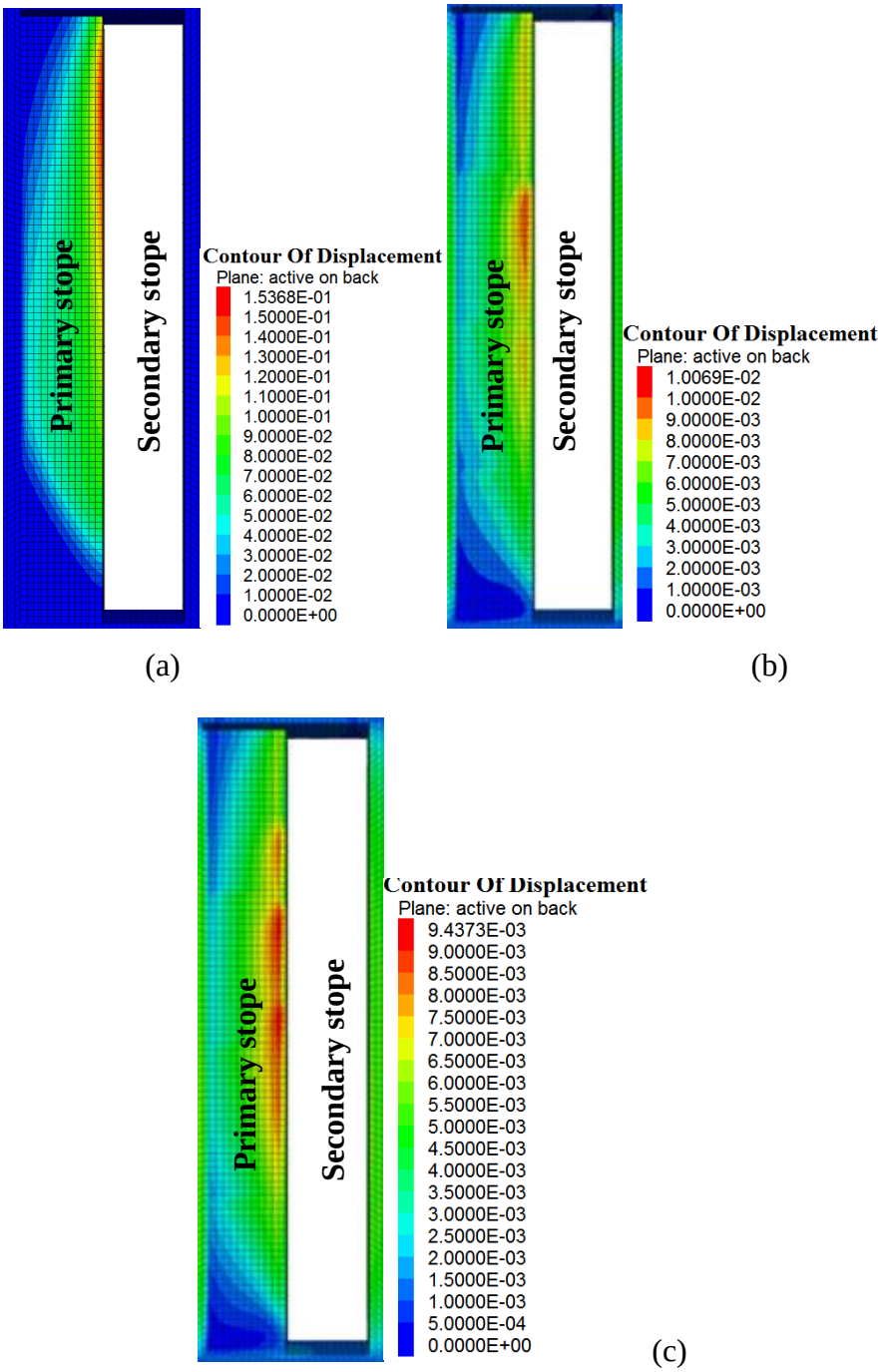

Figure 6-18: Effect of the number of excavation steps to create the secondary stope (removal of the front wall) on the displacements of the backfill in the primary stope: (a) one excavation step (Case 4_1) unstable backfill, (b) four excavation steps (Case 4_4), stable backfill (c) seven excavation steps (Case 4_7) stable backfill with c = 30 kPa

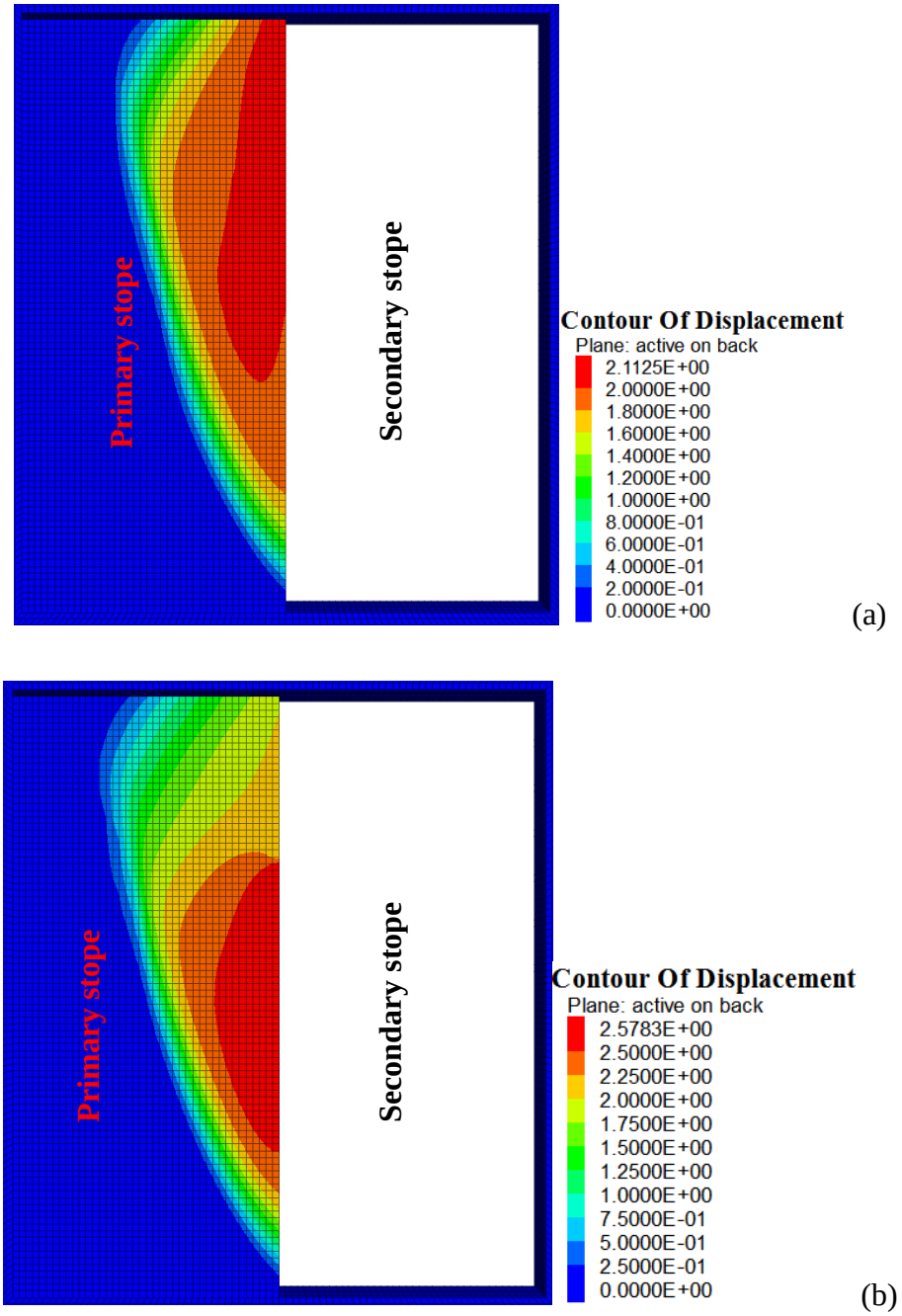

Figure 6-19: Effect of the number of excavation steps to create the secondary stope (removal of the front wall) on the displacements of the backfill in the primary stope: (a) one excavation step (Case 5_1), (b) four excavation steps (Case 5_4), unstable backfill with c = 20 kPa

Figure 6-20 shows the displacements obtained for a stope having a height H = 20 m, B = 6 m, L = 9 m and c = 20 kPa, with the wall removed in one and four steps (Cases 6_1 and 6_4); the backfill is stable in these two cases. It is seen that the maximum total displacement of the open

face δ_{max} = 5.1 mm when the wall is removed in one step and δ_{max} = 4.63 mm when removal is done in four steps; there is thus a very limited effect of the removal sequence for such a stable backfill face. Nonetheless, the location of the maximum displacement is affected by the removal sequence of the front wall, being close to the top for Case 6_1 and near mid-height for Case 6_4.

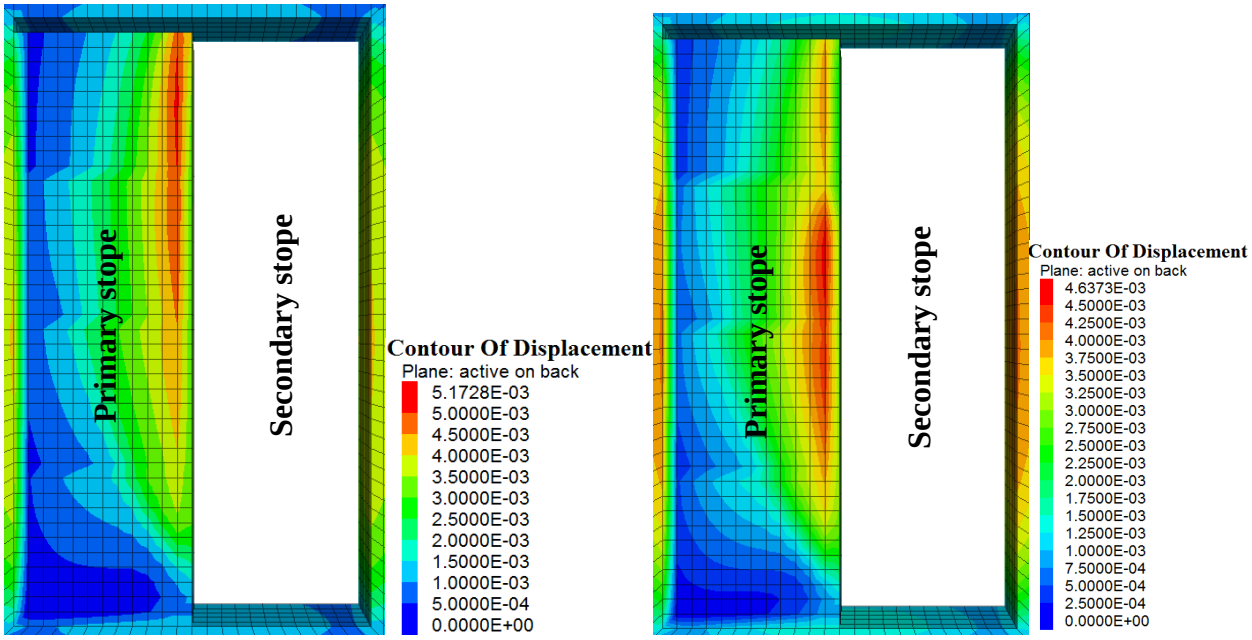

(a) (b)

Figure 6-20: Effect of the number of excavation steps to create the secondary stope (removal of the front wall) on the displacements of the backfill in the primary stope: (a) one excavation step (Case 6_1), (b) four excavation steps (Case 6_4), stable backfill with c = 20 kPa

6.4 Analytical solutions for the required strength of cemented backfill

As was mentioned earlier, various solutions have been proposed to estimate the strength of exposed backfill. Three of these solutions are recalled here, and then compared with results obtained from the numerical simulations.

6.4.1 Original solution of Mitchell et al. (1982)

Figure 6-21 shows the well-known wedge block model used by Mitchell et al. (1982) to develop an analytical solution that gives the factor of safety *FS* of an exposed backfill in a vertical stope. In addition to the *FS*, this solution can also be used to evaluate the required

cohesion *c* for the backfill to be placed in a stope with an open face. These two parameters can be expressed as follows:

$$FS = \frac{\tan \emptyset}{\tan \alpha} + \frac{2cL}{(H - \frac{B \times \tan \alpha}{2})(\gamma L - 2c_b) \sin 2\alpha} \quad (6\text{-}1)$$

$$c = \frac{\gamma H}{2\,(\frac{H}{L} + tan\alpha)} \quad , \quad \text{for } FS = 1 \quad (6\text{-}2)$$

In these equations, α is the angle of failure plane from the horizontal axis ($\alpha = 45° + \frac{\emptyset}{2}$ is assumed); ϕ is internal friction angle (°) of the backfill material; *c* is the backfill cohesion (kPa); c_b is the cohesion (kPa) along the sidewalls and backfill interfaces; γ is the fill unit weight (kN/m^3); *L* is the exposed block length (m); *B* is the block width (m); *H* is the block height (m).

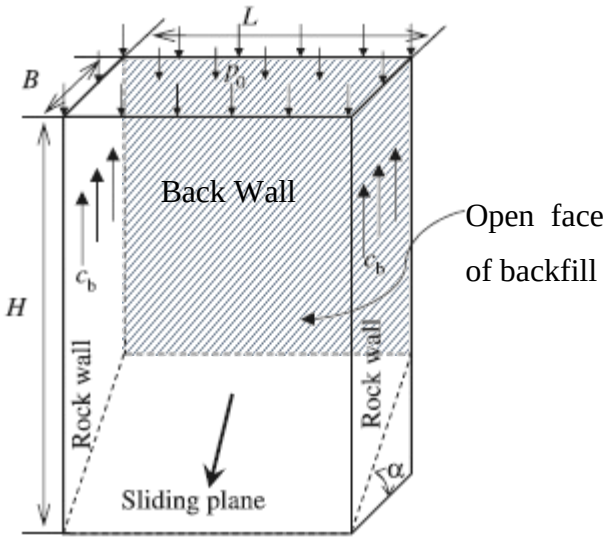

Figure 6-21: Wedge block model for the backfilled stope with an open face (after Mitchell et al. 1982)

This solution applies to backfilled stopes with a high aspect ratio (i.e. $H/B > tan\ \alpha$). Mitchell et al. (1982) assumed that the cohesion c_b along the interfaces between the backfill and two side walls is equal to the cohesion of the backfill *c*. Other characteristics of this solution have been reviewed and discussed by Li and Aubertin (2012, 2014), who have proposed the following variants.

6.4.2 Modified Mitchell (MM) solution

Li and Aubertin (2012) modified the Mitchell et al. (1982) solution, using many of the same assumptions. However, they postulated that the cohesion c_b along the two lateral interfaces between the backfill and the sidewalls could (and often should) be smaller than the backfill cohesion c. They also included a surcharge p_o at the surface of the backfill. When neglecting the effect of tension cracks, this led to the following MM solution for stopes with a high aspect ratio (HAR):

$$FS = \frac{\tan \emptyset}{\tan \alpha} + \frac{2c}{[p_o + (H - \frac{B \times \tan \alpha}{2})(\gamma - 2c_b / L)] \sin 2\alpha} \quad (6\text{-}3)$$

$$c = \frac{(p_o + \gamma(H - (B \times tan\, \alpha)/2)/2}{\left[\left(FS - \frac{\tan \emptyset}{\tan \alpha}\right) \sin 2\alpha\right]^{-1} + r_b\, (H - \frac{B \times \tan \alpha}{2})/L} \quad (6\text{-}4)$$

Where r_b (= c_b/c; from 0 to 1) is the adherence ratio of the fill-rock interfaces.

The Mitchell et al. (1982) solution has also been extended to the case of stopes with a low aspect ratio (LAR, for $H/B < \tan \alpha$). The factor of safety and required cohesion can then be expressed as follows:

$$FS = \frac{\tan \emptyset}{\tan \alpha} + \frac{2c}{[p_o + H(\frac{\gamma}{2} - \frac{c.r_b}{L})] \sin 2\alpha} \quad (6\text{-}5)$$

$$c = \frac{p_o + \gamma(H/2)}{2\left[\left(FS - \frac{\tan \emptyset}{\tan \alpha}\right) \sin 2\alpha\right]^{-1} + r_b H/L} \quad (6\text{-}6)$$

The MM solution was shown to better represent the experimental laboratory testing results provided by Mitchell et al (1982). Its practical application however requires an evaluation of the strength along the fill-rock interface to define the value of c_b (and r_b).

6.4.3 Solution of Li and Aubertin (2014)

The MM solution presented above is based on assumptions that are quite similar to those adopted by Mitchell et al. (1982), thus inheriting some of the same limitations. More recently, Li and Aubertin (2014) presented numerical simulations results obtained with FLAC^{3D} that illustrate the response of exposed backfill in terms of displacements and failure mechanism. The results were used to develop a somewhat different solution, which is summarized here.

This solution is also based on the sliding block model shown in Figure 6-21, considering an upper rectangular block and a lower triangular wedge. The upper block is assumed to move downward along the vertical direction while the lower part moves in a direction parallel to the inclined sliding plane. The analysis of the model stability presented by Li and Aubertin (2014) gives the factor of safety *FS* and the required cohesion *c*, which can be expressed as follows:

$$FS = \frac{\tan\phi}{\tan\alpha} + \frac{c\left(\frac{1}{\cos\alpha} + r_{bs}\frac{H'}{L}\right) + \frac{\left(\frac{\gamma}{M} - p_1\right)\left[\frac{1-\exp(-MH')}{MH'} - 1\right] + \gamma H'/2}{1+L/B}}{\left(p_1 + \frac{\gamma H'}{2}\right)\sin\alpha} \quad (6\text{-}7)$$

$$c = \frac{D'\left(p_o + \gamma\left(H-H'\right) - G'\right) + \frac{(A'\gamma H')}{2}[1+L/B]\sin\alpha - \gamma\left(\frac{C'}{M} + \frac{H'}{2}\right)}{\left(1+\frac{L}{B}\right)B' + D'(H-H')\left(\frac{2r_{bs}}{L} + \frac{r_{bb}}{B}\right)} \quad (6\text{-}8)$$

With $p_1 = p_o - G' + (H-H')\left\{\gamma - c\left(\frac{2r_{bs}}{L} + \frac{r_{bb}}{B}\right)\right\}$ (6-9)

$$G' = \frac{1}{1+\frac{L}{B}}\left\{\gamma(H-H') + (p_O - \frac{\gamma}{M})[1 - \exp(-(H-H')M]\right\} \quad (6\text{-}10)$$

$$A' = FS - \frac{\tan\phi}{\tan\alpha} \qquad B' = \frac{1}{cos\alpha} + r_{bs}\frac{H'}{L} \qquad C' = \frac{1-\exp(-MH')}{MH'} - 1 \quad (6\text{-}11)$$

$$D' = A'\left(1 + \frac{L}{B}\right)sin\alpha + C' \quad H' = B\,tan\alpha \quad M = 2K\,(B^{-1} + L^{-1})tan\delta \quad (6\text{-}12)$$

6.4.4 Comparison with numerical results

A series of numerical simulations have been performed to evaluate the stability of exposed backfill for different conditions and to assess the validity of the three analytical solutions presented above; in these calculations, the wall was removed in a single step. Figure 6-22 shows the variation of the required backfill cohesion *c* (for *FS* = 1) obtained from the Mitchell et al. (1982) solution, the MM solution from Li and Aubertin (2012), and the Li and Aubertin (2014) solution (with r_{bb}= r_{bs} = 1; this corresponds to a condition without interface elements), for specific stope geometries (defined in the caption). The simulations were repeated for each geometry by varying the value of *c* to determine the backfill cohesion required to maintain a stable condition; this critical value is obtained by progressively reducing the value of *c*, from one

simulation to the other, until failure appears. The displacements, stresses and strength/stress ratio are monitored during each simulation to assess the stability of the model. This process was repeated for each stope geometry, for the various conditions considered here. The different numerical outcomes are shown in Figure 6-22 (dots) for stopes with varying length *L* (Fig. 6-22a), width *B* (Fig. 6-22b), and height *H* (Fig. 6-22c). The minimum cohesion obtained from the three analytical solutions is also shown in these graphs.

The simulations results show that the required backfill strength, expressed in terms of cohesion *c* (for a fixed internal friction angle $\phi = 35°$), tends to increase with an increase of the stope length *L*, and to a lesser degree with height *H;* the required cohesion c remains almost unchanged when stope width *B* varies (for the conditions analyzed here). In all cases, the cohesion value given by the solution of Li and Aubertin (2014) is the closest to the numerical results for the base case (i.e. starting value of *L*, *B* and *H*). However, the tendencies observed in Figure 6-22 for the numerical results do not always agree with those of the analytical solutions.

More specifically, it is seen that the MM solution (applied here to cases with a high aspect ratio, HAR) lead to a higher required cohesion for the backfill when *L* and *H* are increased. The Li and Aubertin (2014) solution seems to better capture the effect of *H* (Fig. 6-22c), while the effect of *L* follows an intermediate trend between this solution and the MM solution (Fig. 6-22a); in both graphs, the MM and Mitchell et al. (1982) solutions tend to overestimate the required strength and the cohesion given by that of Li and Aubertin (2014) is underestimated, especially when *L* increases.

The simulations results indicate that the required strength does not change much with stope width *B*, hence following the trend given by the Mitchell et al. (1982) solution that nonetheless largely overestimates the required cohesion. The effect of *B* is not well captured by the 2 other analytical solutions, which give a reduction of *c* when the width increases. Additional calculations have been made for backfilled stopes with a low aspect ratio (LAR, $B > 23$m); it these cases, the required cohesion calculated using the MM solution is close to the value obtained using numerical simulations (results not shown here; see Appendix E for details in Falaknaz, 2014).

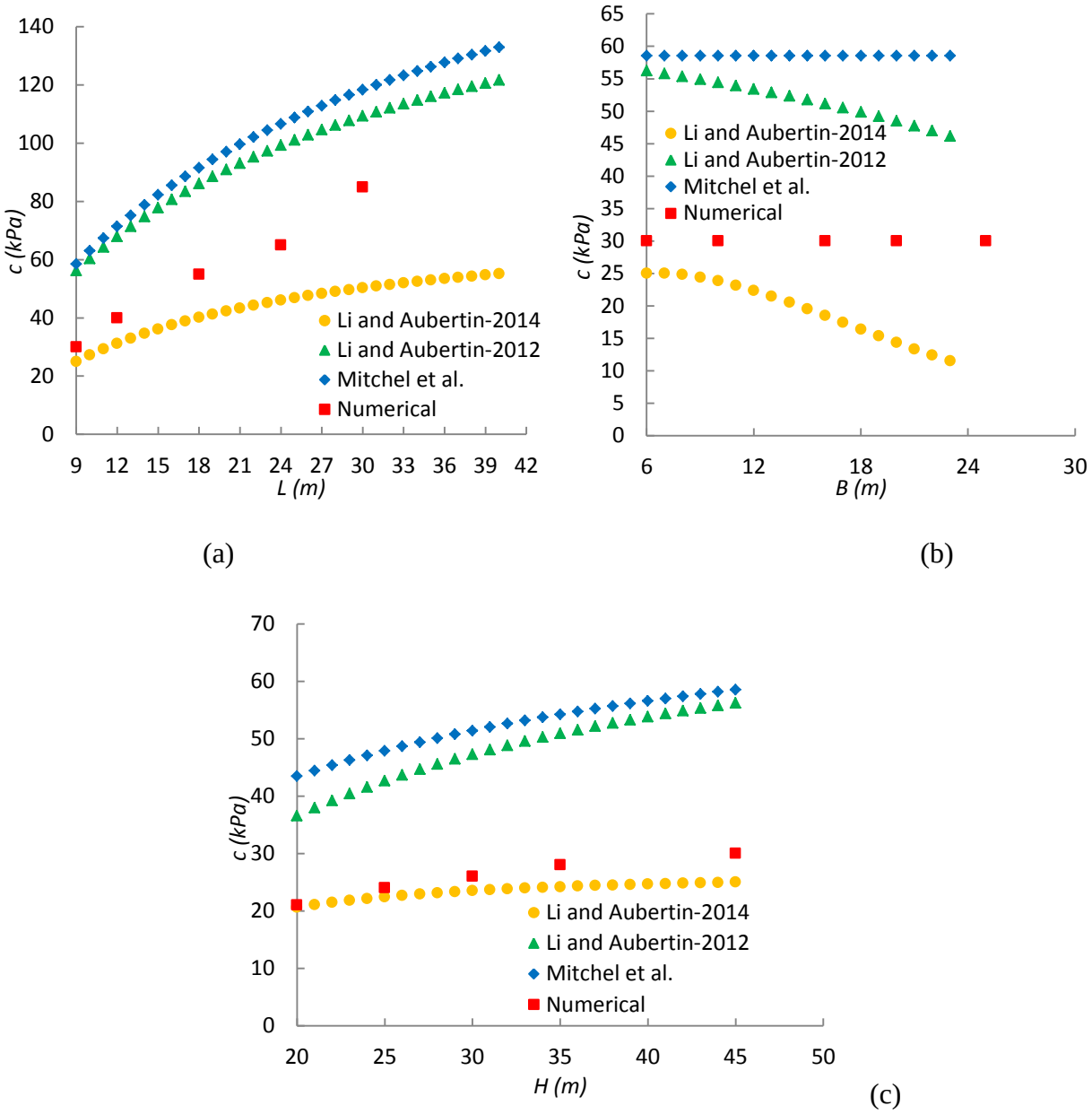

Figure 6-22: Required backfill cohesion c (for FS = 1): (a) variation of stope length, L, (H = 45m, B = 6 m), (b) variation of stope width, B, (L = 9m, H = 45m), (c) variation of stope height, H, (L = 9m, B = 6m); Results obtained from three analytical solutions and numerical simulations (with a zero tensile strength cut-off)

It thus appears, based on these numerical simulations, that none of the three solutions considered here can properly capture the variation of the required cohesion as a function of the stope geometry. More work is thus required to better define analytically this critical value for various geometrical characteristics of mine stopes with exposed backfill.

The angle of the sliding plane, α, was also evaluated for all simulated cases where instability occurred (for the critical value of c, AWR in a single step). The main results shown in Figure 6-23 indicate that the apparent sliding plane makes an angle α between 47° and 64°. Many of these values are lower than the critical angle commonly used for the sliding plane angle, i.e. α = 62.5° for ϕ = 35° (defined for plane strain conditions). The results indicate that this sliding plane angle α may vary with the stope geometry, as its value is affected by changing values of L, B, or H (for the other dimensions remaining constant).

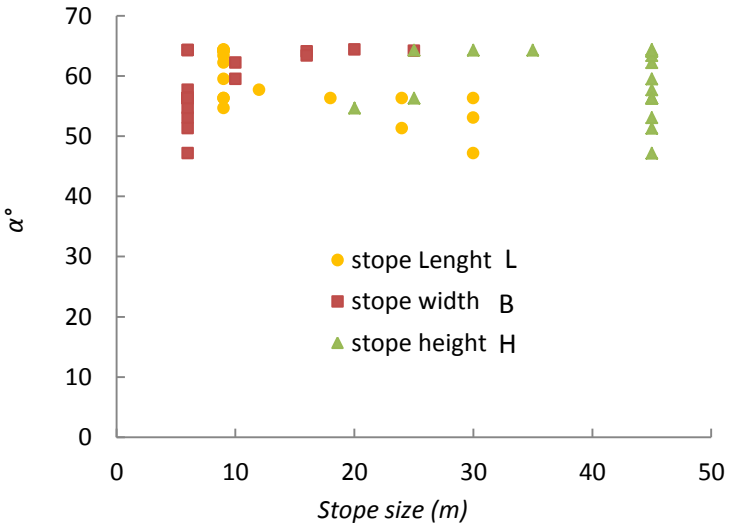

Figure 6-23: Variation of the sliding plane angle α with stope sizes (L, B, H) obtained from the numerical simulations for stope with an open face (base values *L=9m*, *B=6m*, *H=45m)*

6.5 Discussion

The numerical code FLAC^{3D} has been used here to assess the effect of creating a secondary stope immediately next to a primary backfilled stope, focusing on the stress distribution and backfill displacement upon removal of the wall. The results illustrate how the opening geometry (i.e. height, length and width) and backfill cohesion affect the stresses and displacements in the backfilled stope with an open face.

The simulations specifically show that when the supporting (front) wall is removed, the arching effect can be significantly reduced. The horizontal stresses acting on the walls in the primary stope then become much smaller than those obtained before wall removal, particularly when the backfill cohesion is low. The results nonetheless indicate that the normal stresses along

the back wall are not nil, as was postulated to develop the analytical solutions of Mitchell et al. (1982) and Li and Aubertin (2012, 2014). The value of this horizontal stress, normal to the back wall, is higher when the backfill cohesion is sufficiently large to maintain stability of the exposed backfill. This suggests that the shear resistance due to frictional stresses along this back wall should be included in a representative analytical solution.

The simulations results also provide information on the required strength (cohesion) of the exposed backfill when the stope length L and height H are increased. These numerical calculations furthermore suggest that the minimum cohesion is not influenced much by the stope width B (for the cases studied here).

Comparisons between numerical and analytical results indicate that the solutions proposed by Mitchell et al. (1982) and Li and Aubertin (2012) tend to overestimate the required strength of backfill, while the one proposed by Li and Aubertin (2014) tends to underestimate this cohesion, particularly when L and B become much larger than the base values used in the calculations.

The simulations further show that the excavation sequence (i.e. number of steps for removing the front wall) can also influence the displacements and the required strength of the exposed backfill. When the value of c is relatively low and the backfill face is unstable, increasing the number of steps to remove the wall leads to increased displacements and a reduction of FS (strength/stress ratio). However, when the value of c is sufficiently large ($\geq$ 20 kPa for most cases simulated here), increasing the number of steps to remove the front wall leads to reduced displacements and increased FS.

The simulations results also indicate that the sliding plane angle α may vary with the stope geometry and backfill cohesion. In many cases, the value of α obtained from the 3D simulations is lower than the theoretical critical angle used in the analytical solutions (developed for plane strain conditions).

Some notes of caution should be mentioned when considering the results presented here. As stated above, the numerical simulations were performed without considering interface elements between the backfill and the rock walls; this corresponds to a condition with $\delta = \phi'$ (= 35°) and $c = c_b$. This is why $r_{bs} = r_{bb} = 1$ has been used in the calculations made with the analytical solutions of Li and Aubertin (2012, 2014). However, experimental evidence suggests that the

cohesion along rock-backfill interfaces may be smaller than that of the cemented backfill (Fall et al. 2010). This aspect has not been taken into account here.

The backfill strength has been expressed here using the Coulomb criterion, with a tension cut-off. A zero tensile strength cut-off was applied for the backfill in these simulations. As stated above, this conservative assumption was used because there is a lack of data on the actual tensile strength of cemented backfills. Nonetheless, as most of the unstable zones tend to fail in tension, it would be quite useful to evaluate the response of backfilled stopes with an open face using more realistic tensile strength values; it can be expected (from ongoing work) that this would reduce the required strength of cemented backfills.

It should also be acknowledged that the Coulomb criterion, and the corresponding elasto-plastic model, may not always be representative of the response of cemented backfill (Li et al. 2010). Also the Coulomb parameters, c and ϕ', are used here to define the strength/stress ratio (or *FS*), while others, like Mitchell et al. (1982), have been using the uniaxial compressive strength (UCS) to express the critical conditions leading to instability; if needed, the relationship between UCS and (c , ϕ') could be applied to express *FS* in terms of the former parameter.

Additional factors can also influence the stresses and displacements in exposed backfill. These include the backfill friction angle, dilation angle, stope inclination, and conditions along the stope walls, which are being considered in ongoing work.

6.6 Conclusion

This paper presents the main results of a numerical and analytical investigation of the behavior of exposed backfill in mine stopes (with an open face). The main factors considered in the numerical simulations include the stope geometry, backfill cohesion, and excavation sequence to remove the front wall. The results indicate that the arching effect is significantly reduced in the back filled stope after removal of the front wall. The results also show that non-negligible contact stresses exist along the fill-wall interfaces, on the three remaining walls, after front wall removal; this observation is not in line with assumptions adopted to develop the analytical solutions proposed by Mitchell et al. (1982) and Li et al. (2012, 2014). This behavior thus needs to be reconsidered for further development of more appropriate solutions.

The results presented here also show that higher backfill strength is required for stopes with a higher length or height. The stability of the exposed backfill face appears to be little affected by the stope width, for the cases analysed here.

The results further show that for a given stope geometry, removing the front wall in more than one step (i.e. progressive removal) can influence negatively the backfill displacement and factor of safety (*FS*) when the cohesion is relatively week.

The comparison between numerical results and analytical solutions tends to indicate that the existing solutions do not necessarily follow the trends given by the former when the geometry of the stope is changed. Therefore, improvements may be required to give more realistic values of the required backfill cohesion.

Acknowledgements

The authors acknowledge the financial support from NSERC, from the partners of the Industrial NSERC Polytechnique-UQAT Chair on Environment and Mine Wastes Management (2006-2012) and from the Research Institute on Mines and the Environment (RIME UQAT-Polytechnique; http://rime-irme.ca/).

References

Arjang, B. (2004). Database on Canadian in situ ground stresses. CANMET Division Report MMSL, 01-029 (TR).

Belem, T., Benzaazoua, M., and Bussière, B. (2000). Mechanical behaviour of cemented paste backfill. *In* Proceedings of 53th Canadian Geotechnical Conference, Montreal, Canada, Vol. 1, pp. 373-380.

Benzaazoua, M., Peyronnard O., Belem T., Fried E., Aurore S., Dublet G. (2010). Key issues related to behaviour of binders in cemented paste backfilling. Proceedings of the 13th International Seminar on Paste & Thickened Tailings (Paste 2010), 3-6 may 2010, Toronto, ON, Keynote paper.

Dirige APE, McNearny RL, Thompson DS. (2009). The effect of stope inclination and wall rock roughness on back-fill free face stability. In: Rock Engineering in Difficult Conditions: Proceedings of the 3rd Canada-US Rock Mechanics Symposium, Toronto, 2009: 9-15.

Emad, M.Z., Mitri, H.S. (2013). Modelling dynamic loading on backfilled stopes in sublevel stoping systems. Rock characterisation, modelling and engineering design methods, Feng Hudson and Tan (Eds), Taylor and Francis Group, London, ISBN 978-1-138-00057-5.

Emad, M.Z., Mitri, H.S., and Kelly, C. (2014). Effect of blast-induced vibration on fill failure in vertical block mining with delayed backfill. Can. Geotech.J. **51**(9): 975-983.

Falaknaz, N., Aubertin, M. and Li, L. (2014). A numerical modelling study to assess the stress distribution in two nearby backfilled openings created in sequence. In: Proceedings of the Canadian geotechnical conference, GeoRegina, Regina, Canada.

Falaknaz, N., Aubertin, M. and Li, L. (2013). Numerical investigation of the stress state in adjacent backfilled mine stopes. In: Proceedings of the Canadian Geotechnical Conference, GeoMontreal, Montreal, Canada.

Fall, M., Nasir, O. (2010). Mechanical behaviour of the interface between cemented tailings backfill and retaining structures under shear loads. Geotechnical and Geological engineering, **28** (6), 779-790.

Hassani, F., and Archibald, J. (1998). Mine backfill. CD-Rom, Canadian Institute of Mine, Metallurgy and Petroleum. Montreal, CIM.

Herget, G. (1988). Stresses in rock. A.A.Balkema, Rotterdam, The Netherland.

Itasca. (2014). FLAC^{3D} version 5.0. Users Manuals. ITASCA Consulting Group, Thresher square East, 708 South Third Street, Suite 310, Minneapolis, Minnesota, USA.

Karima, R., Simangunsongb, G. M., Sulistiantocand, B., and Lopulaland, A. (2013). Stability analysis of paste fill as stope wall using analytical method and numerical modeling in the kencana underground gold mining with long hole stope method. Procedia Earth and Planetary Science, **6**(2013): 474 – 484.

Li, L., Aubertin, M., Simon, R., Bussiere, B., and Belem, T. (2003). Modelling arching effects in narrow backfilled stopes with FLAC. Proc., the 3th Int. FLAC symp, R. Brummer, P. Andrieux, C. Detournay, and R. Hart, eds, A.A.Balkema, Rotterdam, Netherlands, 211-219.

Li, L., Aubertin, M., and Belem, T. 2005. Formulation of a three dimensional analytical solution to evaluate stress in backfilled vertical narrow openings. Can. Geotech. J., **42**(6), 1705-1717.

Li, L., and Aubertin, M. (2009). Numerical investigation of the stress state in inclined backfilled stopes. International Journal of Geomechanics, **9**(2): 52-62.

Li, L., Aubertin, M., Shirazi, A. (2010). Implementation and application of a new elasto-plastic model based on a multiaxial criterion to assess the stress state near underground openings. ASCE International Journal of Geomechanics., **10**(1): 13-21.

Li L, Aubertin M. (2012). A modified solution to assess the required strength of exposed backfill in mine stopes. Can Geotech J, **49**(8): 994-1002.

Li L, Aubertin M. (2014). An improved method to assess the required strength of cemented backfill in underground stopes with an open face. International Journal of Mining Science and Technology, 24: 549–558.

Mitchell, R.J., Olsen, R.S., and Smith, J.D. (1982). Model studies on cemented tailings used in mine backfill. Canadian Geotechnical Journal, **19**(1): 14–28. doi:10.1139/t82-002.

Potvin Y, Thomas E, and Fourie A. (2005). Handbook on mine fill. Australian Centre for Geomechanics, The University of Western Australia, Nedlands, Australia.

Zou, D.H., and Nadarajah, N. (2006). Optimizing backfill design for ground support and cost saving. In Proceedings of the 41st U.S. Rock Mechanics Symposium – ARMA's Golden Rocks 2006 – 50 Years of Rock Mechanics, Golden, Colo.Omnipress.

Veenstra, R. (2013). A design procedure for determining the in situ stresses of early age cemented paste backfill. PhD Thesis, University of Toronto, Canada.

CHAPTER 7 OTHER THREE DIMENSIONAL ANALYSES AND DISCUSSION

7.1 Introduction

Backfilling of underground stopes serves to improve ground control conditions and prevent excessive deformation of the surrounding rock mass, providing a safer working place (Potvin et al. 2005). The stress state in backfilled stopes is a critical issue for its design. In this regard, various studies have shown that the difference in stiffness and strength between filling materials and rock mass can generate stress redistribution from the backfill to the adjacent walls. This stress transfer has been referred to an arching effect (e.g. Knutsson 1981; Mitchell et al. 1982). In recent years, much work has been done to develop analytical solutions to evaluate the stress distribution in isolated backfilled stopes under plane strain (2D) condition (Aubertin et al. 2003; Li and Aubertin, 2008; Pirapakaran, 2008). A few studies have also been developed for 3D conditions (Li et al. 2005, Pirapakaran, 2008; Dirige et al. 2009). Two-dimensional numerical simulations have been used to validate these analytical solutions for vertical stopes (Li et al. 2003). Other conditions have also been simulated, including inclined backfilled stopes (Li et al. 2007; Li and Aubertin, 2009), the effect of filling rate and evolving properties of cemented backfill (El Mkadmi et al. 2014).

The stress state in two adjacent backfilled stopes has recently been investigated under plane strain (2D) conditions, considering the influence of stope geometry and natural stress state in the rock mass (Falaknaz et al. 2013, 2014). However, such 2D analyses are not representative of backfilled stopes with a relatively small length. The 3D stress state in a single stope has been investigated by Veenstra (2013) using FLAC^{3D} but it has not been assessed for neighboring stopes.

This chapter presents results of numerical simulations conducted under three-dimensional conditions to analyse the response of two adjacent stopes created one after the other. The results include an evaluation of the stresses, displacements and strain in the backfill, taking into account various influence factors including the stopes size and depth, and backfill properties. A comparison is made between the results obtained using the 3D numerical models with those

obtained in plane strain condition (2D) as well as with analytical solutions developed for an isolated stope (Li et al. 2005).

7.2 Simulation procedures

The code FLAC^{3D} (Itasca, 2014) was used to assess the stress distribution in and around the underground backfilled stopes. Models with quadrilateral elements were created for the simulations, with a coarser mesh applied to the elastic rock region, while a finer mesh was used inside of the stope and near the walls. The number of elements depends on the stope geometry and model size. The location of the external boundaries was far enough so they do not influence the simulation results, while maintaining the model domain to a realistic size; the model size may vary with the stopes geometry. The horizontal displacements along these two (*x* and *y*) axes were restricted, while vertical displacements (*z* axis) were allowed along the sides of the model. Displacements at the base of the model were prevented along all axes. Gravity was the initial condition applied to the model. The natural horizontal stress σ_h in the rock mass was taken as twice the vertical stress σ_v (i.e. $\sigma_h = K_r\, \sigma_v = 2\, \gamma_r\, z$), based on a typical situation encountered in the Canadian Shield (e.g. Arjang, 2004). The sidewalls of stope were considered rough; There was no (planar) interface element between the backfill and rock mass in models (Li et al. 2003; Li and Aubertin, 2009).

The rock mass and backfill properties are given in Table 7.1, with the stopes geometry. In these calculations, the rock mass is considered homogeneous, isotropic and linearly elastic, with the following properties: E_r = 30 GPa (Young's modulus), υ_r = 0.3 (Poisson's ratio), γ_r = 27 kN/m^3 (unit weight). The properties of the backfill (with and without cement) have been adopted from Belem et al. (2000), Pirapirakan (2008) and Veenstra (2013). The fill behaviour follows an elasto-plastic law with the Mohr-Coulomb criterion. Its mechanical properties are described by *E*, υ, γ, with the effective internal friction angle ϕ', cohesion c', dilation angle $\psi' = 0$ (with $\phi' \neq \psi'$ for a non-associated flow rule).

Table 7.1: Parameters used in the numerical simulations, including stope size and backfill properties (with stope height H = 45.5 m, pillar width D = 8 m, and backfill modulus E = 300 MPa)

Cases		*Width B* (m)	*Length L* (m)	*v*	ϕ' (°)	*c'* (kPa)	*Depth of stope base z* (m)
0 (single stope)	0a(2D)	6	$L = \infty$	0.3	35	0	300
	0b(3D)		60				
1	(3D)	6	6,9,12,18,36,60	0.3	35	0	300
2	2a(2D)	6	$L = \infty$	0.3	35	0	300
	2b(3D)		60				
3	(3D)	6	9	0.3	35	0	300
4	4a(2D)	6	$L = \infty$	0.36, 0.33, 0.3	25, 30, 35	0	300
	4b(3D)		9				
5	5a(2D)	6	$L = \infty$	0.3	35	20, 50	300
	5b(3D)		9				
6	6a(2D)	6	$L = \infty$	0.3	35	0	2000
	6b(3D)		9				
7	7a(2D)	18	$L = \infty$	0.3	35	0	300
	7b(3D)		9				

The model size and boundary conditions were adjusted for all cases to avoid the external boundaries effect on the calculations results. In the case of two neighboring stopes, the first stope is excavated in one step and the backfill is placed in four layers after the rock mass reaches equilibrium under the imposed stresses (including rock weight). The second stope is then excavated in four equal steps and filled in four layers. The stresses, displacements and strains evolve through 9 steps, starting with step 0 at the end of filling (similar to a single stope), followed by 8 steps for the excavation (4 steps) and filling (4 steps) of the second stope. The opening was filled to a height of 45 m, with 0.5 m of void space left at the top. The natural in-situ vertical stress σ_v in the rock mass was obtained by considering the overburden weight for a depth z = 300 m at the base of the opening; the horizontal stress $\sigma_h = 2\sigma_v$ (a value typical of the Canadian Shield). Figure 7-1(a) shows a representative 2D model used to analyse the response of an isolated backfilled stope (Case 0a, in Table 7.1). The horizontal (σ_{hx}) and vertical (σ_{vz}) stresses and horizontal displacement δ_{hx}, under 3D conditions (Case 0b, Table 7.1), were given along three lines within the first stope, i.e. AA′ (vertical central line, VCL), BB′ (along the left wall) and CC′ (along the right wall); the locations of these lines are shown in Figure 7-1(b). Both unbalance force ratio and unbalance force history were used to evaluate whether the system reached equilibrium at each step of excavation and filling. The stress and displacement contours and vectors were also used to assess the backfill and rock mass behavior.

7.3 Behavior of a single stope

Figures 7-2(a) and 7-2(b) show the distribution of the vertical and horizontal stresses in the backfilled stope at the end of filling under plane strain condition (Case 0a). These results show that both the horizontal and vertical stresses tend to be smaller along the walls than in the central part of the stope at a given elevation; the latter is smaller than the overburden pressure (γz). Figures 7-2(c) and 7-2(d) shows a model used for simulation of a single stope with a limited length (L = 60 m) under 3D conditions (Case 0b). The rock mass and backfill properties were similar to those considered for 2D condition (Case 0a). As can be seen, the stress distributions are almost identical to those obtained for plane strain condition ($L >> B$).

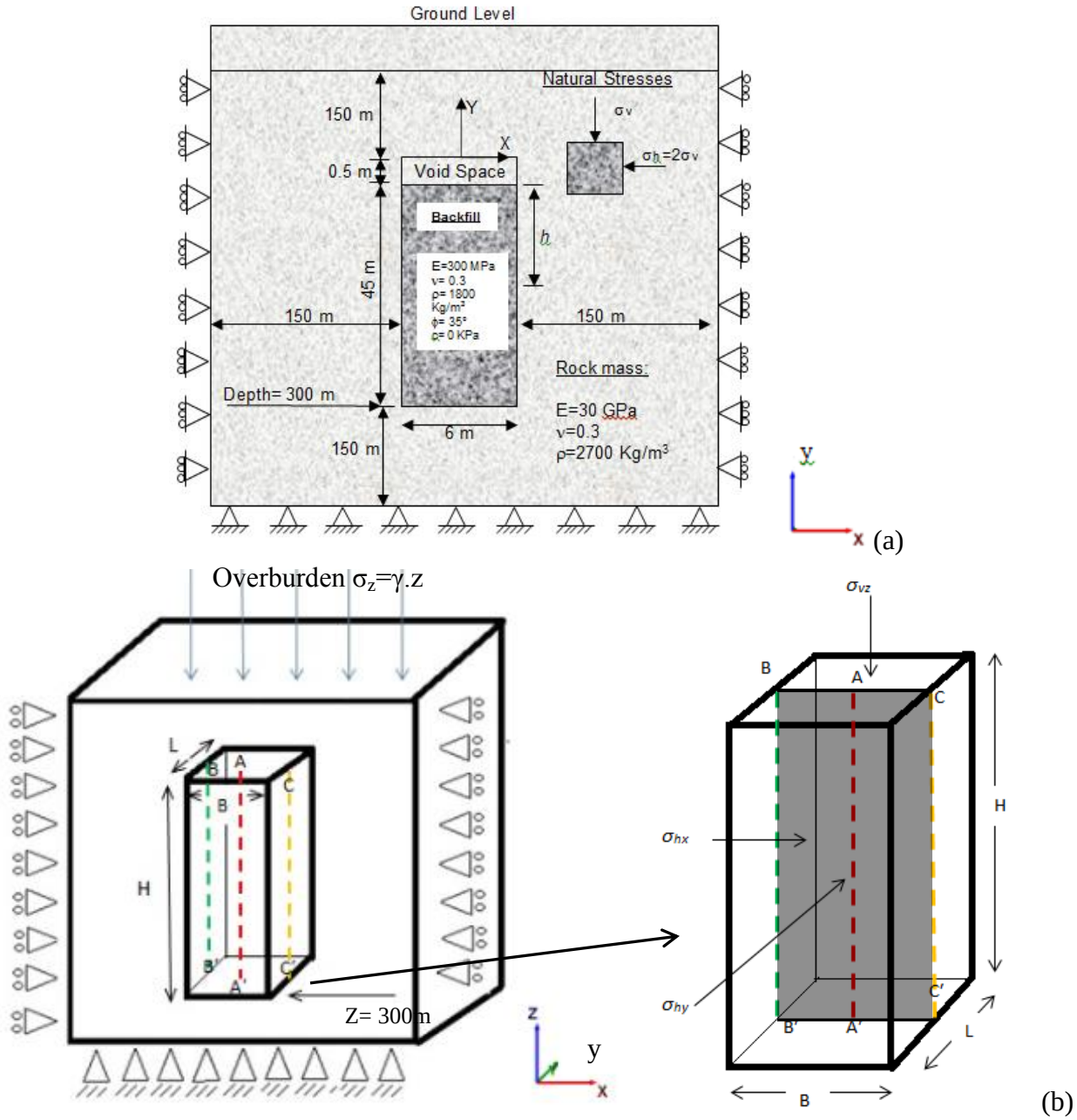

Figure 7-1: Backfilled stope model for the base case: (a) schematic view (not to scale) of the model, with properties and boundary conditions used for the 2D simulations with FLAC (Case 0a), (b) schematic view (not to scale), with axes and boundary conditions used for the simulations with FLAC^{3D}

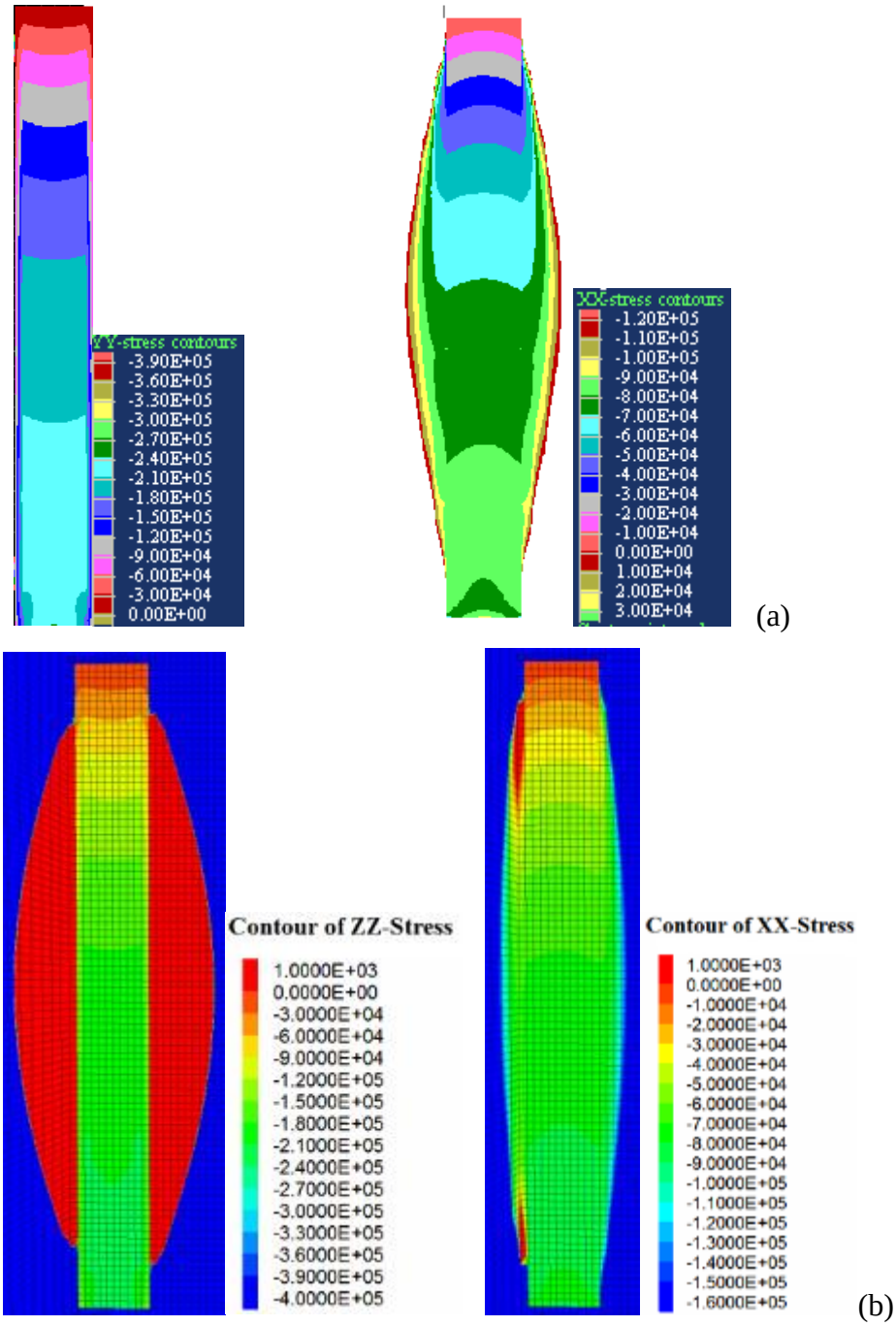

Figure 7-2: Numerical simulation results with isocontours of the vertical stresses σ_{vz} (left side) and horizontal stresses σ_{hx} (right side) for : (a) the 2D simulations with FLAC, (b) the simulations with FLAC ^{3D}; the results are shown along plane BCC′B′ at the end of filling (see Table 7.1 for details)

Figure 7-3 shows the stresses obtained from the numerical simulation and the analytical solution proposed by Li and Aubertin (2008) for plane strain condition (2D) and Li and Aubertin

(2005) for 3D condition. The solution for plane strain condition (2D) can be expressed as follows for the vertical and horizontal stresses at depth *h* (Li and Aubertin, 2008):

$$\sigma_{vx} = \gamma B \left(\frac{1-\exp\left(-\frac{2K\,h\,tan\phi\prime}{B(1-DF)}\right)}{2K\,tan\phi\prime} \right).\left[1 - a\left(\frac{x}{B}\right)^{b}\right] \quad (7\text{-}1)$$

$$\sigma_{h} = \gamma B \left(\frac{1-\exp\left(-\frac{2K\,h\,tan\phi\prime}{B(1-DF)}\right)}{2tan\phi\prime} \right) \quad (7\text{-}2)$$

In these equations (as specified in pervious chapters), *B* is the stope width (m); *K* is the earth pressure coefficient in the backfill, which is taken as the Rankine active coefficient [$K = K_a = \tan^2(45° - \phi'/2)$]; *x* is the distance from the center line of the stope ($x \leq \frac{B}{2}$); *a* and *b* are parameters that control the vertical stress distribution along the width; *DF* is the distribution factor defined as follows:

$$DF = \frac{2^{\left(1-\lambda_1\frac{H}{B}\right)}tan^{-\lambda_2}(\phi_0+\phi\prime)}{2^{b}(b+1)} \quad (7\text{-}3)$$

The values of $b = 3$, $\phi_0 = 50°$, $\lambda_1 = 0.02$ and $\lambda_2 = 0.1$ were obtained from an optimisation technique applied to a series of numerical simulations by Li and Aubertin (2008).

Li et al. (2005) proposed the following 3D analytical solution for vertical backfilled stopes, based on the Marston solution:

$$\sigma_{vh} = \frac{\gamma-\left(\kappa_{13}B^{-1}+\kappa_{24}L^{-1}\right)}{\left(\lambda_{13}B^{-1}+\lambda_{24}L^{-1}\right)}\left(1 - exp\left[-h\left(\left(\lambda_{13}B^{-1} + \lambda_{24}L^{-1}\right)\right]\right)\right) \quad (7\text{-}4)$$

$$\lambda_{13} = K_1\,tan\delta_1 + K_3\,tan\delta_3 \quad (7\text{-}5)$$

$$\lambda_{24} = K_2\,tan\delta_2 + K_4 tan\delta_4 \quad (7\text{-}6)$$

$$\kappa_{13} = c_1 + c_3 + 2c(tan\,\alpha_1 \tan\delta_1 + tan\,\alpha_3 \tan\delta_3) \quad (7\text{-}7)$$

$$\kappa_{24} = c_2 + c_4 + 2c(tan\,\alpha_2 \tan\delta_2 + tan\,\alpha_4 \tan\delta_4) \quad (7\text{-}8)$$

where γ is the fill unit weight (kN/m^3); δ_i and c_i are the friction angle (°) and the cohesion (kPa) of the i^{th} fill-wall interface (i =1, 2, 3, and 4). The value of K_i (i =1- 4) is based on the Rankine' theory (McCarthy, 1988) according to the wall movement condition ($K_i = K_o$, K_a or K_p). α_i (i = 1-4) is the angle of failure plane to the horizontal.

Figures 7-3(a) and 7-3(b) show the distribution of the vertical σ_{vz} and horizontal σ_{hx} stresses along the VCL in an isolated stope obtained under 2D (Case 0a) and 3D (Case 0b) conditions at the end of filling. The stresses obtained from the numerical simulations and analytical solutions are close to each other for 2D and 3D conditions. This result was expected because the stope length was considered large (L = 60 m) for Case 0b. Therefore, the stresses in this isolated backfilled stope was not affected by the third dimension, but will be different for smaller L.

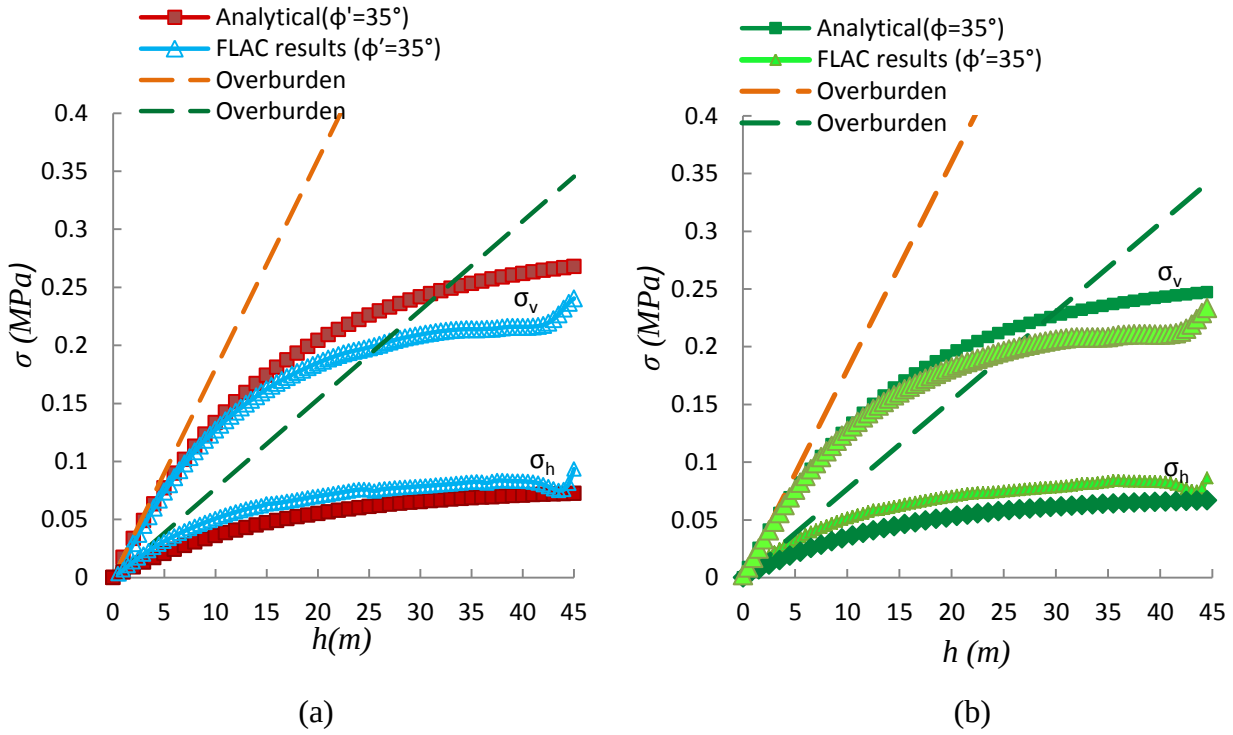

(a) (b)

Figure 7-3: Vertical σ_{vz} (z axis) and horizontal stresses σ_{hx} (x axis) along the VCL of the first backfilled stope for: (a) 2D condition (Case 0a); (b) 3D condition (Case 0b); results obtained using the analytical (Eqs. 7-1 to 7-8) and numerical (using FLAC and FLAC ^{3D}) solutions

It should be noted that the horizontal displacements δ_{hx} of the right (line BB′) and left (line CC′) walls of a single stope obtained with the 3D models are smaller (by about 20 % in this case 0b, i.e. 1.63 cm) than those obtained using the 2D model (about 2.04 cm, Case 0a) as shown in Figure 7-8. Figure 7-4 shows the effect of stope length L on the horizontal σ_{hx} and vertical σ_{vz} stresses along the VCL (line AA′) within isolated backfilled stopes under 3D condition (Case 1), obtained using FLAC^{3D}. In this Case, the stope width B = 6 m and different stope lengths L (= 6 m, 9 m, 12 m, 18 m, 36 m and 60 m) were considered. The horizontal σ_x and vertical σ_v stresses

along the VCL obtained for a stope under plane strain condition (2D, Case 0a), obtained using FLAC, are also shown in this figure. It is first noticed that an increase in the stope length L tends to increase the stresses along the VCL of the stope. These results also indicate that under 3D condition for a given stope width B (= 6 m), a stope length (L = 60 m), tends to generate the similar stress magnitudes to those obtained under plane strain condition (2D).

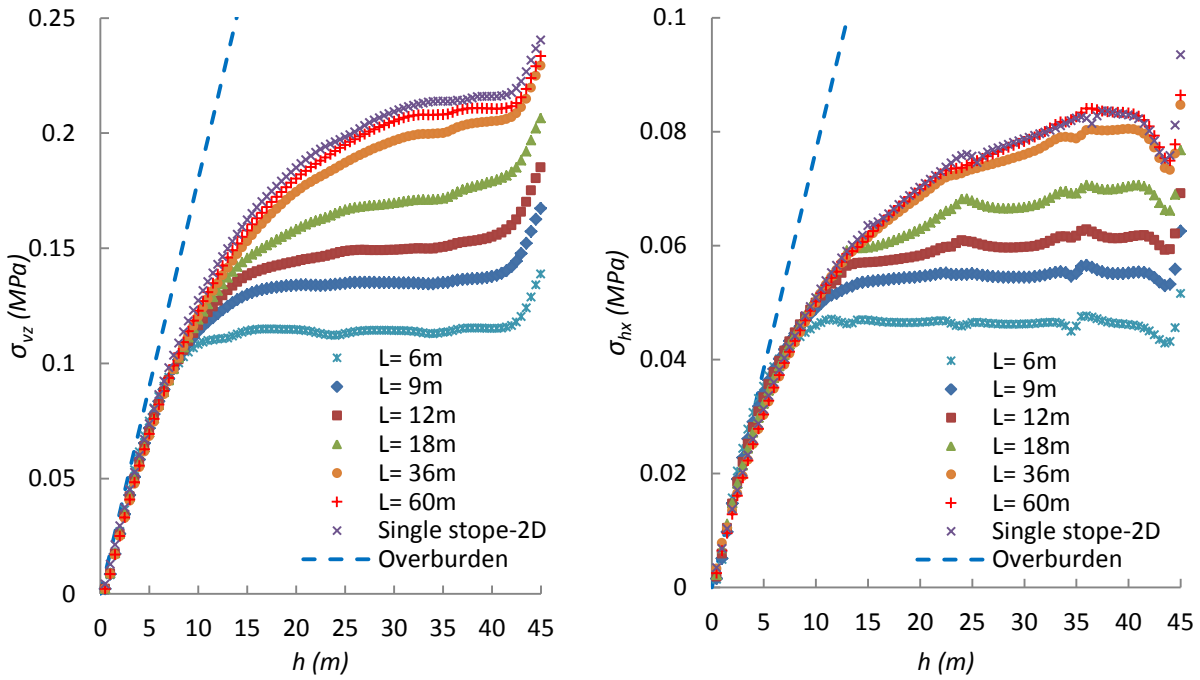

Figure 7-4: Horizontal σ_{hx} (a) and vertical σ_{vz} (b) stresses along VCL (line AA′, along the x and z axes) in the first backfilled stope obtained under 3D conditions with FLAC^{3D} (Case 1) for different stope length L at the end of filling; the results obtained under plane strain condition (2D, Case 0a) are also shown

7.4 Two adjacent stopes

7.4.1 Plane strain

Falaknaz et al. (2013, 2014) showed various results obtained for two neighboring stopes in plane strain condition (Chapters 3, 4 and 5). Figure 7-5 shows the typical results of the vertical and horizontal stress distributions in the first backfilled stope obtained with 2D condition at the end of filling of the second stope. The model size, boundary condition and in-situ natural stresses

are similar to the model shown in Figure 4-2. The stope distance (pillar width) D = 8 m. The results show that both the horizontal and vertical stresses along the VCL at the end of filling of the second stope tend to be smaller than the overburden stresses at a given elevation. It is also seen that the stresses in the second stope are lower than those obtain for the first backfilled stope.

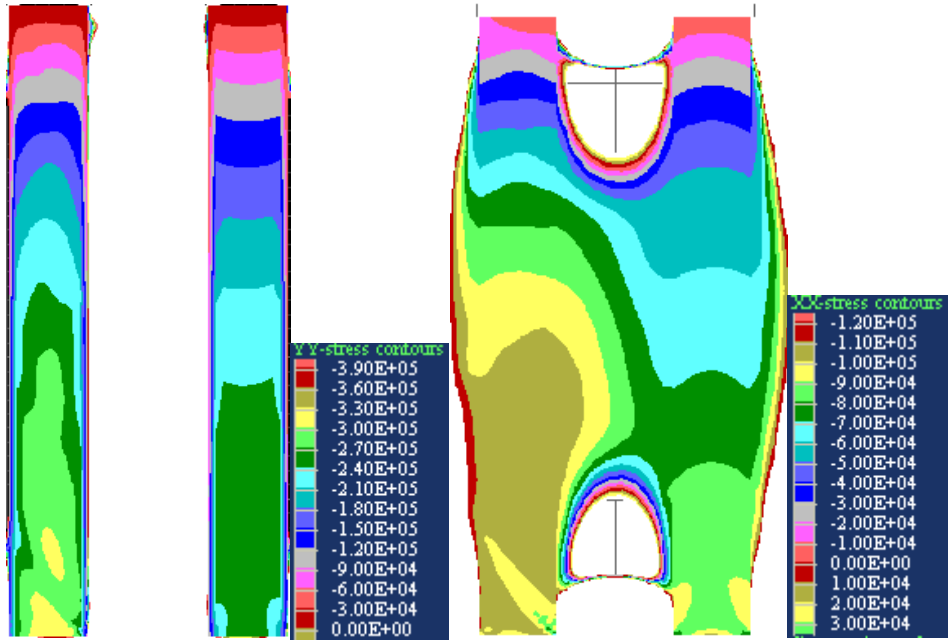

Figure 7-5: Modeling results showing the vertical (left) and horizontal (right) stress distributions obtained using 2D condition in the two adjacent backfilled stopes at the end of filling of the second stope (Case 2a)

7.4.2 3D Conditions

7.4.2.1 Stopes with large length *L*

Figure 7-6a shows a 3D model of two backfilled stopes and the boundary conditions applied to the rock region (Case 2b, Table 7.1).

Stress-state

The horizontal σ_{hx} and vertical σ_{vz} stress distributions are shown in Figure 7-6b and 7-6c for two adjacent stopes each having a length L= 60 m (Case 2b, i.e. compared to plane strain condition).

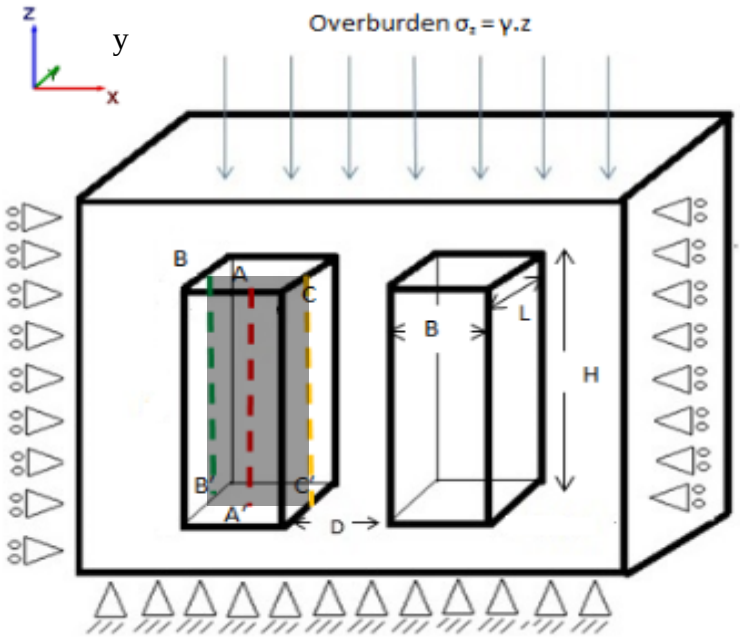

(a)

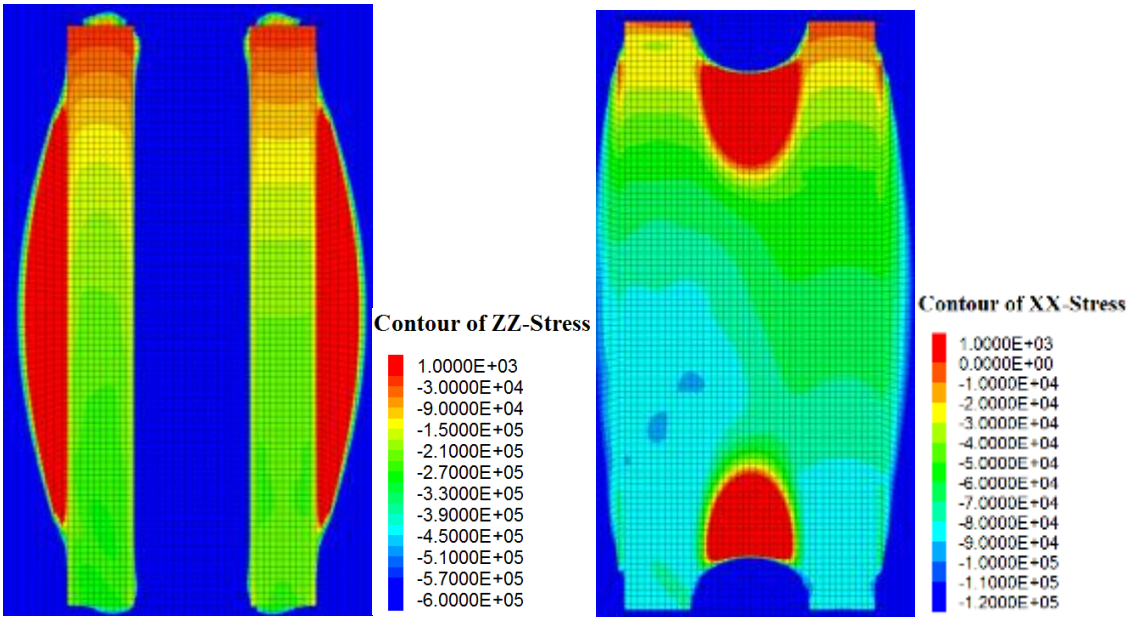

(b) (c)

Figure 7-6: (a) schematic view (not to scale) of the model with two stopes with axes and boundary conditions used for the simulations with FLAC^{3D}; numerical results showing isocontours (Case 2b, L = 60 m) of : (b) the vertical stresses σ_{vz}, and (c) horizontal stresses σ_{hx} (along plane BCC′B′) for two adjacent stopes at the end of filling

The results indicate that there is a significant transfer of the backfill load to the walls in both stopes, which reduces the stresses at depth. The results also show that an arching effect

developed in both stopes, but with different stress states. The stress distributions for the second stope are seen to be fairly similar to those obtained for a single stope (base Case, Figure 7-2b). However, the simulated stresses in the first backfilled stope are quite different from those obtained for a single stope (or for the second stope).

Figure 7-7 compares the stresses along the VCL (line AA′, along axes *x* and *z*) in the two adjacent stopes (Case 2b) and a single stope (Case 0b), obtained using FLAC^{3D}, after excavation and filling of the second stope. The results for two adjacent stopes (Case 2a) and a single stope (Case 0a) under plane strain condition also shown in this figure. It can be seen that the final horizontal σ_{hx} and vertical σ_{vz} stresses along the VCL (line AA′) of the first stope are larger than those obtained for a single stope and for the second backfilled stope after filling of the second stope for both Cases 2a ($L = \infty$) and 2b (L = 60 m).

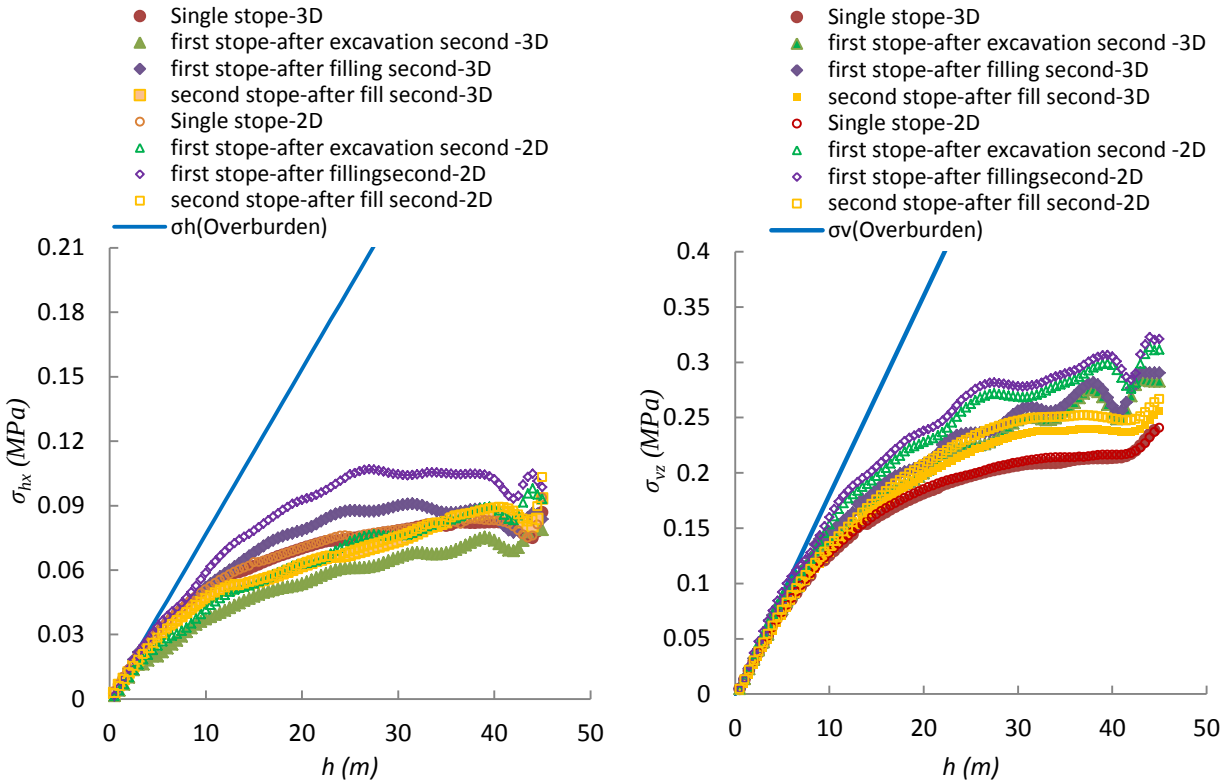

(a) (b)

Figure 7-7: Horizontal σ_{hx} (a) and vertical σ_{vz} (b) stress distributions along the VCL (Line AA′) of the first backfilled stope for 2D (Case 2a) and 3D conditions with L = 60 m (Case 2b) at the end of filling of the second stope; These stresses can be compared with those obtained for a single stope with L = 60 m (Case 0b, Figure 7-3)

It is also seen (Figure 7-7a) that filling of the second stope increases the horizontal stresses σ_{hx} in the first backfilled stope by up to 15% (from 73 kPa to 85 kPa, near mid-height) for Case 2b, while it increases by 25% (from 74 kPa to 98 kPa) for 2D condition (Case 2a). This figure also shows that the horizontal stresses σ_{hx} in the single stope (Case 0a) and second backfilled stope obtained under plane strain (Case 2a) are almost identical to those results obtained using 3D condition with L = 60 m (Cases 2b, 0b), at the end of the filling process. The vertical stresses σ_{vz} along the VCL (Line AA′) of the second stope (Fig. 7-7b) are somewhat higher than those obtained for a single stope, but smaller than those obtained for the first stope under 2D and 3D conditions (after complete excavation and filling of the second stope).

It is also observed that the horizontal stresses σ_{hx} (Fig.7-7a) obtained in plane strain (Case 2a) along the VCL (line AA′) of the first stope are about 20% higher than those simulated under 3D condition (Case 2b, L = 60 m) (in this case, σ_{hx} = 105 kPa for 2D to σ_{hx} = 86 kPa for 3D with L = 60 m) after excavation and filling of the second stope (step 9). The vertical stress σ_{vz} along the VCL (line AA′) goes from σ_{vz} = 278 kPa (Case 2a) to σ_{vz} = 236 kPa (Case 2b) after filling of the second stope. However, the horizontal and vertical stresses along the VCL of the second stope (and for a single stope) are fairly similar for Cases 2a (2D condition) and 2b (3D condition with L = 60 m) after the filling steps of the second stope (step 9).

Displacements and strains

Figure 7-8 shows the simulated displacements δ_{hx} of the walls (Lines BB′ and CC′ along the x-axis) of the first stope for 2D and 3D conditions, after the excavation of the second stope. It can be seen that for the 3D model with L = 60 m (Case 2b), the horizontal displacements δ_{hx} along the left wall (line BB′) of the first stope are smaller than those obtained using 2D models (Case 2a). At mid-height of the left wall, δ_{hx} = 2.15 cm for Case 2a and δ_{hx} = 1.68 cm for Case 2b (3D model); along the right wall (line CC′) δ_{hx} = -0.075 cm for Case 2a and δ_{hx} = -0.13 cm for 3D model (Case 2b) of the first stope. The horizontal strains ε_{hx} in the backfill along the VCL of the first backfilled stope have also been calculated, using a FISH function introduced in FLAC (based on the horizontal displacements between two vertical axes located near each other (see details in Chapter 3). Figure 7-9 shows the evolution of the horizontal strain Case 2a (2D) and Case 2b (3D with L = 60 m). It is seen that, the backfill is initially subjected to positive (compressive) strain during the first two steps of excavation of the second stope (due to wall

movement) for both conditions. Then, the horizontal strains decrease during the next excavation steps. At the end of the excavation process, the maximum horizontal strain ε_{hx} is -0.27% for Case 2b (Figure 7-9b). The maximum horizontal strain ε_{hx} is -0.35% for Case 2a (Figure 7-9a).

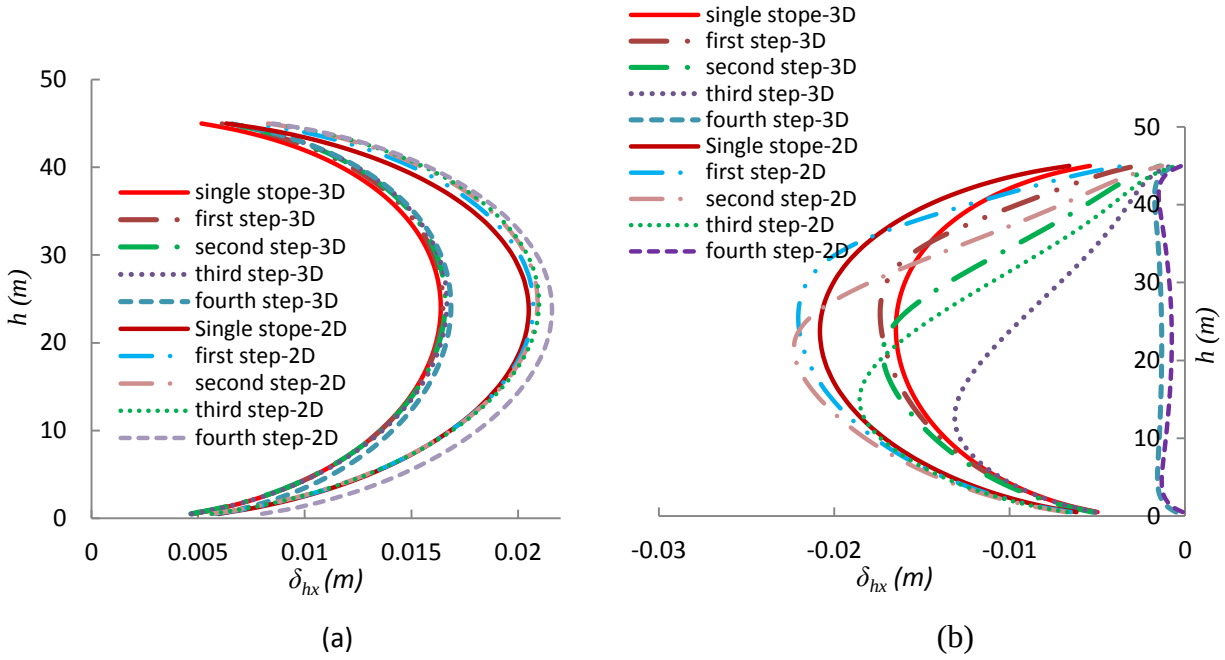

Figure 7-8: Horizontal displacements δ_{hx} along the: (a) left wall (Line BB′), (b) right wall (Line CC′) of the first stope during excavation (4 steps) of the second stope for Case 2a and Case 2b

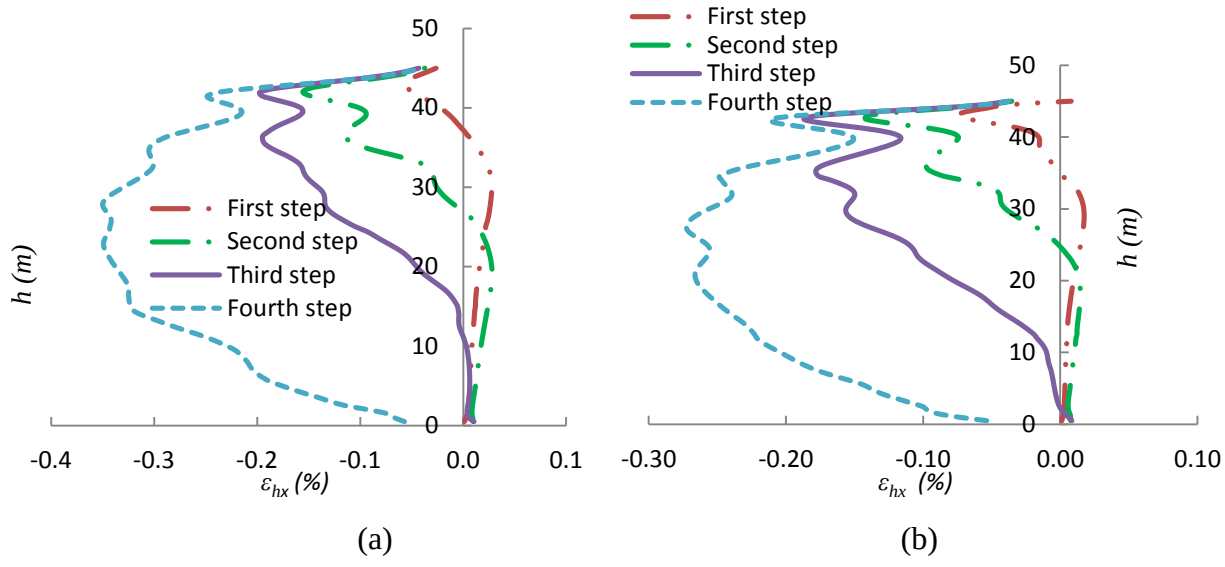

Figure 7-9: Horizontal strains ε_{hx} along the VCL (line AA′) of the first stope during excavation (4 steps) of the second stope: a) Case 2a (2D), and b) Case 2b, 3D with L =60 m

7.4.2.2 Stopes with smaller length *L* - Base Case

Stress state

Figure 7-10 shows the results obtained for two adjacent stopes with L = 9m (Case 3, base case, Table 7.1) with FLAC^{3D} after excavation and filling of the second stope. It can be seen that the horizontal σ_{hx} and vertical σ_{vz} stresses along the VCL (line AA′) obtained for a single stope are identical to those obtained for the second backfilled stope when the two stopes have a limited length (L = 9 m). Also, stresses obtained along the VCL (line AA′) of the first backfilled stope (after excavation of the second stope) are identical to those obtained after filling of the latter. Hence, these results indicate that the horizontal σ_{hx} and vertical σ_{vz} stresses in the first stope are not influenced by filling of the second stope for this case.

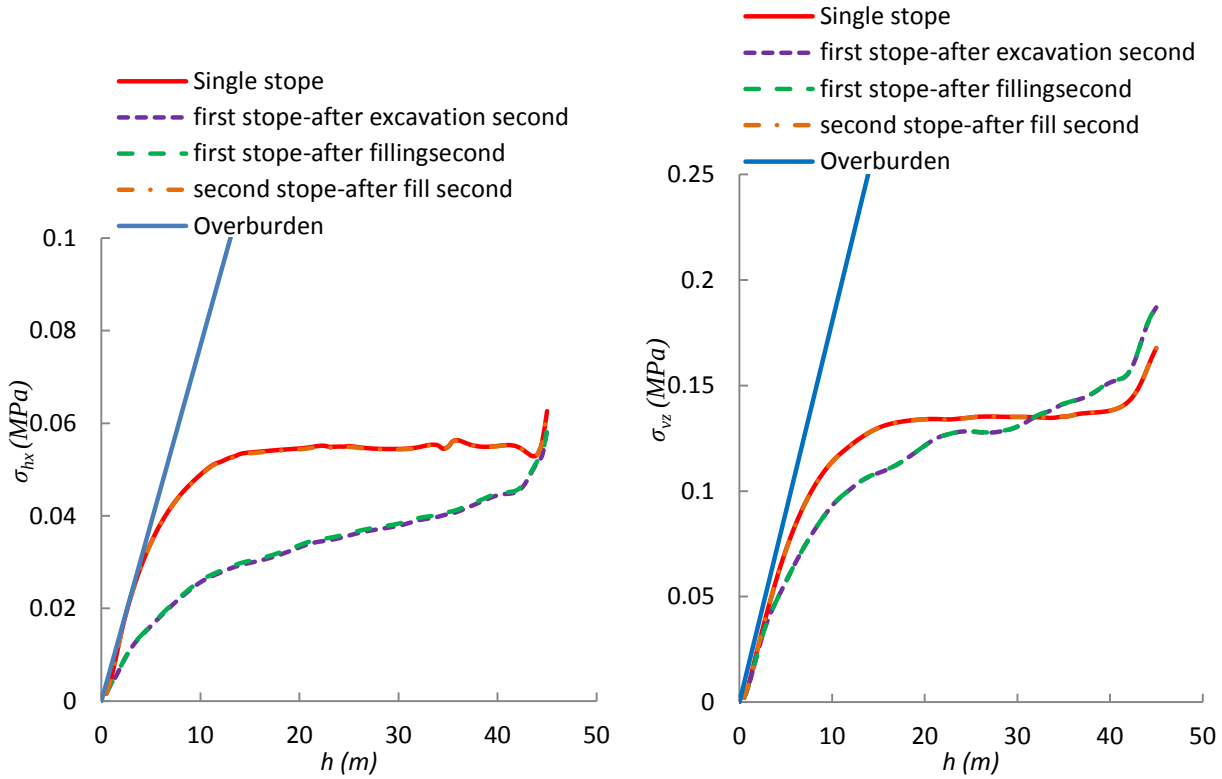

Figure 7-10: Horizontal σ_{hx} (a) and vertical σ_{vz} (b) stresses along the VCL (Line AA′) of the first backfilled stope for a stope, with length L = 9m (Case 3) at the end of filling of the second stope; these stresses are compared with those obtained for a single stope of the same size

Figure 7-10 also shows that the final horizontal σ_{hx} and vertical σ_{vz} stresses along the VCL (line AA′) of the first backfilled stope are somewhat smaller than those obtained for a single

stope and for the second stope. These results further show that the stresses in the first backfilled stope are affected by the stope length L. This is confirmed by the difference between the horizontal σ_{hx} and vertical σ_{vz} stresses in the two stopes with L = 9m (Case 3), and the two long stopes L = 60m (Case 2b, results shown in Figure 7-7). It can be seen that the horizontal stress σ_{hx} in the first backfilled stope (along line AA′) for Case 2b, tends to increase (by up to 30% near mid-height) after filling of the second stope (Fig. 7-7a), while σ_{hx} remains almost unchanged during filling of the second stope for Case 3 (L = 9m, Figure 7-10a).

The vertical stress σ_{vz} along the VCL (line AA′) of the first backfilled stope with L = 60 m (Case 2b) is higher than those obtained for a single stope (Case 0b) and for the second stope (Fig. 7-7b); however, the final vertical stresses σ_{vz} in the first stope with L = 9 m (Case 3) below mid-height are lower than those obtained for a single stope and the second stope (Fig. 7-10b).

Displacements and strains

Figure 7-11 shows the simulated displacements of the walls of the first backfilled stope with length L = 9m (Case 3). It is seen that the horizontal displacement δ_{hx} along the left wall (line BB′) of the first stope (Fig. 7-11a), at mid-height, goes from about 4 mm (step 0, single stope) to 4.4 mm (to the right) during the four excavation steps (of the second stope). Along the right wall (line CC′), the horizontal displacement (Fig.7-11b) is going to the right from -4.2 mm (step 0, single stope) to -2 mm (for the last excavation step). The horizontal displacements of the walls are not affected by the filling process of the second stope (not shown here, Appendix F).

These results also indicate that the horizontal displacements δ_{hx} along the walls of the first backfilled stope are also affected by the stope length L. This is illustrated by the difference between the horizontal displacements in the two stopes with L = 9 m (Case 3), and the two long stopes L = 60 m (Case 2b, results shown in Figure 7-8). It can be seen that the final horizontal displacement δ_{hx} along the left wall (line BB′) of the first backfilled stope for Case 2b (Fig. 7-8a) is about δ_{hx} = 1.63 cm after excavation of the second stope, while δ_{hx} = 0.4 cm for Case 3 (Fig. 7-11a). The displacement δ_{hx} along the right wall (line CC′) of the first backfilled stope is about -0.13 cm for Case 2b (L = 60 m, Figure 7-8b) and δ_{hx} = -0.2 cm for Case 3 (L = 9 m, Figure 7-11b) after excavation of the second stope.

Figure 7-11c shows the evolution of the horizontal strains ε_{hx} for stopes with L = 9 m (Case 3). The backfill in the first stope is subjected to negative strains as a result of wall

displacements. At the end of excavation of the second stope, the maximum horizontal strain ε_{hx} is about 0.03%.

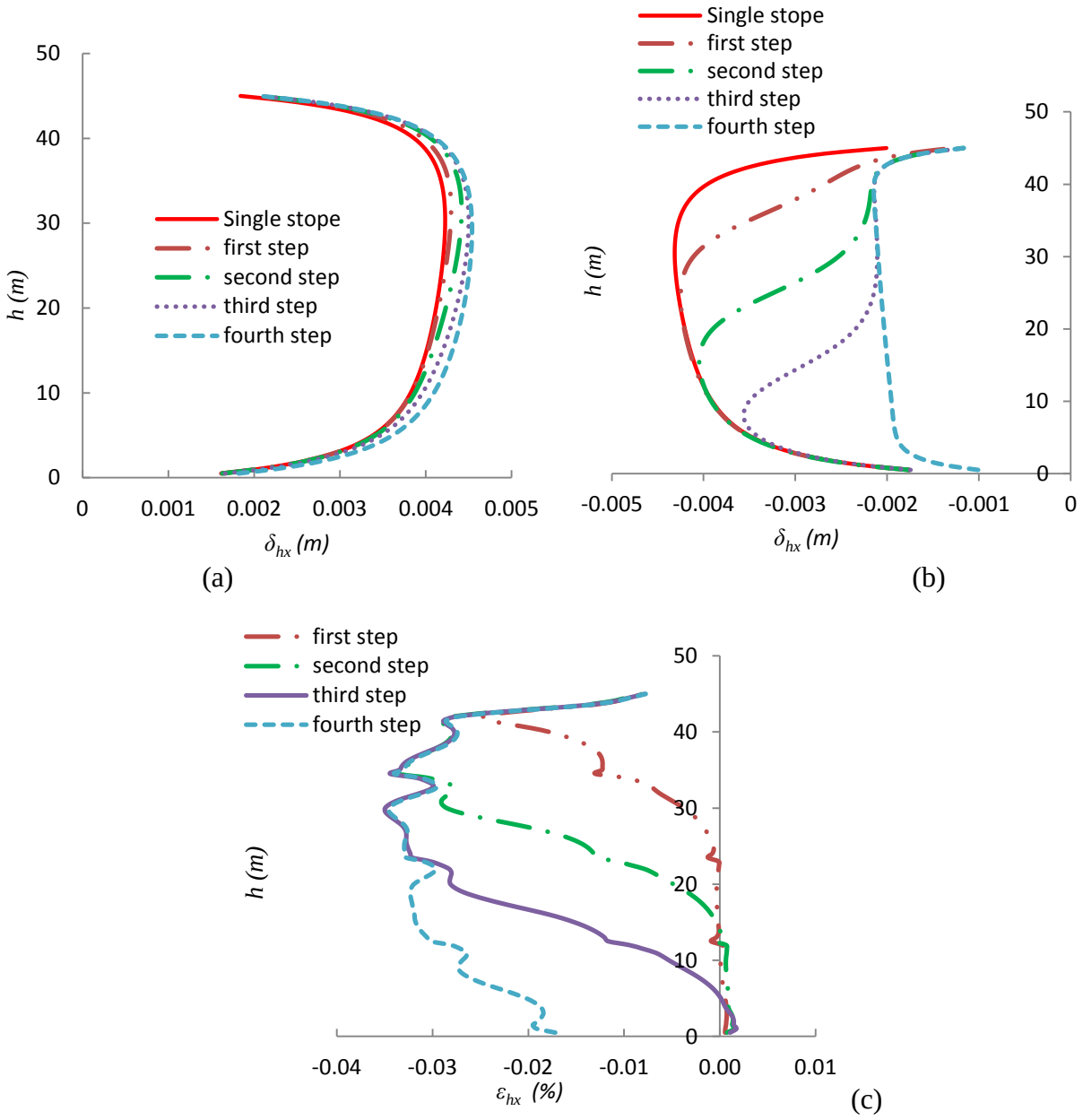

Figure 7-11: Horizontal displacements δ_{hx} obtained along the: (a) left wall (line BB′), and (b) right wall (line CC′); (c) horizontal strains ε_{hx} along the VCL (line AA′); results shown for the first backfilled stope with a length L = 9 m (Case 3) after excavation of the second stope

7.4.3 Effect of other parameters

This section presents the results of a parametric analysis of behavior of two stopes with limited length obtained with FLAC^{3D}. The investigation involves changing one parameter at a time and making comparison between these results, and also those obtained using 2D simulations.

Backfill properties

The influence of the backfill friction angle ϕ' on the stresses in the first backfilled stope is shown in Figure 7-12b for 3D conditions with L = 9 m (Case 4b) at the end of filling of the second stope. It is seen that an increase in the friction angle from 25° to 35º in 3D (Case 4b) tends to decrease the horizontal stresses σ_{hx} along the VCL (line AA′) at mid-height by up to 40% (i.e. by 35 kPa), and the vertical stresses σ_{vz} by up to 10% (i.e. by 126 kPa). The stresses obtained in 2D (Case 4a, $L = \infty$) were compared with those obtained for D conditions with L = 9 m (Case 4b). Figure 7-12a (Case 4a, 2D) shows that as the friction angle increases, the horizontal stresses along the VCL decrease (by up to 30% at the mid-height), while the vertical stresses remain almost unchanged. Hence, for these conditions both stresses are affected by the internal friction angle in 3D (Case 4b), while the friction angle has a limited influence on the vertical stresses under plane strain condition (Case 4a, 2D).

The cohesion c' of cemented backfill is also expected to influence the stress distribution. Simulations results for 3D condition (Case 5b) indicate that an increase in cohesion c' from 0 (Figure 7-12b) to 20 kPa (Figure 7-13b) tends to reduce the horizontal stresses by up to 80% (from 35 kPa to 7 kPa, at mid-height) and vertical stresses by up to 65% (from 126 kPa to 45 kPa) in the first backfilled stope. These results further show that both horizontal σ_{hx} and vertical stresses σ_{vz} along the VCL and walls (not shown here, Appendix F) become almost insensitive to an increase of cohesion c' (from 20 to 50 kPa) (Case 5b). However, the effect of c' is more significant for 2D condition (Case 5a) as seen in Figure 7-13a. In this latter case, an increase of the cohesion c' from 0 (Figure 7-12a) to 20 kPa (Figure 7-13a) tends to reduce the horizontal stresses by about 60% (from 97 kPa to 39 kPa) and vertical stresses by about 55% (from 250 kPa to 113 kPa) in the first backfilled stope at mid-height.

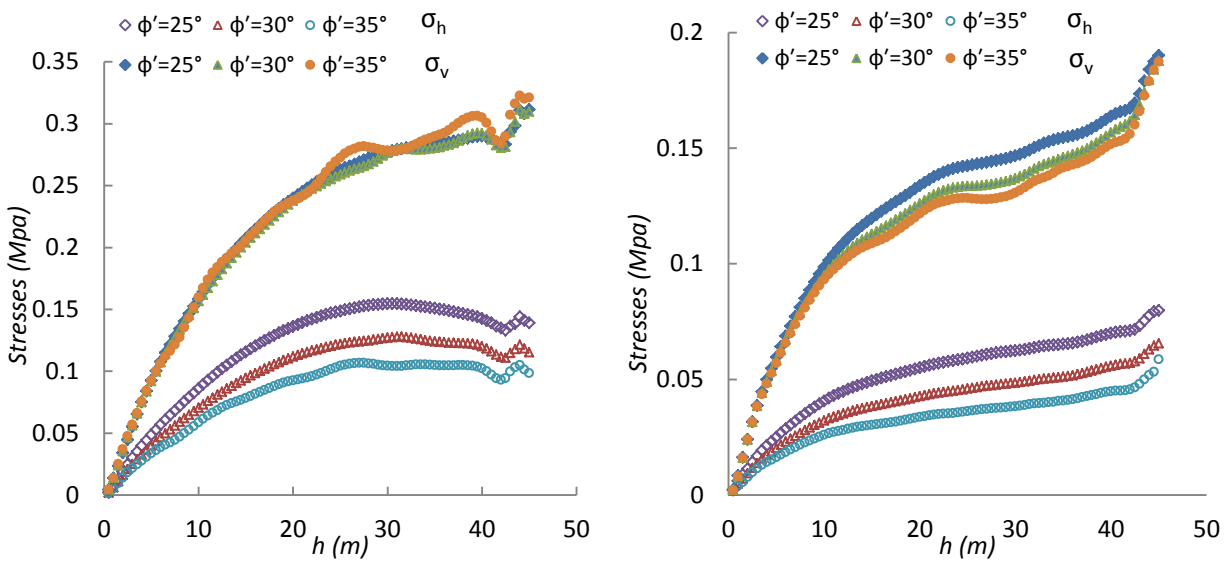

Figure 7-12: Effect of the internal friction angles ϕ' of the backfill on the horizontal σ_{hx} and vertical σ_{vz} stresses along VCL (line AA′) of the first backfilled stope with B = 6m for: (a) Case 4a with $L = \infty$ (2D), (b) Case 4b (3D) with L = 9m

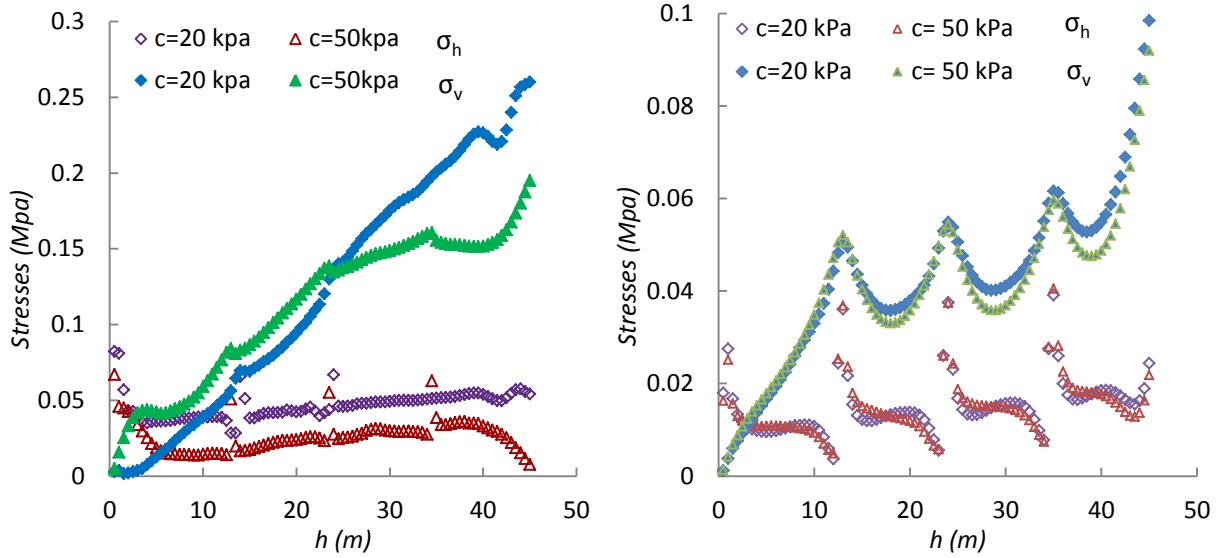

Figure 7-13: Effect of the cohesion c' of the backfill on the horizontal σ_{hx} and vertical σ_{vz} stresses along VCL (line AA′) of the first backfilled stope with B = 6m for: (a) Case 5a with $L = \infty$ (2D), (b) Case 5b (3D) with L = 9m

As the backfill cohesion increases from c' = 20 to 50 kPa (Figure 7-13a), the horizontal stress decreases by up to 35% (from 39 kPa to 25 kPa), while the vertical stress increases by up to 20% (from 113 kPa to 133 kPa at mid-height). In addition, it is seen that both stress distributions along the VCL are irregular, with a trend that becomes wavy. The position of the peaks is related to the sequence of filling (4 steps) when $c' \geq 20$ kPa.

Depth of stopes z

Simulations were also conducted to investigate the influence of the depth of the openings, *z*. The base of the two stopes was located at 300 m and 2000 m below the ground surface (Case 6a, 6b, Table 7.1); this increased the natural stresses proportionally. Figure 7-14b shows the stresses along the VCL and walls (lines BB′, CC′) of the first stope for 3D condition (Case 6b) (located at 2000 m and 300 m) after the excavation and filling of the second stope. It is observed that the horizontal stresses σ_{hx} in the first stope (Case 6b) in 3D are affected by depth, particularly below mid-height where these stresses increase significantly with *z* (by up to 30% along the VCL, line AA′). For instance, near the base of the first stope, σ_{hx} = 46 kPa for *z* = 300 m and σ_{hx} = 63 kPa for *z* = 2000 m, (Case 6b). The same trend can be seen for two adjacent stopes in 2D condition (Figure 7-14a, Case 6a). However, in this latter case, the horizontal stresses in the first stope increase more significantly than those observed for 3D (by a factor of up to 2) along the VCL (from 93 kPa for *z* = 300 m to 158 kPa for *z* = 2000 m, Case 6a). The vertical stresses are much less sensitive to the stope depth for both 2D and 3D conditions.

Stope width B

The effect of stope width *B* was also studied for two adjacent stopes using FLAC^{3D}. For this case (Case 7), the stopes had a width *B* = 18 m (to be compared to *B* = 6m in Case 3) and *D* = 8 m. Figure 7-15b shows the stresses along the VCL (line AA′) of the first stope after filling of the second one with 3D simulation (Case 7b). It is also observed that an increase of the stope width (from 6 m for Case 3 to 18 m for Case 7b) leads to larger horizontal σ_{hx} and vertical stresses σ_{vz}. The stress increase in the first stope can reach up to 50% near the stope base along the VCL (from σ_{vz} = 156 kPa, σ_{hx} = 45 kPa for *B* = 6 m, to σ_{vz} = 270 kPa, σ_{hx} = 96 kPa for *B* = 18 m), after filling the second stope as shown in Figure 7-15b. Under plane strain condition (Case 7a, Figure 7-15a), the same trend can be seen for both stresses in the first stope so that the

horizontal stress increases by a factor of up to 2 along the VCL (from σ_v = 284 kPa, σ_h = 93 kPa for B = 6 m, to σ_v = 566 kPa, σ_h = 182 kPa for B = 18 m).

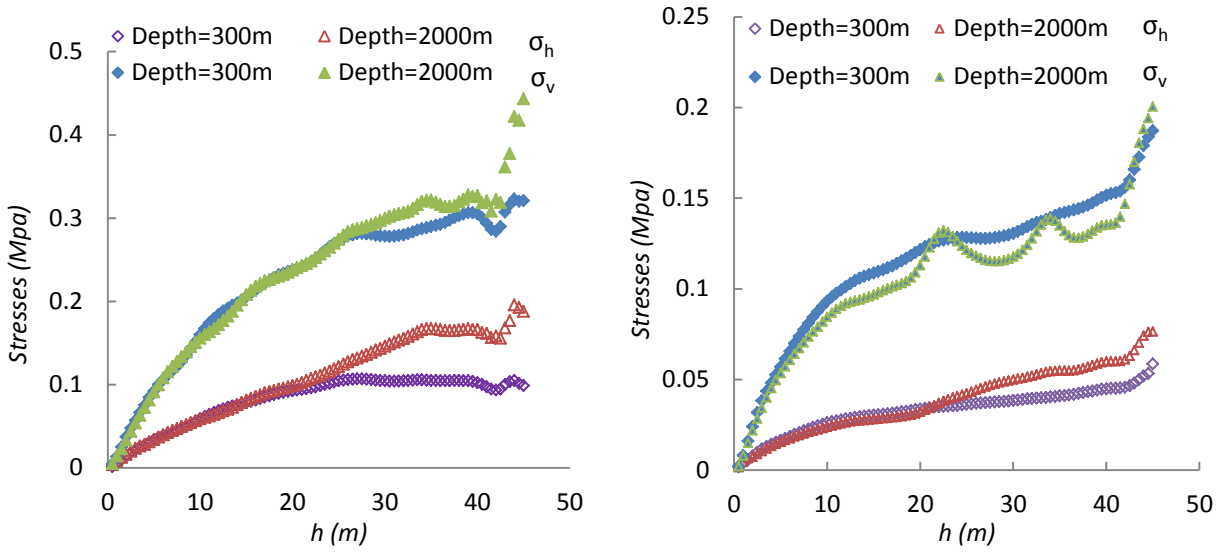

(a) (b)

Figure 7-14: Effect of stope depth z on the horizontal σ_{hx} and vertical σ_{vz} stresses along VCL (line AA′) of the first backfilled stope with B = 6m for: (a) Case 6a with $L = \infty$ (2D), (b) Case 6b (3D) with L = 9m

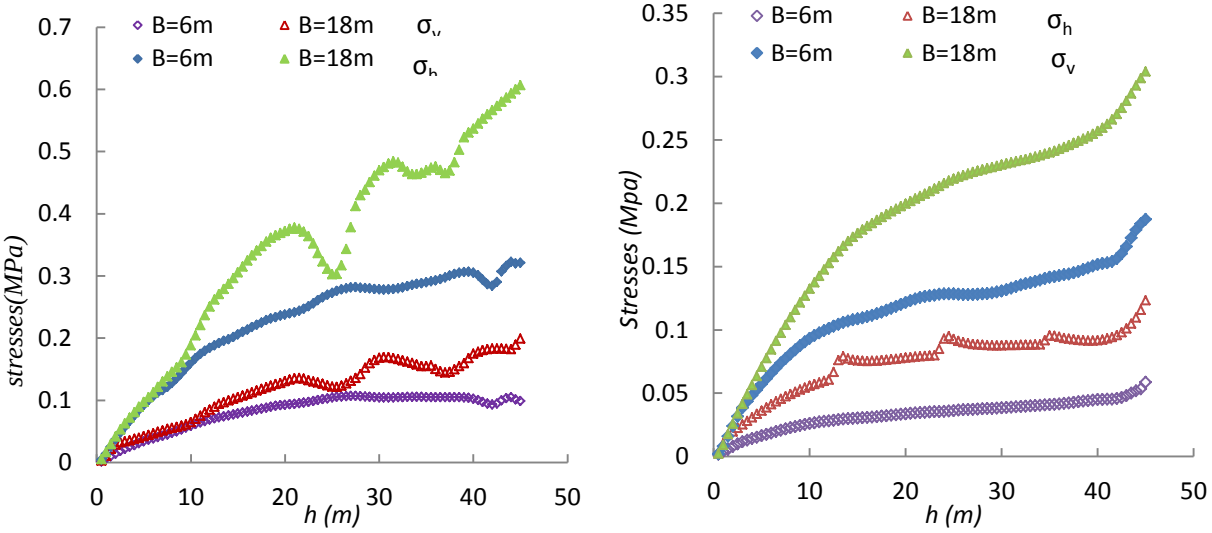

(a) (b)

Figure 7-15: Effect of stope width B on horizontal σ_{hx} and vertical σ_{vz} stresses along VCL (line AA′) of the first backfilled stope with B = 6m for: (a) Case 7a with $L = \infty$ (2D), (b) Case 7b (3D) with L = 9m

7.5 Final remark

This chapter illustrates the main results of numerical investigation of two neighboring backfilled stopes using FLAC and FLAC ^{3D} to evaluate the effect of the third dimension on the stress distribution in the backfill. The numerical modeling indicated comparable modeling results in any of the 2D and 3D simulated stopes. The results indicate that although, the arching effect often dominates the stress distribution in the stopes, the stress distributions are ifferent using the 2D and 3D models. Numerical modeling results for two infinitely long stopes in3D do not entirely agree with those modeling results obtained using 2D, which indicated that, for the same simulated stope sizes, the 2D simulations tend to overestimate the stresses, displacements and horizontal strain in the first backfilled stope.

The parametric analyses using 3D models for two stopes with limited length show that the stope depth and width have almost a similar influence on the stresses in the first backfilled stope with those obtained using 2D simulations. Moreover, these results indicate that the internal friction angle of backfill has influence on both horizontal and vertical stresses of the first backfilled stope with the 3D model, while the horizontal stress is particularly affected by this parameter when the 2D model is used. The results reveal that both stresses in the first backfilled stope are not sensitive to the increase of backfill cohesion (from 20 kPa to 50 kPa) in 3D models, while the stresses decrease with an increase of the cohesion under 2D condition.

Other factors neglected here may need to be taken into account when making a detailed analysis of backfilled openings in 3D, including the dilation of the fill, pillar width, natural stress ratio K_r in the rock mass, rock mass modulus, and elasto-plastic criterion for rock mass. Numerical modeling results in 2D have shown that these factors can in some cases significantly affect the stress distribution in the backfill.

CHAPTER 8 SUMMARY AND GENERAL DISCUSSION

8.1 Main results

Underground mining methods can be divided into three main categories: naturally supported, artificially supported and caving (Brady and Brown, 1993). One of the main methods used for ground support is backfilling. Accurate evaluation of the stress distribution in the rock mass and fill materials is an essential issue for the design underground backfilled stopes and barricades.

One of the approaches available to evaluate the stress distribution in backfilled stopes (and on barricades) is based on the use of analytical solutions. These solutions can provide information at the preliminary phase of mining projects. Two and three-dimensional analytical solutions, based on limit equilibrium conditions, can be used to assess the stress transfer (arching phenomena) to the walls of such backfilled openings, based on the work of Marston (1930) and Terzaghi (1943). In recent years, much effort has been devoted to developing such analytical solutions for evaluating arching effect in backfilled stopes (e.g. Aubertin, et al. 2003; Li et al. 2005; Li and Aubertin, 2008; 2009a, 2009b, 2009c, 2009d, 2009e, 2010; Pirapakaran, 2008; Sing et al. 2011; Ting et al. 2011, 2014).

Another approach to study the stress state in backfilled stopes and on barricades is numerical modeling. Finite Element software (such as SIGMA, PLAXIS) and Finite Difference software (i.e. FLAC, FLAC^{3D}) can be used to assess the stress distribution in backfilled stopes and on barricades more accurately than analytical solutions, as the these can solve more complicated problems than the latter. Numerical models can provide simulations using different constitutive models, input parameters and boundary conditions.

In-situ measurements of stresses and pore water pressures within mine stopes and barricades have also beenreported and compared with calculations results (Knutsson, 1981; Hassani et al. 1996; Belem et al. 2004; Le Roux et al. 2005; Grabinsky et al. 2010; Thompson et al. 2010). These measurements can provide experimental data to validate the numerical and analytical results.

Analytical and numerical solutions are thus commonly used to analyse the behavior and stability of stopes and barricades. In most previous studies, the rock mass has been considered homogeneous, isotropic and linear elastic, while the backfill is assumed to be elasto-plastic and obeys the Mohr-Coulomb criterion. The influence of different parameters, including backfill properties, fill-wall interface characteristics, filling rate and water flow on stress developments within backfilled stopes and on barricades have been studied by different researchers (Li et al. 2005, 2007; Li and Aubertin, 2009, 2010; Helinski et al. 2007, 2010; Pirapakaran, 2008; Fahey et al. 2009). However, there are still many neglected factors that should be considered with numerical and analytical solutions. For instance, all these investigations have neglected the influence of creating and filling more than one stope, with and without an exposed backfill face.

The goal of this thesis was to develop a numerical modeling approach to investigate the stress and strain distributions in two adjacent stopes, without and with an exposed face, considering the influence of different parameters such as backfill properties, stope geometry (height, width), pillar width, natural stress ratio, and rock mass properties.

In order to reach this goal, a series of numerical simulations were carried out using Itasca's FLAC and FLAC^{3D} software, and the internal programming language FISH. Two constitutive models were used for the rock mass (Elastic and Elasto-plastic) to investigate the backfill-rock mass interactions. The general modelling results were first validated using analytical solutions developed for single stopes, considering different numerical modelling conditions (to insure the quality of the simulations). In the next step, two adjacent stopes weresimulated within an elastic rock mass. Additional simulations were also conducted with an elasto-plastic rock mass behavior. Numerical and analytical 3D calculations were also performed to assess the behavior of exposed backfill in mine stopes (with an open face); 3D simulations were also conducted for two adjacent backfilled stopes with limited stope length and a finite pillar size.

As previously stated, the main factors considered in the numerical simulations include the stope geometry, backfill and rock mass properties, stope depth, pillar width, and excavation sequence. The simulations results are presented in terms of stresses, displacements and strains.

The discussion presented in this section refers to the numerical modeling and analytical solutions applied in this study.

Model Validation

A series of numerical simulations were conducted to verify the numerical modelling calculations.

- The total size of the model is a key aspect. The results indicate that the stresses and displacements in the backfilled stope are not affected by the boundary location when these boundaries are located farther than $3D_{max}$ (where D_{max} is the maximum dimension of the excavations) from the openings.

- The results also confirmed that simulation results with more than four steps (for the excavation and filling of the second stope) are practically equivalent; using four steps can then be considered as representative of a good modelling result.

Numerical analyses of two neighboring stopes within an elastic rock mass

Numerical simulations were conducted with FLAC to assess the behavior of two neighboring backfilled stopes and evaluate the effect of backfill properties, stope geometry and depth, pillar width, rock mass parameters and excavation and filling sequence. The stress path along the vertical central line (VCL) of the first stope was also monitored to study the behavior of the backfill during excavation and filling of the second stope. The main result have shown that :

- The stresses distribution in the first backfilled stope can be more complex, and much less uniform, than the one obtained for a single stope, due to a more elaborate loading path associated with the excavation and filling of the second stope. The results also indicate that the final stress distribution in the second stope is almost similar to the one obtained for an isolated stope.

- The stress state in the first backfilled opening varies during the creation of the second one; it is then influenced by the fill material properties. For instance, the simulations indicate that an increase of the internal friction angle ϕ' (from 25º to 35º) of the backfill leads to a decrease of the horizontal stresses. The stresses also diminish with an increase of the backfill cohesion, particularly in the range 1 kPa < c' < 100 kPa; There is also an effect of the backfill dilation angle ψ', but it is usually much less significant.

- The stresses in the first backfilled stope tends to vary with the width, depth and distance between the openings. The results demonstrate that an increase of the width usually decreases the arching effect and increases the stress magnitude in the stopes. A larger depth increases the stresses in the pillar, the displacements of the walls, and the corresponding stresses within the first backfilled stope. The results also show that an increase in the pillar width D between the two stopes influence the stresses of the backfill.

- The results also y show how the stress state in the first backfilled opening varies during the creation of the second one, as a function of the rock mass modulus and natural stresses. A lower elastic modulus usually leads to larger stresses in the first backfilled stope due to larger horizontal displacements δ_h of the walls. The effect of a low rock mass stiffness can be amplified by a greater depth and larger naturel stresses. The results also indicate that higher natural stresses can result in larger horizontal stresses in the first backfilled stope, particularly below the stope mid-height.

- Using related values for the Poisson's ratio, v, and the internal friction angle, ϕ', to establish the backfill properties can influence the results. According to Jaky's (1948) well-known equation (based on ϕ') for the earth pressure coefficient at rest, K_o , these two parameters (v and ϕ') should be related (for consistency and uniqueness of the K_o value) The presented here indicate that such relationship between v and ϕ' may influence the stresses in the stopes, but this effect is generally relatively small.

- The stress distribution within backfilled stopes can also be assessed in terms of the stress path induced by the excavation and filling process. It is shown that the stress paths obtained for different points along the VCL of the first backfilled stope can involve some loading and unloading (in terms of the mean and deviatoric stresses) and intersect the yield surface at various stages. This type of behavior is different from the one observed for a single stope and for the second backfilled stope.

Numerical analyses of two neighboring stopes within an elasto-plastic rock mass

An elastic rock behavior may not reflect its actual response of the rock mass, especially under large natural stresses or for weak/fractured rock. Additional simulations were conducted with FLAC to assess the influence of a non-linear behavior (elasto-plastic EP model) of the rock mass on the stress distribution in neighboring backfilled stopes. The calculations have been performed for two stopes considering various factors, i.e. rock mass shear strength parameters, earth reaction coefficient, stopes geometry, depth and distance, and sequence of excavation and filling. The stress state within the first backfilled stope has been monitored using the stress path along the vertical central line (VCL) to investigate the behavior. The main outcomes of this study indicate that :

- The stresses distributions in the first backfilled stope can be less uniform (particularly below mid-height) than the ones obtained with the elastic (EL) model. The results also reveal that the stress distributions in a single backfilled stope and in the second of two stopes, are fairly similar for the EP and EL models, while higher stresses can be obtained in the first backfilled stope with the EP model.

- When the EP model is used, an increase of stope width B and depth z tend to increase the stress magnitude in the first stope. Also, an increase of the pillar width D tends to decrease the horizontal stress in the first backfilled stope.

- A larger natural stress ratio K_r in the rock mass tends to increase the horizontal stresses in the pillar and the corresponding stresses within the first backfilled stope. A smaller rock mass modulus may also increase the stresses in the backfill and the horizontal displacements δ_h of the rock walls.

- The stress path along the VCL of the first stope shows the effect of the excavation and filling sequence of the second stope. This stress path can be significantly affected by various other influence factors, such as stope depth, natural stress ratio and deformation modulus (and strength parameters) of the rock mass.

Numerical analyses of a backfilled stope with an exposed face

In some mining operations, primary stopes are firts excavated and filled with a cemented backfill; nearby secondary stopes are then excavated so that one of the walls is removed. The stability of the exposed backfill face during adjacent mining is a critical issue that must be analyzed to control the risk for workers and equipment and the associated costs. A numerical investigation was performed with FLAC^{3D} to evaluate the effect of creating a secondary stope immediately next to the primary backfilled stope, focusing on the stress distribution and backfill displacement upon removal of the wall (for an elastic rock mass). The effect of stope geometry, material strength and excavation sequence was also investigated. The results presented in terms of stress, displacements, required strength (cohesion c) and factor of safety FS, were compared with those obtained using analytical solutions. The results indicate that:

- The required strength (cohesion c) of the exposed backfill increases when the stope length *L* and height *H* are increased. The numerical calculations also indicate that the minimum cohesion required is not influenced much by the stope width *B* (for the cases studied here).
- The excavation sequence (i.e. number of steps for removing the front wall) can also influence the displacements and the required strength of the exposed backfill. When the value of cohesion *c* is relatively high ($c > 20$ kPa) and the backfill face is unstable, increasing the number of steps to remove the wall leads to reduction of displacements and an increased *FS* (i.e. strength/stress ratio).
- The sliding plane angle α may vary with the stope geometry and backfill cohesion. The value of α obtained from the 3D simulations is usually lower than the theoretical critical angle used in the analytical solutions.
- The numerical simulations for the backfilled stope with an open face were carried out considering a zero tensile strength cut-off. These results are on the conservative side. It can be expected (based on ongoing work) that the required strength (cohesion) of the cemented backfill would be smaller for a realistic tensile strength.

Three-dimensional analyses of two neighboring stopes

The effect of stope length on the stress state in an existing backfilled stope was investigated using FLAC^{3D}. The results of 2D and 3D simulations were also compared for stopes in an elastic rock mass. Simulations have also been performed to assess the influence of different parameters on the stress distribution, including backfill properties and stope geometry. The results show that :

- A single stope with a given width under 3D conditions tends to generate similar stress magnitudes to those obtained using 2D conditions when the stope length is large enough (L = 60 m, in the cases analyzed here). In the case of two adjacent stopes, the numerical results under 2D conditions tend to overestimate the stresses, displacements and horizontal strains in the first backfilled stope.
- The horizontal and vertical stresses obtained for a single stope in 3D are almost similar to those obtained for the second backfilled stope with a similar size. The horizontal and vertical stresses in the first stope are not influenced much by filling of the second stope under 3D conditions.
- An increase of the fill internal friction angle ϕ' leads to a decrease of both the horizontal and vertical stresses in 3D. The stresses remain unchanged with an increase of the backfill cohesion from 20 to 50 kPa.
- An increase of the stope width and stope depth for the openings with a limited length, tends to increase the stress magnitude in the stopes, particularly within the first backfilled stope.

8.2 Discussion

This thesis presents the results of an extensive numerical investigation that illustrates the influence of creating a second nearby stope on the stresses, displacements, and strains within an existing backfilled stope. The effect of various factors has been analyzed, including the stope geometry, backfill properties, rock mass parameters, excavation sequence and stope position (depth and distance). The results obtained here show that the simulated horizontal and vertical stress distributions in the second stope are usually in a good agreement with those calculated with

the analytical solution previously developed by Li and Aubertin (2008) for a single vertical stope. Therefore, this analytical solution can be used to estimate the stresses in a single stope and in the second of two stopes, for both elastic (EL model) and elasto-plastic (EP model) rock masses. However, this analytical solution may not be appropriate to evaluate the stresses in the first backfilled stope when a new opening is created nearby. The results have also confirmed that the backfill properties (i.e. internal friction angle ϕ and cohesion c), and stope geometry (i.e. width B and length L), have a significant influence on the stresses within the first backfilled stope, for both elastic (EL model) and elasto-plastic (EP model) rock masses. The same trends have been observed by different authors (e.g. Li et al. 2007; Li and Aubertin, 2008, 2009a, 2010a; Pirapakaran, 2008; Veenstra, 2013) working on an isolated backfilled stope excavated in an elastic rock mass, but the ones shown here are the first dealing with neighboring stopes. The numerical results also illustrate the effect of stopes position (i.e. depth z and distance D) on the stresses within the backfill, for both types of rock mass behavior. Different rock mass behavior (and related parameters) may produce different stresses in the first backfilled stope (when the EL and EP models are used). For instance, the stresses in the first backfilled stope are usually less sensitive to an increase in the value of earth reaction coefficient K_r and the rock mass modulus E_r with the EL model than with the EP model. These reponses can be related to the stress paths, which may also depend on the rock mass characteristics. The strains in the first backfilled stope is lower than that obtained using the EL model due to the larger corresponding wall displacements with the EP model. In addition, the stress state of the first backfilled stope along the VCL shows a different tendency for both types of rock mass behavior. It seems that the larger wall displacements with the EP model increases the mean stress so the stress path along the VCL remains under the yield criterion. .

Despite the additional information and insight provided by the simulations results presented in this thesis, it should be recalled here that these calculations are based on many simplifying assumptions. For instance, the effect of a more realistic (irregular) geometry and of actual mining sequence (with excavation of a gallery, or drift, and with small layers followed by larger layers for instance) has not been taken into account in these simulations. Also, previous studies (Li et al. 2007; Pirapakaran, 2008; Li and Aubertin, 2009a; Veenstra, 2013) have shown that the stope inclination may have a significant influence on the stresses distributions (in an isolated stope); the effect of stope inclination has not been assessed in this study. The effect of

excavation and backfilling sequence has been studied here for two adjacent stopes, but more work is still needed to fully investigate this important factor (particularly for cemented backfill with evolving properties). In this study, only one backfill material was considered for the entire stope. In practice, mines commonly use at least two mixtures for the fill (Veenstra, 2013), especially in the case of cemented paste backfills (i.e. with a stronger fill at the base); hence, additional simulations could be performed using different backfill properties along the stopes. Another limitation of this study relates to the use of the Mohr-Coulomb criterion (with a tension cut-off) and the related elasto-plastic model. This may not always be appropriate when dealing with backfills, so another model (such as the MSDPu model proposed by Li et al. 2010; or modified Cam-Clay, used by El Mkadmi et al. 2014) should be used to better consider the volume change and the tensile stresses.

In this dissertation, a zero tensile strength cut-off was used. Additional simulations (not shown here) tend to indicate that the use of a non-zero tension cut-off has a considerable influence on the failure of exposed backfill. The results obtained here nonetheless remains useful as they provide a conservative estimate of the required cohesion for cemented backfill. As there are very few measurements of the tensile strength of cemented backfills, it is difficult at this time to establish a representative value (or range) for the tension cut-off to be used in the model, but it seems clear that this value should not be nil. A lower required strength (cohesion) can be expected for simulations conducted with realistic valuesof the tensile strength.

Recent studies also showed (Pirapakaran, 2008; El Mkadmi et al., 2014) that the use of interface elements along the stope walls can affect the vertical stresses; the effect of such interface elements between the rock mass and backfill was neglected; it was thus assumed that yielding would take place in the much weaker backfill rather than along the rough walls. More work is needed to assess the actual behavior of such interfaces.

Another limitation relates to the rock mass and wall properties, which have been assumed to be unique, isotropic and homogeneous (which is rarely the case in practice). The effect of water, through pore water pressures, consolidation and drainage, are among the other neglected factors, together with the influence of filling rate and backfill strength increase during curing over time.

The results obtained for a backfilled stope with an exposed face (with mature backfill) indicate that the normal stresses along the back wall are not nil, contrarily to the postulate used to develop the analytical solutions of Mitchell et al. (1982) and Li and Aubertin (2012, 2014). The value of this horizontal stress, normal to the back wall, is higher when the backfill cohesion is sufficiently large to maintain stability of the exposed backfill. This suggests that the shear resistance due to frictional stresses along this back wall should be included in a representative analytical solution. In this regard, it can be inferred that in actual backfilled stopes, the value of r_b could be smaller than 1; this would change the results obtained here.

Comparisons between numerical and analytical results obtained for HAR stopes indicate that two of the existing solutions tend to overestimate or one appears to underestimate the required strength of the backfill, when the stope geometry is changed; it was also obsereved that the trends are different between the various solutions. Results obtained for LAR stopes are in better agreement for the numerical simulations and analytical solution (Li and Aubertin, 2014). Improvements would thus be required to give more realistic values for the required backfill cohesion in many situations.

In this study however, only one face of the backfill was exposed. In practice, the cemented backfill is commonly exposed from two sides; hence, additional simulations should be performed considering two exposed faces of backfill.

All the numerical simulations were performed without interface elements, a condition that corresponds $\phi = \delta$ and to a cohesion that is the same along the interface and in the backfill. However, recent results reported by Fall and Nasir (2010) indicate that the cohesion between paste backfill and rough surfaces (brick or concrete materials) may be much smaller than that obtained for the paste fill. Considering this possibility could significantly change the results obtained from the numerical investigation (and from some analytical solutions).

Many of the results presented in this thesis were described based on the engineering judgment of the author.

Another limition of this work lies in the paucity of in-situ measurements. To the author's knowledge, there is no experimental data from field investigations (or even laboratory measurements) available to validate the numerical results for two adjacent stopes, such as those presented here. Although a few in-situ data have been reported (Hassani et al. 1998, 2001;

Grabinsky, 2010; Thompson et al. 2011, 2012), they don't provide the required information to validate such simulations. Therefore, additional work is needed to collect practical data that could be used to calibrate and validate the numerical simulations, based on characterization tests and actual field measurements.

CONCLUSION AND RECOMMENDATIONS

This doctoral thesis presents the results of a numerical investigation on the behavior of two neighboring backfilled stopes created in sequence. The simulations evaluated the effect of backfill properties, rock mass properties, stopes geometry and depth, pillar width, and excavation and filling sequence on the stresses distributions within the backfill. The results indicate that the second backfilled stope tends to behave in a manner similar to a single stope, where arching effects often dominate the stress distribution. The simulated horizontal and vertical stresses in the second stope are in a good agreement with those calculated with the analytical solution previously developed by Li and Aubertin (2008) for a single stope. However, the stress distributions can be quite different in the two neighboring stopes, because the behavior of the first backfilled opening may be significantly influenced by the excavation and filling of the new stope.

The results specifically show how the stresses distributions in the first backfilled opening varies during the creation of the second one and how it is influenced by the fill material properties. For instance, the simulations indicate that an increase of the fill internal friction angle ϕ' (from 25º to 35º) or of the cohesion (c' = 0 to 100 kPa) leads to a decrease of the vertical and horizontal stresses. There is also an effect of the backfill dilation angle ψ', but it is much less significant.

The simulations further illustrate how the stress state in the first backfilled stope may change as a function of width, spacing and depth of the openings. An increase of the stope width B (from 6 m to 18 m) tends to decrease arching effect and to increase the stress magnitude in the stopes (by up to 50% at base of the first stope). A larger depth tends to increase the stresses in the pillar, the displacements of the walls, and the corresponding stresses within the first backfilled stope, which can be raised by factor of up to 2 along the VCL for a depth that goes from 400 m to 2000 m. An increase in the pillar width D between the two stopes can also influence the stress state within the stopes, particularly when a cohesive backfill is used. A thicker pillar tends to decrease the stress magnitude (by up to 50% at mid-height) within the first backfilled stope.

The results obtained with the code FLAC also show that the stresses in the first backfilled opening tends to increase when the rock mass has a lower elastic modulus, due to larger horizontal displacements of the walls. The effect of a low rock mass stiffness can be amplified by a greater depth and larger naturel stresses. Another consideration addressed here is the effect of

using a relationship between Poisson's ratio, v, and the internal friction angle, ϕ', to establish the backfill properties. According to Jaky's (1948) well-known equation for the earth reaction coefficient at rest, K_o, these two parameters should be related. The use of an explicit relationship between v and ϕ' may influence the stress distribution in the stopes, but this effect is generally small.

The stress distribution within backfilled stopes was also assessed in 2D in terms of the stress path induced by the excavation and filling process. It is shown that the stress paths obtained along the VCL of the first backfilled stope can involve loading and unloadingsteps, and intersect the yield surface (Mohr-Coulomb) at various stages. Such unloading and reloading of the backfill in the first stope affects its response, in terms of the induced stress state and yielding condition. This type of behavior is different from the one observed for a single stope and for the second backfilled stope during the excavation and filling steps.

When the rock mass is considered elasto-plastic (EP model), the stresses distributions in adjacent openings can be quite different from those obtained for an elastic (EL model) rock mass behavior, even though the same tendencies are observed. In the former case, the simulations indicate that an increase of the stope width B leads to an increase of the horizontal and vertical stresses, particularly near the first stope base. The stresses tend to diminish with an increase of the pillar width, particularly in the lower part of the first stope. An increase of the stope depth tends to increase the stress magnitude below mid-height of the first stope. A larger natural stress ratio K_r (= σ_h/σ_v) increases displacements of the walls, and the corresponding stresses within the first backfilled stope. A smaller rock mass modulus (and smaller shear strength parameters) typically increases the stresses in the backfill and the horizontal displacements δ_h of the rock walls. The stress paths along the VCL of the first stope are also affected by the above-mentioned parameters.

This thesis also includes new findings related to the stability analysis of an exposed backfill in mine stopes. The main factors considered in the numerical simulations with FLAC^{3D} include the stope geometry, backfill cohesion, and excavation sequence to remove the front wall. The results show that the arching effect is reduced in the backfilled stope after removal of the front wall. The results also indicate that non-negligible contact stresses still exist along the fill-wall interfaces along the three remaining walls, after removal of the front wall. Higher backfill

strength is required to maintain stability for stopes with a higher length or height. When the value of *c* is sufficiently large (≥ 20 kPa for most cases simulated here), increasing the number of steps to remove the front wall leads to reduced displacements and an increased *FS*.

This research also served to underline the effect of the third dimension on the stresses within the backfill and displacements of the wall. The results reveal that the simulations using 2D (plane strain) models often tend to overestimate the stresses and displacements in two adjacent stopes having a limited length. The effect of backfill properties and stope width on the results was also investigated. The results show that both the horizontal and vertical stresses are decreased with an increase of the internal friction angle when the stope length is limited (3D models). The simulations results also indicate that both stresses in the first backfilled stope remain almost unchanged with an increase in the cohesion when the stope length is limited (3D models).

Original contributions and practical applications

The methodology presented in this thesis can be used for mine planning and backfilled stopes design. As stated earlier, the purpose of this study was to assess the response of a backfilled stope when an adjacent opening is created, considering various conditions. The results of this research could have various positive impacts for the mining industry.

The main contributions of this thesis can be summarized as follows:

1. For the first time, a comprehensive numerical study was conducted to simulate the response of two adjacent backfilled stopes created in sequence. This simulations included the effect of backfill properties, stopes geometry and location, rock mass parameters (elastic behavior), and excavation and filling sequence. These simulations lead to
    a. An evaluation of the stresses within the first and second backfilled stopes
    b. An assessment of the rock walls displacements and horizontal strains in the first backfilled stope during creation of the second stope
    c. The identification of parameters that have the more significant influence on the response of two neighboring stopes

d. An evaluation of the influence of stope size and location, and ackfill properties on the behavior of the two adjacent backfilled stopes

2. A novel numerical study of two adjacent stopes was carried out to investigate the effect of an elasto-plastic behavior for the rock mass on the stresses and displacements. This part of the study has shown thatthe modeling approach can be used to evaluate the stresses, displacements and strains in the stopes

3. For the first time, a comprehensive evaluation of the stress path in the first backfilled stope was made to better understand the loading (and unloading) behavior of the backfill and the yielding conditions during creation and filling of the second stope

4. A new series of comprehensive 3D simulations was conducted for exposed cemented backfill, considering various stope geometries and backfill properties. The results of this part of the study allowed:

    a. The determination of the required strength of an exposed backfill in the primary stope as a function of stope geometry

    b. The identification of backfill failure (and mode) that occurs during excavation of a nearby secondary stope

    c. An improve approach for the geoemechanical design of cemented backfill to controlits required strength

5. A first investigation that include a comprehensive comparisonbetween the numerical results for two adjacent stopes under 2D and 3D conditions. This modeling approach could lead to the improved design of backfilled stopes, for more realistic conditions regarding the size and location of two adjacent stopes with a limited length.

Recommendations

In addition to the elements included in this study, several aspects require further research to better assess the behavior of backfill and rock mass in mining stopes. Some of these aspects can be identified as follows:

- Various other factors can influence the simulations results, including the stope inclination, pore water pressure, consolidation, filling rate and rock-backfill

interface properties. It would be useful to evaluate the influence of these parameters on the stresses and strains in the backfill and the displacements of rock walls, in 2D and 3D.

- Other factors neglected in the 3D simulations of two stopes with limited length should to be taken into account, including changes in the dilation angle of the fill, pillar width, natural stress state in the rock mass, and rock mass properties.
- Other constitutive laws suitable for backfills, such as the MSDPu elasto-plastic model (Li et al, 2010b) and the modified Cam-Clay model (used by El Mkadmi et al. 2014) should be considered to overcome some of the limitations of Mohr-Coulomb elasto-plastic model, and assess the effect of a variation of the void ratio andconsolidation in multiple stopes.
- In this thesis, a tensile cut-off of zero (default) was assumed. Hence, the numerical simulations conducted here do not account for the actual value of the tensile strength, which is a property that is seldom determined explicitly. It would thus be useful to conduct tests to determine the tensile strength for cemented backfill and include this value (or other, more realistic values) in simulations as part of future studies.
- It is also beneficial to assess the stress state and displacements when different types of backfill are used (with a plug at the base for instance).
- It is also suggested to simulate backfilled stopes with different rock wall properties, which would be closer to realistic conditions.
- It would also be valuable to simulate stopes with a more realistic geometry (irregular) and with the actual filling sequences.
- It is also recommended to simulate stopes with a sequence that corresponds to actual mining operation methods, which could include the excavation of galleries (drifts) and excavation with small and larger layers.
- An important validation step is missing for these studies. Numerical simulations results should be compared with in-situ measurements, such as those recently

carried out by Hassani et al (1998, 2001), Grabinsky (2010) and Thompson et al. (2011, 2012).

- The comparison between numerical results and analytical solutions on the stability of backfill with an exposed face indicate that existing solutions do not necessarily provide the required strength for different geometry of the stope. Based on the results shown here, it was inferred that the solutions proposed by Mitchell et al. (1982) and Li and Aubertin (2012) tend to overestimate the required strength of backfill, while the one proposed by Li and Aubertin (2014) appears to underestimate this cohesion, particularly when L and B are increased (at least for the conditions considered here). Therefore, improvements of such solutions may be required to give more realistic value of the required backfill strength (after revisiting the basic assumptions used).
- It would also useful to assess the required backfill strength upon removal of two faces of backfill (one of each side) to better simulateactual mining operations.
- The influence of adjacent openings on the stresses acting on barricades and on horizontal pillars made of backfill are other situtations that should be considered.

REFERENCES

Arjang, B. (2004). *Database on Canadian in situ ground stresses*. CANMET Division Report MMSL, 01-029 (TR).

Arjang, B. (1996). *In situ ground stresses in the Abitibi Mining District*. CIM Bulletin, 89(996), 65-71.

Aubertin, M., Li, L., Arnold, S., Belem, T., Bussiere, B., Benzaazoua, M., Simon, R. (2003). *Interaction between backfill and rock mass in narrow Stopes*. SoilRock2003: 12th Panamerican Conference on Soil Mechanics and Geotechnical Engineering and 39th U.S. Rock Mechanics Symposium. 22-26 June 2003, Cambridge, Mass., USA, vol. 1, pp. 1157-1164.

Aysen, A. (2002). *Soil mechanics - Basic concepts and engineering applications*. Lisse: Balkema.

Barrett, J.R. (1973). *Structural Aspects of Cemented Fill Behaviour*. Proceedings of the Jubilee Symposium on Mine Filling. Mount Isa, Australia, 19-22 August, Aus.I.M.M., North West Queensland Branch, pp. 85-91.

Belem, T., Benzaazoua, M., and Bussière, B. (2000). *Mechanical behaviour of cemented paste backfill*. Proceedings of 53th Canadian Geotechnical Conference. Montreal, Canada, V1: 373-380.

Belem, T. Benzaazoua, M. Bussière, B. and Dagenais, A.M. (2002). *Effects of settlement and drainage on strength development within mine paste backfill*, Tailings and Mine Waste'01, Vail, CO, 139-148.

Belem, T., Harvey, A., Simon, R., and Aubertin, M. (2004). *Measurement and prediction of internal stresses in an underground opening during its filling with cemented fill*. Proceedings of the Fifth International Symposium on Ground Support. Perth, Australia. pp. 619–630.

Benzaazoua, M., Peyronnard O., Belem T., Fried E., Aurore S., Dublet G. (2010). *Key issues related to behaviour of binders in cemented paste backfilling.* Proceedings of the 13th International Seminar on Paste & Thickened Tailings (Paste 2010), 3-6 may 2010, Toronto, ON, Keynote paper.

Benzaazoua, M., Bussiere, B., Dermers, I., Aubertin, M., Fried, E., and Blier, A. (2008). *Integrated mine tailings management by combining environmental desulphurization and cemented paste backfill*: Application to mine Doyon. Miner. Eng., 21(4), 330-340.

Benzaazoua, M., Fall, M. and Belem, T. (2004). *A contribution to understanding the hardening process of cemented pastefill*. Minerals Engineering. 17(2): 141-152.

Bieniawski, ZT. (1989). Engineering rock mass classifications. Wiley, New York, 215 pp.

Blight, G.E. (1986). *Pressure exerted by materials stored in silos. Part I: coarse materials.* Géotechnique, 36(1): 33-46.

Bloss, M.L. (1992). *Prediction of cemented rock fill stability design procedures and modelling techniqu*es. PhD Thesis, Department of Mining and Metallurgical Engineering, University of Queensland, Brisbane, Australia, 265.

Brady, B.H.G. and Brown, ET. (2004). *Rock mechanics for underground mining*. 3rd edition. Kluwer, Dordrecht, 628 p.

Brady, A.C. and Brown, J.A. (1993). *Rock mechanics for underground mining* (Seconded). Chapman and Hall, London.

Boumiz A, Vernet C, and Tenoudjit FC. (1996). *Mechanical properties of cement pastes and mortars at early ages – evolution with time and degree of hydration*. Advn. Cem. Bas. Mat. 3: 94-106.

Caceres, C. (2005). *Effect of backfill on longhole open stoping*, MASc Thesis. Mining Engineering, University of British Columbia, 139 pp.

Coulthard, M.A. (1999). *Applications of numerical modelling in underground mining and construction*. Geotech. Geol. Eng. 17(2) : 373-385.

Cowin, S.C. (1977). *The theory of static loads in bins*. J. Applied Mech., 44(3), 409-412.

Darling, P. (2011). *SME Mining Engineering Handbook*, 3rd edition, Society for Mining, Metallurgy, and Exploration, Inc. p. 1583.

DiMaggio, F.L., and Sandler, I.S. (1971). *Material model for granular soils*. Journal of the Engineering Mechanics Division, ASCE, 97(EM3): 935–950.

Dirige, A.P.E, McNearny, R.L, Thompson, DS. (2009). *The effect of stope inclination and wall rock roughness on back-fill free face stability*. In: Rock Engineering in Difficult Conditions: Proceedings of the 3rd Canada-US Rock Mechanics Symposium. Toronto, 2009: 9-15.

El Mkadmi N, Aubertin M, and Li L. (2014). *Effect of drainage and sequential filling on the behavior of backfill in mine stopes*. Can. Geotech. J. 51(1): 1-15.

El Mkadmi, N., E. M., Aubertin, M., and Li, L. (2011). *The effect of transient drainage on the tress state in backfilled mine stopes*. Proc., 2011 Pan-Am CGS Geotech. Conf. University of Toronto, #1139.

Euler, D.S. and Aldrich, P.E.D. (2002). *Arching Effects and Sillmat Behaviour*. Proc. 104th Annual General meeting of the Canadian Institute of Mining Metallurgy & Petroleum, 102-107.

Emad, M.Z., Mitri, H.S., and Kelly, C. (2014). *Effect of blast-induced vibration on fill failure in vertical block mining with delayed backfill*. Can. Geotech.J. 51(9): 975-983.

Emad, M.Z., Mitri, H.S. (2013). *Modelling dynamic loading on backfilled stopes in sublevel stoping systems*. Rock characterisation, modelling and engineering designs methods, Feng Hudson and Tan (Eds), Taylor and Francis Group, London, ISBN 978-1-138-00057-5.

Fahey, M., Helinski, M., Fourie, A. (2011). *Development of specimen curing procedures that account for the influence of effective stress during curing on the strength of cemented mine backfill*. Geotech. Geol. Eng. 29(5), 709-723.

Fahey, M., Helinski, M., and Fourie, A. (2009). *Some aspects of the mechanics of arching in backfilled stopes*. Can. Geotech. J. 46(11), 1322-1336.

Falaknaz, N., Aubertin, M. and Li, L. (2014). *A numerical modelling study to assess the stress distribution in two nearby backfilled openings created in sequence*. In: Proceedings of the Canadian geotechnical conference, GeoRegina, Regina, Canada.

Falaknaz N, Aubertin M and Li L. (2013). *Numerical investigation of the stress state in adjacent backfilled mine stopes*. In: Proceedings of the Canadian geotechnical conference. GeoMontreal, Montreal, QC, 8p.

Fall, M., Nasir, O. (2010). *Mechanical behaviour of the interface between cemented tailings backfill and retaining structures under shear loads*. Geotech. Geol. Eng. 28(6): 779-790.

Geo-Slope. (2008). *Stress-Deformation Modeling with SIGMA/W 2007*. (3e éd.): GEO-SLOPE International Ltd.

Godbout, J., Bussière, B., Aubertin, M., Belem, T. (2007). *Evaluation of cemented paste backfill saturated hydraulic conductivity at early curing time. In* Proceedings of the 60th Canadian Geotechnical Conference and the 8th Joint CGS/IAH-CNC Groundwater Conference, Ottawa, ON, 21–24 October 2007. pp. 2230–2236.

Grabinsky, M.W. (2010). *In situ monitoring for ground truthing paste backfill design*. Proceedings of the 13th International Seminar on Paste and Thickened Tailings. 3-6 May 2010, Toronto, Ontario, Canada.

Grice, T. (2001). *Recent mine developments in Australia*. In MineFill'2001: Proceedings of the 7th International Symposium on Mining with Backfill. pp. 351–357.

Handy, R., and Spangler, M. (2007). *Geotechnical engineering: Soil and Foundation principles and practice.* 5th Ed. McGraw Hill, New York.

Handy, R. (1985). *The arch in soil arching*. J. Geotech. Eng. 111(3): 302–318.

Harrop-Williams, K. (1989). *Arch in soil arching*. J. Geotech. Eng. 11(3):415–419.

Hartman, H.L., Britton S.G., Gentry D.W., Karmis M., Mutmansky J.M., Schlitt, W.J. and Singh, M.M. (1992). *SME mining engineering handbook*, 2nd Edition, Cosponsored by Seeley W. Mudd Memorial Fund of AIME, Published by Society for Mining, Metallurgy, and Exploration, Inc., Littleton, Colorado.

Hassani, F., and Archibald, J. (1998). *Mine backfill*. CD-Rom. Canadian Institute of Mine, Metallurgy and Petroleum.

Hassani, F., Fotoohi, K., and Doucet, C. (1998). *Instrumentation and backfill performance in a narrow Vein Gold Mine*. Int. J. of Rock Mech. And Min. Sci. 35 (4-5), No:106.

Hassani, F., Ouellet, J., and Servant., S. (2001). *In situ measurements in a paste backfill: backfill and rock mass response in the context of rockburst*, 17* International Mining Congress and Exhibition of Turkey, 2001.

Hassani, F., Mortazavi, A., Shabani, M. (2008). *An investigation of mechanisms involved in backfill-rock mass behaviour in narrow vein mining*. The Journal of Southern African Institute of Mining and Metallurgy 108, 463-472.

Helinski, M., Fahey, M., Fourie, A. (2007). *Numerical Modeling of cemented mine backfill deposition*. Journal of Geotechnical and Geoenvironmental Engineering. 133, 10, pp. 1308-1319.

Helinski, M., Fahey, M., Fourie, A. (2010). *Coupled two-dimensional finite element modelling of mine backfilling with cemented tailings*. Can. Geotech. J., 47(11) : 1187-1200.

Helinski M, Fahey M, Fourie A. (2011). *Behaviour of cemented paste backfill in two mine stopes—measurements and modelling*. Journal of Geotechnical and Geoenvironmental Engineering. 137 (2): 171-182.

Herget, G. (1988). *Stresses in rock.* A.A.Balkema, Rotterdam, The Netherland.

Hoek, E. (2007). *Practical rock engineering*. Hoek's Corner (Rock Science). <https://www.rocscience.com/education/hoeks_corner> (Mar. 15, 2014).

Hoek, E., Carranza-Torres, C.T., and Corkum, B. (2002). *Hoek-Brown failure criterion 2002 edition*. In Proceeding of 5th North American Rock Mechanics Symposium, Toronto. 1: pp. 267-273.

Hoek, E., and Brown, E.T. (1980). *Underground Excavations in Rock*. London: Istn Min. Metall.

Hustrulid, W., Qianyuan, Y., and Krauland, N. (1989). *Modeling of cutand- fill mining systems*, Näsliden revisited. Innovation in mining backfill technology. F. P. Hassani, M. J. Scoble, and T. R. Yu, eds, Balkema, Rotterdam, The Netherlands, 147–164.

Iglesia, G,R., Einstein, H.H., and Whitman, R.V.(1999). *Determination of vertical loading on underground structures based on an arching evolution concept*. In Geo-engineering for Underground Facilities. Geo- Institute of the American Society of Civil Engineers (ASCE), Reston, Va. pp 495-506.

Itasca. (2014). *FLAC^{3D} version 5.0*. Users Manuals. ITASCA Consulting Group, Thresher square East, 708 South Third Street, Suite 310, Minneapolis, Minnesota, USA.

Itasca. (2002). *FLAC version 5.0*. Users Manuals. ITASCA Consulting Group. Thresher square East, 708 South Third Street, Suite 310, Minneapolis, Minnesota, USA.

Jaky, J. (1948). *Pressure in silos*. Proceedings of the 2nd International Conference on Soil Mechanics and Foundation Engineering. 1: 103-107. Rotterdam: Balkema.

Kaiser, P.K., Kim, B.H. (2008). *Rock mechanics advances of underground construction and mining*. Keynote lecture, Korea rock mechanics symposium, South Korea, pp 1-16.

Karima, R., Simangunsongb, G. M., Sulistiantocand, B., and Lopulaland, A. (2013). *Stability analysis of paste fill as stope wall using analytical method and numerical modeling in the kencana underground gold mining with long hole stope method*. Procedia Earth and Planetary Science, 6(2013): 474 – 484.

Knutsson, S. (1981). *Stresses in the hydraulic backfill from analytical calculations and in-situ measurements*. In: Proceedings of Conference on Application of Rock Mech. to Cut and Fill Mining. Institution of Mining and Metallurgy, London, 261–268.

Ladanyi, B., and Hoyaux, B. (1969). *A study of the trap-door problem in a granular mass*. Can. Geotech. J., 6(1):1-14.

Li L, Aubertin M. (2014). *A modified solution to assess the required strength of exposed backfill in mine stopes*. Int. J. of Mining science and technology. 24 : 549–558.

Li, L., Dube, J.S., Aubertin, M. (2013). *An extension of Marston's solution for the stresses in backfilled trenches with inclined walls*. Geotech. Geol. Eng. 31: 1027-1039.

Li L, Aubertin M. (2012). *A modified solution to assess the required strength of exposed backfill in mine stopes*. Geotech. Geol. Eng. 49: 994-1002.

Li, L., and Aubertin, M. (2010a). *An analytical solution for the nonlinear distribution of effective and total stresses in vertical backfilled stopes*. Geomechanics and Geoengineering. 5(4): 237-245.

Li, L., Aubertin, M., and Shirazi, A. (2010b). *Implementation and application of a new elasto-plastic model based on a multiaxial criterion to assess the stress state near underground openings*. Int. J. Geomech. 10(1): 13-21.

Li, L., Aubertin, M. (2009a). *Numerical investigation of the stress state in inclined backfilled Stopes*. Int. J. Geomech. 9(2): 52-62.

Li, L., Aubertin, M. (2009b). *A three-dimensional analysis of the total and effective stresses in submerged backfilled Stopes*. Geotech. Geol. Eng. 27(4): 559-569.

Li, L., Aubertin, M. (2009c). *Influence of water pressure on the stress state in backfill with Cohesionless Stopes*. Geotech. Geol. Eng. 27(1): 1-11.

Li, L., Aubertin, M. (2009d). *Horizontal pressure on barricades for backfilled stopes*. Part I: Fully Drained conditions. Can. Geotech. J., 46(1): 37-46.

Li, L., Aubertin, M. (2009e). *Horizontal pressure on barricades for backfilled stopes*. Part II: Submerged conditions. Can. Geotech. J., 46(1): 47-56.

Li, L., Aubertin, M. (2008). *An improved analytical solution to estimate the stress state in subvertical backfilled Stopes*. Can. Geotech. J., 45(10): 1487-1496.

Li, L., Aubertin, M., Shirazi, A., Belem, T., Simon, R. (2007). *Stress distribution in inclined backfilled stopes*. 9th International Symposium in Mining with Backfill. April 29- May 2, 2007, Montreal, Quebec, Canada. Canadian Institute of Mining, Metallurgy and Petroleum (CIM).

Li, L., Aubertin, M., and Belem, T. (2005). *Formulation of a three dimensional analytical solution to evaluate stress in backfilled vertical narrow openings*. *Can. Geotech. J.*, 42(6), 1705-1717.

Li, L., Aubertin, M., Simon, R., Bussiere, B., Belem, T. (2003). *Modelling arching effects in narrow backfilled stopes with FLAC*. Proceedings of the 3th International FLAC symposium. 21-24 October 2003, Sudbury, Ontario, Canada, pp. 211-219.

Le Roux, K.L., Bawden, W.F. and Grabinsky, M.F. (2005). *Field properties of cemented paste backfill at the Golden Giant mine*. Mining Technology. 114, A1-A16.

Marston, A. (1930). *The theory of external loads on closed conduits in the light of latest experiments*. Bulletin 96, Iowa Engineering Experiment Station, Ames, Iowa.

McCarthy, D.F. (1988). *Essential of soil mechanics and foundations: basic geotechnics*. Prentice Hall, Englewwod Cliffs, N.J.

Mitchell, R. (1992). *Centrifuge model studies of fill pressures on temporary bulkheads*. CIM (Canadian Mining and Metallurgical) Bulletin, 85(960): 48-54.

Mitchell, R., and Roettger, J. (1984). *Bulkhead pressure measurements in model fill pours*. Name: CIM Bull.

Mitchell, R., Smith, J., and Libby, D. (1975). *Bulkhead pressures due to cemented hydraulic mine backfills*. Can. Geotech. J., 12(3): 362-371.

Mitchell, R.J. and Wong, B.C. (1982). *Behaviour of Cemented Tailings Sands*. Can. Geotech. J., 19(3): 289-295.

Ouellet, J., Benzaazoua, M., and Servant, S. (1998a). *Mechanical, mineralogical and chemical caracterisation of paste backfill*. Proceeding of the 4th International Conference on Tailings and Mine Waste. Rotterdam, Balkema, pp. 139-146.

Ouellet, J., Bidwell, T.J. and Servant, S. (1998b). *Physical and mechanical characterization of paste backfill by laboratory and in situ testing*. Minefill 98, Proceeding of 6th International Symposium on Mining with Backfill. Brisbane, Australie, pp. 249-253.

Pierce, M.E. (2001). *Stability analysis of paste back fill exposes at Brunswick Mine*. Proceeding of 2nd International FLAC Symposium. Lyon, France, 147-156.

Pierce, M.E. (1997). *Laboratory and numerical analysis of the strength and deformation behaviour of paste backfill*. Master's Thesis, Department of mining engineering, Queen's University, Kingston, Ontario, Canada.

Pirapakaran, K. (2008). *Load-deformation characteristics of minefills with particular reference to arching and stress developments*. PhD Thesis. James Cook University, Australia.

Pirapakaran, K., and Sivakugan, N. (2007). *Arching within hydraulic fill stopes*. Geotech. Geol. Eng. 25(1): 25-35.

Pirapakaran. K, and Sivakugan, N. (2006). *Numerical and experimental studies of arching effects within mine fill stopes*. In: Proceedings of the 6th International Conference on physical modelling in geotechnics, C. W. W. Ng, L. M. Zhang and Y. H. Wang, Eds., Taylor & Francis, Hong Kong, Vol. 2, 1519–1525.

Potvin Y, Thomas E, Fourie A. (2005). *Handbook on mine fill*. Australian Centre for Geomechanics. ISBN 0-9756756-2-1.

Rankine, R.M., and Sivakugan, N. (2007). Geotechnical properties of cemented paste backfill from Cannington Mine, Australia. Geotech. Geol. Eng., 25 (4), 383-393.

Rankine, R.M. (2004). *The geotechnical and static stability analysis of Cannington mine paste backfill*. PhD Thesis. James Cook University, Townsville, Australia.

RocScience (2002). Phase2: 2D finite element program for calculating stresses and estimating support around underground excavations. Toronto, Canada.

Robinsky, EI. (1975). *Thickened discharge – A new approach to tailings disposal*. Canadian Mining Metallurg Bulltein. 68:47–53.

Scoble, M., Piciacchia, L. and Robert, J.M. (1987). *In situ testing in underground backfilled stopes*. CIM Bulletin. 80(903): 33-38.

Singh, S., Shukla, S. and Sivakugan., N. (2011). *Arching in inclined and vertical mine stopes*. Geotech. Geo. Eng. J. 29(5), 685-693. doi:10.1007/s10706-011-9410-4.

Sivakugan, N., Widisinghe, S., and Wang, V. (2014). *Vertical stress determination within backfilled mine stopes*. International Journal of Geomechanics, **14**(5): 06014011.

Sivakugan, N., Widisinghe, S., Wang, V. (2013). *A note on vertical stress determination within the backfilled mine stopes*. Int. J. Geomech, doi:10.1061/(ASCE)GM.1943-5622.0000367.

Smith, J.D., and Mitchell, R.J. (1982). *Design and control of large hydraulic backfill pours*. CIM Bulletin, 75(838): 102–111.

Sobhi, M.A., Li, L., Aubertin, M. (2014). *Numerical investigation of the lateral earth pressure coefficient along the VCL of vertical backfilled stopes*. GeoRegina 2014: Engineering for the Extremes, 67th CGS Conference, Regina, SK.

Spangler, M.G. (1962). *Protection of underground structures by Arch Action Associated with the Imperfect Ditch method of construction*. Proceeding of the symposium on soil-structure interaction. University of Arizona, Tucson, Arizona, pp. 531-546.

Spangler, M.G., and Handy, R.L. (1984). *Soil engineering*. Harper and Row, New York.

Take, W., and Valsangkar, A. (2001). *Earth pressures on unyielding retaining walls of narrow backfill width*. *Can. Geotech. J.*, 38(6): 1220-1230.

Terzaghi, K. (1943). *Theoretical soil mechanics*. John Weily & Sons, New York.

Ting, C.H., S.K. Shukla, and N. Sivakugan. (2011). *Arching in soils applied to inclined mine stopes*. Int. J. Geomech. 11(1): 29-35.

Ting, C.H., Sivakugan, N. Read, W., and Shukla, S.K. (2014). *Analytical expression for vertical stress within an inclined mine stope with non-parallel walls*. Geotech. Geol. Eng. 32: 577-586.

Thomas E.G., and Vance W.E. (1969). *Characteristics of hydraulic fill – Portland cement mixtures*. Proceeding of Rock Mechanics Symposium. Sydney University.

Thompson, B.D., Granbinsky, M.W., Bawden, W.F., Counter, D.B. (2009). *In-situ measurements of cemented paste backfill in longhole stopes*. In Proceedings of the 3rd Canada–US Rock Mechanics Symposium and 20th Canadian Rock Mechanics Symposium (RockEng09). May 2009. Toronto, Ont. Canada. Paper 4061.

Thompson, B., Grabinsky, M., and Bawden, W. (2011). *In situ monitoring of cemented paste backfill pressure to increase backfilling efficiency*. CIM Journal, 2(4): 1-10.

Thompson, B., Bawden W., and Grabinsky, M. (2012). *In situ measurements of cemented paste backfill at the Cayeli Mine*. Can. Geotech. J., 49(7): 755–772.

Van Horn, D. (1963). *A study of loads on underground structures*. Part III, Iowa Engineering Experiment Station.

Veenstra, R. (2013). *A design procedure for determining the in situ stresses of early age cemented paste backfill*. PhD Thesis, University of Toronto, Canada.

Veenstra, R.L., Grabinsky, M.W., and Bawden, W.F. (2013). *An Examination of the Failure Mechanisms in Modeled Cemented Paste Backfill*, World Mining Congress, Montreal. 11-15 August 2013.

Villaescusa, E. (2003). *Global extraction sequence in sublevel stoping*. Twelfth Int. Symp. on Mine Planning and Equipment Selection, Western Australian School of Mines, WA, Australia, (1): 9-17.

Winch, C. (1999). *Geotechnical characteristics and stability of paste backfill at BHP Cannington Mine*. B. E. Hons Thesis, James Cook University, Townsville, Australia.

Wood, D. (1990). *Soil behavior and critical state soil mechanics*. Cambridge university press. ISBN 0-521-33782-8.

Yilmaz, E., Benzaazoua, M., Belem, T., and Bussiere, B. (2009). *Effect of curing pressure on compressive strength development of cemented paste backfill*. Minerals Eng. 22:772-785.

Zoback, M.L. (1992). *First and second order patterns of tectonic stress: The world stress map project*. J. of Geophysical Research. v. 97, p. 11,703–11,728.

Zou, D.H., and Nadarajah, N. (2006). *Optimizing backfill design for ground support and cost saving*. In Proceedings of the 41st U.S. Rock Mechanics Symposium – ARMA's Golden Rocks 2006 – 50 Years of Rock Mechanics, Golden, Colo.Omnipress.

APPENDIX A – MODELLING METHODOLOGY AND VALIDATION

This appendix presents the methodology used to create and validate different models for simulation with FLAC and FLAC^{3D}. Model generation can be performed with the following steps.

1- **Mesh size**:

Size type of elements should be defined to give stable and precise results, for realistic computation time. The influence of different element size (from 0.25 m to 4 m) on the stress within the backfill and horizontal displacement of rock wall was investigated as shown in Figure A-1.

2- **Boundary location:**

The total size of the model is another key aspect, as the location of the external boundaries must not influence the results, while maintaining the model domain to a realistic size. This optimum model size may vary when the stopes geometry changes. The boundaries of the model were located at $1D_{max}$, $2D_{max}$, $3D_{max}$ and $5D_{max}$ (D_{max} is the maximum dimension of the excavation, D_{max}) from the openings. The location of the boundaries has been adjusted for each case. The effect of different boundary locations on the stresses in the first backfilled stope and horizontal displacements of rock wall is presented in Figure A-2.

3- **Number of excavation steps and filling layers**

The number of excavation steps and filling layers may affect the stresses and displacements. Therefore, calculations were made with the backfill is then placed in the first stope in 4, 7 or 10 layers. This is followed by the excavation of the second stope in 4, 7 and 10 steps, and its filling in 4, 7 and 10 layers to study the effect of multistep excavation and filling simulation. The results are shown in Figure A-3.

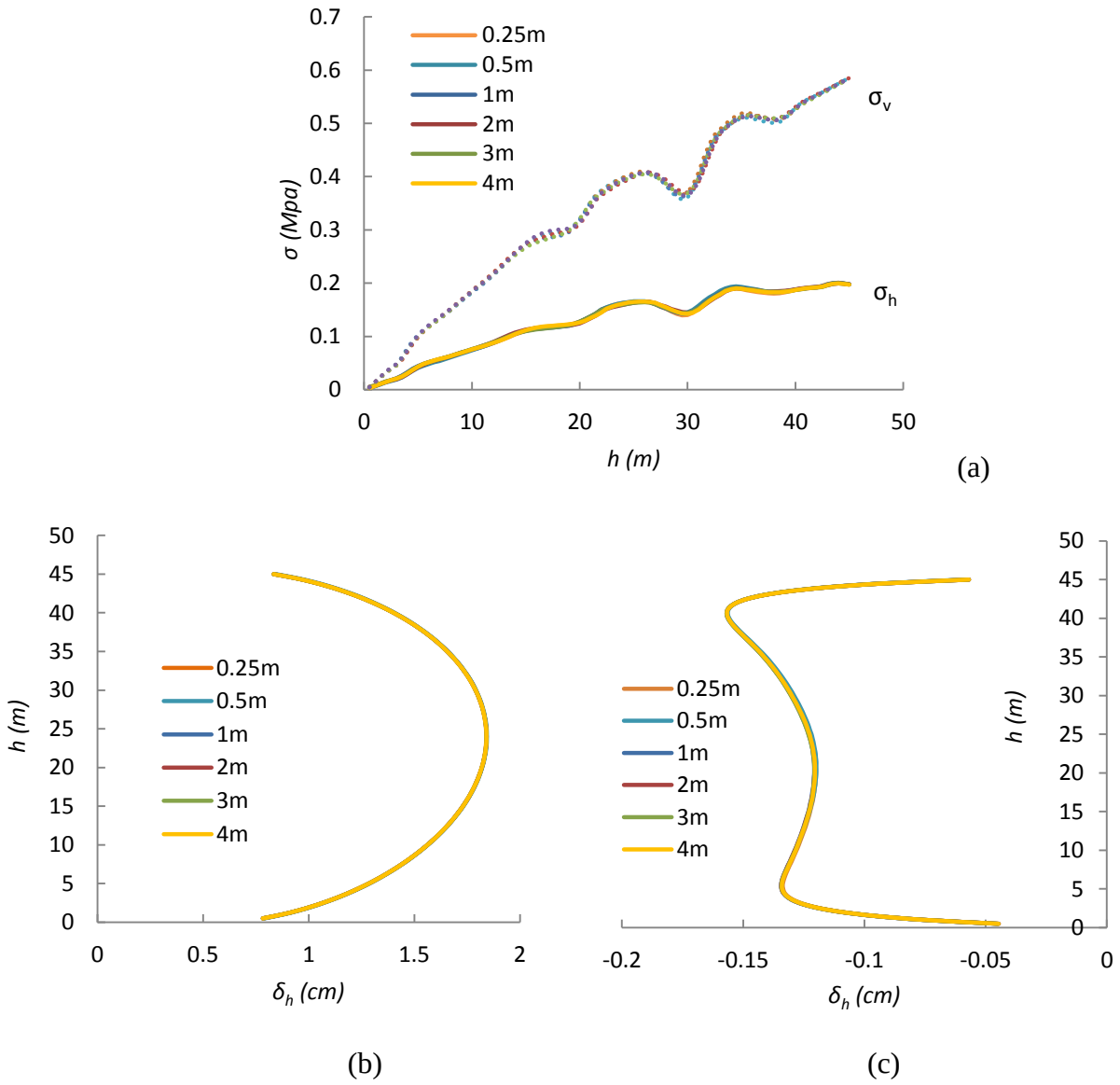

Figure A-1: Influence of mesh size on: a) the horizontal and vertical stresses along the VCL, b) rigth wall and c) left wall displacement of the first back filled stope after excavation and filling of the second stope, with $\phi' = 30^{o}$, $\psi' = 0$, $c' = 0$, $\gamma = 18$ kN/m3, $B = 6$ m, depth=300 m, Case 1b (Chapter 3)

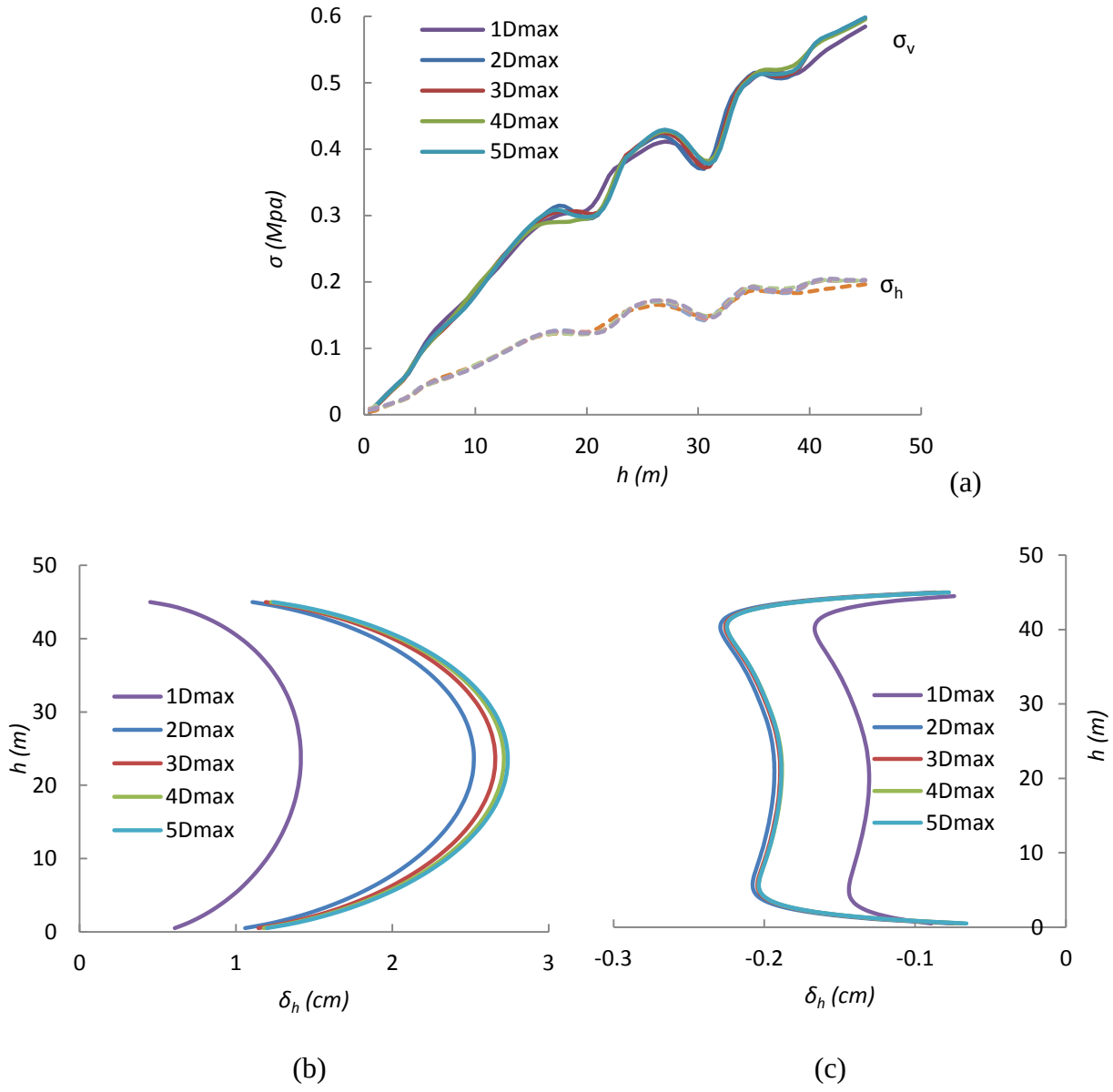

Figure A-2: Influence of boundary location on: a) the horizontal and vertical stresses along the VCL, b) rigth wall and c) left wall displacement of the first back filled stope after excavation and filling of the second stope, with ϕ' = 30º, ψ' = 0, c' = 0, γ = 18 kN/m3, B = 18 m, depth=300 m, Case 1b (Chapter 3)

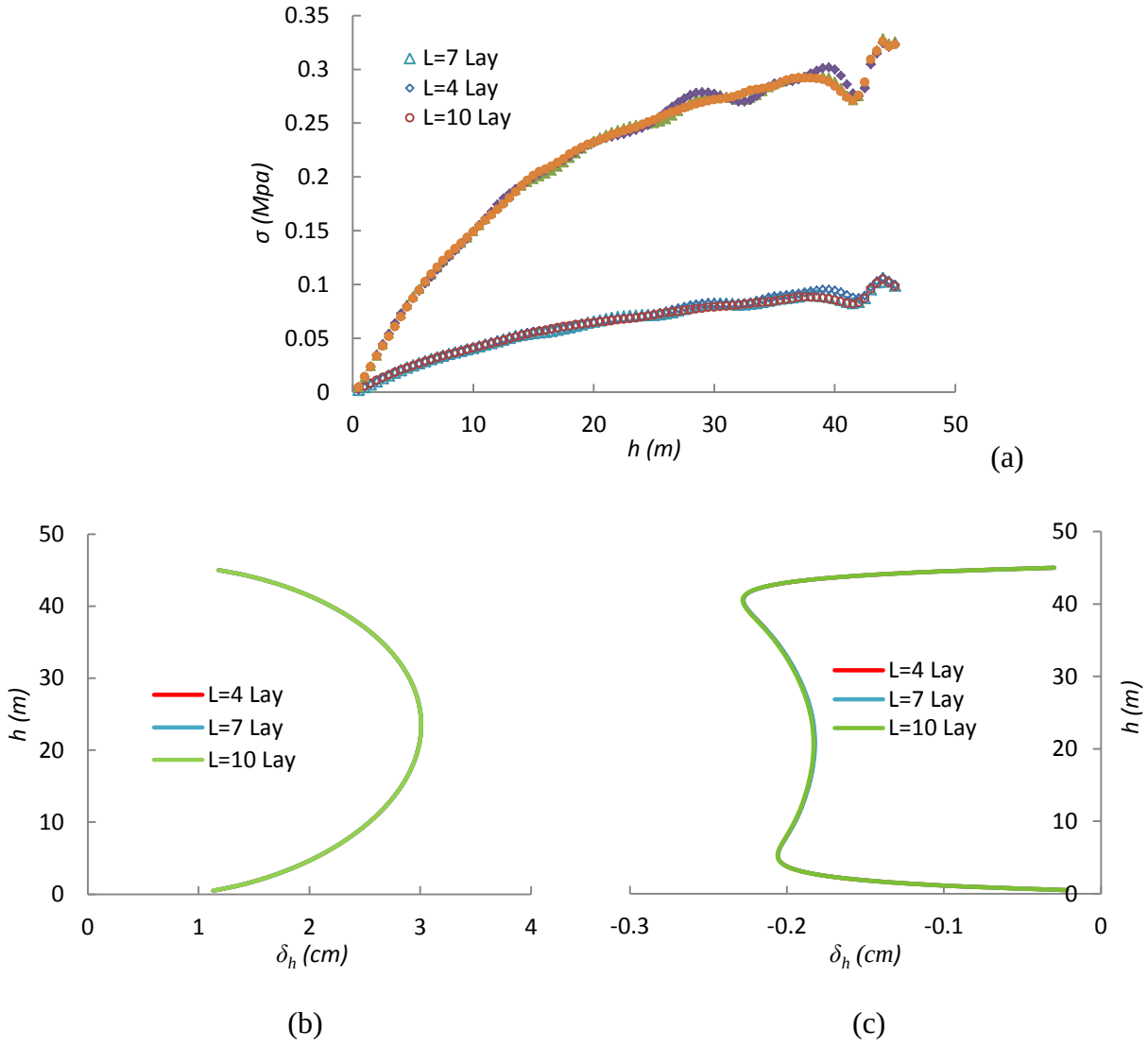

Figure A-3: Influence of multisp excavation and filling on: a) the horizontal and vertical stresses along the VCL, b) rigth wall and c) left wall displacement of the first back filled stope after excavation and filling of the second stope, with ϕ' = 35º, ψ' = 0, c' = 0, γ = 18 kN/m3 (unit weight), B = 6 m, depth=300 m, Case 1b (Chapter 3)

Observation

The results show that the mesh size has little influence on the stresses and displacements in the first backfilled stope. Therefore, the mesh size of 0.5m was selected to obtain accurate results with optimum run time. Also, the results of boundary location indicated that the external boundaries located $3D_{max}$ (150 m) away from the stopes have no influence on the stresses and displacment of the openings. The results also indicate that the stresses obtained along the VCL

and walls of the first stope are almost the same for the different excavation and filling sequences. These results thus suggest that the simulations with four steps for the excavation and filling of the second stope, do provide representative responses.

APPENDIX B - COMPLEMENTARY RESULTS RELATED TO CHAPTER 3

In this section, some complementary results related to Chapter 3, including the vertical displacement δ_v of the first backfilled stope during excavtion and filling of the second stope, the horizontal strain ε_h of the backfill and the effect of stope width B on the vertical displacement of the rock wall and horizontal strain of backfill are presented.

Vertical displacment, δ_v

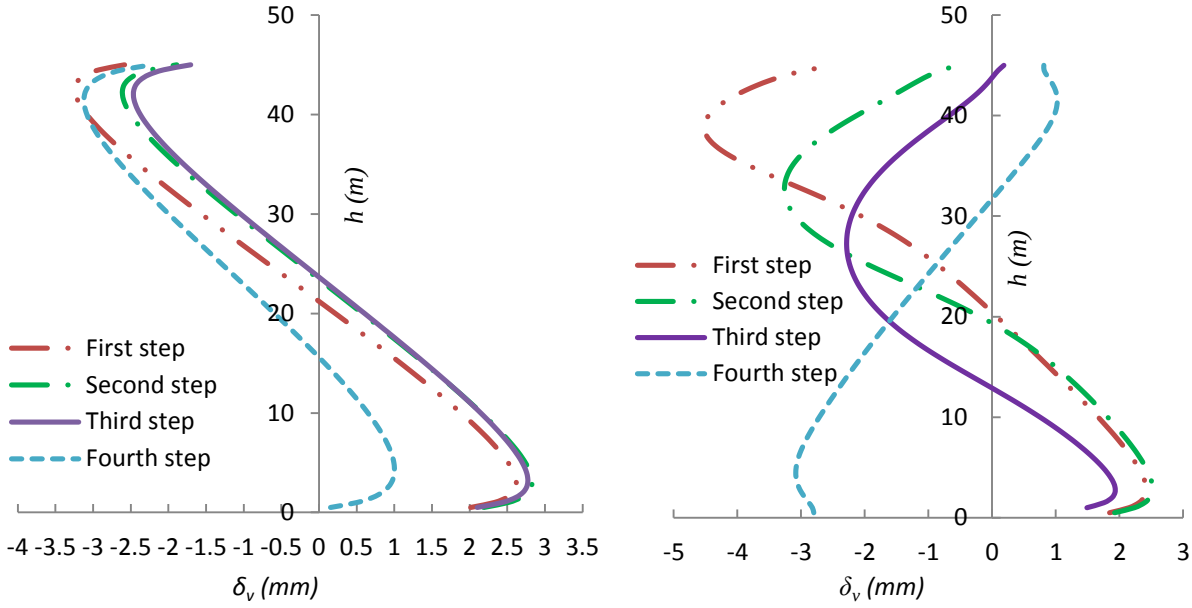

(a) (b)

Figure B-1: Vertical displacements δ_v along the (a) left wall and (b) right wall of the first stope during the excavation (4 steps) of the second stope (Case 1b)

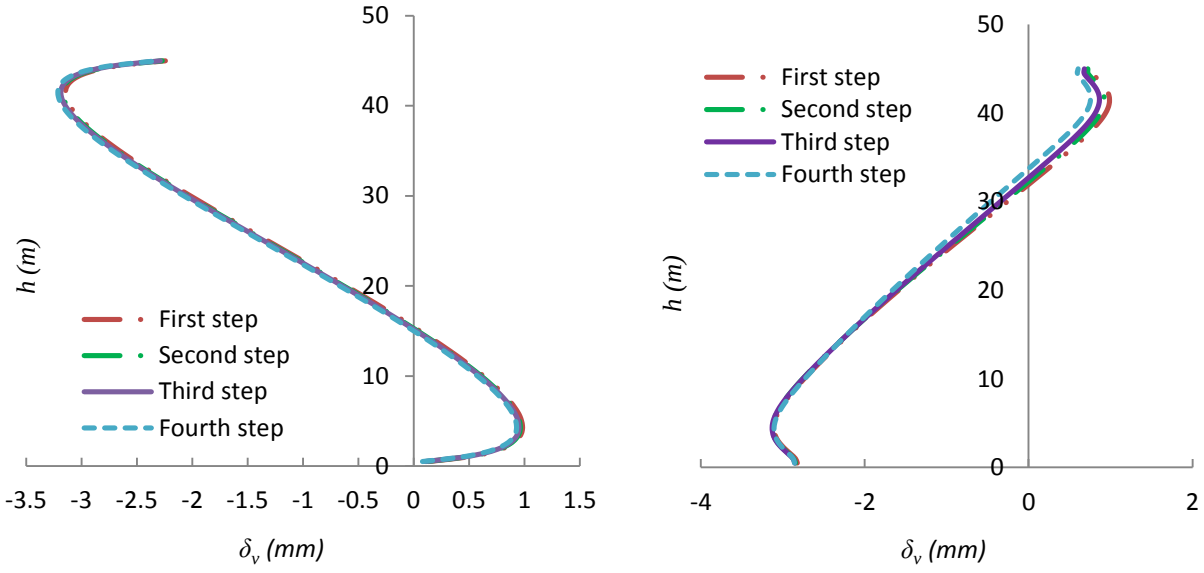

Figure B-2: Vertical displacements δ_v along the (a) left wall and (b) right wall of the first stope during the filling (4 steps) of the second stope (Case 1b)

Effect of stope width, *B*

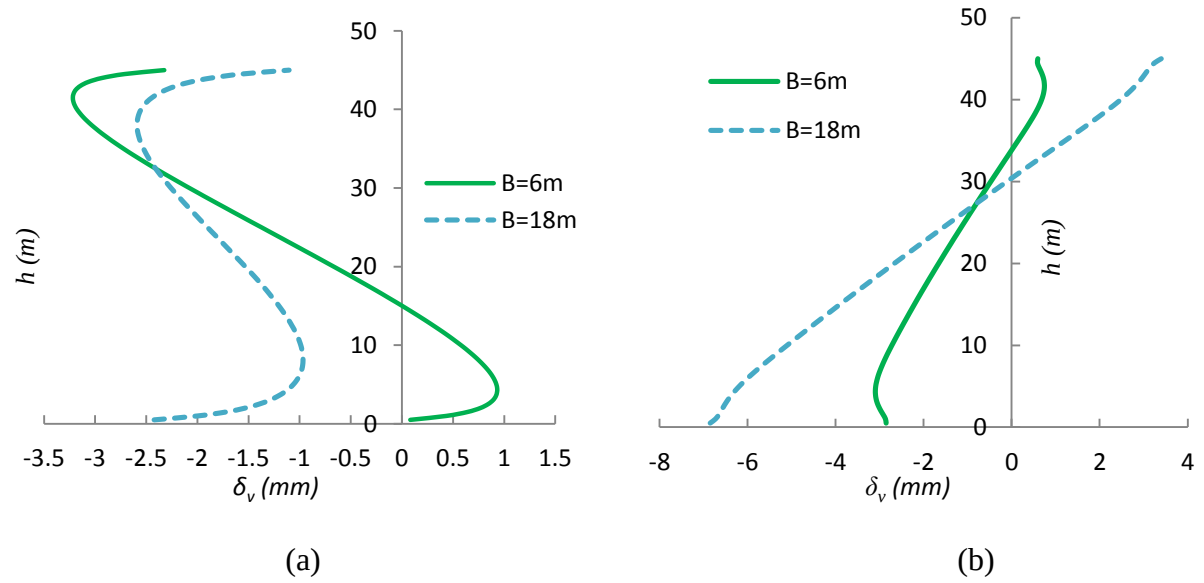

Figure B-3: Vertical displacements δ_v in the first stope along the (a) left wall and (b) right wall after excavation and filling of the second stope (Case 2)

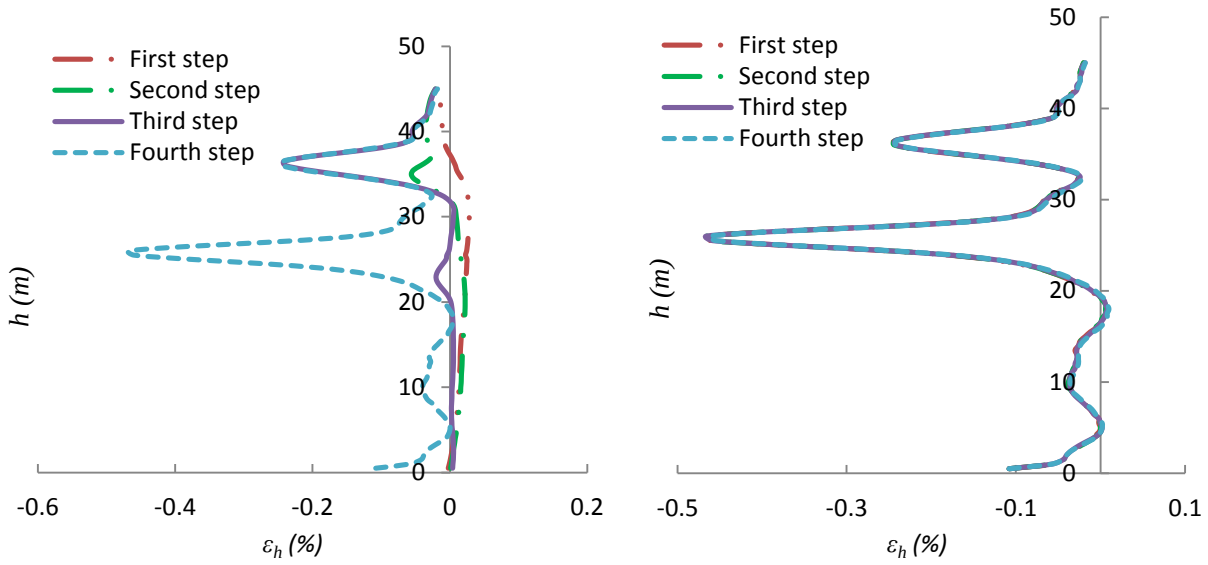

(a) (b)

Figure B-4: Horizontal strain ε_h along the VCL of the first backfilled stope during (a) excavation (4 steps) and (b) filling (4 steps) of the second stope (Case 2)

APPENDIX C - COMPLEMENTARY RESULTS RELATED TO CHAPTER 4

Complementary results related to Chapter 4 are shown in this appendix. The reults include the vertical displacements in the first backfill stope; effect of stope width *B* on the stresses along the VCL of the first backfilled stope, second stope and single stope; effect of pillar width *D*, earth reaction coefficient of rock mass K_r, rock modulus E_r and the stope depth *z* on the stresses along the VCL, walls, rock wall displacement and backfill strain. Also, the stress evolution of the first backfilled stope during excavation and filling of the second stope using independent friction angle ϕ' and Poissoin's ratio v and Eq.4-4 is also presented. Finally, the effect of sequence layer on the stresses along the walls is addressed.

Vertical displacements, δ_v

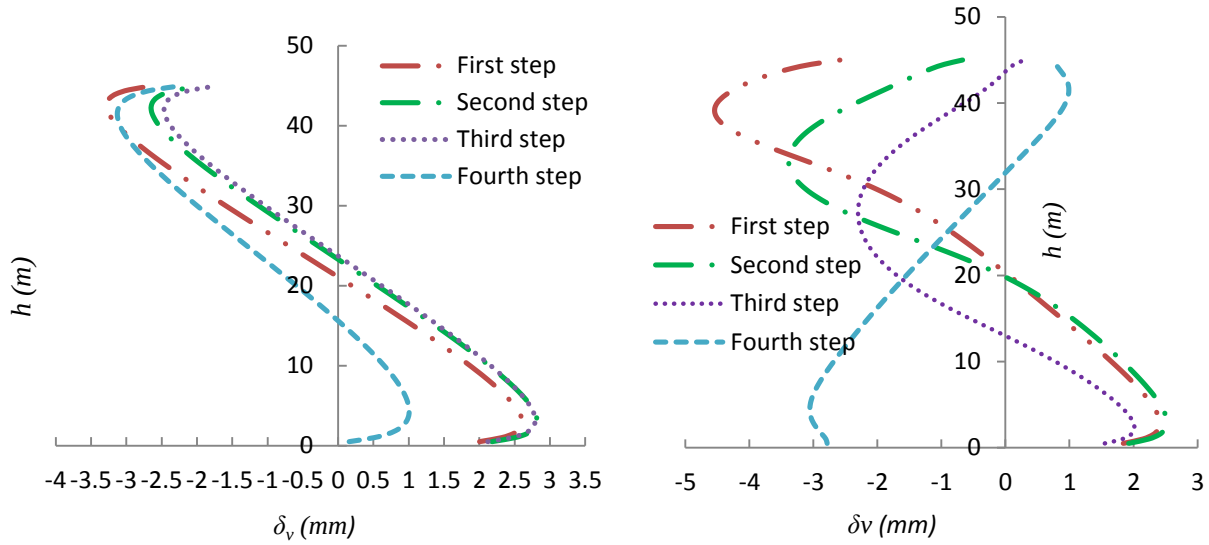

Figure C-1: Vertical displacements δ_v along the: (a) left wall and (b) right wall of the first stope during the excavation (4 steps) of the second stope (Case 0b)

Stresses in first backfilled stope

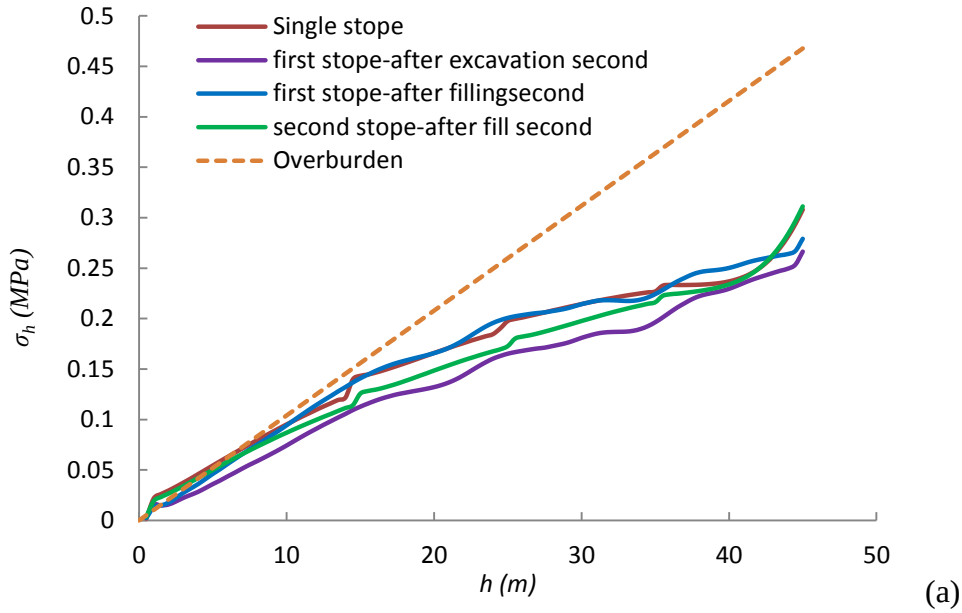

(a)

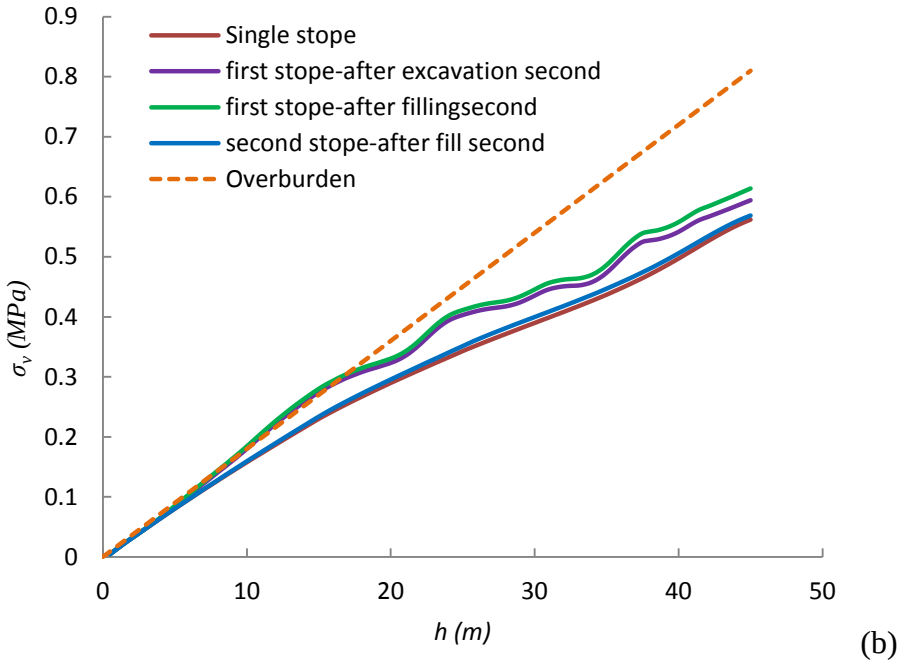

(b)

Figure C-2: Horizontal (a) and vertical (b) stresses along the VCL of the first backfilled stope; the resultants are shown for a single stope (reference case) and for the first and second stopes after excavation and filling of the latter (Case 1)

Effect of pillar width, *D*

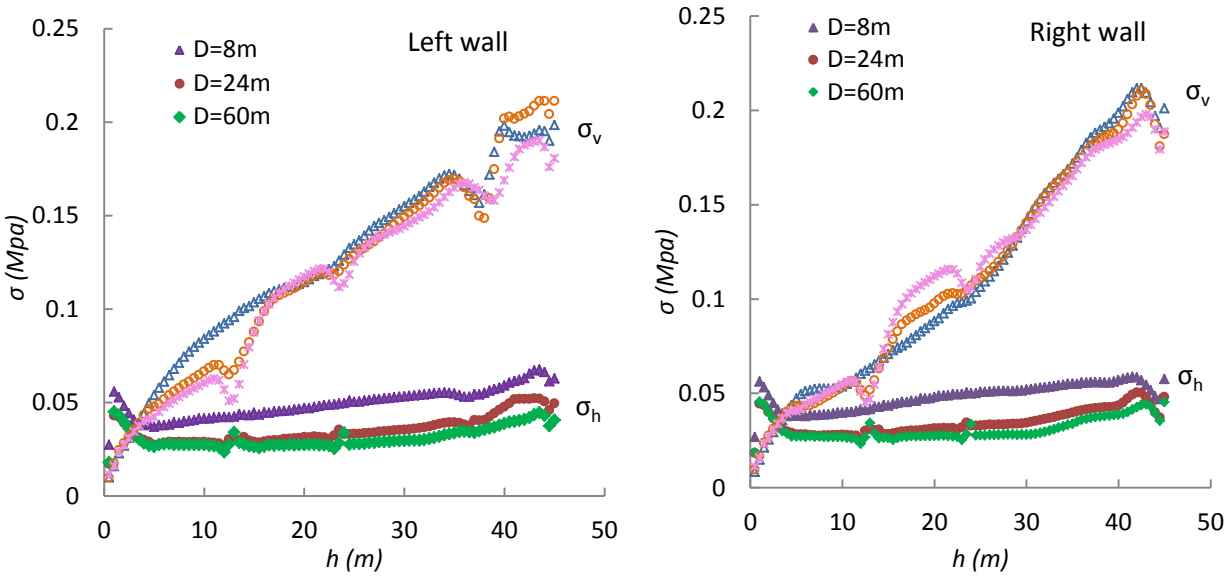

(a)

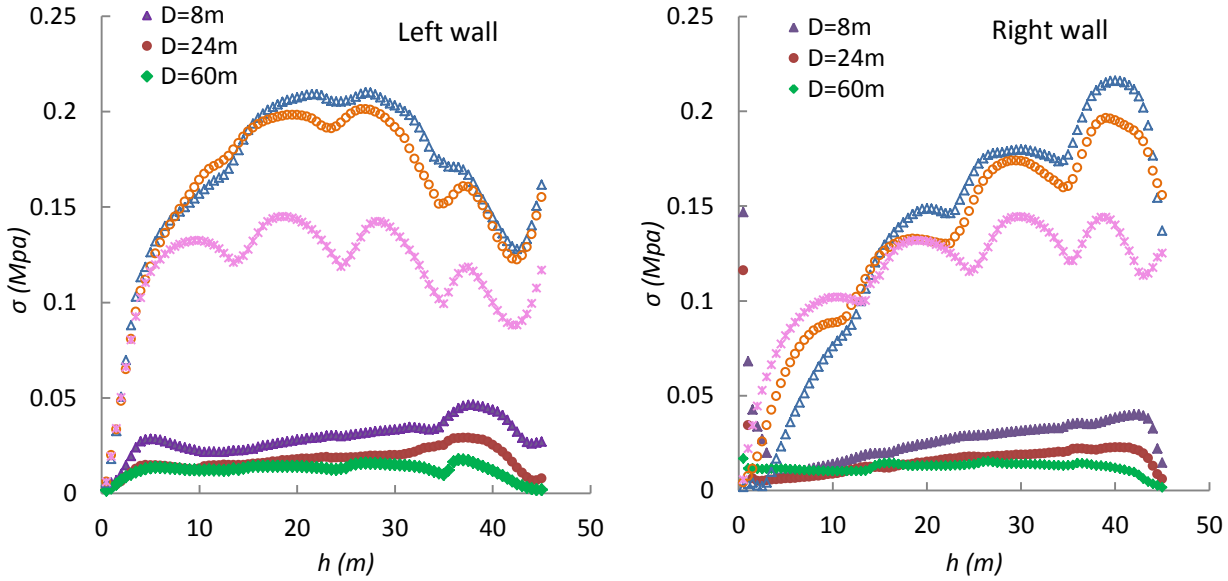

(b)

Figure C-3: Effect of pillar width *D* on the distribution of the vertical and horizontal stresses along the left and right walls of first stope after excavation and filling of the first stope for: (a) Case 3a with c' = 20 kPa; (b) Case 3b with c' = 50 kPa

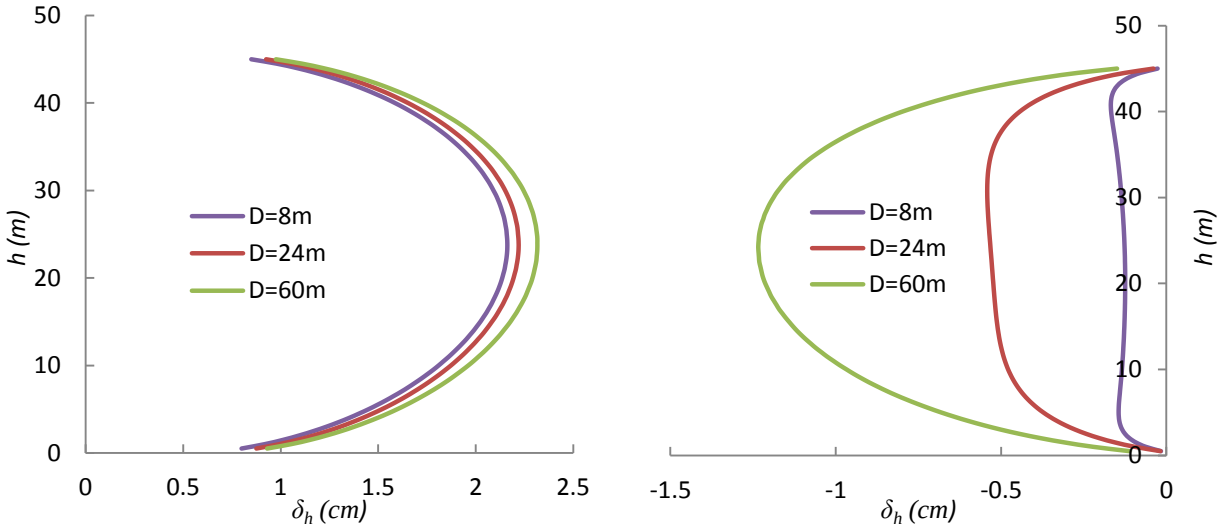

(a) (b)

Figure C-4: Effect of pillar width *D* on the horizontal displacements δ_h in the first stope along the: (a) left wall; (b) right wall after excavation of the first stope for Case 3a with c' = 20 kPa and Case 3b with c' = 50 kPa

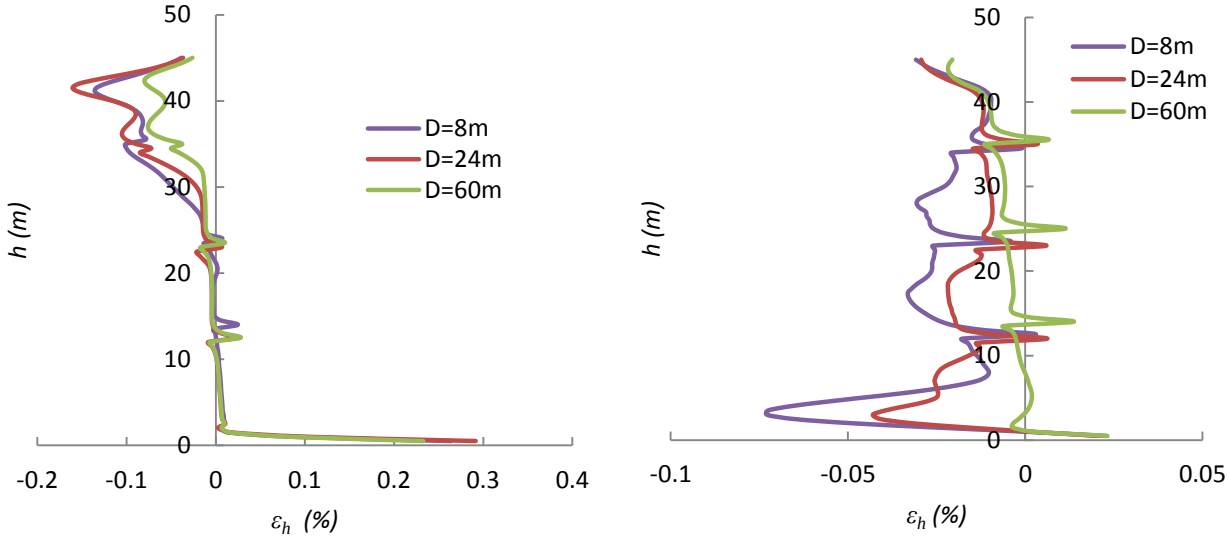

(a) (b)

Figure C-5: Effect of pillar width *D* on the horizontal strain εh in the first stope along the VCL after excavation the first stope for: (a) Case 3a with c' = 20 kPa; (b) Case 3b with c' = 50 kPa

Effect of K_r

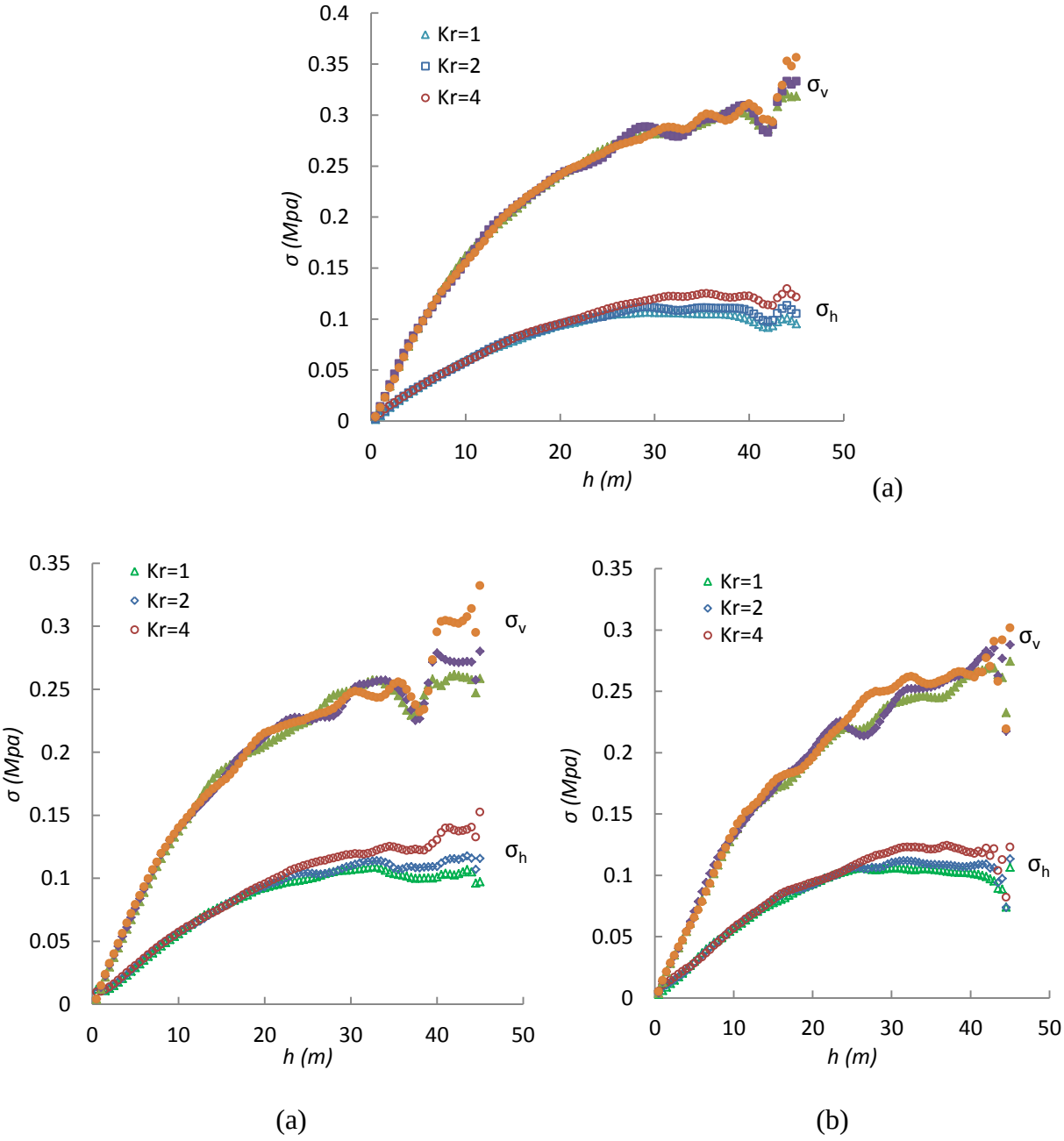

Figure C-6: Effect of K_r on the distribution of the vertical and horizontal stresses in the first stope along the: (a) VCL; (b) left wall; (c) right wall after excavation and filling of the second stope (Case 4)

Effect of E_r

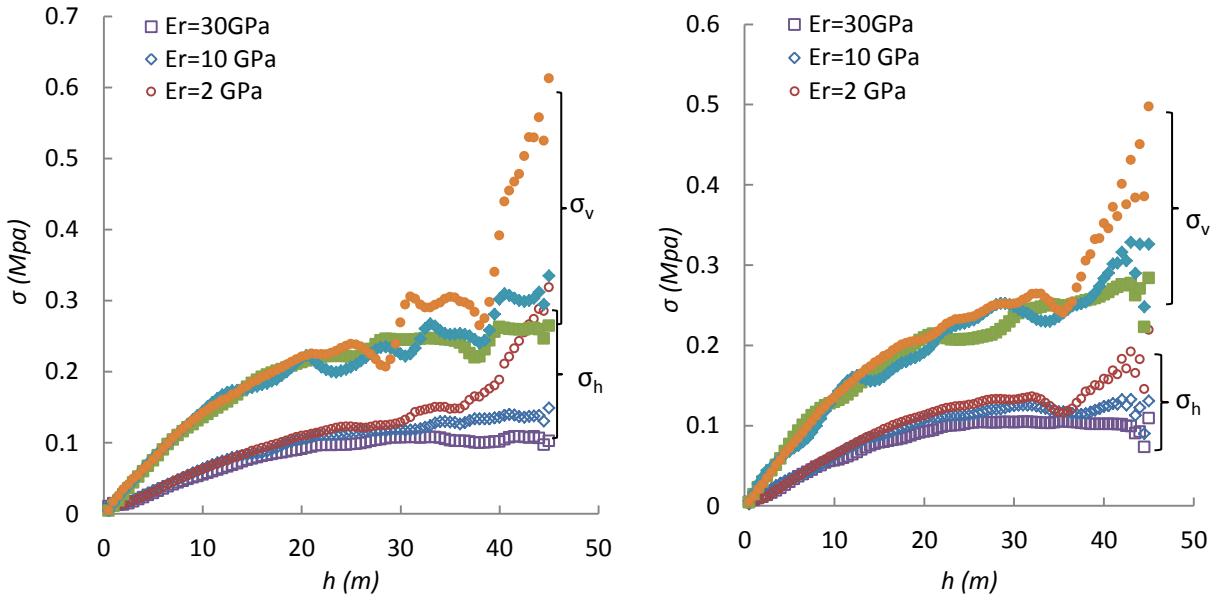

Figure C-7: Effect of rock modulus E_r on the distribution of the vertical and horizontal stresses in the first stope along the: (a) left wall; (b) right wall after excavation and filling of the second stope (Case 5)

Effect of E_r and stope depth z

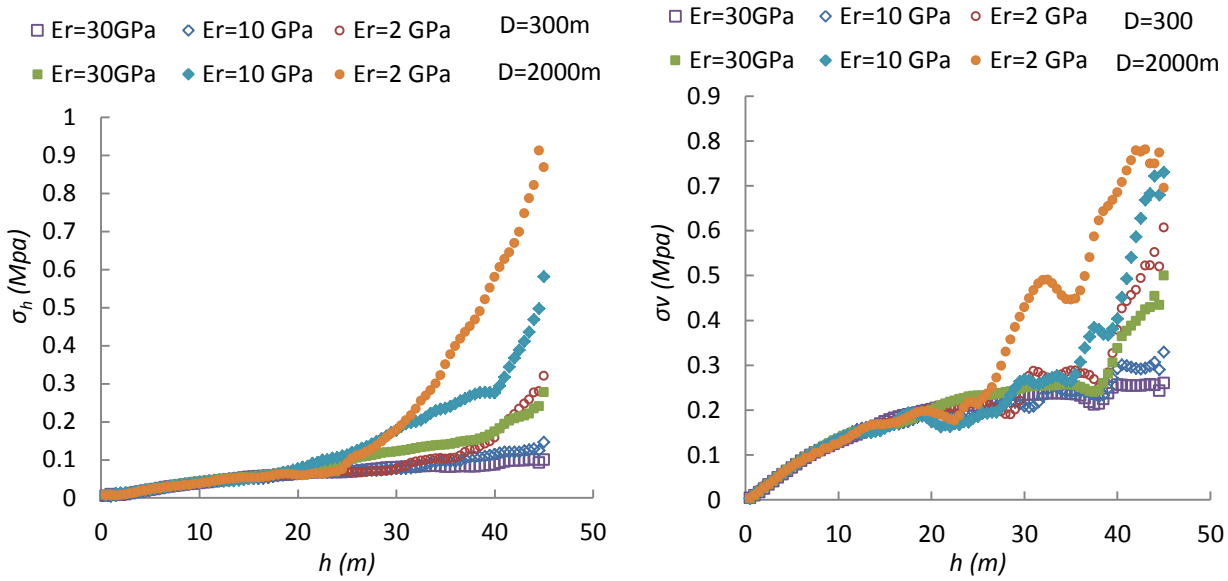

(a)

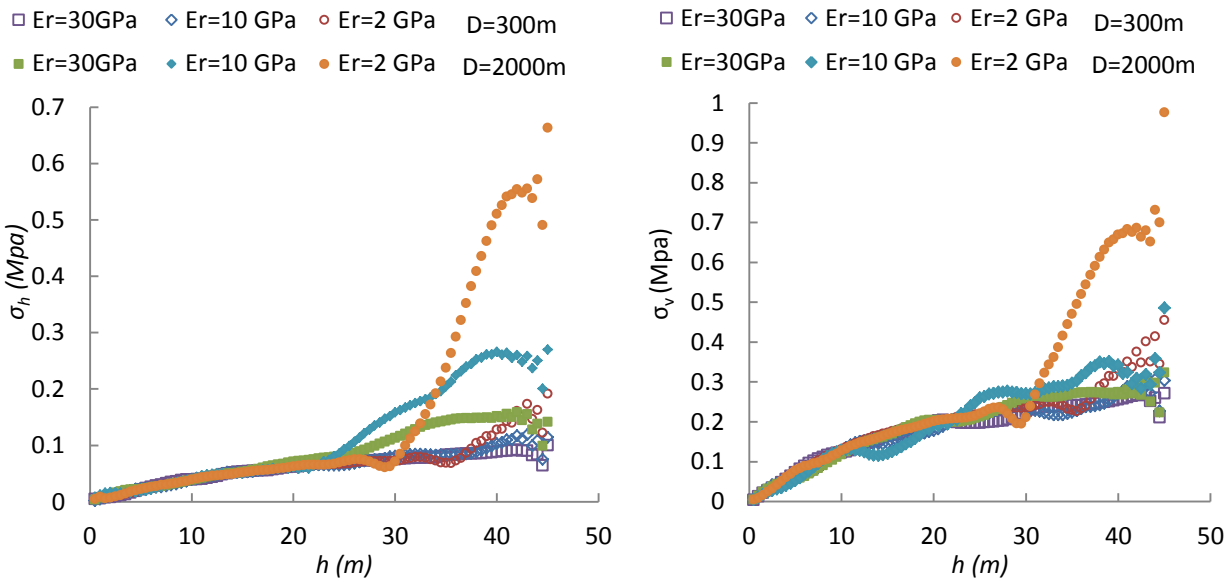

(b)

Figure C-8: Effect of rock modulus E_r and depth z on the distribution of the horizontal (left side) and vertical (right side) stresses in the first stope along the: (a) left wall; (b) right wall in the backfill after excavation of the second stope (Case 6)

Stress evolution using different assumptions

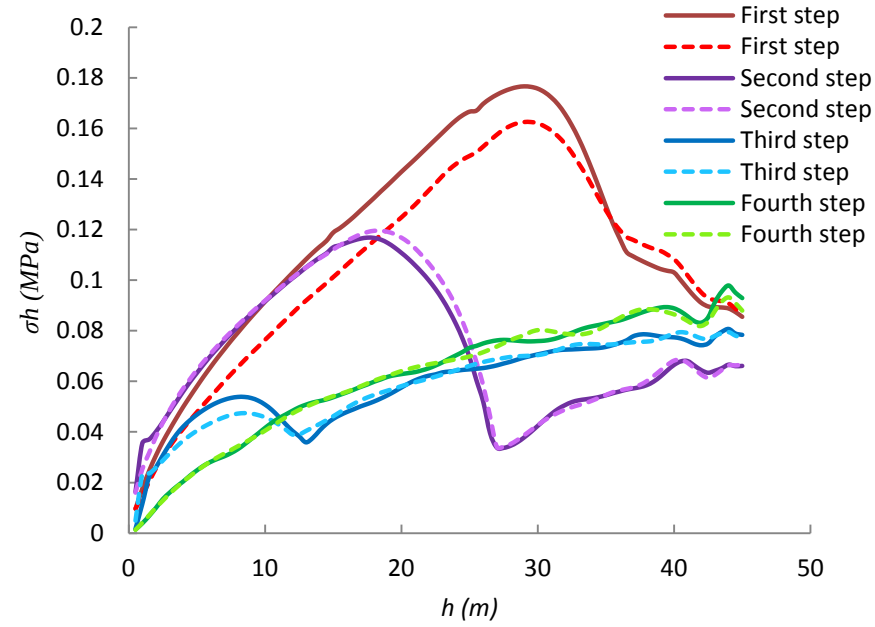

(a)

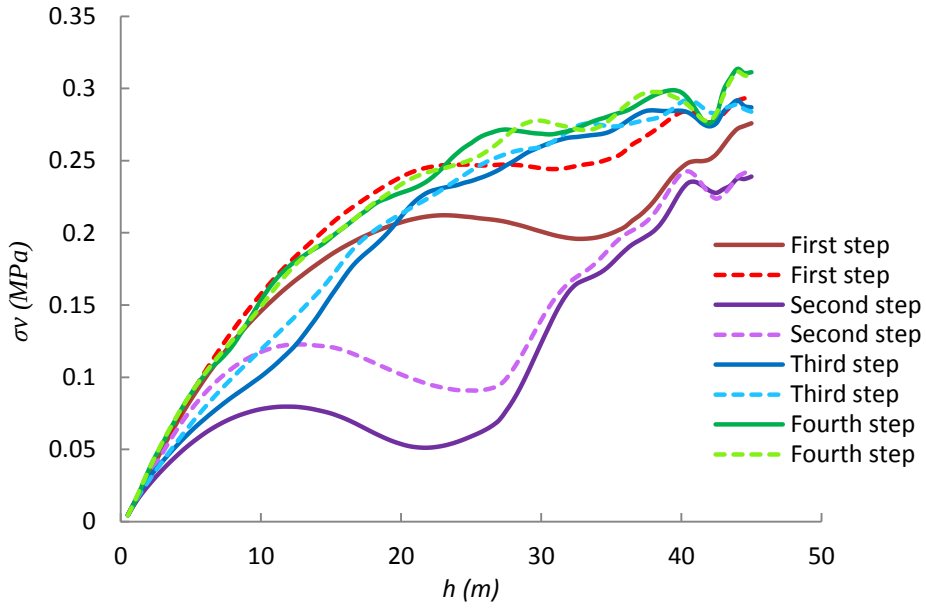

(b)

Figure C-9: Horizontal (a) and vertical (b) stresses along the VCL in the first backfilled stope, using independent v and ϕ' values (Case 7, dash lines) and Eq.4-4 (Case 7, solid lines) after excavation of the second stope

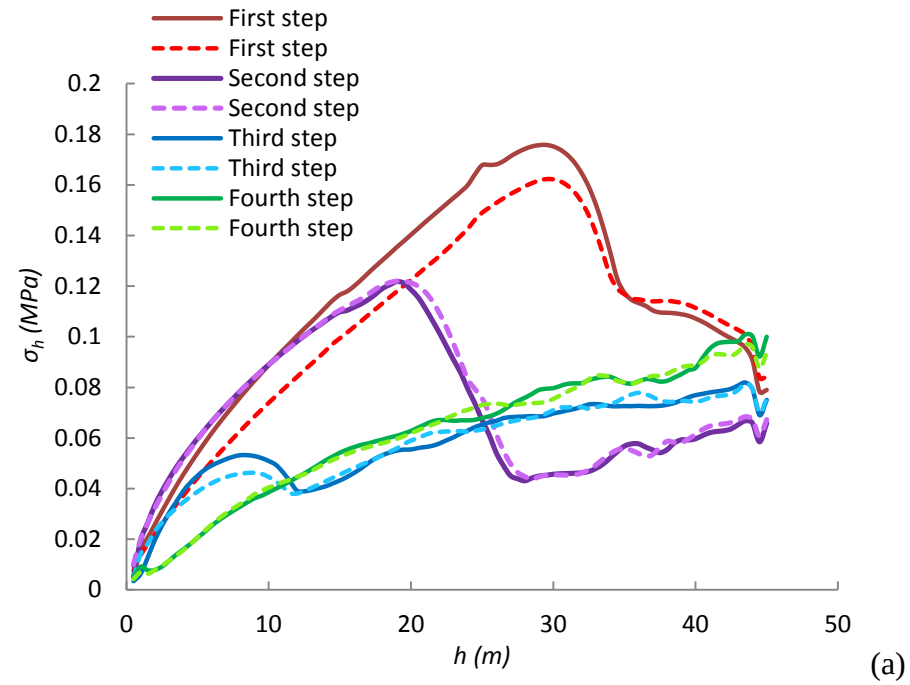

(a)

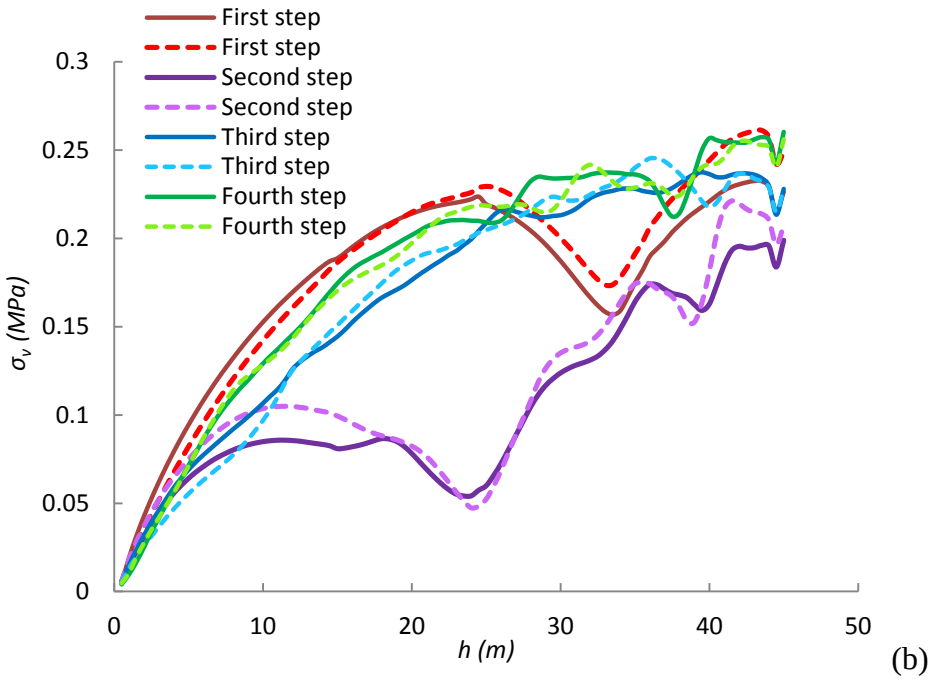

(b)

Figure C-10: Horizontal (a) and vertical (b) stresses along the left wall in the first backfilled stope, using independent v and ϕ' values (Case 7, dash lines) and Eq.4-4 (Case 7, solid lines) after excavation of the second stope

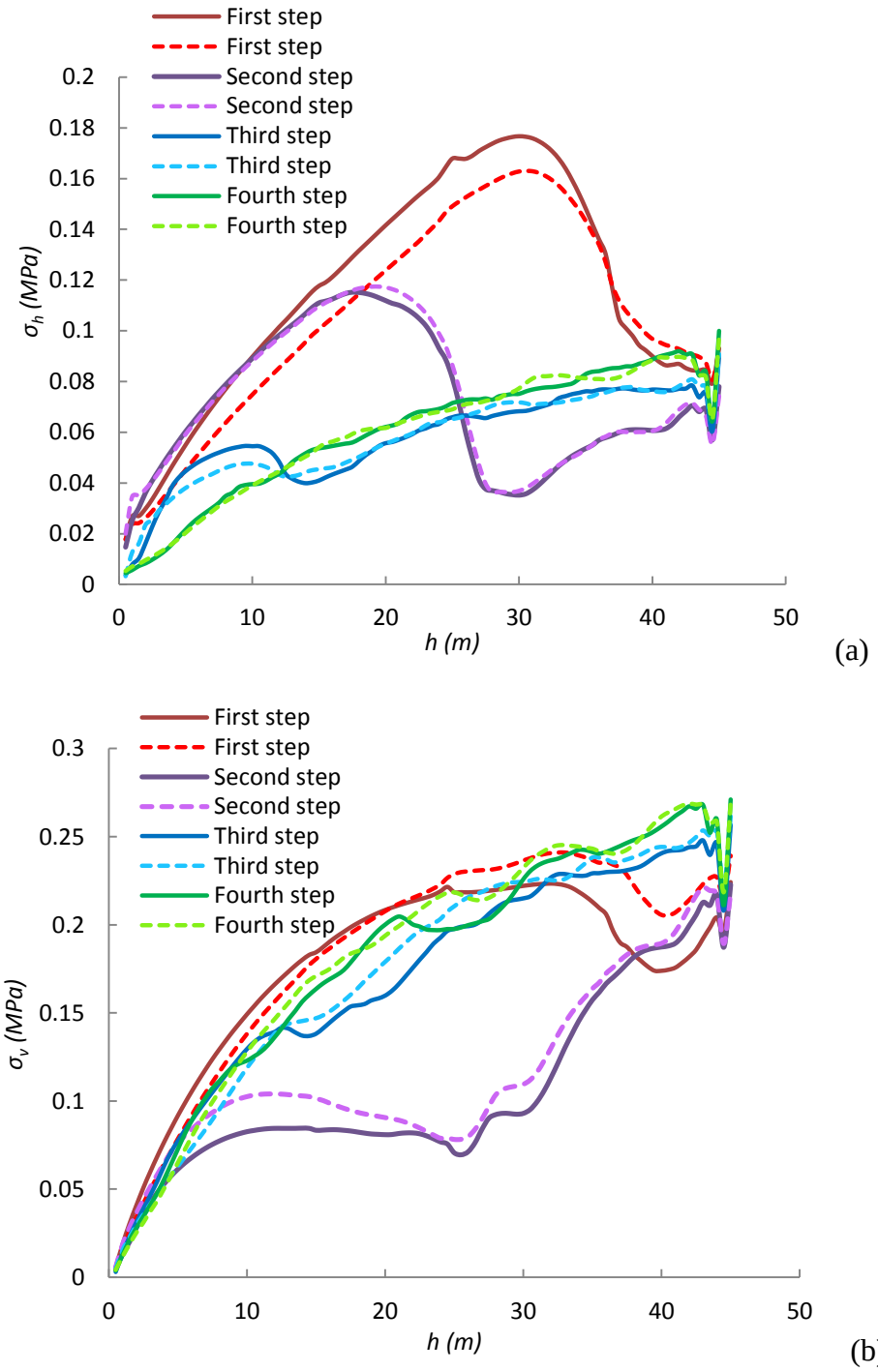

Figure C-11: Horizontal (a) and vertical (b) stresses along the right wall in the first backfilled stope, using independent v and ϕ' values (Case 7, dash lines) and Eq.4-4 (Case 7, solid lines) after excavation of the second stope

Effect of sequence of excavation and filling

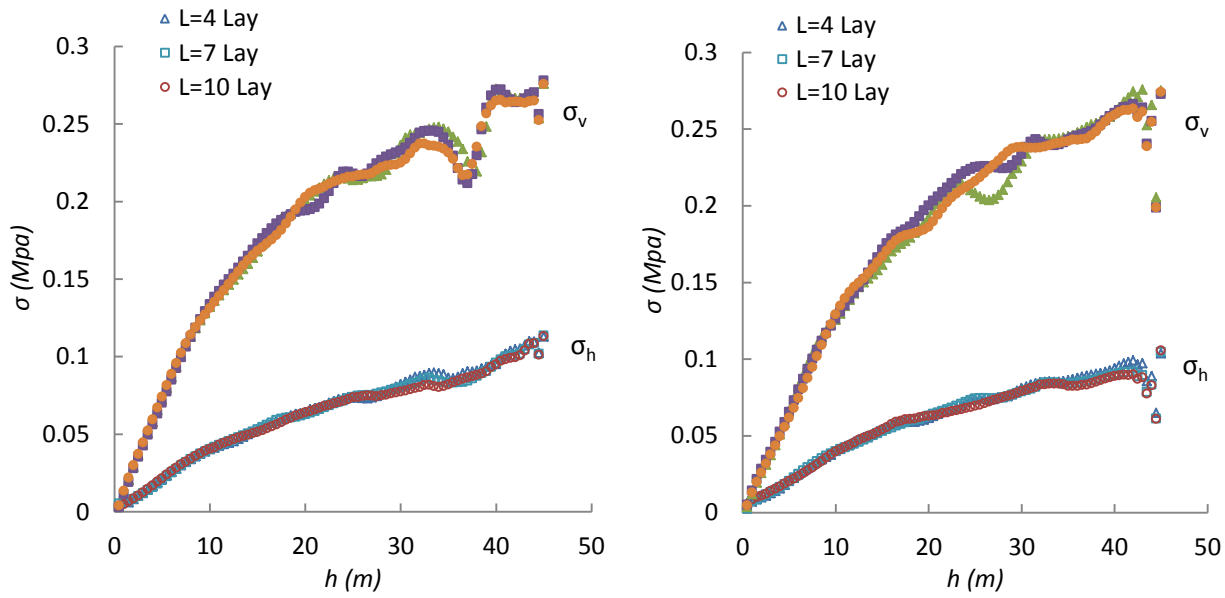

(a) (b)

Figure C-12: Effect of the filling sequence (4 to 10 layers) on the distribution of the vertical and horizontal stresses in the first backfilled stope along the: (a) left wall; (b) right wall (Case 8)

APPENDIX D - COMPLEMENTARY RESULTS RELATED TO CHAPTER 5

In this appendix, complementary results related to Chapter 5 are presented. The reults include the evolution of horizontal and vertical stresses along the walls of the first backfill stope, the stress distribution in the first backfilled stope with an elatic behavior of rock mass, rock wall displacment during the filling of the second stope, the stress path based on the deviatoric stress, effect of stope width B on the stresses along the VCL of the second backfilled stope, and rock wall displacment and backfill strain of the first stope, effect of pillar width D, stope depth z, earth reaction coefficient of rock mass K_r, rock modulus E_r on rock wall displacement and backfill strain is also shown. Finally, the effect of excavation and filling sequence on the stresses in the first backfilled stope is addressed when rock mass behavior is elasto-plastic.

Stress evolution for EP and EL models

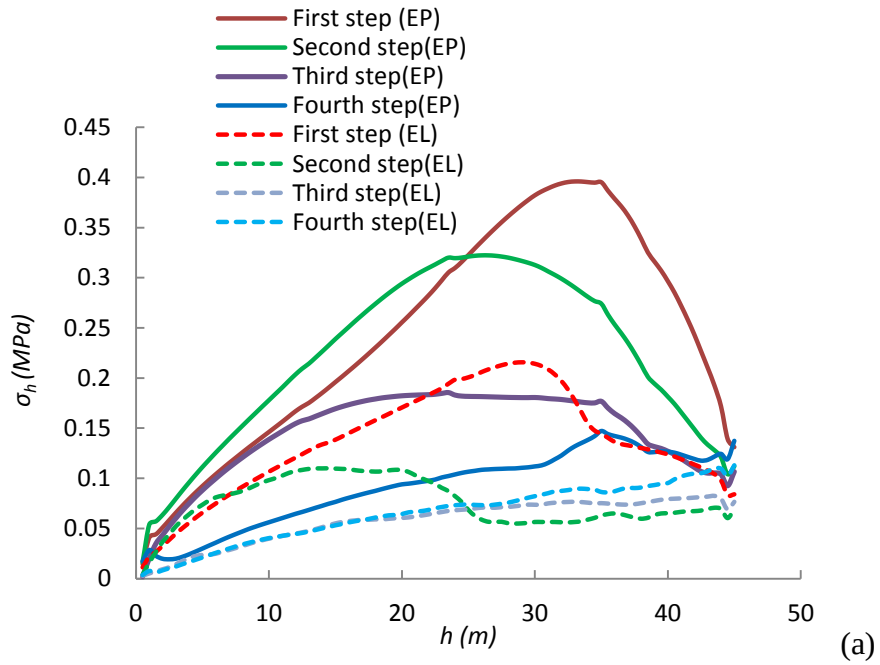

(a)

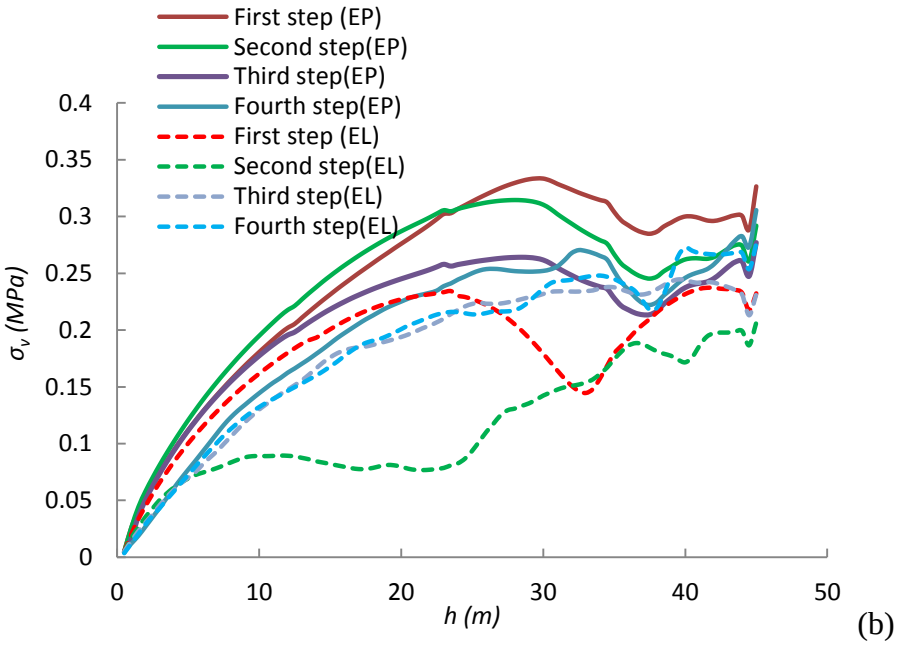

(b)

Figure D-1: Horizontal (a) and vertical (b) stress distributions along the left wall of the first backfilled stope for an elastic (EL, Case 1a) and elasto-plastic (EP, Case 1b) rock mass during the 4 steps of excavating the second stope

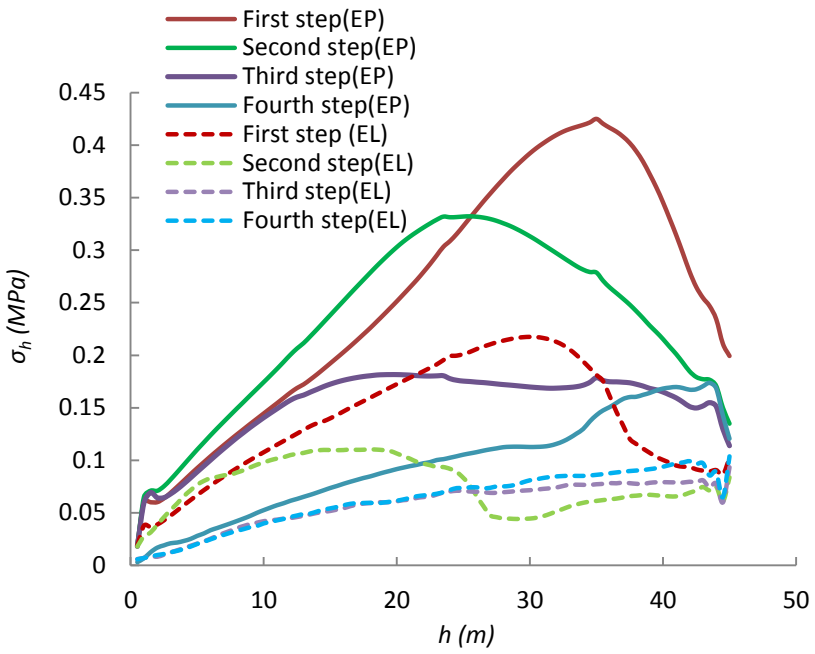

(a)

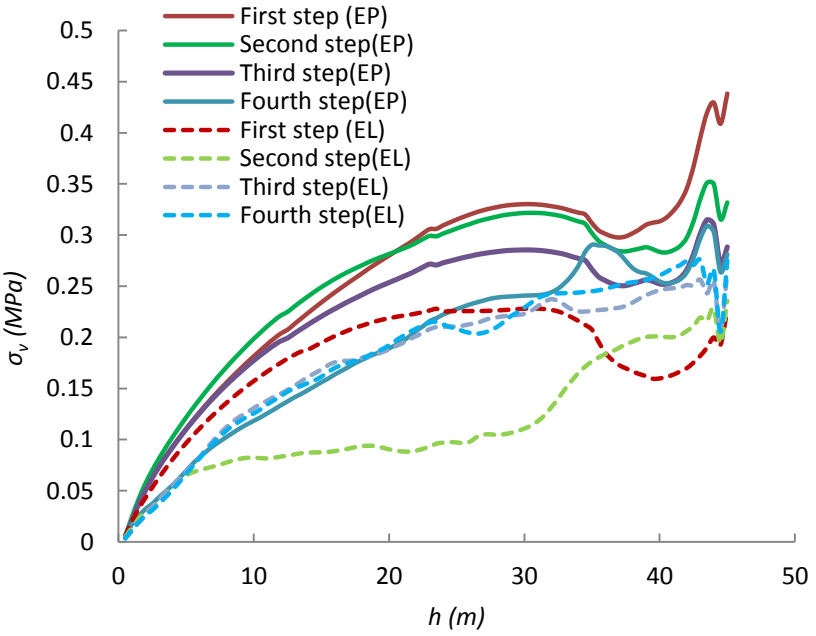

(b)

Figure D-2: Horizontal (a) and vertical (b) stress distributions along the right wall of the first backfilled stope for an elastic (EL, Case 1a) and elasto-plastic (EP, Case 1b) rock mass during the 4 steps of excavating the second stope

Stresses along the VCL of the first backfilled stope for EL model

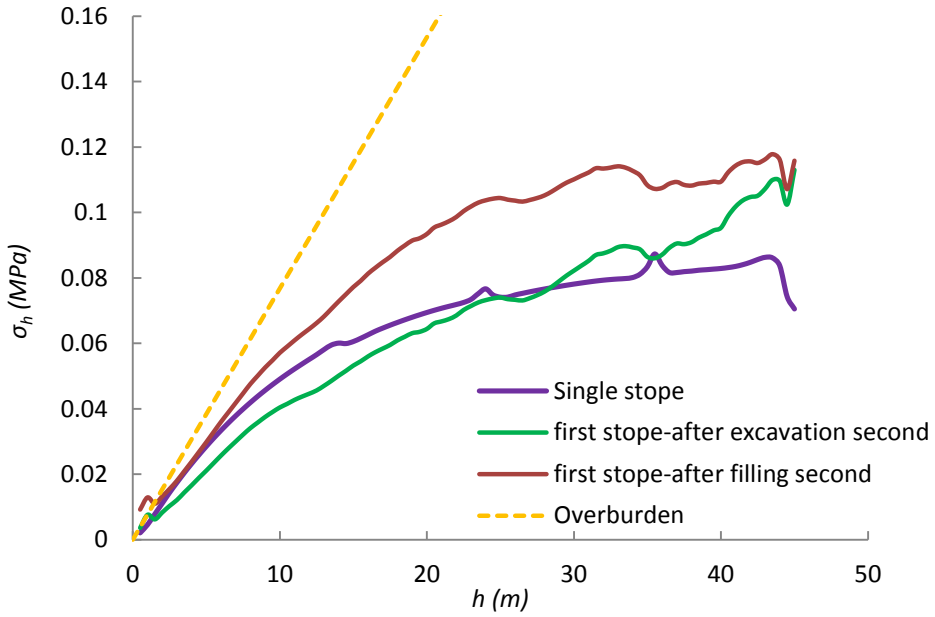

(a)

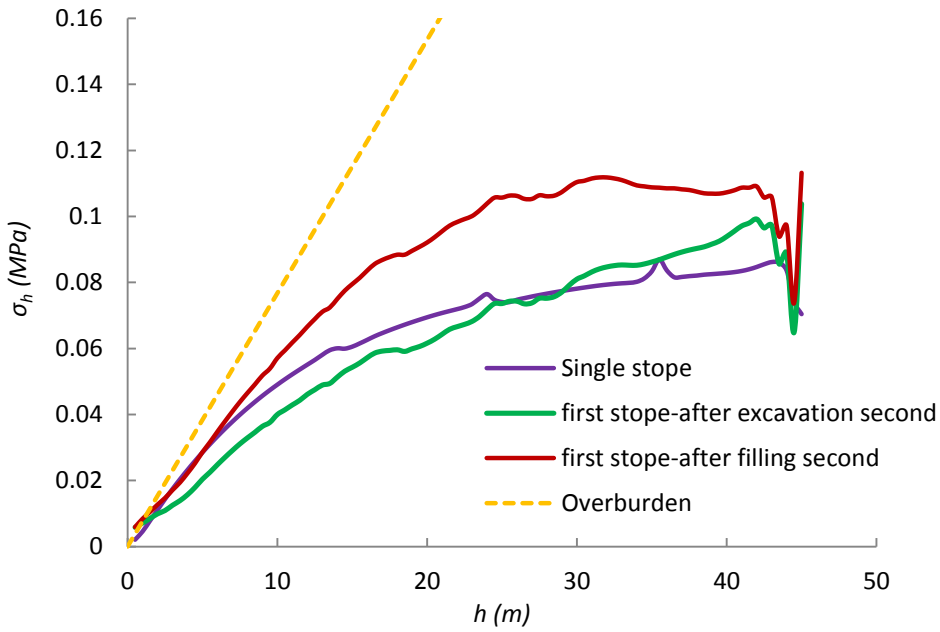

(b)

Figure D-3: Horizontal stress distributions along the: a) left wall; b) right wall of the first backfilled stope, after excavation and filling of the second stope, for an elastic rock mass behavior (EL, Case 1a)

Horizontal displcement of rock walls and stress path

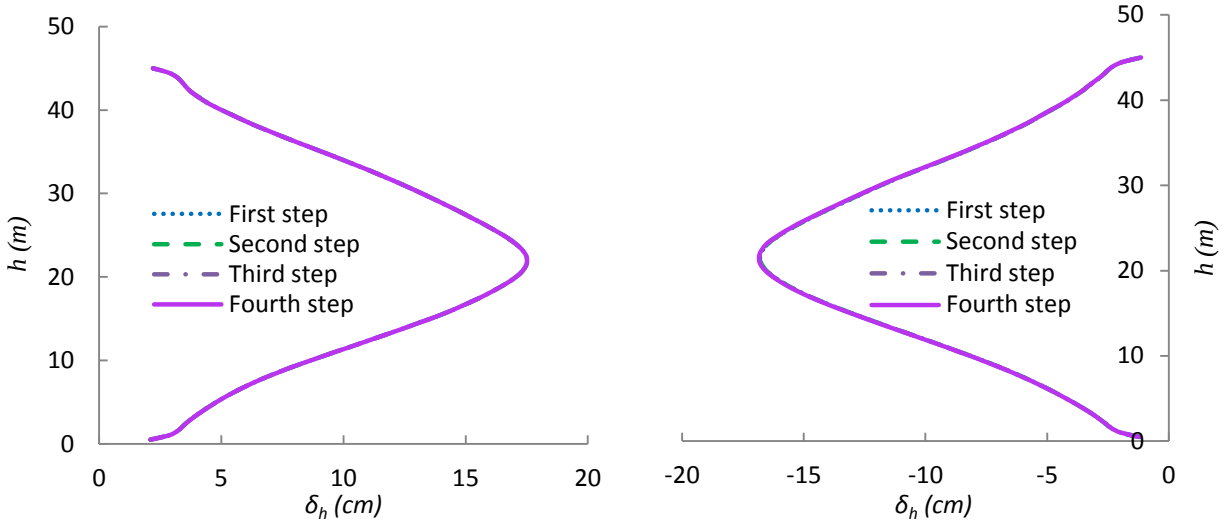

Figure D-4: Horizontal displacements δ_h along the: (a) left wall, (b) right wall of the first stope during filling (4 steps) of the second stope for the EP model (Case 1b)

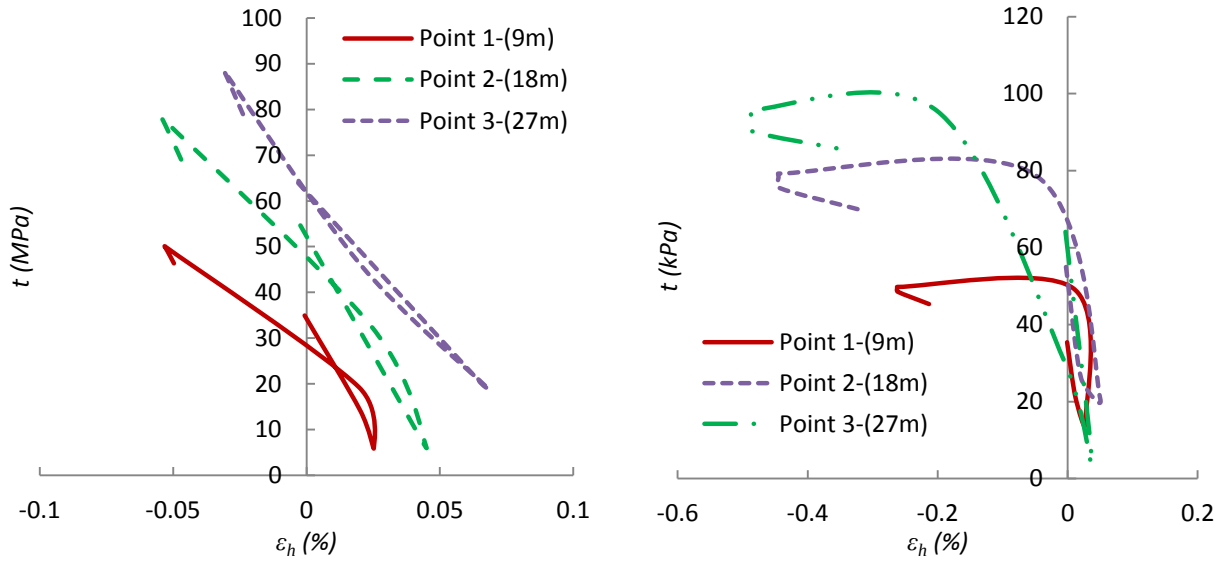

Figure D-5: Deviatoric *s* stresses and horizontal strains ε_h at three different locations (h = 9 m, 18 m, 27 m from the top) along the VCL of the first backfilled stope for: (a) an elasto-plastic rock mass behavior (EP, Case 1b), (b) an elastic rock mass behavior (EL, Case 1a) during the 9 steps (i.e. excavation and filling of the second stope)

Effect of stope width *B*

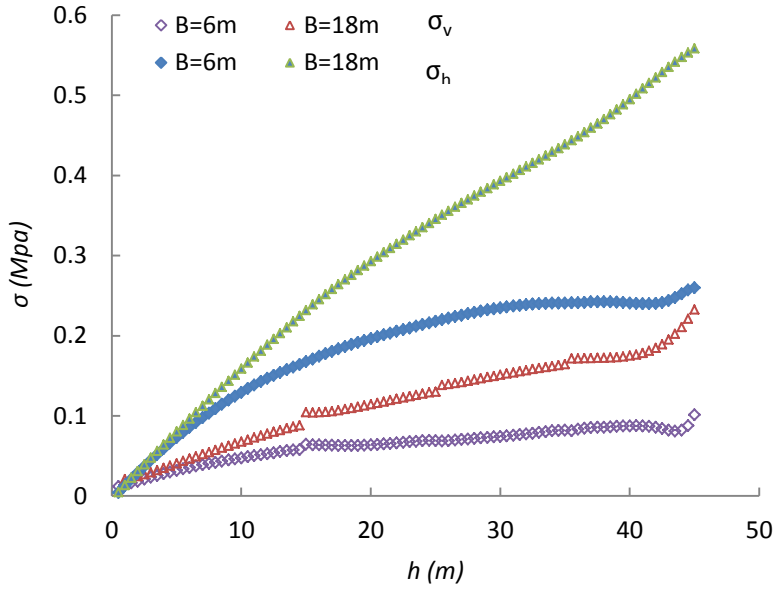

Figure D-6: Effect of stope width *B* on the vertical and horizontal stresses along the VCL of the second backfilled stope for an elasto-plastic rock mass behavior (EP) after excavation and filling of the second stope (Case 2)

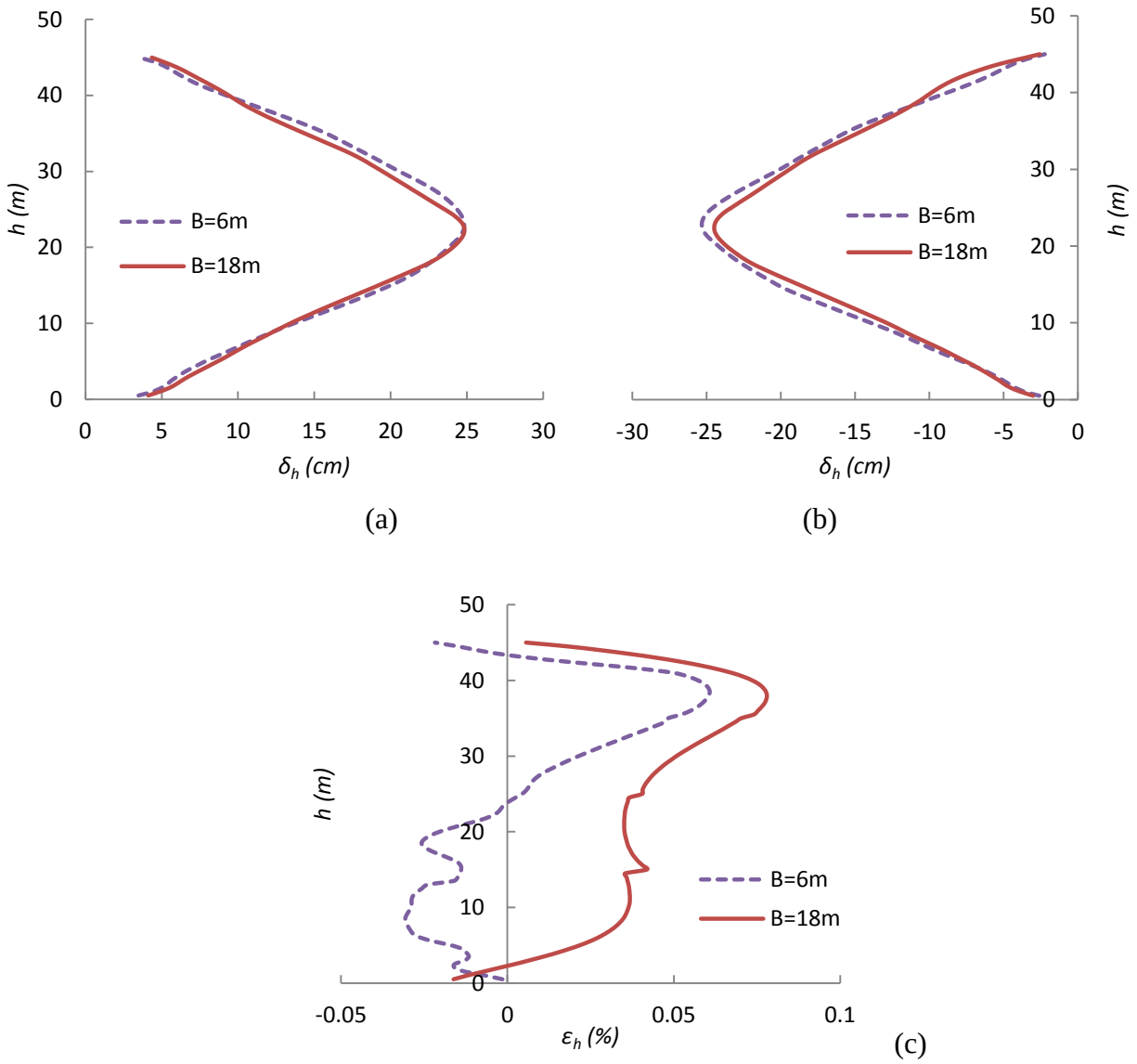

Figure D-7: Effect of stope width B on the horizontal displacements δ_h in the first stope along the: (a) left wall; (b) right wall; (c) horizontal strains ε_h in the backfill along the VCL after excavation and filling of the second stope (Case 2)

Effect of pillar width *D*

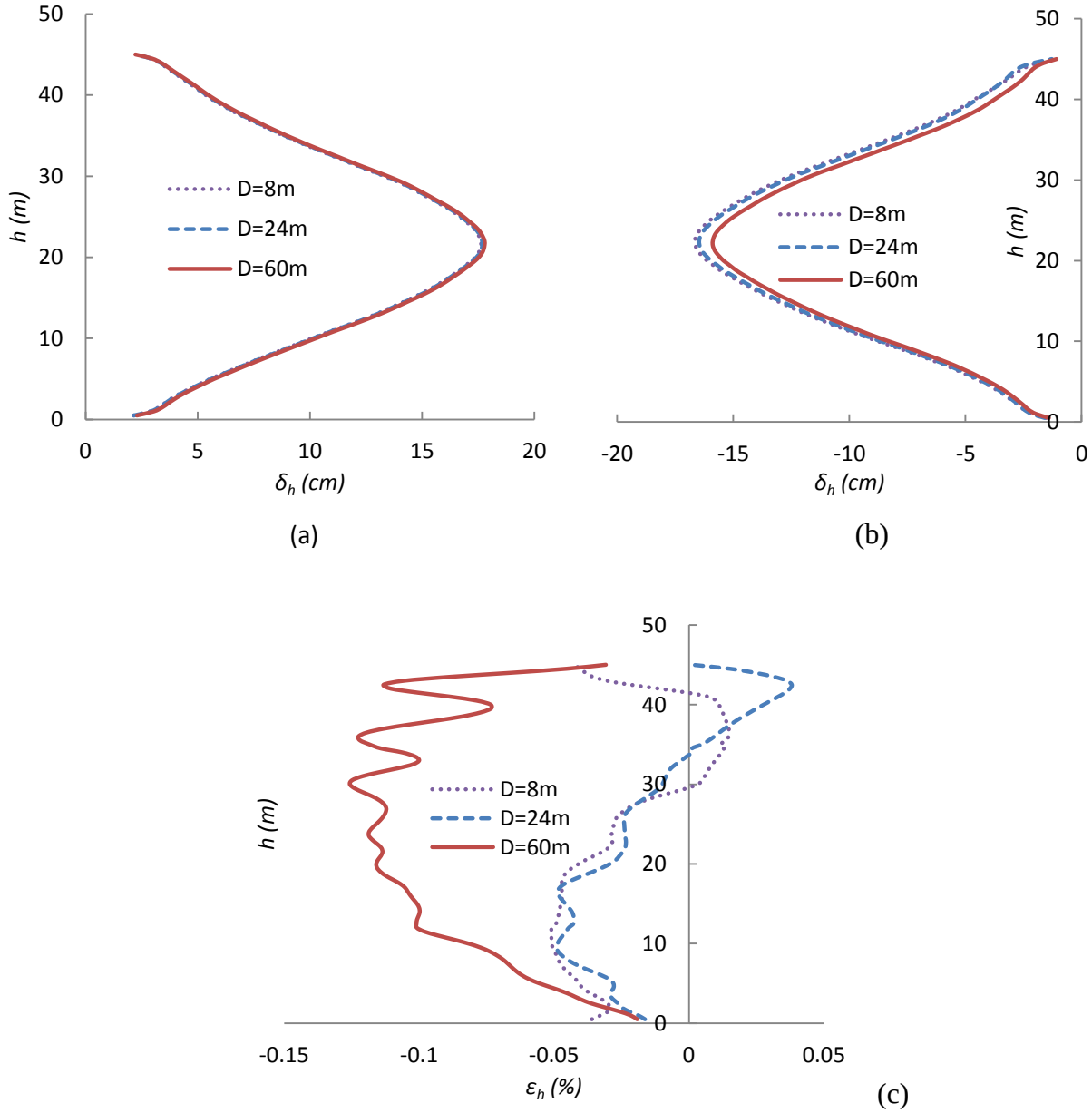

Figure D-8: Effect of pillar width *D* on the horizontal displacements δ_h in the first stope along the: (a) left wall; (b) right wall; (c) horizontal strains ε_h in the backfill along the VCL after excavation and filling of the second stope (Case 3)

Effect of stope depth *z*

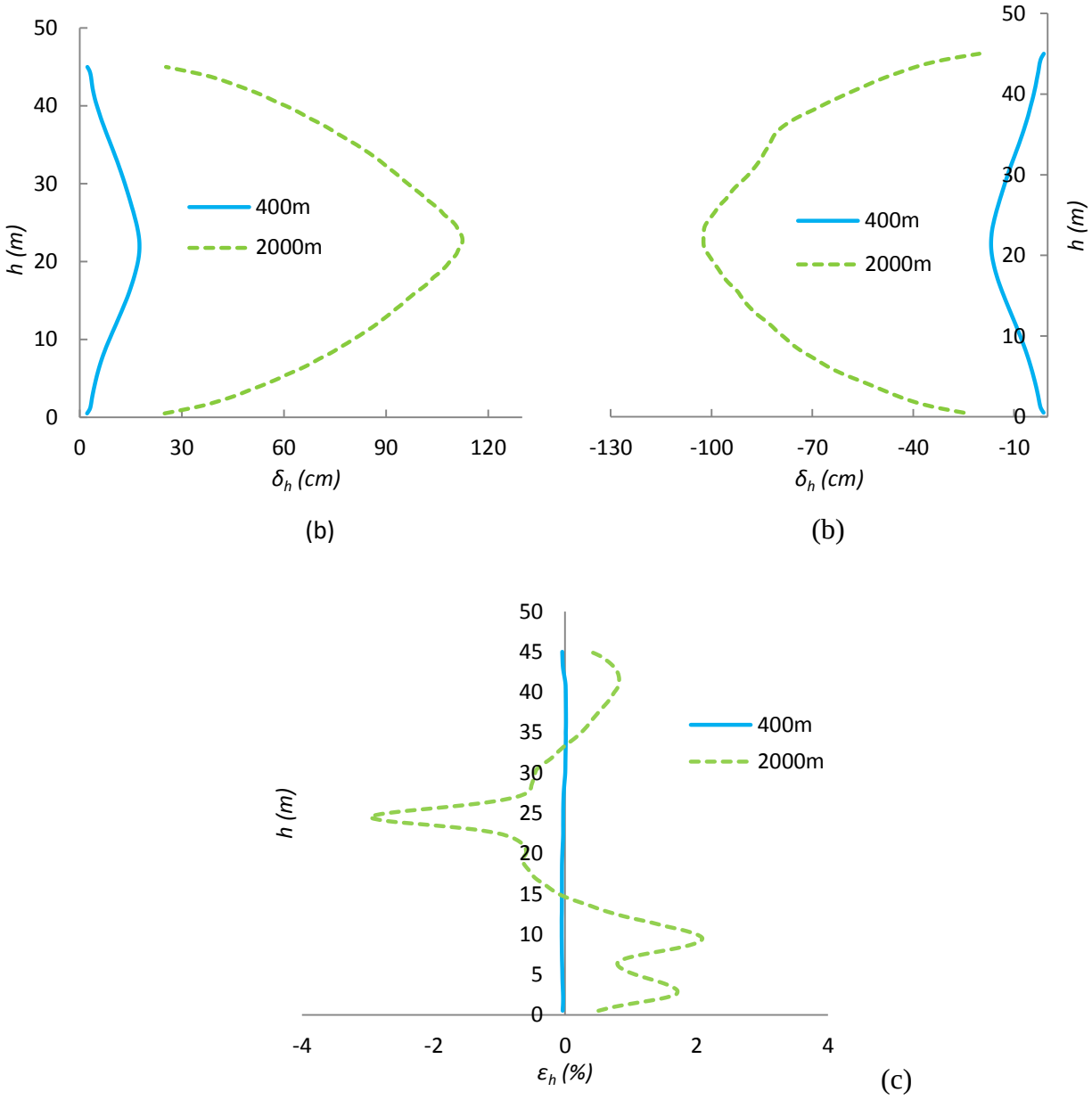

Figure D-9: Effect of stope depth *z* on the horizontal displacements δ_h in the first stope along the: (a) left wall; (b) right wall; (c) horizontal strains ε_h in the backfill along the VCL after excavation and filling of the second stope (Case 4)

Effect of K_r

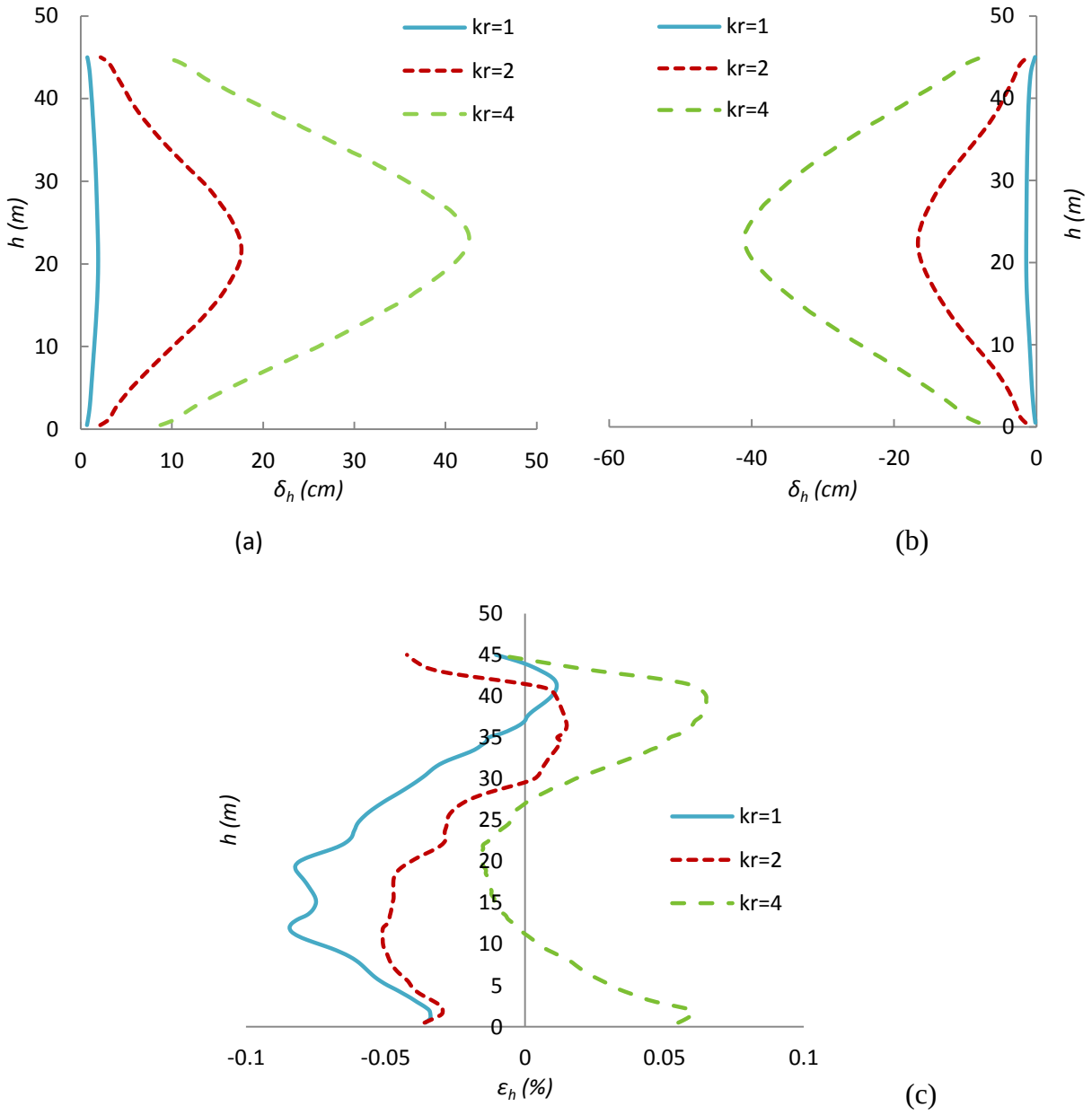

Figure D-10: Effect of K_r on the horizontal displacements δ_h in the first stope along the: (a) left wall; (b) right wall; (c) horizontal strains εh in the backfill along the VCL after excavation and filling of the second stope (Case 5)

Effect of E_r

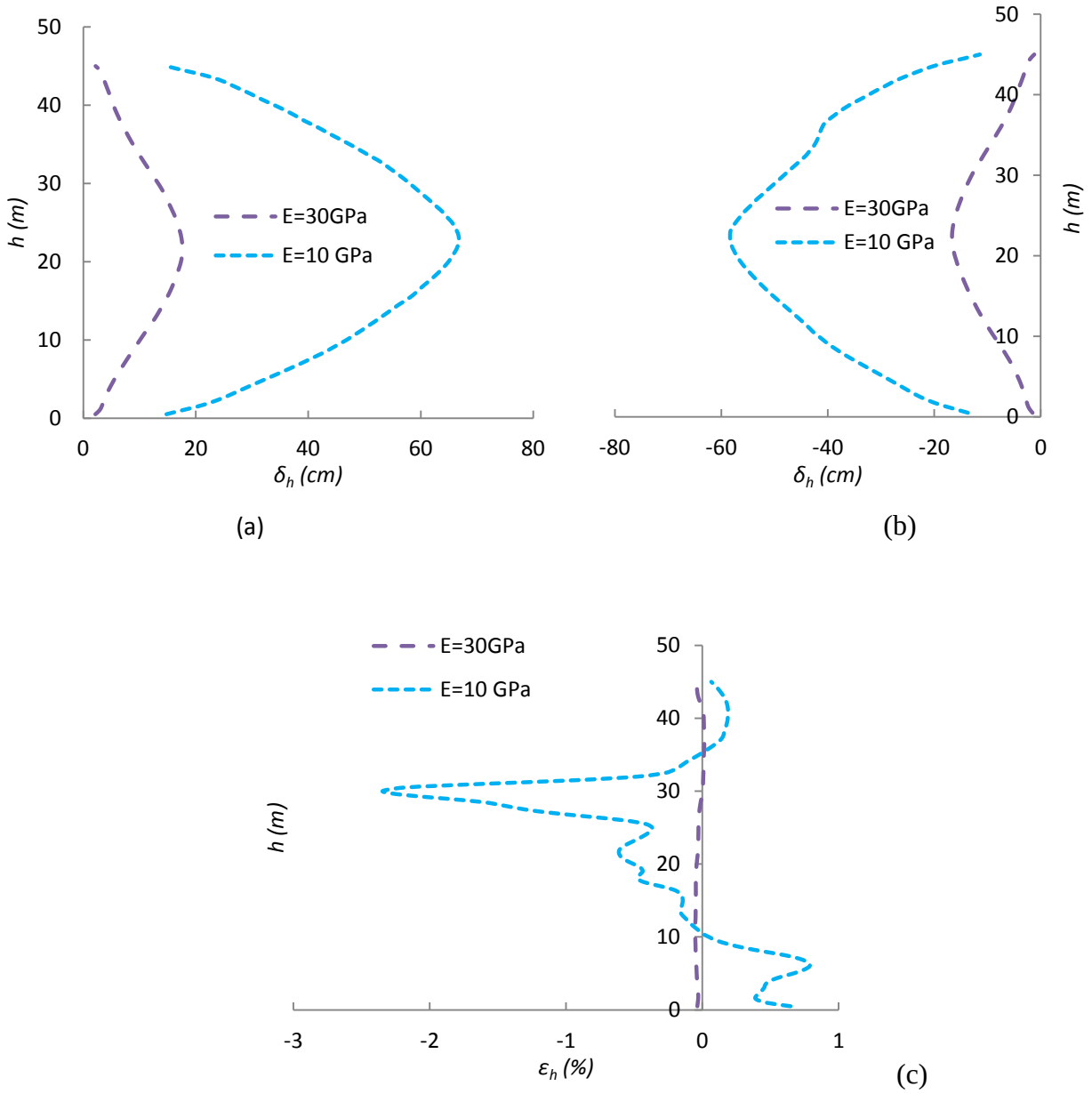

Figure D-11: Effect of rock modulus (strength parameters, c_r, ϕ_r) E_r on the horizontal displacements δ_h in the first stope along the: (a) left wall; (b) right wall; (c) horizontal strains ε_h in the backfill along the VCL after excavation and filling of the second stope (Case 6)

Effect of sequence

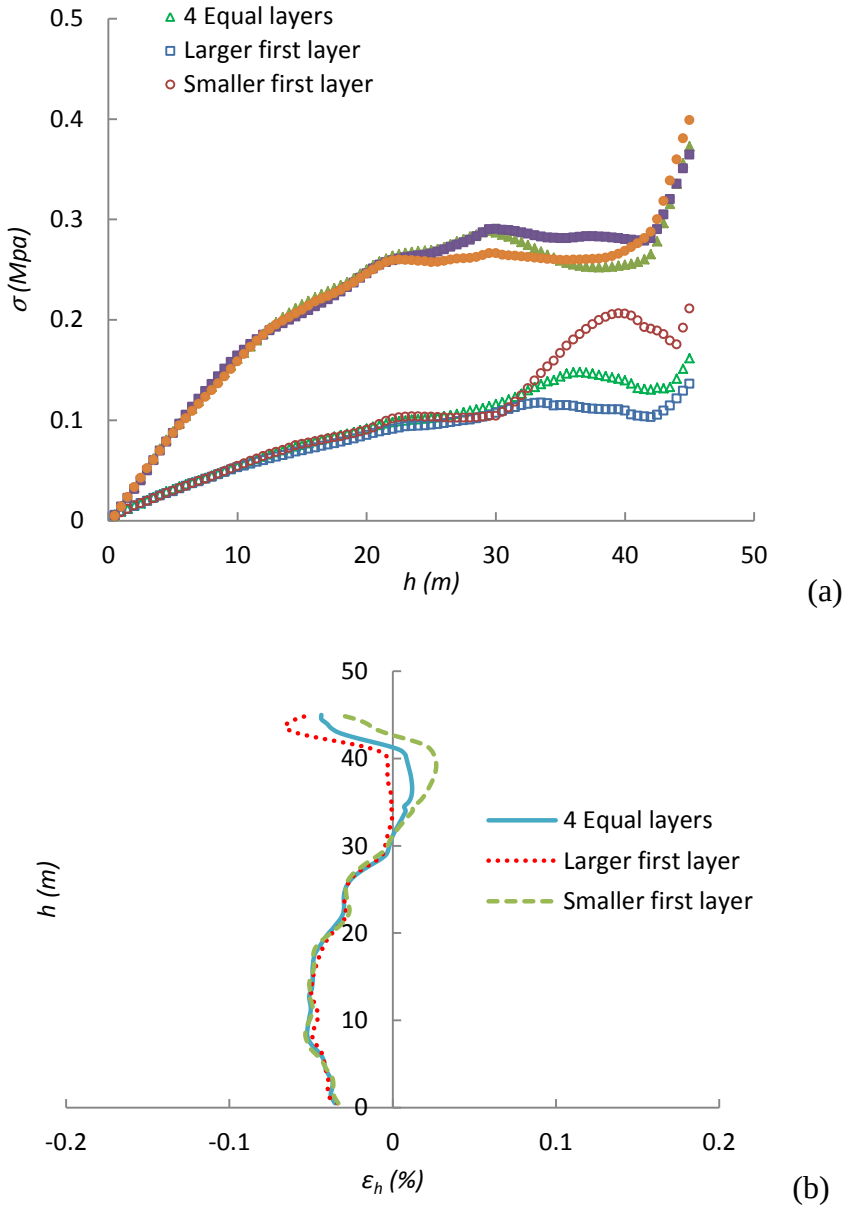

Figure D-12: Effect of the layer height on: (a) the the vertical and horizontal stresses, (b) horizontal strain ε_h in the first backfilled stope along the VCL for B = 6m, D = 8m

APPENDIX E - COMPLEMENTARY RESULTS RELATED TO CHAPTER 6

In this appendix, complementary results related to Chapter 6 are presented. The reults include the horizontal, $S_{yy,}$ and vertical S_{zz} stresses in the primary backfilled stope along the VCL and three walls before (BWR) and after (AWR) removal of the front wall with differnt stope geometry (*L*, *B*, *H*). Also, the effect of the number of excavation steps of the secandary stope on the displacements of the backfill in the primary stope when the front wall removed from top to bottom is shown. In addition, the required backfill cohesion *c* (for *FS* = 1) with variation of stope width, *B* obtained from three analytical solutions for (HAR) and (LAR) conditions is presented.

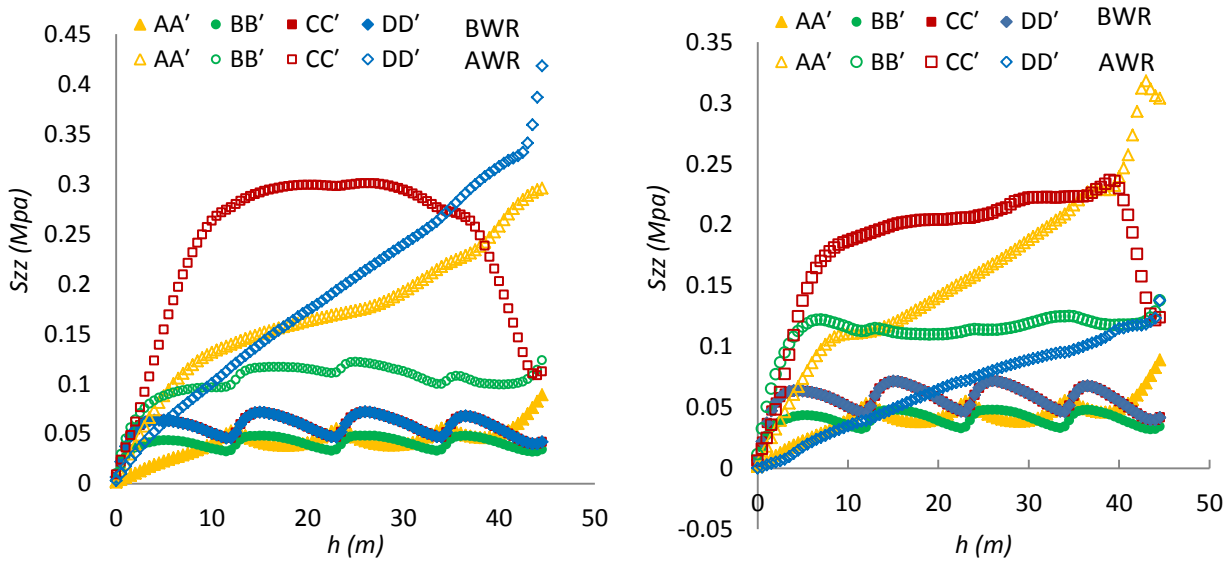

(a) (b)

Figure E-1: Vertical stresses S_{zz} in the primary backfilled stope along the VCL (line AA′), back wall (line CC′), sidewalls (line BB′) and open face (line DD′) before (BWR) and after (AWR) front wall removal: (a) Case $1_{30,85}$, stable backfill (b) Case $1_{30,60,}$ unstable backfill.

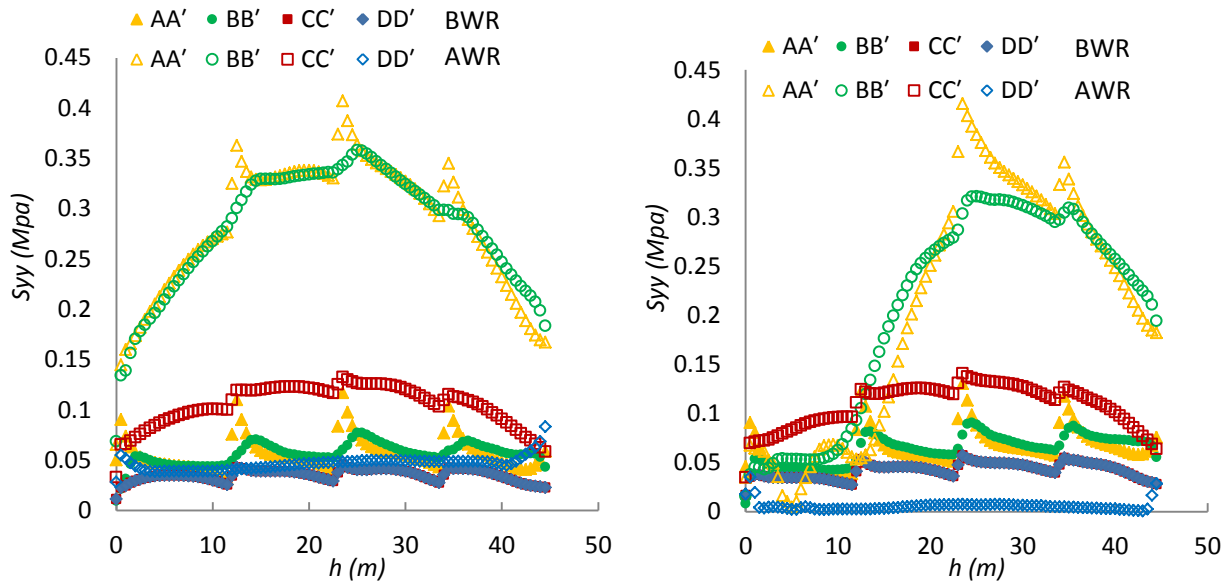

(a) (b)

Figure E-2: Horizontal stresses S_{yy} in the primary backfilled stope along the VCL (line AA′), back wall (line CC′), sidewalls (line BB′) and open face (line DD′) before (BWR) and after (AWR) front wall removal: (a) Case $2_{25,30}$, stable backfill (b) Case $2_{25,20,}$ unstable backfill.

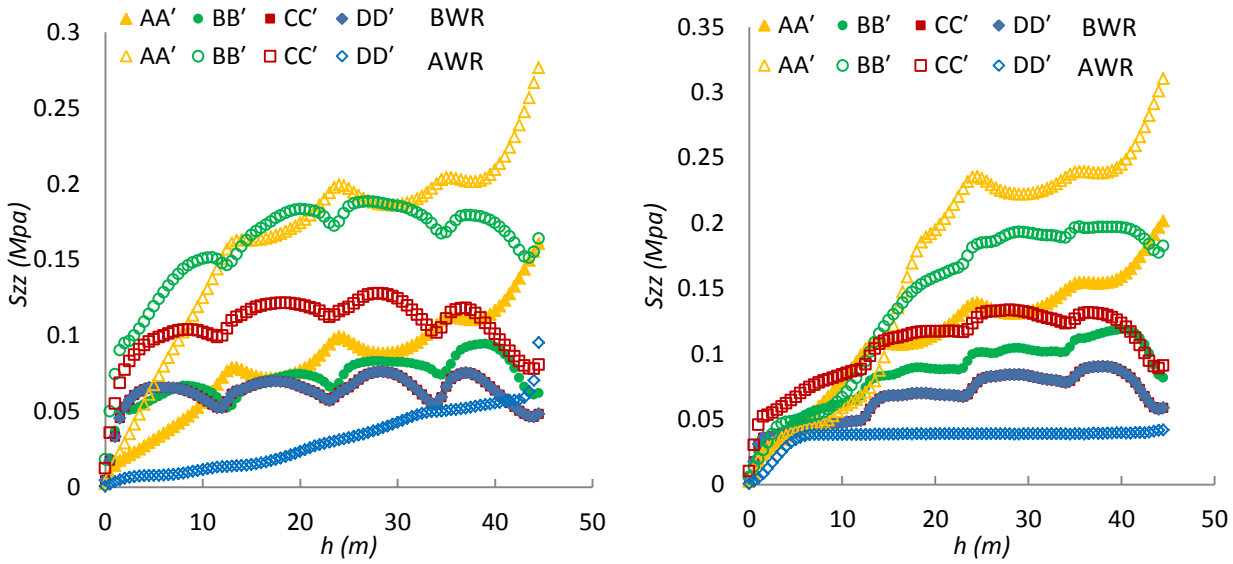

(a) (b)

Figure E-3: Vertical stresses S_{zz} in the primary backfilled stope along the VCL (line AA′), back wall (line CC′), sidewalls (line BB′) and open face (line DD′) before (BWR) and after (AWR) front wall removal: (a) Case $2_{25,30}$, stable backfill (b) Case $2_{25,20,}$ unstable backfill.

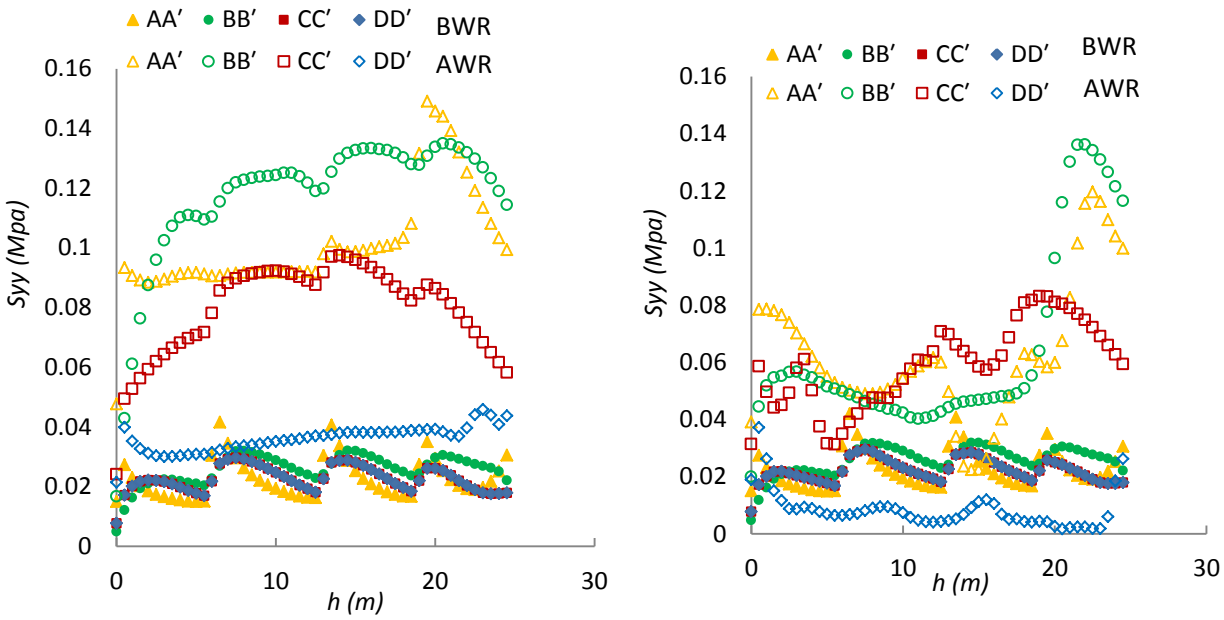

Figure E-4: Horizontal stresses S_{yy} in the primary backfilled stope along the VCL (line AA′), back wall (line CC′), sidewalls (line BB′) and open face (line DD′) before (BWR) and after (AWR) front wall removal: (a) Case $3_{25,24}$, stable backfill (b) Case $3_{25,20,}$ unstable backfill.

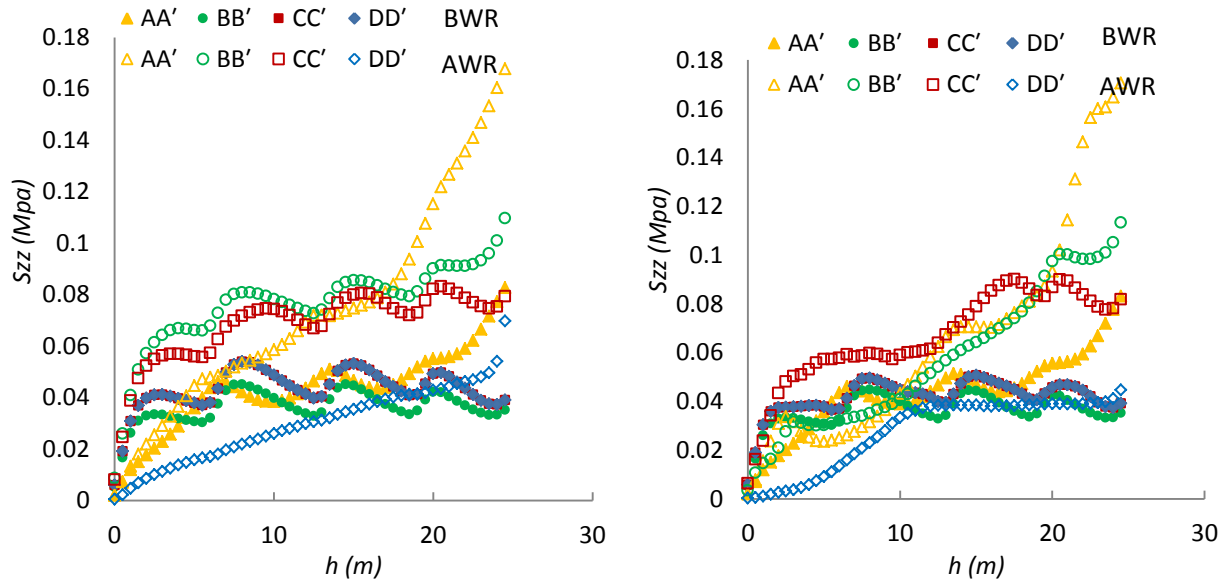

(a) (b)

Figure E-5: Vertical stresses S_{zz} in the primary backfilled stope along the VCL (line AA′), back wall (line CC′), sidewalls (line BB′) and open face (line DD′) before (BWR) and after (AWR) front wall removal: (a) Case $3_{25,24}$, stable backfill (b) Case $3_{25,20,}$ unstable backfill.

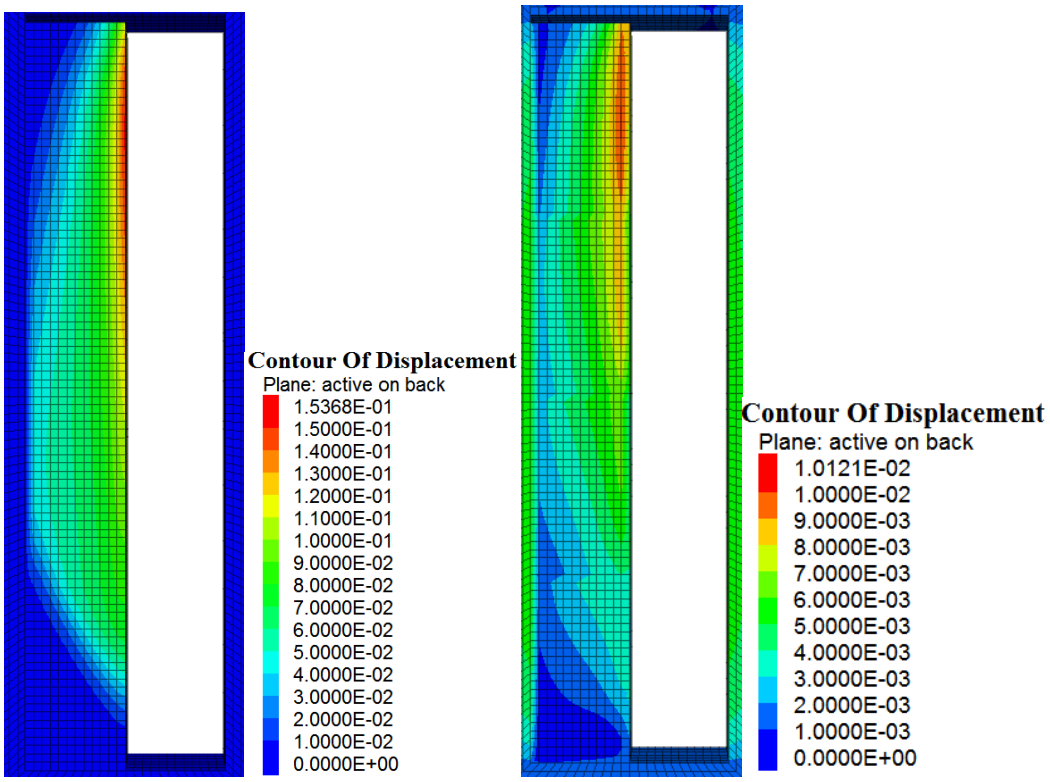

(a) (b)

Figure E-6: Effect of the number of excavation steps to create the secondary stope (removal of the front wall from top to bottom) on the displacements of the backfill in the primary stope: (a) one excavation step (Case 4_1) unstable backfill, (b) four excavation steps (Case 4_4) with c = 30 kPa.

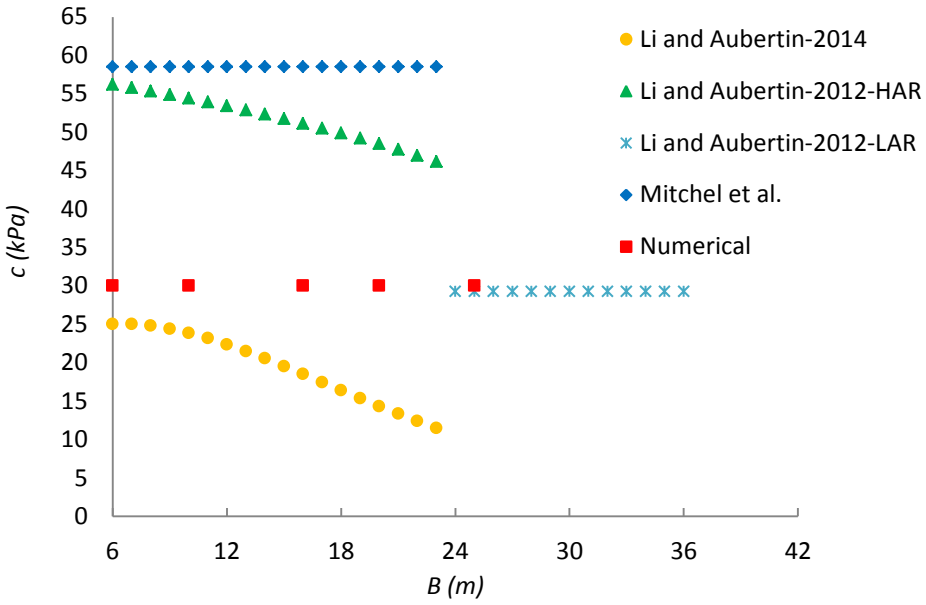

Figure E-7: Required backfill cohesion *c* (for *FS* = 1) with variation of stope width, *B*, (*L* = 9m, *H* = 45m); Results obtained from three analytical solutions for (HAR) and (LAR) conditions and numerical simulations.

APPENDIX F - COMPLEMENTARY RESULTS RELATED TO CHAPTER 7

In this appendix, complementary results related to Chapter 7 are presented. The reults include the horizontal displacements of rock walls after filling of the second stope when the stopes have limited length (3D). Also, the effect of backfill cohesion on the stress distribution along the walls of the first backfilled stope is presented.

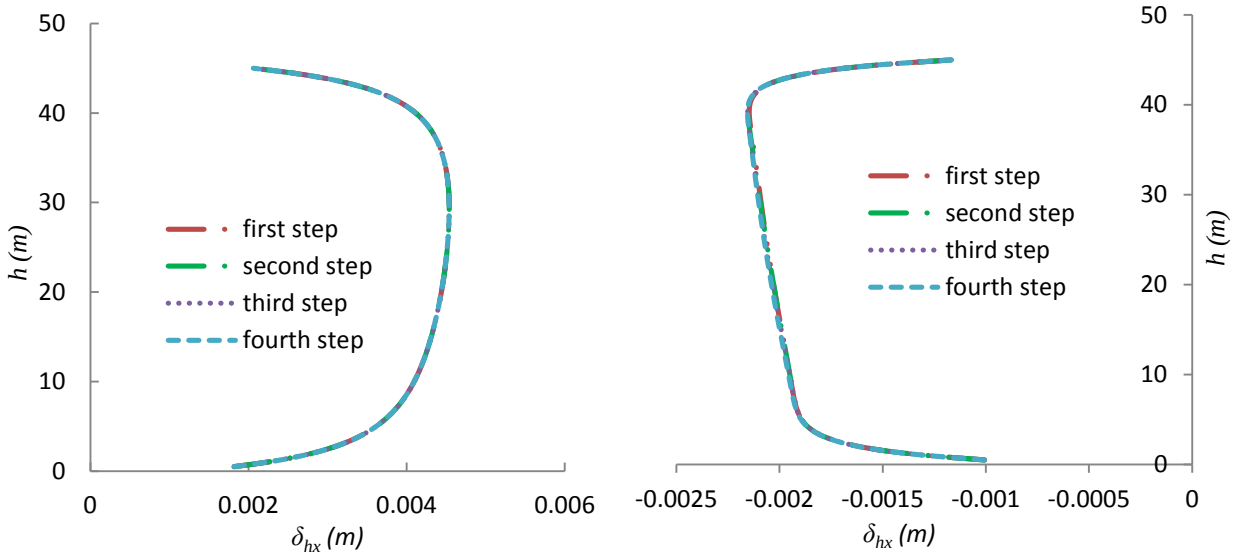

(a) (b)

Figure F-1: Horizontal displacements δ_{hx} obtained along the: (a) left wall (line BB′), and (b) right wall (line CC′) of the first backfilled stope with length L = 9 m (Case 3) after filling of the second stope

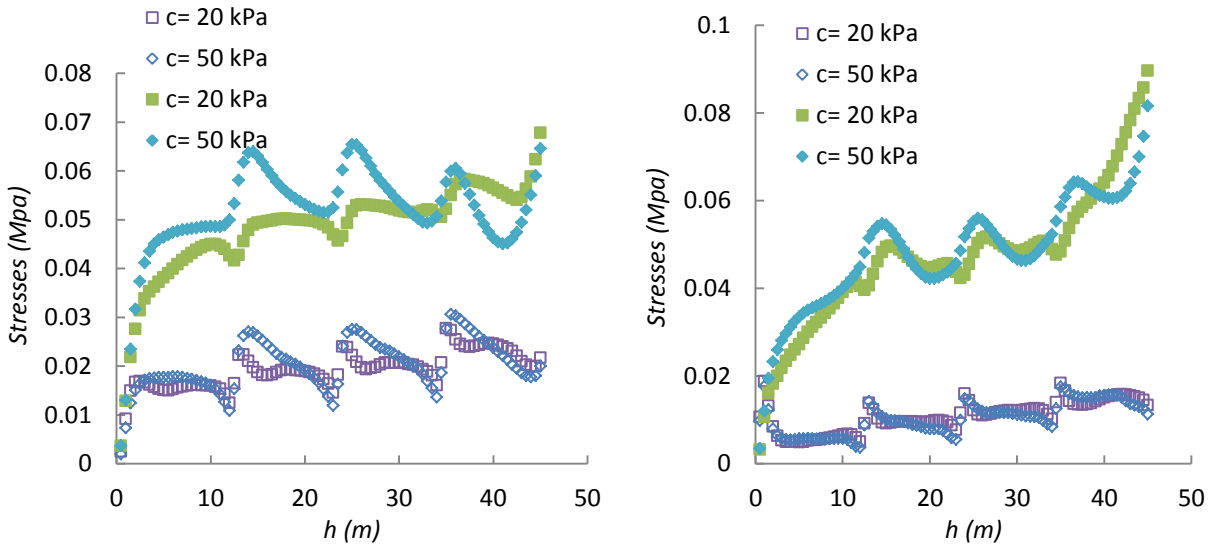

(a) (b)

Figure F-2: Effect of the cohesion c' of the backfill on the horizontal σ_{hx} and vertical σ_{vz} stresses along: (a) left wall (line BB′), (b) right wall (line CC′) of the first backfilled stope having B = 6m, L= 9m for Case 5b (3D)

APPENDIX G – ROCK MASS AND BACKFILL PROPERTIES

References	Young's modulus, *E* (GPa)		UCS (MPa)	
	Rock mass	backfill	Rock or Rock mass	backfill
Belem et al.(2000)	-	0.29-1.14	-	0.53-3.5
Li et al. (2003)	30	0.3	-	-
Rankine (2004)	30	0.2	-	0.1-0.7
Caceres (2005)	72-85	0.3	86-181	8
Pirapakaran (2008)	-	0.025- 0.12	-	0.47-0.9
Belem et al (2002), Belem and Benzaazoua (2008)	20-100	0.3-4	5-240	0.73-1.14
Fahey et al. (2009)	-	0.01-1	-	0.6-1.4
Helinski et al (2007)	-	0.05-0.25	-	0.2-2.5
Veenstra (2013)	-	0.002-0.12	-	0.05-0.8
Emad and Mitri (2013)*	51	2.5	-	-
Emad et al. (2014)*	28-32	4	7.6-11	3

*CRF (cemented or consolidated rock fill)